

Exploring the anti-cancer potential of phytochemicals against oral squamous cell carcinoma and developing their glycosylation strategies with organic Brønsted acid

by

ASWATHY.M.

10CC18A39010

A thesis submitted to the
Academy of Scientific & Innovative Research
for the award of the degree of

DOCTOR OF PHILOSOPHY
in
SCIENCE

Under the combined supervision of

Dr. K. V. RADHAKRISHNAN & Dr. L. RAVI SHANKAR



**CSIR-National Institute for Interdisciplinary
Science and Technology (CSIR-NIIST)
Thiruvananthapuram, Kerala- 695 019, India**



**Academy of Scientific and Innovative Research
AcSIR Headquarters, CSIR-HRDC campus
Sector 19, Kamla Nehru Nagar,
Ghaziabad, U.P. – 201 002, India**

JULY-2023

Dedicated to my beloved Family.....

CSIR- National Institute for Interdisciplinary Science and Technology



(Formerly Regional Research Laboratory)

Council of Scientific & Innovative Research (CSIR)



Industrial Estate P.O., Trivandrum-695 019

Kerala, INDIA

CERTIFICATES

This is to certify that the work incorporated in this Ph.D thesis entitled, “*Exploring the anti-cancer potential of phytochemicals against oral squamous cell carcinoma and developing their glycosylation strategies with organic Brønsted acid*” submitted by *Ms. Aswathy M.*, to the Academy of Scientific and Innovative Research (AcSIR) in fulfilment of the requirements for the award of the Degree of *Doctor of Philosophy in Sciences*, embodies original research work carried out by the student. We further certify that this work has not been submitted to any other University or Institution in part or full for the award of any degree or diploma. Research materials obtained from other sources and used in this research work has been duly acknowledged in the thesis. Images, illustrations, figures, tables etc., used in the thesis from other sources, have also been duly cited and acknowledged.

Aswathy M.

07/06/2023

Dr. K.V. Radhakrishnan

(Supervisor)

07/06/2023

Dr. L. Ravi Shankar

(Co-Supervisor)

07/06/2023

STATEMENTS OF ACCADEMIC INTEGRITY

I, Aswathy M. a Ph.D student of the Accademy of Scientific and Innovative Research (AcSIR) with Registration No. 10CC18A39010 hereby undertake that, the thesis entitled “*Exploring the anti-cancer potential of phytochemicals against oral squamous cell carcinoma and developing their glycosylation strategies with organic Brønsted acid*” has been prepared by me and that the document reports original work carried out by me and is free of any plagiarism in compliance with the UGC Regulations on “*Promotion of Academic Integrity and Prevention of Plagiarism in Higher Educational Institutions (2018)*” and the CSIR guidelines for “*Ethics in Research and in Governance (2020)*”.

July 7, 2023

Aswathy M.

Thiruvananthapuram

It is here by certified that the work done by the student, under our supervision, is plagiarism free in accordance with the UGC Regulations on “*Promotion of Academic Integrity and Prevention of Plagiarism in Higher Educational Institutions (2018)*” and the CSIR guidelines for “*Ethics in Research and in Governance (2020)*”.

Dr. K. V. Radhakrishnan

July 7, 2023

Thiruvananthapuram

Dr. L. Ravi Shankar

July 7, 2023

Thiruvananthapuram

DECLARATION

I, **Aswathy M.**, bearing AcSIR Registration No. 10CC18A39010 declare: that my thesis entitled, “*Exploring the anti-cancer potential of phytochemicals against oral squamous cell carcinoma and developing their glycosylation strategies with organic Brønsted acid*” is plagiarism free in accordance with the UGC Regulations on “*Promotion of Academic Integrity and Prevention of Plagiarism in Higher Educational Institutions (2018)*” and the CSIR guidelines for “*Ethics in Research and in Governance (2020)*”.

I would be solely held responsible if any plagiarised content in my thesis is detected, which is violative of the UGC regulations 2018.

July 7, 2023

Aswathy M.

Thiruvananthapuram

ACKNOWLEDGEMENTS

*It is with great respect that I express my deep sense of gratitude and obligation to my mentors and research supervisors **Dr. K. V. Radhakrishnan** and **Dr. L. Ravi Shankar** for suggesting the research topic and also for their excellent guidance, constant encouragement, and constructive criticism.*

*I am grateful to **Dr. C. Anandharamakrishnan** and **Dr. A. Ajayaghosh**, present and former Directors, National Institute for Interdisciplinary Science and Technology, for providing all infrastructural facilities to carry out this work.*

My sincere thanks are also due to:

- ❖ **Dr. V. Karunakaran** and **Dr. C. H. Suresh**, present and former AcSIR programme coordinator, CSIR-NIIST for the timely help and advice for the academic procedures of AcSIR*
- ❖ **Dr. B. S. Sasidhar**, **Dr. Kaustabh Kumar Maiti**, and **Dr. S. Priya** (my Doctoral Advisory Committee members) for their valuable suggestions and evaluations throughout my Ph. D. period.*
- ❖ **Dr. K. V. Radhakrishnan**, **Dr. P. Sujatha Devi**, **Dr. R. Luxmi Varma**, present and former Heads, Chemical Sciences and Technology Division for their endless support.*
- ❖ **Dr. Jubi John**, **Dr. Kaustabh Kumar Maiti**, **Dr. B. S. Sasidhar**, **Dr. Sunil Varughese**, and **Dr. Sreedevi**, **Dr. A. Kumaran**, Scientists of Organic Chemistry Section for the stimulation and assistance.*
- ❖ **Prof. Ajaikumar B. Kunnumakkara**, IIT-Guwahati for the wonderful collaboration in anti-cancer studies. **Dr. Kishore Banik**, **Ms. Parama Dey**, **Dr. Harsha Chawdary**, **Ms. Uzini Daimary** and **Dr. Mangala Hegde** for the help, suggestions and the support during the pharmacological evaluation.*
- ❖ **Dr. P. Sasikumar** and **Dr. P. Sharathna**, my seniors for teaching me the initial lessons of research.*
- ❖ **Mr. Abhijith**, **Mr. Sangeeth**, **Mr. Shihab Ahammed**, **Mr. Harikrishnan** for helping me to conduct some of the experiments in laboratory.*
- ❖ **Dr. Ajesh Vijayan**, **Dr. Manu M. Joseph**, **Ms. Anuja Joseph**, **Dr. Arunkumar T**, **Dr. Veena K.S**, **Dr. Meenu M.T**, **Dr. Nitha P.R** for the valuable suggestions and support throughout my work.*

- ❖ *Mr. Vijayakumar Swamiyappan, Mr. Sanjay Varma, Mr. Madhukrishnan, Ms. Irfana Jesin for the fruitful discussions and support.*
- ❖ *Mrs. Saumini Mathew for NMR analysis, Mrs. Viji S. for HRMS, Mr. Billu Abraham, Mrs. Susana Paulose and Mr. Vishnu K. Omankuttan for HPLC analysis*
- ❖ *Mrs. Varna Vijayan, Mrs. Natha K.M., Ms. Diya Anil, Mrs. Akhila N.S, Mrs. Seena Davis, Ms. Maria Peter, Ms. Azmi, Ms. Remya, Ms. Anju, Ms. Devika C.P, Ms. Sruthi Vipin, Ms. Sai Sruthy Murali, Ms. Justy, Ms. Gouri, Ms. Athira Ayyappan, Ms. Geethukrishna, Ms. Vrisanka J for helping me to complete some of the lab works.*
- ❖ *Dr. Prabha Bernard, Dr. Shimi M, Dr. Ashitha K.T, Dr. Santhi Manikanda, Dr. Aparana P.S, Dr. Dhanya B.P, Dr. Greeshma Goplan, Dr. Santhini P.V, Ms. Ummmu Jumailah, Dr. Santhi, and Dr. Neethu S. for the help and support*
- ❖ *Dr. Hridya V.K, Ms. Induja, Mr. Nagaraja, Ms. Sorna Rani, Ms. Sreedevi Menon, Mr. Krishnankumar, Dr. Vishnupriya Murali, Dr. Varsha, Dr. Nisha and Mr. Rahul, Mrs. Sheba, Mr. Akhil Krishnan, Mr. Vimalkumar, Ms. Priyadarshini and Dr. Biji for the help and support.*
- ❖ *Dr. Minju Thomas, Dr. Minju Asok, Dr. Silja Abraham, Dr. Nisha Narayanan for their love, care, support, and companionship*
- ❖ *All the present and former members of K.V.R and J.J group and present members of R.S.L group.*
- ❖ *All present and former members of Organic Chemistry Section for their friendship and creative inspirations.*
- ❖ *All my friends at CSIR-NIIST.*
- ❖ *All my teachers in S.N. College, Chengannur for the care and support.*

Words are inadequate to express my feelings for the love, care, support, and encouragement shown by my parents (Mr. Babu P and Mrs. Maniyamma) Brother (Arun B.), Partner (Madhukrishnan M.) and both family members throughout my academic career.

I am grateful to Council of Scientific and Industrial Research (CSIR), New Delhi, for the financial assistance.

And above all, I thank Almighty for all his blessings.

ASWATHY M.

TABLE OF CONTENTS

Certificate	i
Statement of academic integrity	ii
Declaration	iii
Acknowledgement	iv
Table of contents	vi
List of abbreviations	xii
Preface	xv
CHAPTER 1	1-11
Natural Products in Drug Discovery – Advances and Opportunities	
1.1. Introduction	1
1.2. History of modern drug discovery	1-2
1.3. Natural products in cancer treatment	2-5
1.4. Glycosylation reactions	5-6
1.5. Catalytic activators in glycosylation	6
1.6. Biological importance of carbohydrates	6-7
1.7. Conclusions and present of the present study	7-8
1.8. References	9-10
CHAPTER 2	
<i>In-vitro</i> Screening of Pentacyclic Triterpenoids from <i>Dillenia indica</i> Linn. against SAS Oral Squamous Cell Carcinoma	11-68
2.1. Introduction	11-12
2.2. An overview of Dilleniaceae family	12-15
2.3. Phytochemicals reported from <i>Dillenia</i> genus	15-16
2.4. Phytochemistry of <i>Dillenia indica</i> Linn.	16-18
2.5. Pharamacology of <i>Dillenia indica</i>	19-21
2.5.1. Anti-diabetic activity	19
2.5.2. Anti-cancer activity	19
2.5.3. Anti-oxidant activity	19-20
2.5.4. Anti-inflammatory activity	20
2.5.5. Anti-microbial activity	20
2.5.6. Anti-diarrhoeal activity	21
2.5.7. Anthelmintic activity	21

2.5.8. Hepatoprotective activity	21
2.6. Aim and scope of the study	21
2.7. Extraction, isolation and anti-proliferative analysis of the crude extracts	22-25
2.7.1. Plant collection	22
2.7.2. Extraction strategies and isolation procedures	22-25
2.8. Characterisation of compounds	
2.8.1. Compound 1	
2.8.2. Compound 2	
2.8.3. Compound 3	
2.8.4. Compound 4	
2.8.5. Compound 5	25-37
2.8.6. Compound 6	
2.8.7. Compound 7	
2.8.8. Compound 8	
2.8.9. Compound 9	
2.8.10. Compound 10	
2.9. Computational screening of BA and KA	38
2.9.1. QikProp analysis	38-39
2.9.2. Molecular docking	39-40
2.9.3. Molecular dynamics	40-41
2.10. DI inhibited the clonogenic ability of OSCC cells	41-42
2.11. DI induced cell death in OSCC cells	42-43
2.12. Effect of DI in inducing apoptosis in SAS cells	44
2.13. DI induced cell cycle arrest in OSCC cells	44-45
2.14. DI inhibited the migration of OSCC cells	45-46
2.15. DI mediated the expression of critical protein players	46-51
2.16. Conclusions	51
2.17. Experimental section	52-58
2.17.1. Cell Line	52
2.17.2. Reagents	52
2.17.3. Extraction of DI Fruits	52
2.17.4. Isolation of phytochemicals from methanol extract	52-53
2.17.5. Characterization of Phytochemicals	53

2.17.6.	Computational screening and MD simulation	53-54
2.17.7.	Cell Proliferation Assay	54
2.17.8.	Colony-Forming Assay	54
2.17.9.	Cell Death Analysis	54-55
2.17.10.	Live and Dead Assay	55
2.17.11.	Apoptosis Assay	55-56
2.17.12.	Cell Cycle Analysis	56
2.17.13.	Cell Migration Assay	56
2.17.14.	Western Blot Analysis	57
2.17.15.	Statistical Analysis	57
2.18.	Spectral data	57-61
2.19.	References	61-68
CHAPTER 3		
CHAPTER 3A		
	Bioprospecting of Prenyl Flavones and Phenolic Constituents from <i>Artocarpus altilis</i> (Parkinson) Fosberg.	69-91
3A.1.	<i>Artocarpus altilis</i> (Parkinson) Fosberg.	69
3A.2.	Phytochemistry of <i>Artocarpus altilis</i>	69-71
3A.3.	Pharmacological activity of <i>Artocarpus altilis</i>	71-73
3A.3.1.	Antitubercular and Antiplasmodial	71-72
3A.3.2.	Antiatherosclerotic activity	72
3A.3.3.	Anti-microbial activity	72
3A.3.4.	Anti-cancer activity	72
3A.4.	Aim and scope of the study	72-73
3A.5.	Extraction, isolation and characterization of phytochemicals	73
3A.5.1.	Collection of plant material	73
3A.5.2.	Extraction and isolation procedure	73-85
3A.6.	Conclusions	86
3A.7.	Experimental Section	86
3A.7.1.	Extraction of <i>Artocarpus altilis</i>	86
3A.7.2.	Isolation of Phytochemicals from <i>Artocarpus altilis</i> stem bark	86
3A.8.	Spectral Data	87-90
3A.9.	References	90-91

CHAPTER 3B

Exploring the Cytotoxic Effects of Natural Prenylflavones from <i>Artocarpus altilis</i> against SAS Oral Squamous Cell Carcinoma	93-120
3B.1. Introduction	92-94
3B.2. Results and Discussion	94-96
3B.2.1. Evaluation of Anti-proliferative potential of isolated phytochemicals against oral squamous cell carcinoma (OSCC)	94-96
3B.2.2. Computational screening of active candidates AA2 and AA3	96
3B.2.2.1. Molecular docking	96-97
3B.2.2.2. Molecular Dynamics	98
3B.2.3. Effect of AA2 and AA3 in colony formation potential of SAS cells	99
3B.2.4. Effect of AA2 and AA3 in the migration of SAS cells	99-101
3B.2.5. Effect of both AA2 and AA3 in inducing cell death in SAS cells	101-102
3B.2.6. Induction of apoptosis by annexin V assay	102-103
3B.2.7. AA2, AA3 induced cell cycle arrest in SAS OSCC cells	103-104
3B.2.8. Effect of AA2 and AA3 in the expression of critical players	104-109
3B.3. Conclusions	109-110
3B.4. Experimental Section	110
3B.4.1. General experimental procedure	110
3B.4.2. Plant material	110
3B.4.3. Extraction and isolation of phytochemicals	110
3B.4.4. Computational Screening and Molecular Dynamics simulation	110-111
3B.4.5. Cell culture	111
3B.4.6. Cell proliferation MTT assay	111
3B.4.7. Colony formation assay	111-112
3B.4.8. Wound healing assay	112
3B.4.9. PI-FACS analysis	112
3B.4.10. Annexin V assay	113
3B.4.11. Cell cycle analysis	113
3B.4.12. Western blot analysis	113-114
3B.4.13. Statistical analysis	114
3B.5. References	114-120

CHAPTER 4

An Organic Brønsted Acid, Pentacarbomethoxycyclopentadiene (PCCP) Catalysed Stereo-, and Regioselective Glycosidation of Secondary Metabolites in Conjunction with N-Iodosuccinimide **121-167**

4.1. Introduction	121-122
4.2. Results and Discussion	122
4.2.1. Synthetic route of Pentacarbomethoxycyclopentadiene	122-125
4.2.2. Synthesis of <i>n</i> -pentenyl orthoester (NPOE) donors	125-132
4.2.3. Selection of glycosyl acceptors	132
4.2.4. General procedure & optimization BA-mediated Glycosylation	133-151
4.3. Plausible mechanism	151-152
4.4. Conclusions	152
4.5. Experimental Section	153
4.5.1. General Experimental Methods	153
4.5.2. General procedure for BA mediated Glycosylation	153
4.6. Spectral data	153-164
4.7. References	164-167

CHAPTER 5

α/β -Stereo- and Diastereoselective Glycosylation with *n*-Pentenyl Glycoside Donors, Promoted by N-Iodosuccinimide and Catalysed by Chiral Brønsted Acid **168-223**

5.1. Introduction	168-169
5.2. Results and Discussion	169
5.2.1. Synthesis of chiral Brønsted acids, CBA 1, CBA 3 & CBA 4	169-172
5.2.2. Procedure for the synthesis of glycosyl donors 6, 7, and 8	173-177
5.2.3. General procedure for chiral Brønsted acid mediated glycosylation with racemic substrates	178
5.2.4. Mechanistic rationale behind the stereoselectivity of glycosylation	195
5.3. Conclusions	214
5.4. Experimental Section	215
5.5. Spectral data	215-221
5.6. References	221-223

Abstract of the thesis	224
List of publications	225
Papers presented at conferences	226
Attachment of the Photocopy of Publications	

ABBREVIATIONS

Å	:	Angstrom
AA	:	<i>Artocarpus altilis</i>
Bcl-2	:	B-cell lymphoma 2
BSA	:	Bovine serum albumin
Calcd	:	Calculated
Ca ⁺⁺	:	Calcium ion
CC	:	Column chromatography
CDCl ₃	:	Deuterated chloroform
CD ₃ COCD ₃	:	Deuterated acetone
cm	:	Centimeter
COX-2	:	cyclooxygenase 2
CXCR4	:	C-X-C chemokine receptor type 4
°C	:	Degree Celsius
d	:	doublet
DCM	:	Dichloromethane
dd	:	Doublets of doublet
DEPT	:	Distortionless enhancement by polarization transfer
DI	:	<i>Dillenia indica</i>
DMEM	:	Dulbecco's modified eagle's medium
DMSO	:	Dimethyl sulfoxide
DTT	:	Dithiothreitol
EDTA	:	Ethylenediaminetetraacetic acid
EGFR	:	Epidermal growth factor receptor
Equiv.	:	Equivalence
ESI	:	Electrospray ionization
EtOAc	:	Ethyl acetate
FACS	:	Fluorescence-activated cell sorting
FBS	:	Foetal bovine serum
FT-IR	:	Fourier transform infrared
FDA	:	Food and Drug Administration
Fr.	:	Fraction
g	:	Gram

GAPDH	:	Glyceraldehyde 3-phosphate dehydrogenase
h	:	Hour
IUCN	:	International Union for Conservation of Nature
HCl	:	Hydrochloric acid
HEPES	:	4-(2-hydroxyethyl)-1-piperazineethanesulfonic acid
HMBC	:	Heteronuclear multiple bond correlation
HMQC	:	Heteronuclear multiple-quantum correlation
HOMOCOSY	:	Homonuclear Correlation Spectroscopy
HPLC	:	High performance liquid chromatography
HRMS	:	High-resolution mass spectrometry
Hz	:	Hertz
IL-8	:	Interleukin-8
IC ₅₀	:	Half minimal inhibitory concentration
IR	:	Infrared
J	:	Coupling constant
JAK2	:	Janus kinase-2
m	:	Multiplet
M+	:	Molecular ion
MeOH	:	Methanol
mg	:	Milligram
MHz	:	Mega Hertz
mL	:	Millilitre
mM	:	Millimolar
mmol	:	Millimoles
MMPs	:	Matrix metalloproteinases
mTOR	:	Mammalian target of rapamycin
MTT	:	3-(4,5-Dimethylthiazal-2-yl)-2,5-diphenylterazolium bromide
NF- κ B	:	Nuclear factor kappa B
NMR	:	Nuclear Magnetic Resonance
NOESY	:	Nuclear overhauser effect spectroscopy
OSCC	:	Oral squamous cell carcinoma

PBS	:	Phosphate-buffered saline
PDB	:	Protein Data Bank
PI	:	Propidium iodide
PMSF	:	Phenylmethylsulfonyl fluoride
ppm	:	Parts per million
p38 MAPK	:	p38 mitogen-activated protein kinase
RT	:	Room temperature
s	:	Singlet
SDS-PAGE	:	Sodium dodecyl sulfate polyacrylamide gel electrophoresis
STAT	:	Signal transducer and activator of transcription
Sc(OTf) ₃	:	Scandium triflate
t	:	Triplet
TBST	:	Tris-buffered saline (TBS) and Polysorbate 20 (Tween 20)
TLC	:	Thin Layer Chromatography
TMS	:	Tetramethylsilane
TNF	:	Tumor necrosis factor
TRAIL	:	TNF related apoptosis-inducing ligand
α	:	Alpha
β	:	Beta
δ	:	Delta
μL	:	Microlitre
μM	:	Micromolar
UV	:	Ultraviolet
VEGF	:	Vascular endothelial growth factor

PREFACE

Natural products and their structural analogues have extensively contributed to pharmacotherapy owing to the development of novel scaffolds of drugs to treat various human ailments.¹ The rich source of medicinal plants and their applications are well-acknowledged in indigenous traditional systems like Siddha, Ayurveda, Unani, and Allopathy. According to the World Health Organization (WHO), 80% of the global population still put their faith in plant-based medicines for key health care.² Cancer, a multifactorial malaise arises due to the dysregulation of multiple signaling pathways in the body. Currently available options for cancer treatment involve surgical removal, radiation therapy, and chemotherapy are associated with numerous side effects and adverse limitations such as recurrence of tumour, toxicity to normal cells, chemo resistance, and radioresistance. Taxol analogs, vinca alkaloids such as vincristine, vinblastine, and podophyllotoxin analogs, etc. are the FDA approved anti-cancer drugs under clinical practices possessing complementary and overlapping mechanisms to slow down the carcinogenic process. Encouraged with the excellent therapeutic potential of naturally derived compounds in clinics there is recent advancement of researches that emphasized on the development of new drug leads from floras with the aid of sophisticated and innovative techniques.

In **chapter 2**, we attempted to explore the anticancer potential of the fruit extract of the ethnomedicinal plant *Dillenia indica* against oral squamous cell carcinoma (OSCC) and have exclusively attributed the efficacy of the extracts to the presence of two triterpenoids, namely, betulinic acid (BA) and koetjapic acid (KA). Preliminary in vitro screening of both BA and KA unveiled that the entities could impart cytotoxicity and induce apoptosis in OSCC cell lines, which were further well-supported by virtual screening based on ligand binding affinity and molecular dynamic simulations. Additionally, the aforementioned metabolites could significantly modulate the critical players such as Akt/mTOR, NF- κ B, and JAK/STAT3 signaling pathways involved in the regulation of important hallmarks of cancer like cell survival, proliferation, invasion, angiogenesis, and metastasis. The present findings provide insight and immense scientific support and integrity to a piece of indigenous knowledge.

Chapter 3, part A deals with the phytochemical evaluation of ethnomedicinal species, *Artocarpus altilis* (Parkinson) Fosberg from the Western Ghats of India. The plant is a traditionally highlighted flora widely used as a traditional medicine for the treatment of various ailments. The species is enriched with isoprenyl and geranyl substituted flavones. Herein, we

are reporting the detailed chemoprofiling of *Artocarpus altilis*. In part B, we have unveiled the anti-cancer effect of two flavone isolated from the acetone extract of the stem bark of *Artocarpus altilis* (Parkinson) Fosberg for the inhibition and prevention of the growth and multiplication of SAS oral cancer cells. The disclosed bioactive flavonoids artonin E (AA2) and artobiloxanthone (AA3) have isoprenyl substitution and pyranoxanthone moiety respectively. Further, both compounds were optimized with the aid of virtual screening based ligand binding affinity and molecular simulation studies. Additionally, the promising anti-cancer potential of the selected candidates was demonstrated through various apoptotic and metastatic assays and explained the mechanistic evaluation of the molecules in the *in-vitro* system. Further, the mechanistic rationale behind the mode of action was illustrated with immunoblotting analysis and demonstrated changes in the expression of various critical protein players involved in cancer progression and development.

In **chapter 4**, we utilized the organic Brønsted acid, Pentacarbomethoxycyclopentadiene (PCCP), for catalysing the glycosylation with *n*-pentenyl orthoesters (NPOE) of D-glucose and D-galactose in conjunction with *N*-iodosuccinimide (NIS). Benzoyl and benzyl protection in D-glucosyl NPOEs led to 1,2–trans glycosides, while acetyl protection in NPOE led to a mixture of 1,2–cis and trans glycosides with >75% cis selectivity.

Chapter 5 describes a stereoselective glycosylation method catalyzed by (+)-isomenthol ester of pentacarbomethoxycyclopentadiene (PCCP) as chiral Brønsted acid (CBA **1**) with *n*-pentenylglycosides (NPGs) in the presence of *N*-iodosuccinimide as the promoter that offered a chiral recognition of the racemic substrates.

References

- (1) Atanasov, A. G.; Zotchev, S. B.; Dirsch, V. M.; Orhan, I. E.; Banach, M.; Rollinger, J. M.; Barreca, D.; Weckwerth, W.; Bauer, R.; Bayer, E. A.; Majeed, M.; Bishayee, A.; Bochkov, V.; Bonn, G. K.; Braidy, N.; Bucar, F.; Cifuentes, A. Natural Products in Drug Discovery: Advances and Opportunities. *Nat. Rev. Drug Discov.* **2021**, *20* (3), 200–216. <https://doi.org/10.1038/s41573-020-00114-z>.
- (2) Sen, T.; Samanta, S. K. Medicinal Plants, Human Health and Biodiversity: A Broad Review. *Adv. Biochem. Eng. Biotechnol.* **2014**, *147*, 59–110. https://doi.org/10.1007/10_2014_273.

Natural Products in Drug Discovery - Advances and Opportunities

1.1. Introduction

Natural products serve as the single most productive source for the discovery of drugs and pharmaceutical leads. The chemicals derived from microbes, plants, and even animals have been an invaluable source of therapeutic agents, and the structurally diverse phytochemicals with potent biological activities were the most significant among them, which have been extensively documented [1–3]. Polyphenolic compounds, including alkaloids and flavonoids, are some of the pleiotropic phytoconstituents that exhibit promising antitumor activities in a plethora of cellular and animal models [4,5]. In addition, a wide range of polyphenolic secondary metabolites has successively completed different phases of preclinical/clinical trials. For instance, a bioactive ingredient of turmeric, curcumin, is reputed to be an excellent therapeutic agent and is presently under human clinical trials for various chronic diseases such as Alzheimer's disease, cancers of the colon, pancreas, and blood cells, myelodysplastic syndromes, and psoriasis [6,7]. Furthermore, resveratrol, a major phytochemical isolated from grapes and red wine species, has drawn the worldwide attention of many research groups and confronted many key outcomes of preclinical and clinical trials [8,9]. One of the past studies by Newman and Cragg reported that approximately 60% of the current anticancer drugs were isolated from natural products or their structural analogues [10].

1.2. History modern drug discovery

Natural product assisted drug discovery began in ancient times by utilising traditionally highlighted medicinal plant extracts. The successful stories of natural product-aided drug development were instigated by Friedrich Sertürner, who created history in 1803 by isolating morphine, a highly potent analgesic from the unripe seed extract of *Papaver somniferum* (Opium poppy) [11]. Later, in 1874, Wright and co-workers reported the synthesis of heroin (diacetylmorphine) from morphine by boiling with acetic anhydride which led to the conversion of the popular painkiller codeine [12]. The discovery of digitoxin, a cardiotonic glycoside from *Digitalis purpurea* L., improves the cardiac contractibility strength and enhances cardiac conduction [13]. Moreover, digitoxin and analogues have been used to

manage congestive heart failure. In 2004, the FDA approved the anti-malarial drug quinine, isolated from the bark of *Cinchona succirubra* Pav. ex Klotsc had been used to treat various ailments such as malaria, throat diseases, indigestion, fever and cancer [13]. Later, the development of the L-histidine-derived alkaloid Pilocarpine from *Pilocarpus jaborandi* (Rutaceae) for the treatment of chronic open-angle glaucoma and acute angle-closure glaucoma and the oral formulation of Pilocarpine to xerostomia in head and neck cancers are the two legendary contributions of natural products in drug discovery process [13]. Later, in 1998, oral preparation was permitted to manage the autoimmune disease Sjogren's syndrome which causes damage to salivary glands and lacrimal glands. The discovery of Penicillin from *Penicillium notatum* in 1929 by Alexander Fleming is one of the most popular natural product discoveries that contributed to the Nobel prize in Physiology and Medicine in 1945 [13]. Vancomycin is a glycopeptide produced in cultures of *Amycolatopsis orientalis* and was approved by the FDA as an antibiotic drug against wide ranges of gram-positive and gram-negative bacteria [13]. In 2002, Doxorubicin (Adriamycin) was isolated from the fungus *Streptomyces peucetius* and is used to treat lung cancer, bone sarcomas, leukaemia, soft tissue and thyroid cancer. Paclitaxel, the most widely prescribed breast cancer drug, is first isolated from the bark of *Taxus brevifolia*.



Friedrich Sertürner



Pierre Pelletier



Alexander Fleming

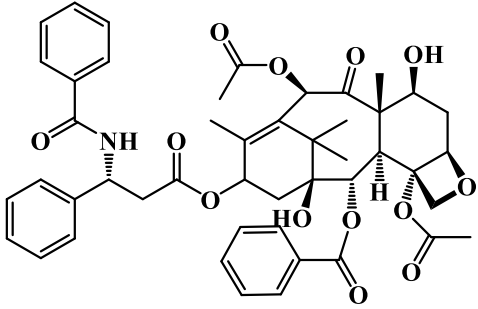
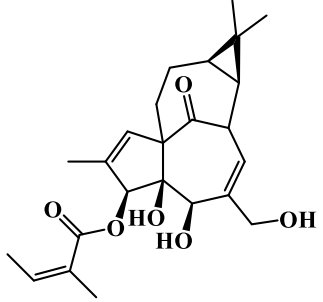
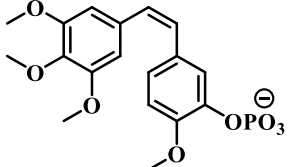
Figure 1.1: Famous personalities in the field of Natural products

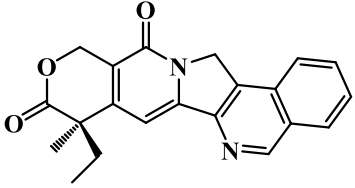
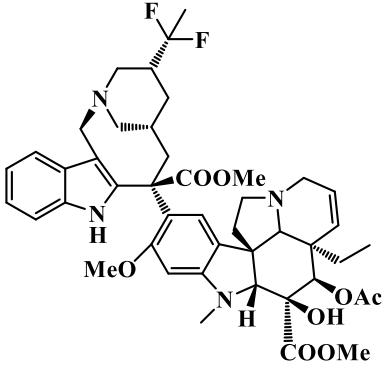
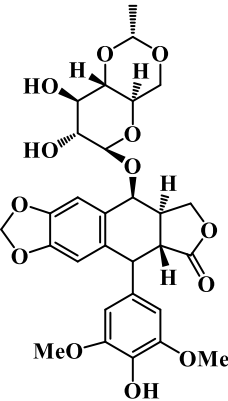
1.3. Natural Products in cancer treatment

Cancer is a multifactorial malaise that arises due to the dysregulation of multiple signaling pathways and their regulated molecules in the body. The conventional treatment modalities for this disease include surgery, radiation, chemo, immuno, and hormone therapies, which associated with numerous side effects and adverse limitations. The standard anti-cancer drugs currently available in the market are nonspecific, cytotoxic, expensive, and inadequate, which necessitates the requirement for alternative medicines that are safe, cost-effective, and

efficacious. Hence, developing alternative approaches for the prevention and treatment of cancer becomes imperative. Some of the anti-cancer drugs derived from plants are summarised in the table (Table 1).

Table 1: Plant Derived anti-cancer drugs

Drug	Structure	Source
Paclitaxel		 <p data-bbox="1078 875 1294 909"><i>Taxus brevifolia</i></p>
Ingenol 3- <i>O</i> -angelate		 <p data-bbox="1046 1323 1278 1357"><i>Euphorbia peplus</i></p>
Combretastatin A-4 phosphate		 <p data-bbox="1038 1682 1302 1715"><i>Combretum caffrum</i></p>

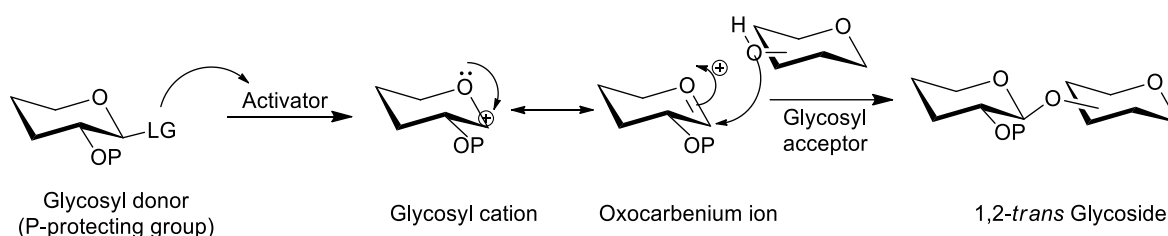
Camptothecin		 <p data-bbox="1023 521 1342 555"><i>Camptotheca acuminata</i></p>
Vinflunine		 <p data-bbox="1050 936 1315 969"><i>Catharanthus roseus</i></p>
Etoposide		 <p data-bbox="1038 1350 1331 1384"><i>Podophyllum peltatum</i></p>

Even though many of the isolated phytochemicals have excellent anti-tumour potential in various cancer cells, limited aqueous solubility of the isolated phytomolecules impedes their bioavailability and challenges their pharmaceutical development, stressing the requirement of various formulation techniques. Glycosides are one of the important categories of natural products, frequently used as the lead compounds for synthesising of new drugs. They have importance in pharmacokinetics and pharmacodynamics by improving the pharmacological properties such as potency, selectivity, solubility and bioavailability. Many biologically active secondary metabolites occur in plants generally as their glycosides, *i.e.* linked with various sugars, which are usually cleaved off during their complex isolation processes, liberating pure aglycone. As part of our ongoing interest in natural products of phytoorigin, we are attaching

the saccharide appendages to the aglycones *via* glycosylation in synthetic carbohydrate chemistry. The re-attachment of aglycones with glycone is a formidable challenge, which arises the problems of stereo, regio and enantioselectivities.

1.4. Glycosylation Reactions

Catalytic glycosylation, introduced by Emil Fischer, has been a reaction of paramount significance in carbohydrate chemistry, which involves coupling a glycosyl donor with a glycosyl acceptor in the presence of a suitable activator (**Scheme 1.1**). Later, numerous research groups made remarkable contributions to improving the glycosidic bond formation by varying glycosyl donor, promoter, catalyst and reaction methodologies [14].



Scheme 1.1: General mechanism for glycosylation with glycosyl acceptor

The commonly used glycosyl donors are shown in the following figure (Figure 2).

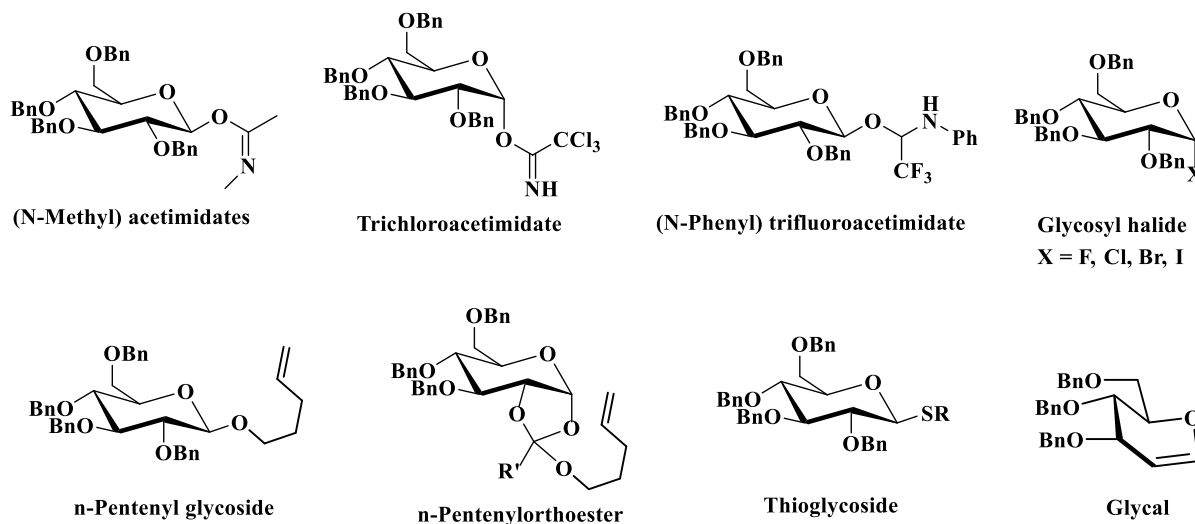


Figure 2: Structure of glycosyl donors

The pioneering synthesis of the glycosyl donor (N-Methyl) acetimidates was reported by Sinay and co-workers in 1976 from glycosyl halides and is utilised for the glycosylation of wide range of a glycosyl acceptors under the activation of p-toluene sulfonic acid [14]. However, the popularity of the donor gained little attention since, its synthesis was reported from glycosyl

halides which itself act as a glycosyl donor. Later, in 1980, Michel and Schmidt were inspired by the attempt of Sinay's group and developed trichloroacetimidate donors, reputed as the most widely used glycosyl donor for chemical glycosylation [14]. The contribution of glycosyl halides as donors in glycosylation strategies is imperative. Mukiyama and co-workers developed glycosyl fluorides, Koenigs and Knorr reported glycosyl bromides, and Helferich and Gootz investigated glycosyl iodides for the glycosylation of various acceptors under various catalytic activation [14]. Orthoesters are well-known intermediates in glycosylation reactions with having a 2-O-acyl group, introduced by Kochetkov and used as glycosyl donors with various acceptor systems [14]. Later, Frasier Reid and co-worker's serendipitous observation lead to the synthesis of *n*-pentenyl glycosyl donors.

1.5. Catalytic activators in glycosylation

It has been observed that the stereoselectivity of glycosylation reactions are considerably affected by the choice of the catalyst. Lewis acids such as SnCl₄, BF₃.Et₂O, ZnCl₂, TMSOTf, etc., are the most commonly used catalysts for chemical glycosylation [14]. Various research groups reported some route catalytic activators for the activation of particular glycosyl donors. BF₃.Et₂O and TMSOTf are popular for the activation of trichloroacetimidate donors, silver salts for glycosyl halides, metal triflates for *n*-pentenyl glycosyl donors and TMSOTf/NIS for thioglycosides etc. [14]. Besides Lewis acid catalysts, Brønsted acid catalysed glycosylation reactions are also reported, which would improve the stereo, regio, selectivities of the reaction [14]. Moreover, the attempts with chiral Brønsted acid catalysts (Figure 1.3) would increase the reactions stereo and diastereoselectivities.

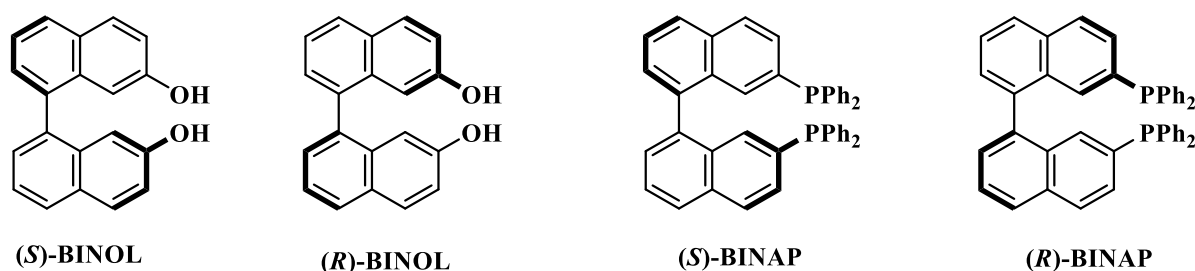
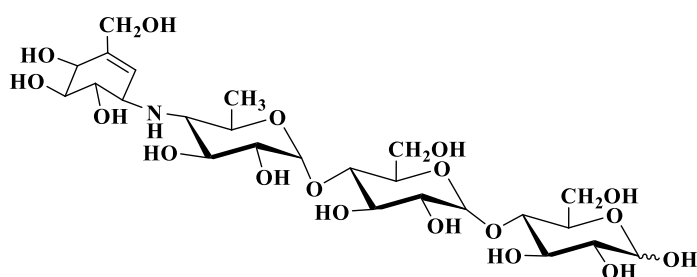


Figure 1.3: Structure chiral Brønsted acid catalyst

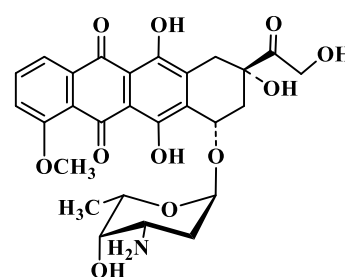
1.6. Biological importance of carbohydrates

Carbohydrate chemistry can be envisioned for synthesising and developing of broad range of drugs and complex therapeutic molecules due to their structural diversity. They also

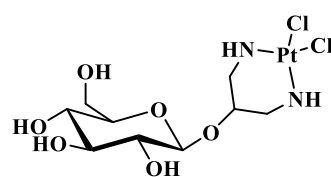
contributed to designing new drugs and vaccines against various malaises including covid-19, malaria, HIV, etc. The greater biological activity of these molecules is explained by their interaction with the proteins inside the human body, which plays a crucial role in cell differentiation, inflammation, immune response, cancer metastasis and pathogen adhesion. Carbohydrate chemistry and glycobiology imparts greater bioavailability, aqueous solubility and pharmacokinetics properties by promoting the development of targeted drug delivery systems. There are several carbohydrate-based drugs are currently available in the market for the treatment of various diseases. Some of them are mentioned below with their function.



Acarbose : Anti-diabetic drug used for type 2 diabetic mellitus



Doxorubicin : Anti-cancer drug



Cis-platin with carbohydrate side chain:
Anti-cancer drug

1.7. Conclusions and present objectives of the study

From the above discussions, it is clear that the role of natural products in modern drug design and discovery is noticeable, especially in various infectious and lifestyle diseases. Among them, cancer is more prominent. Despite the significant advancement in the field of diagnosis and treatment modalities for cancer, it is one of the life-threatening diseases with a substantial rate of morbidity and mortality around the globe. High expense, non-targeted action, toxicity to normal cells, and inefficacy still troubles the potency of the currently existing drugs. Extensive research is being carried out globally to develop nature-based therapeutic drugs that are safe, cost-effective, and nontoxic. With the development of science, the reason behind the biological properties of the medicinal plants has been inspected, and this quest of research

communities has directed to a burst in Phytochemistry, which includes isolation, structural elucidation, biological evaluation, and structural modification.

In this scenario, our focus was mainly on the chemoprofiling and bioprospecting of two traditionally significant medicinal floras, viz. *Dillenia indica* and *Artocarpus altilis*. In the present thesis, we explore the potential of these medicinal plants for the inhibition, prevention and better management of oral squamous cell carcinoma. In chapter 2, we attempted to explore the anti-cancer potential of the fruit extract of the ethnomedicinal plant *Dillenia indica* against oral squamous cell carcinoma (OSCC) and have exclusively attributed the efficacy of the extracts to the presence of two triterpenoids, namely, betulinic acid (BA) and koetjapic acid (KA). Preliminary in vitro screening of both BA and KA unveiled that the entities could impart cytotoxicity and induce apoptosis in OSCC cell lines, which were further well-supported by virtual screening based on ligand binding affinity and molecular dynamic simulations. Additionally, the aforementioned metabolites could significantly modulate the critical players such as AKT/mTOR, NF- κ B, and JAK/STAT-3 signaling pathways involved in the regulation of important hallmarks of cancer like cell survival, proliferation, invasion, angiogenesis, and metastasis. The present findings provide insight, immense scientific support and integrity to a piece of indigenous knowledge. Chapter 3, discusses the phytochemical investigation of *Artocarpus altilis* and the anti-proliferative potential of two isolated flavones, artonin E (AA2) and artobiloxanthone (AA3), against SAS oral cancer cells. Further, both compounds were optimized with virtual-screening based ligand binding affinity and molecular simulation studies. Additionally, we have also demonstrated the promising anti-cancer potential of the selected candidates through various apoptotic and metastatic assays and explained the mechanistic evaluation of the molecules in the *in-vitro* system.

Chapter 4 deals with the synthesis of a unique organic Brønsted acid, 1,2,3,4,5-Pentacarbomethoxycyclopentadiene (PCCP), for catalysing the glycosylation of natural products with *n*-pentenyl orthoesters (NPOE) of D-glucose and D-galactose in conjunction with *N*-iodosuccinimide (NIS).

A stereoselective glycosylation method catalysed by (+)-isomenthol ester of pentacarbomethoxycyclopentadiene (PCCP) as chiral Brønsted acid (CBA 1) with *n*-pentenyl glycosides (NPGs) in the presence of *N*-iodosuccinimide as the promoter discussed in Chapter 5. The aforementioned chiral Brønsted acid has synthesized from PCCP and a natural secondary alcohol, (+)-isomenthol.

References

- [1] S. Henamayee, K. Banik, B.L. Sailo, B. Shabnam, C. Harsha, S. Srilakshmi, V.G.M. Naidu, S.H. Baek, K.S. Ahn, A.B. Kunnumakkara, Therapeutic emergence of rehin as a potential anticancer drug: A review of its molecular targets and anticancer properties, *Molecules*. 25 (2020) 1–26. <https://doi.org/10.3390/molecules25102278>.
- [2] K. Platel, K. Srinivasan, V.H.P. Prakash, J. Prakash, V.K. Singh, S.S. Singh, S.S. Singh, D.K. Singh, M. Wegner, M.S. Ali, I. Azhar, Z. Amtul, V.U. Ahmad, K. Usmanghani, C. Figueiredo, J. Barroso, L. Pedro, J. Scheefeer, N. V. Yanishlieva, E. Marinova, J. Pokorný, A. Karatepe, M. Soylak, L. Elçi, M.E. Lucchesi, F. Chemat, J. Smadja, H. Maarse, L.M. Nijssen, B.P. Hubert, O.G. Vitzthum, K. Garcinol, M. Chapman, R. Stevens, K. Thymoquinone, O. Baritoux, H. Richard, J. Touche, M. Derbesy, M.H. Farzaei, M.R. Shams-Ardekani, Z. Abbasabadi, R. Rahimi, M. Kivanç, A. Akgül, J. Kundu, Y. Surh, S. Shukla, S. Gupta, L.J. Sass, N. Nigam, J. George, Y. Shukla, I. Paur, M.H. Carlsen, B. Lise, C.M. Kaefer, J.A. Milner, S. Yodkeeree, D. Danda, B. Sung, B.B. Aggarwal, Y. Kadoma, Y. Murakami, T. Atsumi, S. Ito, S. Fujisawa, K. Srinivasan, F. Diosgenin, A. Press, N. York, M.N. Dang, M. Takácsová, D. V Nguyen, K. Kristiánová, Traditional Uses of Spices :, *Flavour Fragr. J.* 2 (1999) 1–24.
- [3] S.A. Ali Shah, N. Akhter, B.N. Auckloo, I. Khan, Y. Lu, K. Wang, B. Wu, Y.W. Guo, Structural diversity, biological properties and applications of natural products from cyanobacteria. A review, *Mar. Drugs*. 15 (2017) 1–30. <https://doi.org/10.3390/md15110354>.
- [4] A.B. Kunnumakkara, A.S. Nair, S.A. Kwang, M.K. Pandey, Z. Yi, M. Liu, B.B. Aggarwal, Gossypin, a pentahydroxy glucosyl flavone, inhibits the transforming growth factor beta-activated kinase-1-mediated NF-κB activation pathway, leading to potentiation of apoptosis, suppression of invasion, and abrogation of osteoclastogenesis, *Blood*. 109 (2007) 5112–5121. <https://doi.org/10.1182/blood-2007-01-067256>.
- [5] A.B. Kunnumakkara, B. Sung, J. Ravindran, P. Diagaradjane, A. Deorukhkar, S. Dey, C. Koca, Z. Tong, J.G. Gelovani, S. Guha, S. Krishnan, B.B. Aggarwal, Zylflamend suppresses growth and sensitizes human pancreatic tumors to gemcitabine in an orthotopic mouse model through modulation of multiple targets, *Int. J. Cancer*. 131

- (2012) 292–303. <https://doi.org/10.1002/ijc.26442>.
- [6] S. Gopi, J. Jacob, K. Varma, S. Jude, A. Amalraj, C.A. Arundhathy, R. George, T.R. Sreeraj, C. Divya, A.B. Kunnumakkara, S.J. Stohs, Comparative Oral Absorption of Curcumin in a Natural Turmeric Matrix with Two Other Curcumin Formulations: An Open-label Parallel-arm Study, *Phyther. Res.* 31 (2017) 1883–1891. <https://doi.org/10.1002/ptr.5931>.
- [7] A. Amalraj, K. Varma, J. Jacob, C. Divya, A.B. Kunnumakkara, S.J. Stohs, S. Gopi, A Novel Highly Bioavailable Curcumin Formulation Improves Symptoms and Diagnostic Indicators in Rheumatoid Arthritis Patients: A Randomized, Double-Blind, Placebo-Controlled, Two-Dose, Three-Arm, and Parallel-Group Study, *J. Med. Food.* 20 (2017) 1022–1030. <https://doi.org/10.1089/jmf.2017.3930>.
- [8] M.T.G.-C. and J.C.E. Joao Tomé-Carneiro, Mar Larrosa, Antonio González-Sarrías, Francisco A. Tomás-Barberán, Resveratrol and Clinical Trials: The Crossroad from In Vitro Studies to Human Evidence, *Curr. Pharm. Des.* 19 (2013) 6064–6093. <https://doi.org/10.1097/00002060-199407000-00003>.
- [9] C. Buhrmann, P. Shayan, A. Brockmueller, M. Shakibaei, Resveratrol suppresses cross-talk between colorectal cancer cells and stromal cells in multicellular tumor microenvironment: A bridge between in vitro and in vivo tumor microenvironment study, *Molecules.* 25 (2020) 1–21. <https://doi.org/10.3390/molecules25184292>.
- [10] D.J. Newman, G.M. Cragg, Natural Products as Sources of New Drugs from 1981 to 2014, *J. Nat. Prod.* 79 (2016) 629–661. <https://doi.org/10.1021/acs.jnatprod.5b01055>.
- [11] C. Krishnamurti, S.S.C.C. Rao, The isolation of morphine by serturner, *Indian J. Anaesth.* 60 (2016) 861–862. <https://doi.org/10.4103/0019-5049.193696>.
- [12] Walter Sneader, The discovery of heroin, *Lancet* •. 351 (1998) 1697–1699.
- [13] D.A. Dias, S. Urban, U. Roessner, A Historical overview of natural products in drug discovery, *Metabolites.* 2 (2012) 303–336. <https://doi.org/10.3390/metabo2020303>.
- [14] M.M. Nielsen, C.M. Pedersen, Catalytic Glycosylations in Oligosaccharide Synthesis, *Chem. Rev.* 118 (2018) 8285–8358. <https://doi.org/10.1021/acs.chemrev.8b00144>.

In-vitro Screening of Pentacyclic Triterpenoids from *Dillenia indica* against SAS Oral Squamous Cell Carcinoma

2.1. Introduction

Cancer is one of the leading causes of death worldwide, and according to GLOBOCAN 2018, it accounted for approximately 18.1 million new cases and around 9.6 million deaths globally in 2018. Oral cancer, or its predominant form, oral squamous cell carcinoma (OSCC), is a major cause of morbidity and mortality in India. It is one of the most aggressive malignancies occurring globally, affecting approximately 3,54,864 people yearly and causing 1,77,384 deaths per year [1–5]. Due to its extremely high recurrence rate, the survival rate percentage of oral cancer patients is one of the lowest among all cancer types. Lifestyle factors like chewing tobacco, areca nut, consumption of alcohol, smoking, high intake of red meat, and fermented food are major risk factors for oral cancer and are the prime reason for its high prevalence [2,6–8]. Despite the significant advancement in the diagnosis and treatment of disease, the incidence of oral cancer is rising quickly due to the lack of sensitive diagnostic methods and effective drugs. The conventional treatment modalities of oral cancer, i.e., surgery, radiation therapy (external beam radiotherapy and brachytherapy), and chemotherapy, face numerous limitations such as adverse side effects, high treatment cost, toxicity to healthy cells, chemoresistance, radioresistance, recurrence of the tumour, and so on [2,3,9,10]. Thus, there has been a growing interest in developing nontoxic and cost-effective oral cancer treatments, comprising complementary and alternative therapies. Exploring natural products and their active components, which exhibit significant chemopreventive and chemotherapeutic potential, has been an area of great attraction for researchers worldwide for the last few decades [11–15].

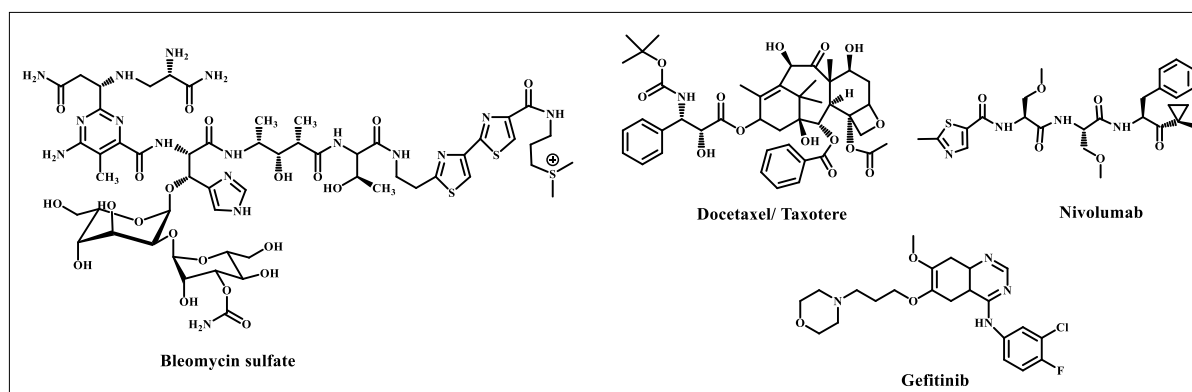


Figure 2.1: FDA approved drugs for oral cancer treatment

The development of new drug molecules from naturally occurring species is a growing area of research at present. The ease of availability of plant species, simple extraction and isolation protocols, purification techniques, favourable safety profile and multiple pharmacological activities hidden in the species are the beneficial features of natural products that contributed to developing more environmentally sound, economical, and effective drug discovery processes. Moreover, the plants are the storehouse of a diverse array of phytochemicals which can be converted into bioactive drug leads in the near future. Hence, the phytochemical profiling of such floras and faunas and identifying their phytoconstituents are essential and necessary for the development of phytochemistry research.

2.2. An overview of Dilleniaceae family

Dilleniaceae is a family of flowering plants with 11 genera and 430 species of woody vines, trees, shrubs, and creepers native to the tropics and subtropics of Australia. The family is remarkable in angiosperm groups because of their variability, floristic diversity and morphological characteristics. *Acrotrema*, *Curatella*, *Davilla*, *Didesmandra*, *Dillenia*, *Doliocarpus*, *Hibbertia*, *Neodillenia*, *Pinzona*, *Schumacheria*, and *Tetracera* are the distinguished genera included in the Dilleniaceae family. Many of the species under the family possess ethnomedicinal significance. They are traditionally highlighted for treating various malaises and infections such as dysentery, hepatitis, arthritis, diabetes, blennorrhagia, gastrointestinal disorders, inflammation, hemorrhoids, wounds, and leishmanial ulcers [16–18]. Various research groups were intrigued by the chemical investigation of phytochemicals from the family Dilleniaceae and identified approximately 130 molecules from different species belonging to the category of flavonoids, terpenoids, lignoids, phenolic derivatives, and other compounds. Among them, flavonoids and terpenoids are identified as the most representative and diversified moieties recognised as the major phytochemicals (Figure 1 & 2). *Dillenia* is a genus that comprises around 100 species, characterized by their attractive flowers and fruits.

According to the Plant List (2013), as many as 175 scientific plant names from the genus *Dillenia* have been recorded, with 58 accepted names and 71 names of synonym species. The genus is named under British botanist, Joannes Jacobus Dillenius, who dedicated his efforts in the chemotaxonomic identification of the genus.

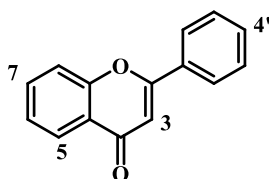
Table 1: *Dillenia* species and their distribution

Sl. No.	<i>Dillenia</i> species	Distribution
1	<i>Dillenia alata</i> (R.Br. ex DC.) Martelli	Maluku Islands, New Guinea, Australia
2	<i>Dillenia albertisiana</i> Martelli.	New Guinea
3	<i>Dillenia albiflos</i> (Ridl.) Hoogland	Peninsula Malaysia
4	<i>Dillenia andreana</i> F.Muell.	Australia
5	<i>Dillenia aurea</i> Sm.	Bangladesh, India, Laos, Thailand
6	<i>Dillenia auriculata</i> Martelli.	New Guinea
7	<i>Dillenia beccariana</i> Martelli.	Borneo
8	<i>Dillenia bracteata</i> Wight	India
9	<i>Dillenia biflora</i> (A.Gray) Guillaumin.	Fiji, Vanuatu
10	<i>Dillenia blanchardii</i> Pierre.	Vietnam
11	<i>Dillenia bolsteri</i> Merr.	Philippines
12	<i>Dillenia borneensis</i> Hoogland.	Borneo
13	<i>Dillenia castaneifolia</i> (Miq.) Martelli ex T.Durand & B.D.Jacks.	New Guinea
14	<i>Dillenia cauliflora</i> Merr.	Philippines
15	<i>Dillenia celebica</i> Hoogland.	Sulawesi
16	<i>Dillenia crenatifolia</i> Hoogland ex Mabb.	Solomon Islands
17	<i>Dillenia cycloperensis</i> Hoogland.	New Guinea
18	<i>Dillenia diantha</i> Hoogland.	Philippines
19	<i>Dillenia eximia</i> Miq.	Thailand
20	<i>Dillenia fagifolia</i> Hoogland.	New Guinea
21	<i>Dillenia ferruginea</i> (Baill.) Gilg.	Seychelles
22	<i>Dillenia fischeri</i> Merr.	Philippines
23	<i>Dillenia grandifolia</i> Wall. ex Hook.f. & Thomson	Peninsula Thailand
24	<i>Dillenia hookeri</i> Pierre.	Indo-China

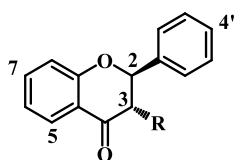
25	<i>Dillenia ingens</i> B.L.Burt.	Solomon Islands
26	<i>Dillenia insignis</i> (A.C.Sm.) Hoogland.	Papua New Guinea
27	<i>Dillenia insularum</i> Hoogland.	New Guinea
28	<i>Dillenia luzoniensis</i> (S.Vidal) Merr.	Philippines
29	<i>Dillenia marsupialis</i> Hoogland.	Philippines
30	<i>Dillenia megalantha</i> Merr.	Philippines
31	<i>Dillenia mansonii</i> (Gage) Hoogland.	India
32	<i>Dillenia monantha</i> Merr.	Philippines
33	<i>Dillenia montana</i> Diels.	New Guinea
34	<i>Dillenia nalagi</i> Hoogland.	Papua New Guinea
35	<i>Dillenia obovata</i> (Blume) Hoogland.	Indo-China
36	<i>Dillenia ochreate</i> (Miq.) Teijsm. & Binn. ex Martelli.	Sulawesi
37	<i>Dillenia ovalifolia</i> Hoogland.	New Guinea
38	<i>Dillenia papyracea</i> Merr.	Philippines
39	<i>Dillenia parkinsonii</i> Hoogland.	Myanmar
40	<i>Dillenia pentagyna</i> Roxb.	India
41	<i>Dillenia philippinensis</i> Rolfe.	Philippines
42	<i>Dillenia pteropoda</i> (Miq.) Hoogland.	Maluku, New Guinea, Philippines
43	<i>Dillenia pulchella</i> (Jack) Gilg.	Borneo, Malaya, Sumatera
44	<i>Dillenia quercifolia</i> (C.T.White & W.D.Francis ex Lane-Poole) Hoogland.	New Guinea
45	<i>Dillenia reifferscheidia</i> Fern.-Vill.	Philippines
46	<i>Dillenia reticulate</i> King.	Philippines
47	<i>Dillenia retusa</i> Thunb.	India
48	<i>Dillenia salomonensis</i> (C.T.White) Hoogland.	Solomon Islands
49	<i>Dillenia scabrella</i> (D.Don) Roxb. Ex Wall.	Indo-China
50	<i>Dillenia schlechteri</i> Diels.	Papuasias
51	<i>Dillenia sibuyanensis</i> (Elmer) Merr.	Philippines
52	<i>Dillenia serrata</i> Thunb.	Sulawesi
53	<i>Dillenia suffruticosa</i> (Griff.) Martelli	Borneo, Malay Peninsula, Sumatra
54	<i>Dillenia sumatrana</i> Miq.	Borneo, Malaya, Sumatera

55	<i>Dillenia talaudensis</i> Hoogland.	Sulawesi
56	<i>Dillenia tetrapetala</i> Joongku Lee, T.B.Tran & R.K.Choudhary.	Vietnam
57	<i>Dillenia triquetra</i> (Rottb.) Gilg.	Madagascar, Sri Lanka
58	<i>Dillenia turbinata</i> Finet & Gagnep.	China, Vietnam

2.3. Phytochemicals reported from *Dillenia* genus

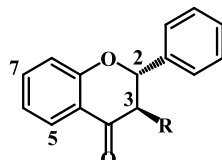


1. 5,7,4'-OH, Apigenin (1)
2. 5, 4'-OH, 7-Gal-OSO₃H (2)
3. 5,4'-OH, 7-OSO₃H (3)
4. 5,7,3',4'-OH, 3-a-L-Ara (4)
5. 3,7,3',4'-OH, 5-OMe (5)
6. 3',5-OH, 4', 3-OMe, 7-O-β-D-Glc (6)
7. 5,7-OH, 4'-OMe, 3-O-β-D-Glc (7)
8. 3,5,7-OH, 3',4'-OMe (8)
9. 3,5,7,4'-OH, 3'-OMe (9)
10. 5-OH, 3'-OMe, 3,7,4'-OSO₃H (10)
11. 5,7,4'-OH, 6-C-Glc (11)
12. 3,5-OH, 7-OMe (12)
13. 5-OH, 3,7-OMe (13)
14. 3,5,7,4'-OH (14)
15. 3,5-OH, 7,4'-OMe (15)
16. 5,4'-OH, 3,7-OSO₃H (16)
17. 5,7,4'-OH, 3-Gal (17)
18. 3,5,7-OH, 4'-O-β-Glc (18)
19. 5,7,4'-OH, 3-Glc (19)
20. 3,5,7-OH, 4'-OMe (20)
21. 5,7,4'-OH, 3-Rha (21)
22. 5,7,4'-OH, 3-OSO₃H (22)
23. 5-OH, 3,7,4'-OSO₃H (23)
24. 3,5,7,3',4'-OH (24)
25. 3,5,3',4'-OH, 7-OSO₃H (25)
26. 3,5,7,3',5'-OH, 4'-OMe (26)
27. 5,7,3',5'-OH, 3-Rha, 4'-OMe (27)
28. 3,5,4'-OH, 7-OMe (28)
29. 3,5,3',4'-OH, 7-OMe (29)
30. 3,7,4'-OH, 5-OMe (30)
31. 3,5,7,3',4',5'-OH (31)
32. 5,7,3',4',5'-OH, 3-Ara (32)
33. 5,7,3',4',5'-OH, 3-Gal (33)
34. 5,7,3',4',5'-OH, 3-O-α-L-Rha (34)
35. 3,5,7,4',5'-OH, 3'-O-α-L-Rha (35)
36. 5,7, 3',4',5'-OH, 3-O-α-L-Rha-SO₃H (36)
37. 5,5'-OH, 3,7,3',4'-OMe (37)
38. 3,5,3'-OH, 7,4'-OMe (38)
39. 5-OH, 7,4'-OMe, 3,3'-OSO₃H (39)
40. 3,5,7,3',4'-OH (40)
41. 5,7,3',4'-OH 3-O-Ara (41)
42. 5,7,3',4'-OH 3-Gal (42)
43. 5,7,3',4'-OH 3-Gal-Ara (43)
44. 5,7,3',4'-OH 3-O-β-D-Glu (44)
45. 5,7,3',4'-OH 3-Glc (45)
46. 5,7,3',4'-OH 3-O-β-D-Rha (46)
47. 5,7,3',4'-OH, 3-O-α-L-Rha (47)
48. 5,7,3',4'-OH, 3-α-L-Rha-(1→6)-Gal (48)
49. 5,7,3',4'-OH, 3-OSO₃H (49)
50. 5,3',4'-OH, 7-OMe, 3-Glc (50)
51. 3,5,4'-OH, 7-OMe (51)
52. 5,4'-OH, 7-OMe, 3-Glu (52)
53. 5,4'-OH, 7-OMe, 3-OSO₃H (53)
54. 5,4'-OH, 6-C-Glc, 7-O-β-D-Glc (54)
55. 5,7,4'-OH, 3-(6-O-p-Cou)-β-D-Glc (55)
56. 5,7,4'-OH, 8-C-Glc (56)
57. 5,7-OH, 8-OMe (57)
58. 5-OH, 7-O-β-D-Glu-(OMe), 8-OMe (58)
59. 5-OH, 7-O-β-D-Glu, 8-OMe (59)



60. 5,7,4'-OH, R = OH (60)

61. 5,7,4'-OH, 3'-OMe, R = OH (61)



62. 5,7-OH, 4'-OMe, R = OH (62)

63. 5,7,3',4'-OH, R = OH (63)

64. 7,3',4'-OH, 5-O-Gal, R = OH (64)

65. 5,7-OH, 8-OMe, R = H (65)

66. 5,7,4'-OH, 3'-OMe, R = OH (66)

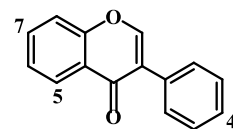
67. 5,7,3'-OH, 4'-OMe, R = OH (67)

68. 5,7,4'-OH, R = H (68)

69. 5,4'-OH, 7-Gal-(1→4)-Glc, R = H (69)

70. 5,7-OH, 4'-O-[4-O-(β-D-Glc)]-β-D-Xyl, R = H (70)

71. 4,5,7,3',4'-OH, 3-O-β-D-Glc (71)



73. 5,7,4'-OH, 3',5'-Diprenyl (73)

74. 5,7,4'-OH, 6,8-Diprenyl (74)

75. 5,7,4'-OH (75)

Ara = Arabinoside; Cou = Coumaroyl; Gal = Galactopyranoside; Glc = Glucopyranoside; Glu = Glucoronide; Rha = Rhamnopyranoside

Figure 2.2.: Structures of flavonoids isolated from Dilleniaceae family

2.4. Phytochemistry of *Dillenia indica* Linn.



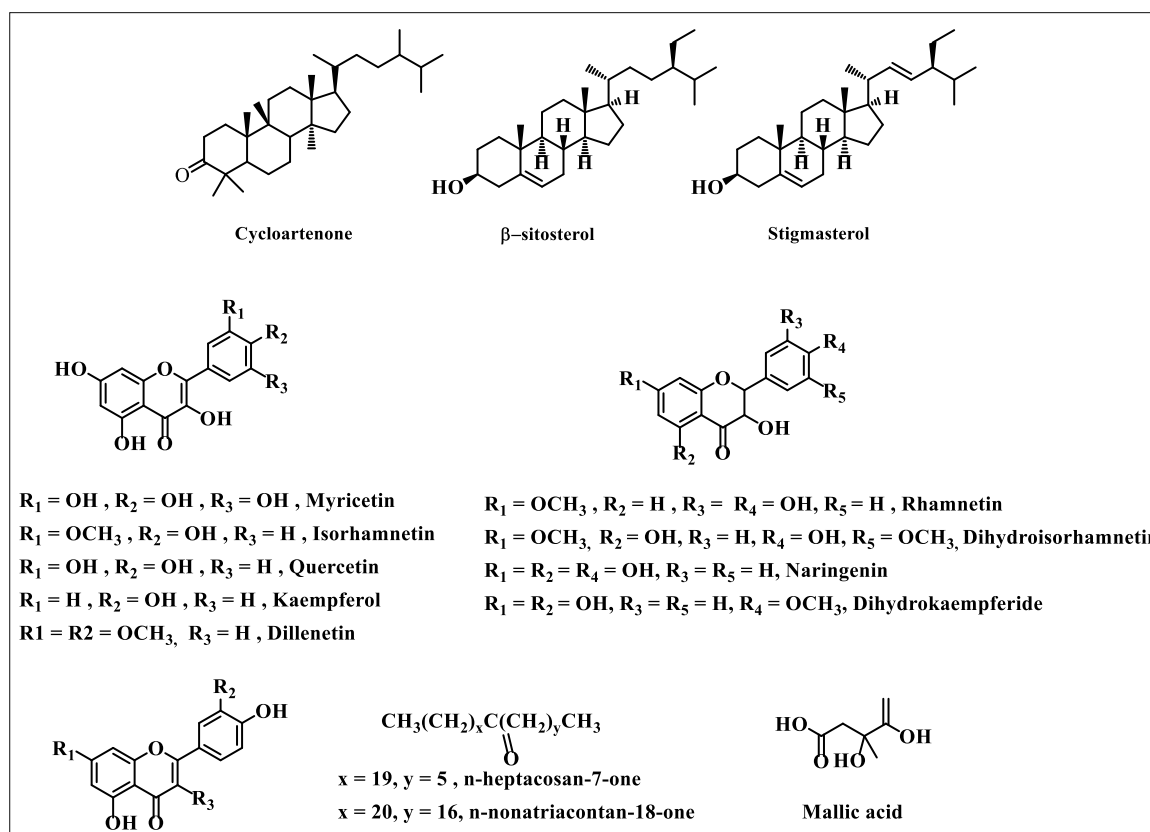
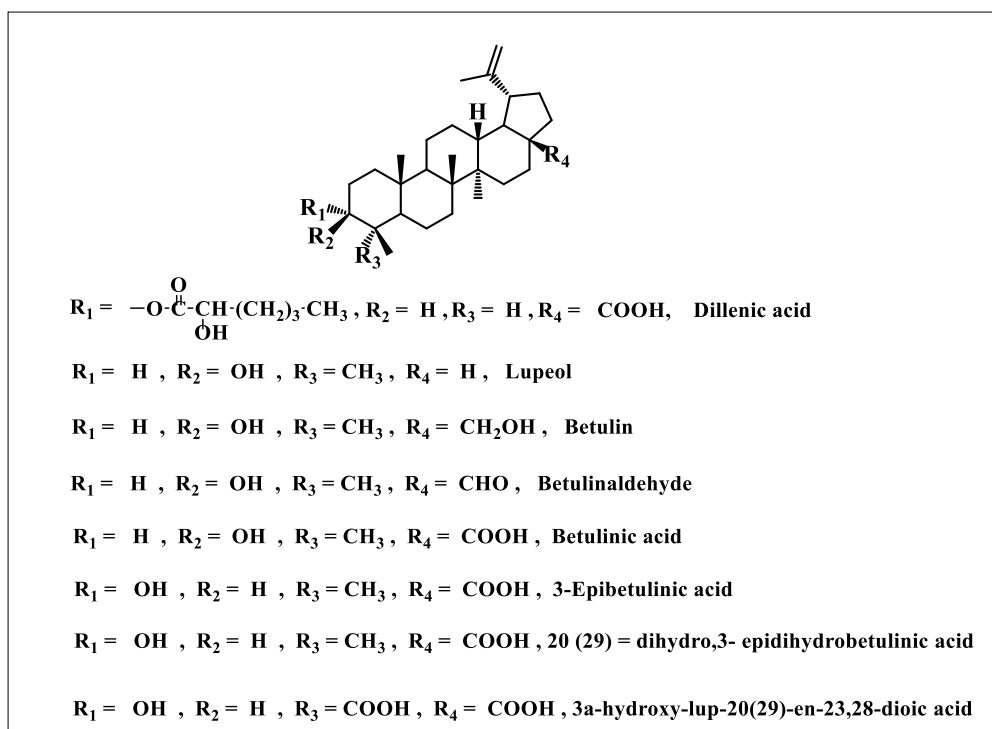
Figure 2.3 : Flower, tree and fruit of *Dillenia indica* (adapted from Indian Biodiversity Portal)

Dillenia indica (DI) Linn. is an evergreen medicinal tree belonging to the family Dilleniaceae and is typically found in the moist forests of the sub-Himalayan region in north-eastern India [19]. It is an important ethnomedicinal fauna described in 1759 by Carl Linnaeus in his *Systema Naturae*'s 10th edition. DI has been prevalently used in Vedas and other ancient relics, Indian traditional, Ayurvedic and Siddha systems of medicine for curing a plethora of ailments such as respiratory, digestive and central nervous system disorders. The plant produces a large number of hard edible fruits, which have to be attracted by mega herbivores like elephants and play the role of the seed disperser for the germination process; hence, the species is popularized under the common name elephant apple. Fruits of the plant are widely used as a traditional medicine among the tribal population of Mizoram for the treatment of mouth ulcers, diarrhoea, and jaundice [19,20]. In addition, it is a common culinary ingredient in Assam and is used for preparing jams, pickles, and curries. Besides, the extracts of leaves, fruits, and bark are found to possess medicinal properties and are given orally to treat diabetes, cancer, and stomach

disorders in the tribal areas of north-eastern India [21,22]. The leaves and bark extracts possess antioxidant potential and are also used as a laxative and an astringent agent [23–26].

Various research groups reported the phytochemical profiling of DI and inferred that the plant is enriched with a substantial amount of tannins, alkaloids, flavonoids and polyphenols and are contributed towards the wide spectrum pharmacological activities [27]. Triterpenoids such as betulinaldehyde, betulinic acid and lupeol were isolated from the stem bark on sequential extraction with petroleum ether, chloroform and methanol. In 2016, Preet Amol Singh and co-workers confirmed the quantitative amount of betulin (2.510% w/w) at the least retention time in the ethyl acetate extracts of DI by HPLC analysis [27]. In addition to these triterpenes and triterpenoids, flavonoids such as dihydro-isorhamnetin, rhamnetin, 5,7-dimethoxyapigenin, 6,7,3'-trihydroxy-2',4'-dimethoxyisoflavan, myricetin, naringenin, kaempferol, and quercetin derivatives are obtained from the stem and pericarp of DI [28,29].

Phytochemical investigations on the fruits of DI revealed that the major constituents in the fruits are phenolics (34%) and polysaccharides. Around 2% of arabinogalactan, a polysaccharide composed of β (1 \rightarrow 4) linked D-galactopyranose units to which the non-reducing L-arabinose units attached to the C3 position reported from the fruit [30]. Moreover, fruits containing total ash (4.45%), tannins (1.2%), acid soluble ash (4.15%), and reducing sugars (3.44%) [30]. Phytochemical profiling of the flower extract of *Dillenia indica* was reported by Tiwari *et al.* and identified 27 bioactive compounds from the methanolic extract of medicinal and pharmaceutical significance [31]. Apart from this, the sequential extraction of the leaves of DI with petroleum ether and chloroform ascertain the presence of β -sitosterol, *n*-hentriacontanol, betulin and betulinic acid. Flavonoids like kaempferol, dihydrokaempferide and 7-glucosides of naringenin were isolated from the dried and fresh leaves of DI.



Structure 2.4: Phytochemicals reported from *Dillenia indica* Linn.

2.5. Pharmacology of *Dillenia indica*

2.5.1. Anti-diabetic activity - Diabetes, a metabolic disorder, is considered a top seven leading cause of death characterised by the elevation of fasting blood glucose levels and affects approximately 8% of the global population. Various research studies and folklore evidence described the anti-diabetic potential of the ethnomedicinal plant DI. In 2011, Sunil Kumar and co-workers reported anti-diabetic and antihyperlipidemic effects of the methanolic leaf extract of DI in streptozotocin-induced diabetic Wistar rats. The study concluded that the corresponding extract may effectively sensitise the insulin receptor, thereby promoting insulin secretion from beta cells and improving the biochemical parameters and abnormalities associated with this malaise [32,33]. Later, in 2016, Kaur *et al.* isolated a new chromane from the DI extract by column chromatography and demonstrated the chromane ameliorates STZ-induced diabetic neuropathy by attenuating oxidative stress-mediated release of pro-inflammatory cytokines which might be responsible for diabetes-induced nerve damage. Moreover, the alcohol and hydro-alcohol extract of DI at a dose of 100, 200, and 400 mg/kg displayed a nephroprotective effect in diabetic rats and also produced a significant diminution of glycemic status, renal parameter, lipid profile, and augmentation of antioxidant enzymes [34]. The therapeutic potential of dried powder of the fruit of DI was also tested in humans at the Government Medical College in Assam. The study inferred that the oral administration of the powder at a dose of 30 g/day twice a day in an interval of half an hour before lunch and dinner significantly reduces both fasting and postprandial blood glucose levels without any side effects [35].

2.5.2. Anti-cancer activity – The anti-cancer activity of the methanolic extract of DI was demonstrated in human leukemic cell lines U937, HL60 and K562. The study revealed that the extract could significantly inhibit the growth and proliferation of leukemic cell lines having IC₅₀ values of 328.80±14.77, 297.69±7.29 and 275.40±8.49 µg/ml against U937, HL60 and K562, respectively. Moreover, the study also concluded that the anti-cancer activity was exclusively attributed to the presence of the pentacyclic triterpenoid, betulinic acid, which was quantitatively present in the methanolic fraction [36]. The IC₅₀ values of betulinic acid in these leukemic cell lines are 13.73±0.89, 12.84±1.23, and 15.27±1.16 mg/ml, respectively [36].

2.5.3. Antioxidant activity - The antioxidant activity of the methanolic extract of DI was determined by various *in-vitro* screening assays such as DPPH radical scavenging assay, total phenolic content and total flavonoids content determination assays. In the DPPH scavenging

assay, the IC₅₀ value of the hydro-alcoholic extract of the leaves of DI was found to be 100.53 µg/ml, which is greater than that of the standard ascorbic acid (IC₅₀ = 58.92 µg/ml) [37]. In 2012, Monjoy Kumar Choudhury and co-workers expressed the *in-vitro* antioxidant activity of the methanol, petroleum and water extracts of DI in terms of the DPPH, hydroxyl radical scavenging activity, superoxide radical scavenging activity, nitric oxide and reductive ability. The study concluded the petroleum extract exhibited greater activity than the polar extracts [38]. Recently, Vijay kumar *et al.*, isolated endophytic fungi from DI and demonstrated the anti-oxidant activity of the crude ethyl acetate extract of the endophytic fungal strain. The anti-oxidant activity of the aforementioned could be explained by the presence of the major phytochemicals such as alkaloids, flavonoids, phenolics, terpene, and saponins and furnishes 50–90% by DPPH and H₂O₂ assay [39].

2.5.4. Anti-inflammatory activity – The ameliorative effect of the hexane, methanol and chloroform fractions of *Dillenia indica* in acetic acid was elucidated in experimental colitis using female Swiss albino mice (25-30 g) via the inhibition of the production of NF-kB [40]. The oral administration of three doses of methanolic extract (800 mg/kg), two doses of both hexane extract (200 mg/kg) and chloroform (200 mg/kg) displayed a significant reduction in macroscopic score, colon myeloperoxidase (MPO), malonaldehyde (MDA) and TNF-α levels. Additionally, Khare *et al.*, investigated the anti-inflammatory activity of the chloroform fraction of the methanol extract of DI by carrageenan-induced rat paw oedema mode. They observed that the fraction showed significant anti-inflammatory activity at 25, 50 and 75 mg/kg doses. However, the effect was more prominent at a high dose of 75 mg/kg than lower dose 25 mg/kg [41].

2.5.5. Anti-microbial activity - Anti-microbial and cytotoxic potential of crude methanolic extract DI was investigated by disc diffusion method. Hexane, carbon tetrachloride, chloroform and methanolic fractions of the methanol extract of the leaves were selected for the study, and three out of the four fractions such as hexane, carbon tetrachloride, chloroform showed moderate anti-bacterial activity against both gram-positive and gram-negative bacteria [42]. In 2014, Jaiswal *et al.*, evaluated the anti-bacterial activity of the aqueous acetone extract (70%) of both fruit and stem bark of DI by agar dilution method and indicated the bark extract possessed minimum inhibitory concentration on all tested bacteria. The remarkable anti-bacterial activity of the extract might be due to the disintegration of cell walls and leakage of genetic material [42].

2.5.6. Antidiarrheal activity - Rahman and co-workers tested the antidiarrheal activity of the methanol extract of the root of DI in young Swiss-albino mice models and reported that as compared with the internal standard loperamide, the administration of 500 mg/kg of extract produced remarkable activity [43]. In 2013, Islam *et al*, reported the beneficial effect of the hot methanolic extract of the stem bark of DI for controlling diarrhoea in experimental animals. The study revealed that the extract could effectively mediate gastrointestinal motility and hypersecretion and enhance gastric transit time, contributing to the activity [44]. The anti-Diarrheal activity of methanolic and aqueous extracts of DI leaves was evaluated by Castor oil-induced diarrhoea mode and demonstrated both extracts at doses of 200 and 400 mg/kg P.O. caused the inhibition of diarrhoea and the prolongation of onset via inhibiting the release of inflammatory mediator [45].

2.5.7. Anthelmintic activity - Anthelmintic activity of the methanolic extract of the bark of DI was performed by using adult earthworms having 3-5 cm length, 0.1-0.2 cm width and 0.8-3.04 weight from the moist soil. Treatment of extracts with different concentrations such as 10, 15, 20, and 25 mg/ml in distilled water with the earthworms produced concentration dependent paralysis and worms' death [46].

2.5.8. Hepatoprotective activity - The ethanolic extract of the leaves of DI exhibited significant carbon tetrachloride-induced hepatotoxicity in albino rats and caused remarkable reduction in the various biochemical parameters [47].

2.6. Aim and Scope of the Study- *Dillenia indica* Linn. is an endemic, critically endangered, and economically important ethnomedicinal flora of the Western Ghats. The fruit of the plant is widely used as a traditional medicine among the tribal communities of Mizoram for the treatment of mouth ulcers and sores, which is undocumented. Because of the lack of awareness of the therapeutic importance of the fruit, most of them are not utilised for medicinal purposes and are wasted. In this context, the present study explores a rational explication of traditional knowledge with scientific criteria, including experimental and theoretical supports. Initially, our efforts are directed towards the anti-proliferative study of the fruit extracts of DI. The bioactivity assessment of the crude extract for inhibiting the growth and proliferation of oral cancer cells SAS encouraged us to identify the phytochemicals in the extract which confer the activity. So, the present chapter discloses the *in-vitro* anti-cancer activity of the crude extracts of DI and its bioactive phytochemicals for the inhibition, prevention and better management of OSCC.

2.7. Extraction, Isolation and anti-proliferation assay of the extracts and phytochemicals

2.7.1. Plant collection

Fruits of DI were collected from Guwahati, Assam, and were identified by the taxonomists of Jawaharlal Nehru Botanical Garden of India (JNTBGRI), Palode, Thiruvananthapuram, Kerala. A voucher specimen number JNTBGRI 93635 was deposited at the herbarium of JNTBGRI, Kerala.

2.7.2. Extraction Strategy and Isolation Procedure

Initially, the sequential extraction of the fruits of DI (900 g) was carried out with methanol (2.5 L) as well as water (500 mL) for 3 days; 45 g of methanol extract (DI-ME Ext) and 11 g of aqueous extract (DI-H₂O Ext) were obtained. As a part of our attempt to validate the integrity of the known medicinal properties popularised among the tribal communities, such as the potential of the fruit of DI to cure mouth ulcers and sores, we first analysed the anti-proliferative potential of the fruit extracts through MTT assay against an oral cancer cell line, SAS. The MTT cell proliferation assay is known to assess the metabolic activity of the cells. The amount of insoluble violet-blue formazan produced via the reduction of MTT tetrazolium salt by mitochondrial dehydrogenases determines the percentage of live cells. In this assay, SAS cells treated with an increasing concentration of DI showed reduced growth and proliferation rates of tumour cells, with IC₅₀ values of 14 and 12 µg/mL for DI-H₂O Ext and DI-ME Ext, respectively (Figure 2.5).

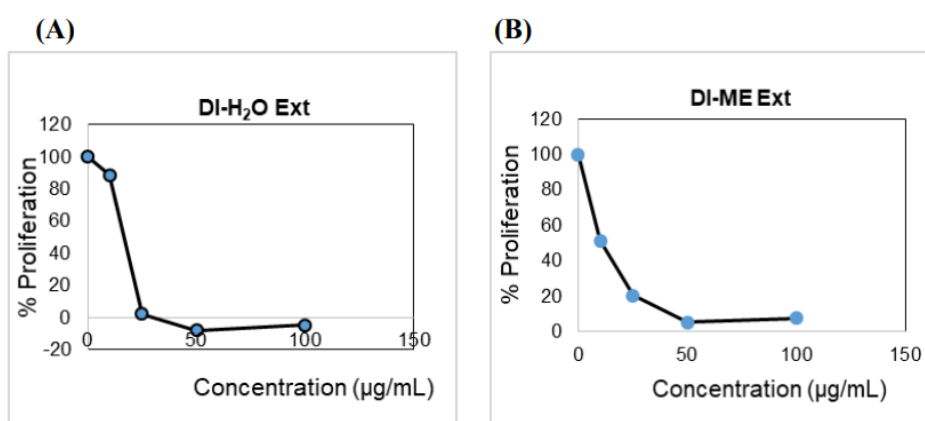


Figure 2.5: Inhibition of the proliferation of SAS cells by: (A) DI-H₂O Ext, with IC₅₀ of 14 µg/mL (B) DI-ME Ext, with IC₅₀ of 12 µg/mL.

Because of our keen interest in divulging the phytochemicals in the species which has conferred the corresponding pharmacological activity, the isolation of molecules from DI-ME

Ext was performed. For this purpose, DI-ME Ext was preferred over DI-H₂O Ext owing to its lower IC₅₀ value. The isolation procedure involved different chromatographic separation techniques, including thin-layer chromatography (TLC), column chromatography (CC) over silica gel (100-200 and 230-400 mesh), sephadex LH-20, and precipitation methods (Figure 3). TLC of the fractions 1-3 obtained on eluting the column with 5% ethyl acetate-hexane showed an interesting spot on charring in McGill solution. After concentration, it was subjected to crystallisation in ethyl acetate-hexane mixture and obtained as a white-needle shaped one. The compound was characterised as β -sitosterol (compound **1**, 10 mg), a phytosterol widely distributed in most plant species. TLC of the 4-8 fractions showed an intense spot on charring in McGill solution, eluted from the column using 10% ethyl acetate in hexane as eluent. Then pooled fractions were concentrated, and subjected to crystallisation hexane ethyl acetate mixture. The compound *n*-hentriacontanol (compound **2**, 7 mg) is a long-chain hydrocarbon obtained as a white solid. TLC of the fraction 9 eluted from the column in 20% ethyl acetate in hexane showed an interesting spot on charring in McGill solution. Then it was subjected to crystallisation using the same solvent yielded Lupeol (compound **3**, 120 mg) TLC of the fractions 10-30 eluted from the column in 30% ethyl acetate in hexane showed an intense spot on charring in McGill solution. It was subjected to column chromatography using silica gel (100-200 mesh) and hexane-ethyl acetate in different polarities as the solvent system, betulinic acid (compound **4**, 4.0 g) was obtained in a white crystalline solid. Fraction pools 30-34 on TLC analysis showed an inactive UV spot identified by charring in McGill solution. Then the fraction pools were combined, concentrated and subjected to column chromatography for purification using sephadex LH-20 in methanol as the eluent, koetjapic acid (Compound **5**, 17 mg) was obtained as a white amorphous solid. TLC of the fractions 35-38 eluted from the column in 50-60% ethyl acetate in hexane showed an intense UV active spot, further purified by repeated column chromatography by using sephadex LH-20 in MeOH yielded ferulic acid (compound **6**, 15 mg). TLC of the fractions 39-41 eluted from the column in 70% ethyl acetate in hexane showed an intense UV active spot. The compound was further purified by sephadex LH-20 column and was crystallised in methanol, palmarumycin JC1 (compound **7**, 40 mg) was obtained. Fraction pools 42-44 on TLC analysis showed an intense UV active spot. Then the fraction pools were combined, concentrated and subjected to column chromatography by silica gel (100-200 mesh) yielding the mixture of compound **8** and compound **9**, which was further purified by using sephadex LH-20 in methanol as the eluent yielded 3-oxykojic acid (compound **8**, 45 mg) and 2-(1,2 dihydroxykojic acid) (compound **9**, 30 mg) respectively. Compound **10** is a common secondary metabolite of many plant species β -sitosterol- β -D-

glucopyranoside (Compound **10**, 20 mg) was obtained from the fraction pool 45-50 as an amorphous solid, which was further purified by precipitation using acetone. All the ten compounds obtained were characterised by various spectroscopic techniques. We could successfully isolate and characterise ten molecules from the methanol extract including sterols, long-chain hydrocarbon, triterpenoids, deoxypreussomerin and aromatic compounds (Figure 2.7). Then, we analysed the anti-proliferative potential of all the isolated molecules against the oral cancer cell line SAS to identify which phytochemical (s) contributed to the pharmacological activity of the crude methanol extract. Surprisingly, two among the ten isolated molecules showed immense cytotoxicity against the SAS cell line. Both these molecules belong to the category of triterpenoids: BA, [(3 β)-3-hydroxy-lup-20(29)-en-28-oicacid], a pentacyclic triterpenoid is reputed as a cytotoxic agent in various malignant tumour cells, and KA is a seco-A-ring oleanane group triterpenoid, hitherto uninvestigated from the species, however, reported from the same genus. The selection strategy of the entities made by preliminary anti-proliferative assay, wherein BA and KA inhibited proliferation at IC₅₀ values of 6 and 20 μ M respectively after 72 h of treatment (Figure 2.31). Characterisation was done with sophisticated NMR techniques, including ¹H and ¹³C (Figure 2.8- 2.30).

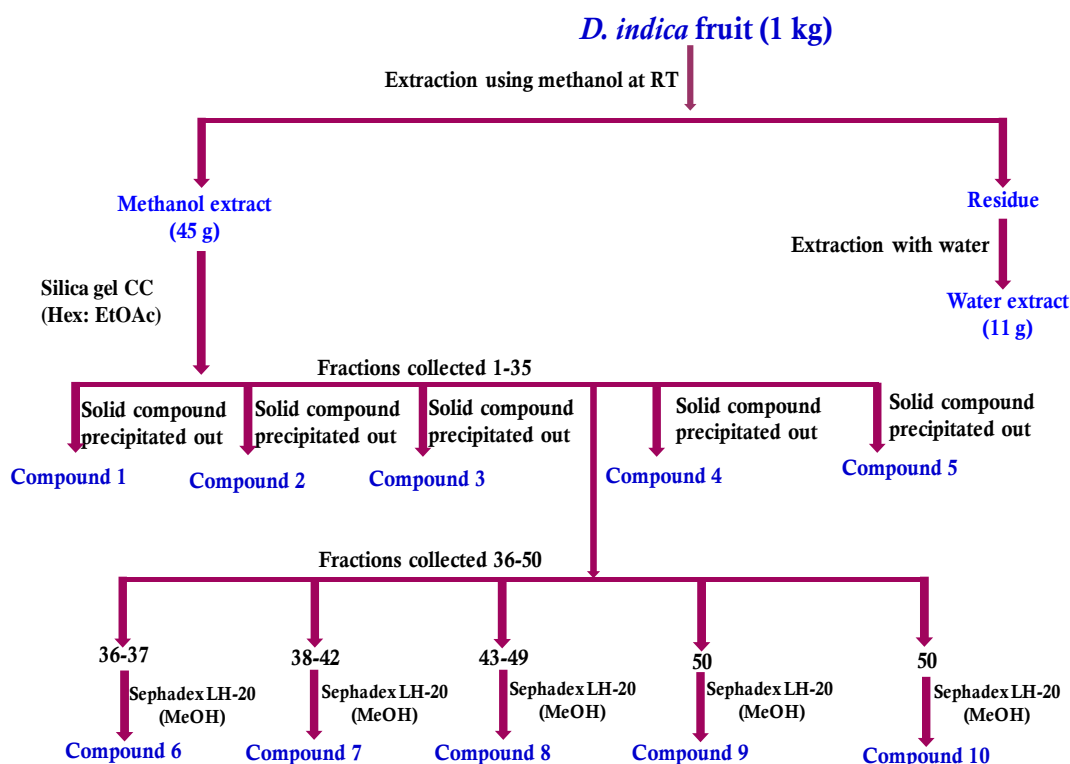


Figure 2.6: Extraction and isolation strategies of *Dillenia indica* fruit

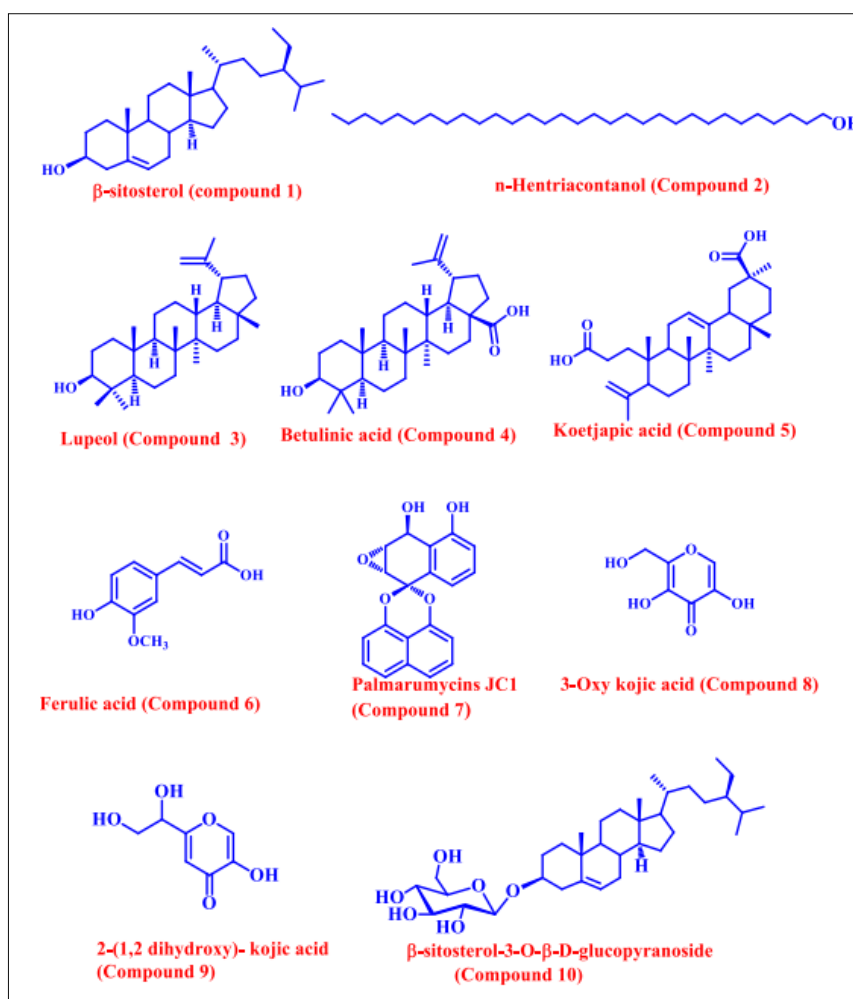


Figure 2.7: Structure of isolated molecules from the fruit of *Dillenia indica*

2.8. Characterisation of Compounds.

2.8.1. Compound 1 (β -sitosterol)

The structure of compound **1** was confirmed through ^1H NMR and ^{13}C NMR, wherein the peak observed at δ 5.37 ppm in the ^1H NMR and δ 121.7, 140.7 ppm in ^{13}C NMR indicated the presence of olefinic proton and carbons respectively. The peak resonated at δ 3.53- 3.54 ppm as multiplet corresponding to methine proton (CH) at the C-3 position bearing OH group.

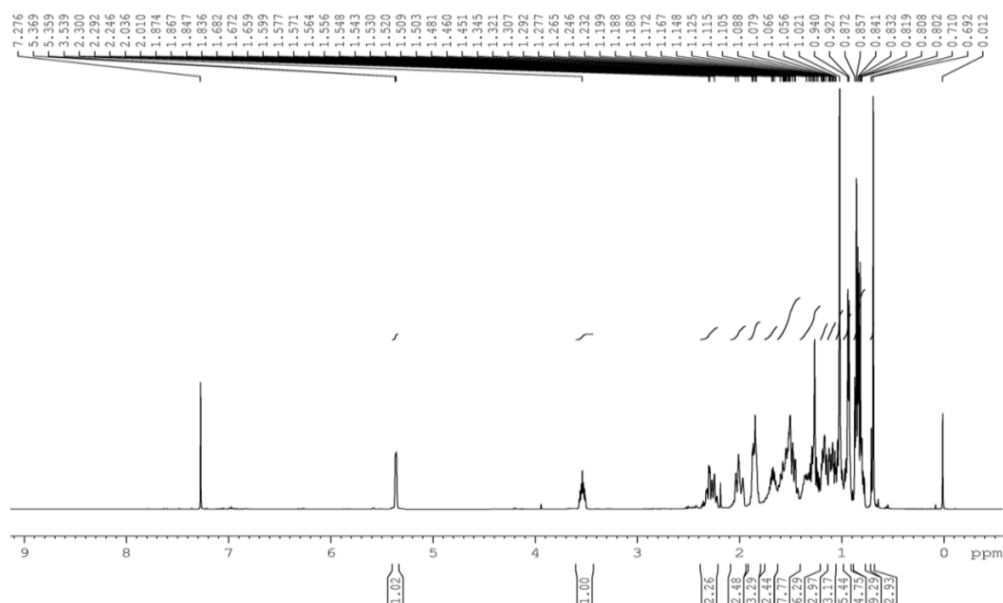


Figure 2.8: ^1H NMR spectra of β -sitosterol (500 MHz, CDCl_3)

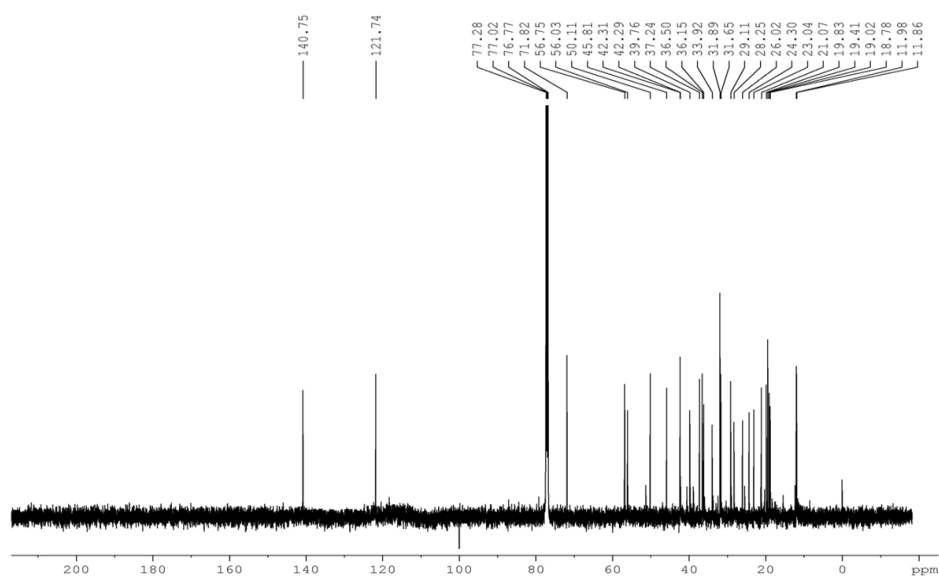


Figure 2.9: ^{13}C NMR spectra of β -sitosterol (125 MHz, CDCl_3)

2.8.2. Compound 2 (n-Hentriacontanol)

Compound 2 is a long-chain hydrocarbon in which the methylene proton directly attached to the hydroxyl group resonated as a triplet at δ 3.64 ppm with a coupling constant of $J = 6.5$ Hz in the ^1H NMR. Similarly, the terminal CH_3 proton resonated as a triplet at δ 0.88 ppm with a coupling constant $J = 6.5$ Hz. Similarly, in ^{13}C NMR spectra, the methylene carbon attached to

the OH group resonated at δ 63.1 ppm. Finally, the structure was confirmed with ESI-HRMS with a molecular ion peak observed at 453.5035(M+H)⁺.

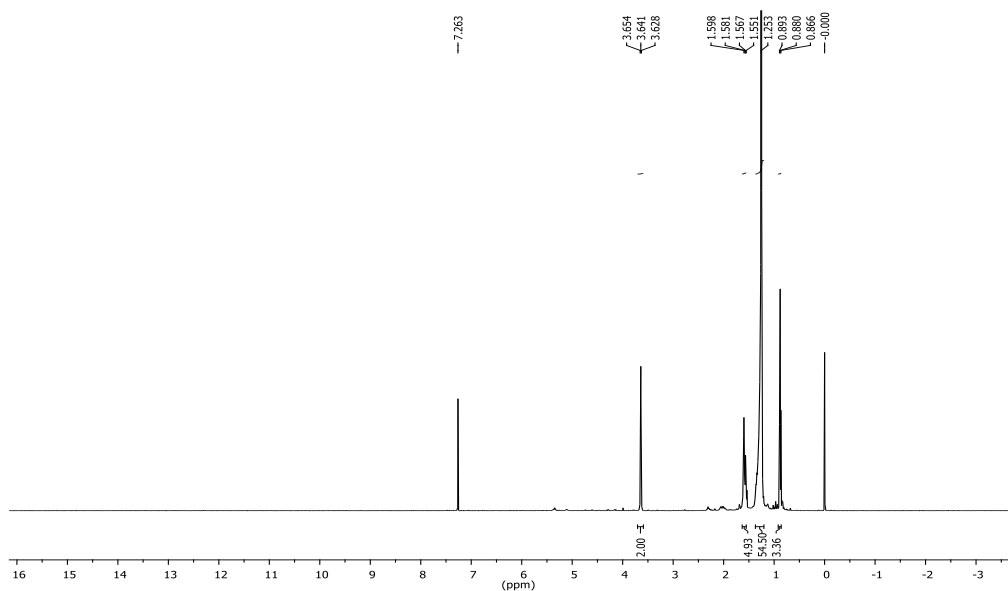


Figure 2.10: ¹H NMR spectra of n-Hentriacontanol (500 MHz, CDCl₃)

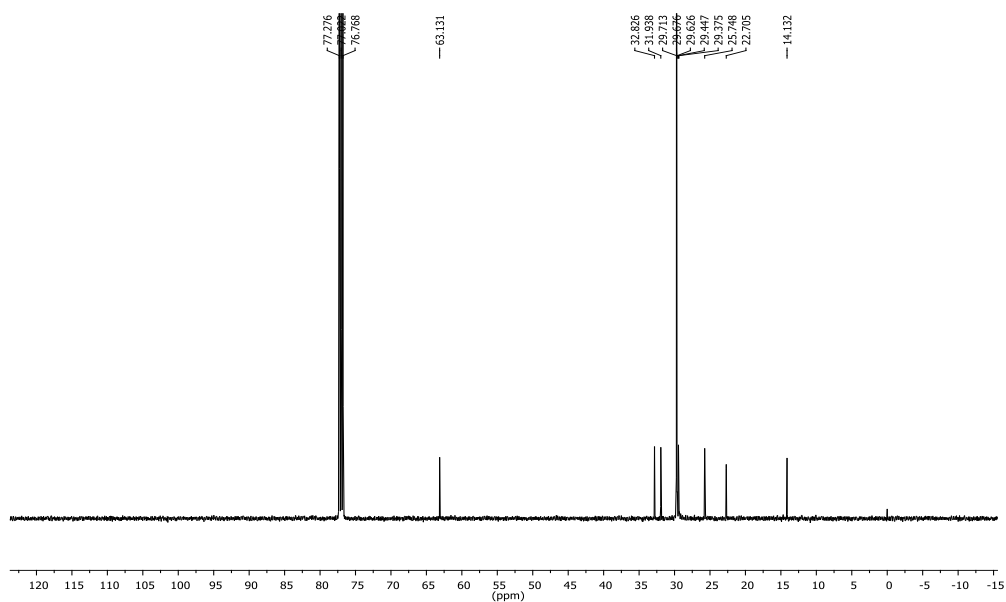


Figure 2.11: ¹³C NMR spectra of n-Hentriacontanol (125 MHz, CDCl₃)

2.8.3. Compound 3 (Lupeol)

The presence of two peaks at chemical shift values δ 4.74 and 4.61 ppm having the same splitting pattern in ^1H NMR spectra, and only one corresponding carbon peak at δ 109.9 ppm in ^{13}C NMR indicated the presence of olefinic CH_2 in the structure of the molecule. Moreover, the methine proton bearing OH group at the A ring resonated as a multiplet at δ 3.21-3.10 ppm, and corresponding carbon resonated at δ 79.1 ppm. Finally, the structure was well in agreement with the literature reference and also following ESI- HRMS spectra, where the molecular ion peak was observed at 427.3939 corresponding to $(\text{M} + \text{H})^+$ ion.

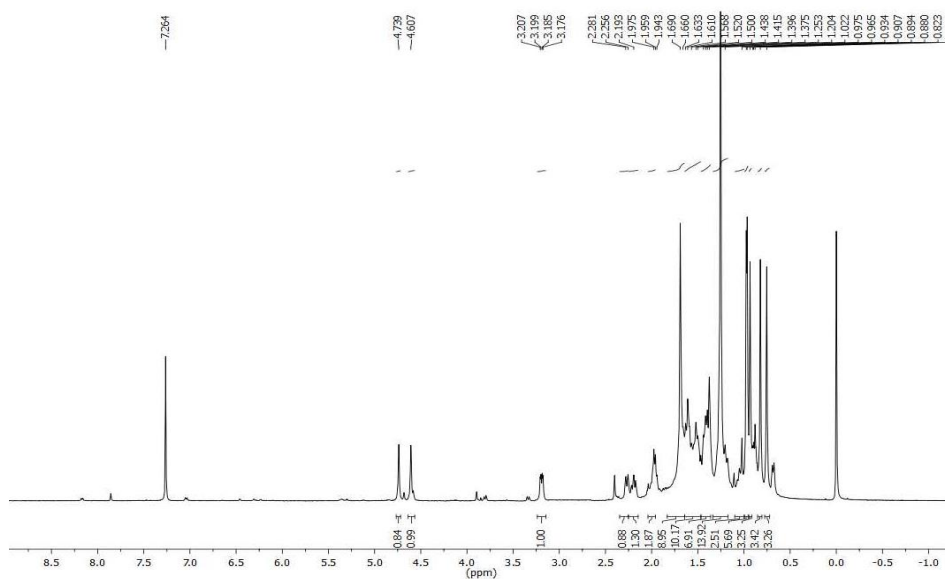


Figure 2.12: ^1H NMR spectra of Lupeol (500 MHz, CDCl_3)

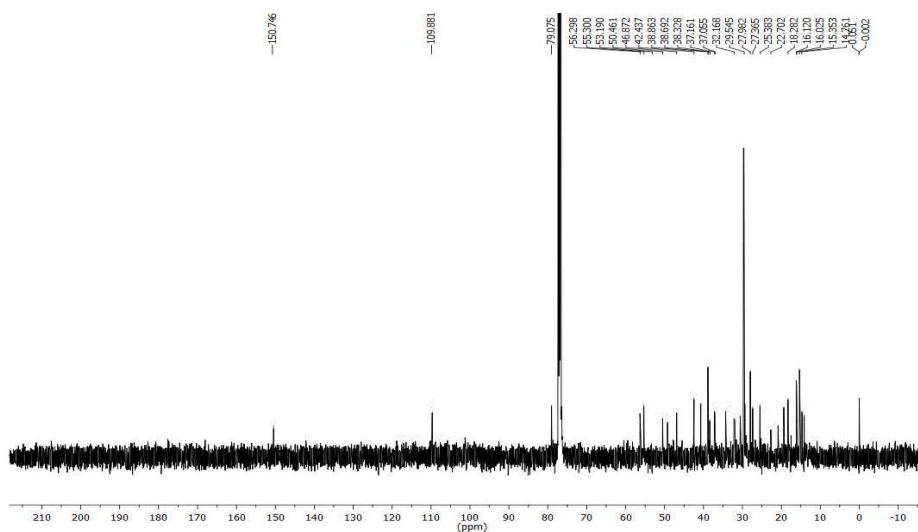


Figure 2.13: ^{13}C NMR spectra of Lupeol (125 MHz, CDCl_3)

2.8.4. Compound 4 (Betulinic acid)

In ^1H NMR, the peak observed at δ 12.07 ppm corresponds to the characteristic of COOH acidic proton. The peak resonated at δ 4.69 and 4.56 ppm, having the same splitting pattern corresponding to the olefinic CH_2 protons. Moreover, the peaks resonated at δ 2.97-2.93 ppm, integrating two protons attributed to the protons directly attached to the carbon-bearing hydroxyl group and an acid group. The peaks resonated at δ 177.7, 150.7, and 110.1 ppm in ^{13}C NMR spectra, indicating the presence of acid carbon and olefinic carbons, respectively. The mass spectra of compound **4** gave a molecular ion peak at 455.3525 ($\text{M}-\text{H}$) $^+$. Finally, the compound was characterised as betulinic acid compared to literature data.

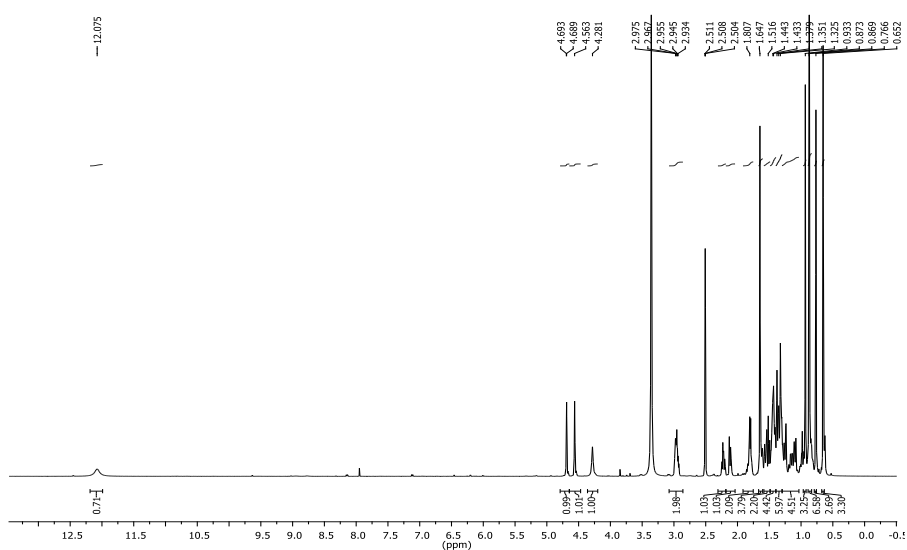


Figure 2.14: ^1H NMR spectra of betulinic acid (500 MHz, $\text{DMSO}-d_6$)

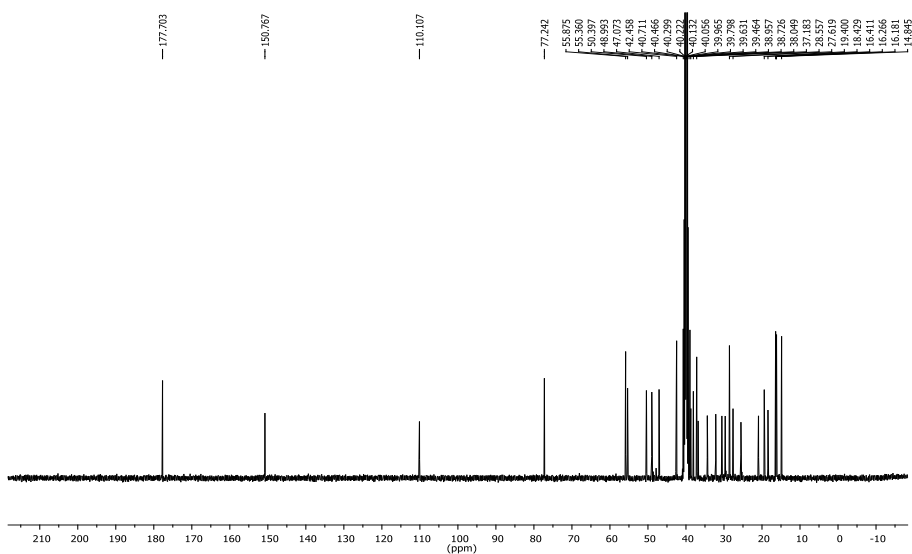


Figure 2.15: ^{13}C NMR spectra of betulinic acid (125 MHz, $\text{DMSO}-d_6$)

2.8.5. Compound 5 (Koetjapic acid)

In ^1H NMR, the peak resonated at δ 5.17 ppm, indicating the presence of an olefinic proton. Signals at δ 4.39 and 4.30 ppm as doublet, each integrating for one proton with coupling constant $J = 4$ Hz, could be attributed to the olefinic CH_2 protons. Signals at δ 2.75-2.73 ppm integrating two protons attributed to the protons which are directly attached to the acid groups. In ^{13}C NMR spectra, the peaks resonated at δ 177.8 and 176.9 ppm, indicating the presence of two acid groups. Signals at δ 147.0, 144.4, 121.9 and 107.9 indicate the presence of olefinic carbons. The mass spectra of compound **5** gave a molecular ion peak at 469.3317 (M-H)⁺. Finally, the compound was confirmed as koetjapic acid compared to literature data.

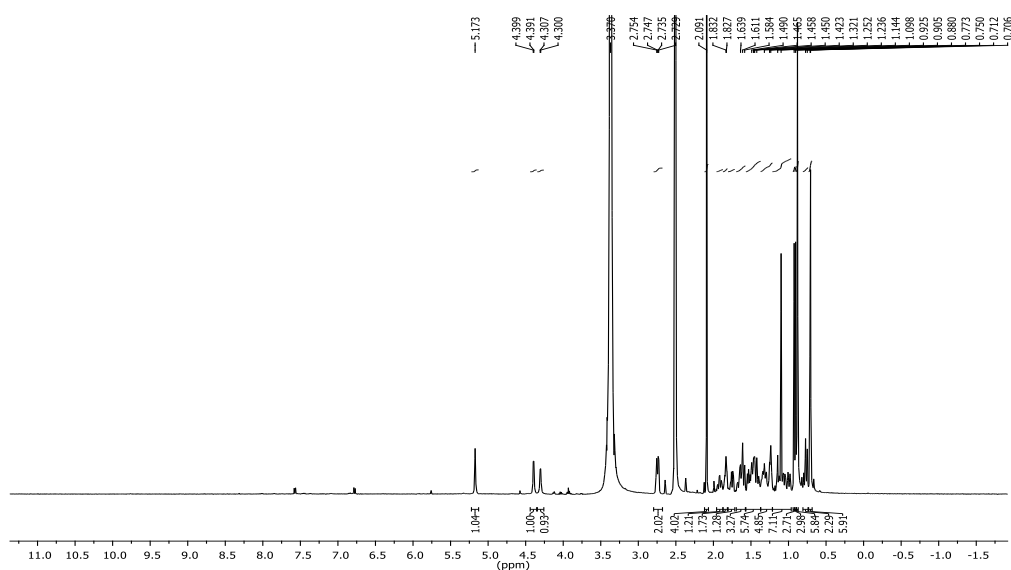


Figure 2.16: ^1H NMR spectra of koetjapic acid (500 MHz, Acetone- d_6)

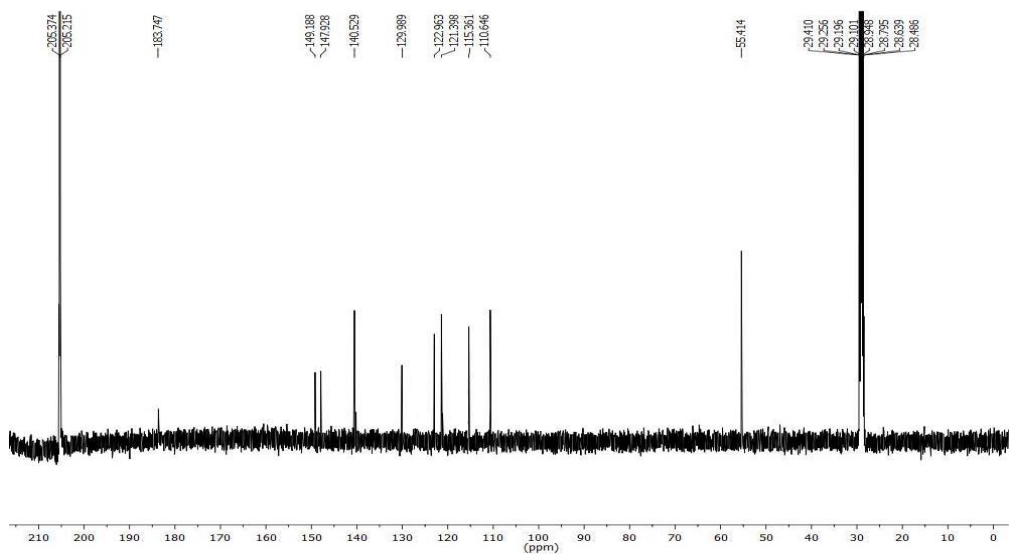


Figure 2.17: ^{13}C NMR spectra of koetjapic acid (125 MHz, Acetone- d_6)

2.8.6. Compound 6 (Ferulic acid)

In the ^1H NMR spectra, the peak resonated at δ 8.27 ppm, indicates the presence aromatic OH proton. The peak resonated at δ 7.62 ppm, and 6.74 ppm resonated as a doublet with a coupling constant of $J = 16$ Hz, corresponding to olefinic protons having trans double bond, which is conjugation with the phenyl ring. Moreover, all three aromatic protons are resonated at δ 7.62, 7.35 and 7.20 ppm as doublet, doublet of doublet, and doublet respectively. In the ^{13}C NMR spectra, the peak at δ 183.7 ppm indicates the presence of acid moiety in the molecule. Finally, the structure was well in agreement with ESI-HRMS and literature reports.

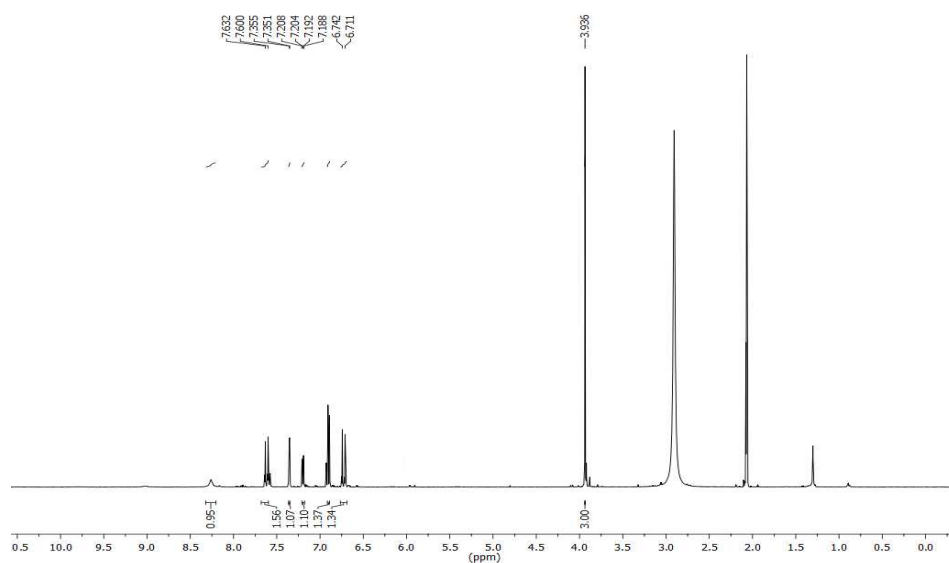


Figure 2.18: ^1H NMR spectra of ferulic acid (500 MHz, Acetone- d_6)

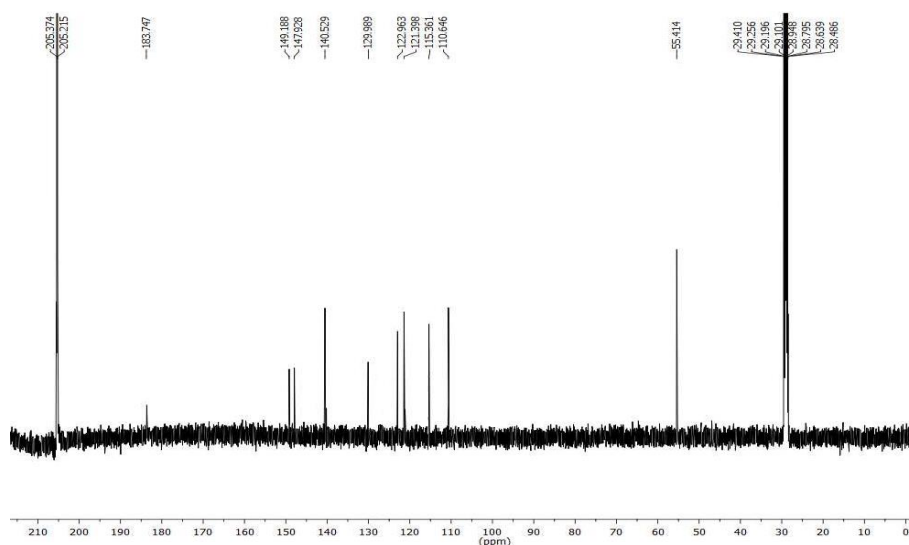


Figure 2.19: ^{13}C NMR spectra of ferulic acid (125 MHz, Acetone- d_6)

2.8.7. Compound 7 (Palmarumycin JC1)

In ^1H NMR, the signal at δ 9.89 ppm indicated the presence of a phenolic hydroxyl group, and nine aromatic protons from the naphthalene and benzene ring resonated in the region δ 7.65-6.96 ppm. The aliphatic hydroxyl group and the proton directly attached to the carbon-bearing hydroxyl group appeared as a singlet. Peaks at δ 5.53 and 5.32 ppm as singlet and at 3.60 and 3.50 ppm as doublet and doublet of doublet each integrating for one proton could be attributed to the protons attached to the epoxide ring. In ^{13}C NMR, the peaks at δ 156.2 ppm indicated the presence of carbon bearing the phenolic hydroxyl group. Signals at δ 147.7 and 144.6 ppm could be attributed to dispiro naphthalene carbon. The relative stereochemistry of the isolated compound was confirmed by the NOESY experiment. In the NOESY spectrum, there is an intense correlation between the secondary aliphatic hydroxyl group and proton directly attached to the epoxide ring, indicating that these protons are in β orientation. The mass spectra of compound 7 exhibit a molecular ion peak at 357.0691 ($\text{M}+\text{Na}$) $^+$. Finally, the compound was confirmed as Palmarumycin JC1 in comparison with literature data.

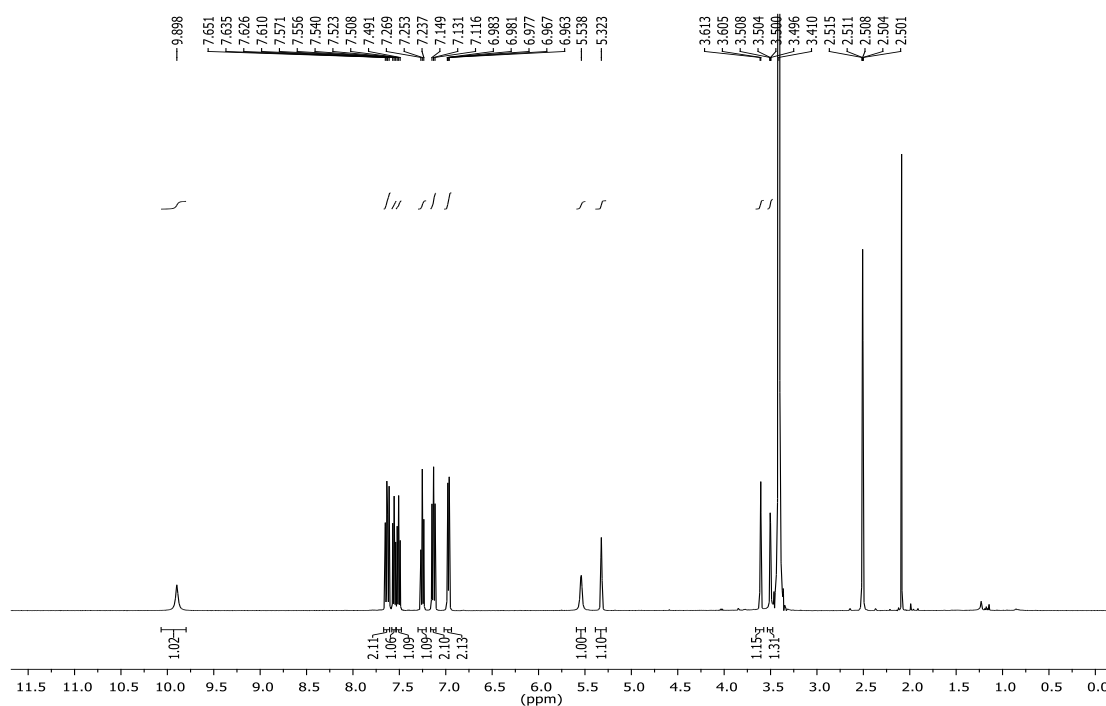


Figure 2.20: ^1H NMR spectra of Palmarumycin JC1 (500 MHz, DMSO-d6)

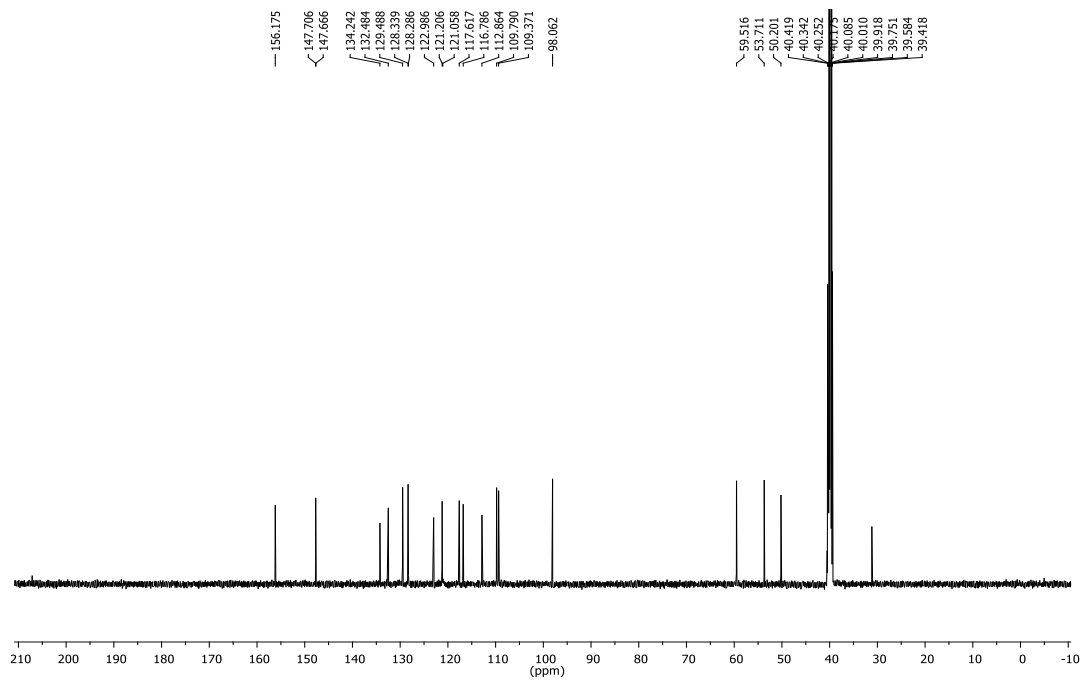


Figure 2.21: ^{13}C NMR spectra of Palmarumycin JC1 (125 MHz, DMSO-d₆)

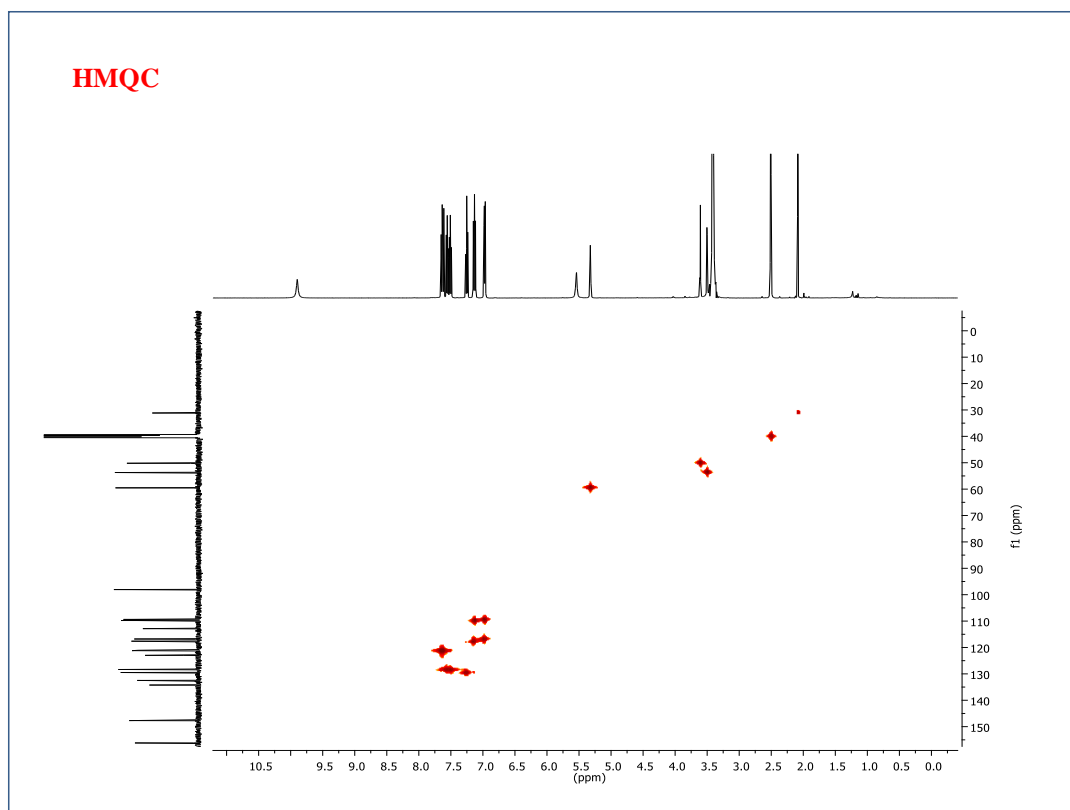


Figure 2.22: HMQC spectra of Palmarumycin JC1

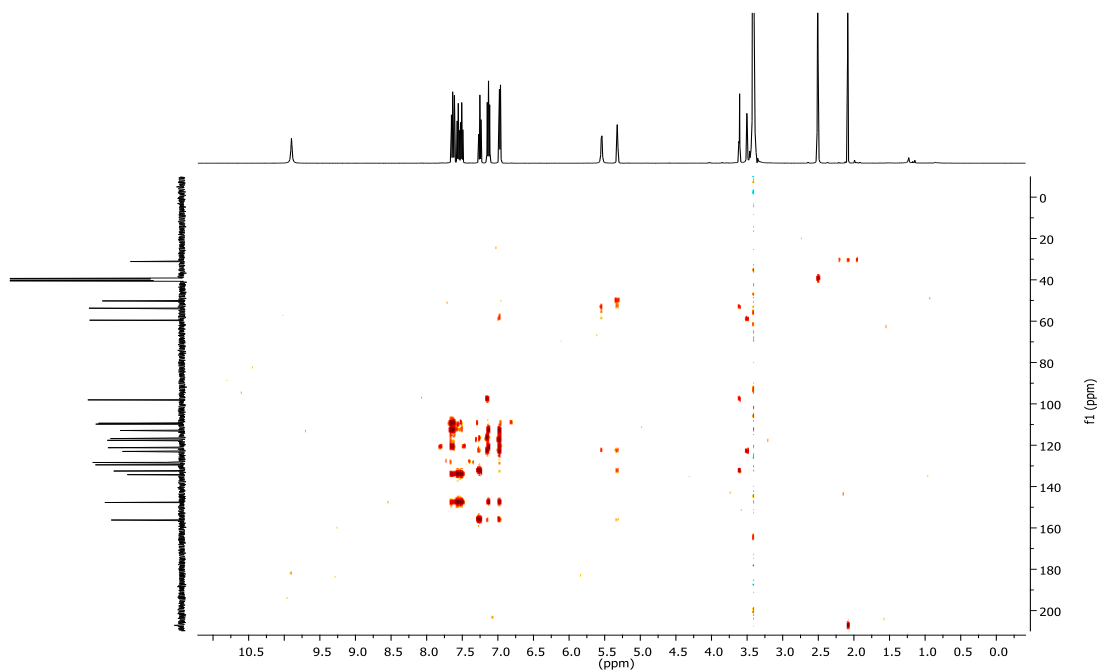


Figure 2.23: HMBC spectra of Palmarumycin JC1

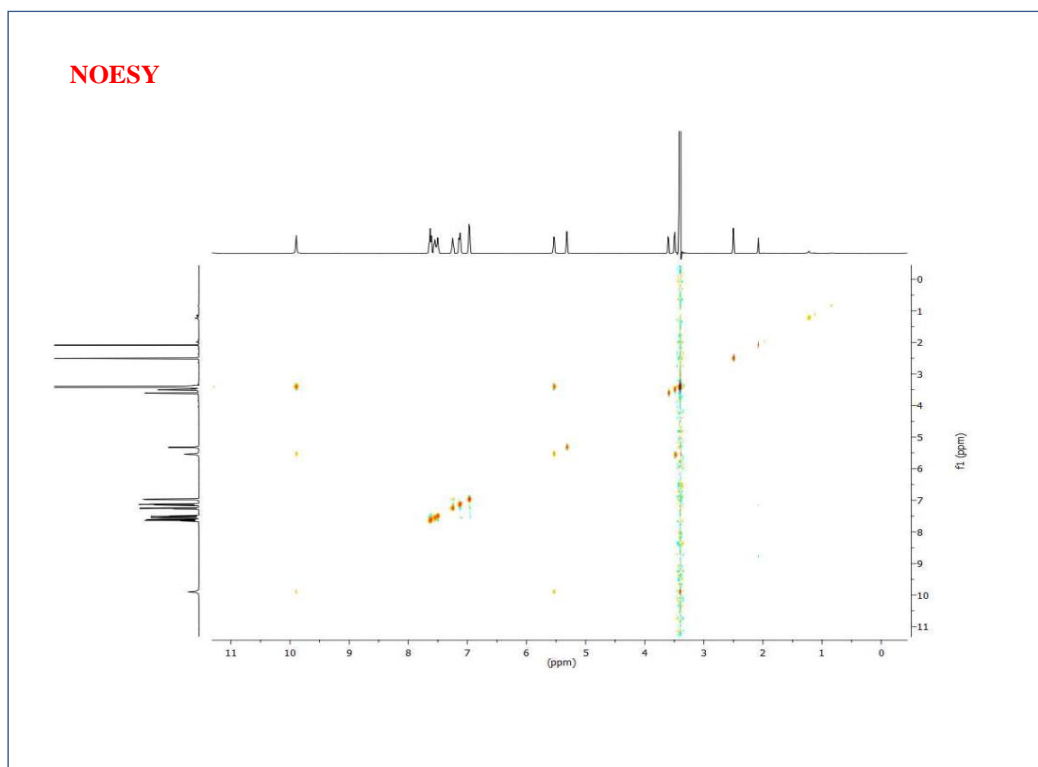


Figure 2.24: NOESY spectra of Palmarumycin JC1

2.8.8. Compound 8 (3-Oxykojic acid)

In ^1H NMR, the signal at δ 8.05 ppm indicated the presence of one aromatic proton. Phenolic hydroxyl protons resonated as a singlet at δ 9.05 and 9.00 ppm. Signal at δ 4.40 ppm as a

doublet with coupling constant $J = 5.5$ Hz could be attributed to methylene CH_2 . In ^{13}C NMR the peaks at δ 169.5 ppm indicated the presence of carbonyl carbon. The mass spectra of compound **8** exhibit molecular ion peak at 157.0137 $(\text{M}-\text{H})^+$. Finally, the compound was confirmed as 3-Oxykojic acid compared to literature data.

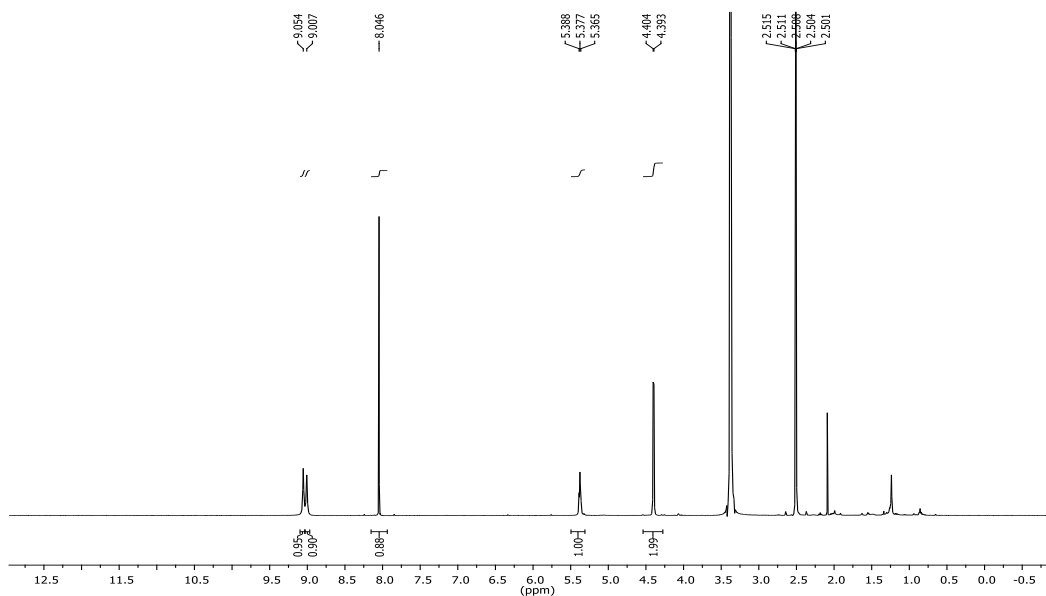


Figure 2.25: ^1H NMR spectra of 3-Oxykojic acid (500 MHz, $\text{DMSO}-d_6$)

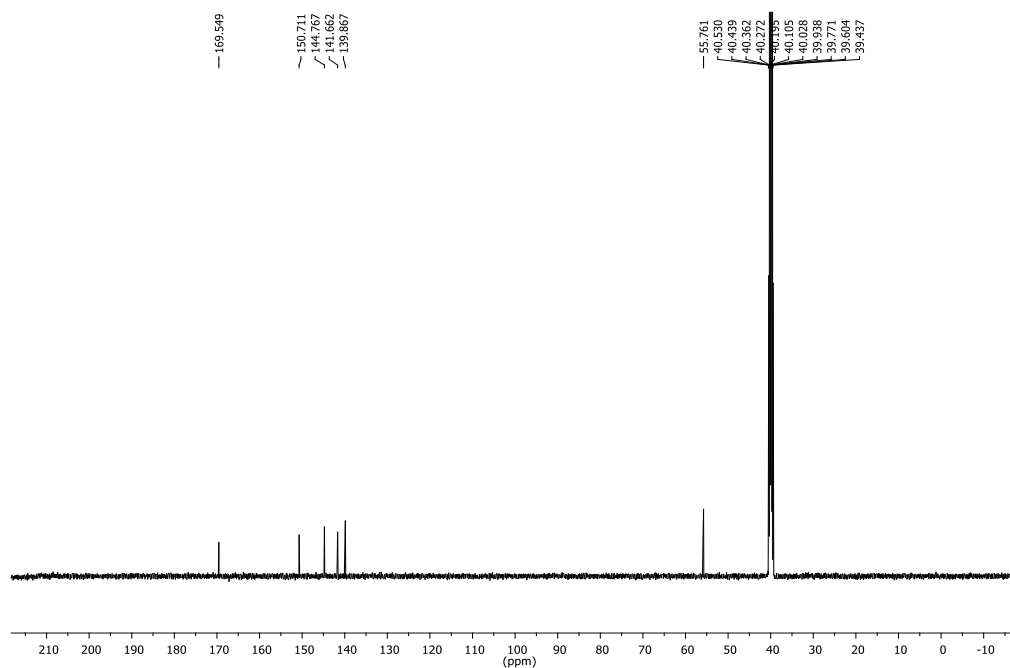


Figure 2.26: ^{13}C NMR spectra of 3-Oxykojic acid (125 MHz, $\text{DMSO}-d_6$)

2.8.9. Compound 9 (2-(1',2'-dihydroxy)-kojic acid)

In ^1H NMR the signal at δ 9.07 ppm indicated the presence of phenolic hydroxyl proton. Two aromatic protons resonated as a singlet at δ 8.03 and 6.34 ppm. Peak observed at δ 4.29 ppm as a doublet with coupling constant $J = 3$ Hz could be attributed to the methylene CH_2 . Methine proton bearing OH group resonated as a doublet at δ 3.17 ppm with a coupling constant of $J = 4.5$ Hz. In ^{13}C NMR, the peaks at δ 174.4 ppm indicated the presence of carbonyl carbon, and the peak at δ 59.9 ppm correspond to methylene carbon. The mass spectra of compound **9** gave a molecular ion peak at 171.0293 $(\text{M}-\text{H})^+$. Finally, the compound was confirmed as 2-(1', 2'-dihydroxy)-kojic acid compared to literature data.

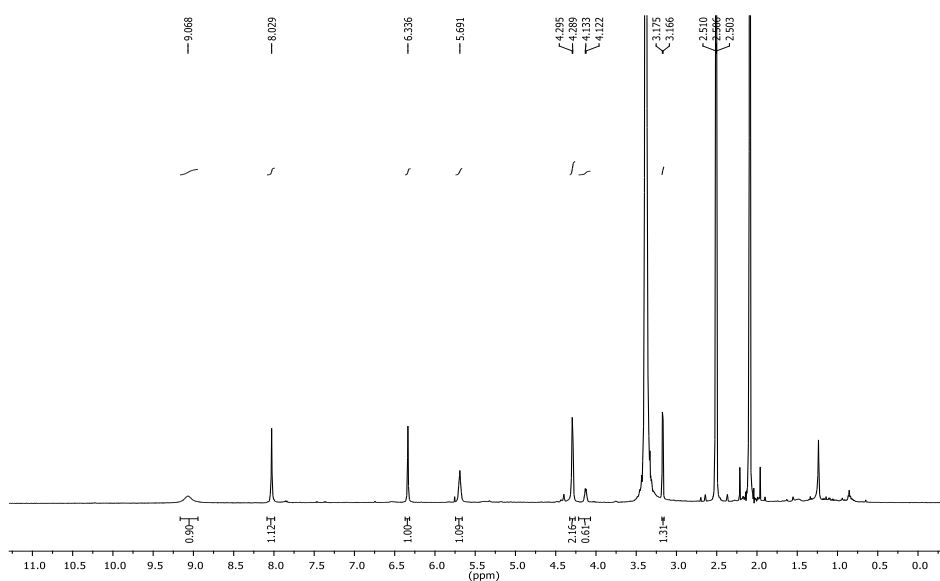


Figure 2.27: ^1H NMR spectra of (2-(1',2'-dihydroxy)-kojic acid) (500 MHz, DMSO-d₆)

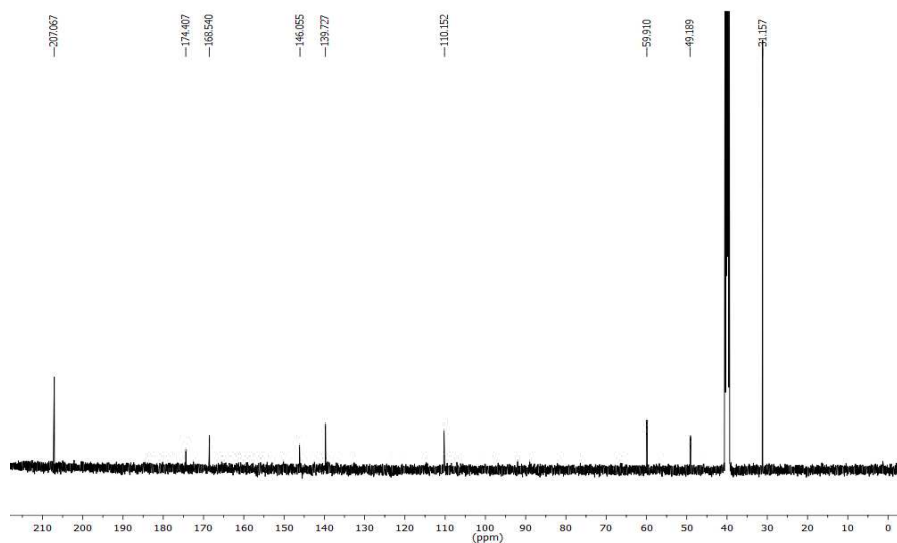


Figure 2.28: ^{13}C NMR spectra of (2-(1',2'-dihydroxy)-kojic acid) (125 MHz, DMSO-d₆)

2.8.10. Compound 10 (β -sitosterol- β -D- glucopyranoside)

The ^1H NMR spectrum of compound **10** showed peaks at δ 0.58, 0.68, 0.71, 0.75, 0.83 and 0.90 ppm corresponding to methyl protons. The methine proton-bearing OH group resonated at δ 3.66 ppm as a multiplet. Peak observed at δ 5.26 ppm as doublet is corresponding to olefinic proton. ^{13}C NMR spectra of compound **10** consist of 29 carbons. The glucose unit contained six carbons, out of which anomeric carbon resonated at δ 100.9 ppm, and methylene carbon appeared at δ 61.7 ppm. The other four carbons of the glucose molecule appeared at 70.0, 75.6, 76.7 and 77.0 ppm.

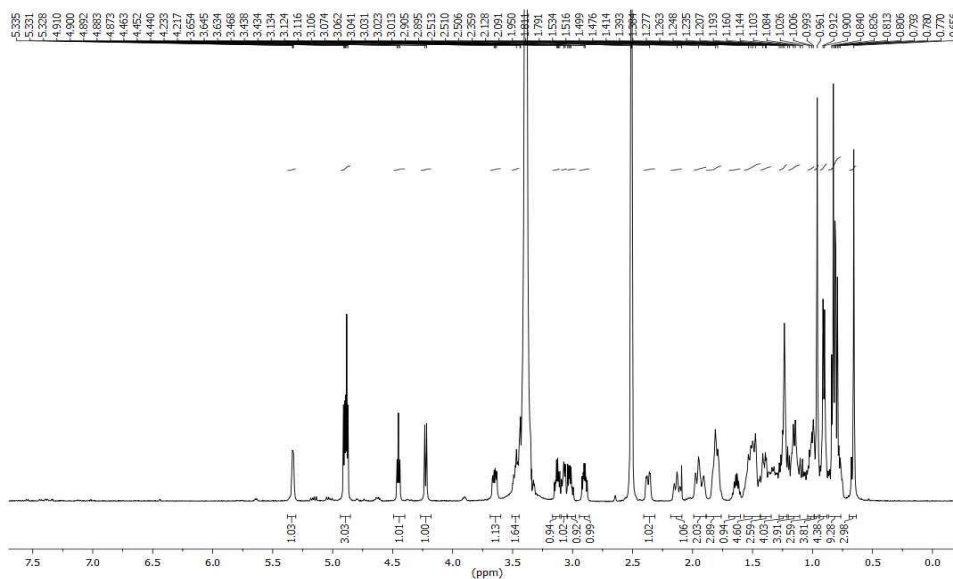


Figure 2.29: ^1H NMR spectra of β -sitosterol- β -D- glucopyranoside (500 MHz, DMSO-d₆)

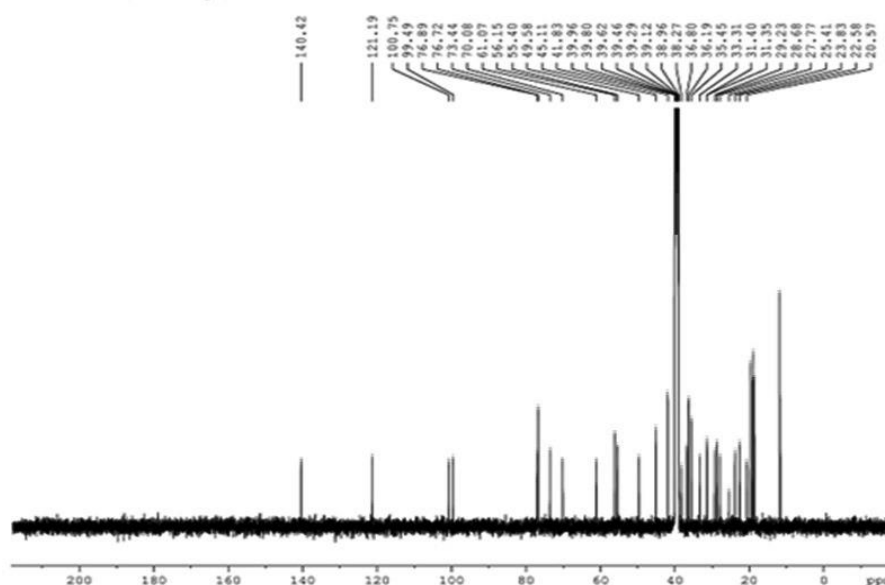


Figure 2.30: ^{13}C NMR spectra of β -sitosterol- β -D- glucopyranoside (125 MHz, DMSO-d₆)

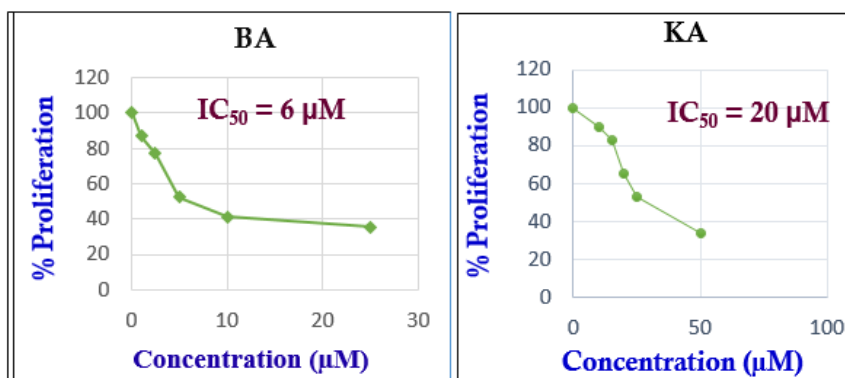


Figure 2.31: Anti-proliferative potential of both BA and KA against SAS cells

2.9. Computational Screening of BA and KA: Next, the screening strategy was further extended to computational simulation tools, where we employed the molecular docking approach to predict the affinity of the previously screened molecules to bind with the selected protein domains involved in regulating the different hallmarks of cancer (Table 2). Moreover, the flexibility and suitability of the molecules inside the binding pocket of the selected receptors were screened by molecular dynamics protocol.

2.9.1. QikProp analysis: In order to check the druggability of the ligands-BA and KA, we carried out the QikProp analysis (Table 1), which predicts the ADME/T properties of the ligands based on the parameters already defined by the software. The important parameters we selected are: #stars (few stars-more drug-like): 0 to 5; M.W. (Molecular Weight): 130.0 to 725.0; HBA (Hydrogen bond acceptor): 2.0 to 20.0; HBD (hydrogen bond donor): 0.0 to 6.0; CNS (Central Nervous System activity): -2 to +2; FISA (hydrophilic component of the SASA on N, O, and H on heteroatoms) 7.0 to 330.0; QPlogS (Aqueous solubility): -6.5 to 0.5; QPlogPo/w (octanol/water partition coefficient): -2.0 to 6.5; QPlogKhsa (binding to human serum albumin): -1.5 to 1.5; % HOA (% human oral absorption): >70, good and Ro5 (Number of violations of Lipinski's rule of five): maximum is 4. From the output values, it is very clear that both the ligands are druggable with few #stars, 2 hydrogen bond donors and 4 hydrogen bond acceptors. The low CNS value and high %HOA indicate their high oral availability with less central nervous system toxicity. The octanol/water partition coefficient and binding to human serum albumin are also indicated the effectiveness of these drugs with only one violation from the Lipinski's rule of five (Ro5).

Table 2. Predicted ADME/T properties of BA and KA

Compound	#stars	MW.	HBA	HBD	CNS	FISA	QPlogS	QPlogPo/w	QPlogKhsa	%HOA	Ro5
BA	0	456.71	3.7	2	-1	95.96	-6.50	6.09	1.31	94.20	1
KA	0	470.69	4	2	-2	160.68	-6.09	6.286	1.11	73.69	1

2.9.2. Molecular Docking: BA was docked against the selected proteins: AKT (Protein Data Bank (PDB) ID: 1O6L), p-AKT, mTOR (PDB ID: 4JSP), p-mTOR, MMP-2 (PDB ID: 3AYU), and VEGF-A (PDB ID: 1FLT) (Table S1). It was found that BA showed a better binding affinity with AKT (D/G-score, -7.5 kcal/mol) and mTOR (D/G-score, -8.4 kcal/mol) (Table 2). In the case of 1O6L, the carboxylate group from the ligand forms H-bonds with polar Thr162 (1.8 and 2.1 Å), while with 4JSP, the carboxylate ion forms a salt bridge with positively charged Lys1452. The salt bridge formation is comparatively stronger and in this case, the ligand is deeply buried inside the binding pocket, thus resulting in maximum binding affinity with 4JSP (Figure 6). Subsequently, KA was docked against NF- κ B (1SVC), p-NF- κ B, mTOR (4JSP), p-mTOR, STAT-3 (6NJS), p-STAT3, CXCR4 (3ODU), COX-2 (5IKQ), survivin (1E31), MMP-2 (1HOV), and VEGF-A (1FLT) (Table 3). Among these, KA showed a better binding affinity with NF- κ B (D/G-score, -7.4 kcal/mol), mTOR (D/G-score, -8.1 kcal/mol), and STAT3 (D/G-score, -6.9 kcal/mol) (Table 1). In the binding pocket of 1SVC, one of the carboxylate ions forms H-bonds with positively charged Lys149 (1.9 and 2.2 Å). With 6NJS, one of the carboxylates forms two salt bridges with positively charged Lys573, Lys574, and one H-bond with Lys574 (2.1 Å), and the other carboxylate ion forms H-bond with Asn567 (2.2 Å). Even though two salt bridges are formed with 6NJS, the positioning of the conformer within the binding pocket is not as deep as in the other two cases, which leads to the comparatively lower score with 6NJS. One of the carboxylate ions from KA forms an H-bond with polar Asn1421 (1.8 Å), while the second carboxylate group forms a salt bridge with positively charged Arg2217, eventually contributing to the maximum affinity with 4JSP (Figure 6). The interaction analysis figured out the stability of the ligands inside the binding pocket of the receptor, which is somewhat more in BA as it is well inside the site.

Table 3: D-score values and residues of BA and KA interacting with selected proteins

	Akt (1O6L)		mTOR (4JSP)			
	D-score (kcal/mol)	interacting residues	D-score (kcal/mol)	interacting residues		
BA	-7.5	Thr162	-8.4	Lys1452		
KA	NF-kB (1SVC)		mTOR (4JSP)		STAT3 (6NJS)	
	D-score (kcal/mol)	interacting residues	D-score (kcal/mol)	interacting residues	D-score (kcal/mol)	interacting residues
	-7.4	Lys149	-8.1	Arg2217	-6.9	Lys573
				Asn1421		Lys574
						Asn567

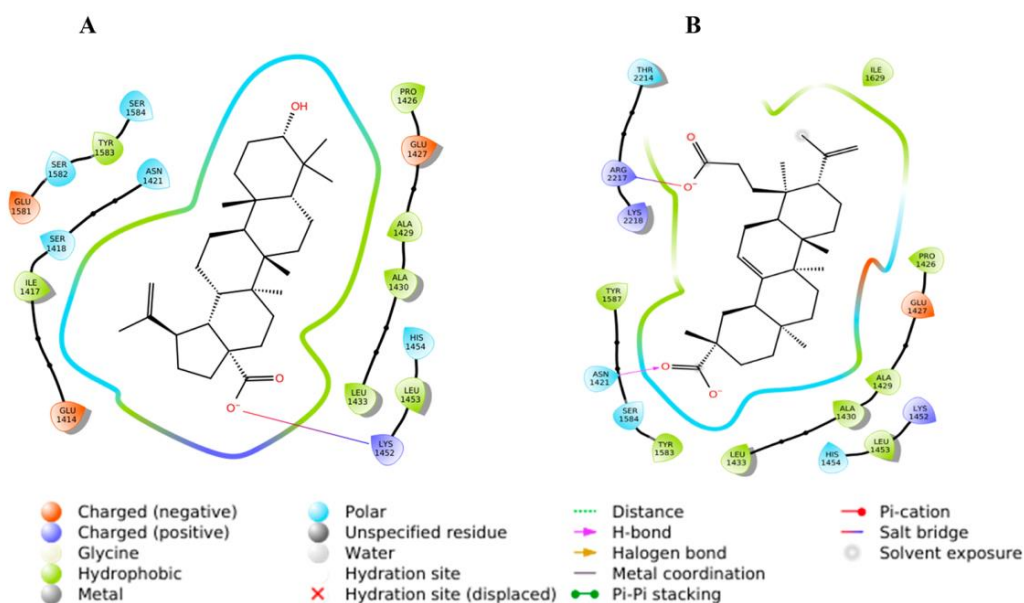


Figure 2.32: 2D interaction diagrams of (A) BA and (B) KA.

2.9.3. Molecular Dynamics. To visualize the suitability and stability of the ligands inside the binding pocket of the receptor, molecular dynamics simulations were carried out for the complexes 4JSP-BA and 4JSP-KA for 10 000 ps under the OPLS-2005 force field. The RMSD plots (Figure 2.33) clearly depicts the stability of the complex.

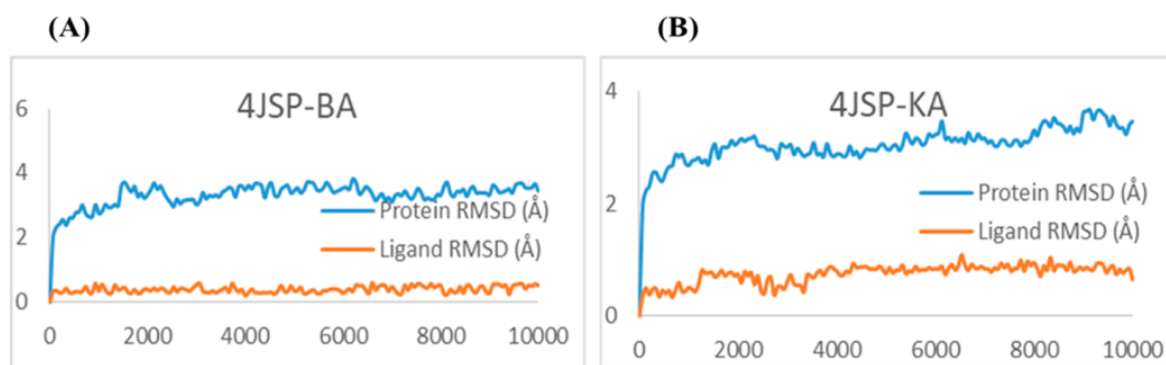


Figure 2.33: RMSD plots of (A) 4JSP-BA and (B) 4JSP-KA

Even though the protein shows an initial fluctuation, it is almost stable under 4 Å during the interaction with the BA and KA, whereas the ligands are stabilized inside the protein throughout the trajectory. 4JSP– BA is comparatively more stable with less root-mean-square fluctuations. The P–L histograms (Figure 2.34) show that the H bonded interactions are the major force of attraction that holds the ligands inside the protein. The simulation event analysis pointed out the H-bond formation of carboxylate ion of BA with positively charged Lys1452, which lasts for 45% of the simulation time, while that with polar Ser1584 lasts for 49% of the simulation time. However, carboxylate ions of KA form Hbond with positive charged Arg2217 (81 and 96%), hydrophobic Tyr1587 (35%), and polar Ser1584 (52%). Some of the KA residues also form water bridges with both of them.

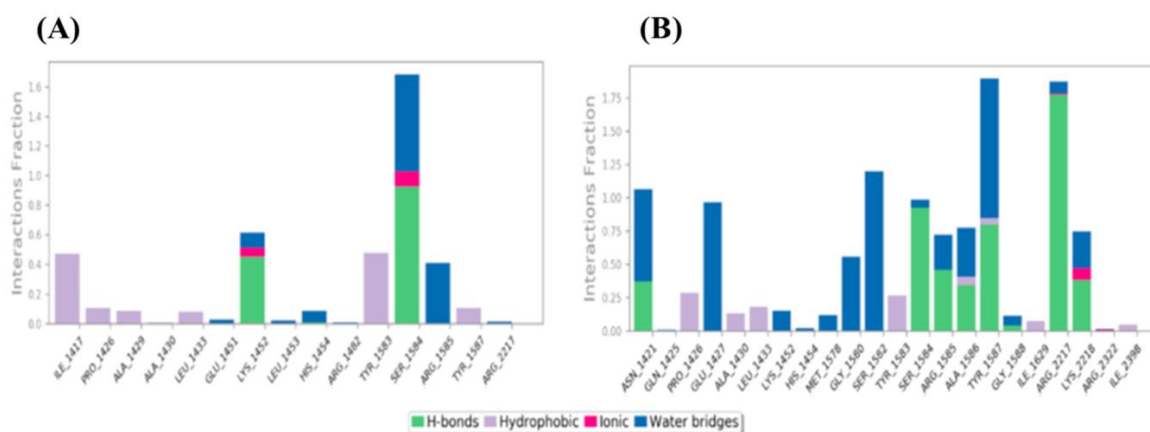


Figure 2.34: P-L interaction histogram of (A) 4JSP-BA and (B) 4JSP-KA

All these factors together subsidize the higher binding affinity of the ligands with mTOR. After evaluating the primary screening based on cancer cell-specific cytotoxicity, followed by molecular docking analysis, the selected candidates were subjected to the next-level studies.

2.10. DI inhibited the clonogenic ability of OSCC cells: We further confirmed the effect of DI on the ability of the individual SAS cells to form colonies by clonogenic assay. Compared with the control, the administration of DI extracts at two different concentrations (10 and 15 µg/mL) caused a significant reduction in the number of colonies. Besides, the treatment of SAS cells with 10 and 15 µM concentrations of both BA and KA was able to reduce the number of colonies in a dose-dependent manner (Figure 2.35). In accordance with the clonogenic assay result, it was inferred that KA was superior to BA for inhibiting the colony-forming ability of SAS cells.

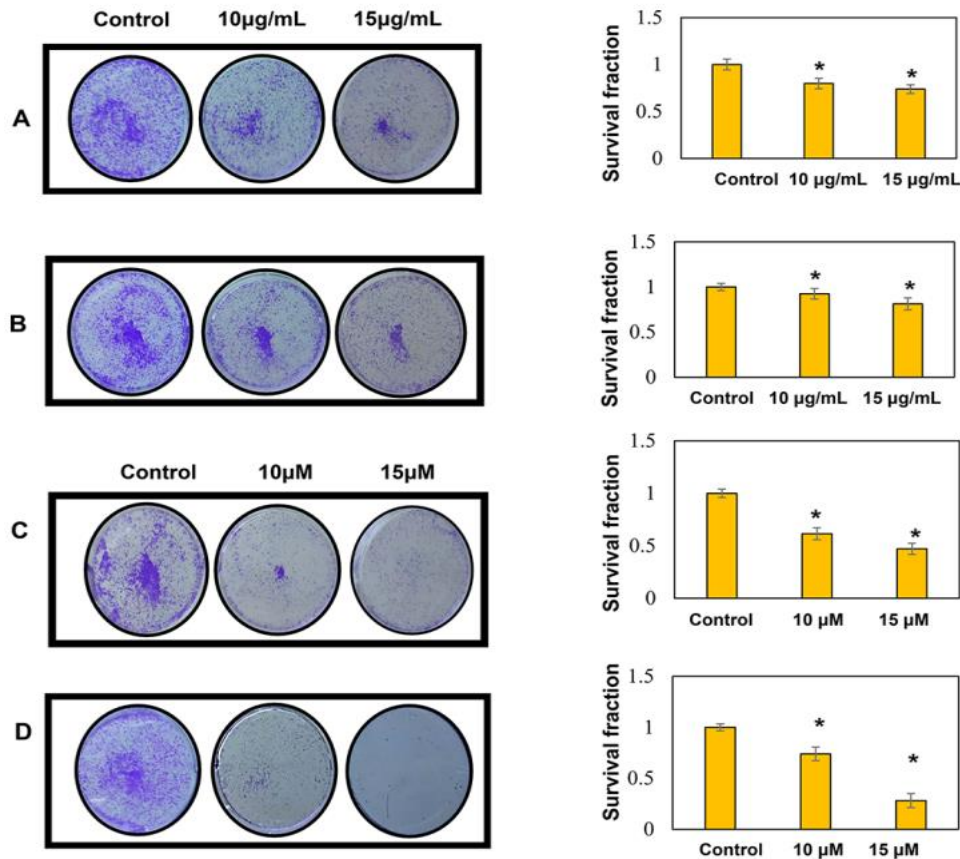
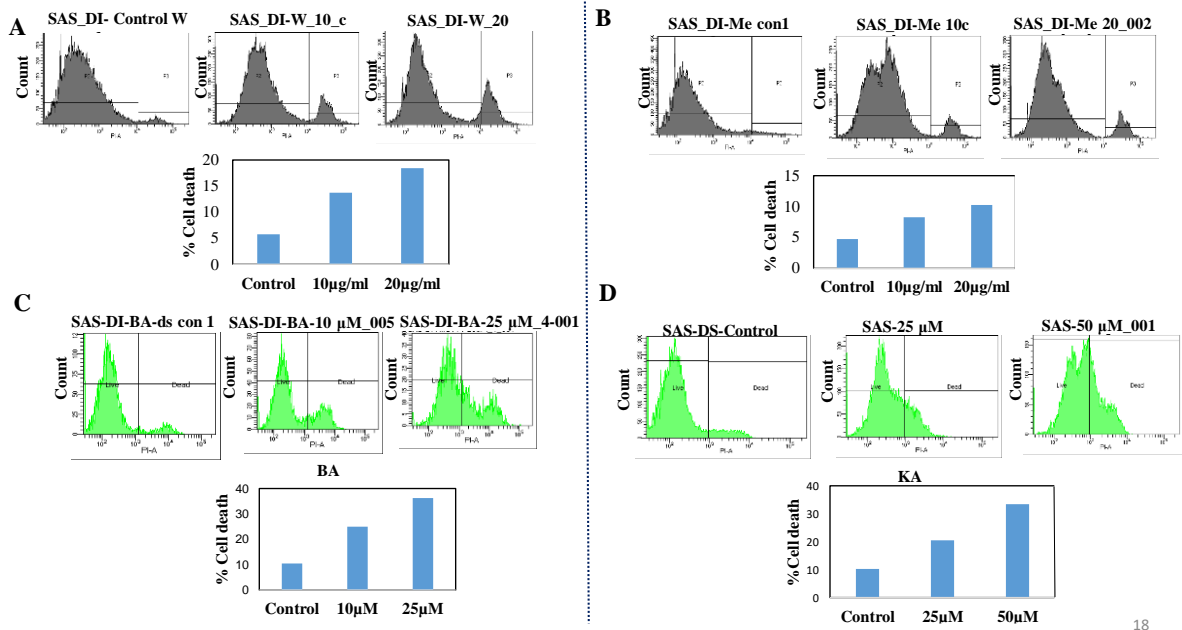


Figure 2.35: Inhibition of clonogenic potential of SAS cells by (A) DI-H₂O Ext (B) DI-ME Ext (C) BA (D) KA. Untreated cells were kept as the control. Quantification of the number of colonies was done with the help of Image J software. Results presented are mean \pm SD of three independent experiments; *, $p < 0.05$ vs control.

2.11. DI induced cell death in OSCC cells: In order to confirm the role of DI in inducing cell death, propidium iodide (PI)-FACS staining was conducted following the treatment of SAS cells with 10 and 20 $\mu\text{g/mL}$ concentrations of both the extracts. Flow cytometric results revealed that the percentage of cell death increased from 14 to 19% in SAS cells treated with DI-H₂O Ext and from 8 to 10% in SAS cells treated with DIME Ext after 72 h compared with the untreated control. A similar strategy was followed for elucidating the death inducing potential of BA and KA. Our results showed that BA increased the percentage of cell death from 25% at 10 μM to 36% at 25 μM , whereas KA increased the percentage of cell death from 20% at 25 μM to 33% at 50 μM , respectively (Figure 2.36).



18

Figure 2.36: Induction of cell death in SAS cells by (A) DI-H₂O Ext, (B) DI-ME Ext, (C) BA, and (D) KA. Cells were treated with the indicated concentrations for 72 h, followed by PI staining and FACS analysis for the cell death profile.

Similarly, in the live and dead assay, treatment with DI led to a dose-dependent toxic effect on OSCC cells (Figure 2.37). Therefore, the results stated that treatment with the extracts, BA and KA resulted in cell death in SAS cells in a dose-dependent manner.

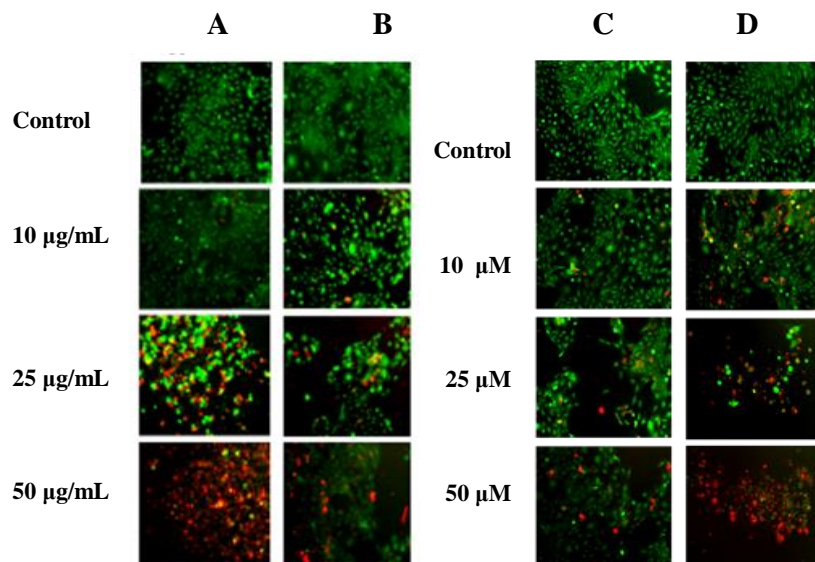


Figure 2.37: Live and dead assay was performed to evaluate the cytotoxic effect of the indicated concentrations of (A) DI-H₂O Ext, (B) DI-ME Ext, (C) BA, and (D) KA on SAS cells.

2.13. Effect of DI in inducing apoptosis in SAS cells: Next, we evaluated the potential of DI in inducing apoptosis in SAS cells using Annexin V assay. SAS cells were treated with 10 and 25 $\mu\text{g}/\text{mL}$ of DI-H₂O Ext and 25 and 50 $\mu\text{g}/\text{mL}$ of DI-ME Ext for 72 h individually. As shown in Figure 7, the percentage of apoptotic cells increased from 1.7% in control to 19.8% under DI-H₂O Ext treatment and from 1% in control to 9% under DI-ME Ext treatment. The percentage of apoptotic cells increased from 3.2% in control to 14.3% in 50 μM BA-treated SAS cells and from 3.2% in control to 12.6% in 50 μM KA treated SAS cells respectively (Figure 2.38). These results indicate that BA treatment causes a statistically evident increase in the number of apoptotic cells thus leading to significant growth inhibition in SAS cells.

2.14. DI induced cell cycle arrest in OSCC cells: To further examine the mechanism of action of DI on SAS cells, the cell cycle distribution was investigated by flow cytometry analysis. We found that the cells upon treatment with different concentrations of DI-H₂O Ext, DI-ME Ext, BA, and KA, showed cell cycle arrest at different phases in comparison to the untreated cells. The SAS cells treated with DI-H₂O Ext and DI-ME Ext exhibited G1 and G2 phase arrest, respectively, while BA and KA treated SAS cells demonstrated S phase arrest. This result indicates that the decrease in cell proliferation and viability of the DI-treated SAS cells may be due to the induction of cell cycle arrest at various phases of the cell cycle (Figure 2.39).

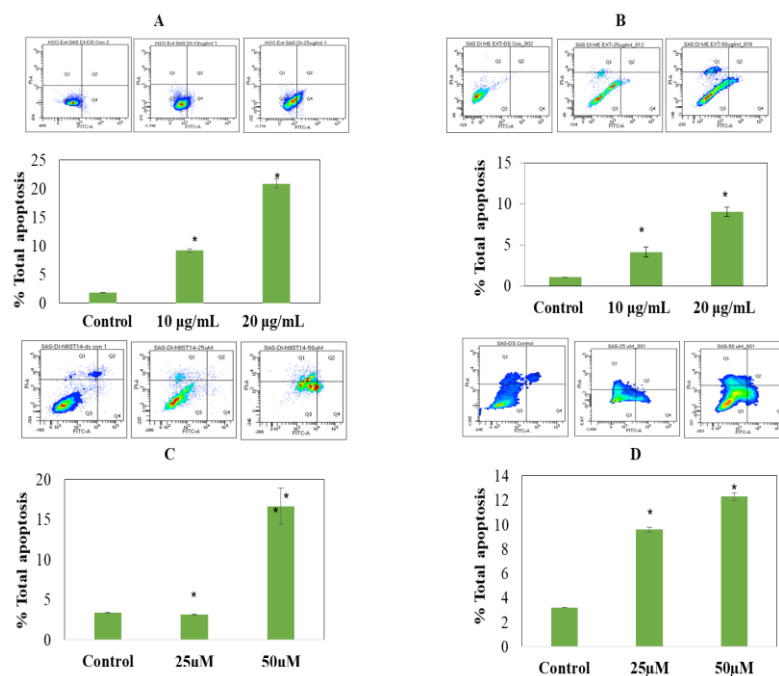


Figure 2.38: Induction of apoptosis in SAS cells upon treatment with (A) DI-H₂O Ext, (B) DI-ME Ext, (C) BA, and (D) KA. Cells were treated with the indicated concentrations for 72 h, followed by Annexin V staining and FACS analysis.

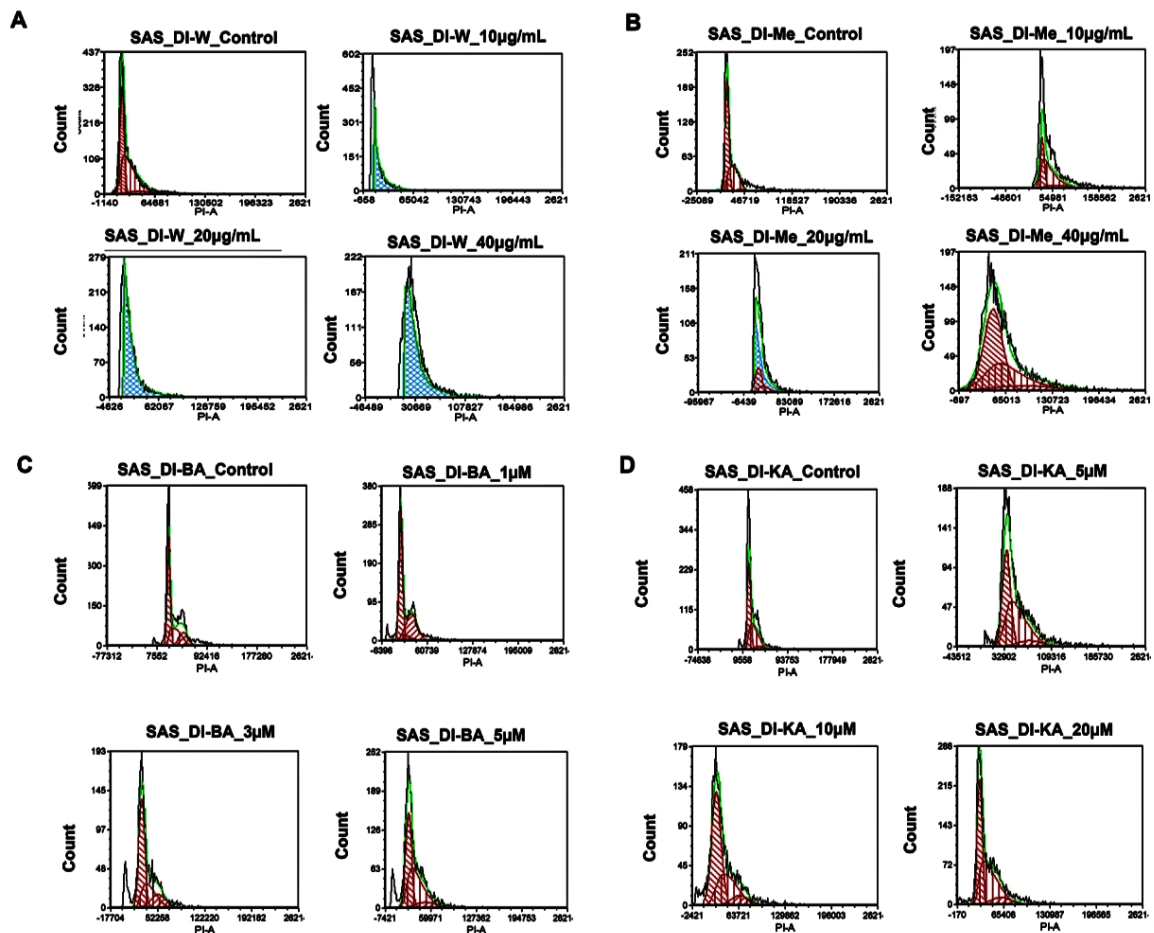


Figure 2.39: Induction of cell cycle arrest in SAS cells by (A) DI-H₂O Ext, (B) DI-ME Ext, (C) BA, and (D) KA. Percentages of each cell cycle phase were obtained using FCS Express software.

2.15. DI inhibited the migration of OSCC cells: The wound healing analysis of SAS cells showed inhibition in the migration of these cells with an increase in the concentration of DI. The images taken at 12 hr in case of DI-H₂O Ext and DI-ME Ext, or 24 hr in case of BA and KA showed that the wound area was completely healed while the treated cells exhibited changes in cell morphology and a significant reduction in the migration of SAS cells compared to the untreated cells. These results indicate that DI controls the migration of SAS cells (Figure 2.40).

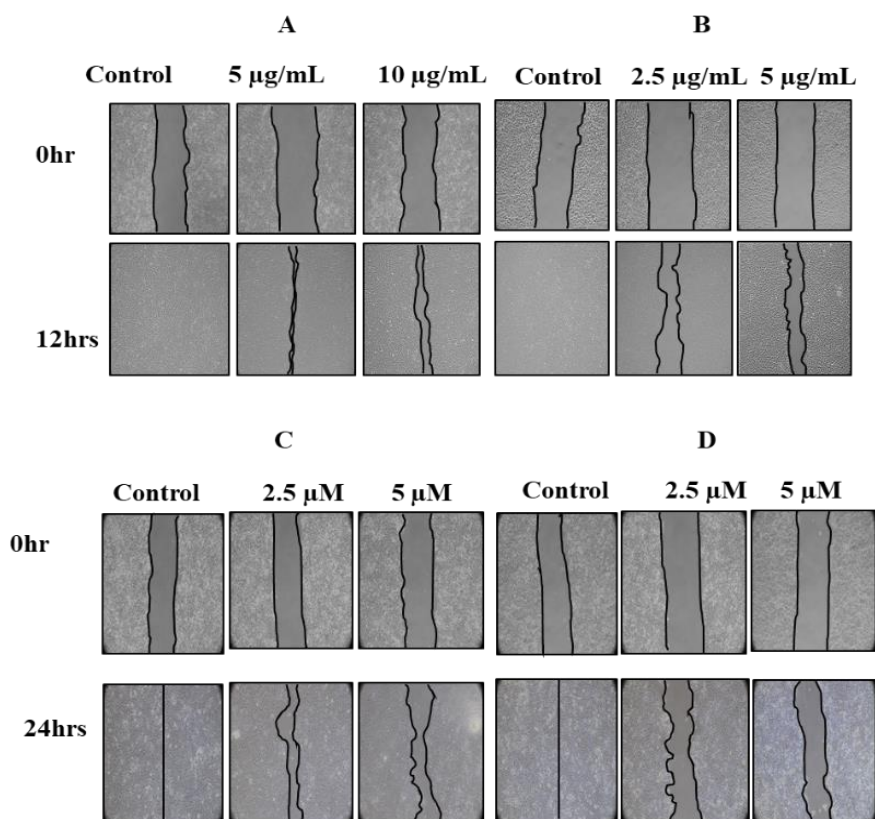


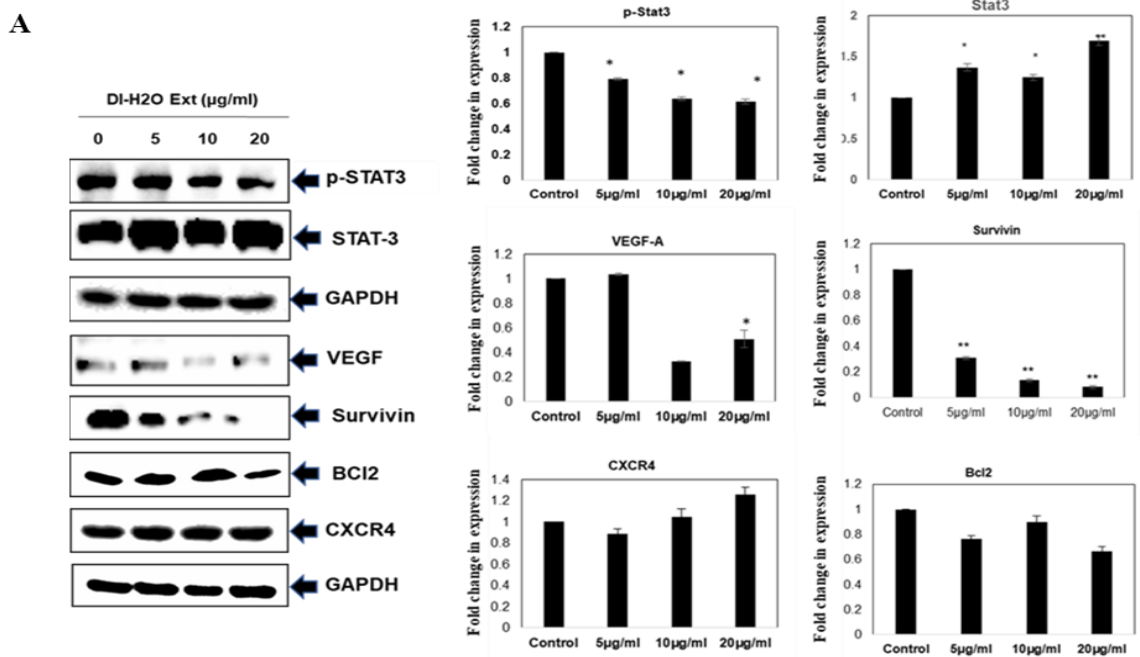
Figure 2.40: Inhibition of the migration of SAS cells upon treatment with (A) DI-H₂O Ext, (B) DI-ME Ext, (C) BA, and (D) KA. Cells were scratch-wounded and then treated with the indicated concentrations, followed by the recording of wound areas at different time points.

2.16. DI mediated the expression of various proteins responsible for survival, inflammation, cell cycle, angiogenesis, migration, and apoptosis of OSCC cells and the involvement of multiple signaling pathways in the mode of action.

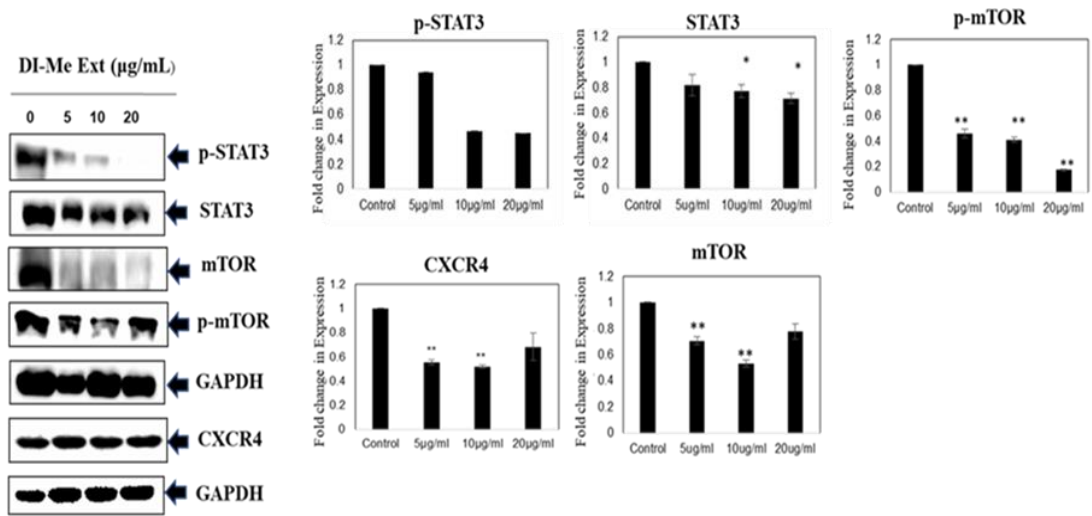
Studies have evidenced that the upregulation of various proteins like MMP-2, COX-2, VEGF, AKT, NF- κ B, CXCR-4, BCL-2, Survivin, mTOR, and STAT-3 are responsible for enhanced proliferation, survival, angiogenesis, invasion and migration in cancer cells. However, the effect of DI on these gene products in human OSCC cells has not yet been elucidated. COX-2 catalyses the first step in the synthesis of prostanooids and is often linked with carcinogenesis and inflammatory diseases. It promotes angiogenesis, migration, invasion of tumors, and deregulates apoptosis. As compared to healthy subjects, a significant upsurge in the expression of COX-2 was seen in cancer patients and patients with premalignant lesions [48–51]. Furthermore, survivin is known to play a critical role in cell survival by regulating cell division and apoptosis. It has been noted that the upregulation of survivin is frequently observed in OSCC samples. This protein is essential for in the development of OSCC and, and it is mostly

associated with the more aggressive form [52]. VEGF-A is a 46 kDa heparin-binding homodimeric glycoprotein. It respectively binds to its receptor to promote endothelial cell differentiation and proliferation. Many studies have demonstrated the increase in the expression of VEGFs in different types of carcinoma. Macrophages, neutrophils, and fibroblasts, upon stimulation by the TGF- β and IL-8, secrete MMPs, and maintain the bioavailability of growth factors, thus promoting cancer cell proliferation. Furthermore, MMPs cleave the FAS receptors, and modulate the function of natural killer cells and the apoptosis mechanism. They are also known to promote angiogenesis and metastasis. Various studies have shown that MMP-2 and MMP-9 are potential diagnostic markers for oral cancer detection [53,54]. In addition, CXCR4 overexpression in cancer cells contributes to tumor growth, proliferation, invasion, angiogenesis, metastasis, relapse, and chemoresistance. CXCR4 antagonism disrupts tumor-stromal interactions, reduces tumor growth and metastatic burden, and sensitizes cancer cells to cytotoxic drugs. CXCR4 is the target for not only therapeutic interference but it is also an important candidate for noninvasive checking of disease progression [55]. Also, BCL-2 family proteins that regulate the intrinsic mitochondrial apoptosis pathway are activated in response to several stress stimuli, including growth-factor deprivation, cytokine-withdrawal, Ca²⁺-flux, or DNA-damage, caused by UV or gamma-irradiation, but they can also contribute to cell death triggered by members of the tumour necrosis factor family member such as FAS, TNF, or TRAIL. Deregulation of BCL-2 protein is a frequent feature of human malignant diseases and causal for therapy resistance [56,57]. NF- κ B plays an essential role in inflammatory and immune responses and controls the expression of multiple genes associated with different hallmarks of cancer. The effect of DI on NF- κ B as well as the diverse gene products regulated by NF- κ B in human OSCC cells has not been elucidated yet. Therefore, in our study, we tried to explicate the effect of DI extracts, BA and KA on the expression of these proteins (Figure 2.41). Our findings revealed that the SAS cells treated with DI-H₂O Ext exhibited downregulation of VEGF-A, survivin and BCL-2 via inhibition of the STAT3 pathway. However, similar trend was not observed in case of CXCR4. In addition, SAS cells treated with DI-ME Ext demonstrated downregulation of p-mTOR (S2448), and p-STAT-3 (S727), the crucial constituents of the AKT/mTOR and JAK/STAT signaling cascade. Besides, this extract was also found to inhibit the expression of CXCR4. Further, Western blot analysis showed that the DI constituents, BA caused dose-dependent downregulation of the expression of VEGF-A and MMP-2 via inhibition of the AKT/mTOR pathway. Similarly, KA was found to reduce the levels of COX-2, survivin, MMP-2 and VEGF-A through modulation of the NF- κ B, mTOR and STAT-3 pathways. A decrease of BCL-

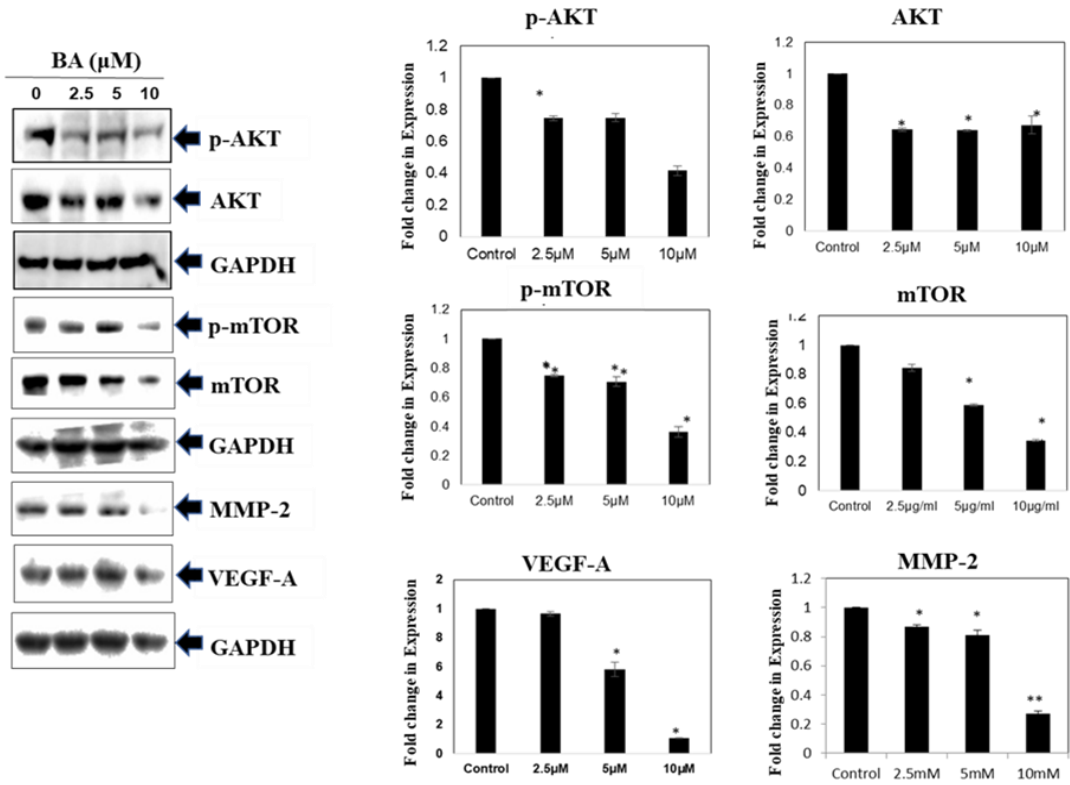
2 expression was observed in DI-H₂O Ext treated SAS cells, indicating that the activation of the mitochondria-dependent apoptotic pathway, at least in part, plays a role in DI-induced apoptosis. AKT1 is a crucial signaling protein involved in cellular survival pathways. It regulates survival by inhibiting apoptosis. The transcription factor NF- κ B is constitutively expressed in head and neck squamous cell carcinoma (HNSCC), and the persistent expression of this protein is one of the root causes of the cancer cell proliferation, survival, invasion, metastasis, and poor survival of patients. Our results showed that the phosphorylated forms of AKT1 and NF- κ B were significantly downregulated upon treatment with BA and KA respectively. It is possible that both the p-AKT1(S473) and p-NF- κ B (S536) proteins are intracellular targets of DI that mediates its cytotoxic effects on SAS cells. Taken together, our results showed that the DI extracts and their active constituents, BA and KA modulated the expression of several critical proteins involved in the development and progression of OSCC. These results provide an insight into the precise mechanism of action of DI and its constituents (Figure 2.42).



B



C



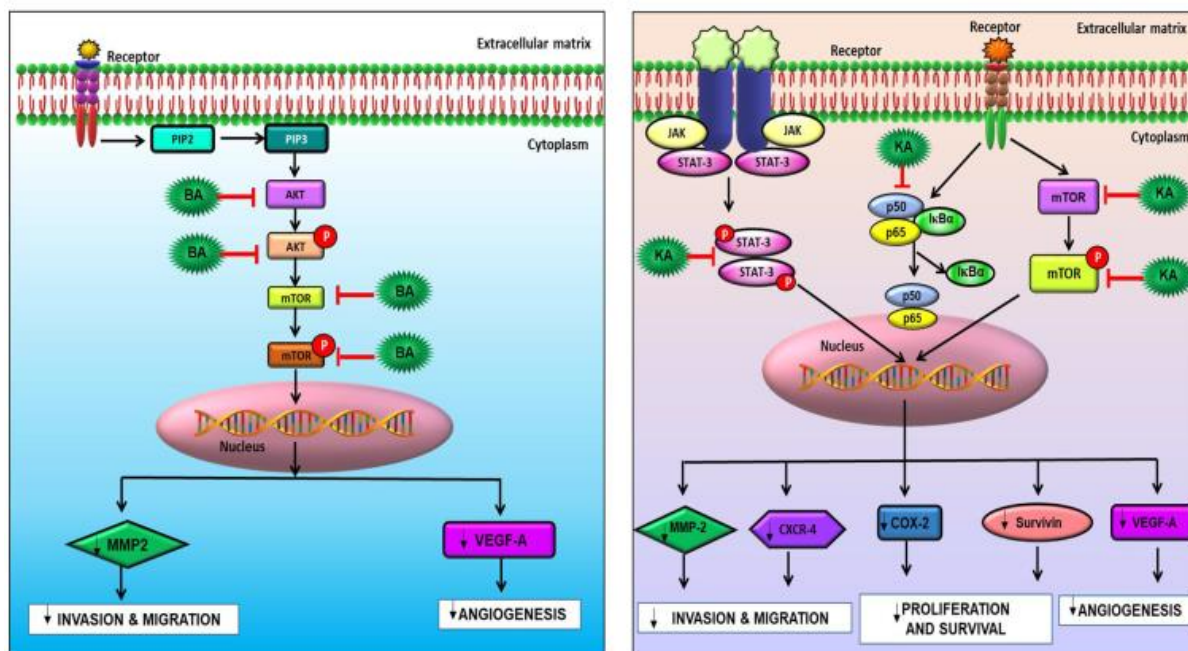


Figure 2.42: Pathway deciphering the proposed mechanistic mode of action with (A) DI-H₂O Ext, (B) DI-ME Ext, (C) BA, and (D) KA treatment in SAS cells.

3.0. CONCLUSION: In summary, we have interpreted indigenous knowledge with scientific criteria and identified new cytotoxic agents against OSCC. The fruit extracts of the ethnomedicinal plant DI might vanquish the adverse side effects of conventional modalities of treatment. In order to recognize the bioactive scaffolds in the plant extract, we performed detailed phytochemical profiling. Ten compounds were isolated and characterized, out of which, five compounds, namely, koetjapic acid, palmarumycin JC1, ferulic acid, 3-oxykojic acid, and 2-(1',2'dihydroxy)-kojic acid, were reported for the first time from this species. All the isolated molecules were screened through preliminary anti-proliferative assay and the leads, BA and KA were identified. They were again subjected to virtual screening based on ligand binding affinity and molecular dynamic simulations for providing theoretical support to the scientific validation. Both of the selected candidates displayed significant anticancer potential *in-vitro* by imparting anti-proliferative, cytotoxic, anti-clonogenic, anti-metastatic, and apoptotic effects. Our findings were further supported by the reduced expression of various proteins involved in the development and progression of OSCC. However, further *in vivo* studies are required to validate our findings and also elucidate the precise mechanism of action, which may provide a basis for developing chemopreventive and chemotherapeutic strategies for the better management of OSCC.

4. EXPERIMENTAL SECTION:

4.1. Cell Line. The OSCC cell line, SAS, was obtained from National Center for Cell Sciences (NCCS, Pune, India). The cells were maintained in DMEM supplemented with 10% heat inactivated FBS and 1% Penstrep. The cells were grown in an incubator under optimum conditions of 5% CO₂ and temperature at 37 °C.

4.2. Reagents. Penstrep, Trypsin EDTA, DMEM medium, and FBS were obtained from Gibco, USA. MTT and PI were obtained from Invitrogen and Sigma-Aldrich respectively, while DMSO used was procured from Merck Life Science Pvt. Ltd. The live and dead assay kit was obtained from Invitrogen, USA. Crystal violet was procured from SRL Pvt. Ltd., India. The Optiblot ECL Detection Kit was procured from Abcam, Cambridge, USA.

4.3. Extraction of DI Fruits. Fruits and leaves of DI were collected in March 2018. These were thoroughly cleaned, dried (in an oven maintained at a temperature of 50 °C for 3 days) and powdered. A 1 kg sample of the powdered fruits was extracted with methanol (2.5 L × 48 h) at room temperature thrice and was filtered. The completion of extraction was checked with TLC. The filtrate was concentrated under reduced pressure using a Heidolph rotary evaporator at a temperature of 50 °C yielded 45 g of crude extract. The residue thus obtained was further extracted with water, lyophilized, and yielded 11 g of aqueous extract.

4.4. Isolation of phytochemicals from methanol extract. TLC of the methanol extract in various combinations of n-hexane-ethyl acetate was studied. The residue was subjected to silica gel (100-200 mesh, Merck) column chromatography (CC) at different compositions of hexane, ethyl acetate, and methanol to afford 50 fractions (fractions 1-50). Each of these pooled fractions was concentrated by removing the solvent under reduced pressure using a Heidolph rotary evaporator. Compound 1 (β-sitosterol, 10 mg) was obtained from fractions 1-3 via CC using 5% ethyl acetate-hexane, which recrystallized as white needle-shaped crystals with the same polarity. Compound 2 (n-hentriacontanol, 7 mg) showed an intense spot in a cerium sulfate/phosphoric acid charring solution and was obtained as a white solid in 10% ethyl acetate-hexane. Compound 3 (lupeol, 20 mg) was isolated from fraction 9 in 20% ethyl acetate-hexane and was further subjected to crystallization. Compound 44 (betulinic acid, 4g) was obtained from 30% ethyl acetate in hexane as white solid, which was identified as the marker compound of the species. Compound 5 (koetjapic acid, 17 mg) was isolated from a pool of fractions 30-34 by Sephadex LH-20 column with methanol as the eluent. TLC of fractions 35-

38 eluted from the column in 50-60% ethyl acetate in hexane showed an intense UV active spot, which was further purified by repeated CC by using sephadex LH-20 in methanol, yielding compound 6 (ferulic acid, 15 mg). Compound 7 (palmarumycins JC1, 40 mg) eluted in 70% ethyl acetate in hexane, which was further purified by using sephadex LH-20 and recrystallized in methanol. Compound 8 (3-oxykojic acid, 45 mg) and compound 99((2-(1',2' dihydroxy)-kojic acid, 30 mg) were obtained as a mixture of both from fractions 42-44, which were further purified by using sephadex LH-20. Compound 10 (β -sitosterol- β -D-glucopyranoside, 30 mg) was obtained from fractions 45-50 as an amorphous solid and was further purified by precipitation using acetone. All molecules were identified by ^1H and ^{13}C and HR-ESIMS spectra.

4.5. Characterization of Phytochemicals. NMR spectra were recorded on Bruker Avance AMX 500 MHz NMR spectrometer. Chemical shift was reported in parts per million using TMS as an internal standard with solvent residual peaks (CDCl_3 : δH -7.26 ppm, δC -77.3 ppm), (DMSO-d_6 : δH -2.50 ppm, δC -39.5 ppm), and (acetone-d_6 : δH -2.05 ppm, δC -29.8 ppm). Multiplicities were given as s (singlet); d (doublet); t (triplet); q (quartet); dd (double doublet); and m (multiplet). Coupling constant (J) was expressed in Hz. Optical rotation was recorded on Jasco P-1020 polarimeter, and absorbance was recorded on a UV 1800 Shimadzu UV Spectrophotometer. Mass spectra were recorded under ESIHRMS at 60,000 resolutions on a Thermo Scientific Exactive Column, and IR spectra were recorded on Bruker Alpha FT-IR spectrometer. All solvents used for UV, IR, MS, and chromatography were purchased from Sigma-Aldrich and Merck (HPLC-grade). For CC, silica gel with different mesh sizes (100-200 and 230-400) and Sephadex-LH 20 were used.

4.6. Computational Screening and Molecular Dynamics Simulation. The optimization and minimization of the proteins, binding site analysis, receptor grid generation, ligand conformation generation, ADME/T screening, molecular docking, and dynamics were done with Schrödinger suite 2020-1. For this, protein preparation wizard, Sitemap, LigPrep, QikProp, Glide XP docking, and Desmond tools were used in Maestro 11.2 interface in OPLS-2005 force field. The crystal structures of the proteins were retrieved from the RCSB Protein Data Bank: protein kinase B, Akt (PDB ID: 1O6L); mammalian target of rapamycin, mTOR (PDB ID: 4JSP); matrix metalloproteinase-2, MMP-2 (PDB ID: 3AYU); vascular endothelial growth factor-A, VEGF-A (PDB ID: 1FLT); nuclear factor kappa-light-chain-enhancer of activated B cells, NF- κ B (PDB ID: 1SVC); signal transducer and activator of transcription 3, STAT-3 (PDB ID: 6NJS); C-X-C chemokine receptor type 4, CXCR-4 (PDB ID: 3ODU),

cyclooxygenase-2, COX-2 (PDB ID: 5IKQ); and survivin (PDB ID: 1E31).⁶² All these proteins were refined by adding hydrogens/missing side chains, optimized, and minimized. The phosphorylated forms of the Akt, mTOR, NF- κ B, and STAT-3 were generated successively by adding a phosphate group to the corresponding serine residues using build structure protocol. Site map analysis was carried out to identify the suitable binding pockets in the case of these receptors, and the grids were generated around site 1 which were used for further docking. The different conformers of the BA and KA were generated using LigPrep module and screened their ADME/T (Absorption, Distribution, Metabolism, and Excretion/Toxicity) properties by QikProp analysis. The docking simulations were done by Glide docking, and the binding affinities were ranked using docking score (D-score) and glide score (G-score). Molecular dynamics simulations further analysed the best ones for 10 000 ps using the Desmond module of Schrödinger suite under OPLS-2005 force field.

4.7. Cell Proliferation Assay: A total of 2×10^3 SAS cells per 100 μ L media were seeded into each well of two 96-well plates and incubated for 24 h. The cells were then treated with different concentrations of the DI-H₂O Ext, DI-ME Ext, BA, and KA individually, and the MTT assay was performed at 0 and 72 h. A 10 μ L aliquot of MTT at a concentration of 5 mg/mL in PBS was added to each well and incubated for 2 h. Next, the cell culture medium was discarded, and 100 μ L of DMSO was added to each well and incubated for 1 h in the dark. Colour conversion of the MTT reaction was measured with a microplate reader at a wavelength of 570 nm. Control cells were defined as 100% proliferation, and the percentage proliferation was calculated to the following formula: (Absorption of treated cells x 100)/(Absorption of control cells (untreated)).

4.8. Colony-Forming Assay: A total of 1×10^3 cells per 2 mL were seeded in a 6-well plate and incubated for 24 h. The cells were then treated with DI-H₂O Ext, DI-ME Ext, BA, and KA separately and incubated for another 24 h. The next day, the media of the wells were replaced with fresh media, and the cells were allowed to form colonies for 9 days. On 9th day, colonies were fixed with ethanol, stained with 0.3% crystal violet (SRL Pvt. Ltd., India) solution for 20 min and washed. Images were captured for each well and the number of colonies was quantified using Image J software.

4.9. Cell Death Analysis: A total of 2×10^4 SAS cells per 2 mL of media were seeded in a 6-well plate and incubated for 24 h, followed by treatment with different concentrations of DI-

H₂O Ext, DI-ME Ext, BA, and KA individually. After 72 h of drug treatment, the media from the wells were collected in labeled 5 x 77 mm² polystyrene test tubes. Adhered cells were washed with PBS, trypsinized, and collected in their respective tubes. The cell suspension was then centrifuged at 4000 rpm for 10 min at 4 °C. After centrifugation, the supernatant was discarded, and the pellet was washed with 1 mL of PBS and centrifuged at 4000 rpm for 10 min, and the step was repeated twice. Finally, the pellet was suspended in 495 µL of PBS, and 5 µL of PI (Sigma-Aldrich) dye was added. The cells were then analysed in BD FACS Diva software. PI dye is impermeable to the live cells as they have an intact cell membrane and thus emit less fluorescence; however, PI can easily penetrate the dead cells because of the damaged plasma membrane, thereby emitting a high red fluorescence.

4.10. Live and Dead Assay: DI-mediated cell death in SAS cells was studied using the Live-Dead assay kit (Invitrogen, USA). The kit contains two fluorescent dyes, calcein-AM and PI. In principle, calcein-AM can enter any cells but labels only live cells. It is converted by cellular cytoplasmic esterases to a highly green-fluorescent calcein. PI is excluded by live cells with an intact membrane but enters dead cells with a broken membrane to stain their nuclei red. Therefore, live cells fluoresce green, whereas dead cells fluoresce red. SAS cells were seeded at 2000 cells per 100 µL of media in 96-well tissue culture plates. After 24 h, the cells were treated with DI-H₂O Ext, DI-ME Ext, BA, and KA individually. Cells were then stained with the live/dead reagent and incubated at 37 °C in the dark for 20 min. Cells were then analysed under an inverted fluorescence microscope (Olympus, Japan).

4.11. Apoptosis Assay. Apoptosis is marked by the translocation and accumulation of the membrane phospholipid phosphatidylserine from the cytoplasmic edge of the membrane to the extracellular surface. The membrane perturbation can be detected by using Annexin V which binds to the phosphatidylserine of the apoptotic cells. A total of 5 × 10⁴ SAS cells per 2 mL of media were seeded in a 6-well plate and incubated for 24 h, followed by treatment with different concentrations of DI-H₂O Ext, DI-ME Ext, BA, and KA individually. After 72 h of drug treatment, the media from the wells were collected in labeled 5 × 77 mm² polystyrene test tubes. Adhered cells were washed with PBS, trypsinized, and collected in their respective tubes. The cell suspension was then centrifuged at 4000 rpm for 10 min at 4 °C. After centrifugation, the supernatant was discarded, and the pellet was washed with 1 mL of PBS and centrifuged at 4000 rpm for 10 min. The PBS was discarded, and 20 µL of binding buffer was added to the tubes and the tubes were centrifuged again. Then the untreated control was divided into unstained (does not contain either PI or Annexin V) and double-stained (contain both the dyes)

tubes, and the positive control was divided into PI-positive and Annexin V-positive tubes. A 2.5 μL aliquot of Annexin V added to all the tubes except the unstained and PI-positive ones and incubated in the dark for 20 min containing different concentrations of DI. The tubes were incubated in dark for 20 min. Centrifugation was done again, and the supernatant is discarded. A 20 μL aliquot of binding buffer is added, and 2.5 μL of PI (Sigma-Aldrich) dye was added. The cells were then analyzed in BD FACS Cell Quest software.

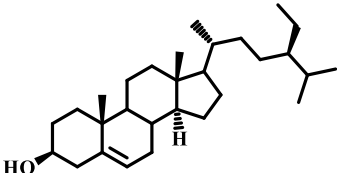
4.12. Cell Cycle Analysis: A total of 2×10^5 SAS cells per 2 mL of media were seeded in a 6-well plate and incubated overnight for cell adhesion. The cells were then treated with different concentrations of DI, and the untreated sample was used as a control. Following 24 h of individual treatment of DI-H₂O Ext, DI-ME Ext, BA, and KA, the media was collected in polystyrene tubes, and the adhered cells were washed with PBS twice. Then, 300 μL of trypsin was added to detach the cells. The detached cells were harvested in their respective tubes and centrifuged at 4000 rpm for 10 min at 4 °C. The supernatant was discarded, and the pellet was washed with 1 mL of PBS and centrifuged at 4000 rpm for 10 min at 4 °C. Then the supernatant was discarded, and 5 mL of 70% ethanol was dropwise added to the pellet under constant vortexing and kept for overnight incubation at 4 °C for fixation. The next day, the suspension was centrifuged at 4000 rpm for 10 min at 4 °C, and the supernatant was discarded. Following the removal of ethanol by centrifugation, the cells were washed twice with PBS and stained with PI/RNase solution for 30 min in the dark. Cell cycle distribution was detected using FACS Celesta (Becton-Dickinson, Franklin Lakes, NJ), and the data were analysed using FCS Express (BD Biosciences). The fluorescence intensity of the stained cells correlates with the amount of DNA they contain.

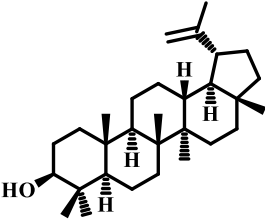
4.13. Cell Migration Assay. A total of 5×10^5 SAS cells per 2 mL of media were seeded in a 6-well plate and incubated for 12 h to form the monolayer. After the monolayer was formed, the media was replaced with serum-free media and incubated for 8 h. Thereafter, the media was removed, and a vertical scratch or wound was made with the help of a 200 μL tip at the center of the well. The wells were then washed with PBS twice to remove the debris. Cells were then treated with different concentrations of DI-H₂O Ext, DI-ME Ext, BA, and KA individually. The untreated cells were used as control. The directional migration of SAS cells was observed under an inverted microscope (Nikon T1-SM, Tokyo, Japan), and images were taken at 0 and 12 or 24 h depending upon the healing timepoint of the wound. Images were compared to quantify the migration of SAS cells after treatment.

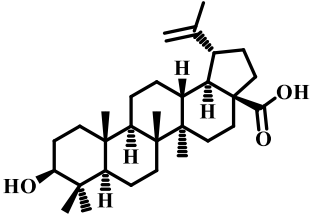
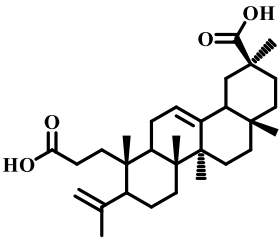
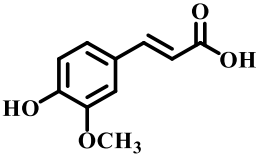
4.14. Western Blot Analysis. A total of 6×10^5 cells per 3 mL of media were seeded in 60 mm culture plates and were allowed to grow for 24 h. The cells were then treated with different concentrations of DI-H₂O Ext, DI-ME Ext, BA, and KA individually and incubated for the next 24 h. Protein was isolated from respective treatment plates using lysis buffer (20 mM HEPES, 2 mM EDTA, 250 mM NaCl, and 0.1% NP40) in the presence of protease inhibitors (2 µg/mL leupeptin hemisulfate, 2 µg/mL aprotinin, 1 mM PMSF, and 1 mM DTT) and quantified using Bradford's reagent. Equal amount of protein (30 µg) was mixed with 5× Laemmli Buffer (250 mM Tris-HCl, 10% SDS, 30% glycerol, 5% β-mercaptoethanol, and 0.02% bromophenol blue) and separated by 12% SDS-PAGE and transferred to nitrocellulose membrane (Biorad) by using a Trans-blot Turbo (Biorad), the membrane was blocked with 5% nonfat skim milk in tris-buffered saline containing 1% tween 20 (TBST). For the phospho-antibodies, the membranes were treated with 5% BSA in tris-buffered saline containing 1% tween 20 to block the nonspecific binding sites. The membranes were then incubated with primary antibodies for MMP-2, COX-2, VEGF-A, Akt1, p-Akt, NF-κB, p-NF-κB, CXCR-4, cyclin D1, Bcl-2, survivin, mTOR, p-mTOR, STAT-3, p-STAT-3, and GAPDH overnight at 4 °C. Afterwards, the blots were washed with 1X TBST buffer and then incubated with horseradish peroxidase conjugated secondary antibody for 2 h at room temperature. The bands representing different proteins were visualized with the help of Clarity Western ECL Substrate (Biorad) in a ChemiDoc XRS System (Biorad). GAPDH was used as the housekeeping control.

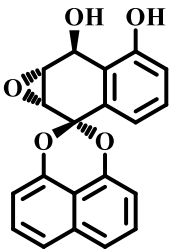
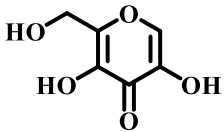
4.16. Statistical Analysis. Statistical analysis was performed using Student's t test. All the data are represented as mean ± standard error (SE). $p < 0.05$ was defined as statistically significant.

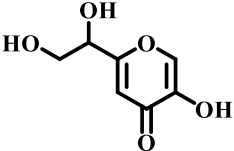
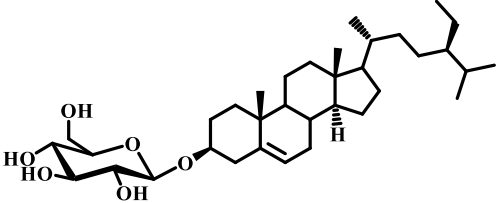
5. Spectral data

<p>Compound 1: β-sitosterol</p> 	<p>Molecular formula: C₂₉H₅₀O</p> <p>FT-IR (Neat) ν_{max}: 3408, 3272, 2935, 2863, 1645, 1459, 1374, 1316, 1257, 1190, 1099, 1054, 1024, 958, 802 cm^{-1}</p> <p>¹H NMR (500 MHz, CDCl₃): δ 5.37 (d, 1H, $J = 5$ Hz), 3.53 - 3.54 (m, 1H), 2.30 - 2.29 (m, 2H), 2.04 - 1.87 (m, 2H), 1.87-1.84 (m, 3H), 1.68 - 1.66 (m, 2H), 1.60 - 1.45 (m, 7H), 1.32 - 1.23 (m, 6H), 1.20 - 1.10 (m, 3H), 1.09 - 1.96 (m, 3H), 1.02 (s,</p>
--	--

	<p>5H), 0.94 - 0.93 (m, 3H), 0.87 - 0.71 (m 9H), 0.69 (s, 3H) ppm.</p> <p>¹³C NMR (125 MHz, CDCl₃): δ 140.8, 121.7, 71.8, 56.8, 56.0, 50.1, 45.8, 42.3, 42.3, 39.8, 37.2, 36.5, 36.2, 33.9, 31.9, 31.7, 29.1, 28.3, 26.0, 24.3, 23.0, 21.1, 19.8, 19.4, 19.0, 18.8, 11.9, 11.9 ppm.</p> <p>HRESI-MS: 415.1097(M+H)⁺</p>
<p>Compound 2: n-Hentriacontanol</p> 	<p>Molecular formula: C₃₁H₆₄O</p> <p>FT-IR (Neat) ν_{\max}: 3318, 2927, 1046 cm⁻¹</p> <p>¹H NMR (500 MHz, CDCl₃): δ 3.65 (t, <i>J</i> = 6.5 Hz, 2H), 1.60 - 1.55 (m, 5H), 1.36 - 1.22 (m, 54H), 0.88 (t, <i>J</i> = 6.5 Hz, 3H) ppm.</p> <p>¹³C NMR (125 MHz, CDCl₃): δ 63.1, 32.8, 31.9, 29.7, 29.6, 29.6, 29.5, 29.4, 25.7, 22.7, 14.1 ppm.</p> <p>HRESI-MS: 453.5035 (M+H)⁺</p>
<p>Compound 3: Lupeol</p> 	<p>Molecular formula: C₃₀H₅₀O</p> <p>FT-IR (Neat) ν_{\max}: 3408, 3272, 2935, 2863, 1645, 1459, 1374, 1316, 1257, 1190, 1099 cm⁻¹</p> <p>¹H NMR (500 MHz, CDCl₃): δ 4.74 (s, 1H), 4.61 (s, 1H), 3.19 (dd, <i>J</i>₁ = 11.5 Hz, <i>J</i>₂ = 4.4 Hz, 2H), 2.28 - 2.17 (m, 2H), 2.03 - 1.94 (m, 2H), 1.69 - 1.66 (m, 9H), 1.63 - 1.61 (m, 10H), 1.59 - 1.37 (m, 20H), 1.25 (s, 3H), 0.97 (s, 3H), 0.96 (s, 3H), 0.93 (s, 3H), 0.82 (s, 3H), 0.75 (s, 3H) ppm.</p> <p>¹³C NMR (125 MHz, CDCl₃): δ 150.7, 109.9, 79.1, 56.3, 55.3, 53.2, 50.5, 46.9, 42.4, 38.9, 38.3, 37.2, 37.1, 32.2, 29.5, 27.9, 25.4, 22.7, 18.3, 16.1, 16.0, 15.3, 14.6, 14.2 ppm.</p> <p>HRESI-MS: 427.3939 (M + H)⁺</p>
<p>Compound 4: Betulinic acid</p>	<p>Molecular formula: C₃₀H₄₈O₃</p> <p>FT-IR (Neat) ν_{\max}: 3428, 3075, 2944, 2671, 1693, 1454, 1440, 1379, 1143cm⁻¹</p>

	<p>¹H NMR (500 MHz, DMSO-d₆): δ 12.08 (s, 1H), 4.69 (d, <i>J</i> = 2Hz, 1H), 4.56 (s, 1H), 4.28 (s, 1H), 3.02 - 2.93 (m, 2H), 2.25 - 2.19 (m, 1H), 2.12 - 2.09 (m, 1H), 1.84 - 1.77 (m, 2H), 1.65 (s, 3H), 1.54 - 1.08 (m, 20H), 0.93 (s, 3H), 0.87 (s, 6H), 0.77 (s, 3H), 0.65 (s, 3H) ppm.</p> <p>¹³C NMR (125 MHz, DMSO-d₆): δ 177.7, 150.8, 110.1, 77.2, 55.9, 55.4, 50.4, 48.9, 47.1, 42.5, 38.9, 38.7, 38.0, 37.2, 36.8, 34.4, 32.2, 30.6, 29.7, 28.6, 27.6, 25.5, 20.9, 19.4, 18.4, 16.4, 16.3, 16.2, 14.8 ppm.</p> <p>HRESI-MS: 455.3525 (M - H)⁺</p>
<p>Compound 5: Koetjapic acid</p> 	<p>Molecular formula: C₃₀H₄₆O₄</p> <p>FT-IR (Neat) ν_{max}: 3440, 2978, 2860, 1706, 1702, 1698, 1694, 1454, 1387, 1281, 1230, 1192, 906 cm⁻¹</p> <p>¹H NMR (500 MHz, DMSO-d₆): δ 5.17 (s, 1H), 4.40 (d, <i>J</i> = 4.5 Hz, 2H), 4.31 (d, <i>J</i> = 4.5 Hz, 1H), 2.74 (dd, <i>J</i>₁ = 9.5, <i>J</i>₂ = 4 Hz, 2H), 1.96 - 1.83 (m, 4H), 1.78 - 1.57 (m, 1H), 1.57 - 1.39 (m, 6H), 1.32 - 1.30 (m, 2H), 1.23- 1.18 (m, 4H), 1.15-0.98 (m, 7H), 0.92 (s, 3H), 0.90 (s, 3H), 0.88 (s, 6H), 0.79 - 0.75 (m, 2H), 0.71 (s, 3H), 0.70 (s, 3H) ppm.</p> <p>¹³C NMR (125 MHz, DMSO-d₆): δ 177.8, 176.9, 146.9, 144.4, 121.8, 107.9, 82.8, 67.6, 55.2, 47.7, 47.5, 46.3, 46.1, 39.6, 39.4, 38.2, 33.3, 32.7, 32.6, 31.2, 30.2, 29.3, 27.6, 26.0, 23.9, 23.6, 23.09, 18.5, 17.6, 17.4, 16.7 ppm.</p> <p>HRESI-MS: 469.3317 (M - H)⁺</p>
<p>Compound 6: Ferulic acid</p> 	<p>Molecular formula: C₁₀H₁₀O₄</p> <p>FT-IR (Neat) ν_{max}: 3436, 2961, 2933, 2872, 1692, 1128, 1074, 1001 cm⁻¹</p>

	<p>¹H NMR (500 MHz, CD₃COCD₃): δ 8.27 (bs, 1H), 7.62 (d, <i>J</i> = 16 Hz, 1H), 7.35 (d, <i>J</i> = 2 Hz, 1H), 7.20 (dd, <i>J</i>₁ = 8.5, <i>J</i>₂ = 2 Hz, 1H), 6.90 (d, <i>J</i> = 8.5 Hz, 1H), 6.74 (d, <i>J</i> = 16 Hz, 1H), 3.94 (s, 3H) ppm. ¹³C NMR (125 MHz, CD₃COCD₃): δ 183.7, 149.2, 147.9, 140.5, 130.0, 122.9, 121.4, 115.4, 110.6, 55.4 ppm.</p> <p>HRESI-MS: 193.0500 (M - H)⁺</p>
<p>Compound 7: Palmarumycin JC1</p> 	<p>Molecular formula: C₂₀H₁₄O₅</p> <p>FT-IR (Neat) ν_{max}: 3050, 1605, 1455, 1409 cm⁻¹</p> <p>¹H NMR (500 MHz, DMSO-d₆): δ 9.90 (s, 1H), 7.63 (dd, <i>J</i>₁ = 12.5, <i>J</i>₂ = 8.5 Hz, 2H), 7.56 (t, <i>J</i> = 7.5 Hz, 1H), 7.51 (t, <i>J</i> = 7.5 Hz, 1H), 7.25 (t, <i>J</i> = 7.5 Hz, 1H), 7.15 - 7.12 (m, 2H), 6.98 - 6.96 (m, 2H), 5.54 (bs, 1H), 5.32 (s, 1H), 3.61 (d, <i>J</i> = 3.5 Hz, 1H), 3.50 (dd, <i>J</i>₁ = 4.5, <i>J</i>₂ = 2.5 Hz, 1H) ppm.</p> <p>¹³C NMR (125 MHz, DMSO-d₆): δ 156.2, 147.7, 147.7, 134.2, 132.5, 129.5, 128.3, 128.3, 122.9, 121.2, 121.0, 117.6, 116.8, 112.9, 109.8, 109.4, 98.1, 59.5, 53.7, 50.2 ppm.</p> <p>HRESI-MS: 357.0691 (M + Na)⁺</p>
<p>Compound 8: 3-Oxykojic acid</p> 	<p>Molecular formula: C₆H₆O₅</p> <p>FT-IR (Neat) ν_{max}: 3271, 3175, 2948, 2668, 1706, 1697 cm⁻¹. ¹H NMR (500 MHz, DMSO-d₆): δ 9.05 (s, 1H), 9.01 (s, 1H), 8.05 (s, 1H), 5.38 (t, <i>J</i> = 5.5 Hz, 1H), 4.40 (d, <i>J</i> = 5.5 Hz, 2H) ppm.</p> <p>¹³C NMR (125 MHz, DMSO-d₆): δ 169.6, 150.7, 144.8, 141.7, 139.8, 55.8 ppm.</p> <p>HRESI-MS: 157.0137 (M - H)⁺</p>
<p>Compound 9: 2-(1,2-Dihydroxy)-kojic acid</p>	<p>Molecular formula: C₇H₈O₅</p> <p>FT-IR (Neat) ν_{max}: 3270, 3175, 3099, 2948, 2668, 1706, 1697 cm⁻¹</p>

	<p>¹H NMR (500 MHz, DMSO-d₆): δ 9.07 (bs, 1H), 8.03 (s, 1H), 6.34 (s, 1H), 5.69 (s, 1H), 4.29 (d, <i>J</i> = 3 Hz, 2H), 4.13 (d, <i>J</i> = 5.0 Hz, 1H), 3.17 (d, <i>J</i> = 4.3 Hz, 1H) ppm.</p> <p>¹³C NMR (125 MHz, DMSO-d₆): δ 174.4, 168.5, 146.1, 139.7, 110.1, 59.9, 49.2 ppm.</p> <p>HRESI-MS: 171.0293 (M – H)⁺</p>
<p>Compound 10: β-sitosterol-β-D-glucopyranoside</p> 	<p>Molecular formula: C₃₅H₆₀O₆</p> <p>FT-IR (Neat) <i>v</i>_{max}: 3400, 2900 cm⁻¹.</p> <p>¹H NMR (500 MHz, DMSO-d₆): δ 5.34 (d, 1H, <i>J</i> = 5Hz), 4.90 - 4.87 (m, 3H), 4.46 - 4.44 (m, 1H), 4.23 (d, <i>J</i> = 8Hz, 1H), 3.64 - 3.63 (m, 1H), 3.47-3.43 (m, 2H), 3.13 - 3.12 (m, 1H), 3.10 - 3.07 (m, 1H), 3.02 - 3.01 (m, 1H), 2.90 - 2.89 (m, 1H), 2.36 - 2.35 (m, 1H), 2.13 - 2.10(m, 1H), 1.95 - 1.94 (m, 2H), 1.81 - 1.79 (m, 3H), 1.53 - 1.51 (m, 1H), 1.51-1.40 (m, 6H), 1.28 - 1.23 (m, 6H), 1.21 - 1.19 (m, 4H), 0.96 (s, 3H), 0.91 (s, 5H), 0.82 (m, 9H), 0.66 (s, 3H) ppm.</p> <p>¹³C NMR (125 MHz, DMSO-d₆): δ 140.4, 121.2, 100.7, 99.5, 76.9, 76.7, 73.4, 70.1, 61.1, 56.1, 55.4, 49.6, 45.1, 41.8, 38.3, 36.8, 36.2, 35.4, 33.3, 31.4, 31.3, 29.2, 28.7, 27.8, 25.4, 23.8, 22.6, 20.6, 19.7, 19.1, 18.9, 18.6, 11.8, 11.6 ppm.</p> <p>HRESI-MS: 577.4013 (M + H)⁺</p>

6. REFERENCES

- [1] H. Sung, J. Ferlay, R.L. Siegel, M. Laversanne, I. Soerjomataram, A. Jemal, F. Bray, Global Cancer Statistics 2020: GLOBOCAN Estimates of Incidence and Mortality Worldwide for 36 Cancers in 185 Countries, CA. Cancer J. Clin. 71 (2021) 209–249. <https://doi.org/10.3322/caac.21660>.
- [2] C. Harsha, K. Banik, H.L. Ang, S. Girisa, R. Vikkurthi, D. Parama, V. Rana, B. Shabnam,

- E. Khatoon, A.P. Kumar, A.B. Kunnumakkara, Targeting akt/mTOR in oral cancer: Mechanisms and advances in clinical trials, *Int. J. Mol. Sci.* 21 (2020) 1–26. <https://doi.org/10.3390/ijms21093285>.
- [3] A.K. Singh, N.K. Roy, D. Bordoloi, G. Padmavathi, K. Banik, A.D. Khwairakpam, A.B. Kunnumakkara, P. Sukumar, Orai-1 and Orai-2 regulate oral cancer cell migration and colonisation by suppressing Akt/mTOR/NF- κ B signalling, *Life Sci.* 261 (2020) 118372. <https://doi.org/10.1016/j.lfs.2020.118372>.
- [4] A.B. Kunnumakkara, C. Harsha, K. Banik, R. Vikkurthi, B.L. Sailo, D. Bordoloi, S.C. Gupta, B.B. Aggarwal, Is curcumin bioavailability a problem in humans: lessons from clinical trials, *Expert Opin. Drug Metab. Toxicol.* 15 (2019) 705–733. <https://doi.org/10.1080/17425255.2019.1650914>.
- [5] A. Devi Khwairakpam, J. Monisha, N.K. Roy, D. Bordoloi, G. Padmavathi, K. Banik, E. Khatoon, A.B. Kunnumakkara, Vietnamese coriander inhibits cell proliferation, survival and migration via suppression of Akt/mTOR pathway in oral squamous cell carcinoma, *J. Basic Clin. Physiol. Pharmacol.* (2019) 1–15. <https://doi.org/10.1515/jbcpp-2019-0162>.
- [6] D. Hanahan, R.A. Weinberg, Hallmarks of cancer: The next generation, *Cell.* 144 (2011) 646–674. <https://doi.org/10.1016/j.cell.2011.02.013>.
- [7] P. Anand, C. Sundaram, S. Jhurani, A.B. Kunnumakkara, B.B. Aggarwal, Curcumin and cancer: An “old-age” disease with an “age-old” solution, *Cancer Lett.* 267 (2008) 133–164. <https://doi.org/10.1016/j.canlet.2008.03.025>.
- [8] W.L. Dissanayaka, G. Pitiyage, P.V.R. Kumarasiri, R.L.P.R. Liyanage, K.D. Dias, W.M. Tilakaratne, Clinical and histopathologic parameters in survival of oral squamous cell carcinoma, *Oral Surg. Oral Med. Oral Pathol. Oral Radiol.* 113 (2012) 518–525. <https://doi.org/10.1016/j.oooo.2011.11.001>.
- [9] N.K. Roy, J. Monisha, G. Padmavathi, H. Lalhruaitluanga, N.S. Kumar, A.K. Singh, D. Bordoloi, M.N. Baruah, G.N. Ahmed, I. Longkumar, F. Arfuso, A.P. Kumar, A.B. Kunnumakkara, Isoform-specific role of akt in oral squamous cell carcinoma, *Biomolecules.* 9 (2019) 1–23. <https://doi.org/10.3390/biom9070253>.
- [10] J. Monisha, N.K. Roy, G. Padmavathi, K. Banik, D. Bordoloi, A.D. Khwairakpam, F.

- Arfuso, A. Chinnathambi, T.A. Alahmadi, S.A. Alharbi, G. Sethi, A.P. Kumar, A.B. Kunnumakkara, NGAL is downregulated in oral squamous cell carcinoma and leads to increased survival, proliferation, migration and chemoresistance, *Cancers (Basel)*. 10 (2018) 1–18. <https://doi.org/10.3390/cancers10070228>.
- [11] S. Henamayee, K. Banik, B.L. Sailo, B. Shabnam, C. Harsha, S. Srilakshmi, V.G.M. Naidu, S.H. Baek, K.S. Ahn, A.B. Kunnumakkara, Therapeutic emergence of rhein as a potential anticancer drug: A review of its molecular targets and anticancer properties, *Molecules*. 25 (2020) 1–26. <https://doi.org/10.3390/molecules25102278>.
- [12] D. Parama, M. Boruah, K. Yachna, V. Rana, K. Banik, C. Harsha, K.K. Thakur, U. Dutta, A. Arya, X. Mao, K.S. Ahn, A.B. Kunnumakkara, Diosgenin, a steroidal saponin, and its analogs: Effective therapies against different chronic diseases, *Life Sci*. 260 (2020) 118182. <https://doi.org/10.1016/j.lfs.2020.118182>.
- [13] E. Khatoon, K. Banik, C. Harsha, B.L. Sailo, K.K. Thakur, A.D. Khwairakpam, R. Vikkurthi, T.B. Devi, S.C. Gupta, A.B. Kunnumakkara, Phytochemicals in cancer cell chemosensitization: Current knowledge and future perspectives, *Semin. Cancer Biol*. 80 (2022) 306–339. <https://doi.org/10.1016/j.semcancer.2020.06.014>.
- [14] K. Banik, A.M. Ranaware, C. Harsha, T. Nitesh, S. Girisa, V. Deshpande, L. Fan, S.P. Nalawade, G. Sethi, A.B. Kunnumakkara, Piceatannol: A natural stilbene for the prevention and treatment of cancer, *Pharmacol. Res*. 153 (2020) 104635. <https://doi.org/10.1016/j.phrs.2020.104635>.
- [15] A.M. Ranaware, K. Banik, V. Deshpande, G. Padmavathi, N.K. Roy, G. Sethi, L. Fan, A.P. Kumar, A.B. Kunnumakkara, Magnolol: A neolignan from the Magnolia family for the prevention and treatment of cancer, *Int. J. Mol. Sci*. 19 (2018) 1–21. <https://doi.org/10.3390/ijms19082362>.
- [16] M.S. Alexandre-Moreira, M.R. Piuvezam, C.C. Araújo, G. Thomas, Studies on the anti-inflammatory and analgesic activity of *Curatella americana* L., *J. Ethnopharmacol*. 67 (1999) 171–177. [https://doi.org/10.1016/S0378-8741\(99\)00009-4](https://doi.org/10.1016/S0378-8741(99)00009-4).
- [17] J.B. Vilar, L.S. De Andrade, K.R. Leite, H.D. Ferreira, L.C. Chen, Assessment of genotoxicity and cytotoxicity of “lixreira” (*Curatella americana* L.) using the prophage λ induction test (SOS inductest), *Brazilian J. Pharm. Sci*. 45 (2009) 491–496. <https://doi.org/10.1590/S1984-82502009000300015>.

- [18] R.L.R.P. Jácome, V.D.C. Oliveira, M.A.T. e Oliveira, M.C.F. Mariano, A.B. de Oliveira, Comparative pharmacognostic study of leaves of *Davilla elliptica* A. St.-Hil. e *D. rugosa* Poir., Dilleniaceae, Rev. Bras. Farmacogn. 20 (2010) 390–396. <https://doi.org/10.1590/S0102-695X2010000300016>.
- [19] H.K. Sharma, L. Chhangte, A.K. Dolui, Traditional medicinal plants in Mizoram, India, Fitoterapia. 72 (2001) 146–161. [https://doi.org/10.1016/S0367-326X\(00\)00278-1](https://doi.org/10.1016/S0367-326X(00)00278-1).
- [20] P.K. Rai, H. Lalramnghinglova, Lesser known ethnomedicinal plants of Mizoram, north east India: An Indo-Burma hotspot region, J. Med. Plants Res. 4 (2010) 1301–1307. <https://doi.org/10.5897/JMPR09.480>.
- [21] J.B. Foo, L. Saiful Yazan, Y.S. Tor, A. Wibowo, N. Ismail, N. Armania, Y.K. Cheah, R. Abdullah, *Dillenia suffruticosa* dichloromethane root extract induced apoptosis towards MDA-MB-231 triple-negative breast cancer cells, J. Ethnopharmacol. 187 (2016) 195–204. <https://doi.org/10.1016/j.jep.2016.04.048>.
- [22] J.B. Foo, L. Saiful Yazan, Y.S. Tor, A. Wibowo, N. Ismail, C.W. How, N. Armania, S.P. Loh, I.S. Ismail, Y.K. Cheah, R. Abdullah, Induction of cell cycle arrest and apoptosis by betulinic acid-rich fraction from *Dillenia suffruticosa* root in MCF-7 cells involved p53/p21 and mitochondrial signalling pathway, J. Ethnopharmacol. 166 (2015) 270–278. <https://doi.org/10.1016/j.jep.2015.03.039>.
- [23] D. Tarak, N.D. Namsa, S. Tangjang, S.C. Arya, B. Rajbonshi, P.K. Samal, M. Mandal, An inventory of the ethnobotanicals used as anti-diabetic by a rural community of Dhemaji district of Assam, Northeast India, J. Ethnopharmacol. 138 (2011) 345–350. <https://doi.org/10.1016/j.jep.2011.08.018>.
- [24] M.H. Abdille, R.P. Singh, G.K. Jayaprakasha, B.S. Jena, Antioxidant activity of the extracts from *Dillenia indica* fruits, Food Chem. 90 (2005) 891–896. <https://doi.org/10.1016/j.foodchem.2004.09.002>.
- [25] P.R.C. Prasad, C.S. Reddy, S.H. Raza, C.B.S. Dutt, Folklore medicinal plants of North Andaman Islands, India, Fitoterapia. 79 (2008) 458–464. <https://doi.org/10.1016/j.fitote.2008.03.007>.
- [26] K. Chatterjee, K.M. Ali, D. De, D.K. Panda, D. Ghosh, Antidiabetic and Antioxidative activity of Ethyl acetate Fraction of Hydromethanolic Extract of Seed of *Eugenia*

- jambolana Linn Through In-Vivo and In-Vitro Study and its Chromatographic Purification, Free Radicals Antioxidants. 2 (2012) 21–30. <https://doi.org/10.5530/ax.2012.2.6>.
- [27] P.A. Singh, N.B. Brindavanam, G.P. Kimothi, V. Aeri, Evaluation of in vivo anti-inflammatory and analgesic activity of *Dillenia indica* f. *elongata* (Miq.) Miq. and *Shorea robusta* stem bark extracts, Asian Pacific J. Trop. Dis. 6 (2016) 75–81. [https://doi.org/10.1016/S2222-1808\(15\)60988-4](https://doi.org/10.1016/S2222-1808(15)60988-4).
- [28] G. Pavanadasivam, M.U.S. Sultanbawa, Chemical investigation of ceylonese plants. Part XII. (+)-3,4',5,7- tetrahydroxy-3'-methoxyflavanone [(+)-dihydroisorhamnetin] and 3,5,7-trihydroxy-3',4'-dimethoxyflavone (dillenetin): Two new natural products from *Dillenia indica* L., J. Chem. Soc. Perkin Trans. 1. (1975) 612–613. <https://doi.org/10.1039/p19750000612>.
- [29] M.B. Alam, A. Ahmed, S. Islam, H.J. Choi, M.A. Motin, S. Kim, S.H. Lee, Phytochemical characterization of *dillenia indica* l. Bark by paper spray ionization-mass spectrometry and evaluation of its antioxidant potential against t-bhp-induced oxidative stress in raw 264.7 cells, Antioxidants. 9 (2020) 1–15. <https://doi.org/10.3390/antiox9111099>.
- [30] N.A. Deshmukh, S. Okram, T. Angami, H. Rymbai, A.K. Jha, Elephant apple (*Dillenia indica*), Minor Fruits Nutraceutical Importance Cultiv. (2017) 409–420.
- [31] A. Gupta, Phytochemical Screening and GC-MS Analysis of Flower Extract of *Dillenia indica*, Biosci. Biotechnol. Res. Commun. 13 (2020) 833–841. <https://doi.org/10.21786/bbrc/13.2/68>.
- [32] S. Kumar, V. Kumar, O. Prakash, Antidiabetic and antihyperlipidemic effects of *Dillenia indica* (L.) leaves extract, Brazilian J. Pharm. Sci. 47 (2011) 373–378. <https://doi.org/10.1590/S1984-82502011000200018>.
- [33] S. Kumar, V. Kumar, O. Prakash, Antidiabetic, hypolipidemic and histopathological analysis of *Dillenia indica* (L.) leaves extract on alloxan induced diabetic rats, Asian Pac. J. Trop. Med. 4 (2011) 347–352. [https://doi.org/10.1016/S1995-7645\(11\)60101-6](https://doi.org/10.1016/S1995-7645(11)60101-6).
- [34] N. Kaur, L. Kishore, R. Singh, *Dillenia indica* L. attenuates diabetic nephropathy via inhibition of advanced glycation end products accumulation in STZ-nicotinamide

- induced diabetic rats, *J. Tradit. Complement. Med.* 8 (2018) 226–238. <https://doi.org/10.1016/j.jtcme.2017.06.004>.
- [35] D. Munmee, S.B. Prasad, Evaluation of hypoglycemic effect of an indian fruit: *Dillenia indica*, *Int. J. Res. Ayurveda Pharm.* 4 (2013) 545–546. <https://doi.org/10.7897/2277-4343.04418>.
- [36] D. Kumar, S. Mallick, J.R. Vedasiromoni, B.C. Pal, Anti-leukemic activity of *Dillenia indica* L. fruit extract and quantification of betulinic acid by HPLC, *Phytomedicine*. 17 (2010) 431–435. <https://doi.org/10.1016/j.phymed.2009.07.010>.
- [37] M.R. Saha, A. Alam, R. Hasan, R. Akter, M. Hossain, E.H. Mazumder, S. Rana, *In-vitro* anti-oxidant activity of the leaves of *Dillenia indica*, *Orient. Pharm. Exp. Med.* 9 (2009) 277–284. <https://doi.org/10.3742/opem.2009.9.4.277>.
- [38] M. Das, B.P. Sarma, G. Ahmed, C.B. Nirmala, M.K. Choudhury, *In-vitro* anti oxidant activity total phenolic content of *Dillenia indica* *Garcinia penducalata*, commonly used fruits in Assamese cuisine, *Free Radicals Antioxidants*. 2 (2012) 30–36. <https://doi.org/10.5530/ax.2012.2.2.6>.
- [39] V. Kumar, I.B. Prasher, Phytochemical Analysis and Antioxidant Activity of Endophytic Fungi Isolated from *Dillenia indica* Linn., *Appl. Biochem. Biotechnol.* (2023). <https://doi.org/10.1007/s12010-023-04498-7>.
- [40] S.J. Somani, L.B. Badgujar, B.K. Sutariya, M.N. Saraf, Protective effect of *Dillenia indica* L. on acetic acid induced colitis in mice, *Indian J. Exp. Biol.* 52 (2014) 876–881.
- [41] P.B. Ravindra kumare khare, A.K. Prasad, Shankul kumar, Satish V Iyer, S.K. Vaidya, Flavonoid and triterpene rich fraction of *Dillenia indica* Linn. leaves: As anti-inflammatory & anti-arthritis activity, *Indo Am. J. Pharm. Res.* 1 (2013) 4653–4659.
- [42] A.S. Apu, M.A. Muhit, S.M. Tareq, A.H. Pathan, A.T.M. Jamaluddin, M. Ahmed, Antimicrobial activity and brine shrimp lethality bioassay of the leaves extract of *Dillenia indica* linn, *J. Young Pharm.* 2 (2010) 50–53. <https://doi.org/10.4103/0975-1483.62213>.
- [43] M.A. Rahman, M. Hasanuzzaman, S.R. Muhuri, A.A. Rahman, Antinociceptive, antidiarrhoeal and GI motility activities of *Dillenia indica* Linn. roots, *Pharmacologyonline*. 1 (2011) 1247–1254.
- [44] M. Monirul Islam, M. Monirul Islam, R. Sharmin Pia, K. Sifath-E-Jahan, J.

- Chowdhury, F. Akter, N. Parvin, S. Akter, Antidiarrheal Activity of *Dillenia Indica* Bark Extract, *Ijpsr*. 4 (2013) 682–688. www.ijpsr.com.
- [45] S. Yeshwante, A. Juvekar, D. Nagmoti, S. Wankhede, A. Shah, R. Pimprikar, D. Saindane, Anti-inflammatory activity of methanolic extracts of *Dillenia indica* L. leaves, *J. Young Pharm.* 1 (2009) 63. <https://doi.org/10.4103/0975-1483.51885>.
- [46] Manjurul Islam Chowdhury, J.A. Md. Mizanur Rahman Moghal, Syed Masudur Dewan, Biological activities of *Dillenia indica* L. bark growing in Bangladesh, *J. Biol. Sci. Opin.* 1 (2013) 45–49. <https://doi.org/10.7897/2321>.
- [47] I.P. Padhya, N.S.K. Choudhary, S.K. Padhy, S. Dash, Effect of *Dillenia indica* leaves against carbon tetrachloride induced hepatotoxicity., *J. Pharm. Chem.* 2 (2008) 24–27.
- [48] A. Zeng, H. Hua, L. Liu, J. Zhao, Betulinic acid induces apoptosis and inhibits metastasis of human colorectal cancer cells in vitro and in vivo, *Bioorganic Med. Chem.* 27 (2019) 2546–2552. <https://doi.org/10.1016/j.bmc.2019.03.033>.
- [49] A. Ferrandez, S.M. Prescott, O. Medical, R.W. Burt, COX-2 and colorectal cancer, *Curr. Pharm. Des.* 9 (2003) 2229–2251.
- [50] B. Liu, L. Qu, S. Yan, Cyclooxygenase-2 promotes tumor growth and suppresses tumor immunity, *Cancer Cell Int.* 15 (2015) 2–7. <https://doi.org/10.1186/s12935-015-0260-7>.
- [51] B. Xiong, T.J. Sun, H.Y. Yuan, M.B. Hu, W.D. Hu, F.L. Cheng, Cyclooxygenase-2 expression and angiogenesis in colorectal cancer, *World J. Gastroenterol.* 9 (2003) 1237–1240. <https://doi.org/10.3748/wjg.v9.i6.1237>.
- [52] M.E. Johnson, E.W. Howerth, Survivin: A bifunctional inhibitor of apoptosis protein, *Vet. Pathol.* 41 (2004) 599–607. <https://doi.org/10.1354/vp.41-6-599>.
- [53] A. Venugopal, T. Uma Maheswari, Expression of matrix metalloproteinase-9 in oral potentially malignant disorders: A systematic review, *J. Oral Maxillofac. Pathol.* 20 (2016) 474–479. <https://doi.org/10.4103/0973-029X.190951>.
- [54] P.S.P. LBeena P. Patel, Shakuntala V. Shah, Shilin N. Shukla, Pankaj M. Shah, Clinical Significance of MMP-2 and MMP-9 in patients with oral cancer, *Head Neck.* 36 (2007) 564–572. <https://doi.org/10.1002/HED>.
- [55] S. Chatterjee, B. Behnam Azad, S. Nimmagadda, The intricate role of CXCR4 in cancer,

1st ed., Elsevier Inc., 2014. <https://doi.org/10.1016/B978-0-12-411638-2.00002-1>.

- [56] R.J. Youle, A. Strasser, The BCL-2 protein family: Opposing activities that mediate cell death, *Nat. Rev. Mol. Cell Biol.* 9 (2008) 47–59. <https://doi.org/10.1038/nrm2308>.
- [57] A. Frenzel, F. Grespi, W. Chmielewski, A. Villunger, Bcl2 family proteins in carcinogenesis and the treatment of cancer, *Apoptosis.* 14 (2009) 584–596. <https://doi.org/10.1007/s10495-008-0300-z>.

Bioprospecting of prenyl flavones and phenolic constituents from *Artocarpus altilis* (Parkinson) Fosberg.

3A.1. *Artocarpus altilis* (Parkinson) Fosberg.

Artocarpus altilis (Parkinson) Fosberg is the primary component of traditional agroforestry systems native to the Pacific and tropical Asia and is widely cultivated throughout the humid tropics. The species is a multifarious agroforestry tree, economically utilized for multiple applications such as staple crops, construction materials, clothing materials, animal feeds, and folk medicines. It belongs to the popular Jackfruit/Moraceae family, which has been recognized as a source of edible, nutritious and starchy fruits. The texture of the moderately ripe fruit of *Artocarpus altilis* is similar to that of baked bread, and it is popularized under the common name breadfruit. The medicinal importance of *Artocarpus altilis* is enormous. It is used for curing chronic ailments such as low blood pressure, tongue thrush, diarrhoea, asthma, skin infections and sciatica. The roasted leaves powder is used as a remedy for enlarging spleen and its juice is used as ear drops.



Figure 3.A.1: Fruit, leaves and tree of *Artocarpus altilis* (Adapted from wikipedia)

3.A.2. Phytochemistry of *Artocarpus altilis*

Artocarpus species are an abundant source of phenolic constituents such as isoprenyl flavonoids, stilbenoids, 2-arylbenzofuran derivatives, and phenolic compounds with oxepine rings [1]. Phytochemical profiling of *Artocarpus altilis* was done by various research groups and identified more than 130 compounds from different parts of the species; among them more than 50% were derived from phenyl propanoid pathway [2]. The detailed phytochemical investigation of the leaves conveyed the chemical composition is different in various organic solvents. Flavonoids were identified as the major constituents in the petroleum and ethyl

acetate leaf extracts, whereas tannins and phenolic compounds are in methanol extract. Wang *et al.*, reported nine geranylated flavones from the ethyl acetate fraction of the methanolic extract of the leaves of *Artocarpus altilis* by silica gel column chromatography, out of which five are novel molecules which are hitherto uninvestigated [3].

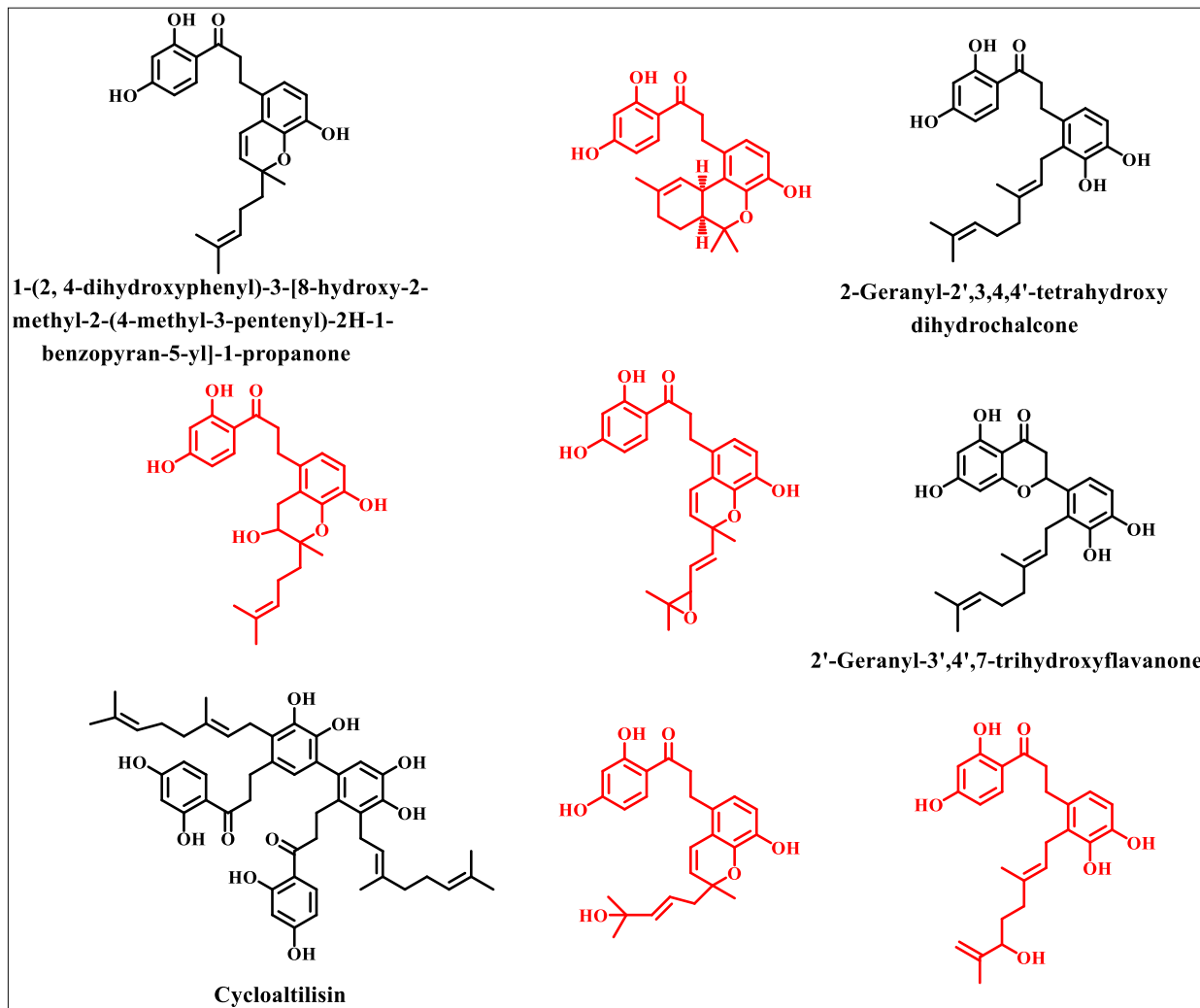


Figure 3.A.2: Geranylated flavones reported from the dried root of *Artocarpus altilis*

In 2007, Boonphong and co-workers reported nine prenylflavones from the dichloromethane extract of the dried root extract of *Artocarpus altilis*. Among them, artocarpin, cycloartocarpin and chaplashin were isolated from the dried root stem, and the remaining six viz, cycloartobiloxanthone, artobiloxanthone, cudraflavone B, cudraflavone C, morusin and artonin E are from root bark [4].

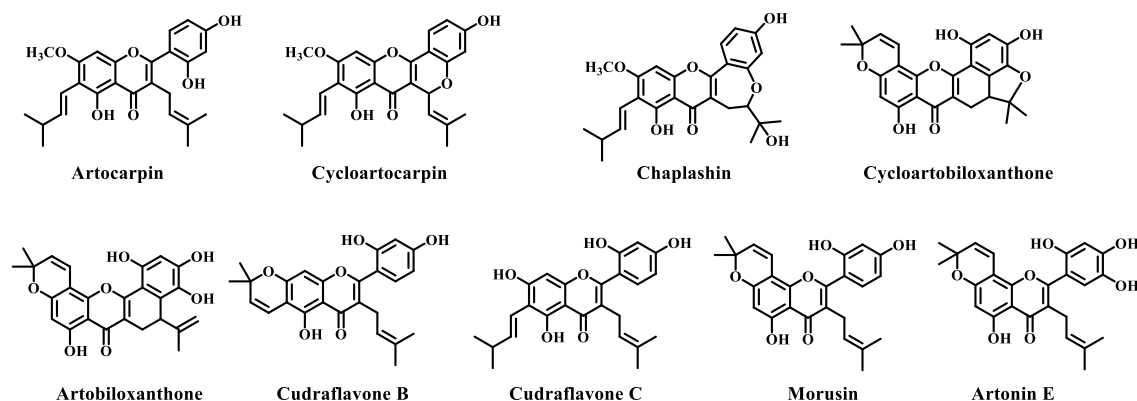


Figure 3.A.3: Prenylflavones reported from the dried root of *Artocarpus altilis*

Later in 2011, Kuete *et al.* reported five molecules from the stem bark of *Artocarpus altilis* such as peruvianursenyl acetate C (1), α -amyrenol (2), sitosterol 3-*O*- β -D-glucopyranoside (3), artonin E (4) & 2-[(3,5-dihydroxy)-(Z)-4-(3-methylbut-1-enyl)phenyl] benzofuran-6-ol (5)[5].

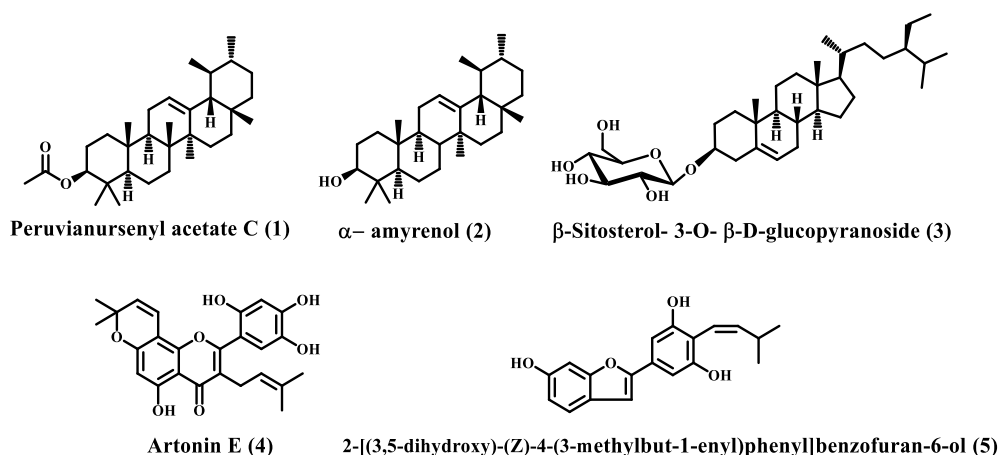


Figure 3.A.4: Structure of phytochemicals reported from the stem bark of *Artocarpus altilis*

Bioactivity-guided isolation from the ethyl acetate extract of the leaves of *Artocarpus altilis* afforded six flavonoids along with β -sitosterol [6]. Moreover, analytical HPLC techniques identify artocarpin as the major phytoconstituents present in the heartwood of *Artocarpus altilis* [7]. The breadfruit's methanol and ethyl acetate extracts contains sterols, phenolics and flavonoids [8].

3.A.3. Pharmacological activity of *Artocarpus altilis*

3.A.3.1. Antitubercular and Antiplasmodial

Natural prenylflavones isolated from the root of *Artocarpus altilis* exhibited anti-tubercular activity against *Mycobacterium tuberculosis* H37Ra and anti-plasmodial activity against

Plasmodium falciparum. Anti-tubercular and anti-plasmodial activities are done by microplate alamar blue assay (MABA) and micro culture radioisotope technique, respectively [4]. All the isolated ones showed moderate cytotoxicity against human oral epidermoid cells (KB) and human breast cancer (BC).

3.A.3.2. Antiatherosclerotic activity

The cytoprotective effect of the ethyl acetate extract of *Artocarpus altilis* was evaluated by Wang and co-workers in U937 cells incubated with oxidized LDL (OxLDL) using the 4-[3-(4-iodophenyl)-2-(4-nitrophenyl)-2H-5-tetrazolio]-1, 3-benzene disulfonate (WST-1) assay [6].

3.A.3.3. Anti-microbial activity

The anti-microbial potential of the fruit extract of *Artocarpus altilis* was tested in various pathogens like *Staphylococcus aureus*, *Pseudomonas aeruginosa*, *Streptococcus mutans* and *Enterococcus faecalis*. The study revealed that fruit's methanolic and ethyl acetate extract effectively reduce the growth of tested pathogens. Among them, methanolic extract exhibited maximum growth inhibition in *Streptococcus mutans* and *Enterococcus faecalis*, having MIC values of 0.90 and 0.6 mg/ml, respectively. Since the ethyl acetate extract showed the maximum zone of inhibition in *Staphylococcus aureus* and *Pseudomonas aeruginosa* with the same MIC value of 0.90 mg/ml [8].

3.A.3.4. Anti-cancer activity

Abdul Jamil and co-workers elucidated the anti-cancer effect of *Artocarpus altilis* in HeLa cervical cancer cells. Compared with the control, the administration of various concentrations of the pulp part extracts inhibit the growth and proliferation of HeLa cells in a concentration-dependent manner after 72 h incubation. Moreover, the extract exhibits cell-specific cytotoxicity in cancer cells only at the tested concentrations [9]. In 2009, Arung et al. reported the anti-cancer properties of *Artocarpus altilis* wood extract in T47D human breast cancer cells *via* inducing apoptosis at the sub-G1 phase. Moreover, they also identified the activity is exclusively attributed to the presence of a major phytochemical artocarpin, in the extract [10].

3.A.4. Aim and scope of the study

Flavonoids are one of the common components in the human diet. The biological properties of flavonoids are immense due to their interaction with multiple cellular targets and free radical scavenging activities. Because of our keen interest in seeking phytochemicals with excellent anti-cancer potential against oral squamous cell carcinoma, we focussed on isolating flavonoids and phenolic compounds. Hence, we selected *Artocarpus altilis* from the Moraceae/Jackfruit family because the family is enriched with phytochemicals especially prenyl/geranyl substituted flavonoids. Even though there are some literature on the isolation of phytochemicals

from the species, it is crucial to conduct more scientific research on edible species that can be further exploited for value-added products in the form of nutraceuticals and health products. Hence, this chapter described the bioprospecting of prenyl flavones and other phenolic compounds from the acetone extract of the stem bark of *Artocarpus altilis*.

3.A.5. Extraction, isolation and characterisation of phytochemicals

3.A.5.1. Collection of plant material

Artocarpus altilis stem bark was collected from Wayanad, Kerala, India and the species was identified by the taxonomist of Jawaharlal Nehru Tropical Botanical Garden of India (J.N.T.B.G.R.I), Palode, Kerala, India. A voucher specimen was deposited in the herbarium repository of J.N.T.B.G.R. I, Palode.

3.A.5.2. Extraction and isolation procedure

Initially, 900 g of the dried, powdered stem bark was subjected to extraction using hexane (2.5L X 3) at room temperature for 3 days. After percolation with hexane, the defatted residue was further subjected to acetone extraction (2.5 L X 3) for 3 consecutive days. The obtained extract was concentrated in a Heidolph rotary Evaporator at reduced pressure to get a crude of 45 g for acetone. The acetone extract thus obtained was subjected to column chromatographic separation over silica gel (100-200 mesh) with diverse gradients of hexane-ethyl acetate polarities offered eleven compounds (Figure 3A.5). The structure of the molecules (Figure 3A.6) was characterised by 1D and 2D NMR techniques along with ESI-HRMS analysis and comparison with literature reports.

The white solid obtained from the purification of fraction pool 1, characterised as β -sitosterol (compound **11**, 20 mg), a phytosterol with a structure similar to cholesterol, is widely distributed in the plant kingdom. The fraction pool 1 was repeatedly column chromatographed with 10% ethyl acetate-hexane mixture, gave compound **12 (110 mg)** as a white crystalline solid soluble in chloroform. A broad signal observed at 1733 cm^{-1} in the IR spectrum of the compound **12** indicating the presence of the ester moiety in the structure. In the ^1H NMR spectrum, one proton resonated at δ 5.10 ppm could be attributed to the presence of an olefinic proton and the proton resonated at δ 4.57 ppm (Figure 3A.6) corresponding to the methine proton directly attached to the ester group. Moreover, the diastereotopic methylene protons from the cyclopropane ring resonated as two peaks at the chemical shift values δ 0.57 and 0.34 ppm. In the ^{13}C NMR spectrum, the peak observed at δ 4.57 ppm 171.0 ppm is the diagnostic

peak of ester carbonyl carbon (Figure 3A.7). Finally, the structure of the molecule was in agreement with ESI-HRMS spectra having molecular ion peak observed at 469.4045, which is the $[M+H]^+$ peak and the compound was identified as cycloartenol acetate.

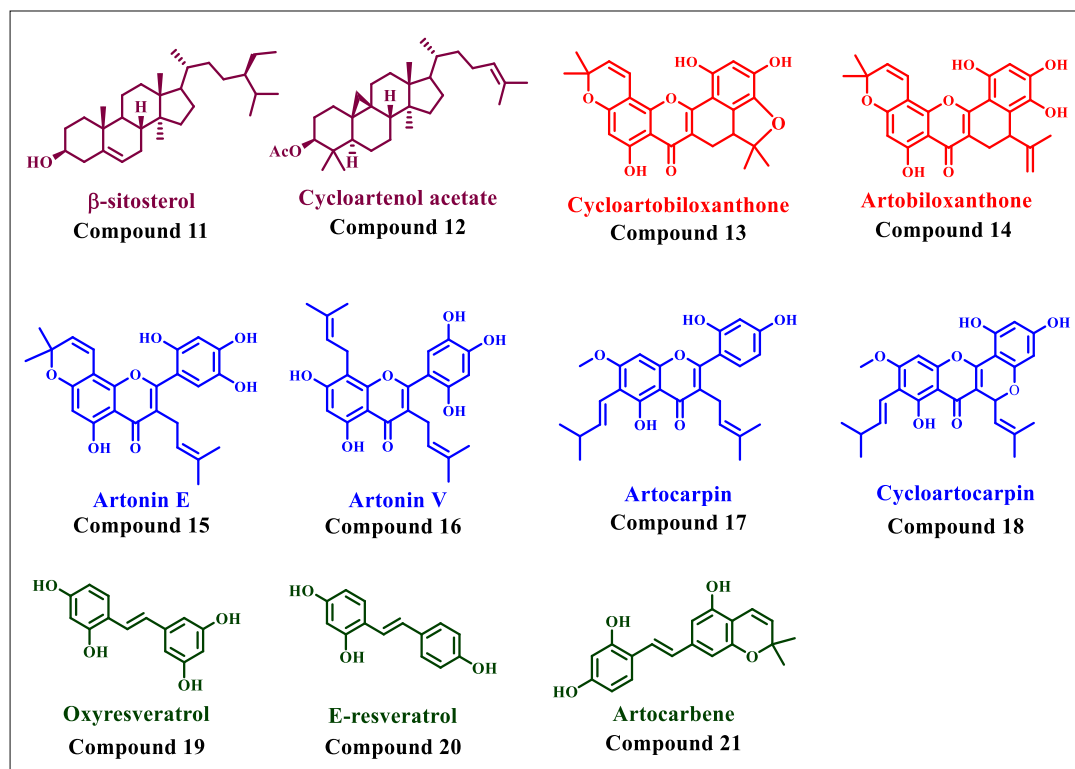


Figure 3A.5: Structure of molecules isolated from the stem bark of *Artocarpus altilis*

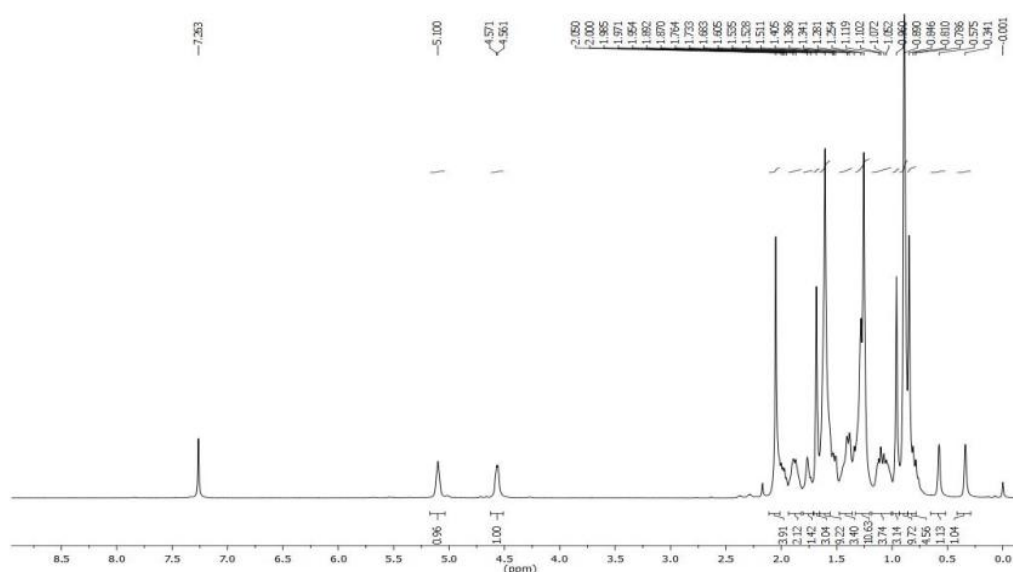


Figure 3A.6: ^1H NMR spectrum of cycloartenol acetate

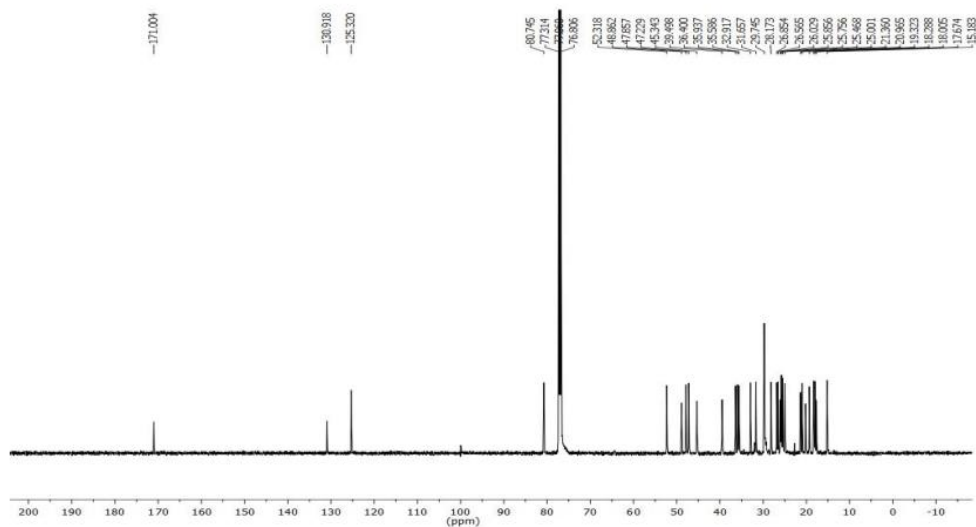


Figure 3A.7: ^{13}C NMR spectrum of cycloartenol acetate

Compound **13**, **cycloartobiloxanthone** (9 mg) was obtained as a yellow solid from fraction pool 2 by sephadex-LH 20 with methanol. The IR spectrum of compound **13** displayed a broad signal at a frequency of 1622 cm^{-1} , which could be attributed to the ester moiety. In the ^1H NMR spectrum (Figure 3A.8), the most deshielded proton resonated at δ 13.39 ppm corresponding to hydrogen bonded (O-H-O) hydroxyl proton. The peak observed at δ 3.21 and 2.31 ppm could be attributed to the methylene proton, which is found to be diastereotopic. Additionally, the methine proton of the furan moiety resonated at δ 3.43 ppm. In ^{13}C NMR, the peak resonated at δ 181.4 ppm is the characteristic peak of carbonyl carbon. The peaks observed at δ 47.5 ppm and δ 20.34 ppm could be attributed to methine and methyl carbons in furan moiety (Figure 3A.9). Finally, the structure was confirmed with ESI-HRMS, where the compound showed molecular ion peak at m/z 435.1438, which is the $[\text{M}+\text{H}]^+$ peak.

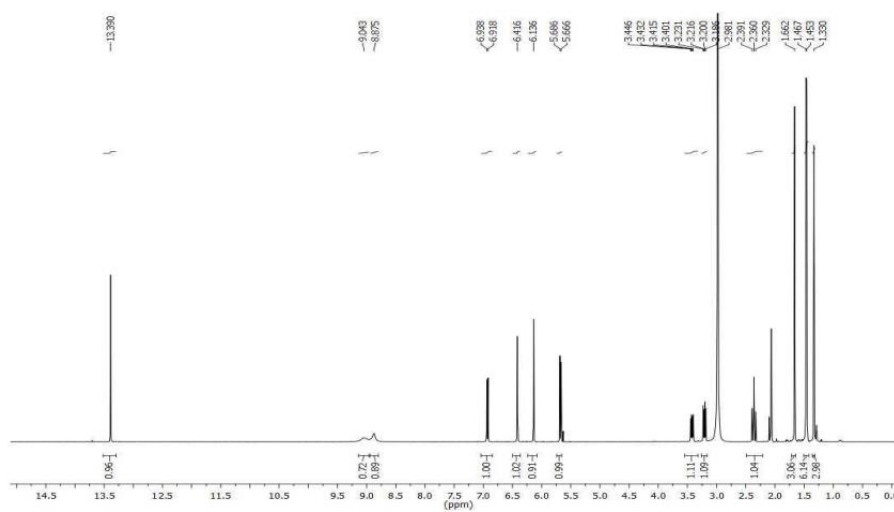


Figure 3A.8: ^1H NMR spectrum of cycloartobiloxanthone

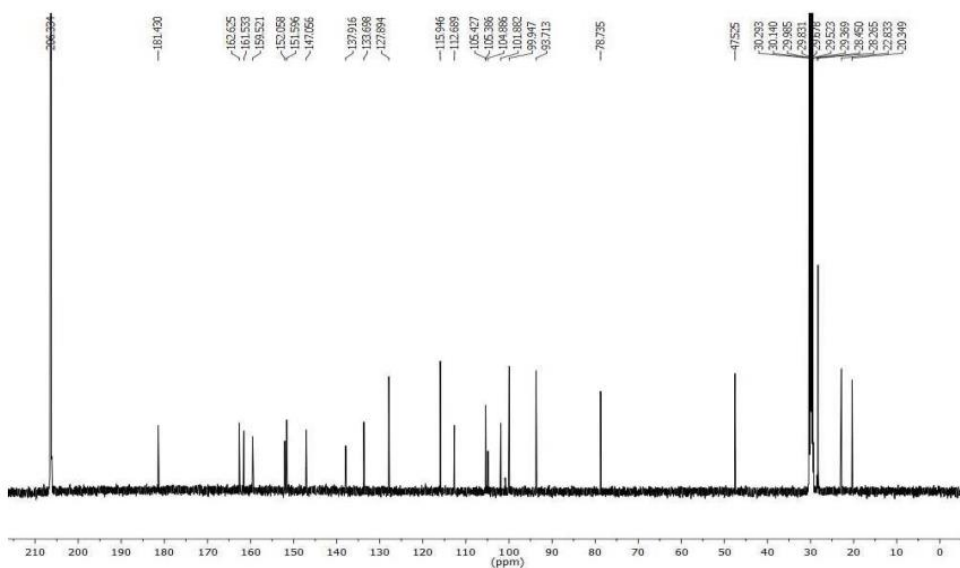


Figure 3A.9: ^{13}C NMR spectrum of cycloartobiloxanthone

Compound **14**, artobiloxanthone (24 mg) was obtained as a dark yellow solid from fraction 38-39, by repeated silica gel column chromatography followed by sephadex-LH 20 column with methanol. In the IR spectrum of compound **14**, a broad peak was observed at 1642 cm^{-1} , corresponding to carbonyl group stretching vibration. In ^1H NMR, the H-bonded hydroxyl proton resonated at δ 12.51 ppm, and the exocyclic methylene protons were resonated at δ 4.82 and 4.58 ppm, respectively. Moreover, the diastereotopic methylene protons resonated at δ 3.44 and 2.67 respectively (Figure 3A.10). In ^{13}C NMR, the carbonyl carbon resonated at δ 180.3 ppm. The peak observed at δ 113.2 ppm corresponds to olefinic methylene carbon (Figure 3A.11). Finally, the mass spectrum of compound **14** displayed molecular ion peak at m/z 435.1441, is the $[\text{M}+\text{H}]^+$ peak. Based on the above spectral data and previous literature reports, the compound was identified as **artobiloxanthone**.

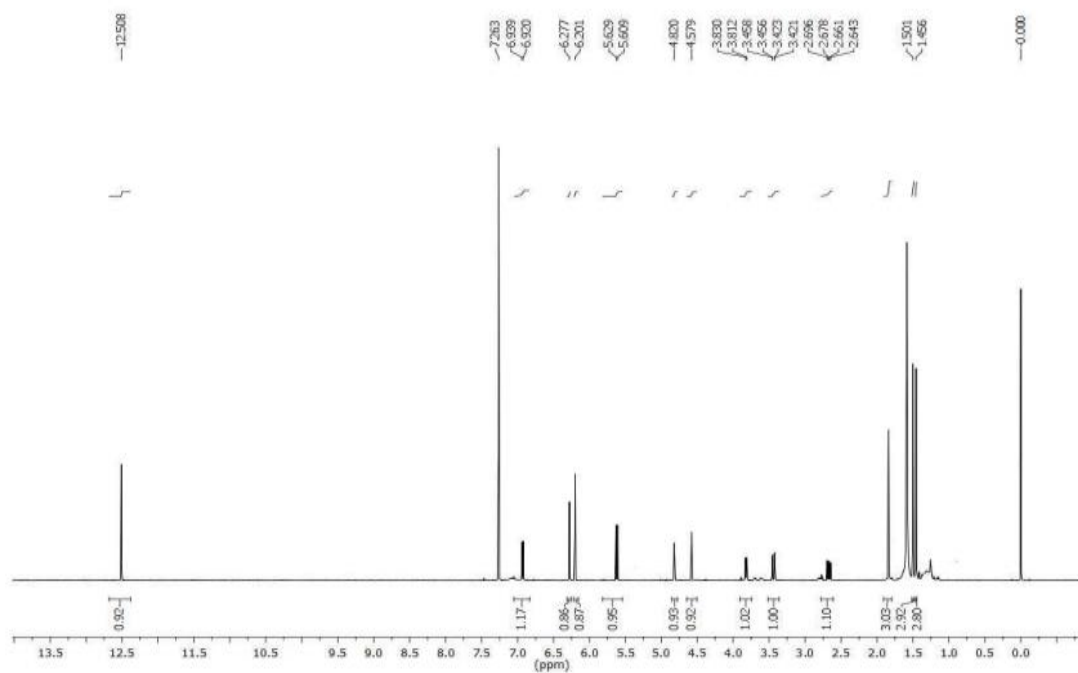


Figure 3A.10: ^1H NMR spectrum of artobioxanthone

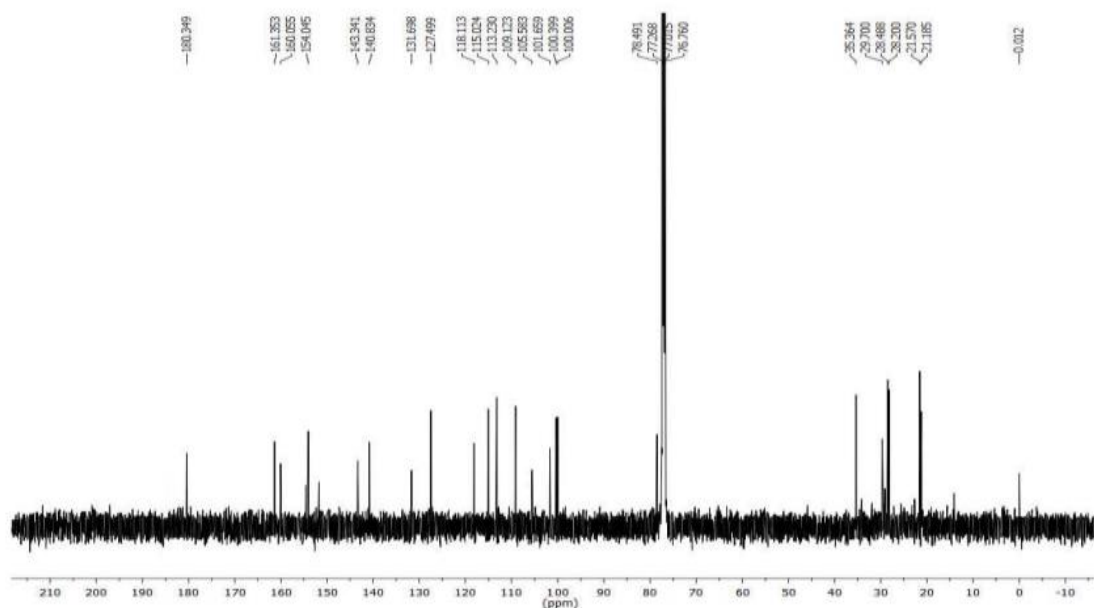


Figure 3A.11: ^{13}C NMR spectrum of artobioxanthone

Fraction pool 4 was obtained by eluting the column with 50% ethyl acetate-hexane. It showed the presence of two UV active spots both charring as yellow colour in p-Anisaldehyde- H_2SO_4 solution. Compound **15** was precipitated as a yellow crystalline solid quantitatively by adding dichloromethane to the fraction pool, which was identified as the marker compound. The ^1H NMR spectra of compound **15** suggest the presence of four phenolic hydroxyl groups resonated as broad singlets at δ values 13.25, 8.34, 8.20 and 7.81 ppm, among them the most deshielded

hydroxyl group at δ 13.25 ppm corresponding to the intramolecular hydrogen-bonded OH of the flavone ring. The olefine, methylene and two methyl protons on the isoprenyl substitution resonated at δ 5.14 (d, $J = 7.0$ Hz, 1H), 3.17 (d, $J = 7.0$ Hz, 2H), 1.59 (s, 3H), 1.48 (s, 3H) ppm respectively (Figure 3A.12). In ^{13}C NMR spectrum, the α,β - unsaturated carbonyl carbon resonated at δ 182.4 ppm (Figure 3A.13). Finally, the structure was in good agreement with ESI-HRMS spectra, where compound **15** displayed a molecular ion peak at m/z 437.16038, which is the $[\text{M}+\text{H}]^+$ peak. And the above described spectral data and compared with the previous literature, compound **15** was identified as **arntonin E**.

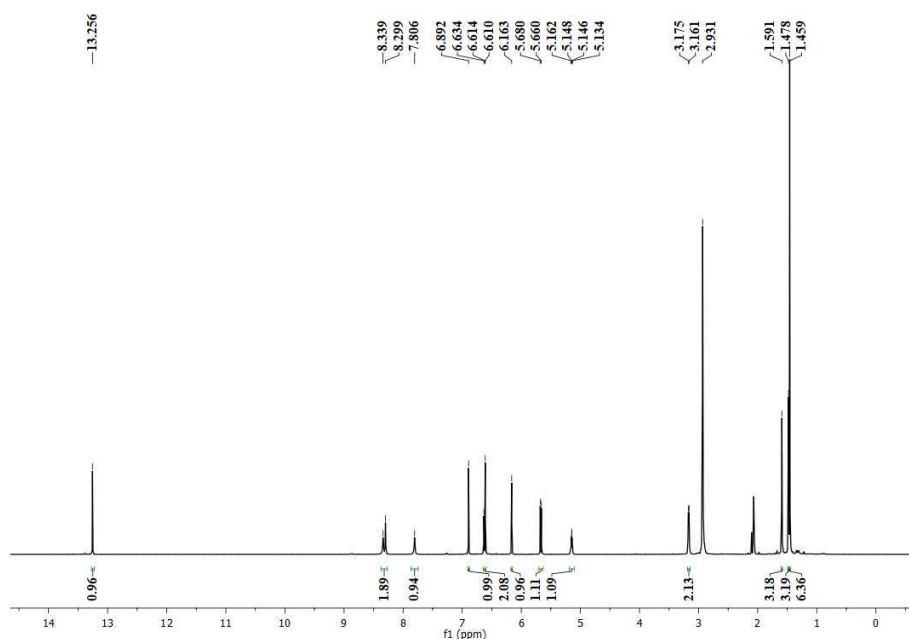


Figure 3A.12: ^1H NMR spectrum of Arntonin E

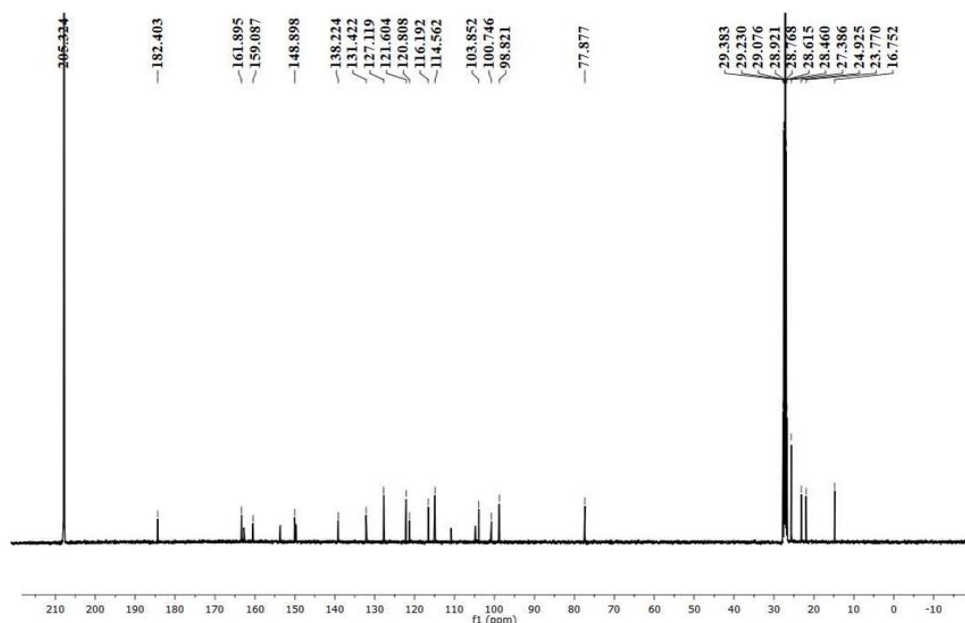


Figure 3A.13: ^{13}C NMR spectrum of Artonin E

The second UV active spot from fraction 4 was purified by repeated column chromatography with 100-200 mesh silica followed by the sephadex LH-20 column. In ^1H NMR spectra, the olefinic protons in the two isoprenyl substitutions resonated as a triplet at δ 5.18, 5.13 ppm respectively with a coupling constant of $J = 7.0$ Hz. Moreover, the four methyl protons on both substitutions resonated at δ 1.62, 1.61, 1.59, 1.43 ppm, respectively (Figure 3A.14). In ^{13}C NMR spectrum, the peak resonated at δ 182.6 ppm corresponding to α , β - unsaturated carbonyl carbon (Figure 3A.15). Finally, the structure was well in agreement with ESI-HRMS spectra, where compound **16** showed a molecular ion peak at m/z 439.1756, which is the $[\text{M}+\text{H}]^+$. Finally, the compound was identified as **artonin V** based on above spectral data and by the previous literature reports.

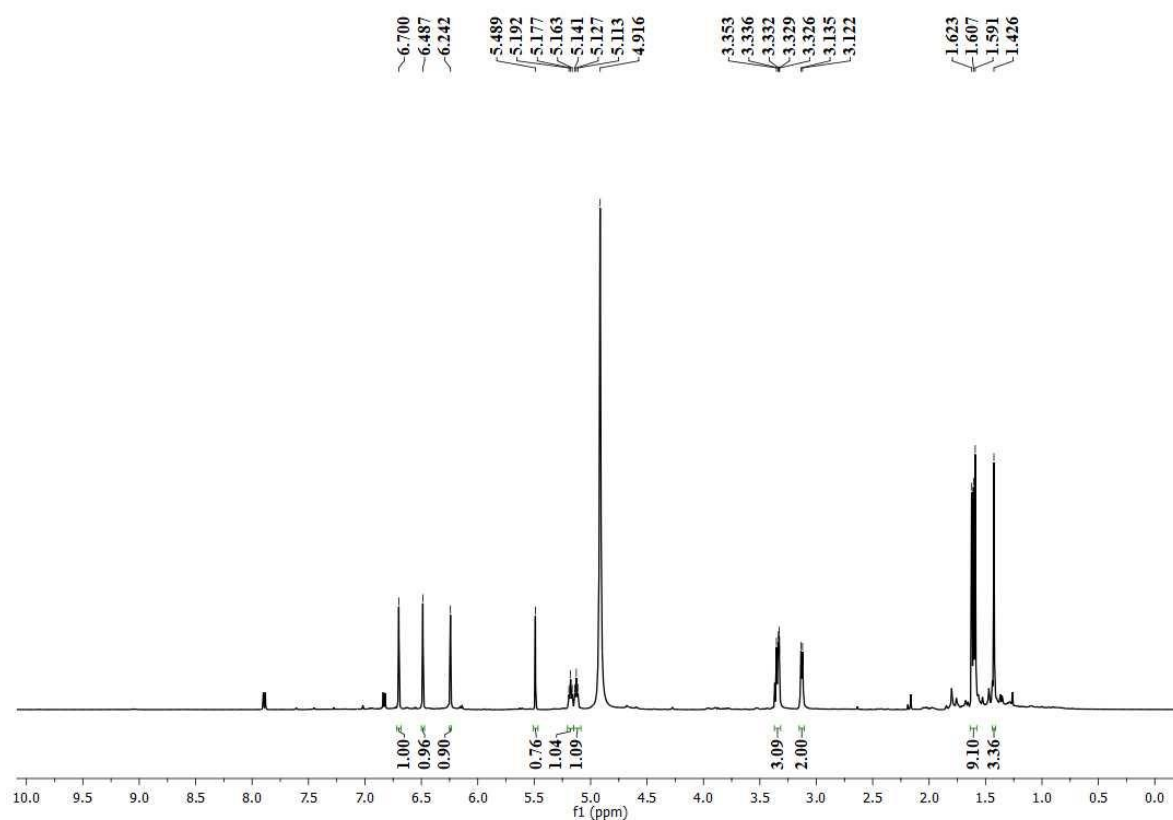


Figure 3A.14: ^1H NMR spectrum of Artonin V

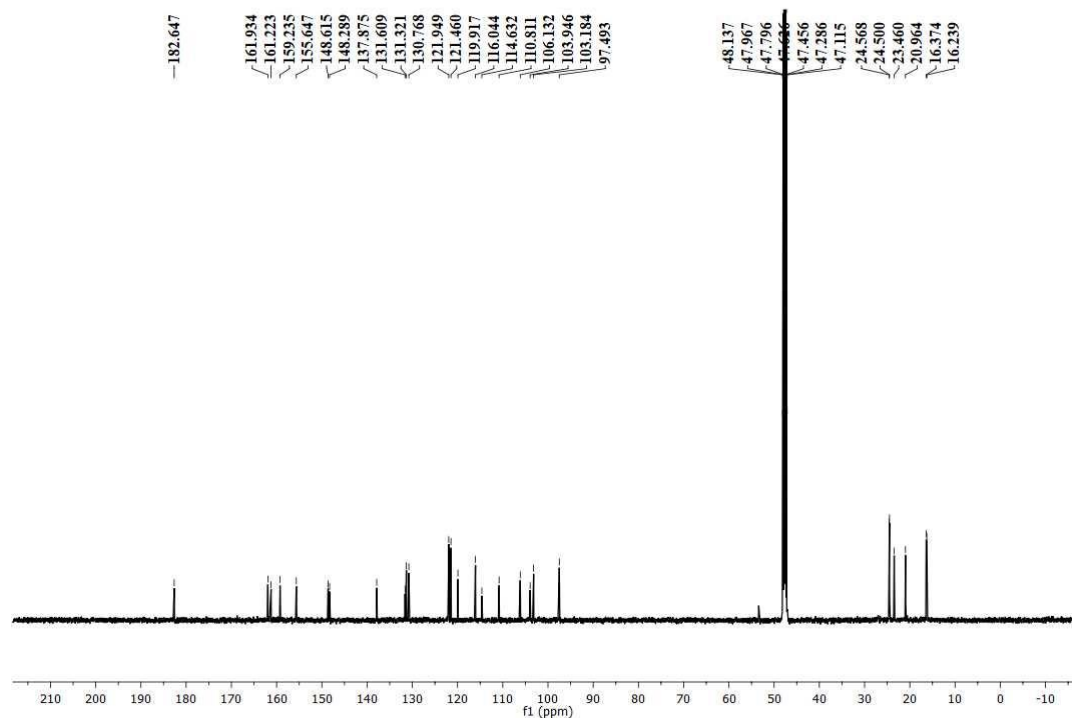


Figure 3A.15: ^{13}C NMR spectrum of Artonin V

Compound **17** was isolated as a yellowish powder from fraction pool 5 (Fraction 64-69). In ^1H NMR spectra, compound **17** showed a peak at the chemical shift value δ 13.43 ppm, which is the diagnostic peak of the flavonoid moiety (Figure 3A.16). The peaks resonated at δ values 6.27 ppm (d, $J = 9.0$ Hz), 5.44-5.41 ppm (1H, m), 1.97 (3H, s), and 1.70 ppm (3H, s) are corresponding to the pirano group γ,γ -dimethyl allyl system. The proton signals of ring B at 6.42 ppm (1H, d, $J = 2.5$ Hz); 6.54 (1H, dd, $J_1 = 2.0$ Hz; $J_2 = 8.5$ Hz); 7.67 (1H, d, $J = 8.5$ Hz) indicate the existence of substitution at positions 2' and 4'. Moreover, the peak resonated at 3.93 ppm as a singlet corresponding to the methoxy group. The peak observed at δ 178.6 ppm is the typical peak of α, β -unsaturated carbonyl carbon (Figure 3A.17). The position of the prenyl substitution was determined by HMBC analysis. The interaction of prenyl group carbon with the chelated OH, indicating the presence of a prenyl group at C-6 in ring A. The final confirmation was made with HRESI-MS compound **17** showed a peak at m/z $[\text{M}+\text{H}]^+$ 435.1808. Based on the above spectra data and previous literature reports the compound is identified as **cycloartocarpin**.

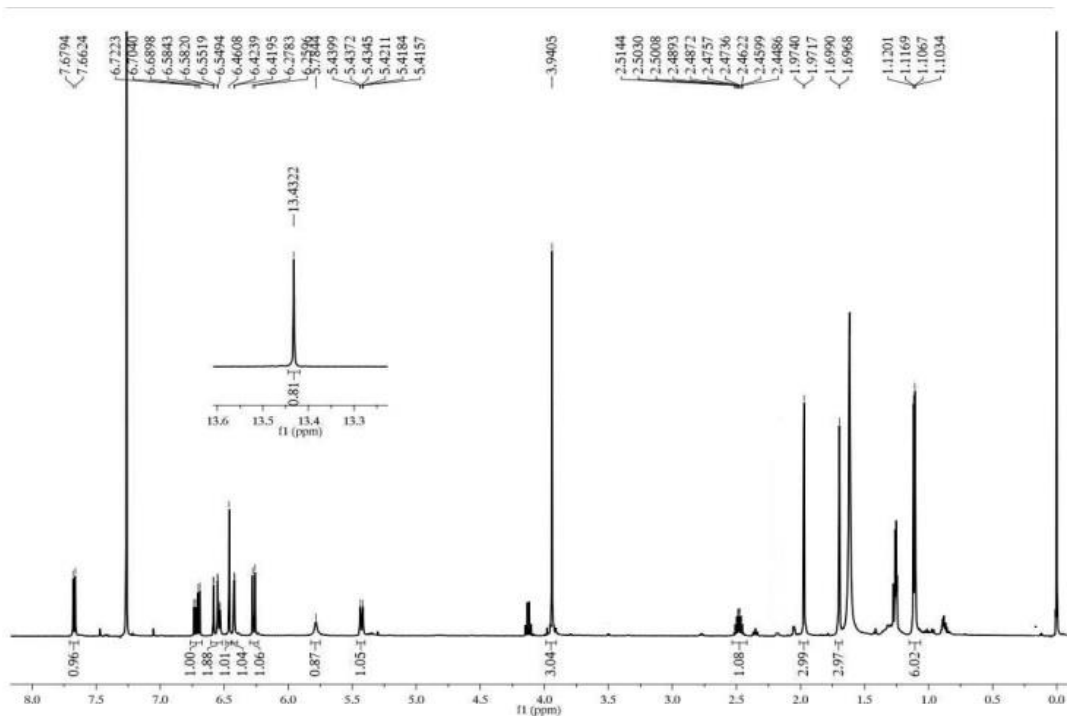


Figure 3A.16: ^1H NMR spectrum of cycloartocarpin

Compound **18** was isolated from the fraction pool 5 as a yellow solid via precipitation with dichloromethane. In the ^1H NMR spectra, a peak resonated at δ 13.98 ppm depicts the presence of a flavonoid moiety (Figure 3A.18). The spectrum also indicates the presence of a trans olefine with two peaks observed at δ 6.76-6.72 ppm as a multiplet and a doublet at δ 6.61 ppm with coupling constant $J = 16.5$ Hz. Moreover, the existence of an isoprenyl substitution was confirmed by a set of olefinic protons resonated at δ 5.16-5.12 ppm as multiplet, which displayed a HOMOCSY relation with a methylene proton resonated at δ 3.14 ppm. The presence of a single methylene group was further confirmed using ^{13}C NMR (Figure 3A.19) and DEPT-135 analysis. Finally, the structure was identified as **artocarpin** from the ESI-HRMS analysis which gave a $(\text{M}+\text{H})^+$ peak at 437.1962.

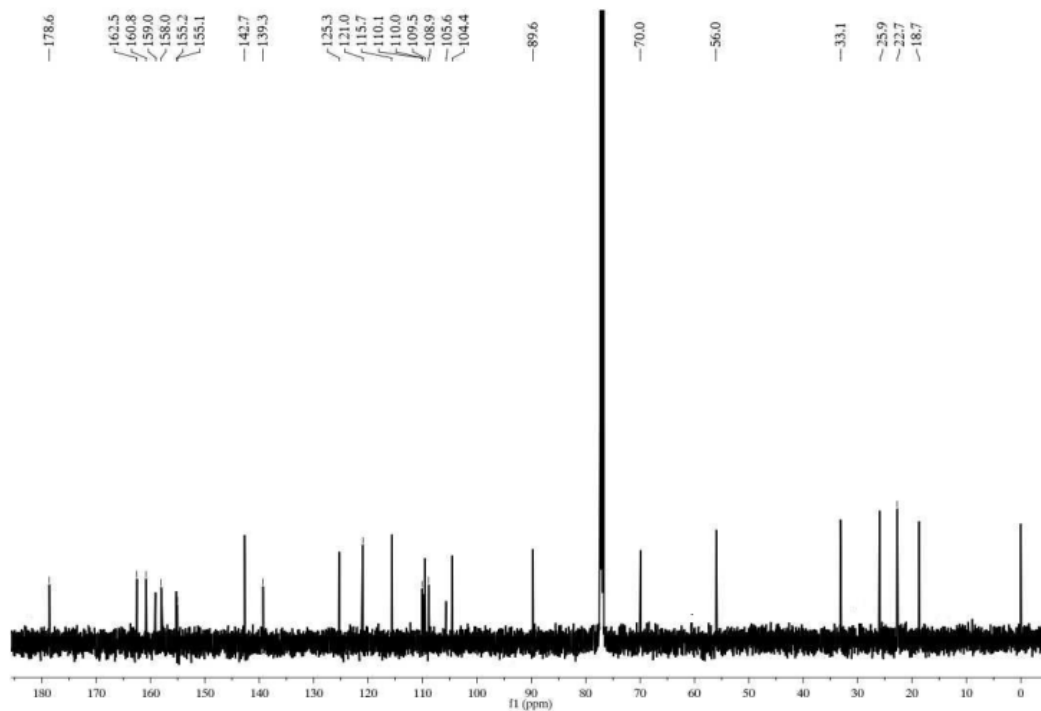


Figure 3A.17: ^{13}C NMR spectrum of cycloartocarpin

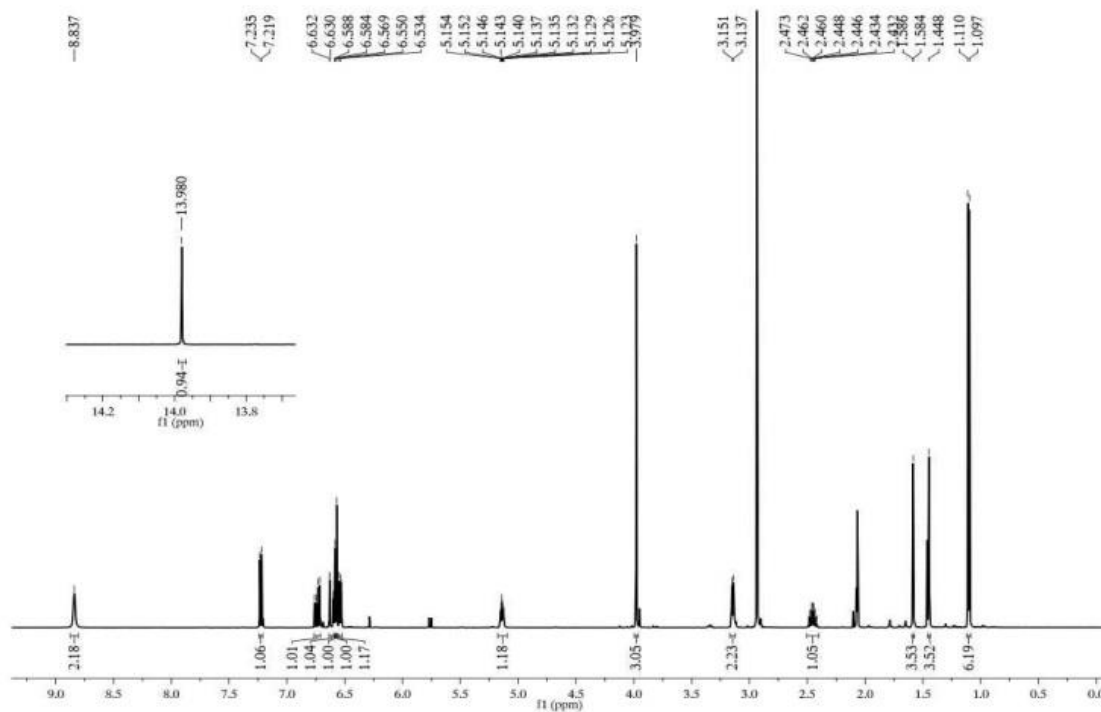


Figure 3A.18: ^1H NMR spectrum of artocarpin

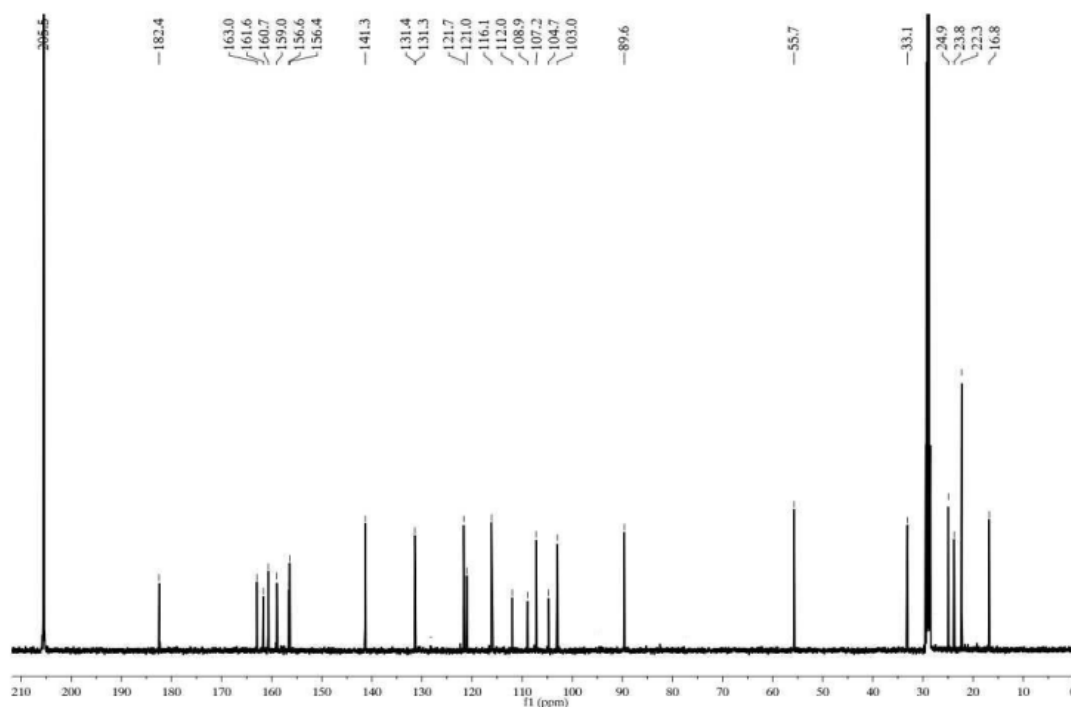


Figure 3A.19: ^{13}C NMR spectrum of artocarpin

Fraction pool 6 obtained by eluting the column with 60% ethyl acetate-hexane showed the presence of a UV-active compound in association with minor impurities. Hence, the fraction was again chromatographed in 230-400 mesh silica and eluting with 50% ethyl acetate-hexane afforded 90 mg of light brownish solid, which was identified as *E*-resveratrol (compound **19**). Structural elucidation of the molecule was done with IR, NMR (^1H & ^{13}C) and HRMS spectra. In the IR spectra, compound **19** showed a broad signal at a stretching frequency 3411 cm^{-1} corresponding to a hydroxyl group. In ^1H NMR, two peaks resonated at δ 8.55 and 8.28 ppm indicating the presence of phenolic hydroxyl groups. The peaks resonated at δ 7.03 and 6.90 ppm as a doublet with a coupling constant $J = 16.5\text{ Hz}$ could be recognised to trans olefinic protons. The aromatic protons at $\text{C}2'$, $\text{C}6'$ and $\text{C}3'$, $\text{C}5'$ are resonated at δ 7.43 and 6.85 ppm respectively, each peaks having two proton integrations and a coupling constant of $J = 8\text{ Hz}$. The remaining two aromatic protons on the $\text{C}2$ and $\text{C}6$ carbon resonated at δ 6.56 ppm as a singlet (Figure 3A.20). In ^{13}C NMR, the peaks observed at δ 158.7 and 157.3 ppm could be attributed to aromatic carbon-bearing hydroxyl group. The trans olefinic carbon resonated at δ 128.2 and 125.9 ppm (Figure.3A.21). Moreover, compound **19** displayed a molecular ion peak at m/z 229.0868 in the ESI-HRMS spectra. From all the spectral data and on comparison with the literature reports the compound was confirmed as ***E*-resveratrol**.

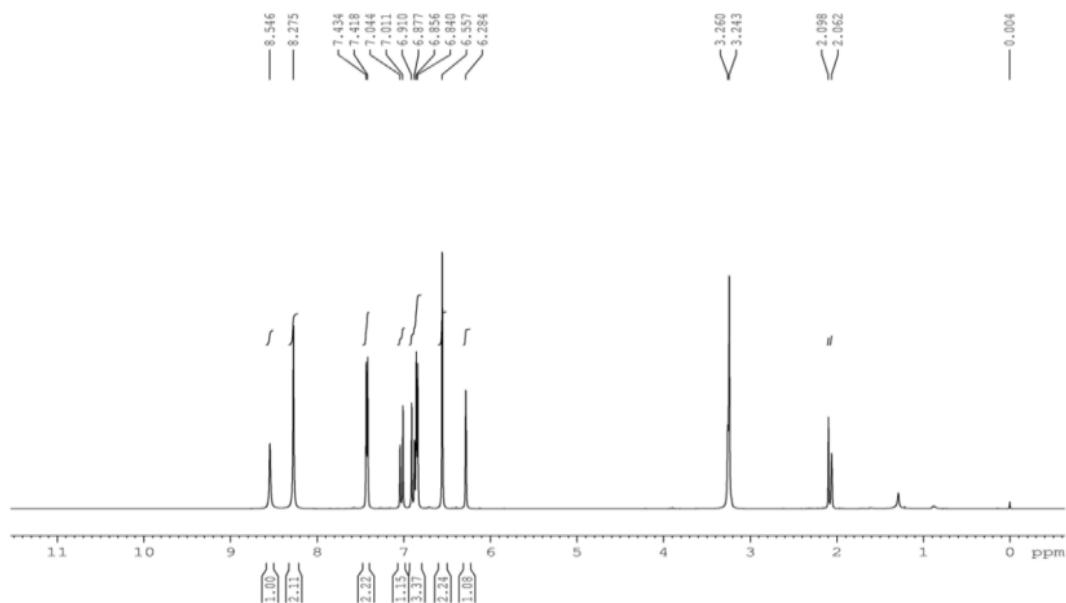


Figure 3A.20: ^1H NMR spectra of *E*-Resveratrol

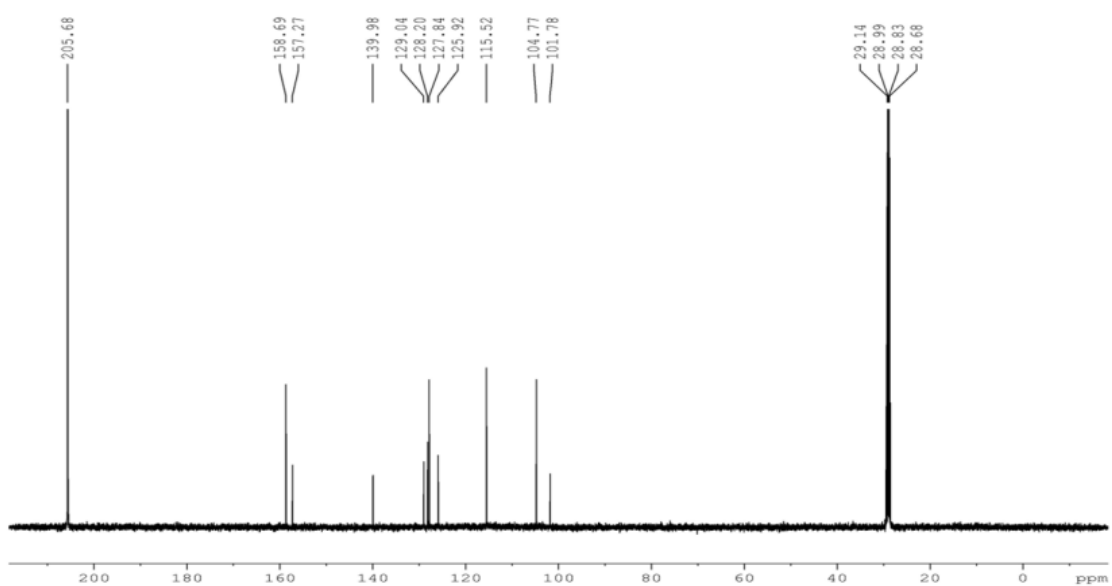


Figure 3A.21: ^{13}C NMR spectra of *E*-Resveratrol

Compound **20** (212 mg) was obtained as a white solid from fraction pool 6, and it was further purified by crystallisation with water. In ^1H NMR spectrum (Figure 3A.22) of compound **20**, peaks resonated at δ 8.75-8.39 ppm indicating the presence of hydroxyl protons. Peaks resonated at δ 7.35 and 6.91 ppm could be attributed to the presence trans olefinic protons. In ^{13}C NMR spectrum, (Figure 3A.23) the peaks resonated at δ 159.5, 159.1 and 156.9 ppm corresponding to aromatic carbons-bearing hydroxyl group. Trans olefinic carbons resonated

at δ 128.3 and 124.4 ppm. Finally, in the ESI-HRMS spectra, compound **20** showed a molecular ion peak at m/z 245.0812, which is the $[M+H]^+$ peak. From all the above spectral data and in comparison with the literature reports, the compound was identified as oxyresveratrol.

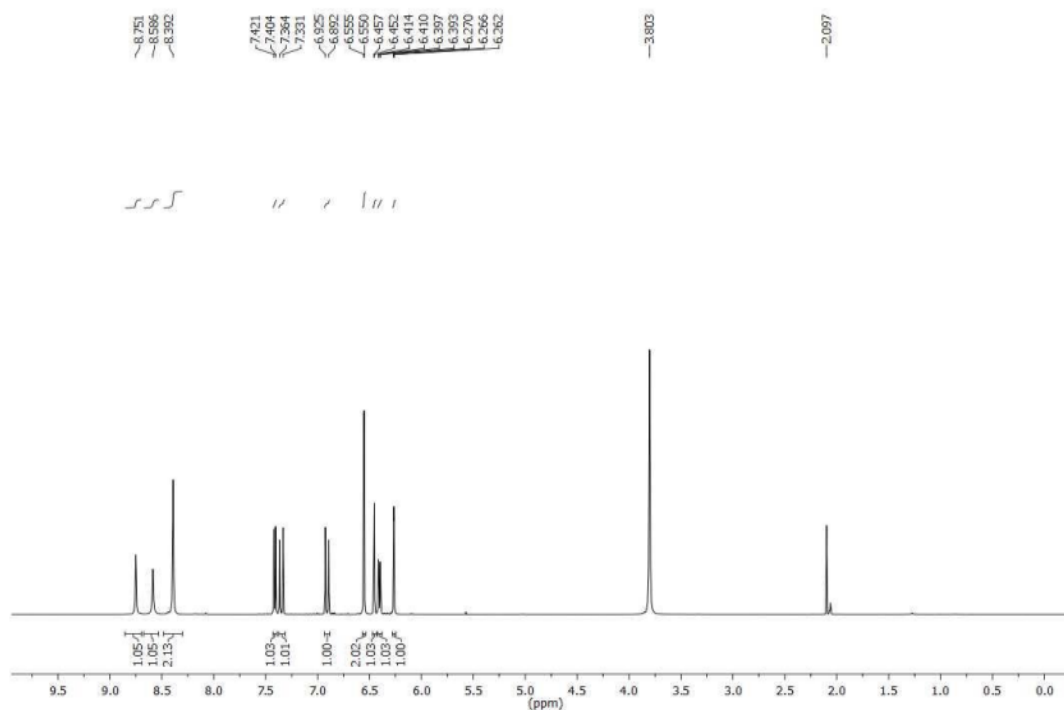


Figure 3A.22: ^1H NMR spectra of Oxyresveratrol

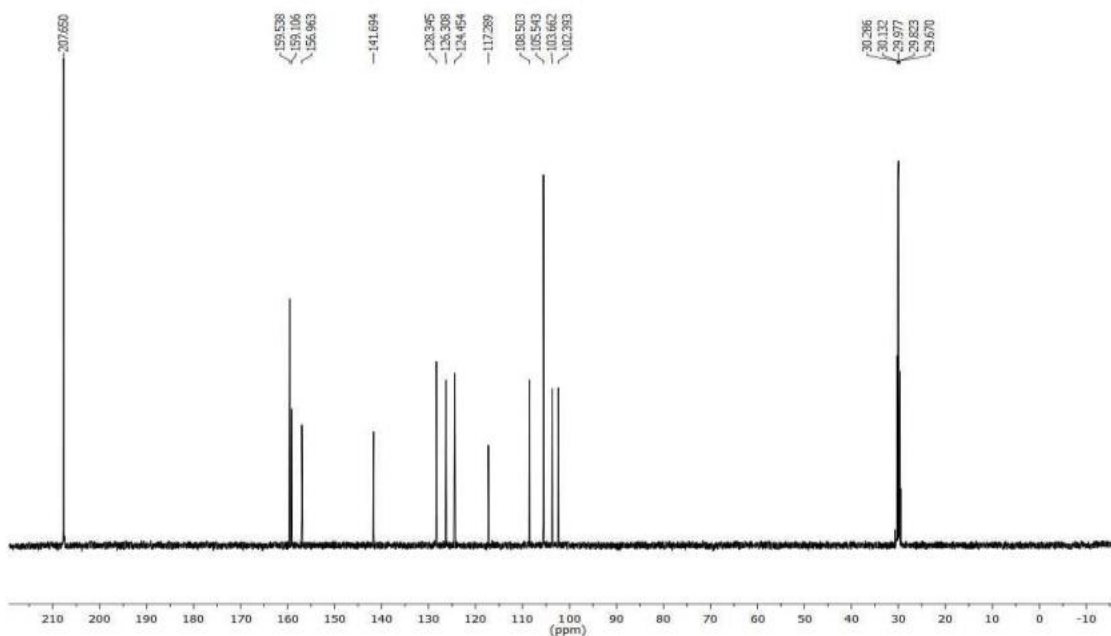


Figure 3A.23: ^{13}C NMR spectra of Oxyresveratrol

3A.6. Conclusion: In this chapter, we have successfully isolated 10 molecules from the stem bark of *Artocarpus altilis* viz., β -sitosterol, cycloartenol acetate, cycloartobiloxanthone, artobiloxanthone, artonin E, artonin V, cycloartocarpin, artocarpin, E-resveratrol, and oxyresveratrol. All the isolated molecules were characterized by 1D and 2D NMR techniques, ESI-HRMS and on comparison with the literature reports.

3A.7. Experimental Section

General experimental details and procedures are discussed in chapter 2.

3A.7.1. Extraction of *Artocarpus altilis*

The stem bark of *Artocarpus altilis* was collected from Wayanad district, Kerala. This material was thoroughly cleaned with water, chopped in to small pieces, and dried in a drier maintained at 50 °C and powdered. The powdered stem bark (900 g) was subjected to sequential extraction with hexane and acetone (2.5 L X 48 h). After extraction, the solvent was removed by Heidolph rotary evaporator under reduced pressure. The acetone extract (45 g) was then column chromatographed with hexane-ethyl acetate mixtures of varying polarity.

5A.7.2. Isolation of phytochemicals from *Artocarpus altilis* stem bark

The acetone extract (45 g) of the stem bark of *Artocarpus altilis* was subjected to column chromatographic separation with 100-200 mesh silica and the system was eluted successively with gradient mixtures of hexane and ethyl acetate of increasing polarities and finally with 30% methanol in ethyl acetate. A total of 30 fractions of approximately 250 mL were collected, and pooled into 6 fraction pools based on their similarity in TLC profile (Figure 3A.24).

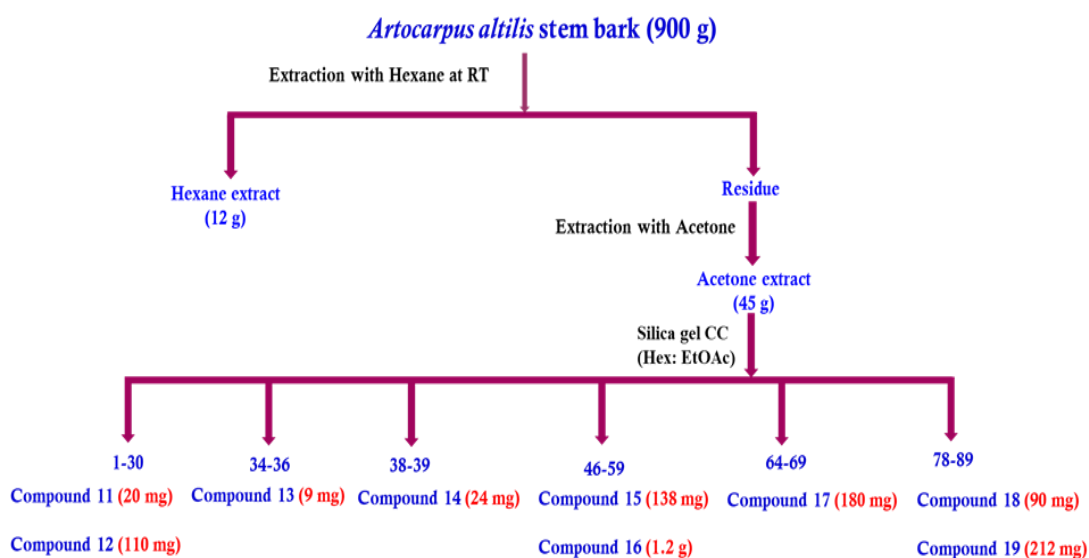
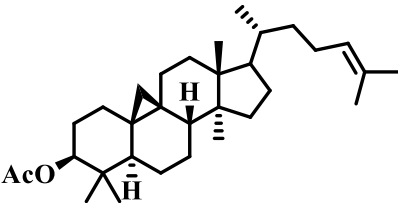
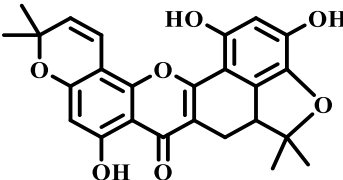
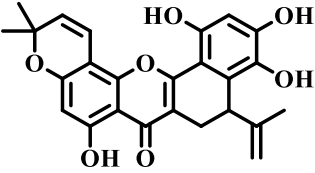
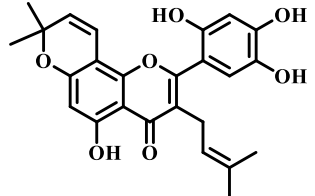
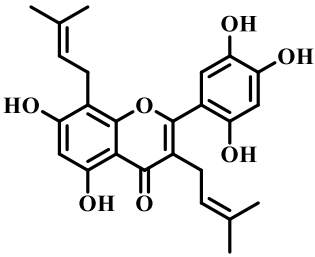
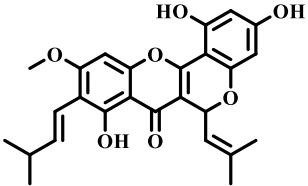
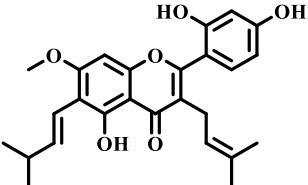


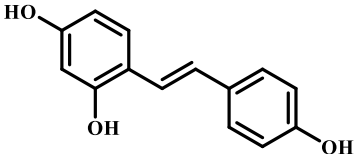
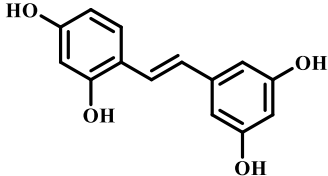
Figure 3A.24: Extraction and isolation of phytochemicals from stem bark of *Artocarpus altilis*.

5A.8. Spectral Data

<p>Compound 12: cycloartenol acetate</p> 	<p>Molecular formula: C₃₂H₅₂O₂</p> <p>FT-IR (Neat) ν_{\max}: 2102, 1733, 1643, 1464, 1372, 1248 cm⁻¹</p> <p>¹H NMR (500 MHz, CDCl₃): δ 5.10 (bs, 1H), 4.57 (d, $J = 5$ Hz, 1H), 2.05 (s, 3H), 2.00-1.95 (m, 1H), 1.89-1.87 (m, 2H), 1.76-1.73 (m, 1H), 1.68 (s, 3H), 1.60-1.51 (m, 9H), 1.40-1.34 (m, 3H), 1.28-1.25 (m, 10H), 1.12-1.05 (m, 4H), 0.96 (s, 3H), 0.89 (s, 9H), 0.81 (s, 3H), 0.58 (bs, 1H), 0.34 (bs, 1H) ppm.</p> <p>¹³C NMR (125 MHz, CDCl₃): δ 171.0, 130.9, 125.3, 80.7, 52.3, 48.9, 47.9, 47.2, 45.3, 39.5, 36.4, 35.9, 35.6, 32.9, 31.7, 29.7, 28.2, 26.9, 26.6, 26.0, 25.9, 25.8, 25.5, 25.0, 21.4, 20.9, 20.2, 19.3, 18.3, 18.0, 17.7, 15.2 ppm.</p> <p>ESI-HRMS: 469.4041 [M+H]⁺</p>
<p>Compound 13: cycloartobiloxanthone</p> 	<p>Molecular formula: C₂₅H₂₂O₇</p> <p>FT-IR (Neat) ν_{\max}: 3404, 3100, 2975, 1640, 1622, 1431 cm⁻¹</p> <p>¹H NMR (500 MHz, CD₃COCD₃): δ 13.39 (s, 1H), 9.04 (s, 1H), 8.88 (s, 1H), 6.93 (d, $J = 10.0$ Hz), 6.42 (s, 1H), 6.14 (s, 1H), 5.68 (d, $J = 10.0$ Hz, 1H), 3.42 (dd, $J_1 = 15.0$ Hz, $J_2 = 7.0$ Hz, 1H), 3.21 (dd, $J_1 = 15.0$ Hz, $J_2 = 7.0$ Hz, 1H), 2.36 (t, $J = 15.0$ Hz, 1H), 1.66 (s, 3H), 1.47 (s, 3H), 1.45 (s, 3H), 1.33 (s, 3H) ppm.</p> <p>¹³C NMR (125 MHz, CD₃COCD₃): δ 181.4, 162.6, 161.5, 159.5, 152.1, 151.6, 147.1, 137.9, 133.7, 127.9, 115.9, 112.7, 105.4, 105.3, 104.9, 99.9, 93.7, 78.7, 47.5, 28.4, 28.3, 22.8, 20.3 ppm.</p> <p>ESI-HRMS: 435.1438 [M+H]⁺</p>
<p>Compound 14: artobiloxanthone</p>	<p>Molecular formula: C₂₅H₂₂O₇</p> <p>FT-IR (Neat) ν_{\max}: 3421, 3150, 2097, 1622, 1431 cm⁻¹</p>

	<p>¹H NMR (500 MHz, CD₃COCD₃): δ 12.51 (s, 1H), 6.93 (d, <i>J</i> = 10 Hz, 1H), 6.28 (s, 1H), 6.20 (s, 1H), 5.62 (d, <i>J</i> = 10.0 Hz, 1H), 4.82 (s, 1H), 4.58 (s, 1H), 3.82 (d, <i>J</i> = 8.5 Hz, 1H), 3.44 (dd, <i>J</i>₁ = 17.5 Hz, <i>J</i>₂ = 1.0 Hz, 1H), 2.67 (dd, <i>J</i>₁ = 17.5 Hz, <i>J</i>₂ = 9.0 Hz, 1H), 1.84 (s, 3H), 1.50 (s, 3H), 1.46 (s, 3H) ppm.</p> <p>¹³C NMR (125 MHz, CD₃COCD₃): δ 180.3, 161.3, 160.1, 154.0, 143.3, 140.8, 131.7, 127.5, 118.1, 115.0, 113.2, 109.1, 105.6, 100.4, 100.0, 78.5, 35.4, 28.5, 28.2, 21.6, 21.2 ppm.</p> <p>ESI-HRMS: 435.1441 [M+H]⁺</p>
<p>Compound 15: artonin E</p> 	<p>Molecular formula: C₂₅H₂₄O₇</p> <p>FT-IR (Neat) ν_{max}: 3423, 3375, 2978, 2912, 1645, 1560, 1356, 1286, 1155 cm⁻¹</p> <p>¹H NMR (500 MHz, CD₃COCD₃): δ 13.26 (s, 1H), 8.34 (s, 1H), 8.30 (s, 1H), 7.81 (s, 1H), 6.89 (s, 1H), 6.64 – 6.59 (m, 2H), 6.16 (s, 1H), 5.67 (d, <i>J</i> = 10.0 Hz, 1H), 5.15 (dd, <i>J</i> = 7.7, 6.4 Hz, 1H), 3.17 (d, <i>J</i> = 7.0 Hz, 2H), 1.59 (s, 3H), 1.47 (d, <i>J</i> = 5.5 Hz, 3H), 1.46 (s, 6H) ppm.</p> <p>¹³C NMR (125 MHz, CD₃COCD₃): δ 182.4, 161.9, 161.3, 159.1, 152.4, 148.9, 148.6, 138.2, 131.4, 127.1, 121.6, 120.8, 116.2, 114.6, 110.6, 104.7, 103.8, 100.7, 98.8, 77.9, 27.4, 24.9, 23.8, 16.7 ppm.</p> <p>ESI-HRMS: 437.16038 [M+H]⁺</p>
<p>Compound 16: artonin V</p> 	<p>Molecular formula: C₂₅H₂₆O₇</p> <p>FT-IR (Neat) ν_{max}: 3413, 3345, 2912, 1632, 1510, 1315, 1294, 1140 cm⁻¹</p> <p>¹H NMR (500 MHz, CD₃COCD₃): δ 6.70 (s, 1H), 6.49 (s, 1H), 6.25 (d, <i>J</i> = 8.4 Hz, 1H), 5.49 (s, 1H), 5.18 (t, <i>J</i> = 7.3 Hz, 1H), 5.13 (t, <i>J</i> = 7.0 Hz, 1H), 3.38 – 3.32 (m, 3H), 3.13 (d, <i>J</i> = 6.9 Hz, 2H), 1.64 – 1.58 (m, 9H), 1.43 (d, <i>J</i> = 6.2 Hz, 4H) ppm.</p>

	<p>^{13}C NMR (125 MHz, CD_3COCD_3): δ 182.6, 161.9, 161.2, 159.2, 155.6, 148.6, 148.3, 137.9, 131.6, 131.3, 130.8, 121.9, 121.5, 119.9, 116.0, 114.6, 110.8, 106.1, 103.9, 103.2, 97.5, 24.6, 24.5, 23.5, 20.9, 16.4, 16.2 ppm.</p> <p>ESI-HRMS: 439.1756 $[\text{M}+\text{H}]^+$</p>
<p>Compound 17: cycloartocarpin</p> 	<p>Molecular formula: $\text{C}_{26}\text{H}_{26}\text{O}_6$</p> <p>FT-IR (Neat) ν_{max}: 3390, 2958, 2866, 1683, 1481, 1471, 1352, 1259, 1149, 1097 cm^{-1}</p> <p>^1H NMR (500 MHz, CD_3COCD_3): δ 13.43 (s, 1H), 7.67 (d, $J = 8.5$ Hz, 1H), 6.74-6.69 (m, 1H), 6.57 (dd, $J_1 = 8.0$ Hz, $J_2 = 1.5$ Hz, 1H), 6.46 (s, 1H), 6.42 (d, $J = 2.5$ Hz, 1H), 6.27 (d, $J = 9.0$ Hz, 1H), 5.78 (s, 1H), 5.44-5.42 (m, 1H), 3.94 (s, 3H), 2.51-2.45 (m, 1H), 1.97 (d, $J = 1.0$ Hz, 3H), 1.70 (d, $J = 1.0$ Hz, 3H), 1.12 (d, $J = 1.5$ Hz, 3H), 1.12 (d, $J = 1.5$ Hz, 3H) ppm.</p> <p>^{13}C NMR (125 MHz, CD_3COCD_3): δ 178.6, 162.5, 160.8, 159.0, 158.0, 155.2, 155.1, 142.7, 139.3, 125.3, 121.0, 115.7, 110.1, 110.0, 109.5, 108.9, 105.6, 104.4, 89.6, 77.3, 77.0, 76.8, 70.0, 56.0, 33.1, 25.9, 22.7, 18.7 ppm.</p> <p>ESI-HRMS: 435.1814 $[\text{M}+\text{H}]^+$</p>
<p>Compound 18: artocarpin</p> 	<p>Molecular formula: $\text{C}_{26}\text{H}_{28}\text{O}_6$</p> <p>FT-IR (Neat) ν_{max}: 3390, 2958, 2866, 1680, 1481, 1471, 1352, 1259, 1205, 1149, 1097 and 979 cm^{-1}</p> <p>^1H NMR (500 MHz, CD_3COCD_3): δ 13.98 (s, 1H), 8.84 (s, 2H), 7.23 (d, $J = 8.5$ Hz, 1H), 6.74 (dd, $J = 16.5$ Hz, 7.0 Hz, 1H), 6.61 (dd, $J = 16.5$ Hz, 1.0 Hz, 1H), 6.59 (d, $J = 2.0$ Hz, 1H), 6.57 (s, 1H), 6.54 (dd, $J = 8.0$ Hz, 2.5 Hz, 1H), 5.16 - 5.12 (m, 1H), 3.98 (s, 3H), 3.14 (d, $J = 7.0$ Hz, 2H), 2.49 - 2.42 (m, 1H), 1.59 (d, $J = 1.0$ Hz, 3H), 1.45 (s, 3H), 1.10 (s, 3H), 1.09 (s, 1H) ppm.</p>

	<p>¹³C NMR (125 MHz, CD₃COCD₃): δ 182.4, 163.0, 161.6, 160.7, 159.0, 156.5, 156.4, 141.3, 131.4, 131.3, 121.7, 121.0, 116.1, 112.0, 108.9, 107.2, 104.7, 103.0, 89.6, 55.7, 33.1, 25.0, 23.8, 22.3, 16.8 ppm.</p> <p>ESI-HRMS: 437.1962 [M+H]⁺</p>
<p>Compound 19: <i>E</i>-resveratrol</p> 	<p>Molecular formula: C₁₄H₁₂O₃</p> <p>FT-IR (Neat) ν_{max}: 3411, 2924, 2858, 1582, 1506, 1440, 1379, 1143 cm⁻¹</p> <p>¹H NMR (500 MHz, CD₃COCD₃): δ 8.55 (s, 1H, -OH), 8.28 (s, 2H, -OH), 7.43 (d, <i>J</i> = 8 Hz, 2H), 7.03 (d, <i>J</i> = 16.5 Hz, 1H), 6.90 (d, <i>J</i> = 16.5 Hz, 1H), 6.85 (d, <i>J</i> = 8 Hz, 2H), 6.56 (s, 2H), 6.28 (s, 1H) ppm.</p> <p>¹³C NMR (125 MHz, CD₃COCD₃): δ 158.7, 157.3, 139.9, 129.0, 128.2, 127.8, 125.9, 115.5, 104.8, 101.8 ppm.</p> <p>ESI-HRMS: 229.0868 [M+H]⁺</p>
<p>Compound 20: oxyresveratrol</p> 	<p>Molecular formula: C₁₄H₁₂O₄</p> <p>FT-IR (Neat) ν_{max}: 3209, 2921, 1589 cm⁻¹.</p> <p>¹H NMR (500 MHz, CD₃COCD₃): δ 8.75 (s, 1H, OH), 8.59 (s, 1H, OH), 8.39 (s, 2H, OH), 7.41 (d, <i>J</i> = 8.5 Hz, 1H), 7.35 (d, <i>J</i> = 16.5 Hz, 1H), 6.91 (d, <i>J</i> = 16.5 Hz, 1H), 6.55 (d, <i>J</i> = 2.1 Hz, 2H, H-2, H-6), 6.45 (d, <i>J</i> = 2 Hz, 1H), 6.40 (dd, <i>J</i>₁ = 8.5, <i>J</i>₂ = 2.5 Hz, 1H), 6.27 (t, <i>J</i> = 2 Hz, 1H) ppm.</p> <p>¹³C NMR (125 MHz, CD₃COCD₃): δ 159.5, 159.1, 156.9, 141.7, 128.3, 126.3, 124.4, 117.3, 108.5, 105.5, 103.7, 102.4 ppm</p> <p>ESI-HRMS: 245.1802 [M+H]⁺</p>

References

- [1] M. Mohanty, Chinmay Pradhan, A Review on Phytochemistry, Bio-Efficacy, Medicinal and Ethno- Pharmaceutical Importance of *Artocarpus altilis*, Int. J. Pharm. Pharm. Res.

- 3 (2015) 219–231.
- [2] N.R. Amarasinghe, L. Jayasinghe, N. Hara, Y. Fujimoto, Chemical constituents of the fruits of *Artocarpus altilis*, *Biochem. Syst. Ecol.* 36 (2008) 323–325. <https://doi.org/10.1016/j.bse.2007.09.007>.
- [3] Y. Wang, K. Xu, L. Lin, Y. Pan, X. Zheng, Geranyl flavonoids from the leaves of *Artocarpus altilis*, *Phytochemistry.* 68 (2007) 1300–1306. <https://doi.org/10.1016/j.phytochem.2007.01.009>.
- [4] S. Boonphong, A. Baramée, P. Kittakoop, Antitubercular and Antiplasmodial Prenylated Flavones from the Roots of *Artocarpus altilis*, *Chiang Mai J. Sci.* 34 (2007) 339–344.
- [5] V. Kuete, P.Y. Ango, G.W. Fotso, G.D.W.F. Kapche, J.P. Dzoyem, A.G. Wouking, B.T. Ngadjui, B.M. Abegaz, Antimicrobial activities of the methanol extract and compounds from *Artocarpus communis* (Moraceae), *BMC Complement. Altern. Med.* 11 (2011) 2–6. <https://doi.org/10.1186/1472-6882-11-42>.
- [6] M.H. Jang, X.L. Piao, J.M. Kim, S.W. Kwon, J.H. Park, Inhibition of cholinesterase and amyloid- β aggregation by resveratrol oligomers from *Vitis amurensis*, *Phyther. Res.* 20 (2006) 1052–1055. <https://doi.org/10.1002/ptr>.
- [7] and P.H. J. Viyoch, S. Buranajaree, F. Grandmottet, S. Robin, D. Binda, C. Viennet, N. Waranuch, Evaluation of the effect of Thai breadfruit's heartwood extract on the biological functions of fibroblasts from wrinkles, *Int. J. Cosmet. Sci.* 32 (2010) 470–473.
- [8] C. Pradhan, M. Mohanty, A. Rout, A.B. Das, K.B. Satapathy, H.K. Patra, Phytoconstituent screening and comparative assessment of antimicrobial potentiality of *Artocarpus altilis* fruit extract, *Int. J. Pharm. Pharm. Sci.* 5 (2013) 840–843.
- [9] M. Mahadi, A. Jamil, S. Ganeson, H. Buhari, R. Abdul, *Artocarpus altilis* extract effect on cervical cancer cells, *Mater. Today Proc.* 5 (2018) 15559–15566. <https://doi.org/10.1016/j.matpr.2018.04.163>.
- [10] E.T. Arung, B.D. Wicaksono, Y.A. Handoko, I.W. Kusuma, D. Yulia, F. Sandra, Anti-cancer properties of diethylether extract of wood from Sukun (*Artocarpus altilis*) in human breast cancer (T47D) cells, *Trop. J. Pharm. Res.* 8 (2009) 317–324. <https://doi.org/10.4314/tjpr.v8i4.45223>.

Exploring the Cytotoxic Effects of Natural Prenylflavones from *Artocarpus altilis* against SAS Oral Squamous Cell Carcinoma

3B.1. Introduction

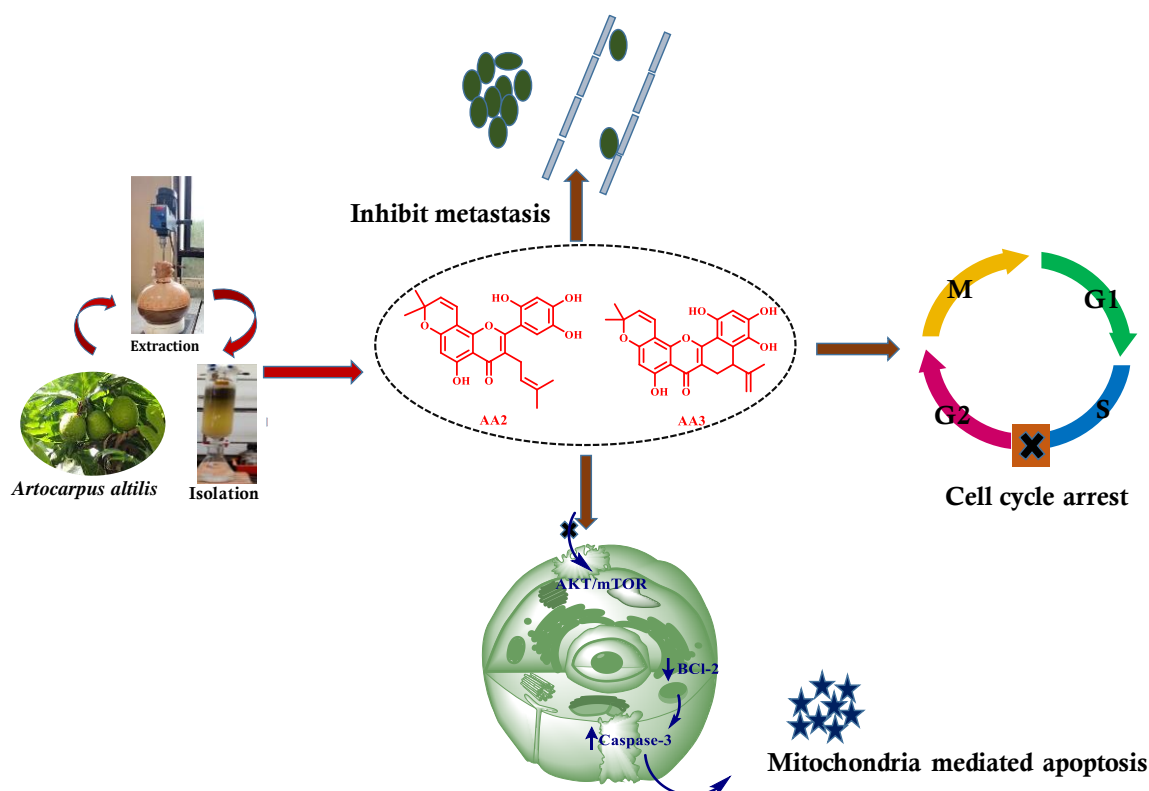
Phytochemicals are the privileged structural motifs recognized for their chemical diversity, structural complexity, and pleiotropic nature and made major contributions to pharmacotherapy from time immemorial. The majority of isolated phytochemicals from numerous ethnomedicinal floras proffer promising anti-cancer potential along with cell-specific toxicity and better efficacy paving the innovation of new chemotherapeutic drugs for the benefit of all humanity [1–3]. The ease of availability of plant species, simple extraction and isolation protocols, purification techniques, favourable safety profile and multiple pharmacological activities hidden in the species are the beneficial features of natural products that contributed to the development of more environmentally sound, economical, and effective drug discovery processes.

Oral cancer, prominently known as oral squamous cell carcinoma (OSCC), is defined as a malignant epithelial neoplasm unveiling squamous differentiation owing to the accumulation of multiple genetic mutations in the cell [4]. OSCC is a common global malignancy, that belongs to a distinct subtype of head and neck squamous cell carcinoma associated with the highest rate of morbidity, mortality, and prevalence [5]. According to Global Cancer Statistics 2018, an estimated number of 354,864 new oral cancer incidences and 177,384 mortality burdens are reported globally in the year 2018 [6]. Smoking tobacco, chewing betel quid, areca nut, drinking alcohols, human papillomavirus infection, high consumption of red meat and fermented foods, etc. are the major etiological factors that contributed to the progression and development of OSCC and are the vital factors for its prevalence [7–10]. The traditional treatment modalities of oral cancer including chemotherapy, radiotherapy, brachytherapy, surgery, and targeted molecular therapy have numerous shortcomings such as adverse side effects, non-specific cell death, recurrence of the tumour, chemoresistance, and radioresistance [11,12]. Hence, the development of personalized, targeted therapies that might block an individual pathway or a combination of pathways must be imperative for the rescue of the development or progression of OSCC. Exploring natural secondary metabolites and their active ingredients having persistent anti-cancer potential embarks the development of new

chemotherapeutic agents and leads to its prevention and curation. In the present scenario, we were intrigued by the tremendous biological potential hidden in these functional moieties and initiated our expedition to the fascinating world of natural products by the isolation of phytochemicals from traditionally highlighted floras for the mitigation and curation of various infectious and lifestyle diseases [13–16]. Previously, we have reported the potential of two bioactive triterpenoids viz., betulinic acid and koetjapic acid from *Dillenia indica* for inhibiting the growth and proliferation of SAS oral cancer cells and illustrated the traditional wisdom with scientific criterion [17].

The traditional knowledge of local millennia is embedded in their empirical observations and cultural traditions are drawn on an impressive array of floras, most of which have not been scrutinized by modern scientific support. The rich biodiversity of the Western Ghats and traditional systems of medicine offered a golden opportunity for the exemplification of natural products for the benefit of all humanity. The genus *Artocarpus* comprises 50 species of evergreen, ramified deciduous trees, economically utilized for multiple applications such as staple crops, construction materials, animal feeds, and folk medicines [18]. Moreover, the genera have been recognized as a source of edible aggregative fruit viz, *Artocarpus heterophyllus*, *Artocarpus camansi*, *Artocarpus hirsutus*, and *Artocarpus altilis*. *Artocarpus altilis* (Parkinson) Fosberg is the primary component of traditional agroforestry systems native to the Pacific and tropical Asia and is widely cultivated throughout the humid tropics. The leaves of the plant are widely used as traditional medicine for curing hypertension, liver cirrhosis, and diabetes [19]. The texture of the moderately ripe fruit is comparable to that of baked bread, it is popularized under the common name breadfruit. The species can produce diverse phytochemical entities, specifically aromatic compounds such as flavonoids, stilbenoids, and arylbenzofurans for host-defense mechanisms and environmental stress conditions [20] [21]. Many of the isolated molecules from *Artocarpus altilis* exhibit a broad range of biological activities such as anti-malarial,[22] anti-bacterial, anti-fungal, anti-tumour and, anti-leukemic activities, etc. Artonin E is an isoprenyl flavone isolated from the stem bark of *Artocarpus altilis* alleviated drug-like behaviour with full acquiescence to Lipinski's rule of five and decent physicochemical properties when compared with 95% of currently available drugs. The molecule is shown to possess several pharmacological activities such as anti-malarial [22,23], anti-cancer [24–27], anti-bacterial [28], and anti-estrogenic activity. The anti-cancer potential of this moiety was demonstrated in various cancer cells such as triple-negative breast cancer cells (MDA-MB-231) [25], MCF-7 [29], leukemia cells (P-388) [30], colon cancer cells (LoVo & HCT116) [24], lung cancer cells (H460, H23, A549 and H292) [31], and

ovarian cancer (SKOV-3) [27]. Artobiloxanthone, an aromatic flavone having a pyran moiety attached to a xanthone ring reported from the stem bark of *Artocarpus nobilis* [32] *Artocarpus lanceifolius* [33] and *Artocarpus altilis* [22]. Herein, we comprehensively explore the chemotherapeutic potential of artonin E and artobiloxanthone isolated from the stem bark of *Artocarpus altilis* for the suppression, prevention, and better management of OSCC (Scheme 1).



Scheme 1: Flavones from *Artocarpus altilis* inhibit AKT/mTOR signaling pathway and induces mitochondria mediated apoptosis

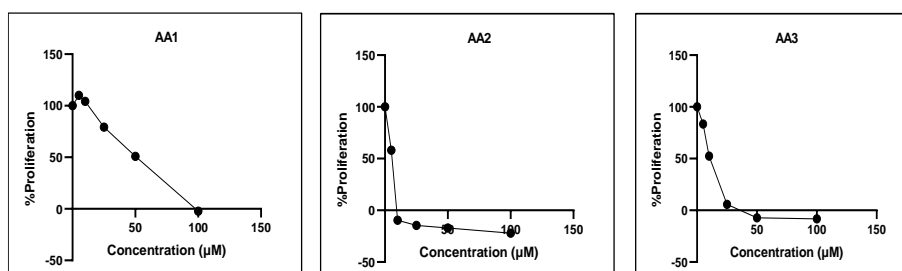
3B.2. RESULTS AND DISCUSSION

3B.2.1. Evaluation of Anti-proliferative potential of isolated phytochemicals against oral squamous cell carcinoma (OSCC)

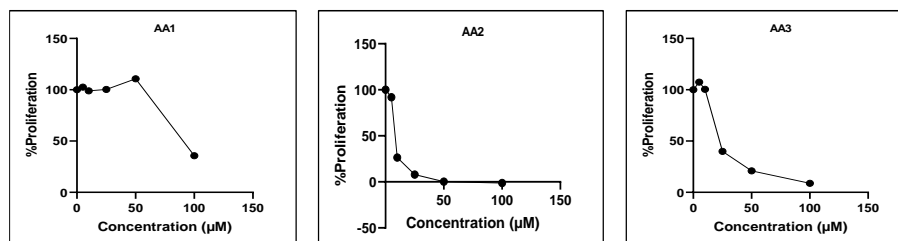
Initially, we analysed the anti-proliferative potential of isolated molecules (discussed in chapter 3A) against human OSCC cell line SAS and esophageal cancer cell line TTn in vitro using MTT assay. The MTT cell proliferation assay is known to measure the viability and metabolic activity of the cells by computing the percentage of live cells from the formazan crystals formed by the reduction of MTT tetrazolium salt. Interestingly, we observed a drastic reduction in cell viability with the increase in the concentration of the treated molecules such as artonin V (AA1), artonin E (AA2), artobiloxanthone (AA3). The IC_{50} values of AA1, AA2, and AA3 in

SAS and TTn were found to be 50 μ M, 6 μ M, 11 Mm in SAS cells and 92 μ M, 8 μ M, and 22 μ M, in TTn cells respectively after 72 hr (Figure 3B.1). Moreover, we analysed the cytotoxic potential of all the molecules against human keratinocyte cells (HaCaT) and are found to be cytotoxic at higher concentrations only. Their IC₅₀ values in HaCaT cells are 92 μ M, 72 μ M, and 70 μ M for AA1, AA2, and AA3 respectively (Table 1). From the MTT proliferation assay, based on the IC₅₀ values we have envisioned that compounds AA2 and AA3 (Figure 3B.2) showed higher potential to inhibit the proliferation of SAS cells than that of TTn even at lower concentrations.

SAS



TTn



HaCaT

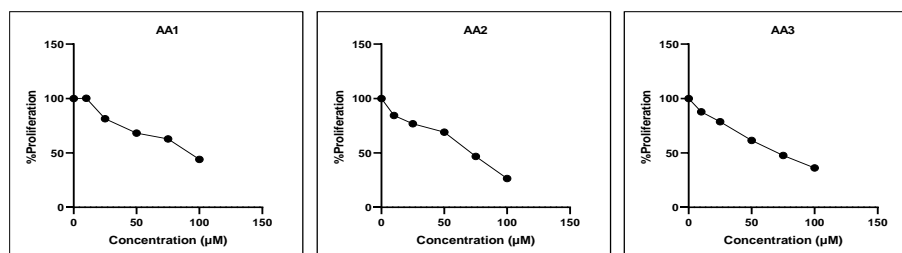


Figure 3B.1: Anti-proliferative potential of the isolated molecules against oral cancer cell lines SAS, TTn and human keratinocyte cell line HaCaT. Anti-proliferative effect of AA1, AA2, and AA3 on oral cancer cells were assessed using MTT assay after 72 hours of treatment. The percentage of proliferation was calculated considering the untreated control as 100% and graph was plotted using Graphpad prism software.

Table 1: Anti-proliferative potential of isolated molecules against various cancer cell lines represented in terms of their IC₅₀ values.

Compounds	IC ₅₀ (μ M)		
	SAS	TTn	HaCaT
AA1	50	92	92
AA2	6	8	72
AA3	11	22	70

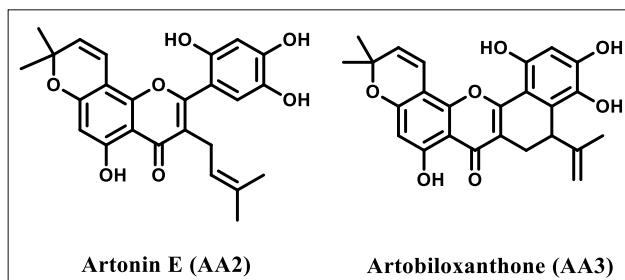


Figure 3B.2: Structure of bioactive molecules against SAS oral cancer cells

3B.2.2. Computational screening of active candidates AA2 and AA3

Next, to provide a rational explanation of the experimental findings with theoretical support, we expanded the screening strategy with computational simulation tools, where we envisage the binding affinity of the bioactive candidates with the selected protein domains involved in regulating different hallmarks of cancer by molecular docking approach. Besides, the molecular dynamics protocols were employed to demonstrate the flexibility and suitability of the molecules inside the binding pocket of the selected receptors.

3B.2.2.1. Molecular docking: Both AA2 and AA3 are docked with different protein domains involved in regulating different stages of cancer such as proliferation, invasion, migration, etc. The ligands AA2 and AA3 were docked against seven selected proteins such as BCL-2 (Protein Data Bank (PDB) ID: 2O21), caspase-3 (PDB ID:1GFW), caspase-9 (PDB ID:1JXQ), p53 (PDB ID:1TUP), COX-2 (PDB ID:1PXX), AKT (PDB ID:1O6L) and mTOR (PDB ID:4JSP). We have observed that AA2 exhibited a better binding affinity with 2O21, 1GFW, and 1JXQ, having a dock score of -8.2 kcal/mol. In the case of 1GFW, the hydrogen bonding interactions between the hydroxyl groups of the ligand AA2 with polar amino acid residue SER209 and hydrophobic PHE250 attributed to the high dock score of -8.2 kcal/mol. While with 1JXQ, the H bond interaction with the amino acid residue PHE294 with the hydroxyl group of AA2 eventually contributed a maximum binding energy of -8.2 kcal/mol. Moreover, the ligand effectively binds with the protein 2O21 via two H bonds with the GLU133 and ALA146 offering a maximum binding energy of -8.2 kcal/mol (Figure 3B.3-3B.5). Similarly, AA3 showed a maximum binding affinity with 1GFW, having a dock score value of -7.9 kcal/mol

and that of -7.8 kcal/mol with 1JXQ and -7.4 kcal/mol with 2O21 respectively (Figure 3B.3-3B.5). The higher binding affinity of the ligand AA3 with these proteins is associated with the H bond interactions of the polar hydroxyl groups in the ligand with the various amino acid residues such as ARG207 and HIS292 (Figure 3B.3-3B.5).

A

B

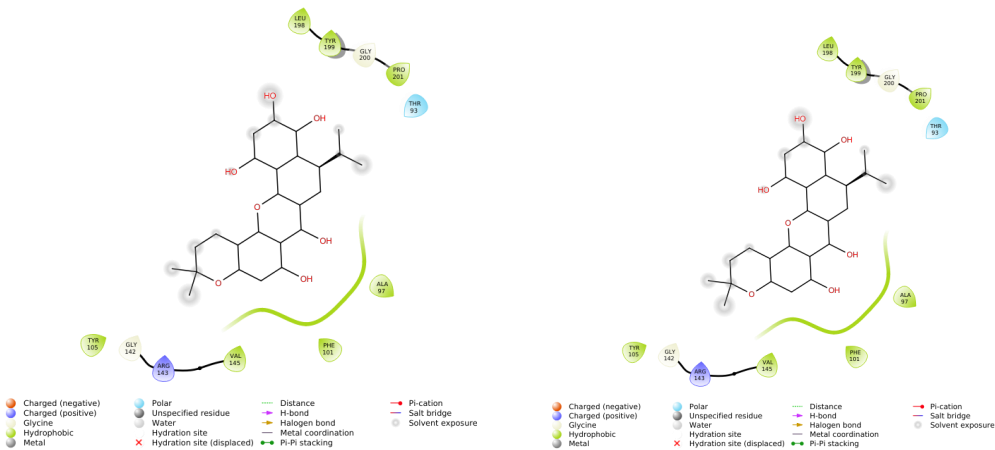


Figure 3B.3: Molecular docking with **2O21** (A) AA2 (B) AA3

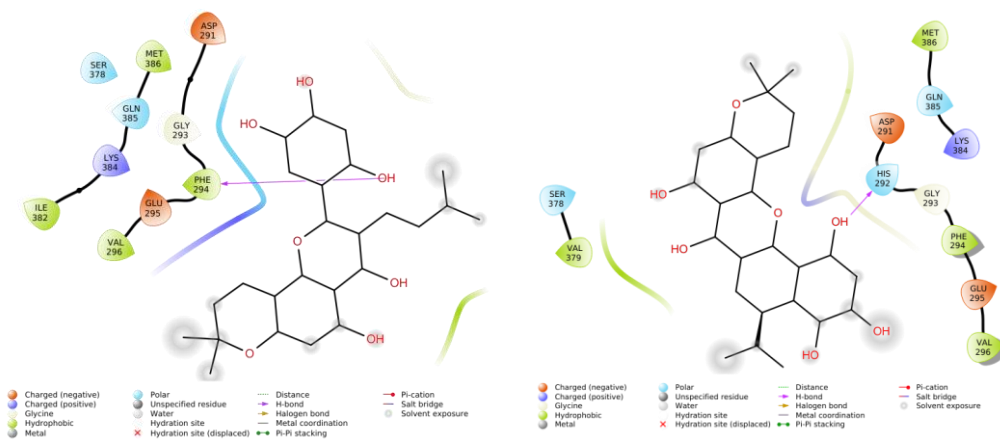


Figure 3B.4: Molecular docking with **1JXQ** (A) AA2 (B) AA3

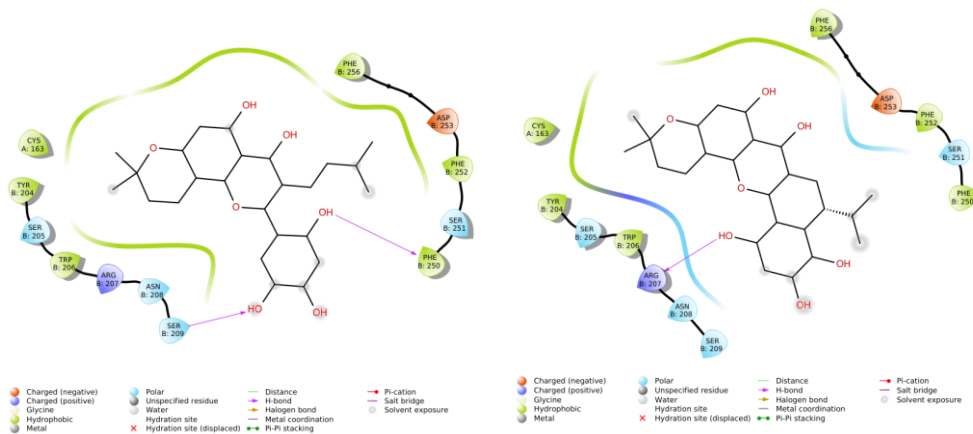


Figure 3B.5: Molecular docking with **IGFW** (A) AA2 (B) AA3

3B.2.2.2. Molecular Dynamics: Further, the molecular dynamics simulations (100ns, OPLS-2005 forcefield) of the protein-ligand complexes, 2O21-AA2 and 2O21-AA3, were carried out to demonstrate the stability and suitability of the complexes formed between the ligands and the protein 2O21 (Figure 3B.6). The RMSD plot consists of dual plots of both protein (left Y axis) and the ligands-AA2/AA3 (right Y axis), clearly distinguished in different colours and adequately labeled. The RMSD plot indicates that the ligands AA2 and AA3 are stable inside the binding pocket of the receptor protein throughout the trajectories. The ligands are highly stable inside the protein's binding pocket with RMSD of less than 1Å. Even though the protein shows fluctuations from the mean position initially, it seems stable at the end of the trajectory with RMSD of less than 5Å. The protein-ligand histogram depicts the H-bond interactions (AA2 with ALA146 and AA3 with ARG106) and hydrophobic interactions are the primary force of interactions that hold the ligands inside the binding pocket of the protein (Figure 3B.7).

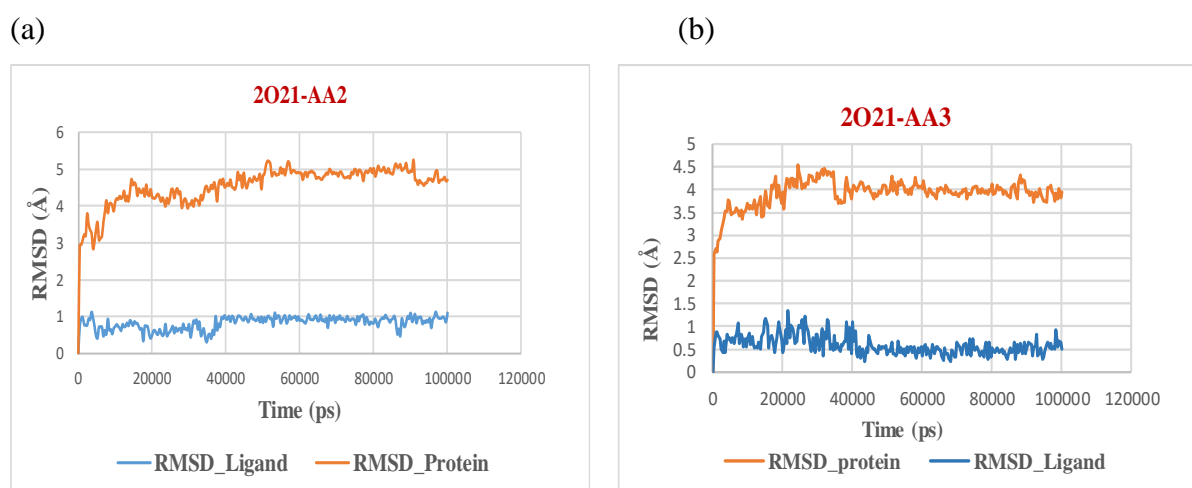


Figure 3B.6: RMSD Plots for the complexes (a) 2O21-AA2 (B) 2O21-AA3

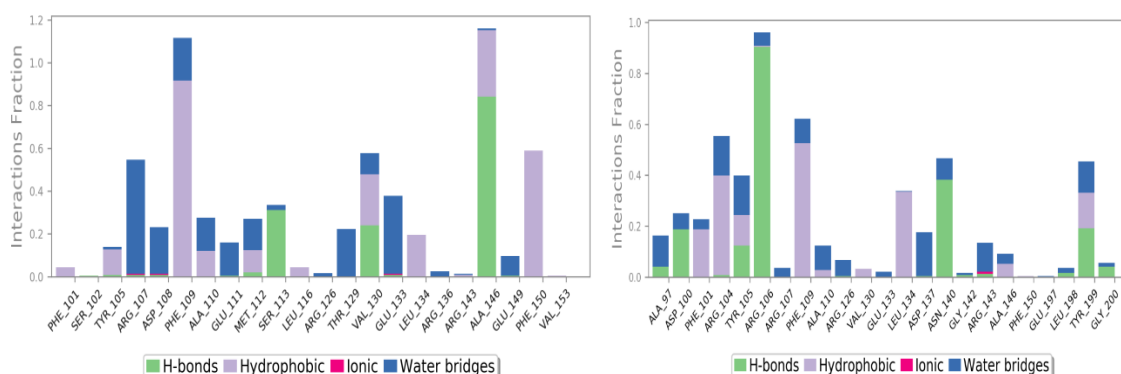


Figure 3B.7: P-L interaction histograms of the complexes, 2O21-AA2 and 2O21-AA3
Based on the cell-specific IC₅₀ values followed by molecular simulation approaches, the selected candidates were subjected to further in-vitro screening assays.

3B.2.3. Effect of AA2 and AA3 in colony formation potential of SAS cells

Next, we performed colony formation assay/ clonogenic assay to evaluate the potential of the active candidates both AA2 and AA3 on the ability of the individual SAS cells to form colonies. As compared with the control, the administration of both AA2 and AA3 unveiled a significant reduction in the formation of colonies in a concentration-dependent manner. In SAS cells treated with AA2, more than 50% of colonies are diminished at a concentration of 2.5 μM and greater than 90% of survival was inhibited followed by the treatment of 5 and 10 μM . Besides, the cells treated with AA3 also reduce the clonogenic potential of SAS cells is not much superior to that of AA2. However, at a concentration of 10 μM , the reduction in the number of colonies was visualized profoundly and become almost vanished at 20 μM . These results together suggest that both AA2 and AA3 (Figure 3B.8) isolated from *Artocarpus altilis* possess potential cytotoxic activities and anti-clonogenic potential against OSCC cells.

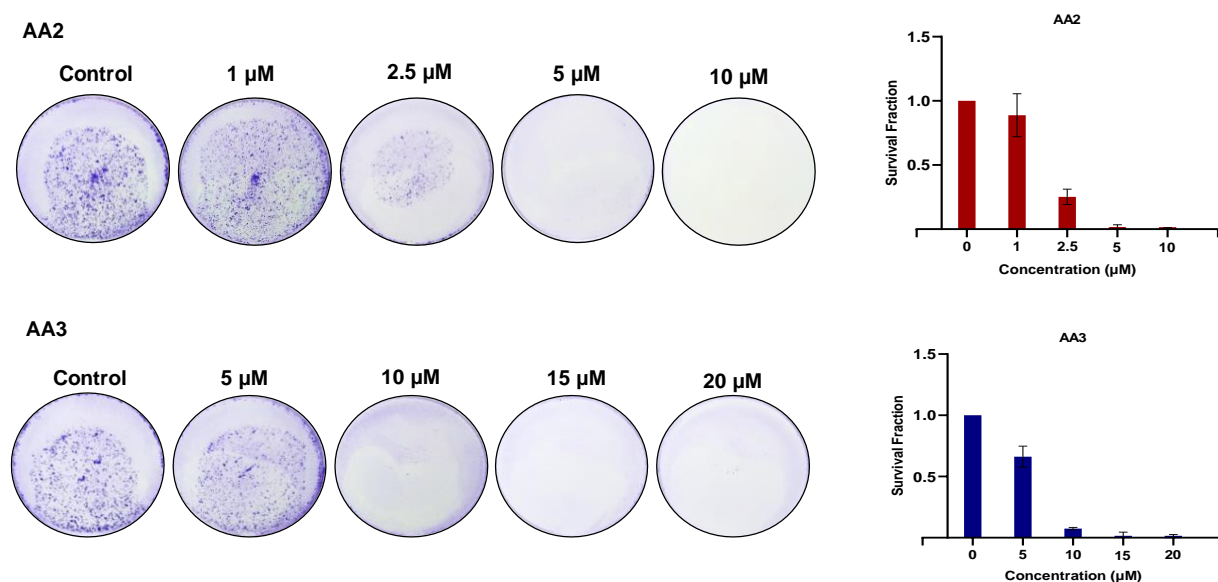


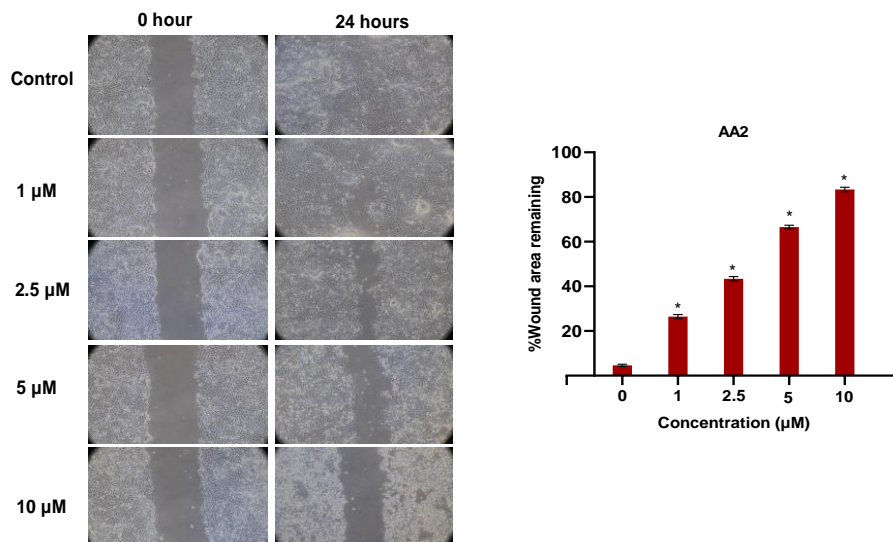
Figure 3B.8: Inhibition of clonogenic potential of SAS cells treated with AA2 and AA3. Quantification of the number of colonies was done with the help of Image J software. Results presented are mean \pm SD of three independent experiments; *, $p < 0.05$ vs control

3B.2.4. Effect of AA2 and AA3 in the migration of SAS cells

Metastasis, a major culprit responsible for cancer-associated mortalities, we have investigated the anti-metastatic potential of both candidates. It is well known the fact that a promising anti-cancer agent should retard the invasion, collective migration, and metastasis of tumour cells. The collective cell migration is allied to embryogenesis, wound repair, cancer metastasis and many other physiological and pathological processes. We next examined the

effect of AA2 and AA3 on the migratory potential of SAS cells. In the scratch assay, it was seen that the control cells without treatment were able to close greater than 90% of the gap created by the 100 μ L tip within 24 hours whereas the cells treated with AA2 and AA3 could not migrate at the same rate. As observed, by the end of 24 hours cells treated with AA2 of 1 μ M were found to have around 25% of wound remaining followed by 40% remaining for 2.5 μ M, over 60% for 5 μ M and over 75% for 10 μ M treated cells. Similarly, AA3 of 5 μ M treated cells remained with over 45% of the gap area, over 60% for 10 μ M cells, over 65% for 15 μ M and 90% of the area remaining to heal for 20 μ M treated cells. These results illustrated that both AA2 and AA3 have substantial potential to inhibit the migration of OSCC cells *in vitro* (Figure 3B.9).

AA2



AA3

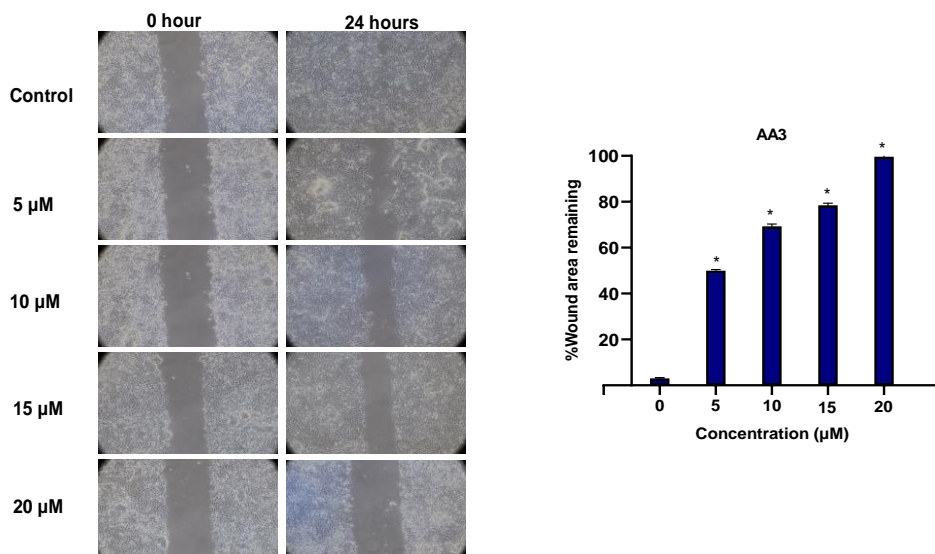


Figure 3B.9: Inhibition of the migration of SAS cells upon treatment with AA2 and AA3. Cells were scratch-wounded and then treated with the indicated concentrations, followed by the recording of wound areas at different time points. Wound area was calculated using Image J software and graph was plotted using Graphpad Prism software. Results were represented as mean \pm SD of three independent experiments and asterisk denotes *, $p < 0.05$ vs control.

3B.2.5. Effect of both AA2 and AA3 in inducing cell death in SAS cells

Evading apoptosis is one of the long-known ‘hallmarks’ of cancer. Therefore, we aimed to understand the effect of AA2 and AA3 on the apoptosis of SAS cells. Firstly, the PI-FACS assay showed that both AA2 and AA3 induced cell death of SAS cells significantly in a concentration-dependent manner. AA2 when treated with 10 μ M was found to induce more than 80% of cell death and AA3 of 20 μ M was found to induce around 8% of cell death. Further, annexin V assay, which is a more specific indicator of apoptosis showed that both AA2 and AA3 remarkably induced apoptosis in a concentration manner (Figure 3B.10).

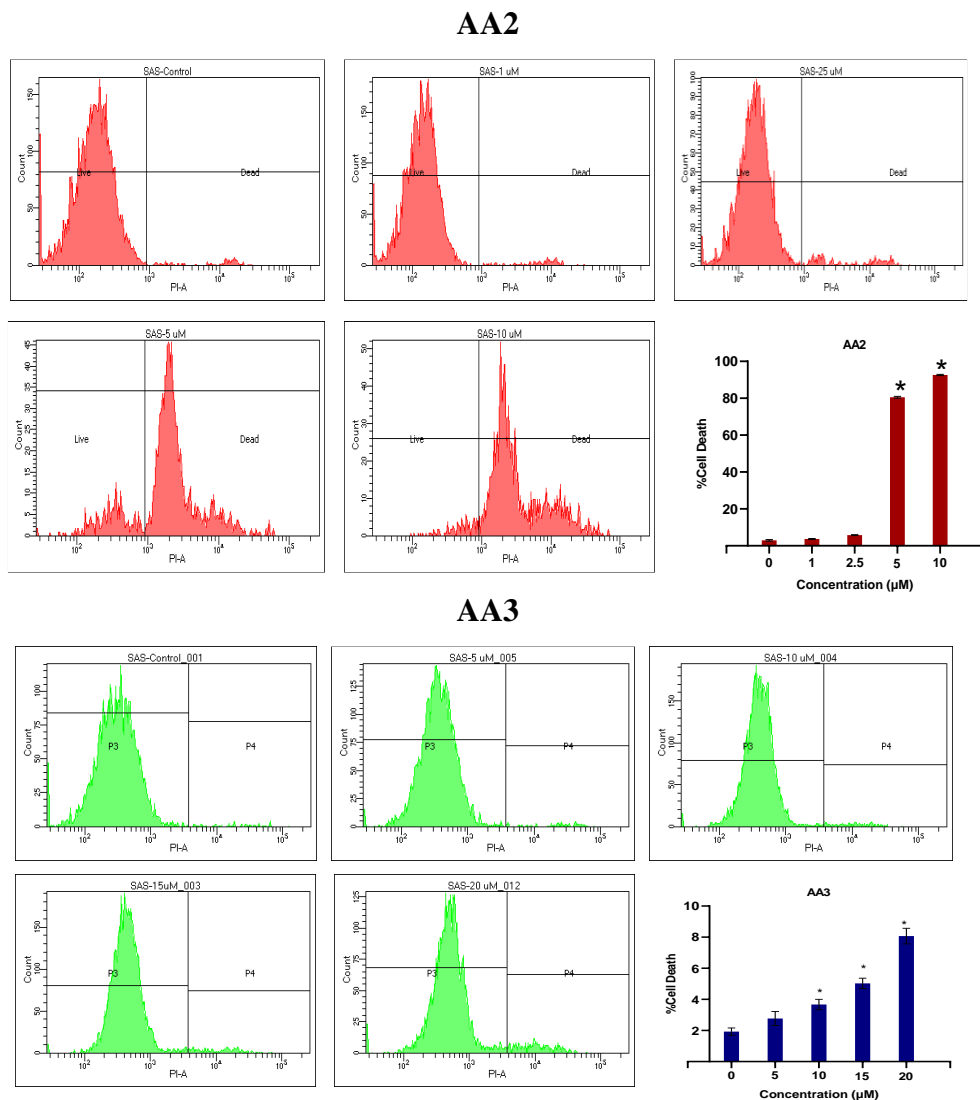
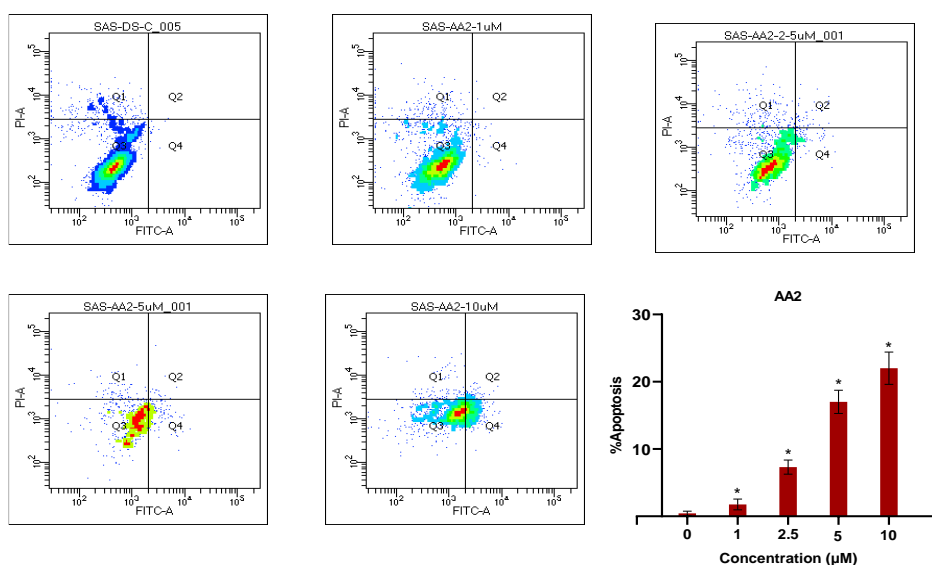


Figure 3B.10: Induction of cell death in SAS cells by AA2 and AA3. Cells were treated with the indicated concentrations for 48 h, followed by PI staining and FACS analysis for the cell death profile. Percentage of cell death was calculated using BDFACS diva software and was plotted using Graphpad Prism software.

3B.2.6. Induction of apoptosis by annexin V assay

Annexin V binding and PI uptake are one of the most frequently used assays to measure apoptosis and necrosis.[34,35]The composition of the healthy cells is comprised of lipids that are asymmetrically distributed on the inner and outer leaflets of the plasma membrane. Phosphatidylserine (PS) is one of such lipids normally located at the inner leaflets of the plasma membrane and its translocation to the external leaflets implemented the process of initiation of apoptosis [36]. Annexin V is a 36-kDa calcium-binding protein showing greater binding affinity with PS and the fluorescently labeled Annexin V can be used to detect PS and that could be used to distinguish cells from apoptosis and necrosis. Hence, we evaluated the potential of AA2 and AA3 in inducing apoptosis by annexin V staining. As compared with the control, the administration of SAS with different concentrations of AA2 increases the percentage of apoptotic cells in a dose-dependent manner. In SAS cells treated with 2.5 μM of AA2 causes 8% of apoptosis that was enhanced to 18% at 5 μM and 22% at 10 μM respectively. Similarly, in AA3 treatment, the percentage of apoptotic cells increases from 8% at 5 μM to 18% at 10 μM , 26% at 15 μM and 30% at 20 μM respectively (Figure 3B.11). Taken together both results, AA2 and AA3 treatment furnishes a statistically evident increase in the number of apoptotic cells thus leading to significant inhibition in the growth of SAS cells.

AA2



AA3

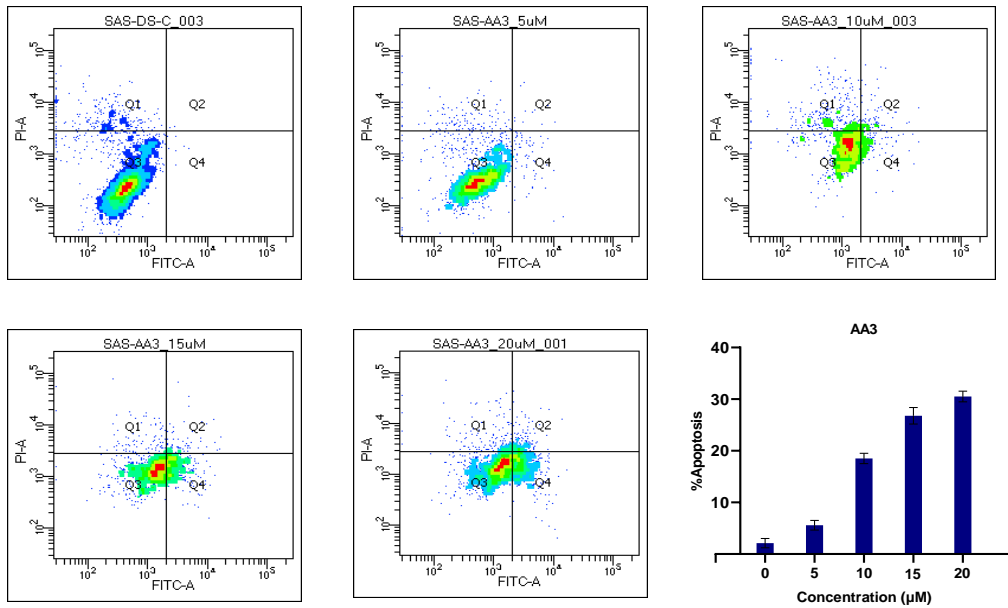
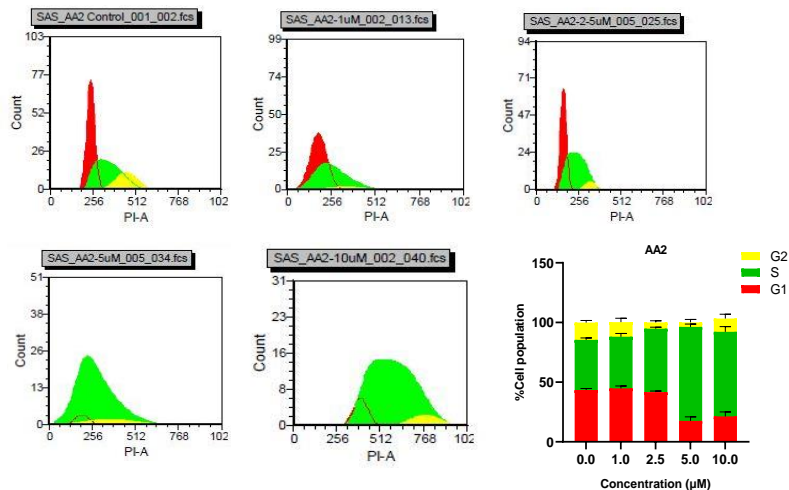


Figure 3B.11: Induction of apoptosis by annexin V assay. Cells were treated with the indicated concentrations for 48 h, followed by Annexin V staining and FACS analysis. The percentage of cells in apoptotic phase was analysed using FACS diva software and is plotted using Graphpad prism software. Statical significance was calculated and * represents p value is less than 0.05.

3B.2.6. AA2, AA3 induced cell cycle arrest in SAS OSCC cells

As AA2 and AA3 inhibited cell proliferation and induced apoptosis, we further examined their control over the cell cycle progression of SAS cells. PI-based flow cytometry analysis showed that both AA2 and AA3 induced S-phase arrest. We observed that after the treatment of AA2 and AA3 percentage of the cell population in the S-phase was increased significantly in a concentration-dependent manner indicating the arrest of these cells at the S-phase (Figure 3B.12).

AA2



AA3

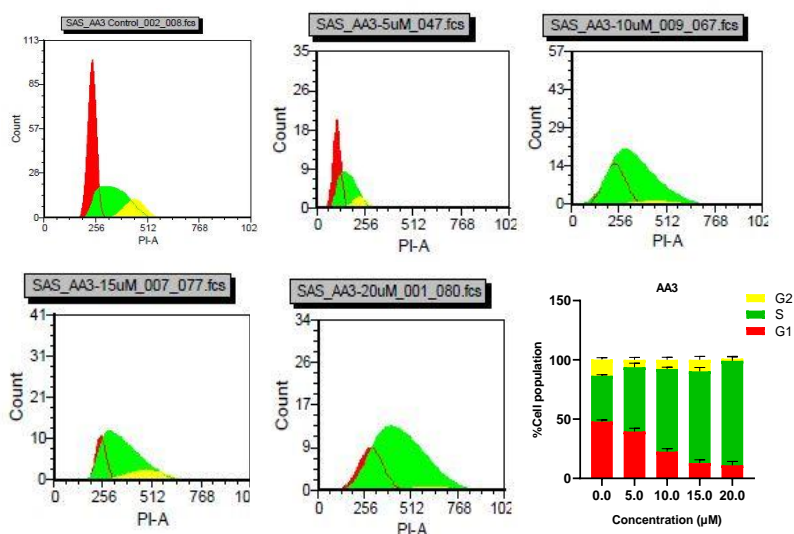


Figure 3B.12: Induction of cell cycle arrest in SAS cells by AA2 and AA3. Percentages of each cell cycle phase were obtained using FCS Express software. Percentage of cell population in each phase was plotted using Graphpad prism software.

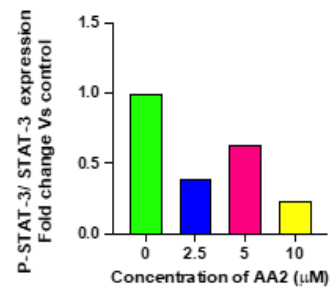
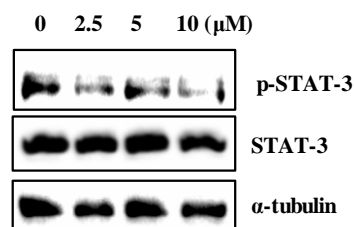
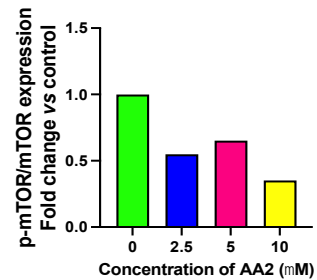
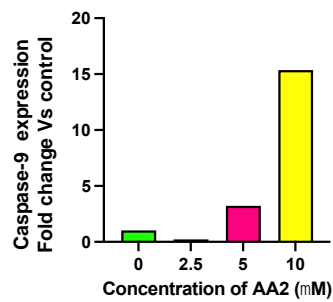
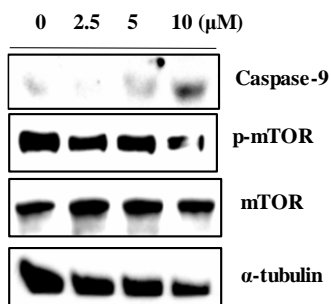
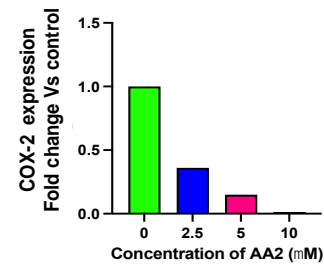
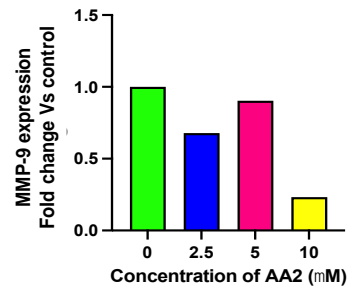
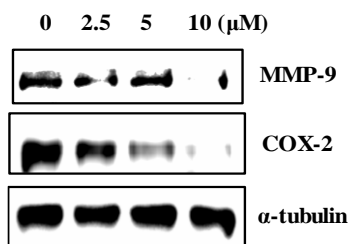
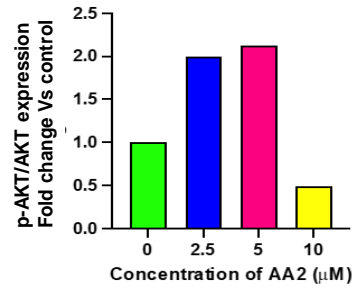
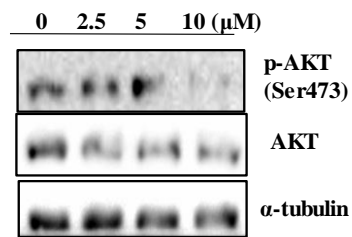
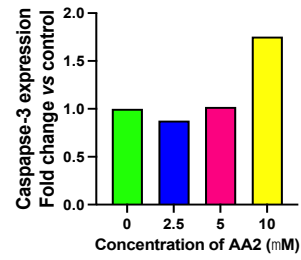
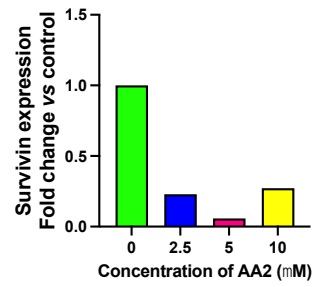
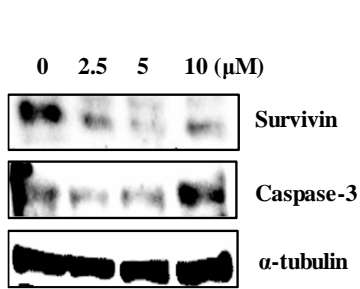
3B.2.7. Effect of AA2 and AA3 in the expression of critical players responsible for survival, inflammation, cell cycle, angiogenesis, migration, and apoptosis of OSCC Cells and the involvement of multiple signaling pathways in the mode of action

The membrane proteins such as MMP-9, COX-2, VEGF, AKT, BCl-2, Survivin, mTOR, and STAT-3 are involved in the various hallmarks of cancers and the overexpression of these receptors responsible for the proliferation, angiogenesis, survival, migration and invasion in cancer cells [37,38]. To the best of our knowledge, the role of AA2 and AA3 on these gene products in human oral squamous cell carcinoma is hitherto uninvestigated. COX-2, the rate-limiting enzyme catalyses the synthesis of prostaglandins and thromboxanes and is frequently associated with regulation and carcinogenesis in several tumours. It promotes angiogenesis, metastasis and deregulates apoptosis in cancer cells and the significant elevation in the expression of COX-2 is highly expressed in various cancers like breast, lung, colorectal and squamous cell carcinoma [39]. AKT is a serine or threonine kinase that plays a pivotal role in the regulation of numerous processes associated with the progression and development of cancer. AKT is overexpressed in many human tumours and thereby promotes cancer cell growth, metabolism, survival, angiogenesis and metastasis [40]. In oral cancer patients, an elevation in the expression of proteins such as PI3K, AKT, and mTOR is frequently observed in the tumour tissues [41]. Ribosomal protein S6 (RPS6), a downstream effector of the

mammalian target of rapamycin pathway (mTOR), is triggered with the early event of the tumour progression, hence it is treated as a potential biomarker for the early detection of OSCC [42]. Survivin is a unique member of the inhibitor of apoptosis and is intuitively associated with cell survival and apoptosis [43]. Furthermore, cellular proliferation, vascular permeability and endothelial cell migration, etc. are accelerated by the fundamental regulator of angiogenesis known as VEGF. It is a heparin-binding cellular protein mainly involved in vascular permeability, hence the inhibition of VEGF expression leads to decreased cell proliferation and tumour progression [44]. The role of VEGF in OSCC samples was elucidated by various research groups such as the level of VEGF can be used as a tool for monitoring cancer progression. Moreover, various studies have shown that MMP-2 and MMP-9 are potential diagnostic markers for oral cancer detection [45].

To propose a detailed mechanism underlying the action of the bioactive candidates in the various events of cancer progression, western blot analyses were employed. The critical protein players such as survivin, caspase-3, caspase-9, MMP-9, S6, p-S6, mTOR, p-mTOR, AKT, p-AKT, VEGF, COX-2, Bcl-2, STAT-3, p-STAT-3 are selected along with the positive control α -tubulin for immunoblotting analysis. Apoptosis/ programmed cell death is the main mechanism involved in the progression and homeostasis in normal tissue through the elimination of unnecessary cells and caspase cascades are involved in both extrinsic and intrinsic pathways of apoptosis. Here, we observed that both AA2 and AA3 treatment triggered mitochondria-mediated apoptosis by the upregulation in the expressions of both caspase-3 and caspase-9 cascades. Moreover, both compounds treatment causes a down-regulation in the expression of anti-apoptotic proteins BCL-2. AA2 and AA3 were found to inhibit the expression of critical players such as survivin, S6, phospho S6, phospho STAT-3, and COX-2 indicating a reduction in the survival potential of SAS cells. Besides, the decrease in p-AKT and p-mTOR was found to be in line with the increased expression of apoptotic genes. Further, reduced expression of COX-2, VEGFA and MMP-9 after the treatment of AA2 and AA3 compared to untreated control cells indicated that these compounds inhibited migration and invasion of SAS cells (Figure 3B.13 & Figure 3B.14). Taken together, immunoblotting results showed that AA2 and AA3 triggered apoptosis, reduced survival and migratory potential of SAS cells by inhibiting Akt/mTOR signaling (Figure 3B.15).

AA2



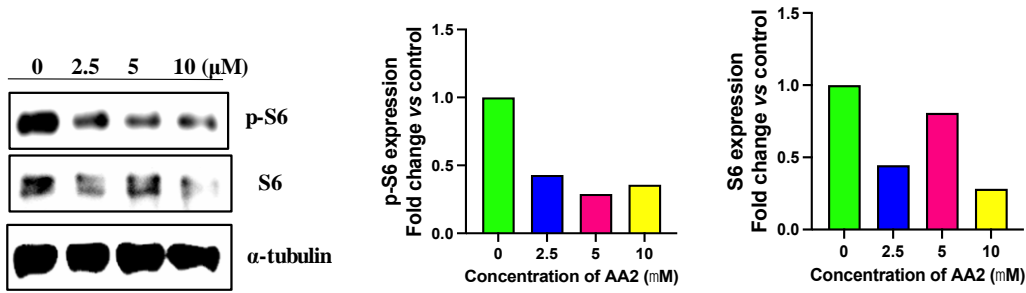
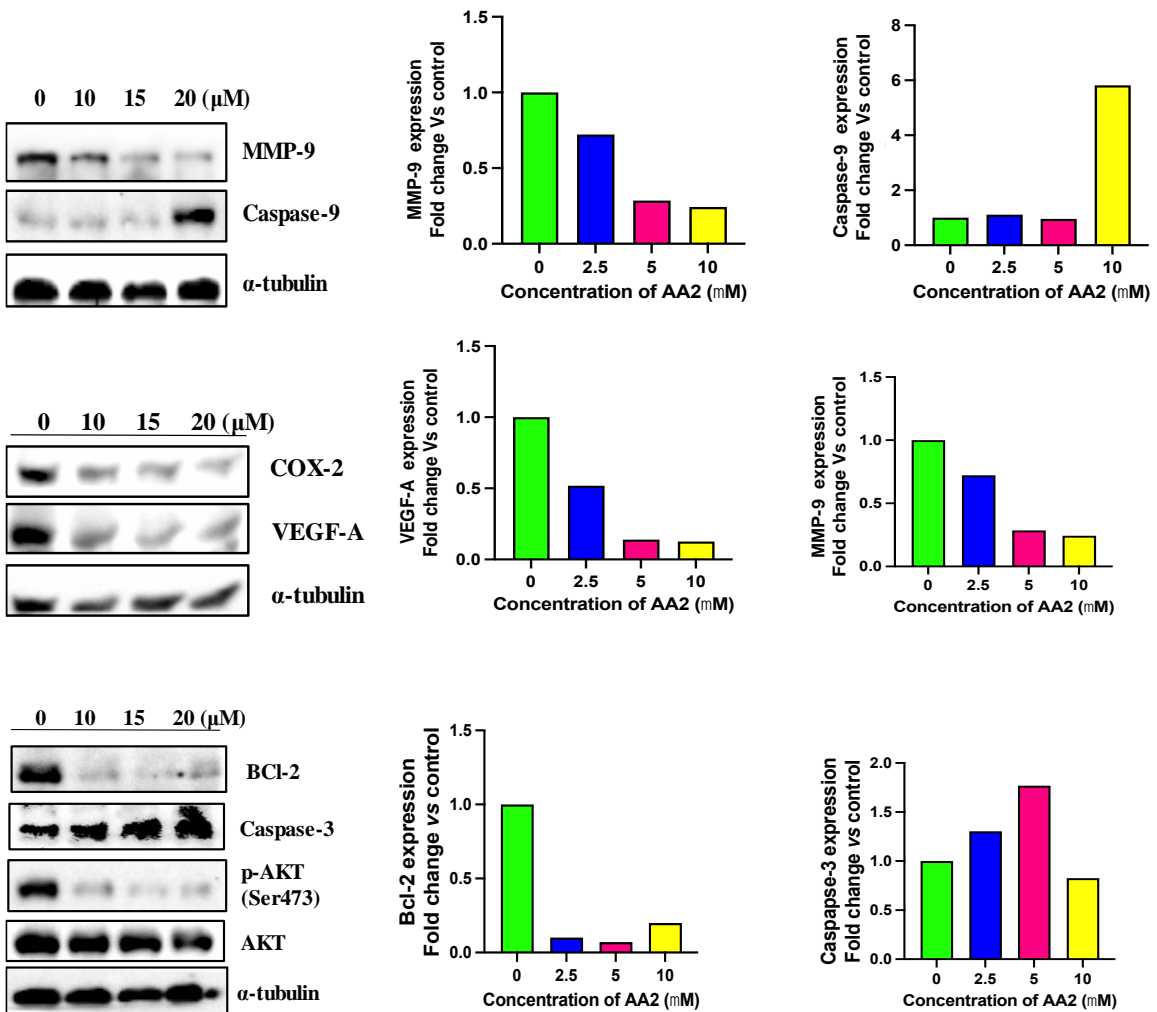


Figure 3B.13: Expression of various proteins in SAS cells upon treatment with AA2 as examined by Western blot analysis. α - tubulin was used as housekeeping control

AA3



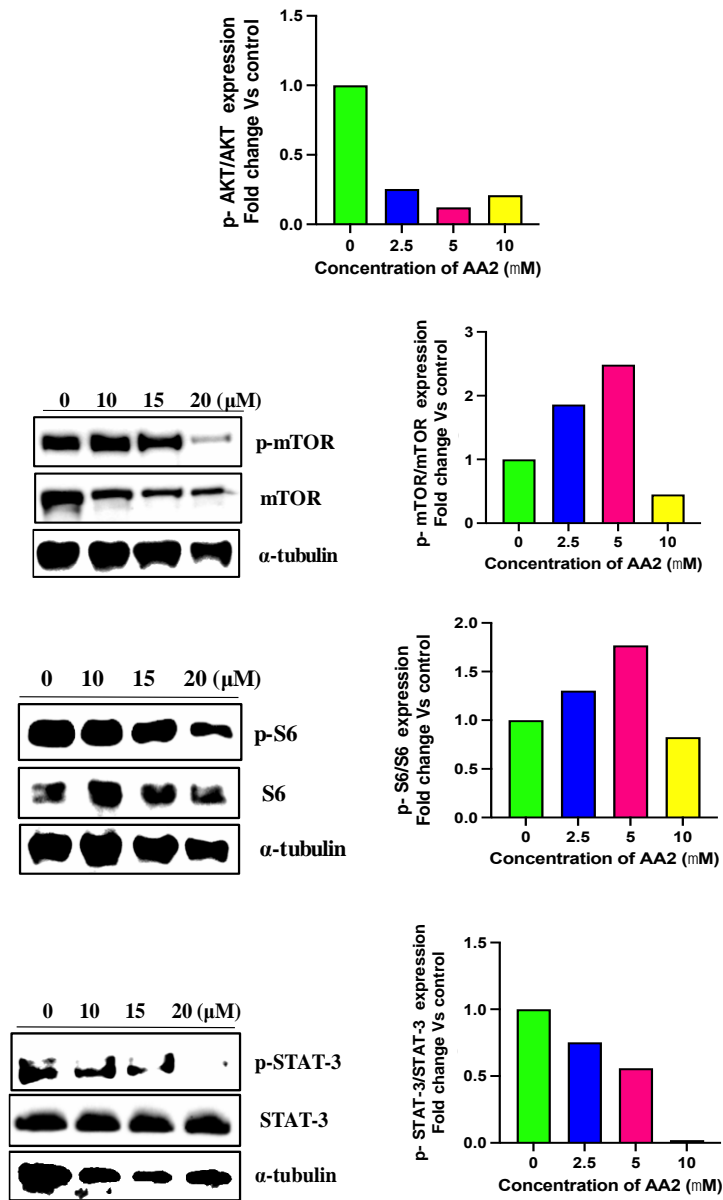


Figure 3B.14: Expression of various proteins in SAS cells upon treatment with AA3 as examined by Western blot analysis. α - tubulin was used as housekeeping control.

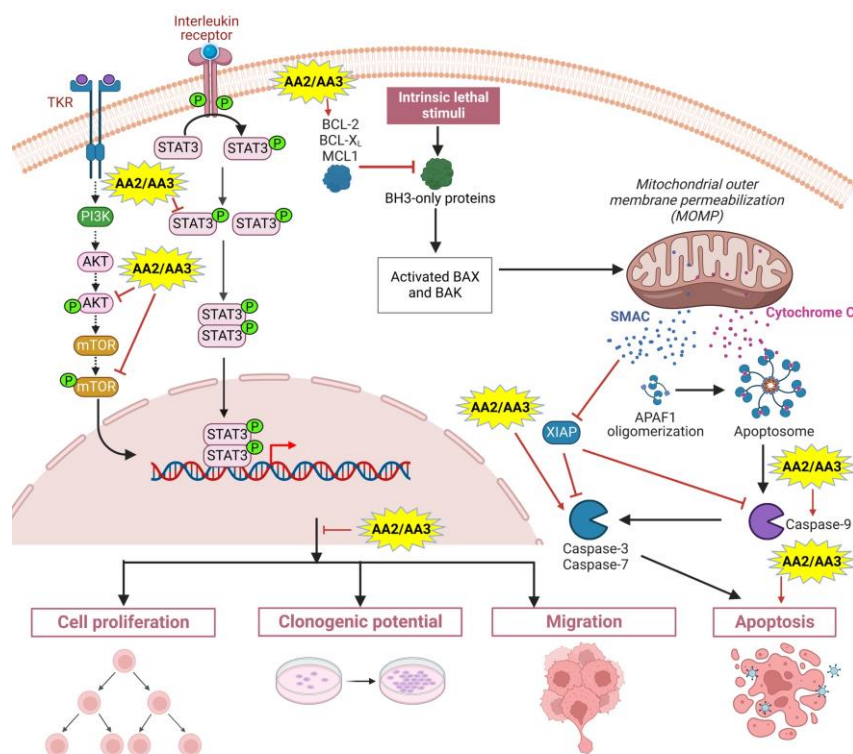


Figure 3B.15: Pathway deciphering the mechanistic mode of action with AA2 and AA3 treatment in SAS cells.

3B.3. Conclusions

We have unveiled the anti-cancer effect of two flavone isolated from the acetone extract of the stem bark of *Artocarpus altilis* (Parkinson) Fosberg for the inhibition and prevention of the growth and multiplication of SAS oral cancer cells. The disclosed bioactive flavonoids artonin E (AA2) and artobiloxanthone (AA3) have isoprenyl substitution and pyranoxanthone moiety respectively. Both AA2 and AA3 effectively inhibited the proliferation of SAS cells having an IC_{50} value of 6 μ M and 12 μ M respectively after 72 hr. The preliminary in-vitro screening was further supported with insilico molecular modeling approaches such as molecular docking and molecular dynamics simulations. Additionally, the various in-vitro screening assays viz, clonogenic assays, PI- FACS analysis, wound healing assay, annexin V staining, and western blot analysis were performed to demonstrate the anti-cancer effect of the ubiquitous candidates. Moreover, the mechanistic rationale behind the mode of action was illustrated with immunoblotting analysis and demonstrated changes in the expression of various critical protein players involved in cancer progression and development. The downregulation of the expression of the anti-apoptotic protein BCL-2 and the activation of caspases including caspase-3 and caspase-9 substantiates the induction of apoptosis and cell death by regulating mitochondria-

mediated apoptotic pathway. The downregulation in the expression of the proteins such as AKT, p-AKT, mTOR, p-mTOR, STAT-3, and p-STAT-3 indicated the involvement of the AKT/ mTOR signaling pathway in their mode of action.

3B.4. Experimental Section

3B.4.1 General Experimental Procedure: The ^1H (500 MHz) and ^{13}C (125 MHz) NMR spectra were recorded on Bruker ASCENDTM- 500 MHz NMR spectrometer. Chemical shifts are expressed in δ (ppm) parts using TMS as an internal standard with solvent deuterated CHCl_3 (CDCl_3) having residual peaks at $\delta_{\text{H}} -7.26$ ppm, $\delta_{\text{C}} -77.30$ ppm and with deuterated acetone (CD_3COCD_3) having residual peaks at $\delta_{\text{H}} -2.05$ ppm, $\delta_{\text{C}} -29.70$ and 206.70 ppm respectively. Coupling constants in Hz with Multiplicity (s (singlet); d (doublet); t (triplet); q (quartet); dd (double doublet); and m (multiplet). Mass spectra were recorded with Agilent QTOFG6545 spectrometer at 50,000 resolutions using ESI mode. Column chromatography was performed by using 100-200 and 230-400 mesh silica (Merck, Darmstadt, Germany) and Thin Layer Chromatography (TLC) by Merck precoated silica gel F₂₅₄ plates. Spots were detected on TLC under UV light and by charring the TLC plate after spraying with p-anisaldehyde-sulphuric acid solution. Reagents were purchased at the highest commercial quality and used without further purification. All solvents used for column chromatography were purchased from Merck.

3B.4.2. Plant Material: The stem bark of *Artocarpus altilis* was collected from Calicut, Kerala, India. The plant material was identified by the taxonomists of Jawaharlal Nehru Botanical Garden of India (JNTBGRI), Palode, Thiruvananthapuram, Kerala.

3B.4.3. Extraction and Isolation of Phytochemicals

The pulverised material (900 g) was subjected to sequential extraction with hexane, acetone and ethanol at room temperature for 3 days. The corresponding crude extracts were concentrated using a Heidolph rotary evaporator at a temperature of 50 °C afforded hexane (5g, 0.5%), and acetone (45 g, 5.0%) respectively. The bioactive candidates AA2 and AA3 were isolated and purified from the acetone extracts using conventional silica gel column chromatography and characterized by various NMR techniques (discussed in chapter 3A).

3B.4.4. Computational Screening and Molecular Dynamics Simulation: The minimization of the proteins and the ligands, receptor grid generation and molecular docking were done with Autodock Vina (Eberhardt et al., 2021). All the analysis and visualizations were done using Chimera 1.13 and Maestro13.5.(Pettersen et al., 2004). The crystal structures of the proteins were retrieved from the RCSB protein databank. All these proteins were refined by adding hydrogens/missing side chains, charges, and minimized. Grids were generated around the

whole proteins, and different conformers of the ligands were chosen at different sites for their binding. The conformer, which shows maximum affinity to a specific site of the protein, with maximum dock score and minimum RMSD, is taken as the best pose. The binding affinities of the ligands to a specific receptor were ranked using dock scores. To depict the stability of these protein-ligand complexes and their interactions, molecular dynamics simulations were done for 100ns using Desmond module of Schrödinger suite under OPLS-2005 force field. (Desmond Molecular Dynamics System, D. E. Shaw Research, New York, NY, 2021. Maestro-Desmond Interoperability Tools, Schrödinger, New York, NY, 2021.)

3B.4.5. Cell culture

SAS (human squamous cell carcinoma of tongue) and TTn (human squamous cell carcinoma of esophagus) cell lines were generously gifted by Prof. Renu Wadhwa, AIST, Japan. These cell lines were maintained in Dulbecco's Minimum Essential Medium (DMEM; Gibco™; Life Technologies, NY, USA) with 10% fetal bovine serum (FBS; Gibco®, NY, USA) and 1X Pen-Strep (Invitrogen, CA, USA). The cells were cultured and maintained at 37 °C, 5% CO₂ and 95% humidity unless otherwise stated.

3B.4.6. Cell proliferation MTT assay

MTT assay was performed to examine the cytotoxic effect of AA2 and AA3 on SAS and TTn cells. Cells were trypsinized and approximately 2000 cells were seeded in 96-well plates per well and incubated for 24 hours at 37°C in a CO₂ incubator. Cells were then treated with various concentration as indicated and incubated for 72 hours. Cells treated with vehicle control were considered as control for the analysis. After the incubation period, 10µl of 5mg/ml of MTT (Sigma-Aldrich, Missouri, USA) was added to each well to the culture medium and incubated for 4 hours. The culture medium was discarded and 100µl of DMSO (Merck, Darmstadt, Germany) was added to all the wells. The absorbance was measured at 575nm after the completion of 1h at room temperature. The absorbance was normalized using 0 hour reading and percentage of proliferation was calculated considering the control as 100%.

3B.4.7. Colony formation assay

To evaluate the effect of compounds, AA2 and AA3, on the clonogenic potential of OSCC cells, colony formation assay was conducted. Briefly, SAS cells were seeded at a density of 500 cells per well in a 6-well plate and cultured in 2mL DMEM medium with 10 % FBS. After 24 hours of seeding, 1, 2.5, 5 and 10 µM of AA2 or AA3 was added to each well. Untreated cells were considered as control followed by 24 hours incubation. The media was then removed and replaced with fresh media of 2mL and cultured for 10 days. Fresh medium was added as

required. The plates were thoroughly washed with 1X PBS thrice and the cells were fixed with 70% ethanol. Ethanol was removed and plates were washed again with 1X PBS and stained with 0.01% (w/v) crystal violet (SRL Pvt. Ltd., Mumbai, India). Plates were again washed several times gently to remove the excess stain using 1X PBS. The images of each well were captured. Plating efficiency and survival fraction was calculated using the formula:

PE, Plating efficiency = (Number of colonies counted/ Number of cells plated) × 100

SF, Survival fraction = (PE of treated sample/ PE of control) × 100

3B.4.8. Wound healing assay

Next, we evaluated the effects of AA2 and AA3 on the migratory potential of SAS cells using scratch assay. For this, approximately SAS cells 5×10^5 cells were seeded per well of 6 well plates and allowed them to form a monolayer. The medium was then replaced with serum-free DMEM medium to inhibit the proliferation of cells. The cells were incubated in serum free medium for 6-8 hours for the adaptation. A scratch was then introduced across the monolayer using a 100 μ L tip. The detached cells and debris were washed using 1X PBS and then treated with the either AA2 or AA3 of 1, 2.5, 5, and 10 μ M concentrations. The plates were then monitored every 2 hours until the migration is completed in the control (untreated) wells. Images were captured at different time intervals and analysed using image J software (NIH, USA). The percentage of wound area remaining was then plotted using Graphpad Prism 9.0.

3B.4.9. PI-FACS analysis

Then we performed the propidium iodide (PI) based fluorescence-activated cell sorting (FACS) assay to determine the effect of AA2 and AA3 on the SAS cell death rate. The SAS cells were seeded at the density of 5×10^4 cells per well in a 6 well plate and incubated for 24 hours. The cells were treated with 1, 2.5, 5, and 10 μ M of AA2 or 5, 10, 15, 20 μ M of AA3 to the plate. Untreated was considered to be control. All the plates were then incubated for 48 hours. The media was collected in the respective labelled polystyrene test tubes (5x77mm). The cells were trypsinized and collected in the respective labelled polystyrene test tubes. These suspensions were centrifuged at 4000 rpm for 10 mins at 4°C. Supernatant was discarded, and the pellet was washed with 1X PBS and centrifuged at 4000 rpm for 10 minutes. This step was repeated three times. The pellet was then suspended in 495 μ l of PBS followed by the addition of 5 μ l of PI (Sigma-Aldrich, Missouri, USA). The cells were then analysed in flow cytometer (BD FACS Celesta™, Becton-Dickinson, New Jersey, USA). The percentage of dead cells in each condition was plotted using Graphpad Prism 9.0.

3B.4.10. Annexin V assay

We performed annexin V assay to determine the percentage of cells undergoing apoptosis after the treatment of AA2 and AA3. SAS cells were seeded at the density of 5×10^4 cells/well of 6 well plate. After 24 hours of incubation, the cells were treated with various concentrations of AA2 (1, 2.5, 5, and 10 μM) or AA3 (5, 10, 15, 20 μM) for 48 hours. The cells which were not treated were considered as control. After completion of 48 hours, medium was collected from all the wells in the respective labelled polystyrene test tubes. The cells were trypsinized and washed thrice with 1X PBS and pelleted at 4000 rpm for 10mins at 4°C . The control cells were divided as stained (stained with both PI and annexin V) and unstained. All the tubes with treated cells and control (stained) cells were incubated with 2.5 μL of annexin and incubated for 20 minutes. The cells were then treated with PI. These stained cells were analysed using flow cytometer (BD FACS Celesta™, Becton-Dickinson, New Jersey, USA). The percentage of cell population stained with both PI and annexin in each condition were plotted using Graphpad Prism 9.0.

3B.4.11. Cell cycle analysis

In the next step, we performed flow cytometry assisted cell cycle analysis using PI to understand the effect of AA2 and AA3 on cell cycle progression of SAS cells. Briefly, 2×10^5 cells were plated in 6 well plates and allowed to divide for 24 hours. Subsequently, the cells were collected by trypsinization and washed with 1X PBS three times. The cells were then fixed with 75% ethanol overnight at -20°C . Care was taken not to form the cell clumps during ethanol addition. Ethanol was later removed by washing with 1X PBS and centrifugation at 4000 rpm for 10 minutes. The cells were stained with Propidium Iodide (PI)/RNase solution and incubated for 20 minutes in the dark. After 20 minutes, cells were analyzed using flow cytometer (BD FACSCelesta™, Becton-Dickinson, New Jersey, USA). The percentage of cells in each phase of the cell cycle was analyzed using FCS express software and plotted using Graphpad Prism 9.0.

3B.4.12. Western blot analysis

Next, we performed immunoblotting analysis to understand the molecular mechanism behind the AA2 and AA3 anti-cancer activities. Cells were seeded at the density of 1×10^5 cells in each well of 6 well plate and incubated at 37°C incubator for 24 hours. The cells were treated with different concentrations of AA2 (2.5, 5, and 10 μM) or AA3 (10, 15, and 20 μM) and untreated was considered as control. Total protein lysates were prepared using lysis buffer (2 mM EDTA, 20 mM HEPES buffer, 0.1% (v/v) Triton-X100, 250 mM NaCl and protease inhibitors

including 2 µg/mL Aprotinin, 1 mM DTT, 2 µg/mL Leupeptin hemisulfate and 1 mM PMSF). Concentration of protein in the lysates were analysed using Bradford protein assay (Bio-rad, California, USA). Equal concentrations of total protein were then loaded on to 10% on a 15% sodium dodecyl sulfate (SDS)-polyacrylamide gel with 5X Laemmli Buffer and ran at a voltage of 90 V. The proteins were then transferred on to a nitrocellulose membrane and blocked using 5% non-fat dry milk (Amulya, India). The membrane was then probed with respective primary antibodies for overnight at 4⁰ C followed by three times wash with 1X TBST for 10 minutes each at room temperature. The membrane was then incubated for 2 hours with secondary antibody conjugated with horseradish peroxidase. the mebrane was again washed thrice with 1XTBST to remove unbound residual secondary antibodies. The blots were developed by adding Clarity Western ECL substrate (Bio-Rad, California, USA) and ChemiDoc™ XRS System (Bio-Rad, California, USA). Housekeeping genes GAPDH or α -tubulin was used as loading control.

3B.4.13. Statistical analysis

All the experiments were repeated three times and Student's t-test was employed. The data are represented as mean and standard deviation. The statistical significance p-value < 0.05 as '**', p-value < 0.01 as '***', p-value < 0.001 as '****', was denoted as statistically significant.

References

- [1] E. Khatoon, K. Banik, C. Harsha, B.L. Sailo, K.K. Thakur, A.D. Khwairakpam, R. Vikkurthi, T.B. Devi, S.C. Gupta, A.B. Kunnumakkara, Phytochemicals in cancer cell chemosensitization: Current knowledge and future perspectives, *Semin. Cancer Biol.* 80 (2022) 306–339. <https://doi.org/10.1016/j.semcancer.2020.06.014>.
- [2] K. Banik, A.M. Ranaware, C. Harsha, T. Nitesh, S. Girisa, V. Deshpande, L. Fan, S.P. Nalawade, G. Sethi, A.B. Kunnumakkara, Piceatannol: A natural stilbene for the prevention and treatment of cancer, *Pharmacol. Res.* 153 (2020) 104635. <https://doi.org/10.1016/j.phrs.2020.104635>.
- [3] A.B. Kunnumakkara, P. Anand, B.B. Aggarwal, Curcumin inhibits proliferation, invasion, angiogenesis and metastasis of different cancers through interaction with multiple cell signaling proteins, *Cancer Lett.* 269 (2008) 199–225. <https://doi.org/10.1016/j.canlet.2008.03.009>.
- [4] S.A. Gharat, M. Momin, C. Bhavsar, Oral squamous cell carcinoma: Current treatment

- strategies and nanotechnology-based approaches for prevention and therapy, *Crit. Rev. Ther. Drug Carrier Syst.* 33 (2016) 363–400. <https://doi.org/10.1615/CritRevTherDrugCarrierSyst.2016016272>.
- [5] C. Harsha, K. Banik, H.L. Ang, S. Girisa, R. Vikkurthi, D. Parama, V. Rana, B. Shabnam, E. Khatoon, A.P. Kumar, A.B. Kunnumakkara, Targeting akt/mTOR in oral cancer: Mechanisms and advances in clinical trials, *Int. J. Mol. Sci.* 21 (2020) 1–26. <https://doi.org/10.3390/ijms21093285>.
- [6] F. Bray, J. Ferlay, I. Soerjomataram, R.L. Siegel, L.A. Torre, A. Jemal, Global cancer statistics 2018: GLOBOCAN estimates of incidence and mortality worldwide for 36 cancers in 185 countries, *CA. Cancer J. Clin.* 68 (2018) 394–424. <https://doi.org/10.3322/caac.21492>.
- [7] P. Chaturvedi, A. Singh, C. Chien, Tobacco related oral cancer, 2142 (2019) 1–10. <https://doi.org/10.1136/bmj.l2142>.
- [8] P. Chen, Q. Mahmood, G.L. Mariottini, T. Chiang, K. Lee, Adverse Health Effects of Betel Quid and the Risk of Oral and Pharyngeal Cancers, *Biomed Res. Int.* 2017 (2017) 1–24.
- [9] J.T. Reidy, E.E. McHugh, L.F.A. Stassen, A review of the role of alcohol in the pathogenesis of oral cancer and the link between alcohol-containing mouthrinses and oral cancer., *J. Ir. Dent. Assoc.* 57 (2011) 200–202.
- [10] V.J. Coglianò, R. Baan, K. Straif, Y. Grosse, B. Lauby-secretan, F. El Ghissassi, V. Bouvard, Preventable Exposures Associated With Human Cancers, *JNCI J. Natl. Cancer Inst.* (2011) 1827–1839. <https://doi.org/10.1093/jnci/djr483>.
- [11] A.K. Singh, N.K. Roy, D. Bordoloi, G. Padmavathi, K. Banik, A.D. Khwairakpam, A.B. Kunnumakkara, P. Sukumar, Orai-1 and Orai-2 regulate oral cancer cell migration and colonisation by suppressing Akt/mTOR/NF- κ B signalling, *Life Sci.* 261 (2020) 118372. <https://doi.org/10.1016/j.lfs.2020.118372>.
- [12] J. Monisha, N.K. Roy, G. Padmavathi, K. Banik, D. Bordoloi, A.D. Khwairakpam, F. Arfuso, A. Chinnathambi, T.A. Alahmadi, S.A. Alharbi, G. Sethi, A.P. Kumar, A.B. Kunnumakkara, NGAL is downregulated in oral squamous cell carcinoma and leads to

- increased survival, proliferation, migration and chemoresistance, *Cancers (Basel)*. 10 (2018) 1–18. <https://doi.org/10.3390/cancers10070228>.
- [13] A. Valsan, M.T. Meenu, V.P. Murali, B. Malgija, A.G. Joseph, P. Nisha, K.V. Radhakrishnan, K.K. Maiti, Exploration of Phaeanthine: A Bisbenzylisoquinoline Alkaloid Induces Anticancer Effect in Cervical Cancer Cells Involving Mitochondria-Mediated Apoptosis, *ACS Omega*. (2023). <https://doi.org/10.1021/acsomega.3c01023>.
- [14] M.T. Meenu, G. Kaul, M. Shukla, K.V. Radhakrishnan, S. Chopra, Cudraflavone C from *Artocarpus hirsutus* as a Promising Inhibitor of Pathogenic, Multidrug-Resistant *S. aureus*, Persisters, and Biofilms: A New Insight into a Rational Explanation of Traditional Wisdom, *J. Nat. Prod.* 84 (2021) 2700–2708. <https://doi.org/10.1021/acs.jnatprod.1c00578>.
- [15] M.T. Meenu, G. Kaul, A. Akhir, M. Shukla, K.V. Radhakrishnan, S. Chopra, Developing the Natural Prenylflavone Artocarpin from *Artocarpus hirsutus* as a Potential Lead Targeting Pathogenic, Multidrug-Resistant *Staphylococcus aureus*, Persisters and Biofilms with No Detectable Resistance, *J. Nat. Prod.* 85 (2022) 2413–2423. <https://doi.org/10.1021/acs.jnatprod.2c00621>.
- [16] M.T. Meenu, A.R. Cherian, D.R. Sherin, A.R. Nair, T.K. Manojkumar, K.V. Radhakrishnan, A. Varghese, A protoberberine alkaloid based ratiometric pH-responsive probe for the detection of diabetic ketoacidosis, *Dye. Pigment.* 194 (2021) 109636. <https://doi.org/10.1016/j.dyepig.2021.109636>.
- [17] M. Aswathy, K. Banik, D. Parama, P. Sasikumar, C. Harsha, A.G. Joseph, D.R. Sherin, M.K. Thanathu, A.B. Kunnumakkara, R.K. Vasu, Exploring the cytotoxic effects of the extracts and bioactive triterpenoids from *dillenia indica* against oral squamous cell carcinoma: A scientific interpretation and validation of indigenous knowledge, *ACS Pharmacol. Transl. Sci.* 4 (2021) 834–847. <https://doi.org/10.1021/acspsci.1c00011>.
- [18] U.B. Jagtap, V.A. Bapat, *Artocarpus*: A review of its traditional uses, phytochemistry and pharmacology, *J. Ethnopharmacol.* 129 (2010) 142–166. <https://doi.org/10.1016/j.jep.2010.03.031>.
- [19] M.H. Jang, X.L. Piao, J.M. Kim, S.W. Kwon, J.H. Park, Inhibition of cholinesterase and

- amyloid- β ; aggregation by resveratrol oligomers from *Vitis amurensis*, *Phyther. Res.* 20 (2006) 1052–1055. <https://doi.org/10.1002/ptr>.
- [20] T. Nomura, Y. Hano, M. Aida, Isoprenoid-substituted flavonoids from *Artocarpus* plants (moraceae), *Heterocycles.* 47 (1998) 1179–1205. [https://doi.org/10.3987/REV-97-SR\(N\)9](https://doi.org/10.3987/REV-97-SR(N)9).
- [21] E.H. Hakim, S.A. Achmad, L.D. Juliawaty, L. Makmur, Y.M. Syah, N. Aimi, M. Kitajima, H. Takayama, E.L. Ghisalberty, Prenylated flavonoids and related compounds of the Indonesian *Artocarpus* (Moraceae), *J. Nat. Med.* 60 (2006) 161–184. <https://doi.org/10.1007/s11418-006-0048-0>.
- [22] S. Boonphong, A. Baramée, P. Kittakoop, Antitubercular and Antiplasmodial Prenylated Flavones from the Roots of *Artocarpus altilis*, *Chiang Mai J. Sci.* 34 (2007) 339–344.
- [23] T. Suhartati, Yandri, J.F. Suwandp, S. Hadi, In vitro and in vivo antiplasmodial activity of oxyresveratrol and artonine isolated from two *Artocarpus* plants in Indonesia, *Orient. J. Chem.* 26 (2010) 825–830.
- [24] K. Yangnok, S. Innajak, R. Sawasjirakij, W. Mahabusarakam, R. Watanapokasin, Effects of Artonin E on Cell Growth Inhibition and Apoptosis Induction in Colon Cancer LoVo and HCT116 Cells, *Molecules.* 27 (2022) 2095. <https://doi.org/10.3390/molecules27072095>.
- [25] I.C. Etti, R. Abdullah, A. Kadir, N.M. Hashim, S.K. Yeap, M.U. Imam, F. Ramli, I. Malami, K.L. Lam, U. Etti, P. Waziri, M. Rahman, The molecular mechanism of the anticancer effect of Artonin E in MDA-MB 231 triple negative breast cancer cells, *PLoS One.* 12 (2017) 1–20. <https://doi.org/10.1371/journal.pone.0182357>.
- [26] C. Bailly, Anticancer mechanism of artonin E and related prenylated flavonoids from the medicinal plant *Artocarpus elasticus*, *Asian J. Nat. Prod. Biochem.* 19 (2021) 45–57. <https://doi.org/10.13057/biofar/f190202>.
- [27] M.A. Rahman, F. Ramli, H. Karimian, F. Dehghan, N. Nordin, H.M. Ali, S. Mohan, N.M. Hashim, Artonin E induces apoptosis via mitochondrial dysregulation in SKOV-3 ovarian cancer cells, *PLoS One.* 11 (2016) 1–23. <https://doi.org/10.1371/journal.pone.0151466>.

- [28] A. Zajmi, N. Mohd Hashim, M.I. Noordin, S.A.M. Khalifa, F. Ramli, H. Mohd Ali, H.R. El-Seedi, Ultrastructural study on the antibacterial activity of artonin e versus streptomycin against *Staphylococcus aureus* strains, *PLoS One*. 10 (2015) 1–12. <https://doi.org/10.1371/journal.pone.0128157>.
- [29] I. Etti, R. Abdullah, A. Kadir, Apoptosis-Inducing Effect of Artonin E in Breast Cancer, in: *Curr. Underst. Apoptosis - Program. Cell Death*, 2018: pp. 1–12. <https://doi.org/10.5772/intechopen.79205>.
- [30] C. Properties, I. Musthapa, J. Latip, H. Takayama, L.D. Juliawaty, E.H. Hakim, Natural Product Communications Prenylated Flavones from *Artocarpus lanceifolius* and their, *Nat. Prod. Commun.* 4 (2009) 927–930.
- [31] K. Plaibua, V. Pongrakhananon, P. Chunchacha, B. Sritularak, P. Chanvorachote, Effects of artonin e on migration and invasion capabilities of human lung cancer cells, *Anticancer Res.* 33 (2013) 3079–3088.
- [32] U.L.B. Jayasinghe, T.B. Samarakoon, B.M.M. Kumarihamy, N. Hara, Y. Fujimoto, Four new prenylated flavonoids and xanthenes from the root bark of *Artocarpus nobilis*, *Fitoterapia*. 79 (2008) 37–41. <https://doi.org/10.1016/j.fitote.2007.07.014>.
- [33] E.H. Hakim, S.A. Achmad, L.D. Juliawaty, L. Makmur, Y.M. Syah, N. Aimi, M. Kitajima, H. Takayama, E.L. Ghisalberti, Prenylated flavonoids and related compounds of the Indonesian *Artocarpus* (Moraceae), *J. Nat. Med.* 60 (2006) 161–184. <https://doi.org/10.1007/s11418-006-0048-0>.
- [34] J. Eberhardt, D. Santos-Martins, A.F. Tillack, S. Forli, AutoDock Vina 1.2.0: New Docking Methods, Expanded Force Field, and Python Bindings, *J. Chem. Inf. Model.* 61 (2021) 3891–3898. <https://doi.org/10.1021/acs.jcim.1c00203>.
- [35] E.F. Pettersen, T.D. Goddard, C.C. Huang, G.S. Couch, D.M. Greenblatt, E.C. Meng, T.E. Ferrin, UCSF Chimera - A visualization system for exploratory research and analysis, *J. Comput. Chem.* 25 (2004) 1605–1612. <https://doi.org/10.1002/jcc.20084>.
- [36] C.P.M. Reutelingsperger, W.L. Van Heerde, Annexin V, the regulator of phosphatidylserine-catalyzed inflammation and coagulation during apoptosis, *Cell. Mol. Life Sci.* 53 (1997) 527–532. <https://doi.org/10.1007/s000180050067>.

- [37] A. Komoriya, B.Z. Packard, M.J. Brown, M.L. Wu, P.A. Henkart, Assessment of caspase activities in intact apoptotic thymocytes using cell-permeable fluorogenic caspase substrates, *J. Exp. Med.* 191 (2000) 1819–1828. <https://doi.org/10.1084/jem.191.11.1819>.
- [38] L.C. Crowley, B.J. Marfell, A.P. Scott, N.J. Waterhouse, Quantitation of apoptosis and necrosis by annexin V binding, propidium iodide uptake, and flow cytometry, *Cold Spring Harb. Protoc.* 2016 (2016) 953–957. <https://doi.org/10.1101/pdb.prot087288>.
- [39] H. Pei, W. Guo, Y. Peng, H. Xiong, Y. Chen, Targeting key proteins involved in transcriptional regulation for cancer therapy: Current strategies and future prospective, 2022. <https://doi.org/10.1002/med.21886>.
- [40] K.R. Kampen, Membrane proteins: The key players of a cancer cell, *J. Membr. Biol.* 242 (2011) 69–74. <https://doi.org/10.1007/s00232-011-9381-7>.
- [41] A. Ferrandez, S.M. Prescott, O. Medical, R.W. Burt, COX-2 and colorectal cancer, *Curr. Pharm. Des.* 9 (2003) 2229–2251.
- [42] S. Revathidevi, A.K. Munirajan, Akt in cancer: Mediator and more, *Semin. Cancer Biol.* 59 (2019) 80–91. <https://doi.org/10.1016/j.semcancer.2019.06.002>.
- [43] D.M. Ferreira, T.J. Neves, L.G.C.A. Lima, F.A. Alves, M.D. Begnami, Prognostic implications of the phosphatidylinositol 3-kinase/Akt signaling pathway in oral squamous cell carcinoma: overexpression of p-mTOR indicates an adverse prognosis, *Appl. Cancer Res.* 37 (2017) 1–8. <https://doi.org/10.1186/s41241-017-0046-4>.
- [44] R. Chaisuparat, S. Rojanawatsirivej, S. Yodsanga, Ribosomal Protein S6 Phosphorylation is Associated with Epithelial Dysplasia and Squamous Cell Carcinoma of the Oral Cavity, *Pathol. Oncol. Res.* 19 (2013) 189–193.
- [45] M.E. Johnson, E.W. Howerth, Survivin: A bifunctional inhibitor of apoptosis protein, *Vet. Pathol.* 41 (2004) 599–607. <https://doi.org/10.1354/vp.41-6-599>.
- [46] B.K.& F.K.& M.J.F.& M.M.& M.T. Andisheh-t, Upregulation of serum vascular endothelial growth factor and matrix metalloproteinase-3 in patients with oral squamous cell carcinoma, *Tumor Biol.* (2014) 1–5. <https://doi.org/10.1007/s13277-014-1753-z>.

[47] P.S. Patel, Original article clinical significance of mmp-2 and mmp-9 in patients with oral cancer, *Head Neck*. (2007) 564–572. <https://doi.org/10.1002/hed>.

An Organic Brønsted acid, Pentacarbomethoxycyclopentadiene (PCCP) catalysed Stereo-, and Regioselective Glycosidation of Secondary metabolites in Conjunction with *N*-iodosuccinimide

4.1. Introduction

The success and efficiency of glycosidation reactions depends on several factors, starting from protecting groups to match-mismatch between glycosyl donors and acceptors [1,2]. Though there are number of methods available for glycosidation, based on different types of donors, there exists the need to have a robust method for stereoselective and regioselective glycosidation [3]. Pioneering studies from a number of laboratories suggests that O-2 protecting group has a profound influence on the control and extent of stereoselective glycosidation [3–5]. Reports also points to the fact that the results of glycosidation reactions cannot be predicted based on reactivity of donors and acceptors alone [6].

As part of our ongoing interest in natural products of phyto-origin, attaching the saccharide appendages to the aglycones with complete regio- and stereoselectivity is a formidable challenge and requires more focused investigation. Fraser-Reid *et al.* have utilized the nuanced activation of donors and donor-acceptor matching to simplify the oligosaccharide assembly utilizing *n*-pentenyl glycosyl donors (NPGs) and *n*-pentenyl orthoesters (NPOEs) [7–9]. The versatile use of NPG and NPOE by utilizing Lewis acids such as ytterbium and scandium triflates are also reported by Fraser-Reid *et al.* [10–12]. In this context, we were impressed by the pioneering report by Lambert *et al.* on synthesis of an organic Brønsted acid, pentacarbomethoxycyclopentadiene (PCCP, Fig. 1), which is efficiently utilized for catalysing various organic reactions [13]. They have also shown that the pKa of PCCP can be manipulated by changing the five ester groups leading to chiral and achiral PCCP derivatives [14]. There is only sporadic information available on utilizing organic Brønsted acid for saccharide coupling [15–19]. We have initiated our studies on utilizing PCCP (**A/B**, Figure. 4.1), the unique organic Brønsted acid for glycosidation reaction using NPOEs, the preliminary results of our investigations are discussed in this chapter.

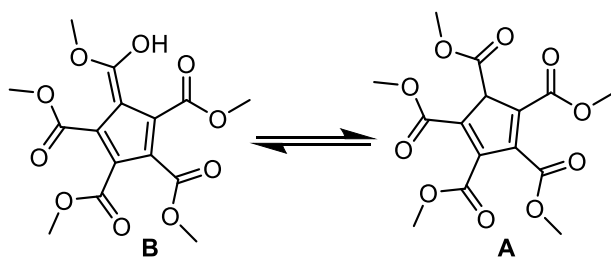


Figure. 4.1 Structure of organic Brønsted acid pentacarbomethoxycyclopentadiene (PCCP).

4.2. Results and Discussion

4.2.1. Synthetic route of Pentacarbomethoxycyclopentadiene (PCCP)

PCCP can be easily synthesized from readily available starting materials such as dimethyl malonate (DMM) and dimethyl acetylene dicarboxylate (DMAD). This synthetic strategy involves two steps that are summarized in the following scheme (Scheme 1). The initial step is the formation of the regioisomer 1,1,2,3,4,5,6,7-octacarbomethoxycycloheptadiene by the combination of DMM (1 equiv.) and DMAD (3 equiv.). In the second step, the formed regioisomer was heated under reflux with aqueous potassium acetate followed by acidification with conc. HCl to generate PCCP as a crystalline solid (60%).

4.2.1.1. Preparation of 1,1,2,3,4,5,6,7-Octacarbomethoxycycloheptadiene

Portion-wise addition of 2.5 mL of equal parts (by weight) of pyridine and acetic acid to a stirred solution of 38 g (0.27 mol) of dimethyl acetylene dicarboxylate (DMAD) and 11.7 g (0.09 mol) of dimethyl malonate in 60 ml of absolute ether resulted in an exothermic reaction. After the vigorous reaction had subsided, the dark red mixture was heated under reflux for 2 h. The resulting solid was collected, washed with ether, and dried with anhydrous sodium sulphate. Then the material was dissolved in minimum volume of methanol, filtered and dried under vacuum. The structure assigned to the product (mixture of two isomers, a and b) was confirmed by the spectral analysis including ^1H NMR and ^{13}C NMR. In ^1H NMR spectrum, the stereogenic protons in both (a) and (b) are resonated at different chemical shifts. The asymmetric proton in (a) resonated as a singlet in the region of δ 4.72 ppm, whereas in (b) it was as a doublet at δ 5.15 ppm. Moreover, all the methoxy protons were resonated at δ 3.88 - 3.69 ppm (Figure 4.2). In ^{13}C NMR, the carbonyl carbon of the ester moieties was resonated at δ 162.5-170.3 ppm. The stereogenic carbons were resonated at δ 44.3 and 34.7 ppm (Figure 4.3).

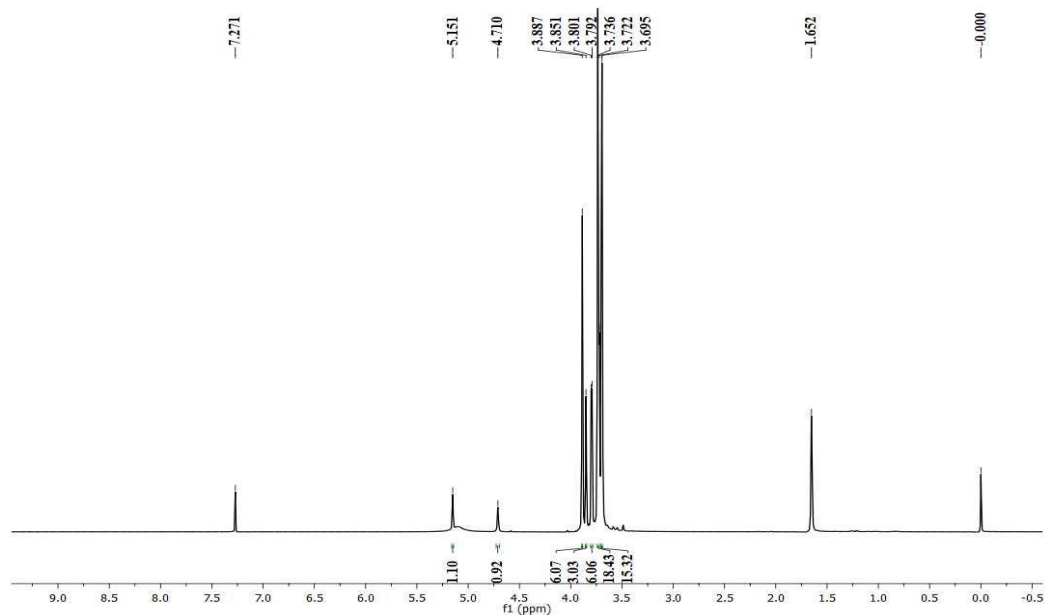


Figure 4.2: ^1H NMR spectrum of the regioisomer (a) and (b)

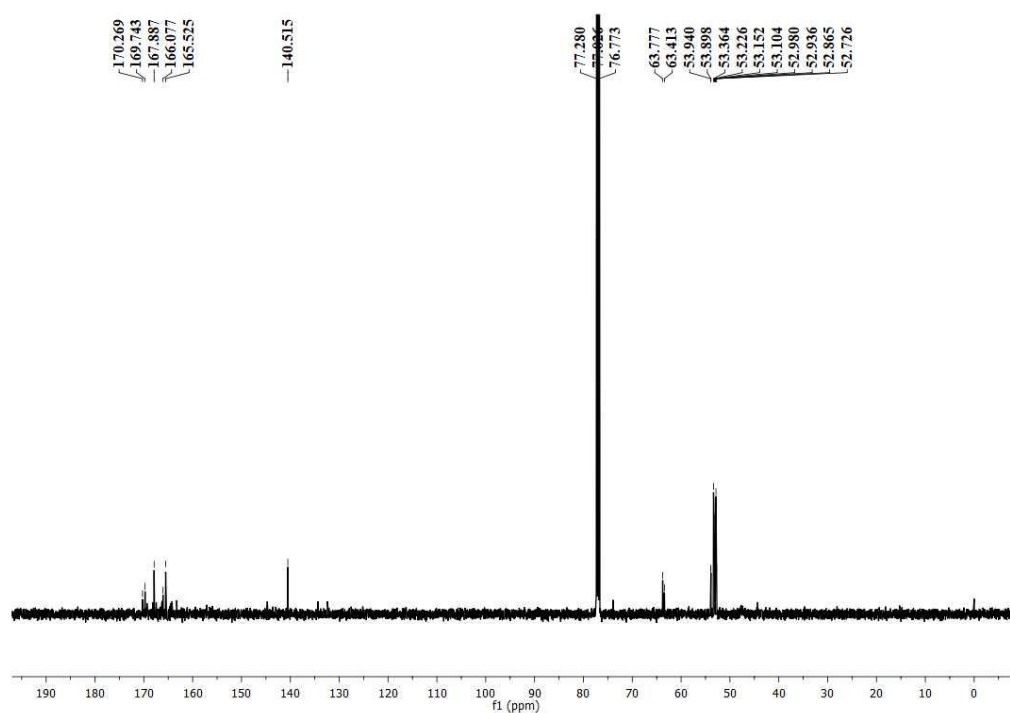
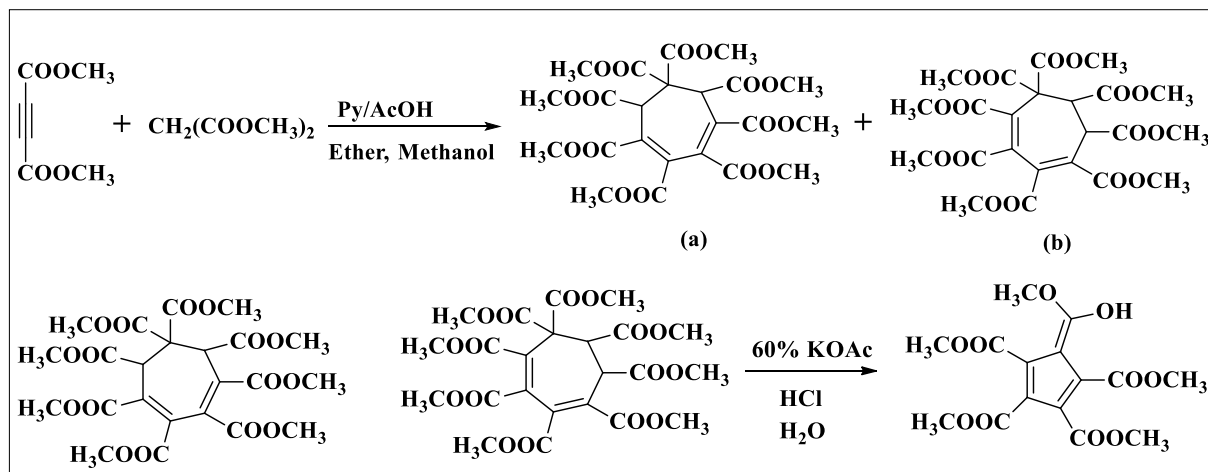


Figure 4.3: ^{13}C NMR spectrum of the regioisomer (a) and (b)

4.2.1.2. Preparation of 1,2,3,4,5-pentacarbomethoxycyclopentadiene (PCCP)

To the regioisomer (10 g), 16.5 g of KOAc (60% KOAc) was added and stirred for 5 h, which results in precipitation of the potassium salt of the Brønsted acid. The resulting salt was acidified with conc. HCl, filtered and dried under vacuum. In the ^1H NMR spectrum, the methoxy protons resonated as a singlet in the region of δ 4.03 - 3.79 ppm. The -OH proton is

highly deshielded due to the intramolecular hydrogen bonding with one of the ester moiety which is observed in the region of δ 20.11 ppm (Figure 4.4). In ^{13}C NMR, peaks resonated between δ 173.0 to 164.3 ppm indicates the presence of ester carbonyl group. The methoxy carbons resonated between δ 51.4 and 55.1 ppm. The olefinic carbons resonated between δ 109.2 to 134.3 ppm (Figure 4.5).



Scheme 1: Two stage synthesis of Pentacarbomethoxycyclopentadiene

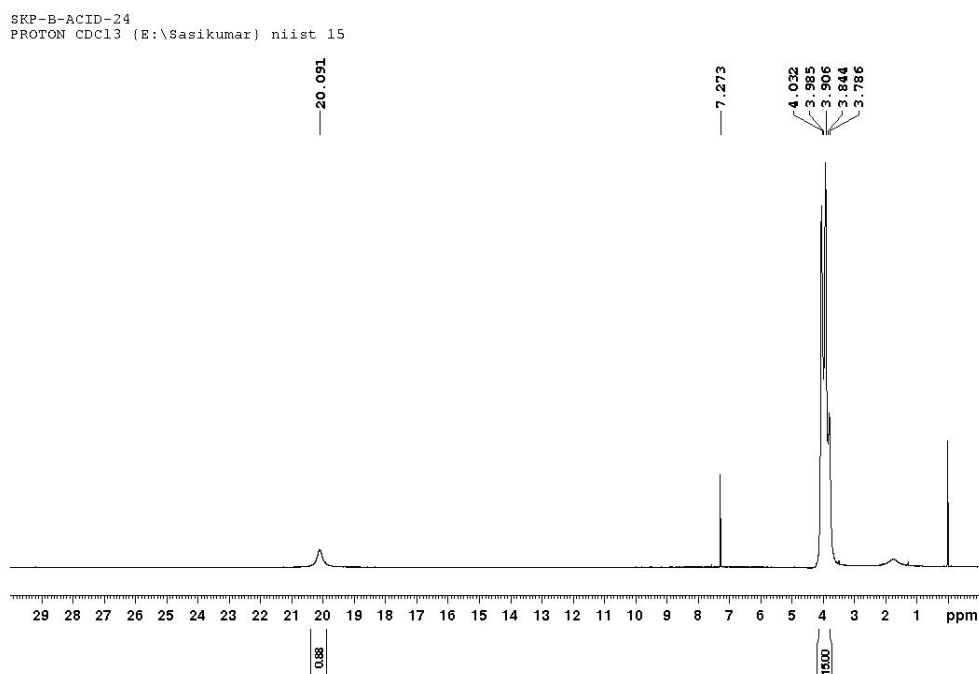


Figure 4.4: ^1H NMR spectra of PCCP

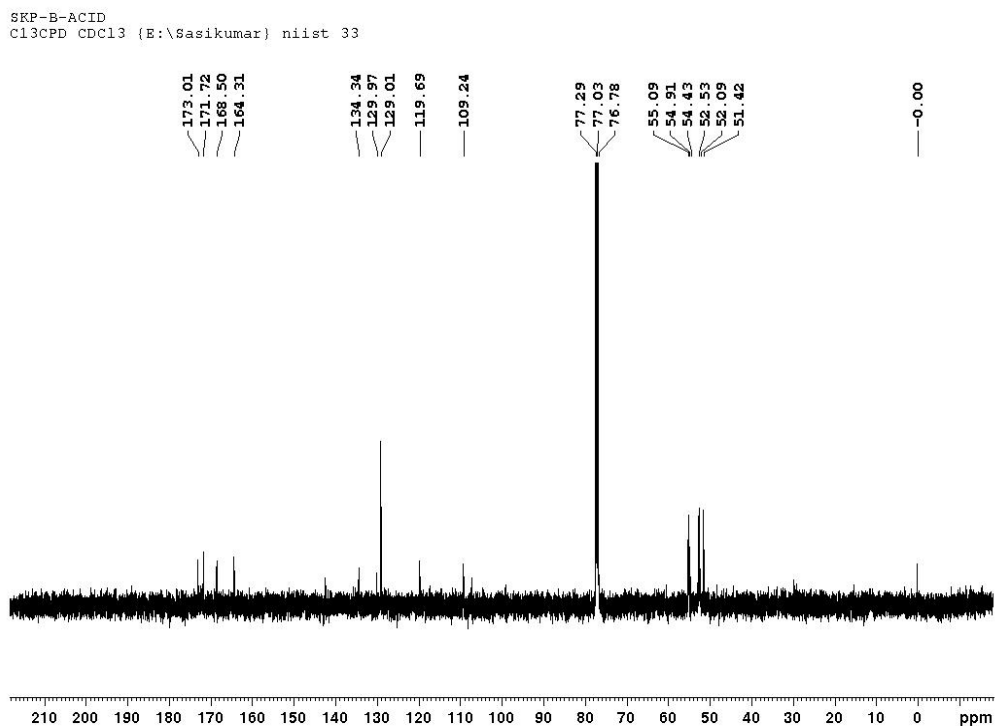


Figure 4.5: ^{13}C NMR spectra of PCCP

4.2.2. Synthesis of *n*-pentenyl orthoester (NPOE) donors

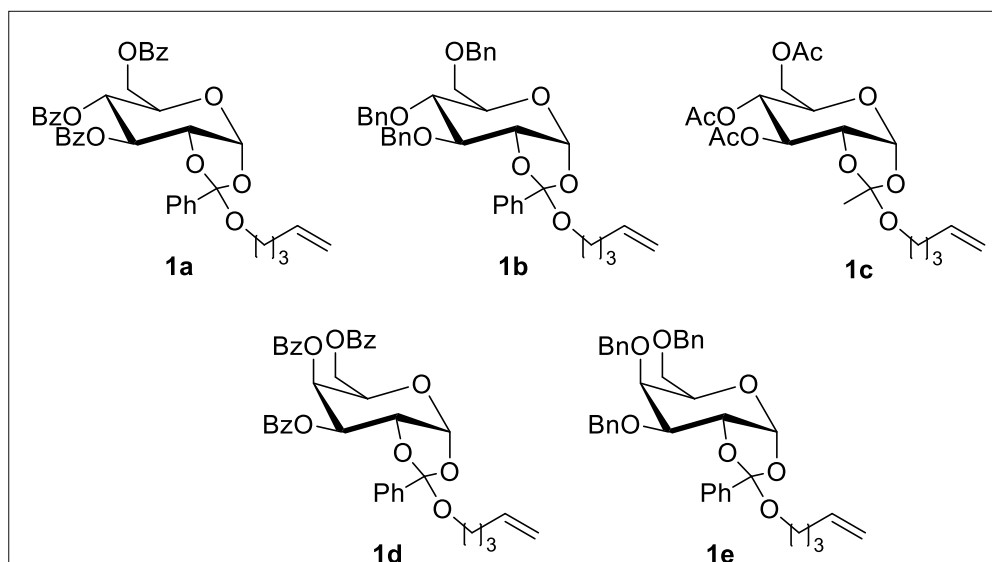


Figure 4.6: Structure of glycosyl donors

3,4,6-Tri-*O*-benzoyl- β -D-glucopyranose-1,2-(pent-4-enyl orthobenzoate)-1a

D-Glucose (20.5 g, 0.114 mol) was dissolved in pyridine (250 mL) and cooled to 0 °C. Benzoyl chloride (86.0 ml, 0.740 mol) was added slowly to the mixture with constant stirring and continued the reaction for 24 h at room temperature. After completion of the reaction by analysing TLC, the excess benzoyl chloride in the reaction mixture was quenched with ice

water. Then the solid residue was dissolved in DCM and treated with 2N HCl, saturated aqueous NaHCO₃, washed with water, dried with anhydrous sodium sulphate, and concentrated to afford crude pentabenzoylate of glucose in 83% yield. The crude material (10 g, 0.014 mol) was dissolved in freshly distilled DCM (60 ml) and cooled to 0 °C. 33% HBr/AcOH (55 ml, 0.982 mol) was added and the mixture was stirred at 0 °C to rt for 3 h. After the complete disappearance of pentabenzoylate, the mixture was diluted with ice-cold water and DCM. Then the organic layer was washed with water, saturated aqueous NaHCO₃, dried over anhydrous sodium sulphate, and concentrated to obtain crude 2,3,4,6-tetra-*O*-benzoyl-β-D-glucopyranosyl bromide in 92% yield. The crude glycosyl bromide (6.0 g, 0.009 mol) was dissolved in dry DCM (30 ml), and 2,6-lutidine (2.92 ml, 0.027 mol), 4-pentenol (2.81 ml, 0.027 mol), and tetra-butyl ammoniumiodide (3.36 g, 0.009 mol) were added. The reaction mixture was refluxed under argon atmosphere overnight. After the complete disappearance of the glycosyl bromide, the reaction mixture was dissolved in more DCM and washed with saturated copper sulphate solution, water, dried over anhydrous sodium sulphate and concentrated. The product **1a** was obtained as colorless syrup in 76% by silica gel column chromatography using 20% EtOAc-Hex as an eluent system.

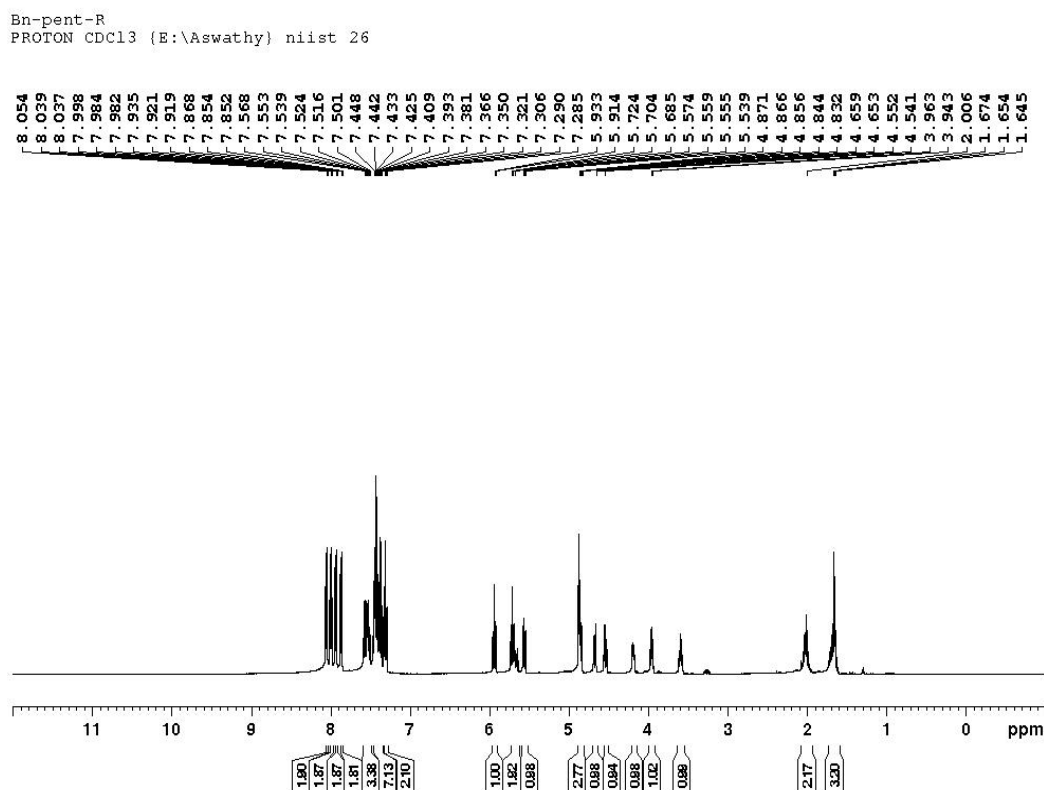


Figure 4.7: ¹H NMR spectra of **1a**

Bn-Pent-R
Cl3CPD CDC13 (E:\Aswathy) niist 3

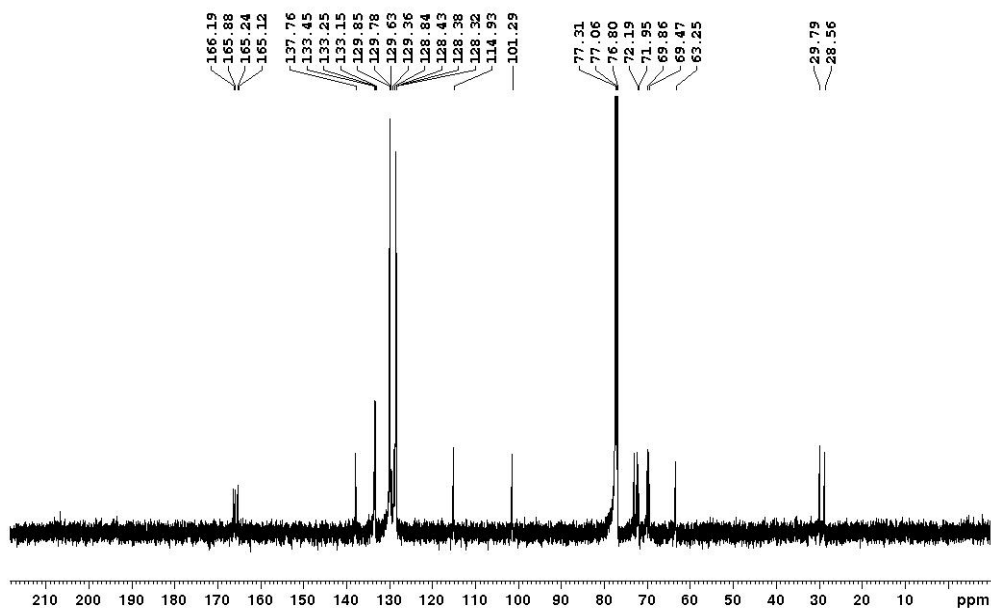


Figure 4.8: ^{13}C NMR spectra of **1a**

The same protocol was also applied for the synthesis of galactose donor **1d**.

GMA-41-1
PROTON CDC13 (E:\Greeshma) niist 5

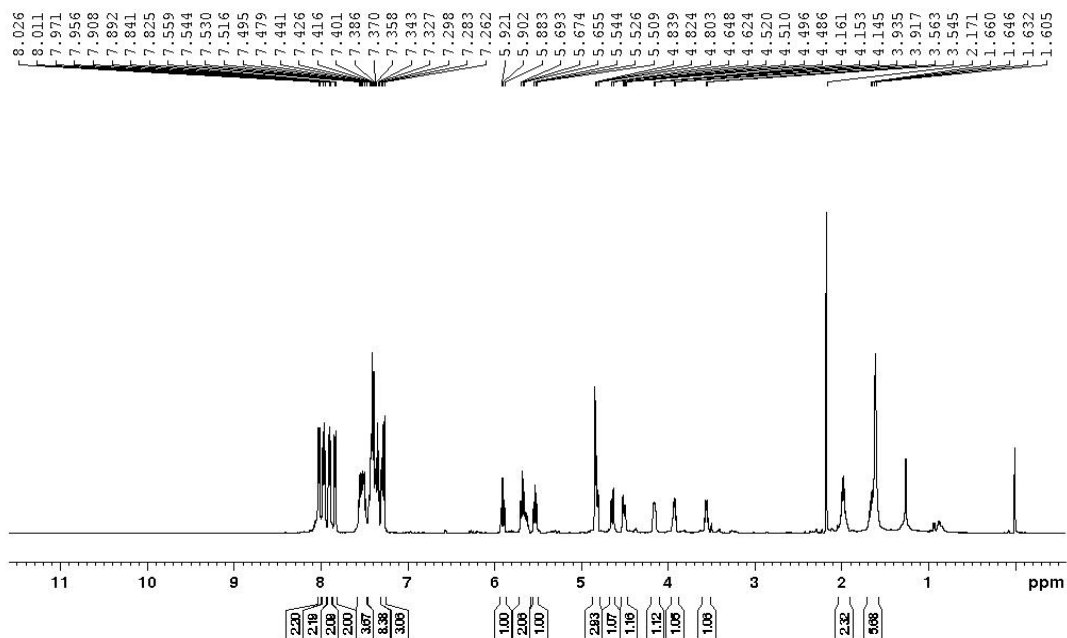


Figure 4.9: ^1H NMR spectra of **1d**

AM-41-1
Cl3CPD CDCl3 {E:\Aswathy} niist 11

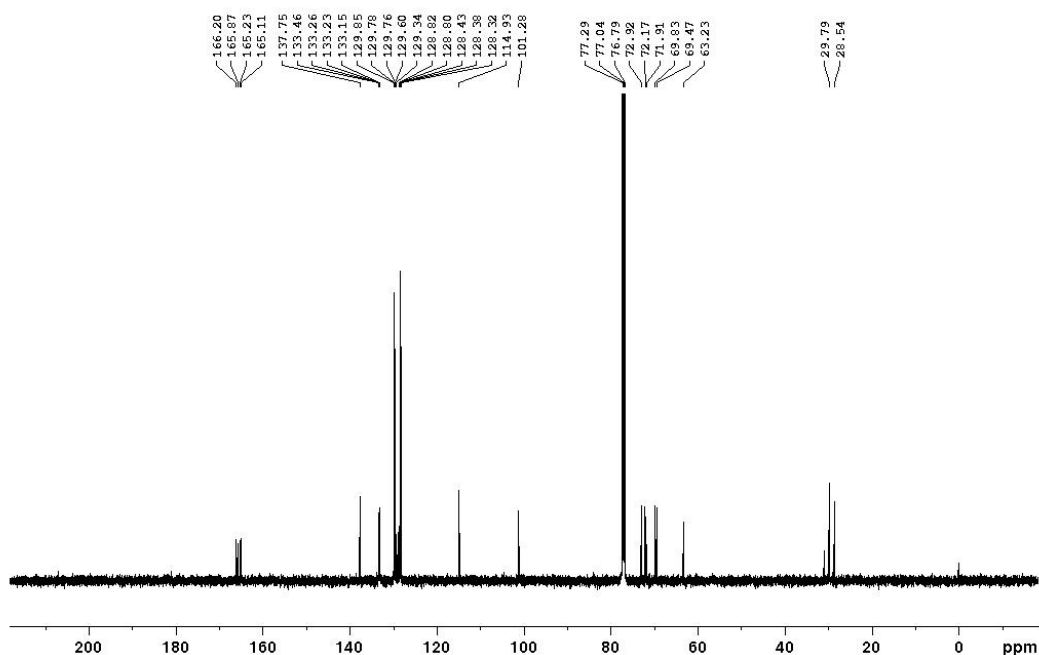


Figure 4.10: ^{13}C NMR spectra of **1d**

The donor **1a** thus obtained was further subjected to desertification by freshly prepared NaOMe solution for 10 min. The crude mixture thus obtained was purified by column chromatography (EtOAc: Hex – 6:4) to afford a colourless syrup, triol. The resultant triol (2.0 g, 0.006 mol) was dissolved in anhydrous *N,N*-dimethyl formamide (30 ml), and sodium hydride (1.36 g, 0.057 mol) was added in portion-wise to the reaction mixture and stirred at rt for 20 min. Benzyl bromide (3.03 ml, 0.025 mol) was slowly added to the reaction mixture in an ice bath, and continued stirring for 2 hr and diluted with DCM. Excess sodium hydride in the reaction mixture was quenched with the careful addition of ice-cold water, washed with water, dried with anhydrous sodium sulphate, and concentrated. The product **1b** was obtained by column chromatography as colourless syrup.

Bz-pent-R
PROTON CDCl3 (E:\Aswathy) niist 27

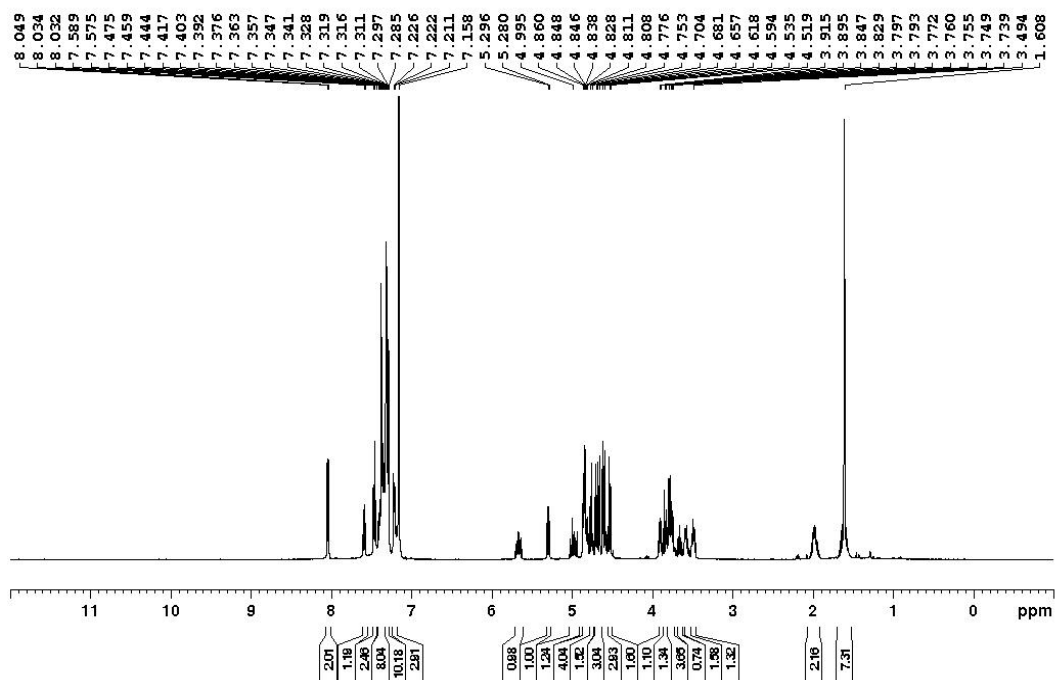


Figure 4.11: ^1H NMR spectra of **1b**

Bz-Pent-R
C13CPD CDCl3 (E:\Aswathy) niist 57

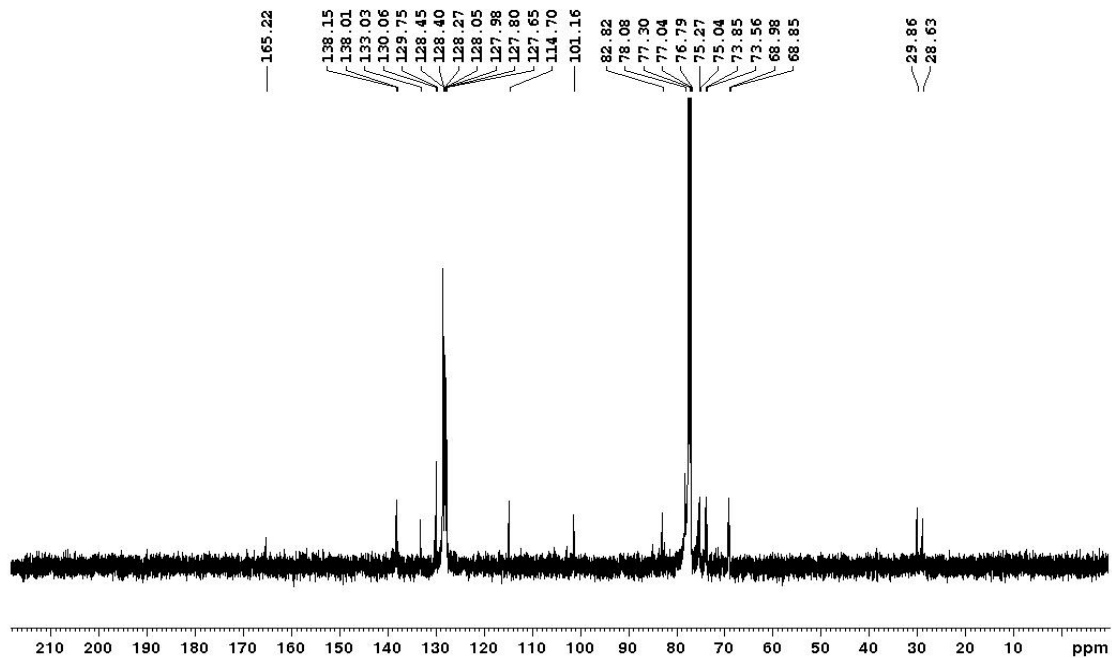


Figure 4.12: ^{13}C NMR spectra of **1b**

The glycosyl donor **1e** obtained from **1d** by applying the same synthetic protocol.

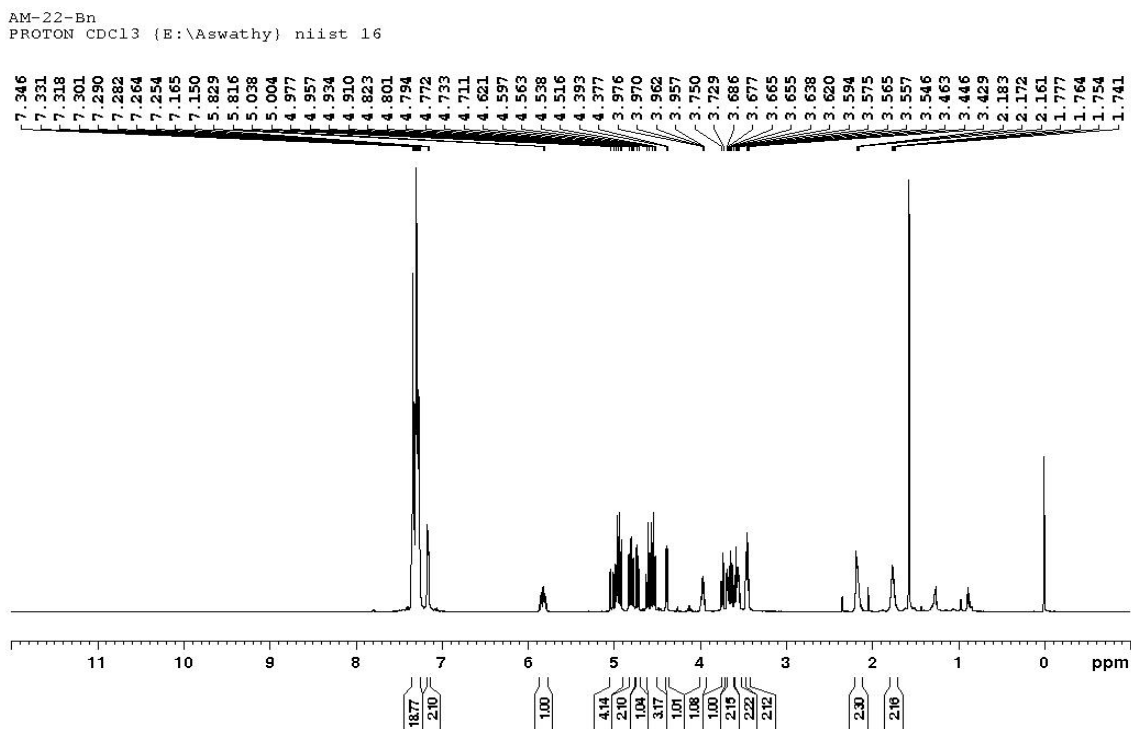


Figure 4.13: ^1H NMR spectra of **1e**

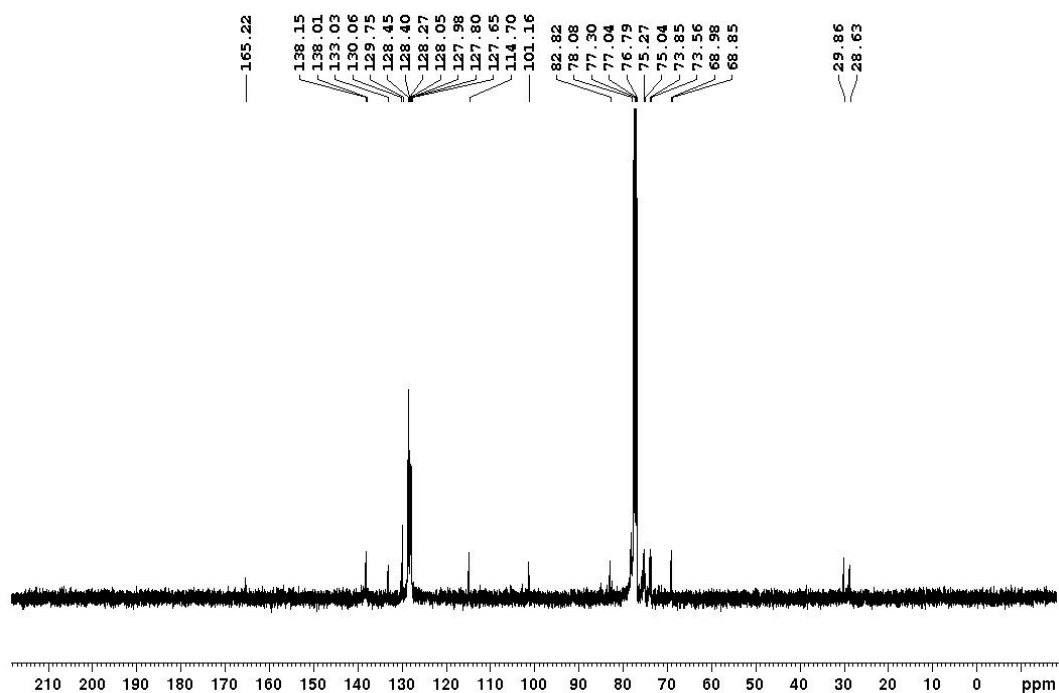


Figure 4.14: ^{13}C NMR spectra of **1e**

For the synthesis of **1c**, D-glucose (2.0 g, 0.011 mol) was dissolved in pyridine (25 ml) and cooled to 0 °C, acetic anhydride (6.82 ml, 0.072 mol) was added slowly to the mixture with constant stirring, and kept the reaction overnight at room temperature. The reaction mixture

was quenched with ice-cold water after completion of the reaction as indicated by TLC. The solid residue was dissolved in DCM and treated with 2N HCl followed by saturated aqueous NaHCO₃. The product was washed with water, dried with anhydrous sodium sulphate, and concentrated to afford crude pentaacetate of glucose in 85% yield. The crude material (2 g, 0.005 mol) was dissolved in freshly distilled DCM (20 ml) and cooled to 0 °C, 33 % HBr/AcOH (19.9 ml, 0.333 mol) was added and the reaction mixture was stirred at 0 °C to rt for 6 h. After analysing TLC, the reaction mixture was diluted with ice-cold water and DCM. Then the organic layer was washed with water, saturated NaHCO₃, dried with anhydrous sodium sulphate and concentrated to obtain crude 2,3,4,6-tetra-*O*-acetyl-β-D-glucopyranosyl bromide in 90 % yield. The crude glycosyl bromide (1.0 g, 0.002 mol) was dissolved in dry DCM (15 ml), and 2,6-lutidine (0.85 ml, 0.007 mol), 4-pentenol (0.75 ml, 0.007 mol), and tetra butyl ammonium iodide (0.898 g, 0.002 mol) were added. The reaction mixture was refluxed under argon atmosphere overnight. After the complete disappearance of the glycosyl bromide, the reaction mixture was dissolved in excess DCM and washed with saturated copper sulphate solution, water, dried and concentrated. The product **1c** was obtained as colourless oil in 80% yield by column chromatography using 40 % EtOAc-Hex as an eluent system.

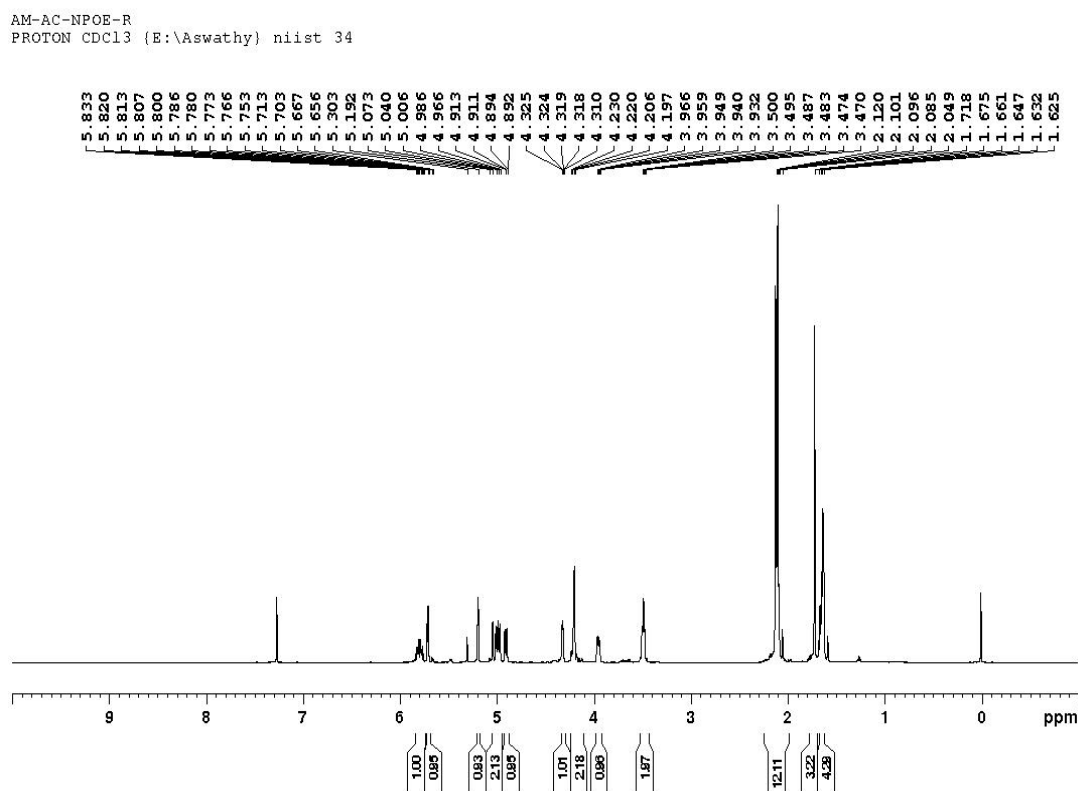


Figure 4.15: ¹H NMR spectra of **1c**

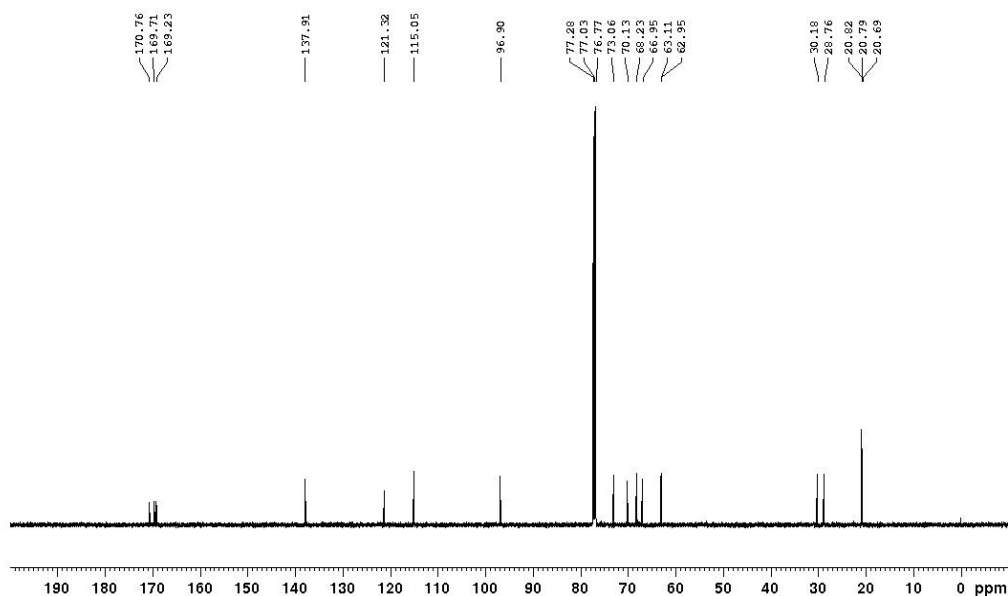


Figure 4.16: ^{13}C NMR spectra of **1c**

4.2.3. Selection of glycosyl acceptors

In the present study, we mainly chose those molecules that possess hydroxyl group and isolated from plant sources. Some of these molecules were isolated in our lab itself including isomenthol and betulinic acid and some others were purchased from TCI chemicals (Figure 4.17). The remaining sugar acceptors are synthesized from D-glucose and D-ribose based on previous literature reports.[1,2]

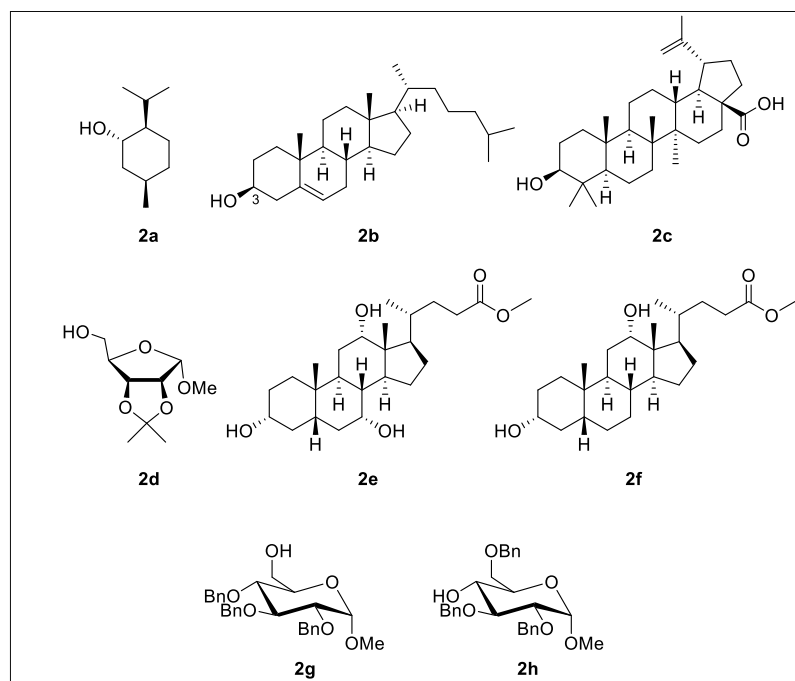
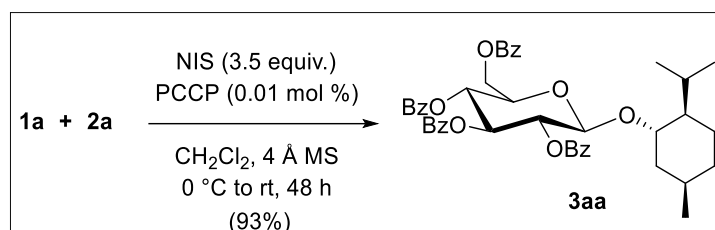


Figure 4.17: Structure of various glycosyl acceptors

4.2.4. General procedure & optimization BA-mediated Glycosylation

Our initial experiment involved glycosidation using benzoyl (Bz) protected NPOE of D-glucose (**1a**, Fig. 2) with a naturally occurring secondary alcohol (+)-isomenthol (**2a**, Fig. 2), a major component of the wild mint *Mentha arvensis*, a species of flowering plant in the mint family Lamiaceae. Reaction of **1a** and **2a** in the presence of a catalytic amount of PCCP (0.01 mol%) and NIS (3.5 equiv.) in dichloromethane at 0 °C to room temperature afforded the glycoside **3aa** (Scheme 2) in moderate yield, even after stirring the reaction mixture for 24 h. Hence, we optimized the reaction conditions by varying the time, temperature, and solvents (Table 1).



Scheme 2: PCCP catalyzed glycosidation of **2a** with NPOE **1a**

Further optimization of the glycosylation strategy by varying solvent, temperature, etc. did not further improve the glycoside formation, all the conditions are summarized in the Table 1.

Entry	Solvents	Time/ Temperature	Product / Yield
1	DCM	30 min / RT	No reaction
2	DCM	1 h / RT	No reaction
3	DCM	2 h / RT	No reaction
4	DCM	6 h / RT	No reaction
5	DCM	12 h / RT	3aa / 10%
6	DCM	24 h / RT	3aa / 27%
7	DCM	24 h / 0 °C - RT	3aa / 68%
8	DCM	48 h / 0 °C - RT	3aa / 93%
9	Acetonitrile	48 h / 0 °C - RT	3aa / 58%
10	Toluene	48 h / 0 °C - RT	3aa / 49%
11	DCM	24 h / -20 °C - RT	3aa / 19%

Table 1: Optimization table for BA mediated glycosylation by varying time, temperature and solvents.

The optimized reaction condition for glycosidation of **2a** (1 equiv.) with **1a** (1.5 equiv.) in the presence of PCCP (0.01 mol%), NIS (3.5 equiv.) in dichloromethane (9 mL) and 4 Å molecular sieves (powdered), under inert atmosphere, from 0 °C to room temperature for a duration of 48 h afforded 1,2-trans glycoside **3aa** in 93 % yield (Scheme 1). The structure of the product was confirmed by ¹H, ¹³C NMR and ESI-HRMS analysis. In ¹H NMR the anomeric proton at C-1 found to be resonated at δ 4.79 ppm with a coupling constant of $J = 8.0$ Hz, indicating the configuration of β glycoside (Figure 4.18). Moreover, the anomeric carbon (C-1) resonated at

δ 101.4 ppm (Figure 4.19). Finally, the product was confirmed by ESI-HRMS, where **3aa** showed a molecular ion peak at m/z 757.2995 which is the $(M+Na)^+$ peak.

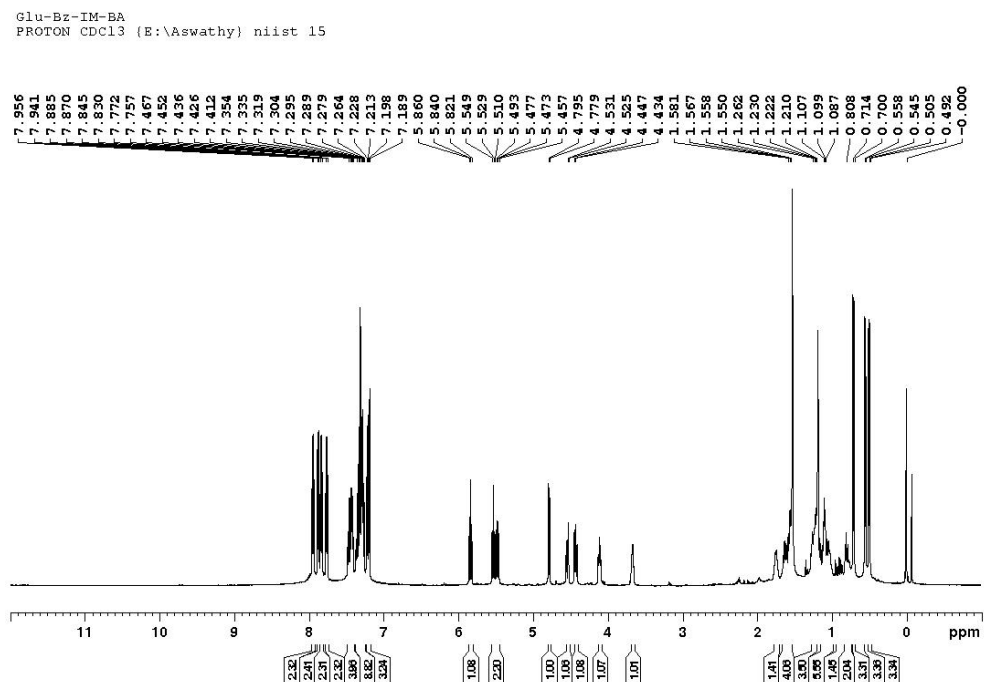


Figure 4.18: ^1H NMR spectra of **3aa**

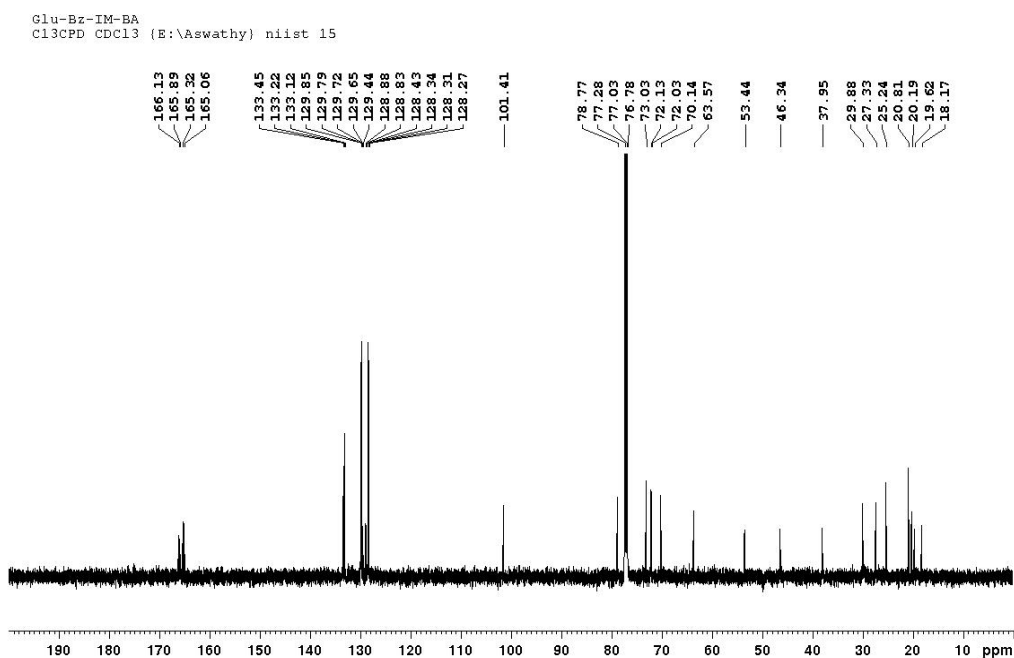
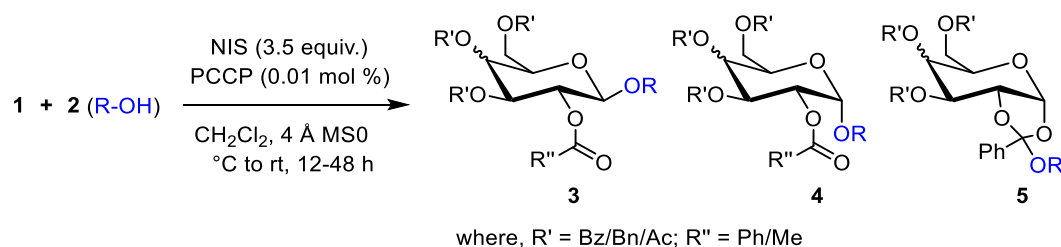


Figure 4.19: ^{13}C NMR spectra of **3aa**

The first successful glycosidation reaction with catalytic PCCP and NIS prompted for investigation of substrate scope of the reaction with D-glucose NPOEs bearing benzyl, benzoyl and acetyl protection, and various aglycones comprising natural products cholesterol **2b**, betulinic acid **2c**, methyl cholate **2e**, deoxymethyl cholate **2f**, and methyl-glycoside acceptors **2d**, **2g-h** (Figure.4.15), which afforded trans glycosides **3** in good to excellent yields (**entry 1-5, Table 1**). The effect of protecting groups on the stereochemical outcome of glycosidation was apparent. Benzoyl (**1a**) and benzyl (**1b**) protected NPOEs selectively afforded 1,2-trans glycosides **3**, whereas, acetyl protected NPOE **1c** led to 1,2-cis and trans glycoside mixture of **4ce:3ce** (1:0.3) and **4cf:3cf** (1:0.33) (**entry 6-7, Table 1**). However, NPOEs bearing benzoyl, benzyl protection on D-galactose (**1d** and **1e**) with the aforementioned aglycones, invariably, led to formation of 1,2-orthoester adducts (**entry 8-13, Table 2**). The glycosylated products/1,2-orthoesters were identified from the coupling constants of the anomeric protons in the ¹H NMR spectra. Anomeric protons of the 1,2-orthoester products exhibit a coupling constant of 5-5.5 Hz, compared to 1,2-trans and 1,2-cis glycosides that exhibit 7-9 and 1-4 Hz, respectively.

Table 2. Substrate scope of glycosidation reactions catalyzed by PCCP using NPOE donors^a



Entry	Glycosyl Donor	Glycosyl acceptor	Product(s)	Yield ^b (%)
1	1a	2b	3ab	76 (94)
2	1a	2c	3ac^c	71 (89)
3	1a	2e	3ae^c	96
4	1b	2a	3ba	79 (90)
5	1b	2e	3be^c	91 (93)
6	1c	2e	3ce:4ce^c (0.3:1)	92
7	1c	2f	3cf:4cf^c (0.33:1)	92
8	1d	2f	5df^c	68 (85)
9	1d	2h	5dh	93
10	1e	2c	5ec^c	63 (91)

Entry	Glycosyl Donor	Glycosyl acceptor	Product(s)	Yield ^b (%)
11	1e	2d	5ed	67 (86)
12	1e	2f	5ef^c	61 (76)
13	1e	2g	5eg	92

^a Reaction conditions: To the mixture of **1** (1.5 equiv.), **2** (16 to 28 mM, 1 equiv.) in CH₂Cl₂ (10 mL) at 0 °C, under 4 Å MS, PCCP (0.01 mol%, 0.3 mM in CH₂Cl₂), NIS (3.5 equiv.) were added, and slowly warmed to room temperature. ^b Isolated yields by column chromatography (yields in parenthesis represent values based on recovered **2**). ^c C3 position glycosidated.

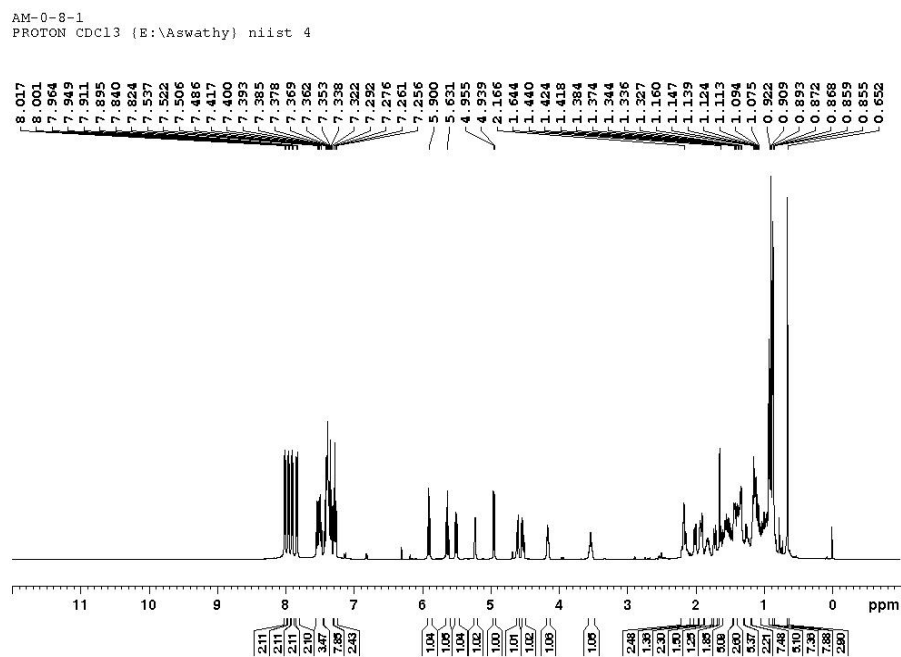


Figure 4.20: ¹H NMR spectra of **3ab**

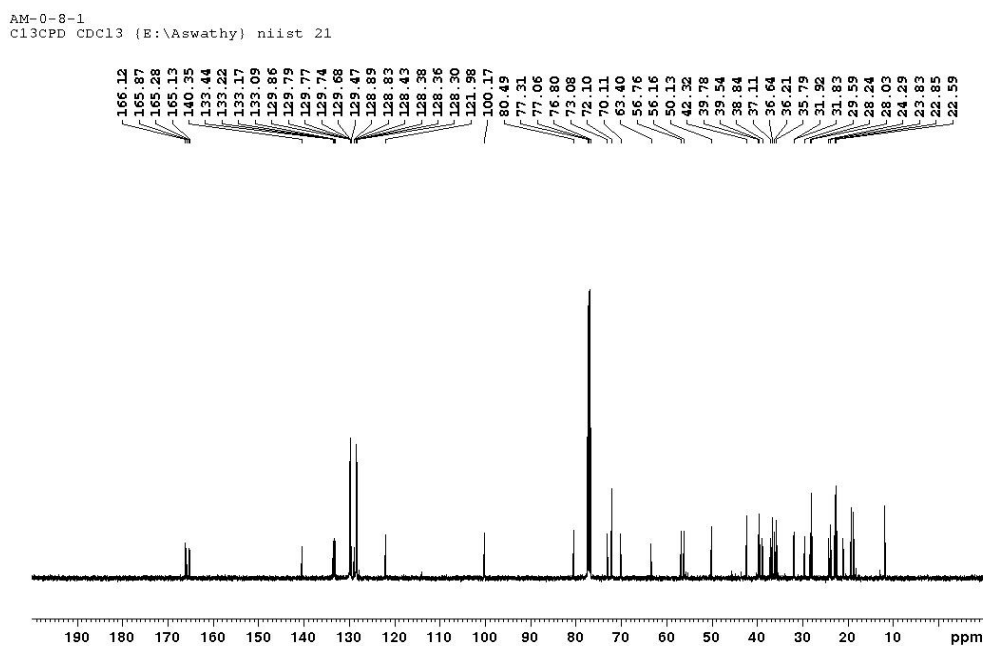


Figure 4.21: ¹³C NMR spectra of **3ab**

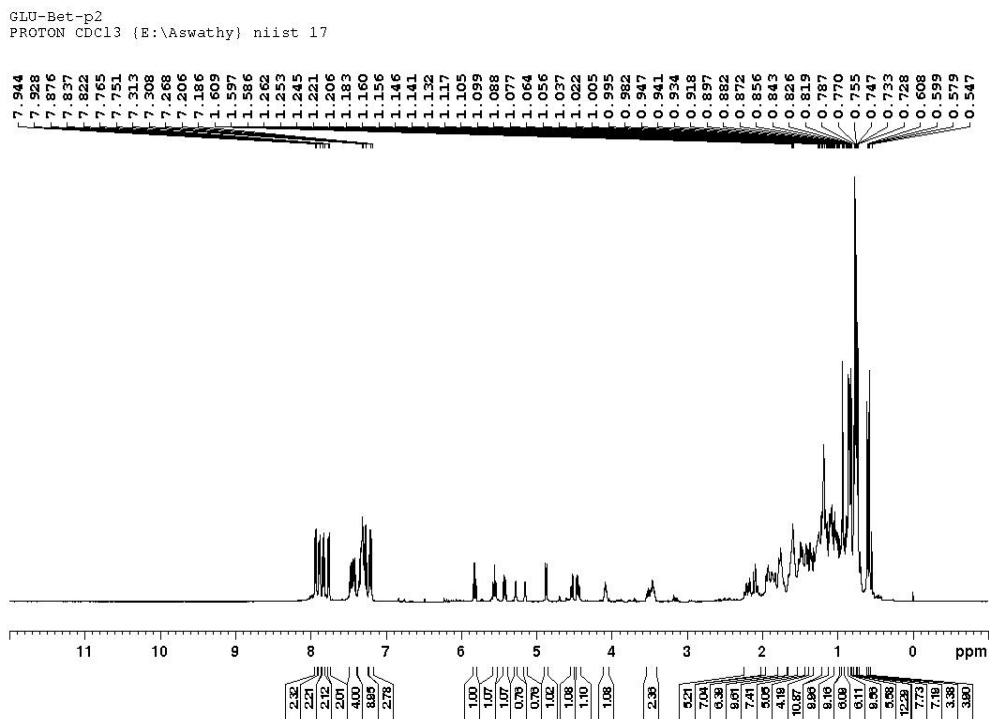


Figure 4.22: ^1H NMR spectra of **3ac**

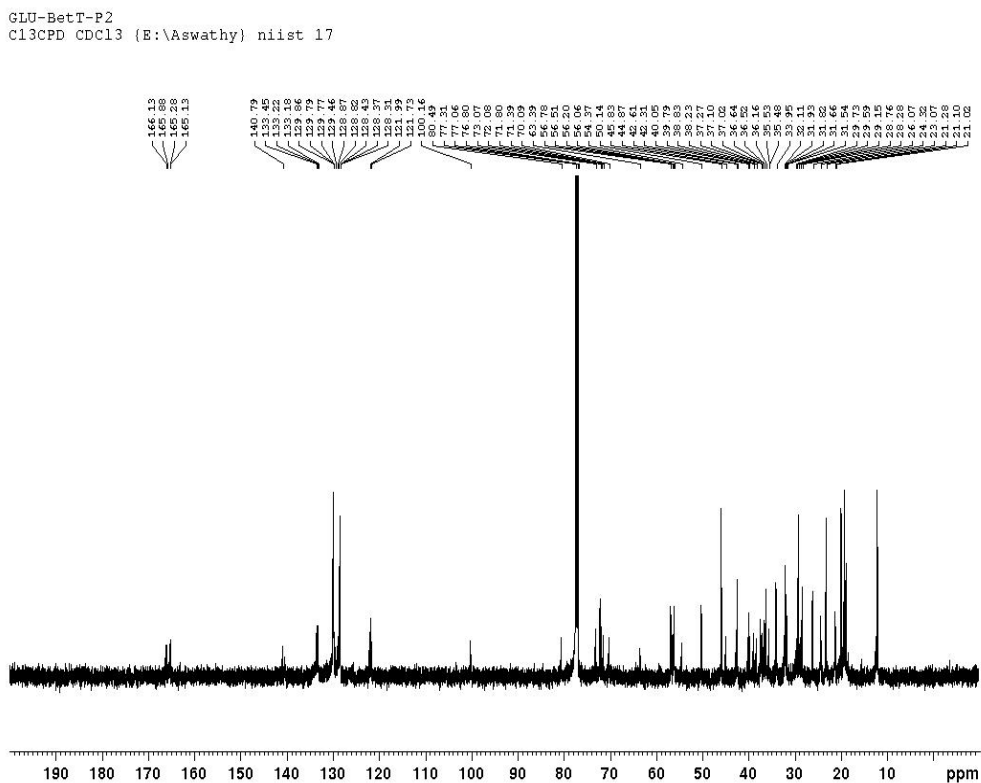


Figure 4.23: ^{13}C NMR spectra of **3ac**

The reactivity order of the three OH groups in cholic acid was investigated by various research groups [20,21]. In the present study, a regioselective glycosidation of **2e** with **1a** at C3 position

was the only product observed in 96% yield. Compound **3ae** was confirmed by comparison with respective chemical shifts in ^{13}C NMR spectra of hydroxy bearing carbons of **2e**, which are 71.9, 68.4, and 73.0 ppm for C3, C7, and C12, respectively. The chemical shifts of C3, C7, and C12 of **3ae** are 80.7, 68.0, and 72.8 ppm, respectively, which confirms the C3 regioselectivity of the glycosidation (Figure 4.24- 4.26). A similar ^{13}C NMR chemical shift analysis was carried out to confirm the C3 regioselectivity of the products **3ac**, **3be**, **3ce**, **4ce**, **3cf**, **4cf**, **5df**, **5ec**, and **5ef**.

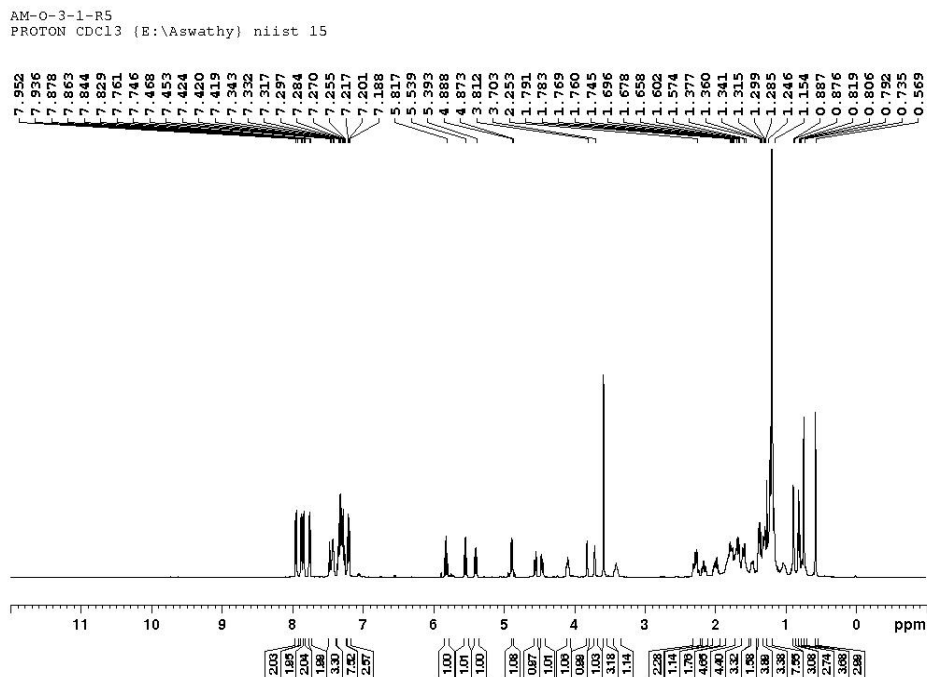


Figure 4.24: ^1H NMR spectra of **3ae**

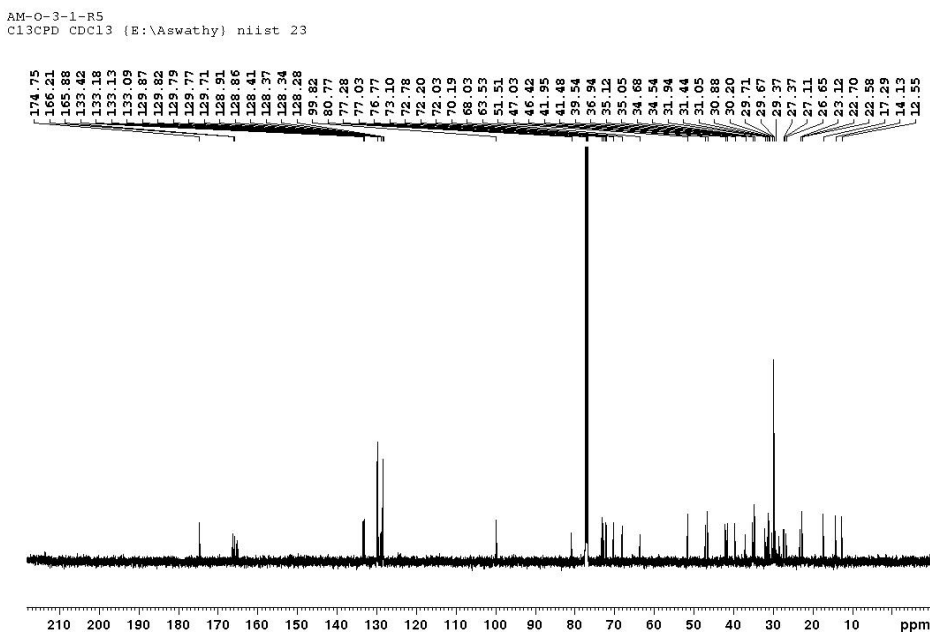


Figure 4.25: ^{13}C NMR spectra of **3ae**

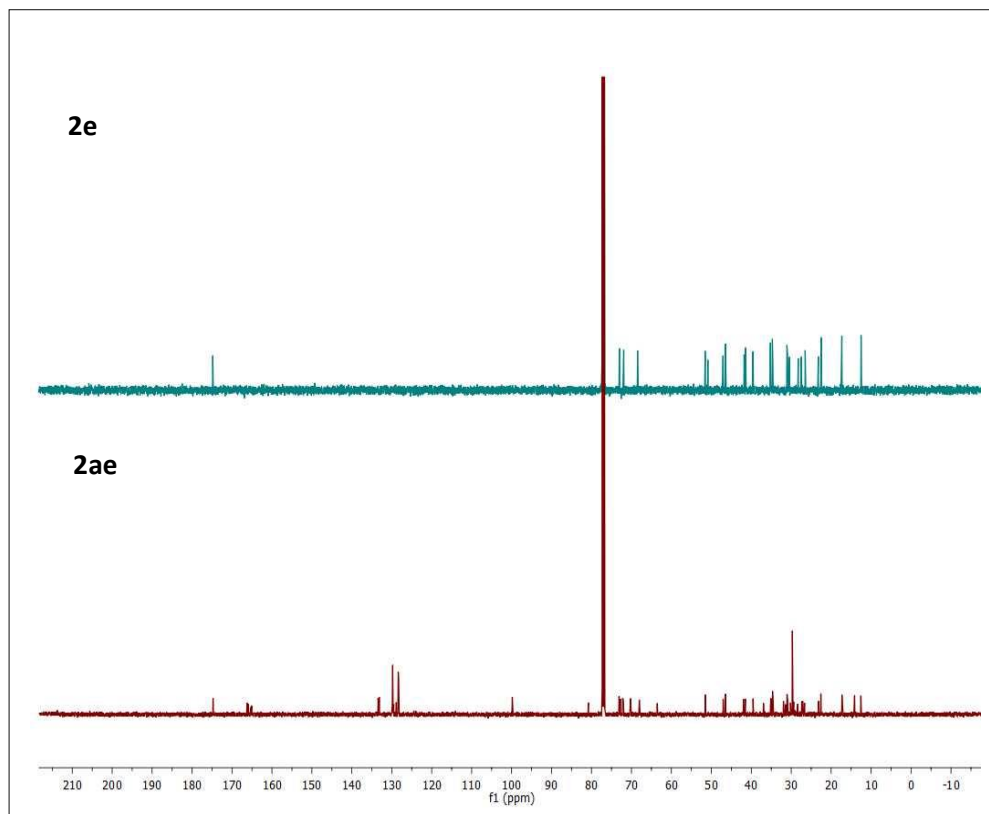


Figure 4.26: Comparison of the ^{13}C NMR spectra of compound **3ae** vs **2e**

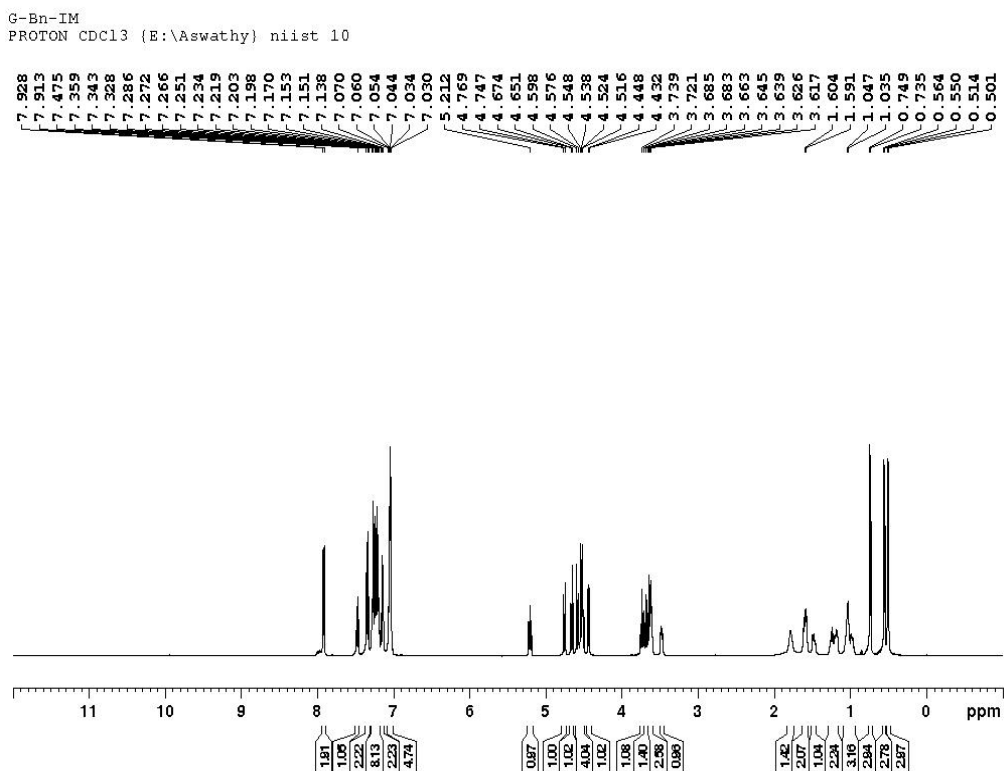


Figure 4.27: ^1H NMR spectra of compound **3ba**

G-Bn-IM
C13CPD CDCl3 (E:\Aswathy) niist 10

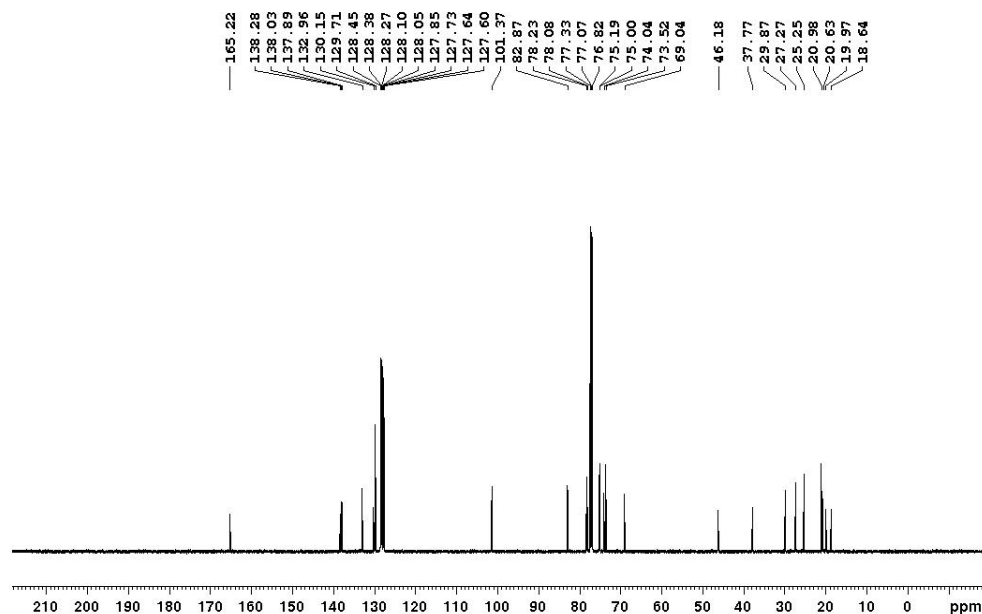


Figure 4.28: ¹³C NMR spectra of compound 3ba

AM-AB-22-4
PROTON CDCl3 (E:\Aswathy) niist 14

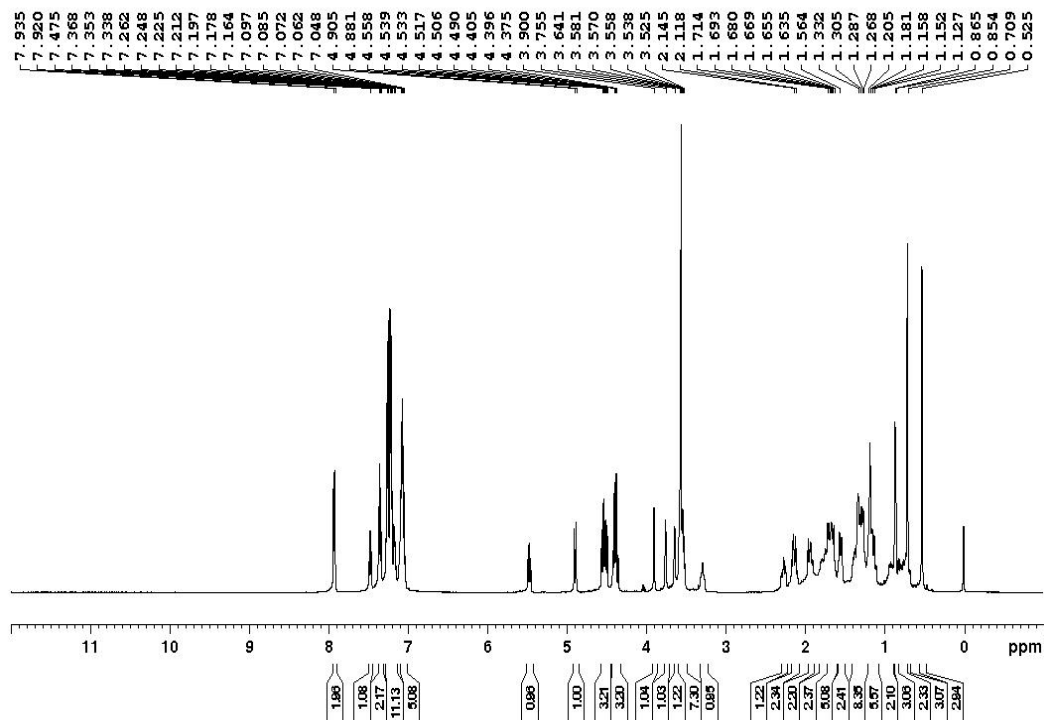


Figure 4.29: ¹H NMR spectra of compound 3be

AM-AB-22-4
 C13CPD CDC13 (E:\Aswathy) niist 19

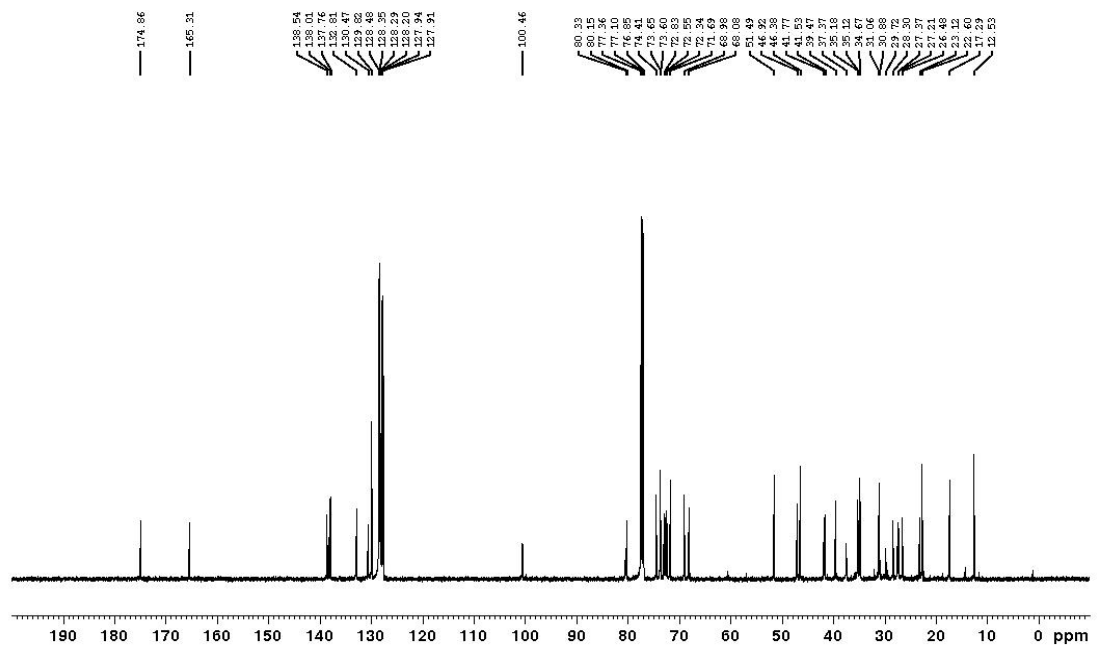


Figure 4.30: ¹³C NMR spectra of compound **3be**

AM-AB-51-R2
 PROTON CDC13 (E:\Aswathy) niist 44

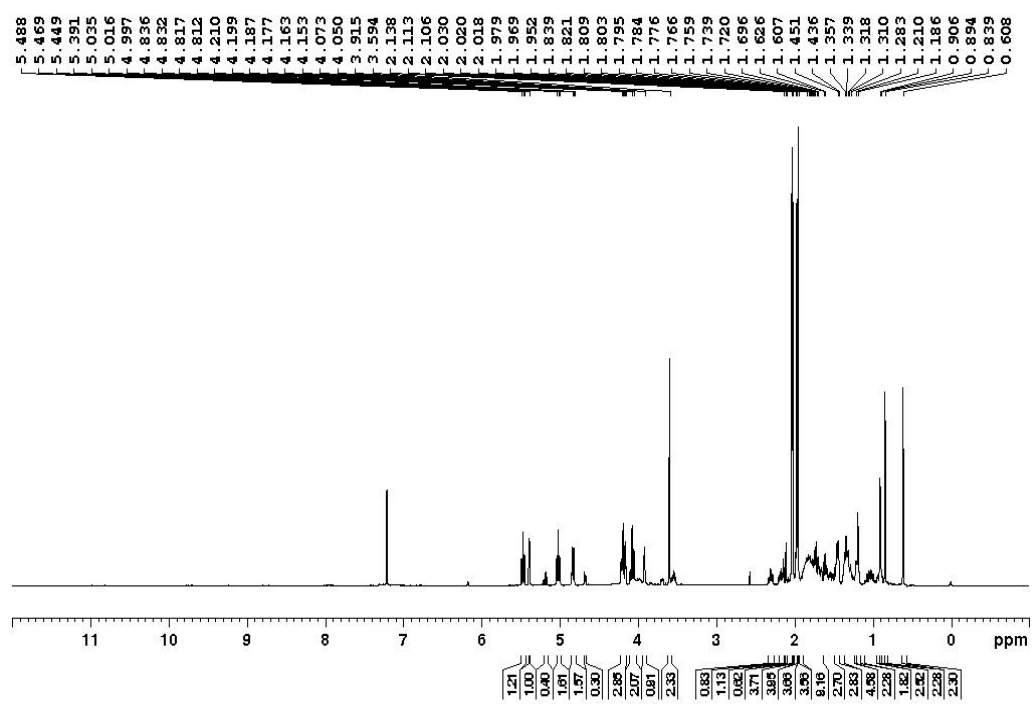


Figure 4.31: ¹H NMR spectra of mixture of **3ce** and **4ce**

AM-AB-51-R2
Cl3CPD CDCl3 (E:\Aswathy) niist 44

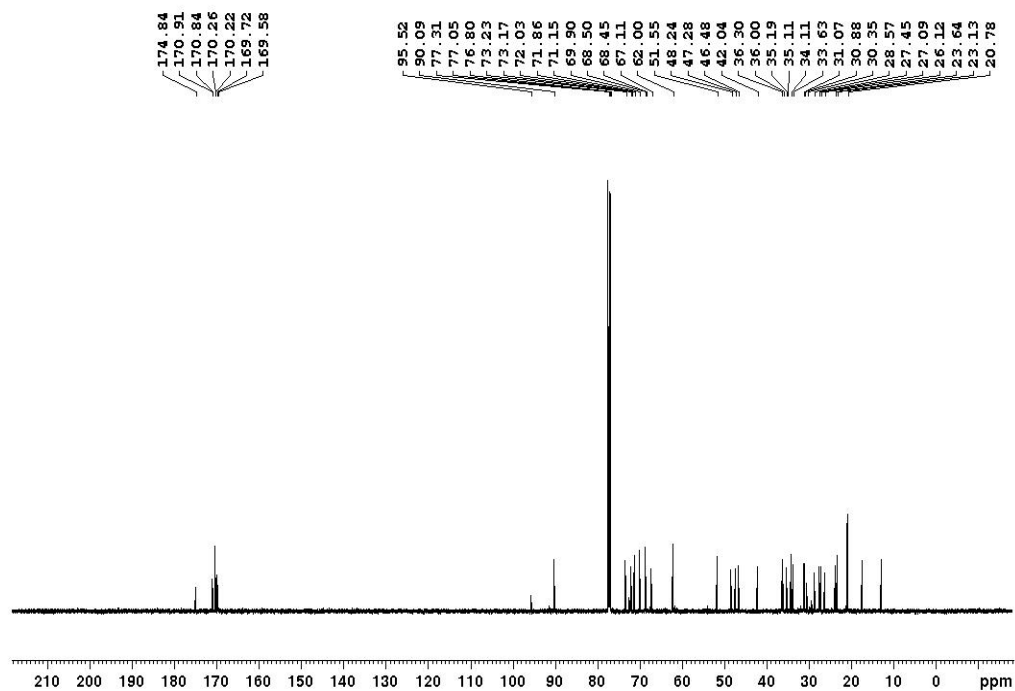


Figure 4.32: ^{13}C NMR spectra of mixture of **3ce** and **4ce**

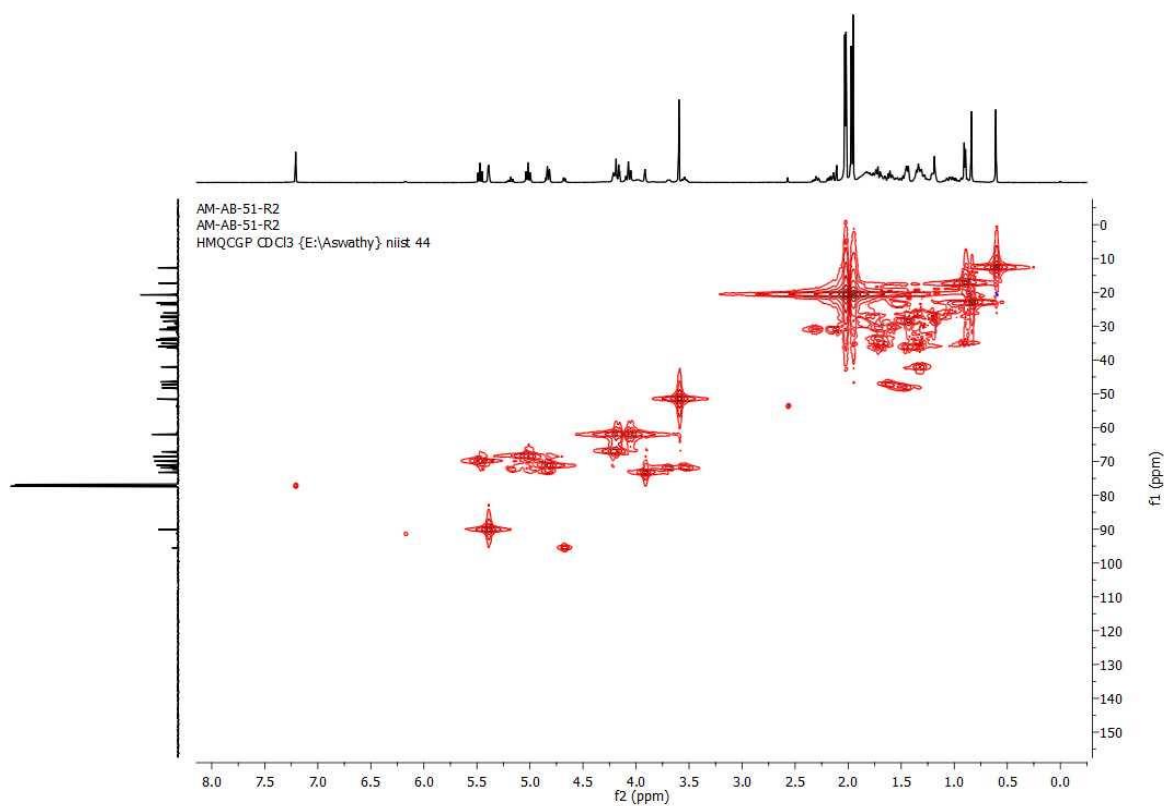


Figure 4.33: HMQC spectra of mixture of **3ce** and **4ce** to ascertain β and α configuration, respectively.

AM-64-BA-4
PROTON CDCl3 {E:\Aswathy} niist 48

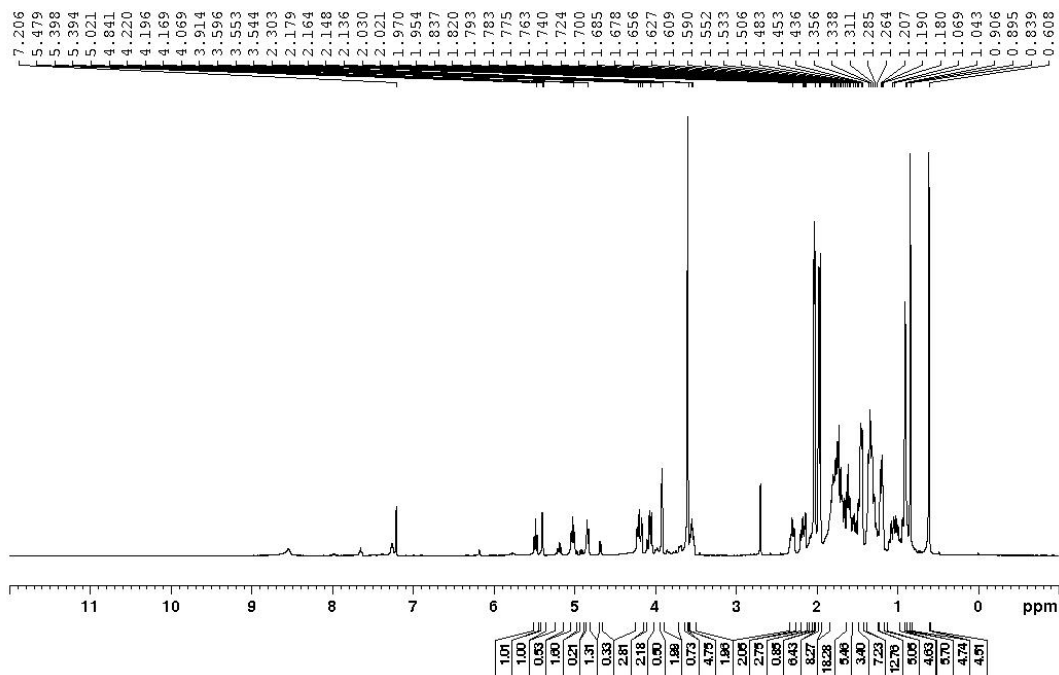


Figure 4.34S: ¹H NMR spectra of mixture of **3cf** and **4cf**

AM-64-BA-4
C13CPD CDCl3 {E:\Aswathy} niist 10

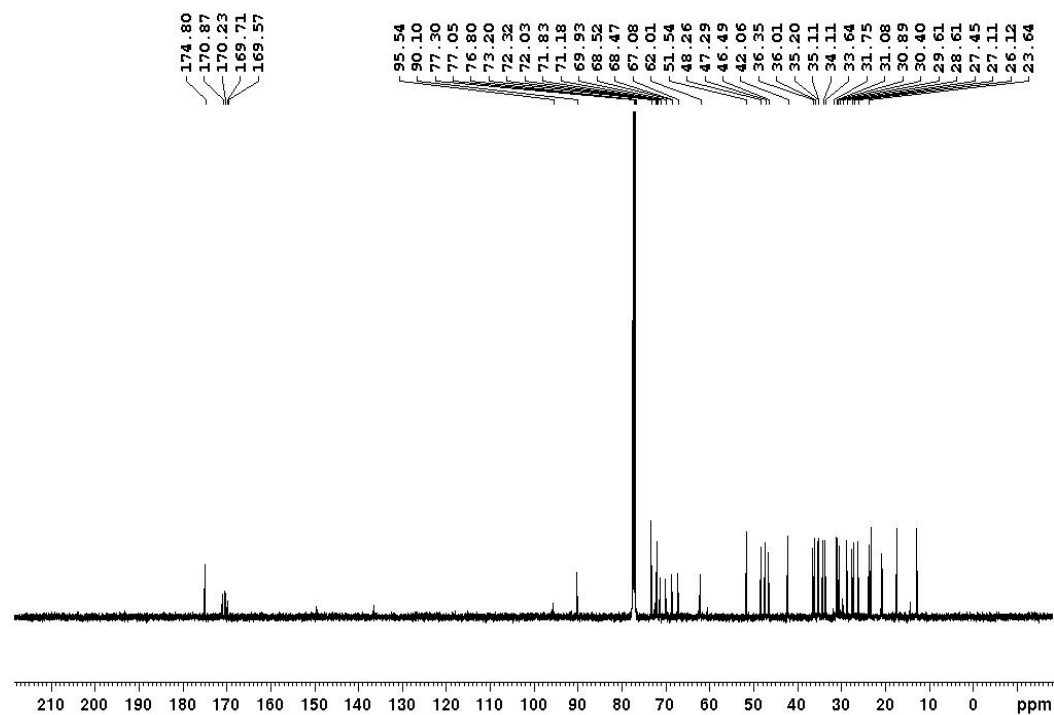


Figure 4.35: ¹³C NMR spectra of mixture of **3cf** and **4cf**

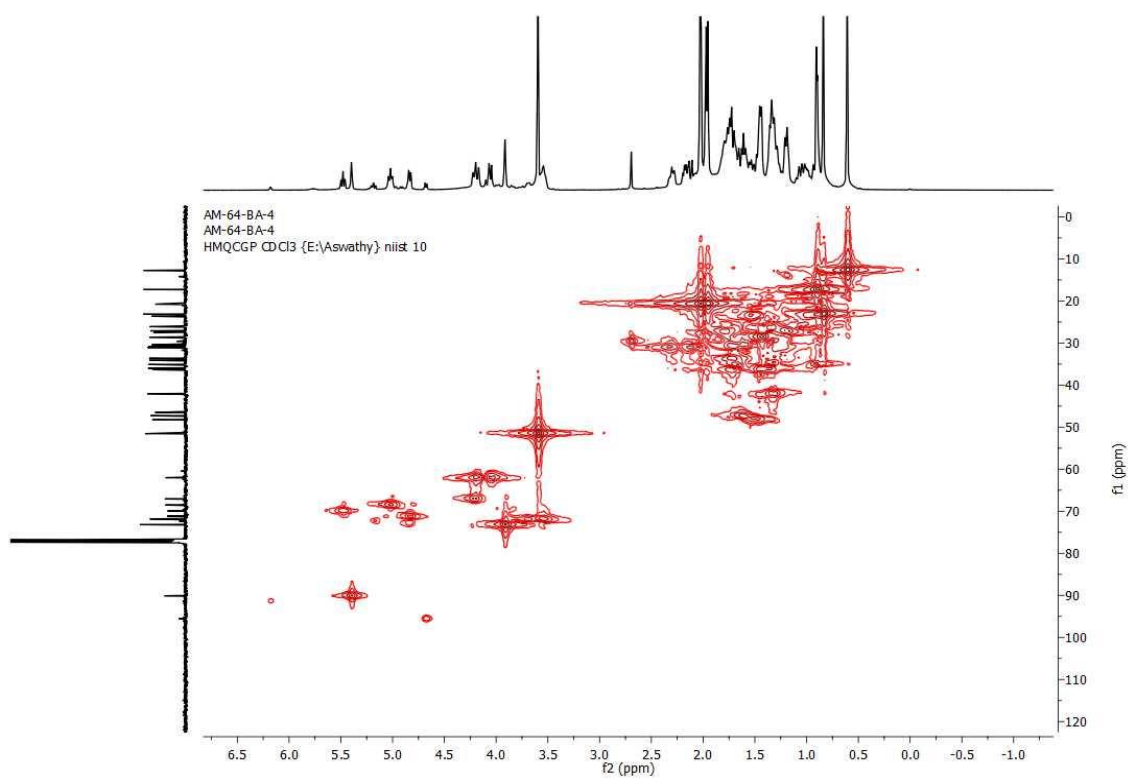


Figure 4.36: HMQC spectra of mixture of **3ce** and **4ce** to ascertain β and α configuration, respectively

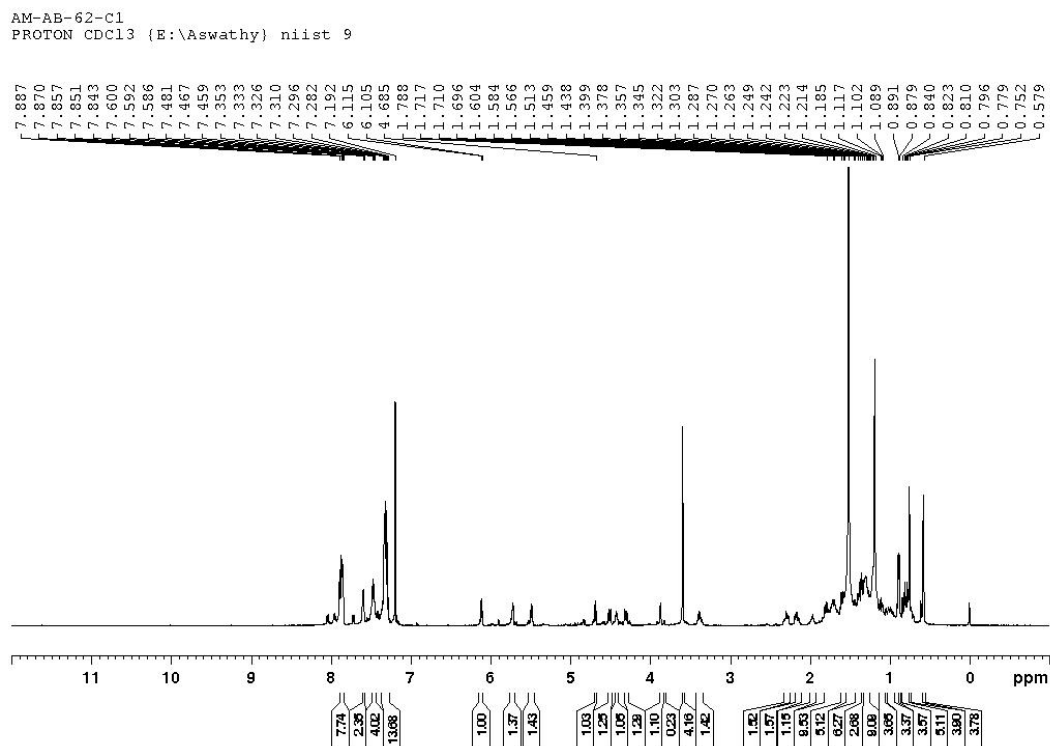


Figure 4.37: ^1H NMR spectra compound **5df**

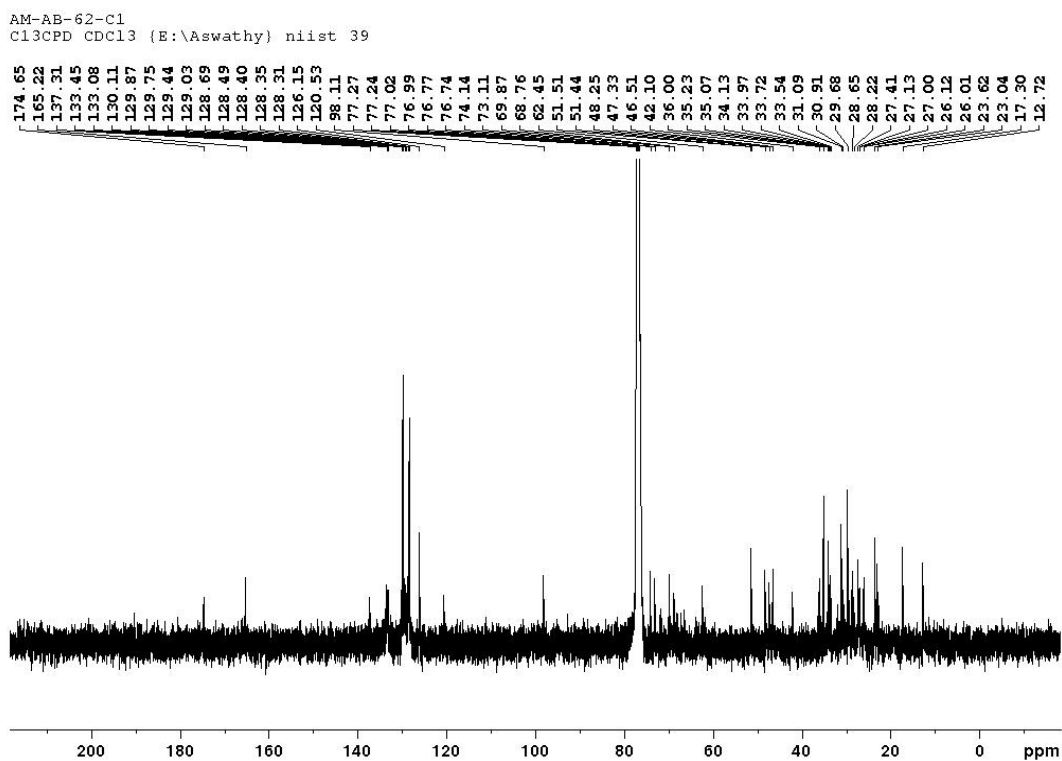


Figure 4.38: ^{13}C NMR spectra compound **5df**

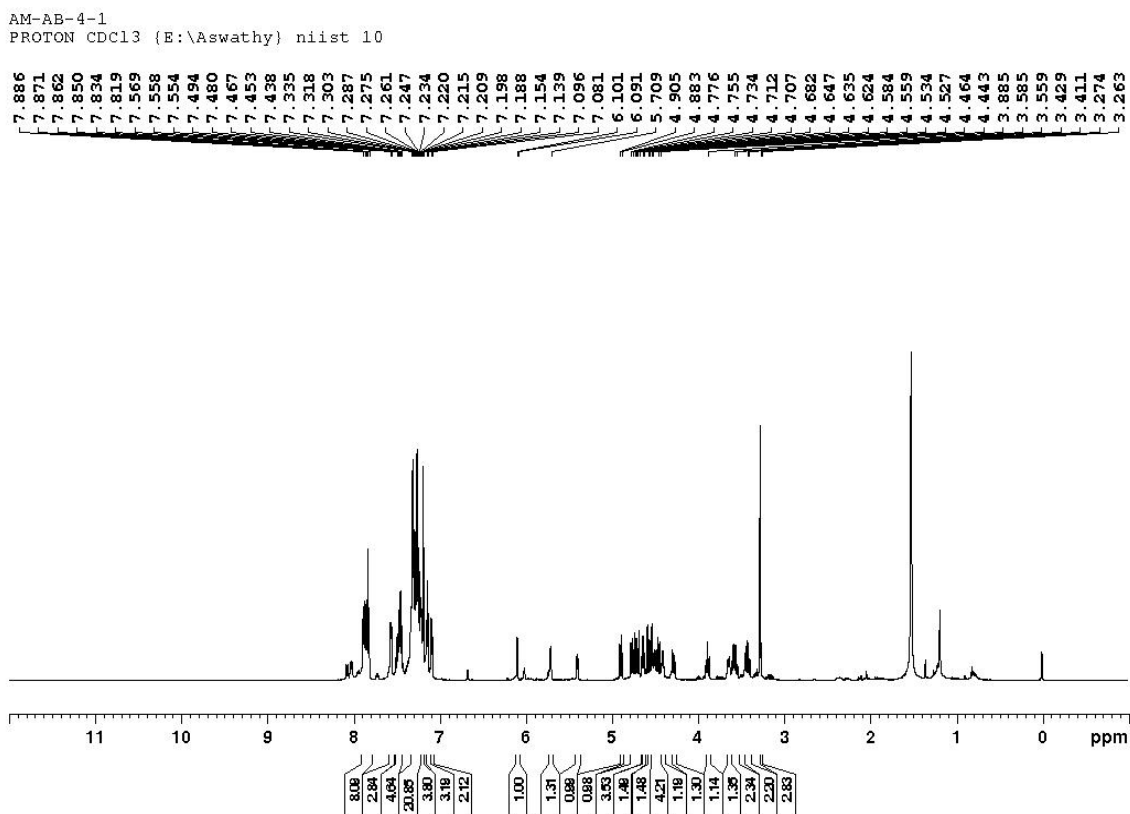


Figure 4.39: ^1H NMR spectra compound **5dh**

AM-AB-4-1
C13CPD CDCl3 (E:\Aswathy) niist 11

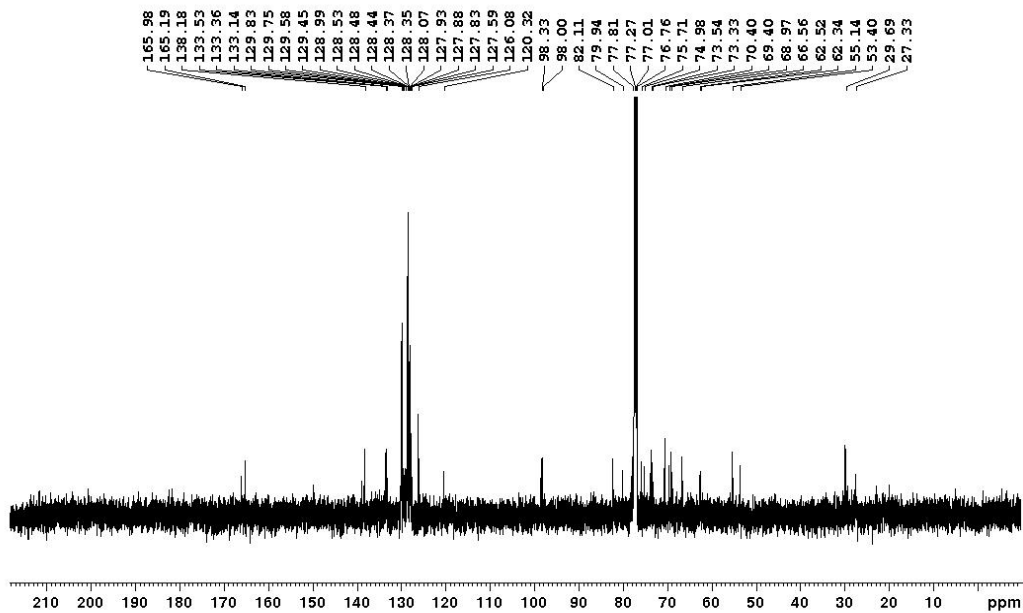


Figure 4.40: ¹³C NMR spectra compound 5dh

AM-AB-20-4
PROTON CDCl3 (E:\Aswathy) niist 37

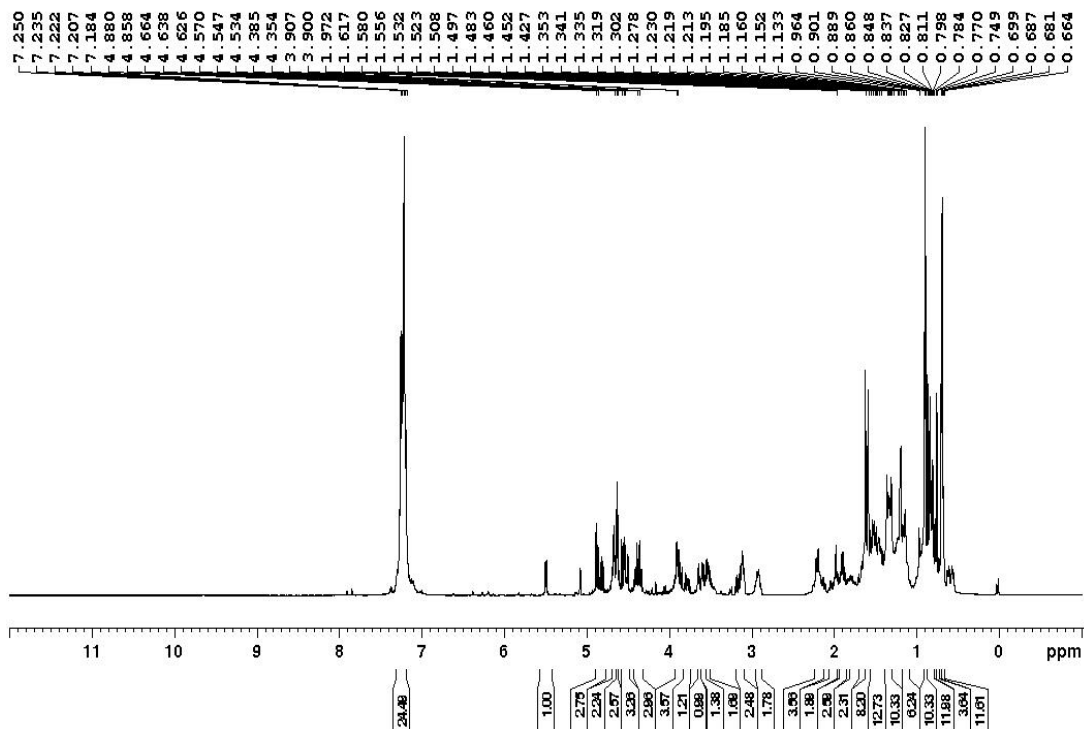


Figure 4.41: ¹H NMR spectra compound 5ec

AM-AB-20-4
 C13CPD CDCl3 (E:\Aswathy) niist 7

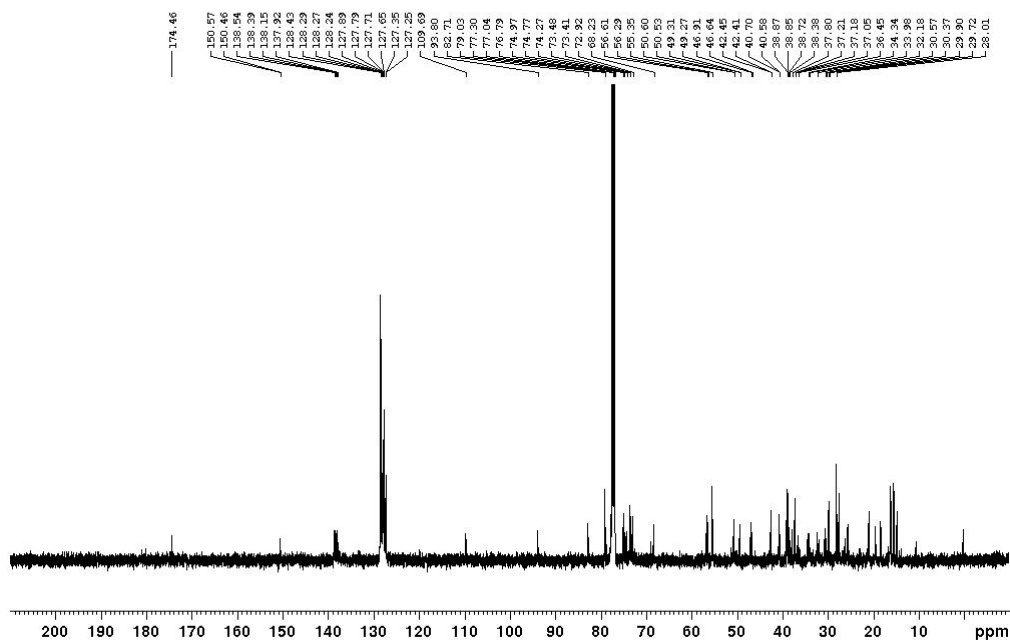


Figure 4.42: ^{13}C NMR spectra compound 5ec

AM-AB-10-1
 PROTON CDCl3 (E:\Aswathy) niist 10

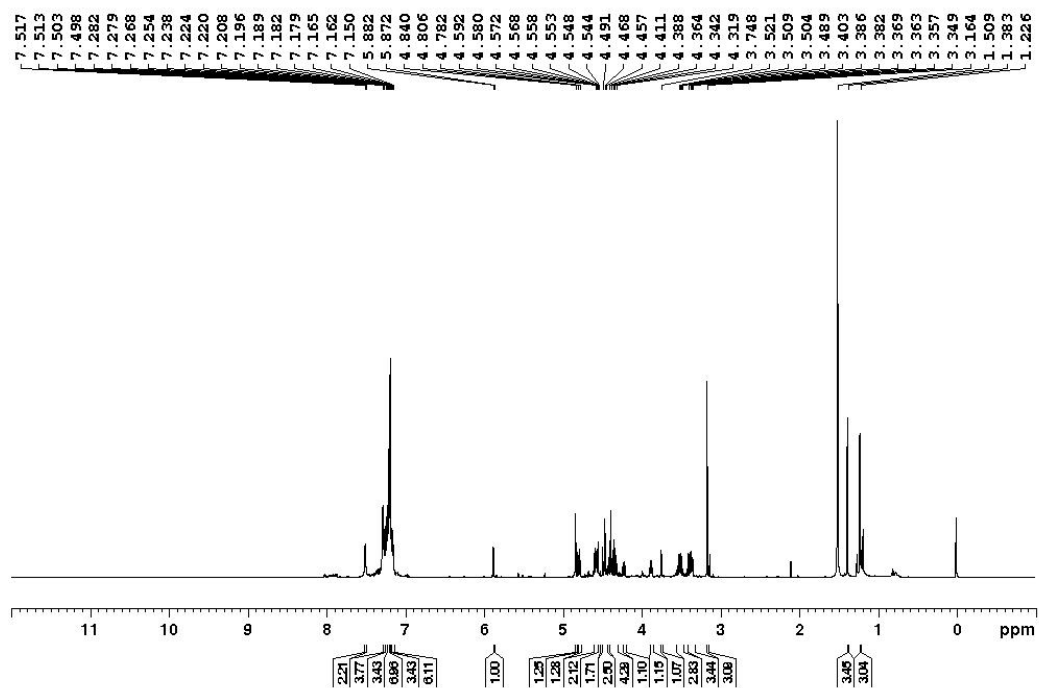


Figure 4.43: ^1H NMR spectra of Compound 5ed

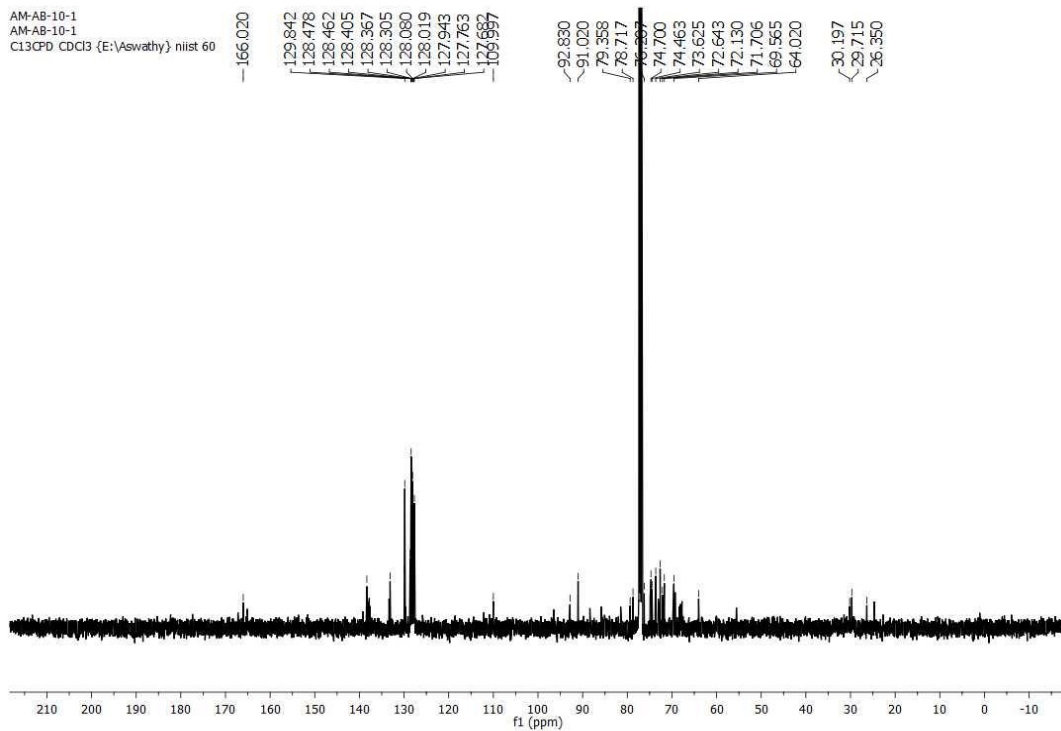


Figure 4.44: ^{13}C NMR spectra of Compound **5ed**

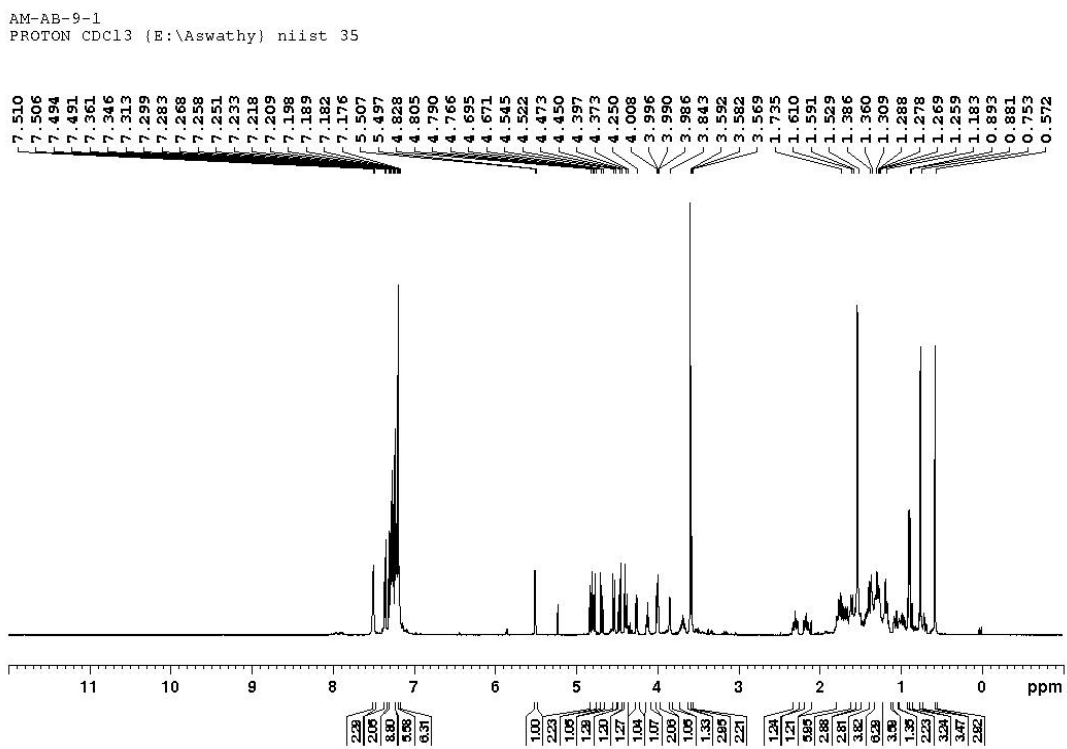


Figure 4.45: ^1H NMR spectra of Compound **5ef**

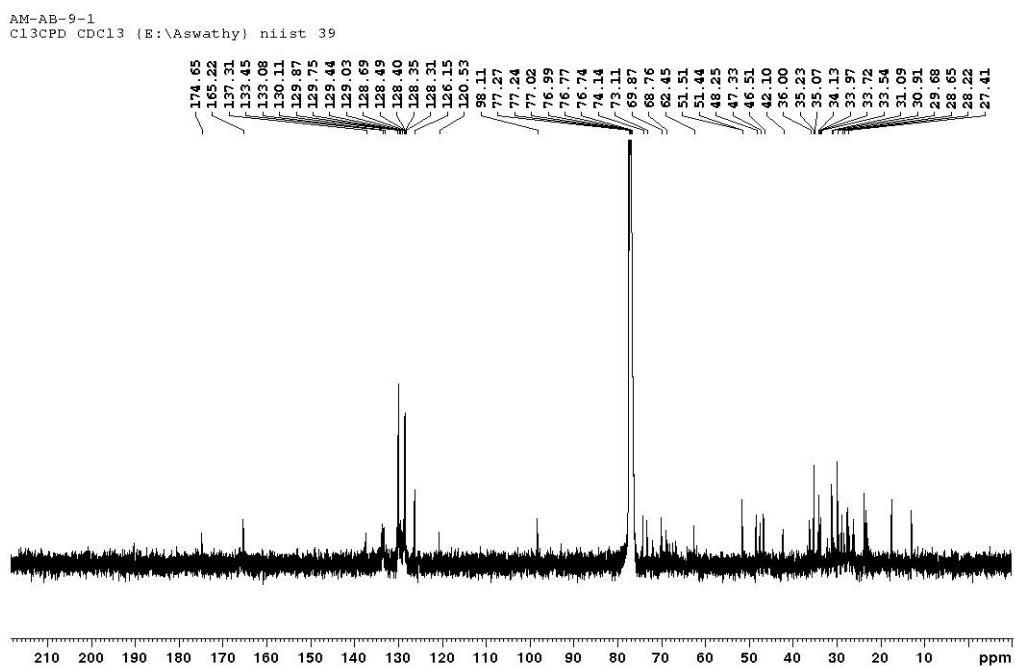


Figure 4.46: ^{13}C NMR spectra of Compound **5ef**

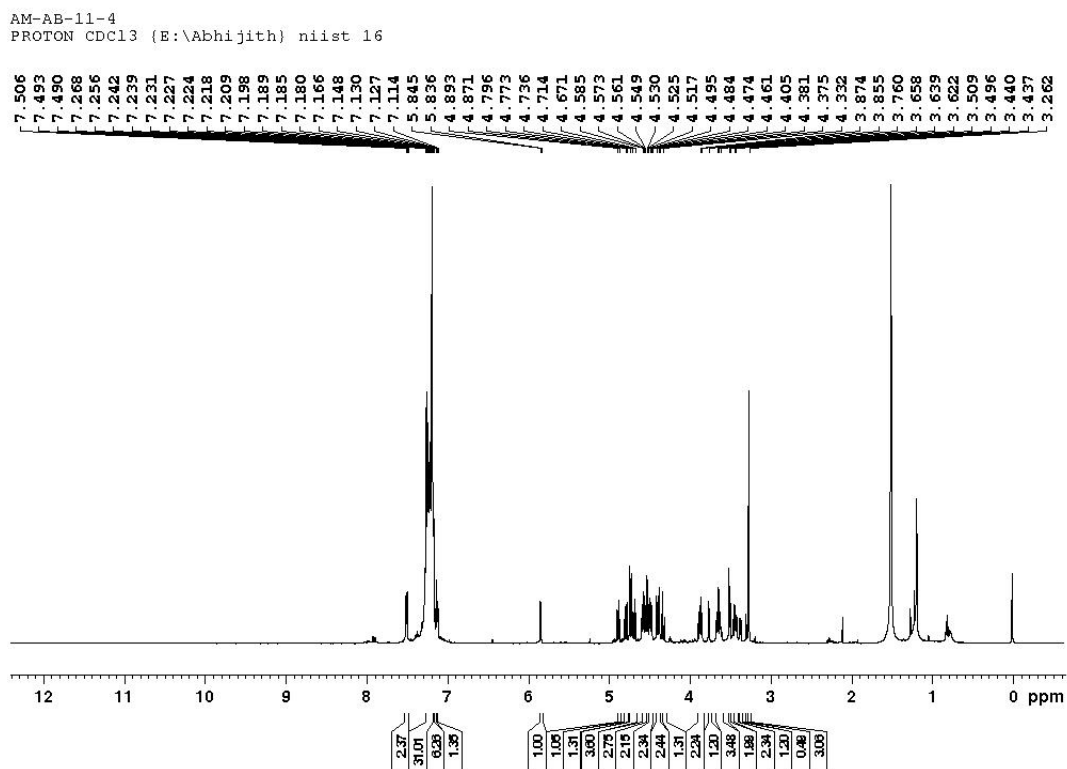


Figure 4.47: ^1H NMR spectra of Compound **5eg**

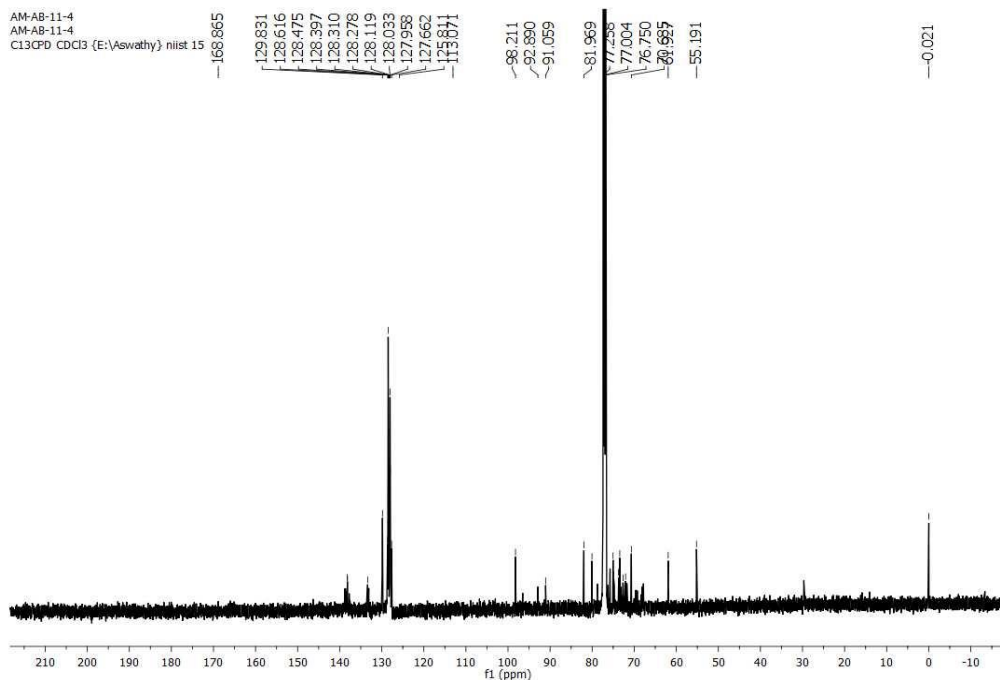
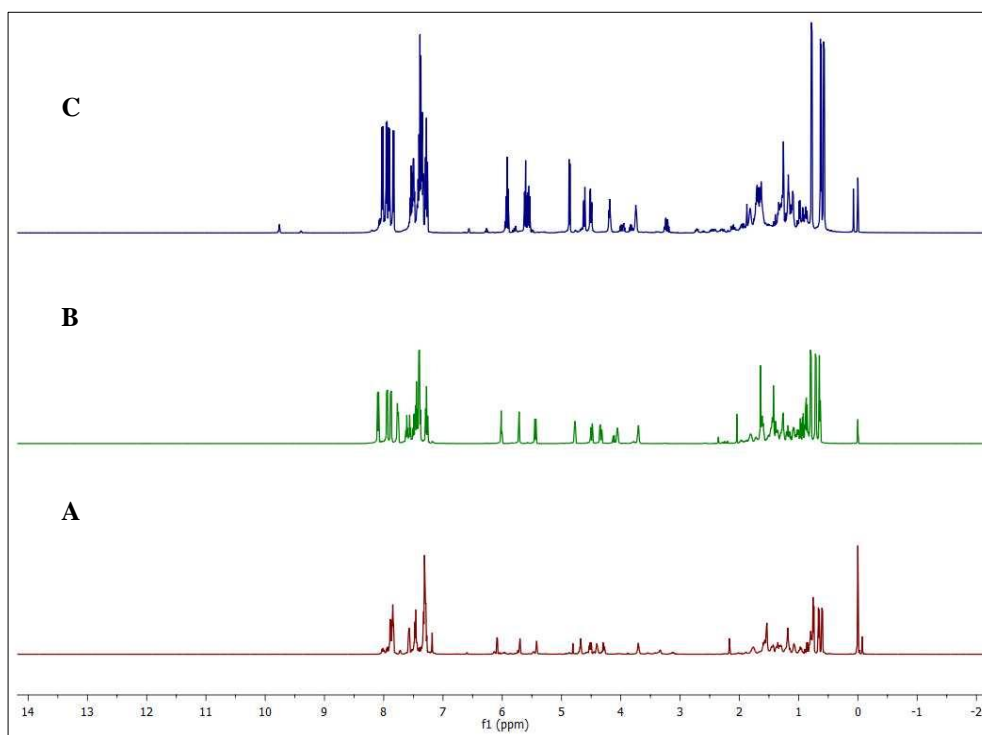


Figure 4.48: ^{13}C NMR spectra of Compound **5eg**

Additionally, experiments were conducted with common Lewis acids (10 mol%) in conventional glycosidation of **2a** with **1a** to ascertain the efficiency of PCCP catalyst. Reactions catalyzed by $\text{Sc}(\text{OTf})_3$ and $\text{Yb}(\text{OTf})_3$ afforded 1,2-orthoester adduct **5aa** in 90 and 93% yields, respectively (Figure 4.42), similar to a report by Fraser-Reid *et al.*,^[6] interestingly, $\text{Zn}(\text{OTf})_3$ afforded the 1,2-trans glycoside **3aa** in 85% yield.



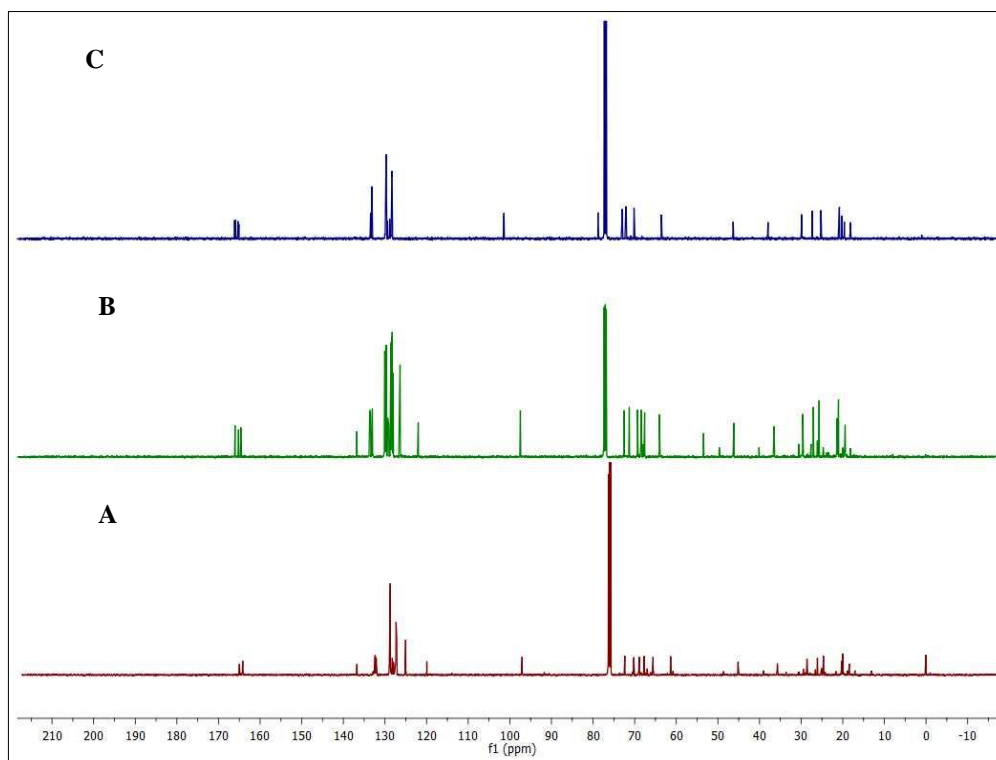


Figure 4.42: Comparison of the ^1H & ^{13}C NMR spectra of glycosylation of **2a** with **1a** catalyzed by various metal triflates. (A) $\text{Sc}(\text{OTf})_3$ gives **5aa** (B) $\text{Yb}(\text{OTf})_3$ gives **5aa** (C) $\text{Zn}(\text{OTf})_3$ gives **3aa**

4.3. Plausible mechanism

Control experiments were conducted to decipher the role of PCCP in conjunction with NIS in the glycosidation reaction, where attempts with either PCCP (0.01 mol%) or NIS (3.5 equiv.) resulted in no reaction, which shows that activation of NIS by PCCP as the driving force behind generation of iodonium ion. Interestingly, repetition of the optimized reaction condition by replacing PCCP with other Brønsted acids viz. BINAP or triflic acid at 10 mol% did not yield the glycosidated product. Fraser-Reid *et al.* described that the activation of NPOE results in the initial formation of oxocarbenium (**I**) and dioxolenium (**III**) cations, which are interchanged via trioxolenium (**II**) ion (Scheme 2) [22]. The second role of PCCP, perhaps, is to enhance the nucleophilicity of the acceptor by hydrogen bonding similar to chiral phosphoric acids,[23] resulting in 1,2-trans glycoside bond formation with **I** or **II** or **III** to afford **3** by $\text{S}_{\text{N}}2$ attack, the steric difference in C2 benzoyl ester versus acetyl ester can be the reason behind 1,2-cis-selectivity with **1c** donor for the formation of **4**. The rationale behind formation of 1,2-orthoester **5** from **1d/1e** could be owing to an intramolecular stabilization of oxocarbenium ion (**I**) from C4 ether or ester, which ensue nucleophilic addition by acceptor alcohol on disarmed

C2 ester **IV**. As reported by Fraser-Reid *et al.* on reactivity of NPOEs in the presence of Lewis acids [6], Sc(OTf)₃ and Yb(OTf)₃ afforded 1,2-orthoester adduct **5aa**. However, the rationale behind the formation of 1,2-trans glycoside **3aa** in the presence of Zn(OTf)₃ can be attributed to the spontaneous release of triflate, due to sheer size of zinc compared to the other two metals, followed by formation of a glycosyl triflate intermediate[24] from oxocarbenium ion **I** and subsequent nucleophilic S_N2 attack by the alcohol acceptor (Figure 4.43).

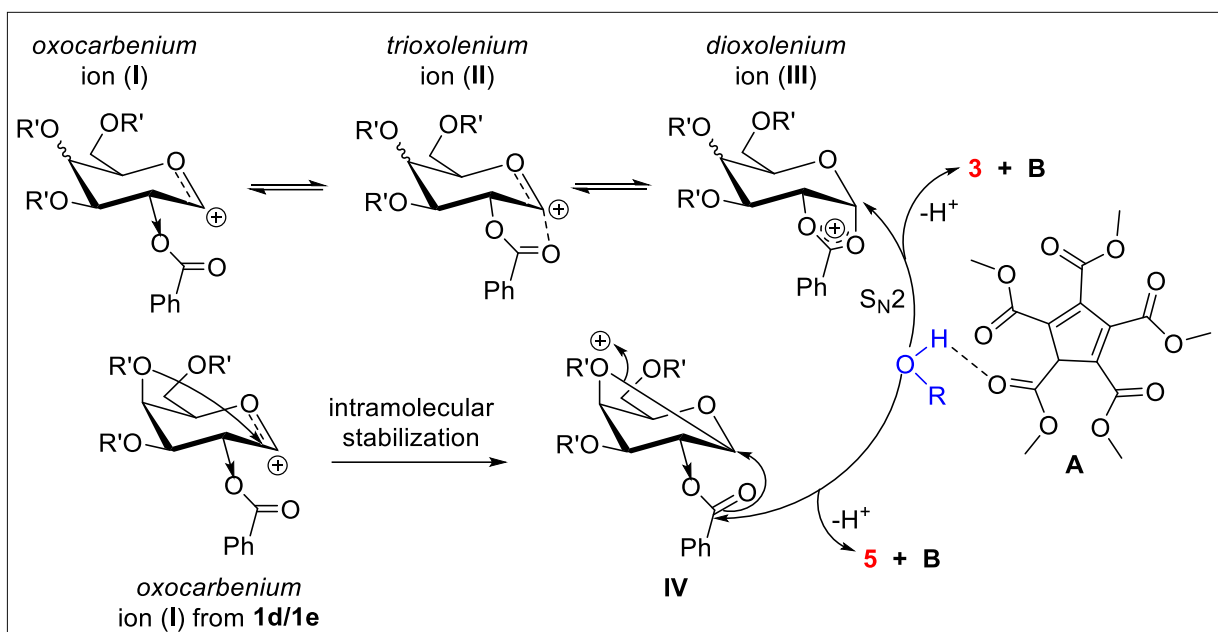


Figure 4.43: Plausible mechanism

4.4. Conclusion

In conclusion, our preliminary investigation in utilizing the organic Brønsted acid PCCP for catalysing the glycosidation with NPOEs in conjunction with NIS led to the formation of 1,2-trans glycosides with *D*-glucose, and variation of C2 position with acetyl group led to *cis* selectivity. However, the *D*-galactose based-NPOEs, afforded 1,2-orthoester products, and a reasonable mechanism behind the reactivity difference with donors is provided. Lewis acids such as Sc(OTf)₃ and Yb(OTf)₃ afforded 1,2-orthoester product in contrary to reaction with PCCP catalyst and *D*-glucosyl NPOEs **1a/1b/1c**. To maintain the utility of the method towards glycosidation of natural products, attempts with cholic acid derivatives afforded a C3 regioselectivity and 1,2-trans stereoselectivity in excellent yields. Though the glycosidation with *D*-galactosyl donors led to 1,2-orthoesters, our preliminary studies showed the utility of PCCP in glycosidation with *D*-glucosyl NPOEs.

4.5. Experimental Section

4.5.1. General Experimental Methods:

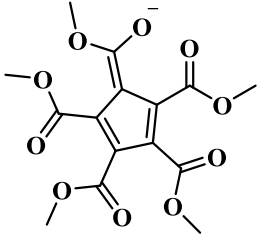
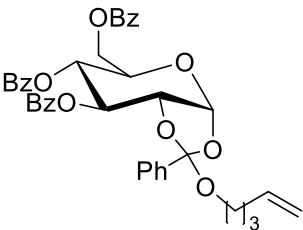
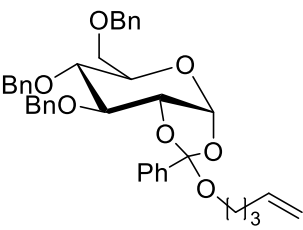
All the reagents that were purchased are of the highest quality and used without further purification. Freshly distilled dichloromethane over calcium hydride was used for the reactions. Reactions were monitored by Merck precoated silica gel F₂₅₄ TLC plates and visualized by a short wavelength UV lamp and by charring the TLC plate after spraying with 15% sulphuric acid in methanol. Gravity column chromatography was performed using silica (100-200 mesh, 230-400 mesh), and mixtures of ethyl acetate-hexane were used for elution. NMR spectra were recorded on a Bruker Ascend™ 500 MHz spectrometer (500 MHz for ¹H NMR, 125 MHz for ¹³C{¹H} NMR). The chemical shifts (δ) are given in ppm and referenced to the internal standard TMS. ¹H NMR coupling constants (J) are reported in Hertz (Hz) and multiplicities are indicated as s (singlet), d (doublet), t (triplet), m (multiplet), dd (doublet of doublets), etc. HR-ESI-MS data were obtained from a Thermo Scientific Exactive mass spectrometer with Orbitrap analyser and the ions are given in m/z.

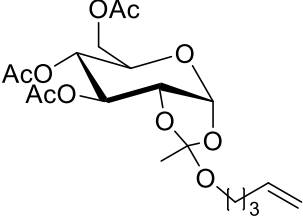
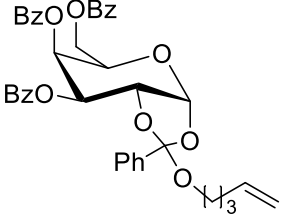
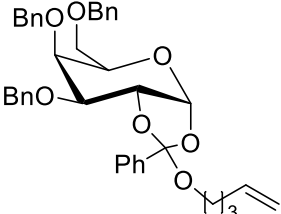
4.5.2. General procedure for BA mediated Glycosylation

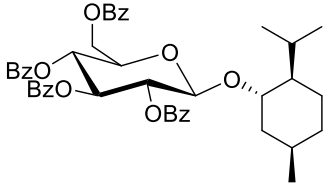
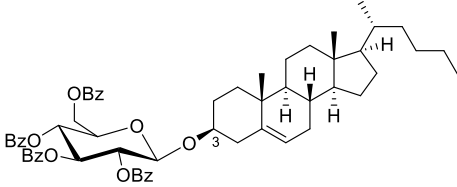
Glucose NPOE **1** (0.479 mmol, 1.5eq) and acceptor **2** (0.320 mmol, 1eq) were azeotroped together with freshly distilled toluene. The resulting dry syrup was redissolved in freshly distilled CH₂Cl₂ (9 mL) and cooled to 0°C. N-iodosuccinimide (NIS) (1.121 mmol, 3.5 eq) and powdered 4A^o molecular sieves were added, stirred for 10 min and then BA (0.01 mol %) in CH₂Cl₂ was added. The reaction mixture was kept at 0°C- RT for 24-48 h, quenched with 10 % Na₂S₂O₃ and saturated NaHCO₃ aqueous solutions. Then the molecular sieves were filtered, washed with CH₂Cl₂. The organic layer was thus collected washed with water, brine and dried. The crude residue was further subjected to conventional silica gel column chromatography using ethyl acetate-hexane as mobile phase.

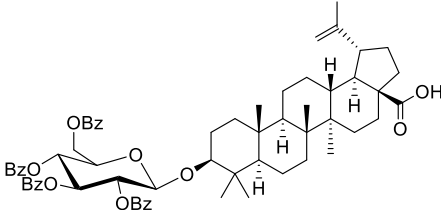
4.6. Spectral data

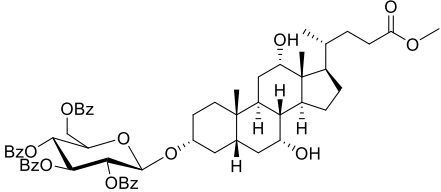
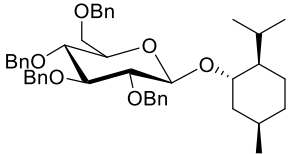
PCCP	¹H NMR (500 MHz, CDCl ₃): δ 3.78, 3.91, 3.98, 4.03 (s, 15H), 20.11 (s, 1H) ppm. ¹³C NMR (125 MHz, CDCl ₃): δ 173.0, 171.0, 168.5, 164.3, 134.3, 129.0, 119.7, 109.2, 55.1, 54.9, 52.5, 51.4 ppm. ESI-HRMS: 355.0656 [M-H] ⁺ (Observed)
-------------	---

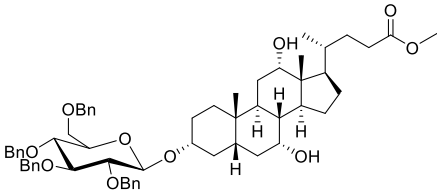
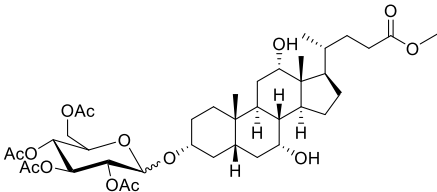
	355.0670 [M-H] ⁺ (Calculated)
<p>Compound 1a</p> 	<p>¹H NMR (500 MHz, CDCl₃): δ 8.07–8.03 (m, 2H), 8.01 – 7.97 (m, 2H), 7.95 – 7.91 (m, 2H), 7.88–7.84 (m, 2H), 7.54 (m, 4H), 7.47 – 7.34 (m, 8H), 7.30 (dd, <i>J</i>₁ = 13.0 Hz, <i>J</i>₂ = 5.3 Hz, 2H), 5.93 (t, <i>J</i> = 9.7 Hz, 1H), 5.73 – 5.62 (m, 2H), 5.56 (dd, <i>J</i>₁ = 9.7 Hz, <i>J</i>₂ = 7.9 Hz, 1H), 4.88 – 4.82 (m, 3H), 4.67 (dd, <i>J</i>₁ = 12.1 Hz, <i>J</i>₂ = 3.2 Hz, 1H), 4.53 (dd, <i>J</i>₁ = 12.1 Hz, <i>J</i>₂ = 5.3 Hz, 1H), 4.21 – 4.16 (m, 1H), 3.95 (m, 1H), 3.58 (m, 1H), 2.05 – 1.90 (m, 2H), 1.72 – 1.63 (m, 3H) ppm. ¹³C NMR (125 MHz, CDCl₃): δ 166.2, 165.9, 165.2, 165.1, 137.8, 133.4, 133.2, 133.1, 129.8, 129.8, 129.6, 128.9, 128.4, 128.4, 128.3, 114.9, 101.3, 73.0, 72.2, 72.0, 69.9, 69.4, 63.3, 29.8, 28.6 ppm.</p>
<p>Compound 1b</p> 	<p>¹H NMR (500 MHz, CDCl₃): δ 8.05 – 8.03 (m, 2H), 7.59 (t, <i>J</i> = 7.4 Hz, 1H), 7.46 (t, <i>J</i> = 7.7 Hz, 2H), 7.42 – 7.39 (m, 2H), 7.38 (s, 3H), 7.36 (m, 2H), 7.34 (m, 2H), 7.33 – 7.29 (m, 9H), 7.21 (m, 2H), 7.16 (s, 4H), 5.66 (m, 1H), 5.32 – 5.27 (m, 1H), 5.04 – 4.93 (m, 1H), 4.86 – 4.84 (m, 2H), 4.83 - 4.80 (m, 1H), 4.71 – 4.66 (m, 3H), 4.62 – 4.56 (m, 2H), 4.56 – 4.49 (m, 2H), 3.93 – 3.88 (m, 1H), 3.87 – 3.82 (m, 2H), 3.79-3.72 (m, 3H), 3.69 – 3.61 (m, 1H), 3.60 – 3.54 (m, 1H), 3.51 – 3.46 (m, 1H), 2.04 – 1.92 (m, 2H), 1.68 – 1.55 (m, 2H) ppm. ¹³C NMR (125 MHz, CDCl₃): δ 165.2, 138.0, 133.0, 129.7, 128.4, 128.3, 128.0, 127.8, 127.6, 114.7, 101.2, 82.8, 78.1, 75.0, 73.8, 73.6, 69.0, 29.9, 28.6 ppm.</p>
<p>Compound 1c</p>	<p>¹H NMR (500 MHz, CDCl₃): δ 5.84 – 5.75 (m, 1H), 5.71 (d, <i>J</i> = 5.1 Hz, 1H), 5.19 (s, 1H), 5.00 (m, 2H),</p>

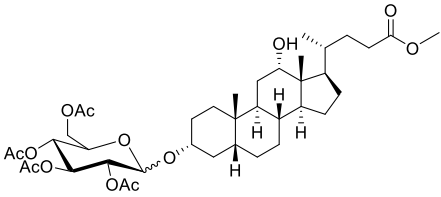
	<p>4.93 – 4.88 (m, 1H), 4.32 (dd, $J_1 = 5.4$ Hz, $J_2 = 2.4$ Hz, 1H), 4.23 – 4.16 (m, 2H), 3.98 – 3.91 (m, 1H), 3.48 (m, 2H), 2.18 – 2.04 (m, 12H), 1.72 (s, 3H), 1.69 – 1.56 (m, 4H) ppm. ^{13}C NMR (125 MHz, CDCl_3): δ 170.8, 169.7, 169.2, 137.9, 121.3, 115.0, 96.9, 73.1, 70.1, 68.2, 66.9, 63.1, 62.9, 30.2, 28.8, 20.8, 20.8, 20.7 ppm</p>
<p>Compound 1d</p> 	<p>^1H NMR (500 MHz, CDCl_3): δ 8.02 (d, $J = 7.7$ Hz, 1H), 7.96 (d, $J = 7.7$ Hz, 2H), 7.90 (d, $J = 7.7$ Hz, 2H), 7.83 (d, $J = 7.6$ Hz, 2H), 7.52 (m, 4H), 7.39 (m, 8H), 7.32 – 7.25 (m, 3H), 5.90 (t, $J = 9.6$ Hz, 1H), 5.65 (m, 2H), 5.53 (t, $J = 8.8$ Hz, 1H), 4.86 – 4.79 (m, 3H), 4.64 (d, $J = 11.9$ Hz, 1H), 4.50 (dd, $J_1 = 12.0$ Hz, $J_2 = 5.0$ Hz, 1H), 4.19 – 4.11 (m, 1H), 3.93 (dd, $J_1 = 15.4$ Hz, $J_2 = 6.4$ Hz, 1H), 3.55 (dd, $J_1 = 15.8$ Hz, $J_2 = 7.1$ Hz, 1H), 1.97 (m, 2H), 1.67 – 1.57 (m, 5H) ppm. ^{13}C NMR (125 MHz, CDCl_3): δ 166.2, 165.9, 165.2, 165.1, 137.7, 133.5, 133.2, 133.1, 129.8, 129.8, 129.8, 129.6, 129.3, 128.8, 128.4, 128.4, 128.3, 114.9, 101.3, 72.9, 72.2, 71.9, 69.8, 69.5, 63.2, 31.0, 29.8, 28.5 ppm.</p>
<p>Compound 1e</p> 	<p>^1H NMR (500 MHz, CDCl_3): δ 7.33 (t, $J = 7.0$ Hz, 6H), 7.31 – 7.25 (m, 13H), 7.16 (d, $J = 7.3$ Hz, 2H), 5.87 – 5.77 (m, 1H), 5.04 – 4.89 (m, 4H), 4.80 (dd, $J_1 = 14.7$ Hz, $J_2 = 11.0$ Hz, 2H), 4.72 (d, $J = 11.0$ Hz, 1H), 4.57 (m, 3H), 4.38 (d, $J = 7.8$ Hz, 1H), 4.00 – 3.92 (m, 1H), 3.74 (d, $J = 10.6$ Hz, 1H), 3.67 (dd, $J_1 = 10.8$ Hz, $J_2 = 4.7$ Hz, 1H), 3.63 (d, $J = 9.0$ Hz, 1H), 3.56 (m, 2H), 3.45 (t, $J = 8.4$ Hz, 2H), 2.20 – 2.14 (m, 2H), 1.75 (m, 2H) ppm. ^{13}C NMR (125 MHz, CDCl_3): δ 165.2, 138.0, 133.0, 129.7, 128.4, 128.3, 128.0, 127.8, 127.6, 114.7, 101.2, 82.8, 78.1, 75.0, 73.8, 73.6, 69.0, 29.9 ppm.</p>
<p>Compound 3aa</p>	<p>^1H NMR (500 MHz, CDCl_3): δ 7.95 (d, $J = 7.5$ Hz, 2H), 7.88 (d, $J = 7.5$ Hz, 2H), 7.84 (d, $J = 7.5$ Hz, 2H),</p>

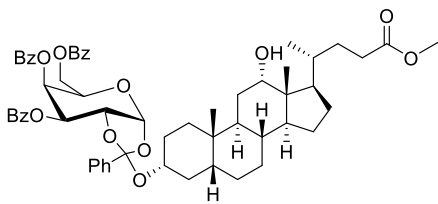
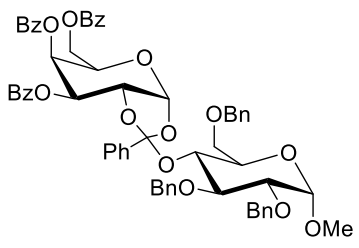
	<p>7.76 (d, $J = 7.5$ Hz, 2H), 7.48-7.41 (m, 4H), 7.37-7.26 (m, 8H), 7.23-7.19 (m, 3H), 5.84 (t, $J = 10.0$ Hz, 1H), 5.53 (t, $J = 10.0$ Hz, 1H), 5.47 (t, $J = 8.0$ Hz, 1H), 4.79 (d, $J = 8.0$ Hz, 1H), 4.56-4.53 (dd, $J_1 = 12.0$ Hz, $J_2 = 3.0$ Hz, 1H), 4.45-4.41 (dd, $J_1 = 12.0$ Hz, $J_2 = 6.5$ Hz, 1H), 4.13-4.09 (m, 1H), 3.68-3.65 (m, 1H), 1.78-1.72 (m, 1H), 1.65-1.54 (m, 4H), 1.28-1.21 (m, 3H), 1.59-1.14 (brd, 1H), 1.12-1.08 (m, 2H), 1.06-1.00 (m, 2H), 0.95-0.85 (m, 1H), 0.82-0.76 (m, 1H), 0.71 (d, $J = 7.0$ Hz, 3H), 0.55 (d, $J = 7.0$ Hz, 3H), 0.50 (d, $J = 7.0$ Hz, 3H) ppm. ^{13}C NMR (125 MHz, CDCl_3): δ 166.1, 165.9, 165.3, 165.1, 133.5, 133.2, 133.1, 129.9, 129.8, 129.7, 129.4, 128.9, 128.8, 128.4, 128.3, 128.3, 128.2, 101.4, 78.8, 73.0, 72.1, 72.0, 70.1, 63.6, 53.4, 46.3, 37.9, 29.9, 27.3, 25.2, 20.8, 20.2, 19.6, 18.2 ppm.</p> <p>ESI-HRMS: 757.2995 ($\text{M}+\text{Na}$)$^+$ (Observed) 757.2989 ($\text{M}+\text{Na}$)$^+$ (Calculated)</p>
<p>Compound 3ab</p> 	<p>^1H NMR (500 MHz, CDCl_3): δ 8.01 (d, $J = 8.0$ Hz, 2H), 7.96 (d, $J = 7.5$ Hz, 2H), 7.90 (d, $J = 8.0$ Hz, 2H), 7.83 (d, $J = 8.0$ Hz, 2H), 7.55-7.47 (m, 3H), 7.43-7.32 (m, 7H), 7.29-7.26 (m, 2H), 5.90 (t, $J = 9.5$ Hz, 1H), 5.63 (t, $J = 9.5$ Hz, 1H), 5.52-5.48 (dd, $J_1 = 8.0$ Hz, $J_2 = 1.5$ Hz, 1H), 5.22 (d, $J = 4.5$ Hz, 1H), 4.95 (d, $J = 8.0$ Hz, 1H), 4.62-4.59 (dd, $J_1 = 12.0$ Hz, $J_2 = 3.5$ Hz, 1H), 4.54-4.51 (dd, $J_1 = 12.0$ Hz, $J_2 = 6.0$ Hz, 1H), 4.18-4.14 (m, 1H), 3.55-3.51 (m, 1H), 2.19-2.12 (m, 2H), 2.02-1.99 (m, 1H), 1.93-1.90 (m, 2H), 1.86-1.78 (m, 1H), 1.73-1.70 (m, 1H), 1.63-1.46 (m, 5H), 1.44-1.33 (m, 8H), 1.26-1.21 (m, 2H), 1.17-1.05 (m, 7H), 1.06-0.94 (m, 5H), 0.92 (d, $J = 6.5$ Hz, 3H), 0.89 (s, 3H), 0.87 (d, $J = 2.0$ Hz, 3H), 0.86 (d, $J = 2.0$ Hz, 3H), 0.65 (s, 3H) ppm. ^{13}C NMR (125 MHz, CDCl_3): δ 166.1, 165.9, 165.3, 165.1, 140.3, 133.4, 133.2, 133.2, 133.1, 129.9,</p>

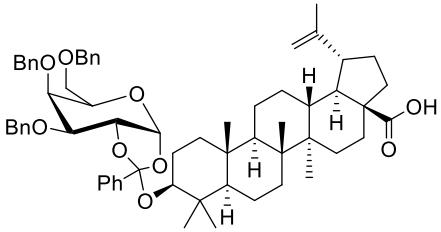
	<p>129.8, 129.8, 129.7, 129.7, 129.5, 128.9, 128.8, 128.4, 128.4, 128.4, 128.3, 122.0, 100.2, 80.5, 73.1, 72.1, 70.1, 63.4, 56.8, 56.2, 50.1, 42.3, 39.8, 39.5, 38.8, 37.1, 36.6, 36.2, 35.8, 31.9, 31.8, 29.6, 28.2, 28.0, 24.3, 23.8, 22.8, 22.6, 21.0, 19.3, 18.7, 11.9 ppm.</p> <p>ESI-HRMS: 987.5047 (M+Na)⁺ (Observed) 987.5023 (M+Na)⁺ (Calculated)</p>
<p>Compound 3ac</p> 	<p>¹H NMR (500 MHz, CDCl₃): δ 7.94 (d, <i>J</i> = 8.0 Hz, 2H), 7.88 (d, <i>J</i> = 7.0 Hz, 2H), 7.83 (d, <i>J</i> = 7.5 Hz, 2H), 7.76 (d, <i>J</i> = 7.0 Hz, 2H), 5.82 (t, <i>J</i> = 9.5 Hz, 1H), 5.58-5.54 (m, 1H), 5.44-5.40 (m, 1H), 5.23 (m, 1H), 5.15 (brd, 1H), 4.87 (d, <i>J</i> = 7.5 Hz, 1H), 4.54-4.51 (dd, <i>J</i>₁ = 12.0 Hz, <i>J</i>₂ = 3.0 Hz, 1H), 4.47-4.43 (dd, <i>J</i>₁ = 12.0 Hz, <i>J</i>₂ = 6.0 Hz, 1H), 4.09-4.07 (m, 1H), 3.51-3.44 (m, 2H), 2.22-2.16 (m, 2H), 2.12-2.06 (m, 2H), 1.95-1.93 (m, 1H), 1.93-1.90 (m, 2H), 1.89-1.86 (m, 2H), 1.83-1.81 (m, 1H), 1.79-1.74 (m, 3H), 1.66-1.54 (m, 8H), 1.52-1.47 (m, 4H), 1.43-1.42 (m, 2H), 1.39 (brs, 2H), 1.37-1.32 (m, 4H), 1.32-1.29 (m, 2H), 1.27-1.20 (m, 8H), 1.16-1.15 (brs, 2H), 1.15-1.13 (m, 2H), 1.12-1.10 (m, 2H), 1.09-1.06 (m, 6H), 1.03-0.94 (m, 8H), 0.93 (s, 3H), 0.92-0.87 (m, 5H), 0.86-0.84 (brd, 9H), 0.83-0.82 (brd, 1H), 0.79 (brs, 2H), 0.77 (brs, 6H), 0.76 (s, 3H), 0.75 (s, 3H), 0.73 (brd, 3H), 0.61 (s, 3H), 0.37 (s, 3H) ppm. ¹³C NMR (125 MHz, CDCl₃): δ 177.2, 166.1, 165.9, 165.3, 165.1, 140.8, 140.3, 133.4, 133.2, 133.1, 129.9, 129.8, 129.7, 129.6, 129.5, 128.9, 128.8, 128.4, 128.3, 128.3, 128.3, 122.0, 121.7, 100.2, 80.5, 73.1, 72.1, 71.8, 71.4, 70.1, 63.4, 56.8, 56.5, 56.2, 56.1, 54.4, 50.1, 45.8, 42.3, 40.1, 39.8, 38.8, 38.2, 37.3, 37.1, 37.0, 36.6, 36.5, 35.4, 33.9, 31.9, 31.6, 31.5, 29.1, 28.3, 26.1, 24.3, 24.2, 23.1, 21.3, 21.1, 21.0, 19.8, 19.4, 19.3, 19.1, 18.8, 12.3, 12.1, 12.0, 11.8 ppm.</p>

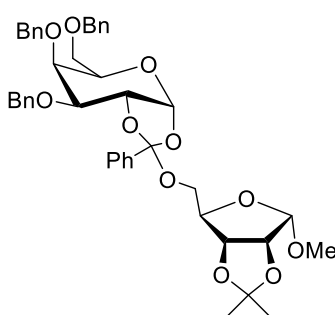
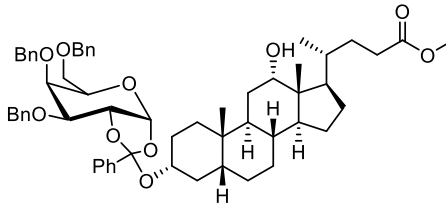
	<p>ESI-HRMS: 1033.5109 (M-H)⁺ (Observed) 1033.5107 (M-H)⁺ (Calculated)</p>
<p>Compound 3ae</p> 	<p>¹H NMR (500 MHz, CDCl₃): δ 7.94 (d, <i>J</i> = 7.5 Hz, 2H), 7.87 (d, <i>J</i> = 7.5 Hz, 2H), 7.84 (d, <i>J</i> = 7.5 Hz, 2H), 7.75 (d, <i>J</i> = 7.5 Hz, 2H), 7.47 (t, <i>J</i> = 7.0 Hz, 1H), 7.44-7.40 (m, 2H), 7.36-7.26 (m, 7H), 7.20 (t, <i>J</i> = 8.0 Hz, 2H), 5.82 (t, <i>J</i> = 9.5 Hz, 1H), 5.54 (t, <i>J</i> = 10.0 Hz, 1H), 5.39 (t, <i>J</i> = 8.5 Hz, 1H), 4.88 (d, <i>J</i> = 7.5 Hz, 1H), 4.56-4.53 (dd, <i>J</i>₁ = 12.0 Hz, <i>J</i>₂ = 3.0 Hz, 1H), 4.47-4.43 (dd, <i>J</i>₁ = 12.0 Hz, <i>J</i>₂ = 6.0 Hz, 1H), 4.11-4.07 (m, 1H), 3.81 (brs, 1H), 3.70 (brs, 1H), 3.58 (s, 3H), 3.42-3.38 (m, 1H), 2.30-2.23 (m, 2H), 2.18-2.13 (m, 1H), 2.03-1.96 (m, 2H), 1.85-1.75 (m, 4H), 1.72-1.64 (m, 4H), 1.60-1.57 (m, 3H), 1.48-1.46 (m, 2H), 1.37-1.34 (m, 4H), 1.32-1.21 (m, 9H), 1.08-1.00 (m, 2H), 0.88 (d, <i>J</i> = 5.5 Hz, 3H), 0.81 (t, <i>J</i> = 6.5 Hz, 3H), 0.74 (s, 3H), 0.57 (s, 3H) ppm. ¹³C NMR (125 MHz, CDCl₃): δ 166.2, 165.9, 165.3, 165.1, 133.4, 133.2, 133.1, 133.0, 129.9, 129.8, 129.8, 129.7, 129.7, 129.5, 128.9, 128.8, 128.4, 128.3, 128.3, 128.2, 99.8, 80.8, 73.1, 72.8, 72.2, 72.0, 70.2, 68.0, 63.5, 51.5, 47.3, 46.4, 41.9, 41.5, 39.5, 36.9, 35.1, 34.7, 34.5, 31.9, 31.4, 31.0, 30.9, 30.2, 29.7, 29.4, 27.4, 27.1, 26.7, 23.1, 22.7, 22.6, 17.3, 14.1, 12.5 ppm.</p> <p>ESI-HRMS: 1023.4525 (M+Na)⁺ (Observed) 1023.4507 (M+Na)⁺ (Calculated)</p>
<p>Compound 3ba</p> 	<p>¹H NMR (500 MHz, CDCl₃): δ 7.92 (d, <i>J</i> = 7.5 Hz, 2H), 7.48 (t, <i>J</i> = 7.5 Hz, 1H), 7.34 (t, <i>J</i> = 8.0 Hz, 2H), 7.29-7.18 (m, 9H), 7.17-7.14 (m, 3H), 7.07-7.03 (m, 5H), 5.21 (t, <i>J</i> = 8.5 Hz, 1H), 4.76 (d, <i>J</i> = 11.0 Hz, 1H), 4.66 (d, <i>J</i> = 11.5 Hz, 1H), 4.59 (brd, 1H), 4.54 (d, <i>J</i> = 5.0 Hz, 1H), 4.54-4.50 (m, 1H), 4.44 (d, <i>J</i> = 8.0 Hz, 1H), 3.74 (t, <i>J</i> = 9.0 Hz, 1H), 3.71-3.66 (t, <i>J</i> = 9.5 Hz, 2H), 3.64 (brd, 1H), 3.62 (brd, 1H), 3.49-3.47 (m, 1H),</p>

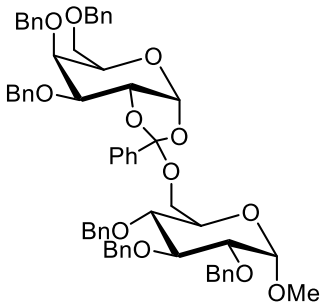
	<p>1.80-1.77 (m, 1H), 1.62-1.57 (m, 2H), 1.51-1.46 (m, 1H), 1.27-1.16 (m, 2H), 1.08-0.96 (m, 1H), 0.74 (d, $J = 7.0$ Hz, 3H), 0.56 (d, $J = 6.5$ Hz, 3H) ppm. ^{13}C NMR (125 MHz, CDCl_3): δ 165.2, 138.3, 138.0, 137.9, 133.0, 130.2, 129.7, 128.5, 128.4, 128.3, 128.1, 128.1, 127.9, 127.7, 127.6, 127.6, 101.4, 82.9, 78.2, 78.1, 75.2, 75.0, 74.0, 73.5, 69.0, 46.2, 37.8, 29.9, 27.3, 25.3, 21.0, 20.6, 20.0, 18.6 ppm.</p> <p>ESI-HRMS: 715.3606 ($\text{M}+\text{Na}$)⁺ (Observed) 715.3611 ($\text{M}+\text{Na}$)⁺ (Calculated)</p>
<p>Compound 3be</p> 	<p>^1H NMR (500 MHz, CDCl_3): δ 7.93 (d, $J = 7.5$ Hz, 2H), 7.48 (t, $J = 7.5$ Hz, 1H), 7.37-7.34 (m, 2H), 7.28-7.15 (m, 11H), 7.10-7.03 (m, 5H), 5.47 (t, $J = 9.0$ Hz, 1H), 4.89 (d, $J = 11.6$ Hz, 1H), 4.57-4.48 (m, 3H), 4.43-4.34 (m, 3H), 3.90 (s, 1H), 3.75 (s, 1H), 3.64 (s, 1H), 3.59-3.50 (m, 7H), 3.30 (m, 1H), 2.32-2.23 (m, 1H), 2.13 (m, 3H), 1.93 (m, 3H), 1.81-1.60 (m, 8H), 1.55 (brd, 2H), 1.43-1.23 (m, 9H), 1.23-1.06 (m, 6H), 0.98-0.88 (m, 2H), 0.86 (d, $J = 5.5$ Hz, 3H), 0.84-0.74 (m, 2H), 0.72 (s, 3H), 0.53 (s, 3H) ppm. ^{13}C NMR (125 MHz, CDCl_3): δ 174.9, 165.3, 138.5, 138.0, 137.8, 132.8, 130.5, 129.8, 128.5, 128.4, 128.3, 128.2, 127.9, 127.8, 127.7, 127.6, 127.6, 100.5, 80.2, 74.4, 73.7, 73.6, 72.8, 72.6, 72.3, 71.7, 69.0, 68.1, 51.5, 46.9, 46.4, 41.8, 41.5, 39.5, 37.4, 35.2, 35.1, 34.8, 34.67, 31.1, 30.9, 28.3, 27.4, 27.2, 26.5, 23.1, 22.6, 17.3, 12.5 ppm.</p> <p>ESI-HRMS: 981.5133 ($\text{M}+\text{Na}$)⁺ (Observed) 981.5129 ($\text{M}+\text{Na}$)⁺ (Calculated)</p>
<p>Mixture of compound 3ce and 4ce</p> 	<p>^1H NMR (500 MHz, CDCl_3): δ 5.47 (t, $J = 9.5$ Hz, 1.34H), 5.39 (d, $J = 2.5$ Hz, 1.0H), 5.18 (t, $J = 9.5$ Hz, 0.50H), 5.02 (m, 2H), 4.85-4.81 (m, 2H), 4.68 (d, $J = 8.0$ Hz, 0.30H), 4.21-4.15 (m, 4H), 4.07 (t, $J = 12.5$ Hz, 2H), 3.92 (brs, 1H), 3.70-3.67 (m, 0.5H), 3.59 (s, 3H),</p>

	<p>3.57-3.52 (m, 1H), 2.23-2.27 (m, 1H), 2.19-2.14 (m, 1H), 2.11 (brd, 1H), 2.03-2.02 (d, $J = 5.0$ Hz, 11H), 1.97-1.95 (m, $J = 8.5$ Hz, 11H), 1.91-1.77 (m, 5H), 1.76-1.72 (m, 3H), 1.69-1.65 (m, 2H), 1.63-1.58 (m, 2H), 1.55-1.48 (m, 1H), 1.45-1.44 (m, 3H), 1.38-1.19 (m, 9H), 1.07-0.98 (m, 2H), 0.89 (d, $J = 6.0$ Hz, 3H), 0.84 (s, 3H), 0.61 (s, 3H) ppm. $^{13}\text{C}\{1\text{H}\}$ NMR (125 MHz, CDCl_3): δ 177.9, 177.8, 174.9, 170.9, 170.3, 169.7, 95.5 (β), 90.1 (α), 73.3, 73.1, 72.0, 71.8, 71.1, 69.9, 68.5, 68.4, 67.1, 62.0, 51.5, 48.2, 47.2, 46.5, 42.0, 36.2, 36.0, 35.2, 35.1, 34.1, 33.6, 31.1, 30.9, 30.3, 29.6, 28.5, 27.4, 27.1, 26.1, 23.6, 23.1, 20.8, 20.7, 20.7, 20.6, 20.6, 17.3, 12.7 ppm.</p> <p>ESI-HRMS: 775.3881 ($\text{M}+\text{Na}$)⁺ (Observed) 775.3881 ($\text{M}+\text{Na}$)⁺ (Calculated)</p>
<p>Mixture of compound 3cf and 4cf</p> 	<p>^1H NMR (500 MHz, CDCl_3): δ 5.48 (t, $J = 10.0$ Hz, 1.09H), 5.39 (d, $J = 2.1$ Hz, 1.0H), 5.23-5.16 (m, 0.48H), 5.02 (t, $J = 10.0$ Hz, 1.64H), 4.84-4.82 (m, 1.39H), 4.68 (d, $J = 8.0$ Hz, 0.33H), 4.22-4.17 (m, 2.10H), 4.10-4.04 (m, 2.10H), 3.91 (s, 1.93H), 3.60 (s, 5.28H), 3.56-3.52 (m, 1.97H), 2.33-2.27 (m, 2.18H), 2.20-2.14 (m, 2.75H), 2.03 (d, $J = 4.5$ Hz, 7.33H), 1.97-1.95 (m, 7.61H), 1.84-1.66 (m, 18.49H), 1.63-1.59 (m, 5.19H), 1.55-1.51 (m, 2.89H), 1.48-1.44 (m, 8.13H), 1.36-1.24 (m, 13.25H), 1.21-1.19 (m, 4.96H), 1.10-0.93 (m, 6.29H), 0.90 (d, $J = 6.0$ Hz, 5.42H), 0.84 (s, 5.35H), 0.61 (s, 5.14H) ppm. $^{13}\text{C}\{1\text{H}\}$ NMR (125 MHz, CDCl_3): δ 174.8, 170.9, 170.2, 169.7, 95.5 (β), 90.1 (α), 73.2, 71.8, 71.2, 69.9, 68.5, 67.1, 62.0, 51.5, 48.2, 47.3, 46.5, 42.0, 36.3, 36.0, 35.2, 35.1, 34.1, 33.6, 31.1, 30.9, 30.4, 28.6, 27.5, 27.1, 26.1, 23.6, 23.1, 20.8, 20.7, 20.7, 20.6, 17.3, 12.7 ppm.</p> <p>ESI-HRMS: 759.3951 ($\text{M}+\text{Na}$)⁺ (Observed)</p>

	759.3932 (M+Na) ⁺ (Calculated)
<p>Compound 5df</p> 	<p>¹H NMR (500 MHz, CDCl₃): δ 7.87 (d, <i>J</i> = 7.5 Hz, 2H), 7.82 (d, <i>J</i> = 7.6 Hz, 2H), 7.79 (d, <i>J</i> = 7.5 Hz, 2H), 7.64-7.60 (m, 2H), 7.46 – 7.38 (m, 5H), 7.35-7.20 (m, 13H), 6.25 (d, <i>J</i> = 4.8 Hz, 1H), 5.68-5.63 (m, 1H), 5.49 (t, <i>J</i> = 5.0 Hz, 1H), 5.09-5.03 (m, 1H), 4.90 (t, <i>J</i> = 5.2 Hz, 1H), 4.48 (dd, <i>J</i>₁ = 11.5 Hz, <i>J</i>₂ = 6.8 Hz, 1H), 4.38-4.34 (m, 1H), 4.26 (dd, <i>J</i>₁ = 11.5 Hz, <i>J</i>₂ = 5.2 Hz, 1H), 3.81 (s, 1H), 3.77 (s, 1H), 3.70 (m, 1H), 3.56 (s, 3H), 2.39 (d, <i>J</i> = 15.5 Hz, 1H), 2.26 (m, 2H), 2.16-2.09 (m, 2H), 2.00-1.95 (m, 1H), 1.81-1.75 (m, 3H), 1.70 (dd, <i>J</i>₁ = 20.1 Hz, <i>J</i>₂ = 13.2 Hz, 2H), 1.64-1.59 (m, 2H), 1.59-1.53 (m, 3H), 1.40-1.36 (m, 2H), 1.34 (d, <i>J</i> = 7.6 Hz, 3H), 1.19 (t, <i>J</i> = 9.0 Hz, 3H), 1.16 (s, 3H), 1.12 (s, 2H), 1.08-0.98 (m, 2H), 0.91 (t, <i>J</i> = 6.8 Hz, 1H), 0.85 (d, <i>J</i> = 6.1 Hz, 4H), 0.80 (t, <i>J</i> = 7.6 Hz, 5H), 0.55 (s, 3H) ppm. ¹³C{¹H} NMR (125 MHz, CDCl₃): δ 174.6, 165.2, 137.3, 133.4, 133.2, 133.1, 129.9, 129.7, 128.5, 128.5, 128.4, 128.4, 128.3, 128.3, 126.1, 120.5, 98.1, 74.1, 73.2, 73.2, 73.1, 69.9, 68.8, 62.4, 51.5, 51.4, 48.3, 48.2, 47.3, 46.5, 35.1, 34.0, 33.7, 33.5, 31.9, 31.1, 30.9, 29.7, 28.6, 27.4, 27.1, 27.0, 26.1, 26.0, 23.6, 23.0, 17.3, 12.7 ppm.</p> <p>ESI-HRMS: 1007.4574 (M+Na)⁺ (Observed) 1007.4558 (M+Na)⁺ (Calculated)</p>
<p>Compound 5dh</p> 	<p>¹H NMR (500 MHz, CDCl₃): δ 7.89-7.81 (m, 9H), 7.58-7.55 (m, 3H), 7.47 (m, 7H), 7.35-7.18 (m, 32H), 7.14 (s, 2H), 7.09 (d, <i>J</i> = 7.5 Hz, 2H), 6.10 (d, <i>J</i> = 5.0 Hz, 1H), 5.72 – 5.70 (m, 1H), 5.40 (dd, <i>J</i>₁ = 6.1 Hz, <i>J</i>₂ = 4.1 Hz, 1H), 4.89 (d, <i>J</i> = 10.9 Hz, 1H), 4.77 (d, <i>J</i> = 10.7 Hz, 1H), 4.71 (dd, <i>J</i>₁ = 14.3 Hz, <i>J</i>₂ = 11.6 Hz, 3H), 4.65 – 4.62 (m, 2H), 4.57 (d, <i>J</i> = 12.1 Hz, 2H), 4.53 (d, <i>J</i> = 3.3 Hz, 1H), 4.50 (dd, <i>J</i>₁ = 11.4 Hz, <i>J</i>₂ = 6.7 Hz,</p>

	<p>2H), 4.45 (d, $J = 10.7$ Hz, 2H), 4.41 (dd, $J_1 = 11.2$ Hz, $J_2 = 5.7$ Hz, 2H), 4.28 (dd, $J_1 = 11.4$ Hz, $J_2 = 5.8$ Hz, 1H), 3.88 (t, $J = 9.2$ Hz, 1H), 3.64 (d, $J = 8.1$ Hz, 2H), 3.62-3.53 (m, 3H), 3.46-3.39 (m, 3H), 3.27 (s, 3H) ppm. $^{13}\text{C}\{^1\text{H}\}$ NMR (125 MHz, CDCl_3): δ 165.2, 138.2, 133.4, 129.8, 129.7, 128.5, 128.4, 128.4, 128.1, 127.9, 127.8, 126.1, 120.3, 98.0, 82.1, 79.9, 75.7, 75.0, 73.5, 73.3, 70.4, 69.4, 69.0, 66.6, 55.1 ppm.</p> <p>ESI-HRMS: 1065.3698 ($\text{M}+\text{Na}$)⁺ (Observed) 1065.3673 ($\text{M}+\text{Na}$)⁺ (Calculated)</p>
<p>Compound 5ec</p> 	<p>^1H NMR (500 MHz, CDCl_3): δ 7.97 (d, $J = 7.4$ Hz, 2H), 7.54 (t, $J = 7.4$ Hz, 1H), 7.39 (t, $J = 7.8$ Hz, 2H), 7.31-7.25 (m, 5H), 7.23 (d, $J = 6.6$ Hz, 4H), 7.19 (s, 1H), 7.15-7.11 (m, 3H), 7.10 (dd, $J_1 = 12.3$ Hz, $J_2 = 5.0$ Hz, 3H), 5.59 (d, $J = 10.0$ Hz, 1H), 4.92 (d, $J = 11.3$ Hz, 1H), 4.67 (s, 1H), 4.63-4.58 (m, 1H), 4.55 (d, $J = 11.9$ Hz, 2H), 4.50-4.46 (m, 2H), 4.44 (d, $J = 12.9$ Hz, 2H), 4.39 (d, $J = 4.3$ Hz, 1H), 4.22 (s, 1H), 4.12 (dd, $J_1 = 10.0$ Hz, $J_2 = 2.1$ Hz, 1H), 3.70 (t, $J = 8.8$ Hz, 1H), 3.65 (dd, $J_1 = 9.1$ Hz, $J_2 = 5.4$ Hz, 1H), 3.12 (dd, $J_1 = 11.4$ Hz, $J_2 = 4.8$ Hz, 1H), 2.93 (td, $J_1 = 10.7$ Hz, $J_2 = 4.8$ Hz, 1H), 2.23-2.17 (m, 1H), 2.11 (m, 1H), 1.90 (dd, $J_1 = 17.3$ Hz, $J_2 = 8.2$ Hz, 2H), 1.62 (s, 3H), 1.60-1.51 (m, 4H), 1.50-1.41 (m, 4H), 1.41-1.31 (m, 5H), 1.30 (s, 2H), 1.18 (s, 1H), 1.16-1.08 (m, 2H), 0.99 (d, $J = 8.9$ Hz, 1H), 0.94 (t, $J = 5.3$ Hz, 2H), 0.90 (dd, $J_1 = 7.0$ Hz, $J_2 = 4.4$ Hz, 6H), 0.87-0.84 (m, 3H), 0.84-0.76 (m, 3H), 0.75 (s, 3H), 0.68 (s, 3H) ppm. $^{13}\text{C}\{^1\text{H}\}$ NMR (125 MHz, CDCl_3): δ 174.5, 150.6, 150.5, 138.5, 138.4, 138.2, 137.9, 128.4, 128.3, 128.3, 128.2, 127.9, 127.8, 127.7, 127.6, 127.3, 109.7, 93.8, 82.7, 79.0, 75.0, 74.8, 73.5, 72.9, 68.2, 56.6, 56.3, 55.4, 50.5, 49.3, 46.9, 42.4, 40.7, 40.6, 38.9, 38.7, 38.4, 37.8, 37.2, 34.3, 32.2, 30.6,</p>

	<p>29.7, 28.0, 27.4, 25.5, 20.9, 19.4, 18.3, 16.1, 15.9, 15.4, 14.7, 14.6 ppm.</p> <p>ESI-HRMS: 1015.5708 (M+Na)⁺ (Observed) 1015.5700 (M+Na)⁺ (Calculated)</p>
<p>Compound 5ed</p> 	<p>¹H NMR (500 MHz, CDCl₃): δ 7.51 (dd, <i>J</i>₁ = 7.2 Hz, <i>J</i>₂ = 2.2 Hz, 3H), 7.29-7.14 (m, 27H), 5.88 (d, <i>J</i> = 4.9 Hz, 1H), 4.85-4.76 (m, 3H), 4.60-4.52 (m, 4H), 4.50 - 4.44 (m, 2H), 4.42-4.30 (m, 4H), 4.24-4.20 (m, 1H), 3.88 (t, <i>J</i> = 6.8 Hz, 1H), 3.75 (s, 1H), 3.57-3.46 (m, 3H), 3.42-3.34 (m, 3H), 3.16 (s, 3H), 1.38 (s, 3H), 1.22 (d, <i>J</i> = 4.7 Hz, 3H) ppm. ¹³C{¹H} NMR (125 MHz, CDCl₃): δ 166.0, 138.3, 133.13, 129.9, 129.8, 128.6, 128.5, 128.5, 128.4, 128.4, 128.3, 128.1, 128.0, 127.9, 127.9, 127.8, 127.7, 110.0, 92.8, 91.0, 79.4, 78.7, 76.2, 74.7, 74.5, 73.6, 72.6, 72.1, 71.7, 69.6, 64.0, 30.2, 29.7, 26.4 ppm.</p> <p>ESI-HRMS: 763.3109 (M+Na)⁺ (Observed) 763.3094 (M+Na)⁺ (Calculated)</p>
<p>Compound 5ef</p> 	<p>¹H NMR (500 MHz, CDCl₃): δ 7.50 (dd, <i>J</i>₁ = 7.6 Hz, <i>J</i>₂ = 1.8 Hz, 2H), 7.35 (d, <i>J</i> = 7.3 Hz, 2H), 7.32-7.18 (m, 20H), 5.50 (d, <i>J</i> = 4.7 Hz, 1H), 4.84-4.75 (m, 2H), 4.68 (d, <i>J</i> = 12.1 Hz, 1H), 4.54 (t, <i>J</i> = 10.7 Hz, 1H), 4.47 (dd, <i>J</i>₁ = 11.7 Hz, <i>J</i>₂ = 4.7 Hz, 1H), 4.41-4.35 (m, 1H), 4.27-4.23 (m, 1H), 4.12 (m, 1H), 4.02-3.97 (m, 2H), 3.84 (s, 1H), 3.69 (m, 1H), 3.59 (s, 3H), 3.58 (d, <i>J</i> = 6.7 Hz, 3H), 2.30 (m, 1H), 2.15 (m, 1H), 1.79-1.65 (m, 5H), 1.63-1.56 (m, 3H), 1.50-1.38 (m, 4H), 1.35 (d, <i>J</i> = 8.7 Hz, 3H), 1.33-1.22 (m, 6H), 1.22-1.13 (m, 3H), 1.06 (d, <i>J</i> = 15.6 Hz, 1H), 1.04-0.92 (m, 2H), 0.89 (d, <i>J</i> = 6.1 Hz, 3H), 0.76 (d, <i>J</i> = 9.3 Hz, 4H), 0.57 (s, 3H) ppm. ¹³C{¹H} NMR (125 MHz, CDCl₃): δ 174.6, 165.2, 137.3, 133.4, 133.1, 129.9, 129.7, 128.3, 126.1, 120.5, 98.1, 76.8, 76.7, 74.1, 73.2, 73.2, 73.1, 69.9,</p>

	62.4, 51.4, 48.2, 46.5, 42.1, 36.0, 35.1, 34.0, 31.1, 30.9, 29.7, 28.6, 27.4, 26.0, 23.6, 23.0, 17.3, 12.7 ppm. ESI-HRMS: 965.5199 (M+Na) ⁺ (Observed) 965.5180 (M+Na) ⁺ (Calculated)
Compound 5eg 	¹H NMR (500 MHz, CDCl ₃): δ 7.53-7.47 (m, 3H), 7.27-7.22 (m, 16H), 7.22-7.19 (m, 10H), 7.19-7.17 (m, 10H), 7.16 (d, <i>J</i> = 8.7 Hz, 5H), 7.14-7.11 (m, 3H), 5.84 (d, <i>J</i> = 4.8 Hz, 1H), 4.88 (d, <i>J</i> = 10.9 Hz, 1H), 4.78 (d, <i>J</i> = 11.6 Hz, 1H), 4.73 (d, <i>J</i> = 10.8 Hz, 2H), 4.68 (d, <i>J</i> = 12.1 Hz, 1H), 4.59-4.56 (m, 2H), 4.56-4.53 (m, 1H), 4.53-4.51 (m, 2H), 4.48 (dd, <i>J</i> ₁ = 11.1 Hz, <i>J</i> ₂ = 6.0 Hz, 2H), 4.40 (d, <i>J</i> = 3.5 Hz, 1H), 4.38 (d, <i>J</i> = 3.3 Hz, 1H), 4.32 (d, <i>J</i> = 11.8 Hz, 1H), 3.87 (dd, <i>J</i> ₁ = 17.3 Hz, <i>J</i> ₂ = 8.0 Hz, 2H), 3.76 (s, 1H), 3.62 (dt, <i>J</i> ₁ = 10.3 Hz, <i>J</i> ₂ = 7.0 Hz, 4H), 3.50 (d, <i>J</i> = 6.6 Hz, 2H), 3.47-3.40 (m, 3H), 3.37 (dd, <i>J</i> ₁ = 7.0 Hz, <i>J</i> ₂ = 2.5 Hz, 1H), 3.26 (s, 3H) ppm. ¹³C{¹H} NMR (125 MHz, CDCl ₃): δ 164.6, 138.8, 138.4, 138.2, 138.1, 133.4, 129.8, 128.6, 128.5, 128.4, 128.3, 128.3, 128.1, 128.0, 127.9, 127.6, 98.2, 92.9, 91.1, 82.0, 80.0, 75.8, 75.8, 75.0, 74.9, 74.8, 73.7, 73.6, 73.4, 72.7, 72.0, 70.7, 61.9, 55.2 ppm. ESI-HRMS: 1023.4297 (M+Na) ⁺ (Observed) 1023.4295 (M+Na) ⁺ (Calculated)

References

- [1] S. Manabe, Y. Ito, Optimizing Glycosylation Reaction Selectivities by Protecting Group Manipulation, *Curr. Bioact. Compd.* 4 (2008) 258–281. <https://doi.org/10.2174/157340708786847861>.
- [2] B. Fraser-Reid, J.C. Lopez, K. V. Radhakrishnan, M. Mach, U. Schlueter, A. Gomez, C. Uriel, Reciprocal donor acceptor selectivity (RDAS): A new concept for “matching” donors with acceptors, *Can. J. Chem.* 80 (2002) 1075–1087. <https://doi.org/10.1139/v02-137>.

- [3] M.M. Nielsen, C.M. Pedersen, Catalytic Glycosylations in Oligosaccharide Synthesis, *Chem. Rev.* 118 (2018) 8285–8358. <https://doi.org/10.1021/acs.chemrev.8b00144>.
- [4] G. Sureshkumar, S. Hotha, Propargyl 1,2-orthoesters as glycosyl donors: stereoselective synthesis of Propargyl 1,2-orthoesters as glycosyl donors: stereoselective synthesis of 1,2-trans glycosides and disaccharides, *Tetrahedron Lett.* 48 (2007) 6564–6568. <https://doi.org/10.1016/j.tetlet.2007.07.015>.
- [5] B. Fraser-Reid, J.C. Lopez, K. V. Radhakrishnan, M. Mach, U. Schlueter, A.M. Gomez, C. Uriel, Unexpected role of O-2 “protecting” groups of glycosyl donors in mediating regioselective glycosidation, *J. Am. Chem. Soc.* 124 (2002) 3198–3199. <https://doi.org/10.1021/ja012383m>.
- [6] K.N. Jayaprakash, S.R. Chaudhuri, C.V.S.R. Murty, B. Fraser-Reid, Regioselective strategies mediated by lanthanide triflates for efficient assembly of oligomannans, *J. Org. Chem.* 72 (2007) 5534–5545. <https://doi.org/10.1021/jo070018t>.
- [7] M. Mach, U. Schlueter, F. Mathew, B. Fraser-Reid, K.C. Hazen, Comparing n-pentenyl orthoesters and n-pentenyl glycosides as alternative glycosyl donors, *Tetrahedron.* 58 (2002) 7345–7354. [https://doi.org/10.1016/S0040-4020\(02\)00671-3](https://doi.org/10.1016/S0040-4020(02)00671-3).
- [8] Z. Yang, W. Lin, B. Yu, Rearrangement of sugar 1,2-orthoesters to glycosidic products: A mechanistic implication, *Carbohydr. Res.* 329 (2000) 879–884. [https://doi.org/10.1016/S0008-6215\(00\)00242-1](https://doi.org/10.1016/S0008-6215(00)00242-1).
- [9] J.G. Allen, B. Fraser-Reid, n-Pentenyl glycosyl orthoesters as versatile intermediates in oligosaccharide synthesis. The proteoglycan linkage region, *J. Am. Chem. Soc.* 121 (1999) 468–469. <https://doi.org/10.1021/ja9832358>.
- [10] T. Buskas, E. Söderberg, P. Konradsson, B. Fraser-Reid, Use of n -Pentenyl Glycosides as Precursors to Various Spacer Functionalities, *J. Org. Chem.* 65 (2000) 958–963. <https://doi.org/10.1021/jo9909554>.
- [11] B. Fraser-Reid, P. Konradsson, D.R. Mootoo, U. Udodong, Direct elaboration of pent-4-enyl glycosides into disaccharides, *J. Chem. Soc. Chem. Commun.* (1988) 823–825. <https://doi.org/10.1039/c39880000823>.
- [12] A. Arasappan, B. Fraser-Reid, n -Pentenyl Glycoside Methodology in the

- Stereoselective Construction of the Tetrasaccharyl Cap Portion of Leishmania Lipophosphoglycan, *J. Org. Chem.* 61 (1996) 2401–2406. <https://doi.org/10.1021/jo9520102>.
- [13] T.H.L. Chirag D. Gheewala, Bridget E. Collins, An aromatic ion platform for enantioselective Brønsted acid catalysis, *Science* (80-.). 351 (2016) 961–965. https://doi.org/10.1142/9781783268993_0002.
- [14] C.D. Gheewala, M.A. Radtke, J. Hui, A.B. Hon, T.H. Lambert, Methods for the Synthesis of Functionalized Pentacarboxycyclopentadienes, *Org. Lett.* 19 (2017) 4227–4230. <https://doi.org/10.1021/acs.orglett.7b01867>.
- [15] D. Benito-Alifonso, M.C. Galan, Brønsted- and Lewis-Acid-Catalyzed Glycosylation, in: *Sel. Glycosylations Synth. Methods Catal.*, Wiley-VCH Verlag GmbH & Co. KGaA, Weinheim, Germany, 2017: pp. 155–172. <https://doi.org/10.1002/9783527696239.ch8>.
- [16] D.J. Cox, M.D. Smith, A.J. Fairbanks, Glycosylation Catalyzed by a Chiral Brønsted Acid, *Org. Lett.* 12 (2010) 1452–1455. <https://doi.org/10.1021/ol1001895>.
- [17] L. Meng, P. Wu, J. Fang, Y. Xiao, X. Xiao, G. Tu, X. Ma, S. Teng, J. Zeng, Q. Wan, Glycosylation Enabled by Successive Rhodium(II) and Brønsted Acid Catalysis, *J. Am. Chem. Soc.* 141 (2019) 1–6. <https://doi.org/10.1021/jacs.9b04619>.
- [18] D. Liu, S. Sarrafpour, W. Guo, B. Goulart, C.S. Bennett, Matched/Mismatched interactions in chiral brønsted acid-catalyzed glycosylation reactions with 2-deoxy-sugar trichloroacetimidate donors, *J. Carbohydr. Chem.* 33 (2014) 423–434. <https://doi.org/10.1080/07328303.2014.927882>.
- [19] S. Traboni, E. Bedini, A. Silipo, G. Vessella, A. Iadonisi, Solvent-Free Glycosylation from per-O-Acylated Donors Catalyzed by Methanesulfonic Acid, *European J. Org. Chem.* 2021 (2021) 5669–5676. <https://doi.org/10.1002/ejoc.202101121>.
- [20] X. HU, Z. ZHANG, X. ZHANG, Z. LI, X. ZHU, Selective acylation of cholic acid derivatives with multiple methacrylate groups, *Steroids.* 70 (2005) 531–537. <https://doi.org/10.1016/j.steroids.2004.11.015>.
- [21] P.S. Dangate, C.L. Salunke, K.G. Akamanchi, Regioselective oxidation of cholic acid and its 7 β epimer by using o-iodoxybenzoic acid, *Steroids.* 76 (2011) 1397–1399.

<https://doi.org/10.1016/j.steroids.2011.07.009>.

- [22] B. Fraser-Reid, S. Grimme, M. Piacenza, M. Mach, U. Schlueter, Orthoesters versus 2-O-acyl glycosides as glycosyl donors: Theoretical and experimental studies, *Chem. - Eur. J.* 9 (2003) 4687–4692. <https://doi.org/10.1002/chem.200304856>.
- [23] T. Kimura, M. Sekine, D. Takahashi, K. Toshima, Chiral Brønsted acid mediated glycosylation with recognition of alcohol chirality, *Angew. Chemie - Int. Ed.* 52 (2013) 12131–12134. <https://doi.org/10.1002/anie.201304830>.
- [24] E.T. Sletten, Y.J. Tu, H.B. Schlegel, H.M. Nguyen, Are Brønsted Acids the True Promoter of Metal-Triflate-Catalyzed Glycosylations? A Mechanistic Probe into 1,2-cis-Aminoglycoside Formation by Nickel Triflate, *ACS Catal.* 9 (2019) 1–30. <https://doi.org/10.1021/acscatal.8b04444>.

α/β -Stereo- and Diastereoselective Glycosylation with *n*-Pentenyl Glycoside Donors, Promoted by *N*-Iodosuccinimide and Catalysed by Chiral Brønsted Acid

5.1. Introduction

Hydrolysis of the glycosidic bond by glycosidases or glycosylation by glycosyltransferases is governed by acid-base catalysis by amino acids Asp, Glu and Tyr as the catalytic residues in the active site [1,2]. It is intuitive that Brønsted acid (BA) can take the role of enzymes when used with appropriate glycosyl donors for synthetic glycosylation. Activation of glycosyl donors by Lewis acids is dominant in glycosylation compared to BA-based promoters that were employed, in general, for 1-hydroxy and trichloroacetimidate glycosyl donors [3-8]. Sulfuric acid immobilized on silica as BA in combination with *N*-iodosuccinimide (NIS) was utilized in activation of a thioglycoside for the synthesis of a tetrasaccharide fragments [9,10]. Further, glycosylation attempts were made with chiral BA (CBA) activation with an aim to achieve α/β -stereoselectivity, which include a tetrazole-amino acid ionic liquid [7], chiral binaphthol (BINOL) phosphoric acids [11-13], and peptide bearing carboxylic acid groups in combination with MgBr₂ Lewis acid [14].

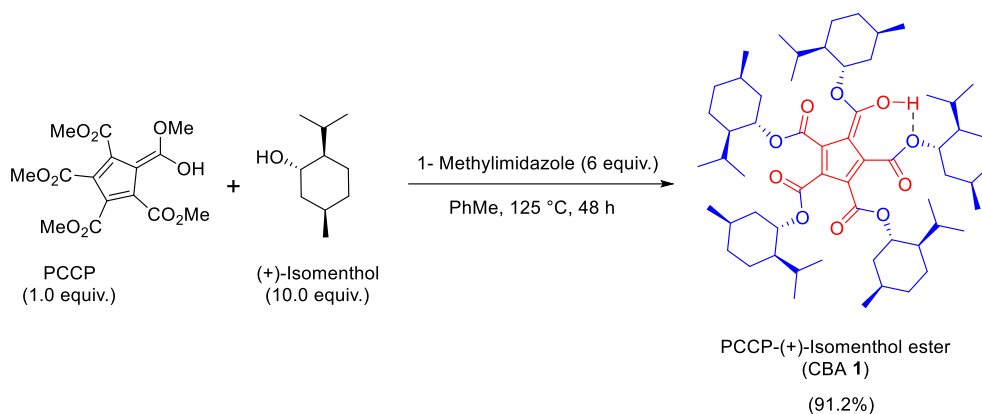
Recently, we reported the catalytic utility of the BA-PCCP (pentacarbomethoxycyclopentadiene) for stereoselective glycosylation with *n*-pentenyl orthoesters (NPOE) of D-glucose and D-galactose in the presence of *N*-iodosuccinimide (NIS) [15]. Oxidative hydrolysis of *n*-pentenyl glucoside (NPG) with *N*-bromosuccinimide to a hemiacetal is an outcome of a serendipitous observation by Fraser-Reid, which led to the inception of NPG and NPOE glycosyl donors [16]. BA-PCCP catalysis was a pioneering contribution by Lambert et al., who prepared the chiral version of this BA by appending naturally occurring (-)-menthol as an ester and showed its utility in Mukaiyama-Mannich and oxocarbenium aldol reactions in an enantioselective manner [17]. Toshima *et al.* utilized chiral BINOL phosphoric acid as BA that resulted in enantioselective catalysis for glycosylation with trichloroacetimidate donors, affording excellent α/β -stereo- and diastereoselectivity [11]. Inspired by these two reports, we present herein our preliminary findings on stereoselective glycosylation with NPG donor in the presence of NIS, by efficient chiral catalysis from (+)-isomenthol ester of PCCP, which offered

chiral recognition of racemic aglycones viz. menthol, benzylic alcohols, and Boc-protected serine.

5.2. Results and Discussion

5.2.1. Synthesis of chiral Brønsted acids, CBA 1, CBA 3 & CBA 4

1,2,3,4,5-Pentacarbomethoxycyclopentadiene (300 mg, 0.842 mmol, 1.0 equiv.), (+)-isomenthol (1.316 g, 10.0 equiv.), and 1-methylimidazole (0.403 mL, 5.052 mmol, 6.0 equiv.) were dissolved in toluene (10.0 mL). The reaction was heated in an ace pressure tube at a temperature of 125 °C (Scheme 1). The reaction mixture was cooled after 48 h to room temperature and concentrated. The crude mixture was purified by CC using a gradient combination of MeOH/DCM (2 → 5%). The purified material was subsequently acidified with 3 M HCl (3 x 10 mL), dried with anhydrous Na₂SO₄, and concentrated in vacuum to yield a black syrupy liquid, then it was dissolved in a small amount of hexane (10 mL), stirred with 200 mg of activated charcoal for 20 min, and filtered through celite-545® to yield a white solid (750.57 mg, 91.2% yield). The structure of the molecule was confirmed with ¹H NMR, ¹³C NMR, and ESI-HRMS analysis.



Scheme 1: Synthesis of CBA 1 from PCCP and (+)-isomenthol.

Similarly, we have synthesized the other two chiral Brønsted acids CBA 3 and CBA 4.

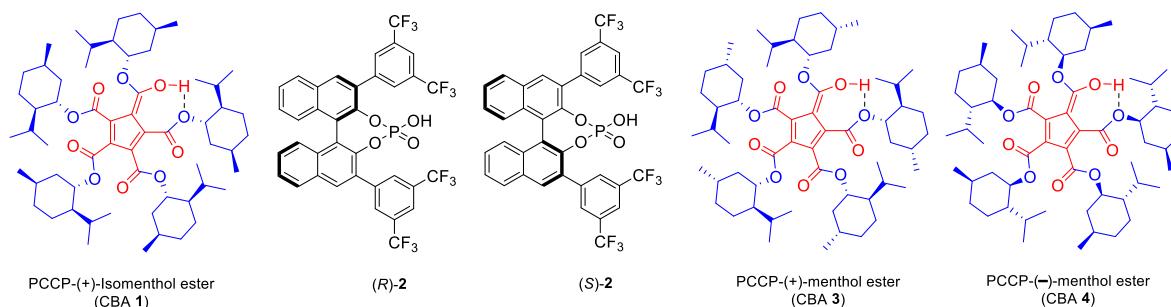


Figure 5.1: Structure of CBAs

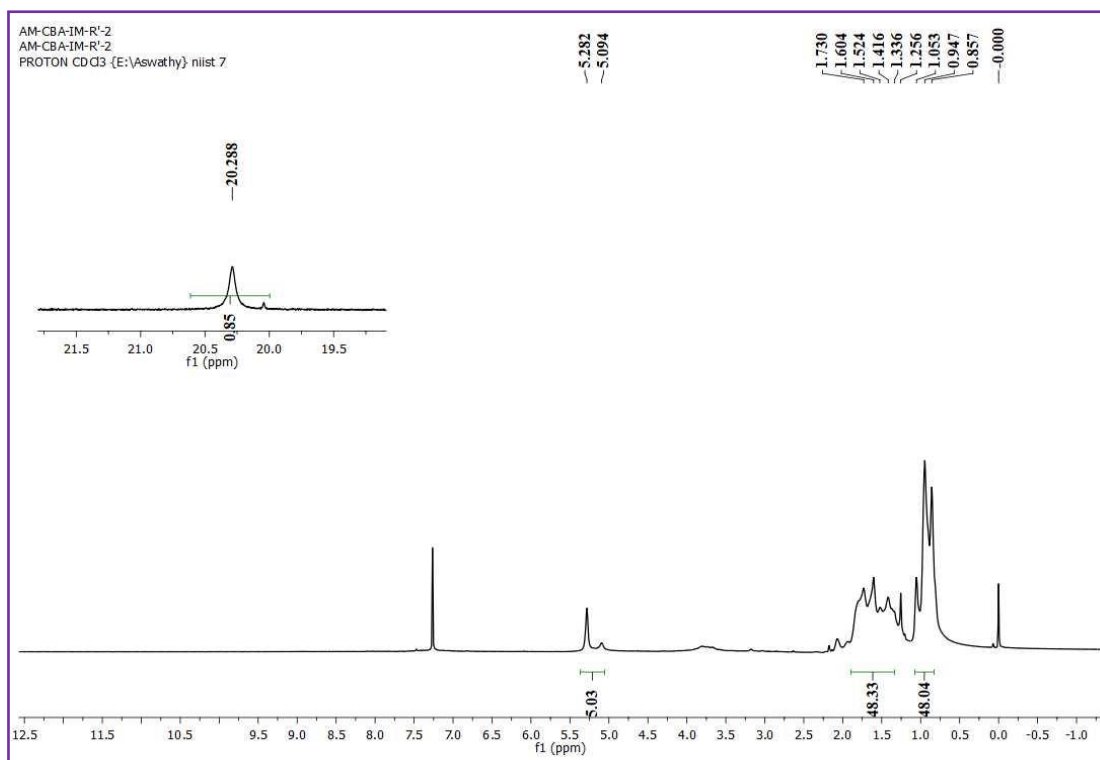


Figure 5.2: ¹H NMR spectra of CBA **1**

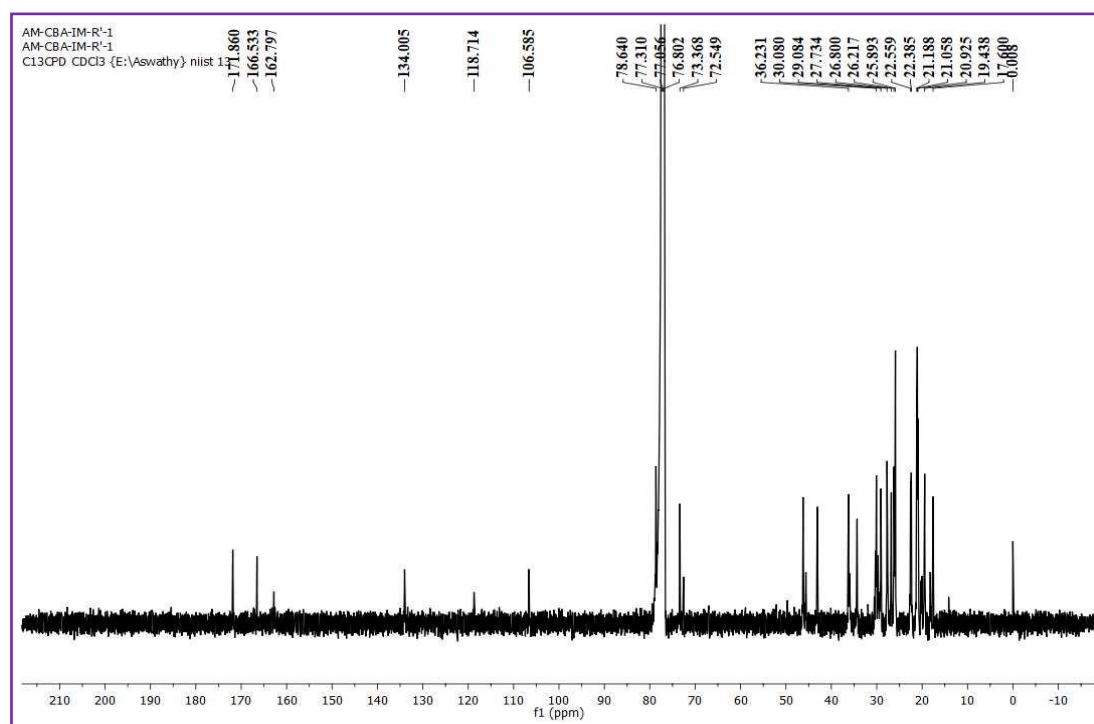


Figure 5.3: ¹³C NMR spectra of CBA **1**

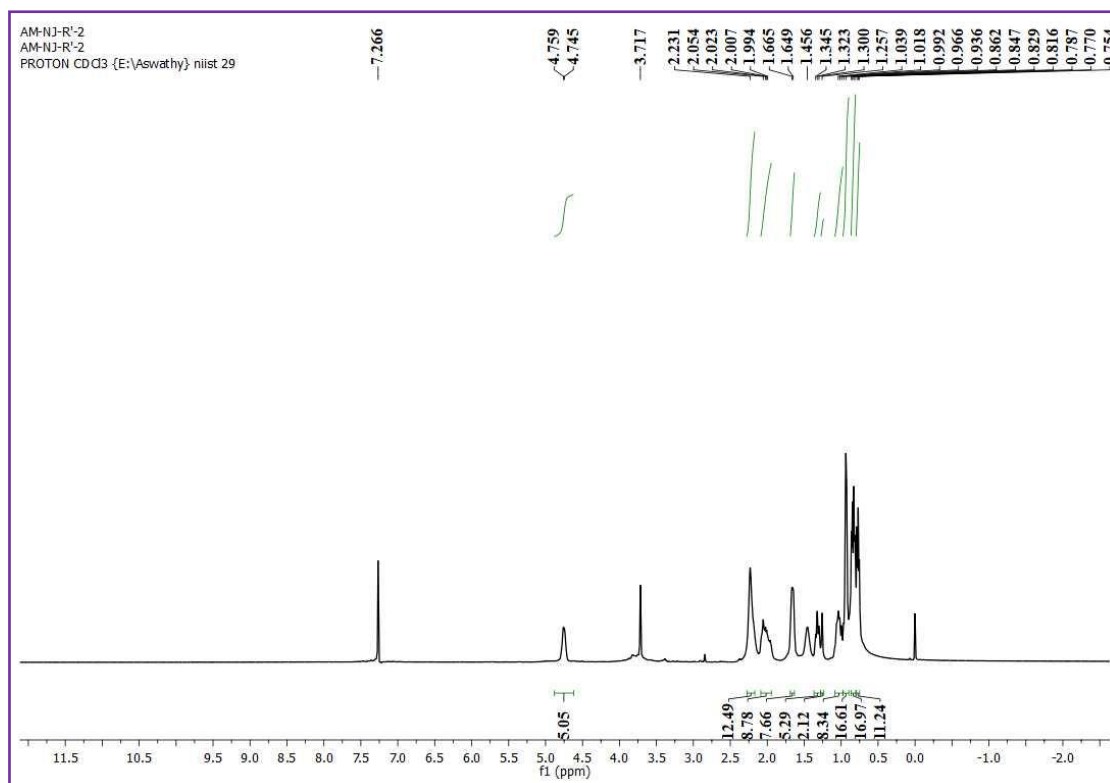


Figure 5.4: ¹H NMR spectra of CBA 3

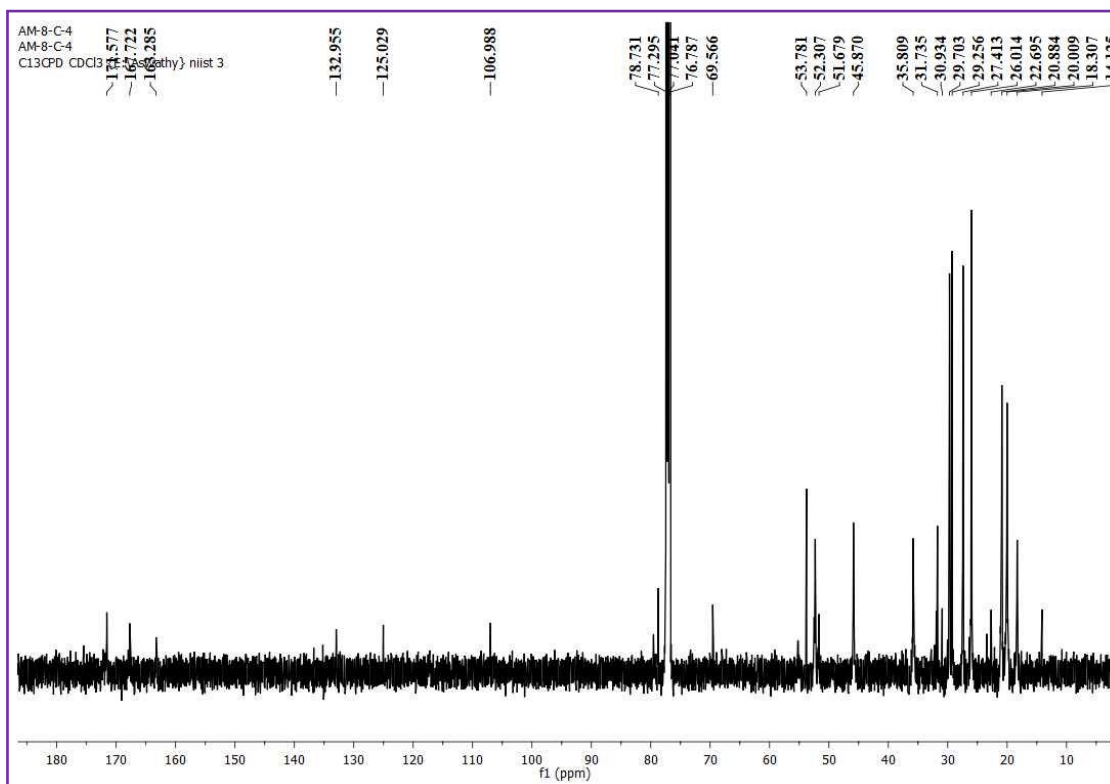


Figure 5.5: ¹³C NMR spectra of CBA 3

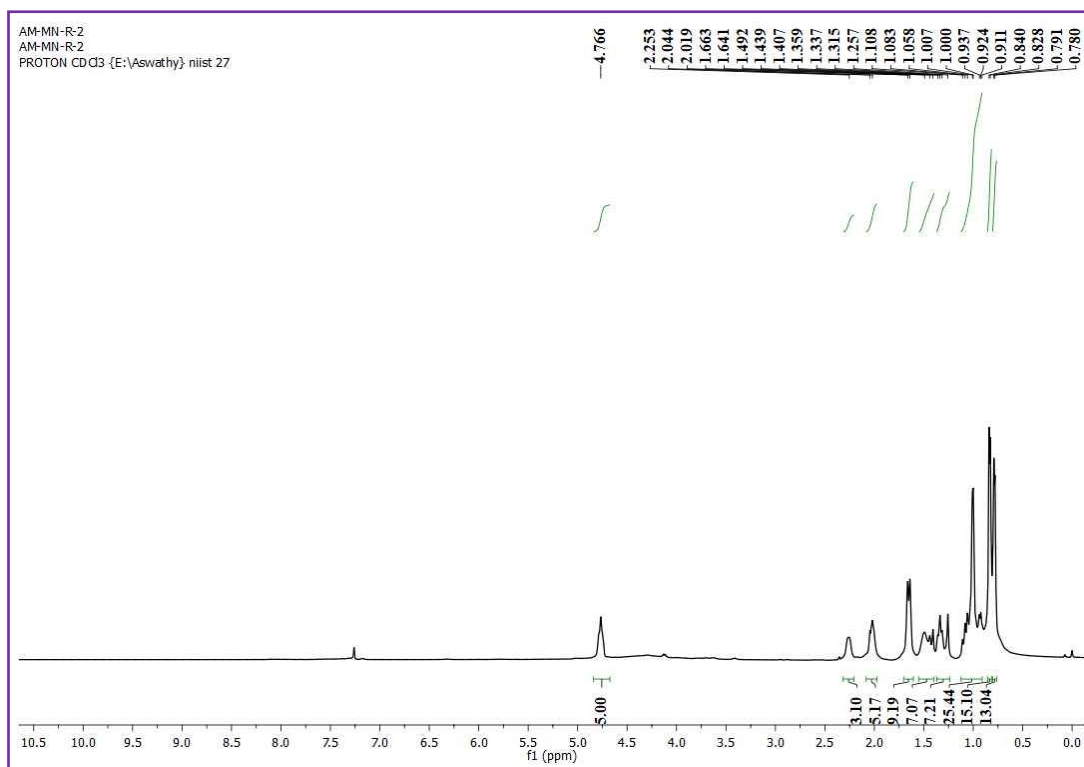


Figure 5.6: ^1H NMR spectra of CBA 4

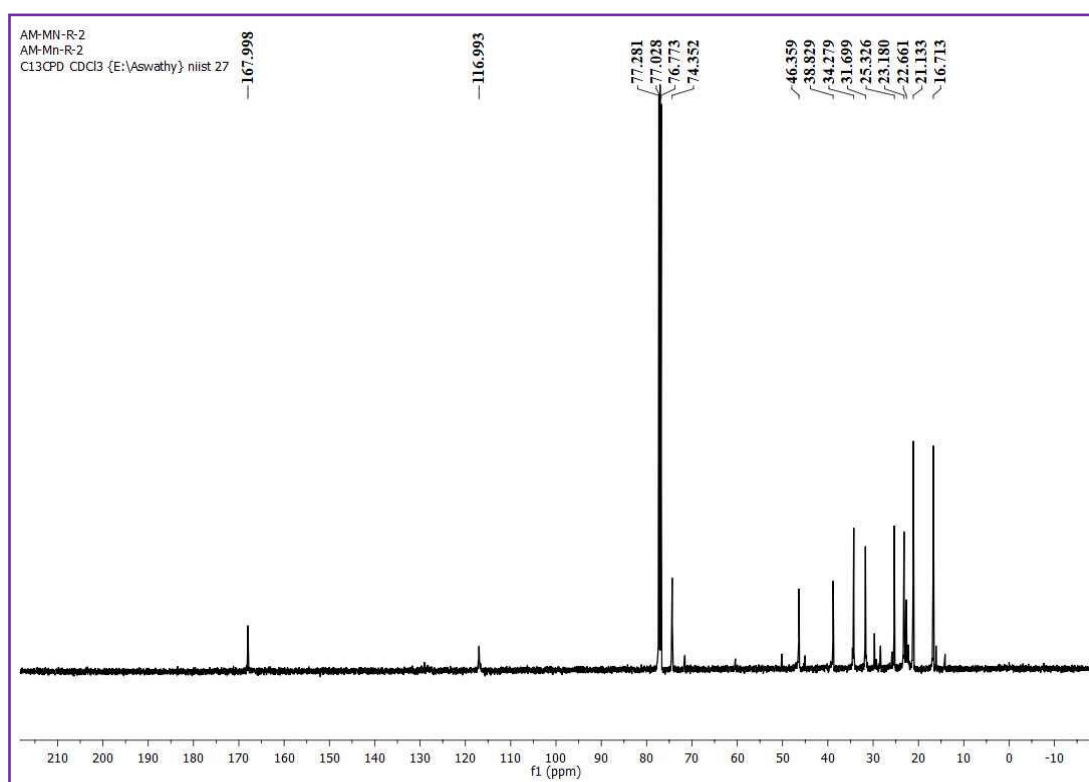
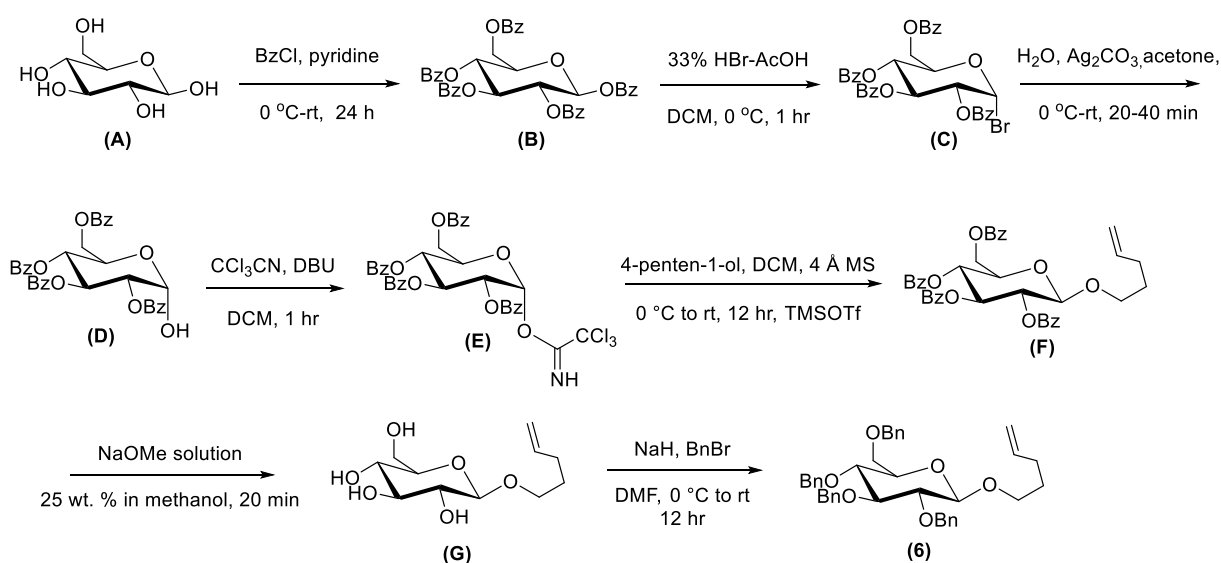


Figure 5.7: ^{13}C NMR spectra of CBA 4

5.2.2. Procedure for the synthesis of glycosyl donors **6**, **7**, and **8**

D-Glucose (5.0 g, 0.03 mol) was dissolved in pyridine (30 mL) and cooled to 0 °C. Benzoyl chloride (19.33 mL, 0.17 mol) was slowly added to the mixture with constant stirring and kept the reaction at room temperature for 24 h. After completion of the reaction, as indicated by TLC, the excess benzoyl chloride in the reaction mixture was quenched with ice-cold water. The resulting solid residue was dissolved in DCM and treated with 2 N HCl, saturated aqueous NaHCO₃, washed with water, dried with anhydrous Na₂SO₄, and concentrated to afford crude pentabenzoate of D-glucose **B** in 83% yield. The product **B** (5 g, 0.01 mol) was dissolved in freshly distilled DCM (30 mL), cooled to 0 °C and 33% HBr/AcOH (27.77 mL, 0.464 mol) was slowly added to the reaction mixture and stirred at room temperature for 1 h. After the complete consumption of **B**, the mixture was quenched with ice-cold water, and the organic layer was washed with water and saturated aqueous NaHCO₃, dried over anhydrous Na₂SO₄, and concentrated to obtain crude 2,3,4,6-tetra-*O*-benzoyl- α -D-glucopyranosyl bromide **C** in 92% yield, which was directly used for the next step without further purification. To the solution of **C** (5 g, 0.01 mol) in acetone (20 mL) at 0 °C in an ice bath, 0.5 mL of water was added, followed by addition of Ag₂CO₃ (1.672 g, 0.01 mol) portion-wise to the mixture. After completion of the reaction, as indicated by TLC, the mixture was filtered, concentrated and purified by CC with EtOAc:hexane (3:7) and obtained **D** in 85% yield. Compound **D** (4.028 g, 0.01 mol) and trichloroacetonitrile (2.37 mL, 0.024 mol) were dissolved in freshly distilled DCM (15 mL), and then DBU (103 μ L) was added to the mixture at 0 °C. After 1 h, the reaction mixture was washed with water, and the organic layer was dried over anhydrous Na₂SO₄ and concentrated. The crude mixture thus obtained was further subjected to silica gel CC using 30% EtOAc: Hexane as eluent, which resulted in **E** as a white crystalline solid. Thus the obtained **E** (4.568 g, 0.006 mol) was further treated with 4-penten-1-ol (765 μ L, 0.01 mol) in freshly distilled DCM (5 mL) and cooled to 0 °C, 4 Å powdered MS was added followed by the addition TMSOTf (15 mol%) in DCM after 10 min and stir the mixture at room temperature for 12 h. After the complete consumption of the starting material, powdered MS were filtered off and the mixture was extracted with DCM, washed the organic layer with brine and dried over anhydrous Na₂SO₄ and concentrated. The compound **F** was obtained as a white crystalline solid after CC using 20% EtOAc: Hexane as mobile phase. Debenzoylation of **F** was carried out by treatment with NaOMe solution in 25 wt% in MeOH that resulted in the formation of **G**, which was further purified by CC with gradient of polarities from EtOAc to EtOAc-methanol (10%). The resultant **G** (1.120 g, 0.0045 mol) was dissolved

in dry DMF (20 mL) and sodium hydride (1.08 g of 60% dispersion in oil, 0.045 mol) was slowly added to the mixture in an ice bath and allowed to stir at room temperature for 20 min. Benzyl bromide (2.95 mL, 0.025 mol) was added portion-wise to the reaction mixture and continued to stir for 12 h. The excess sodium hydride and benzyl bromide were quenched by the slow addition of water, and the mixture was extracted with DCM. The organic layer was washed with water, brine and dried with anhydrous Na_2SO_4 . The product, *n*-pentenyl glucoside **6** was obtained as a colourless oil in 72% yield by CC using the mobile phase as 10% EtOAc: hexane. The overall reactions are summarised in the following scheme (Scheme 2). Similarly, the glycosyl donors **7** and **8** were synthesized from D-mannose and D-galactose, respectively.



Scheme 2: Synthesis of the glycosyl donor **6** from D-glucose

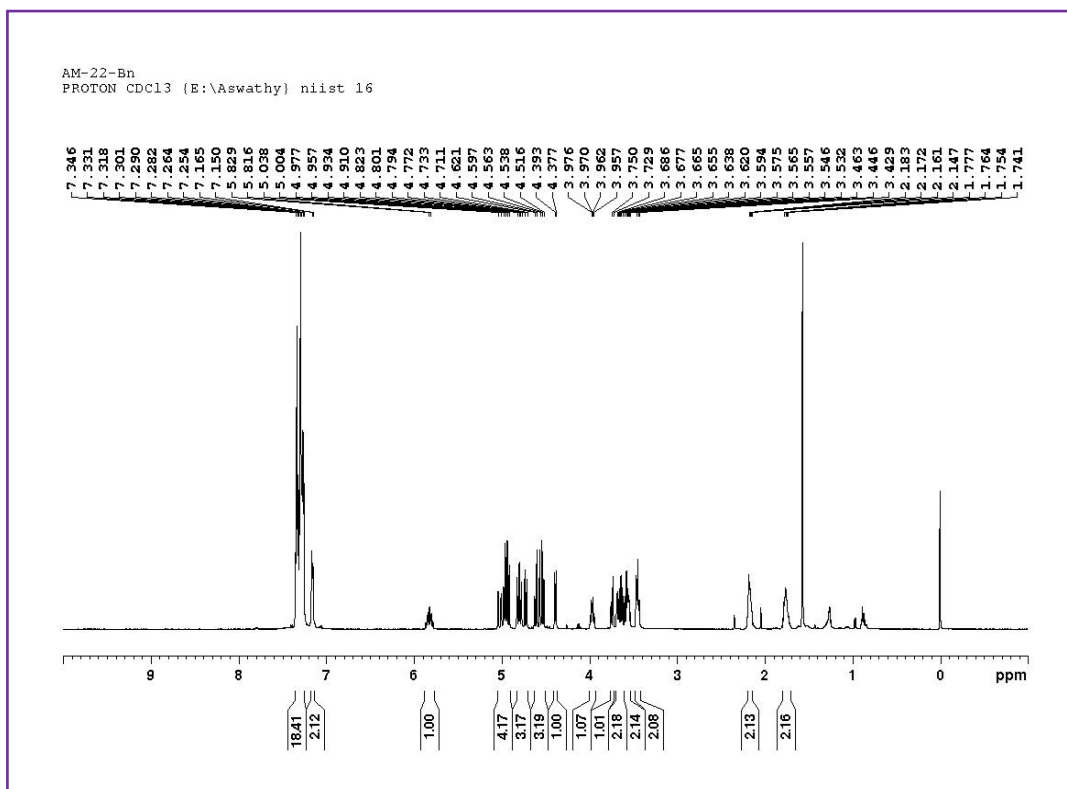


Figure 5.8: ^1H NMR spectra of NPG 6

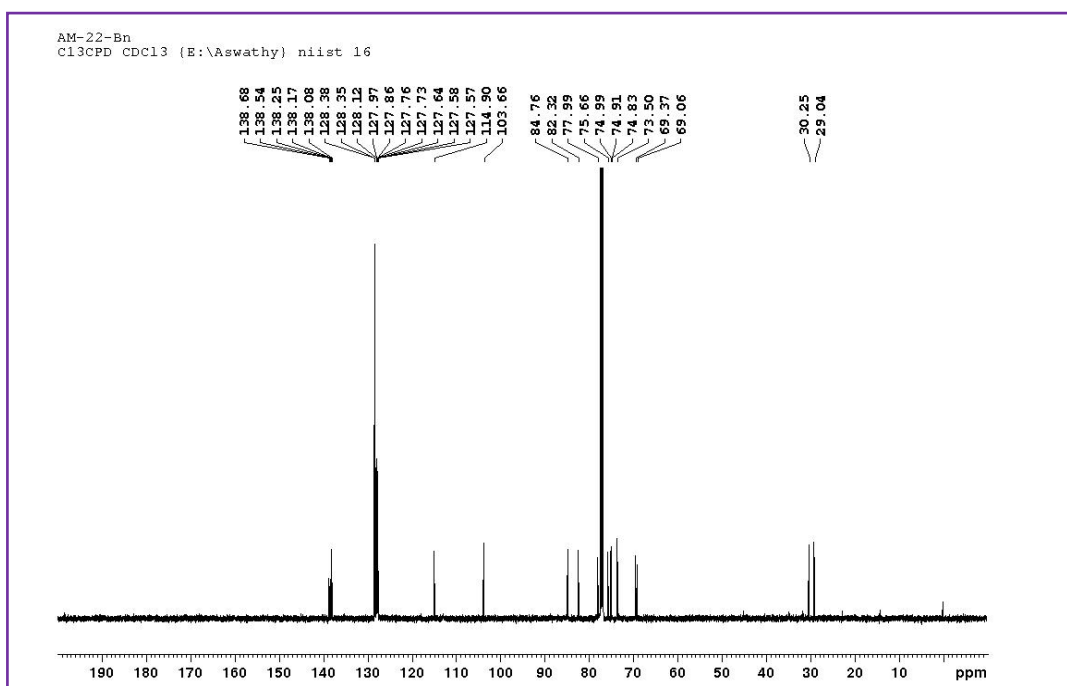


Figure 5.9: ^{13}C NMR spectra of NPG 6

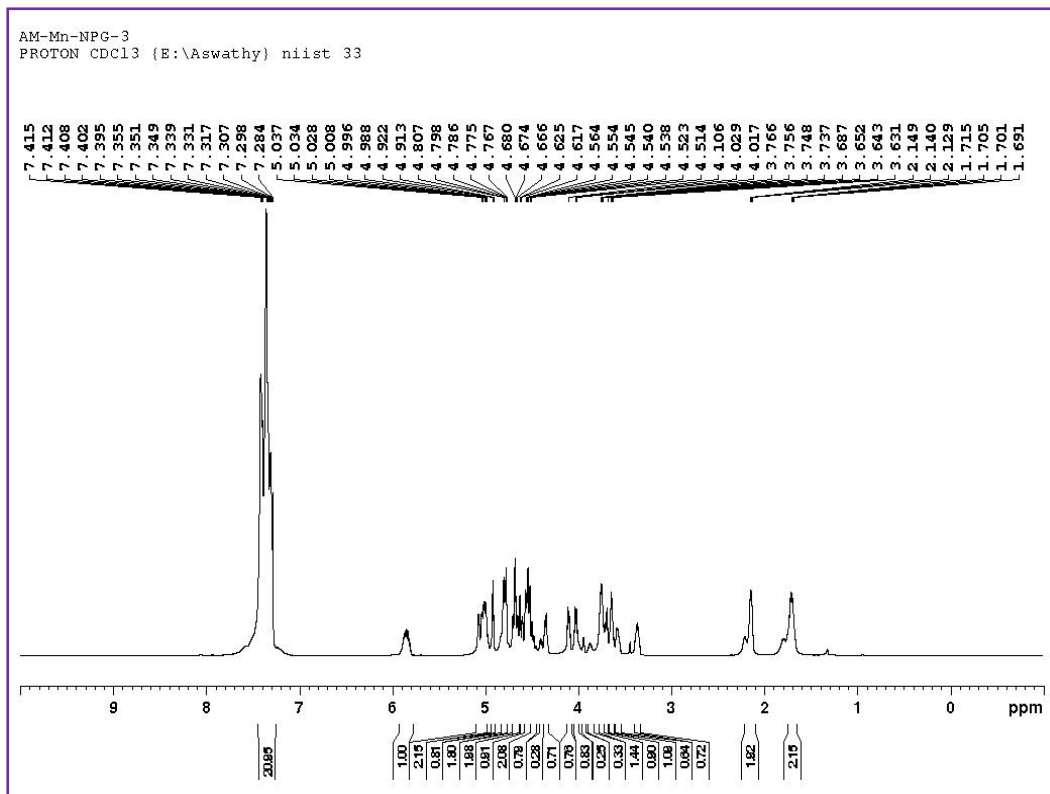


Figure 5.10: ^1H NMR spectra of NPG 7

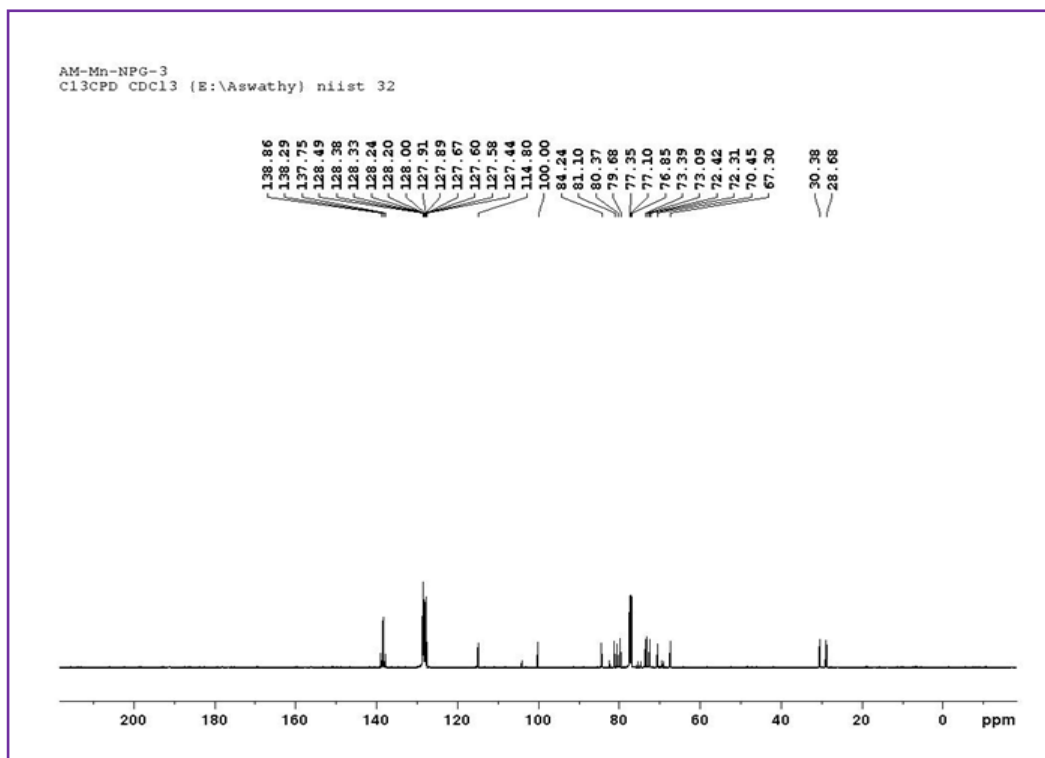


Figure 5.11: ^{13}C NMR spectra of NPG 7

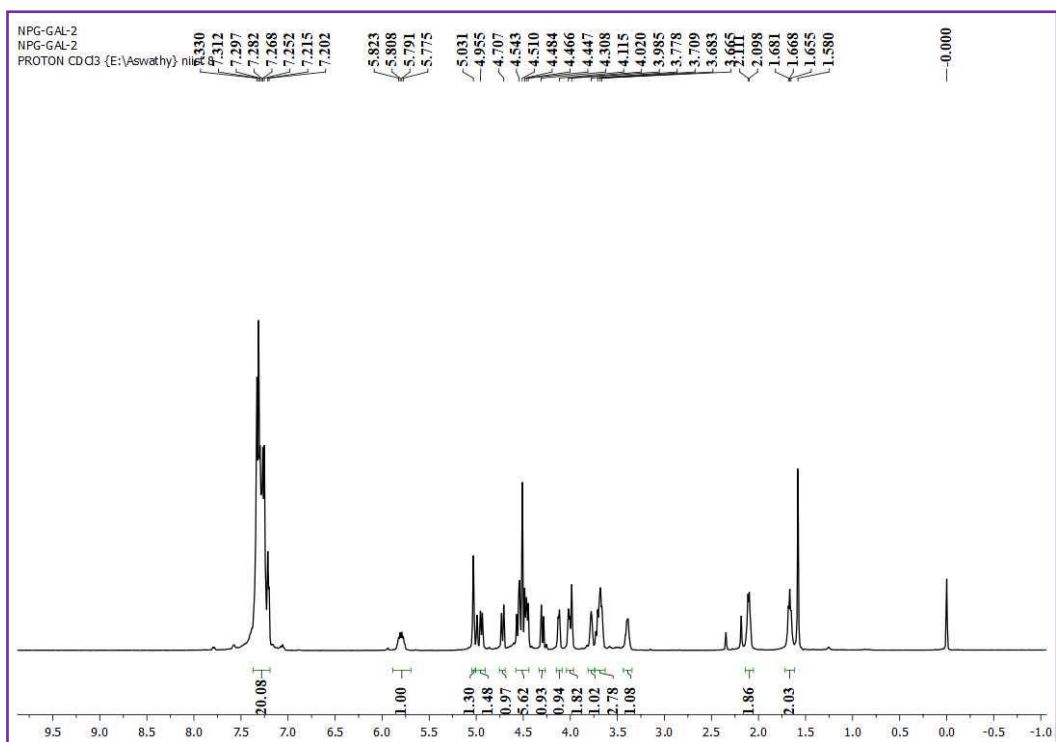


Figure 5.12: ^1H NMR spectra of NPG 8

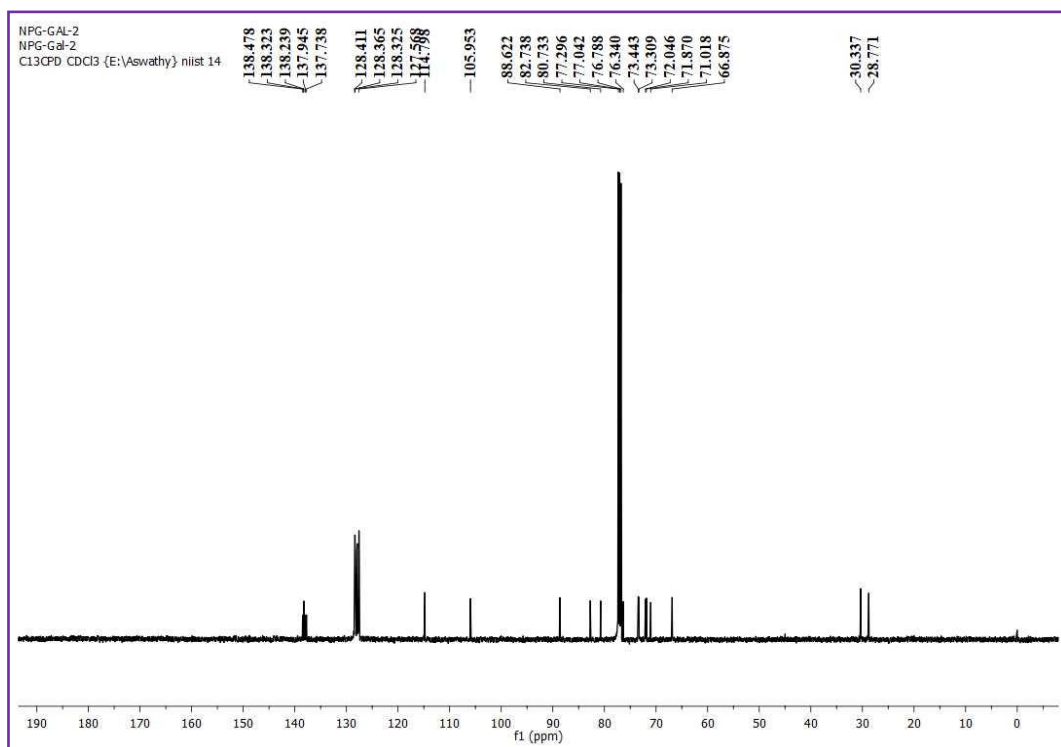


Figure 5.13: ^{13}C NMR spectra of NPG 8

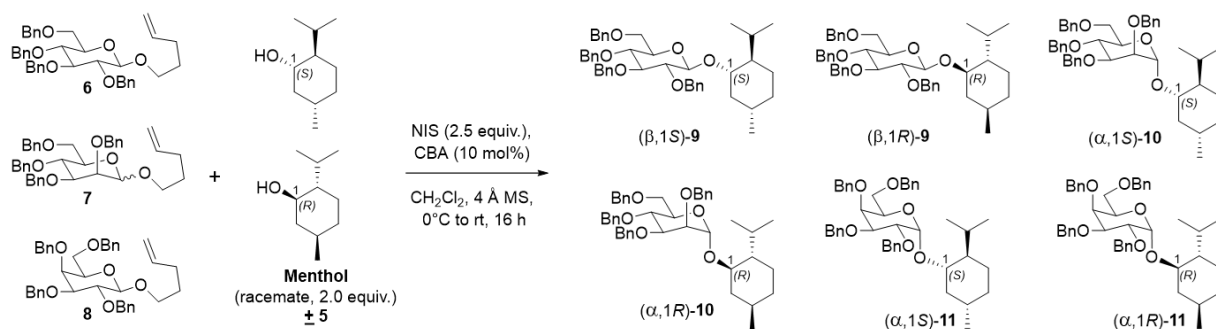
5.2.3. General procedure for chiral Brønsted acid mediated glycosylation with racemic substrates

N-Pentenyl glycosides (**6/7/8**) (100 mg, 0.164 mmol, 1.0 equiv.) and acceptor \pm **5/** \pm **12/** \pm **13/** \pm **14** (2.0 equiv.) were azeotroped together with freshly distilled toluene (3 mL) thrice on rotavapour and dried under high vacuum. The resulting dry syrup was redissolved in freshly distilled DCM (9 mL) and cooled to 0 °C. *N*-Iodosuccinimide (NIS) (92.39 mg, 0.4107 mmol, 2.5 equiv.) and powdered 4 Å molecular sieves were added, stirred for 10 minute and then CBA **1** (10 mol%) in DCM was added, and the reaction mixture was slowly warmed to room temperature. After 16 h, the reaction mixture was quenched with 10% aqueous Na₂S₂O₃ and saturated NaHCO₃ solutions, filtered and washed with DCM. The organic layer was washed with water, brine and dried with anhydrous Na₂SO₄. The crude residue was further subjected to CC using EtOAc-hexane as the mobile phase affording the corresponding diastereomeric mixture. The diastereomeric ratio was determined by computing the area percentage of both the peaks in the HPLC chromatogram and by comparison with the retention times of respective glycosides of each individual enantiomer and / or from the integration of the anomeric protons in ¹H NMR spectra, identified by their respective chemical shifts of the glycosides with pure enantiomers and HMQC spectra.

CBA **1** (Figure 1) was synthesized from PCCP and (+)-isomenthol as per the reported procedure.²⁰ Racemic menthol **5** was chosen as the acceptor for exploring the chiral recognition in CBA **1**-catalyzed glycosylation reaction. The initial glycosylation attempt was performed with benzyl-protected glucosyl-NPG **6** and **5** in the presence of NIS and CBA **1** (10 mol%), under the optimized reaction conditions of our previous report with BA-PCCP,¹⁸ which afforded β -glycoside **9** in 92% yield (entry 1, Table 1). The diastereomeric ratio of (β , 1*S*)-**9** and (β , 1*R*)-**9**, determined by computing the area percentage of both the peaks in the HPLC chromatogram and by comparison with the retention times of respective glycosides of each enantiomer of menthol, were found to be 86.83% and 13.17%, respectively (entry 1, Table 1). Thus, apart from β -selectivity with CBA **1**, chiral recognition of the racemic menthol favouring glycosylation of (+)-menthol afforded (β ,1*S*)-**9** with a diastereomeric excess of 74%. Glycosylation with mannosyl-NPG **7** (α , β mixture) in the presence of CBA **1** afforded glycoside **10** with the expected α -stereoselectivity (entry 2, Table 1). It is interesting to note that glycosylation with the less studied galactosyl-NPG **8** produced α -stereoselectivity for glycoside **11** (entry 3, Table 1). Once again, chiral recognition favoured glycosylation of (+)-menthol to afford diastereoselective products (α ,1*S*)-**10** and (α ,1*S*)-**11**, with both showing a diastereomeric excess of 69% (entry 2 & 3, Table 1). The results of glycosylation with CBA **1**

motivated us to compare its role in α/β -stereo- and diastereoselectivity with other chiral and non-chiral BAs under the optimized glycosylation conditions.¹⁸ Galactosyl-NPG **8** is rarely explored for glycosylation reactions compared to NPGs **6** & **7**. Hence, glycosylation with NPG **8** and BINOL-derived chiral phosphoric acid catalysts (*R*)-**2** and (*S*)-**2** (Figure 1) were attempted, which also afforded α -glycoside like CBA **1**; however, the diastereoselectivity was poor and slightly favoured glycosylation of (-)-menthol (entry 4 & 5, Table 1). Glycosylation attempt with NPG **8** in the presence of Lewis acid activator Sc(OTf)₃, a conventional activator for NPG donors,²¹ and BAs such as achiral PCCP and triflic acid afforded no stereoselectivity (entry 6-8, Table 1). To assess the importance of the selection of (+)-isomenthol in CBA synthesis, CBA **3** and CBA **4** (Figure 1) were synthesized from (+)-menthol and (-)-menthol, respectively, and subjected to glycosylation with NPG **7**. NPG **7** was chosen to study the effect of steric hindrance of the β -face of oxocarbenium ion on glycosylation outcome, in the presence of both CBA **3** and CBA **4** catalysts, the expected α -glycosides were formed, albeit with no diastereoselectivity.

Table 1. Glycosylation reaction of benzyl protected NPGs **6/7/8** and racemic menthol **5**.



Entry	Donor	Activator	Yield (%) ^b	Yield (%) ^c					
				(β,1S)-9	(β,1R)-9	(α,1S)-10	(α,1R)-10	(α,1S)-11	(α,1R)-11
1	6	1	92	86.83%	13.17%	-	-	-	-
2	7	1	85	-	-	84.74%	15.26%	-	-
3	8	1	94	-	-	-	-	84.46%	15.54%
4	8	(<i>R</i>)-2	90	-	-	-	-	40.14%	59.86%
5	8	(<i>S</i>)-2	83	-	-	-	-	45.67%	54.33%
6	8	Sc(OTf) ₃	86	No stereoselectivity					
7	8	PCCP	73	No stereoselectivity					
8	8	CF ₃ SO ₃ H	35	No stereoselectivity					
9	7	3	90	-	-	54.23%	45.77%	-	-
10	7	4	85	-	-	45.89%	54.11%	-	-

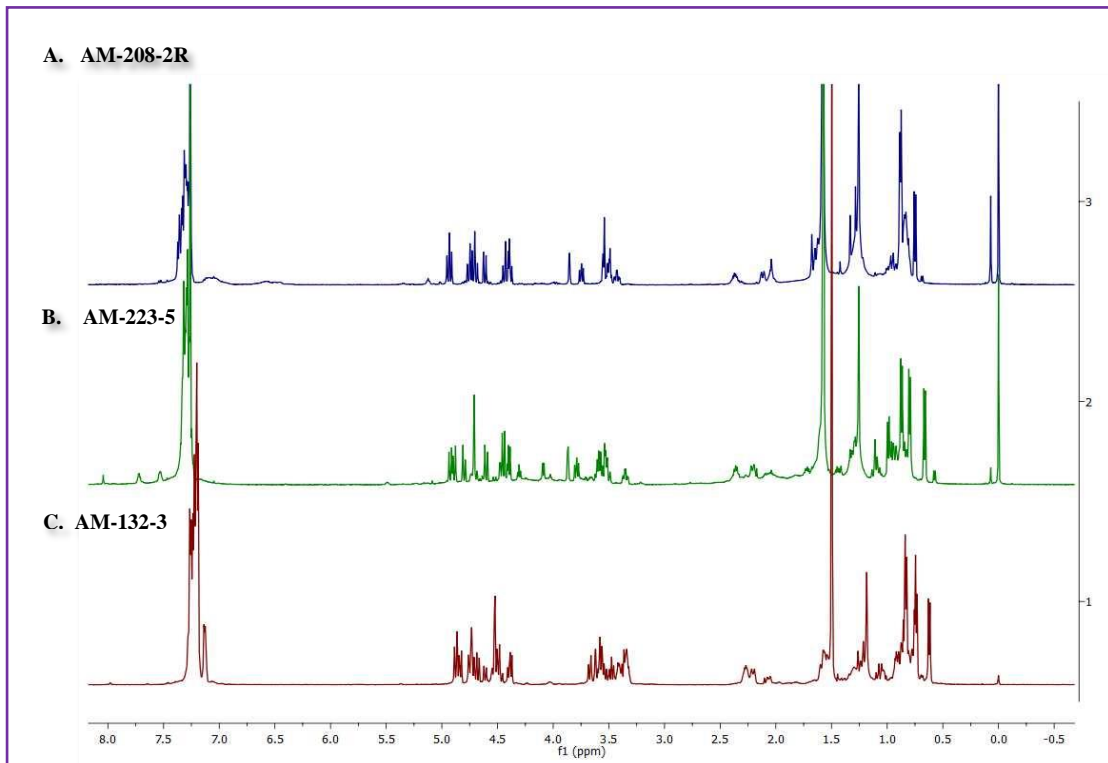


Figure 5.14: ^1H NMR of glycosides (A) (β , 1*R*)-**9** (B) (β , 1*S*)-**9** (C) mixture of (β , 1*S*)-**9** and (β , 1*R*)-**9**

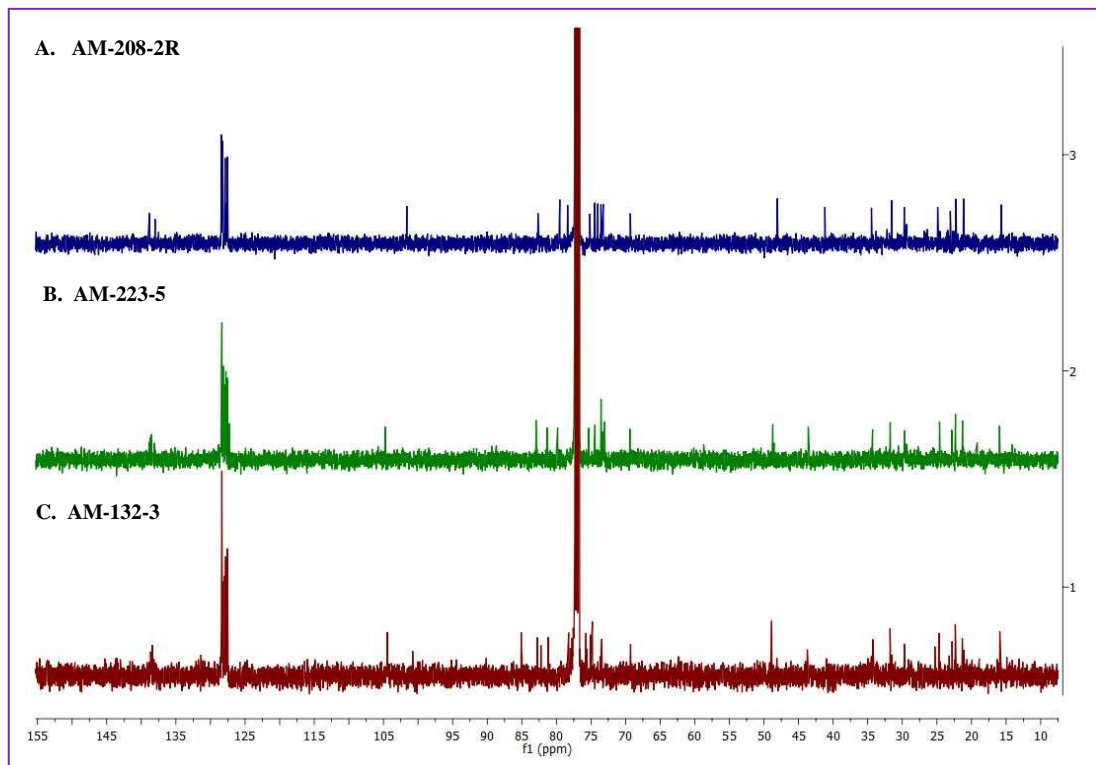


Figure 5.15: ^{13}C NMR of glycosides (A) (β , 1*R*)-**9** (B) (β , 1*S*)-**9** (C) mixture of (β , 1*S*)-**9** and (β , 1*R*)-**9**

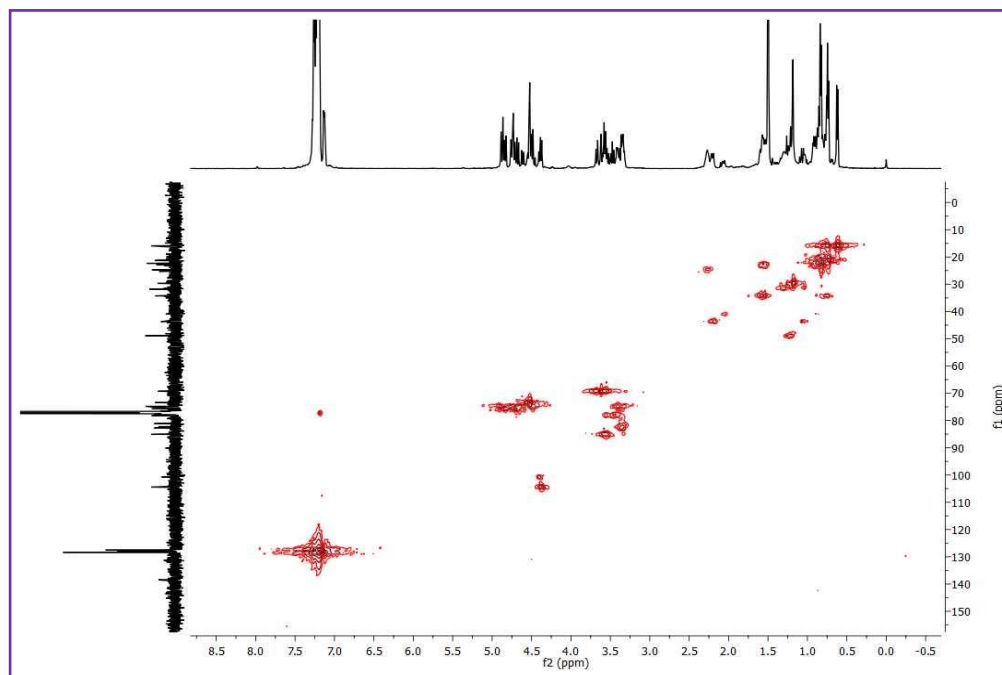


Figure 5.16: HMQC of diastereomeric mixture of (β , 1*S*)-**9** and (β , 1*R*)-**9**

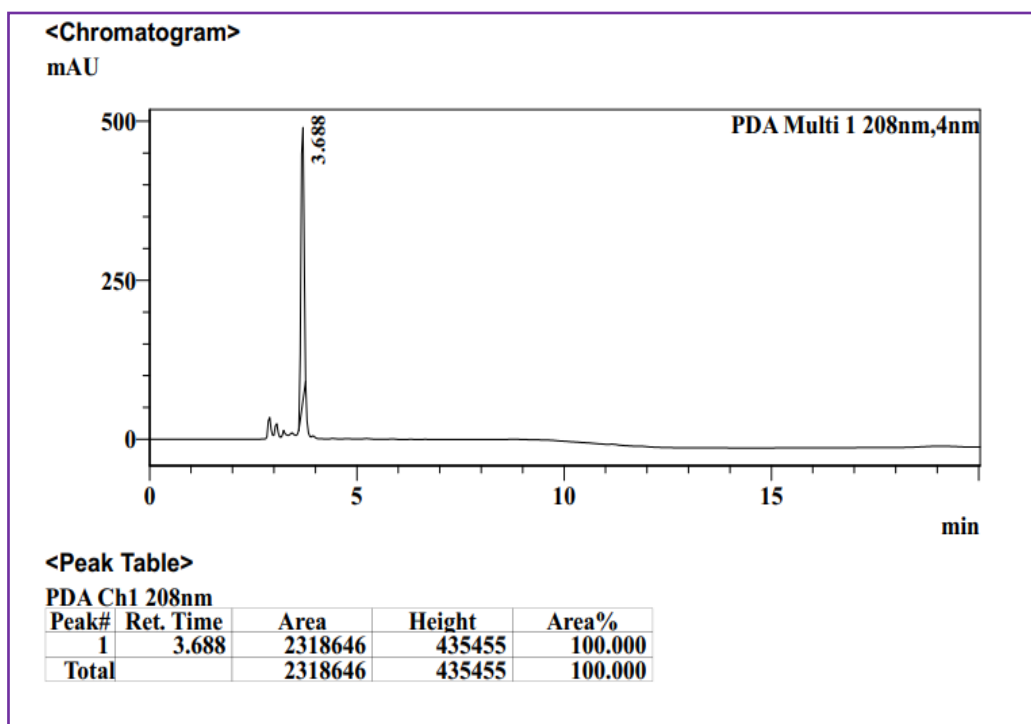


Figure 5.17: HPLC chromatograms of (β , 1*S*)-**9**

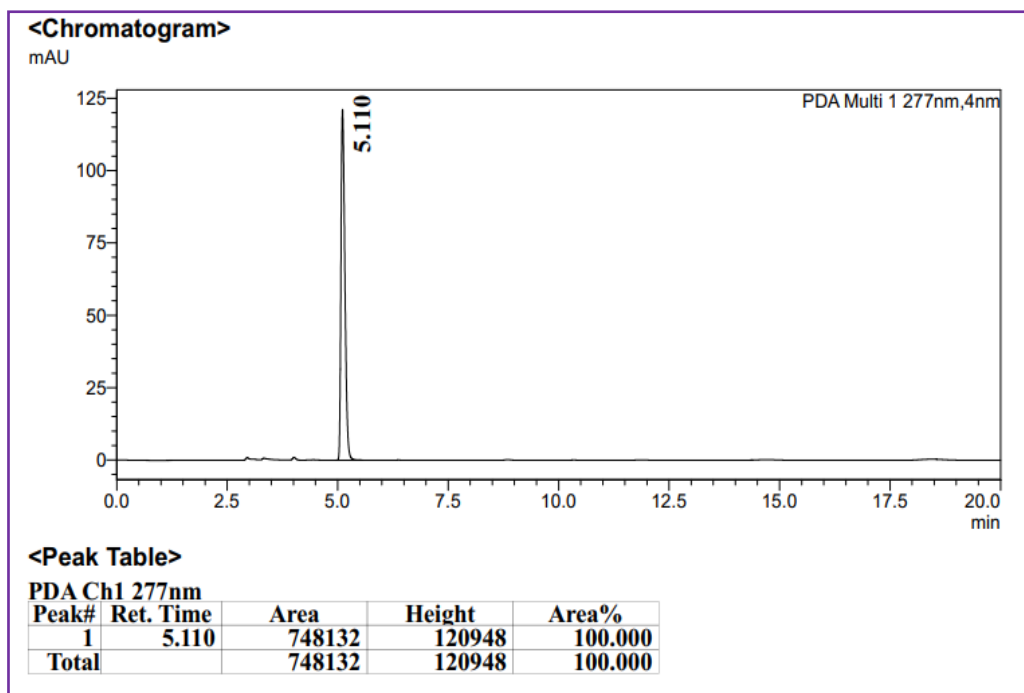


Figure 5.18: HPLC chromatograms of (β , 1*R*)-**9**

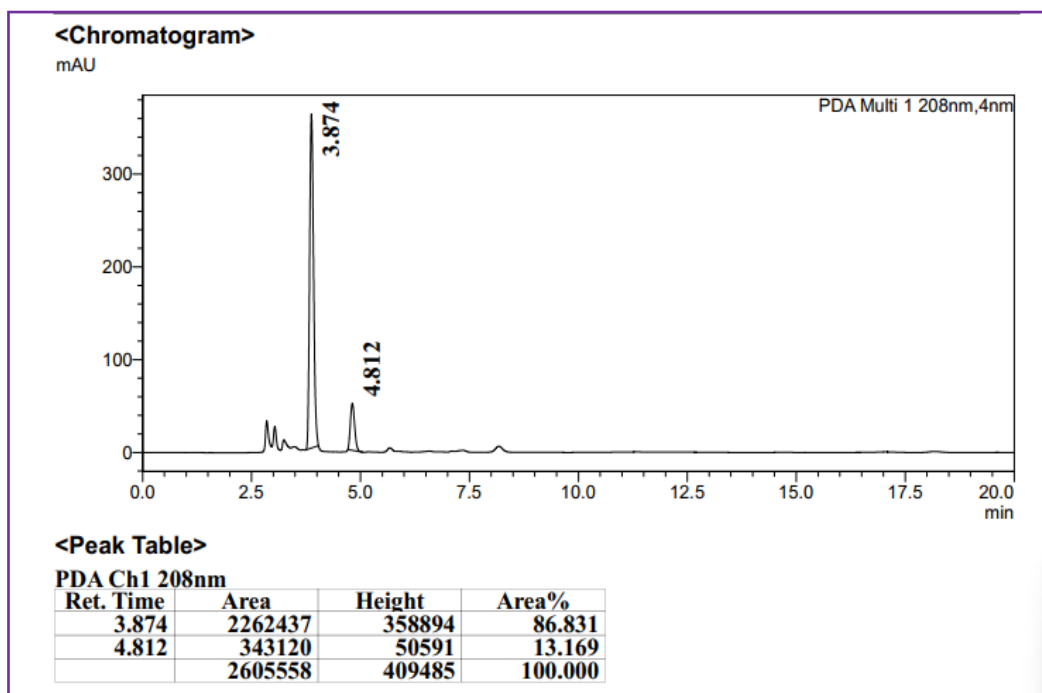


Figure 5.19: HPLC chromatograms of diastereomeric mixture of (β , 1*S*)-**9** and (β , 1*R*)-**9**

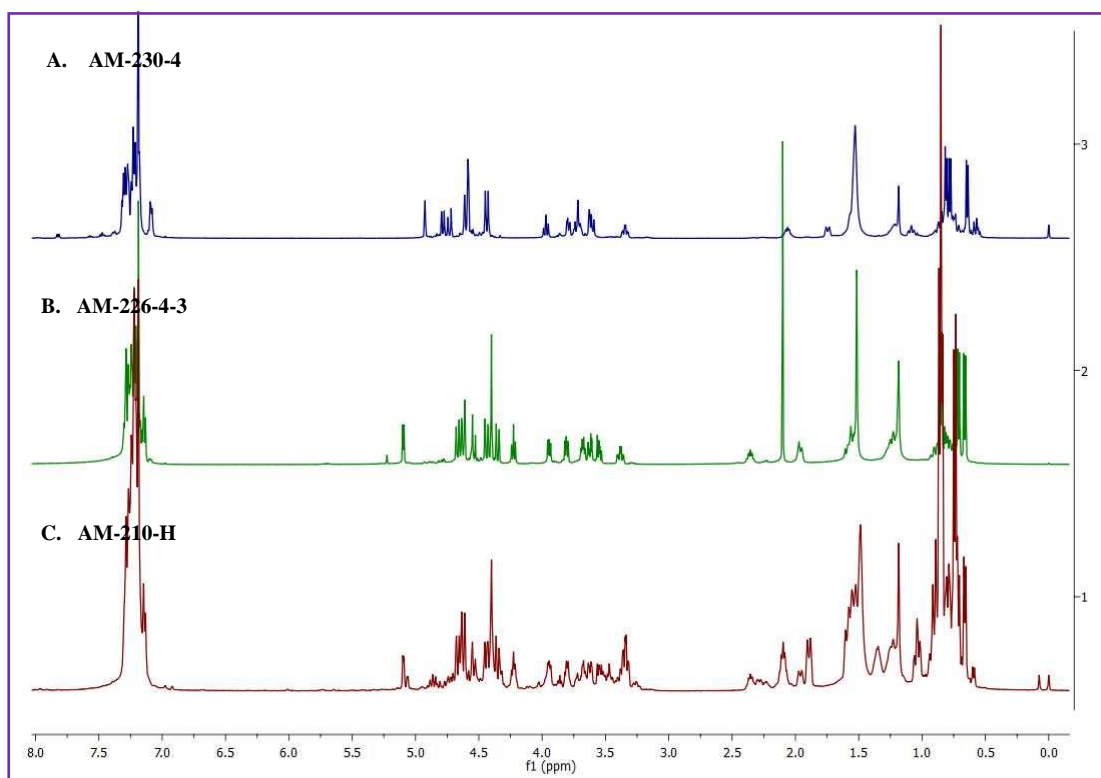


Figure 5.20: ^1H NMR of glycosides (A) ($\alpha,1R$)-**10** (B) ($\alpha,1S$)-**10** (C) mixture of ($\alpha, 1S$)-**10** and ($\alpha, 1R$)-**10**

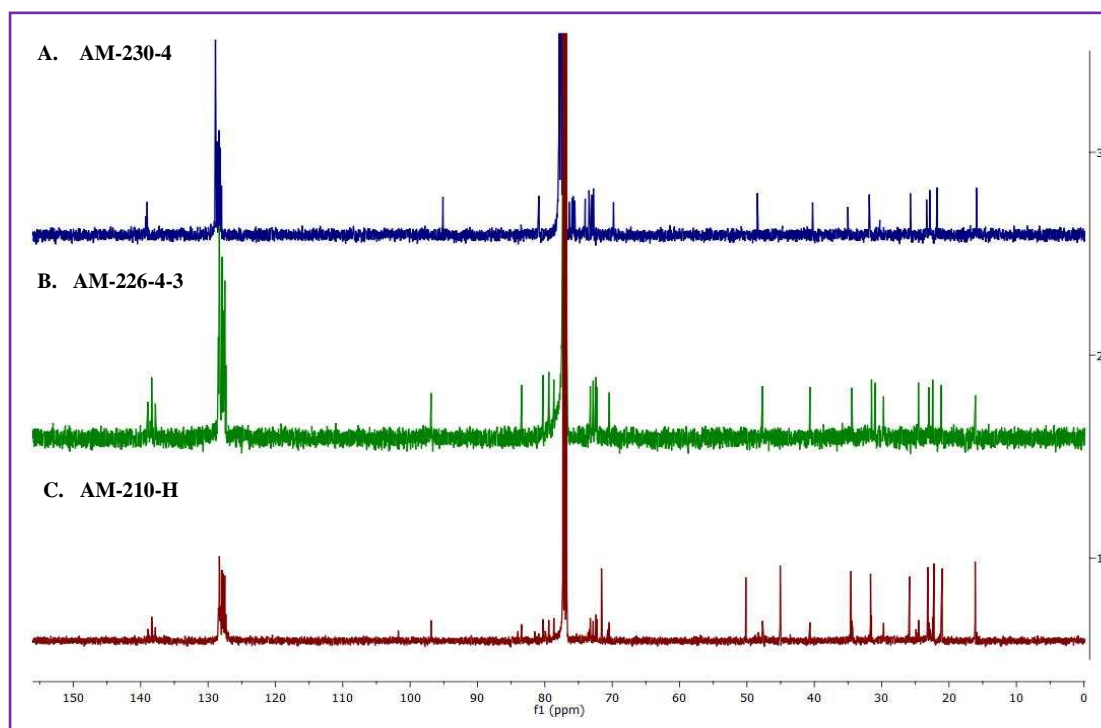


Figure 5.21: ^{13}C NMR of glycosides (A) ($\alpha,1R$)-**10** (B) ($\alpha,1S$)-**10** (C) mixture of ($\alpha, 1S$)-**10** and ($\alpha, 1R$)-**10**

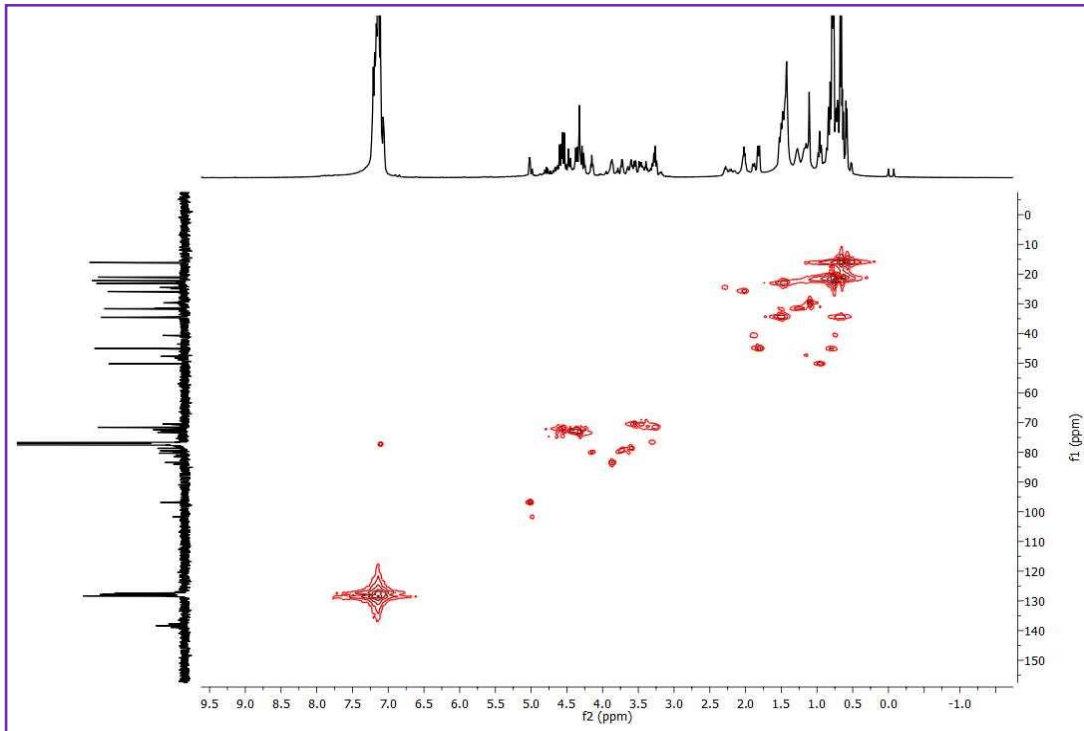


Figure 5.22: HMQC of diastereomeric mixture of (α , 1*S*)-**10** and (α , 1*R*)-**10**

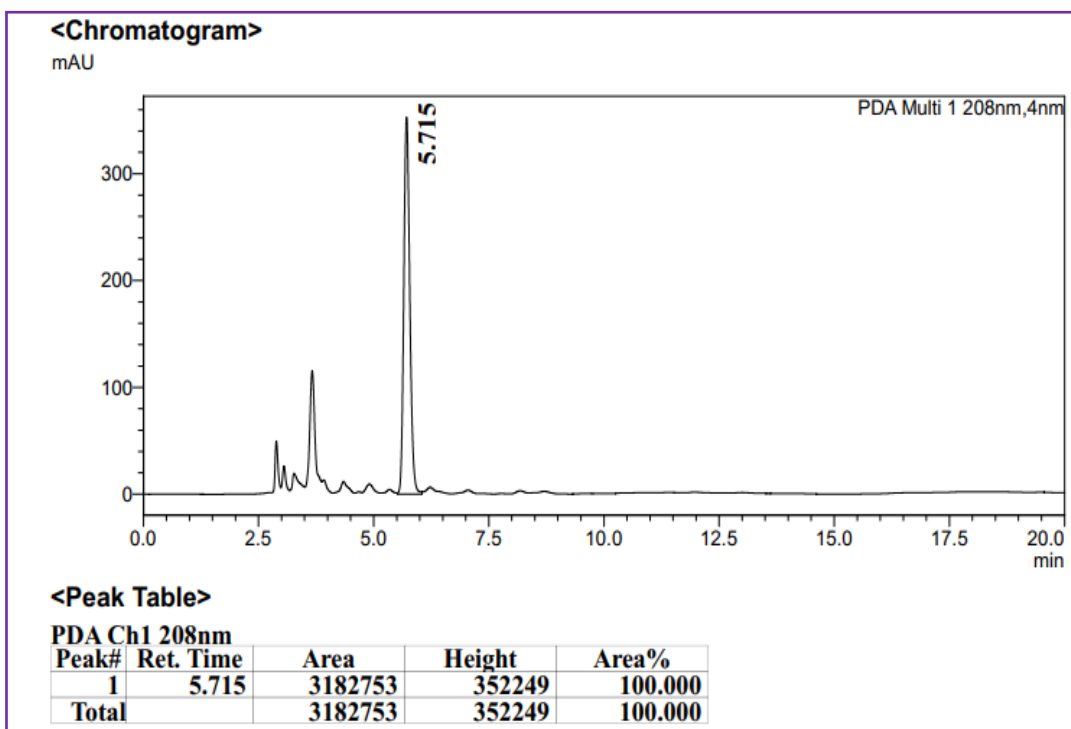


Figure 5.23: HPLC chromatogram of (α , 1*S*)-**10**

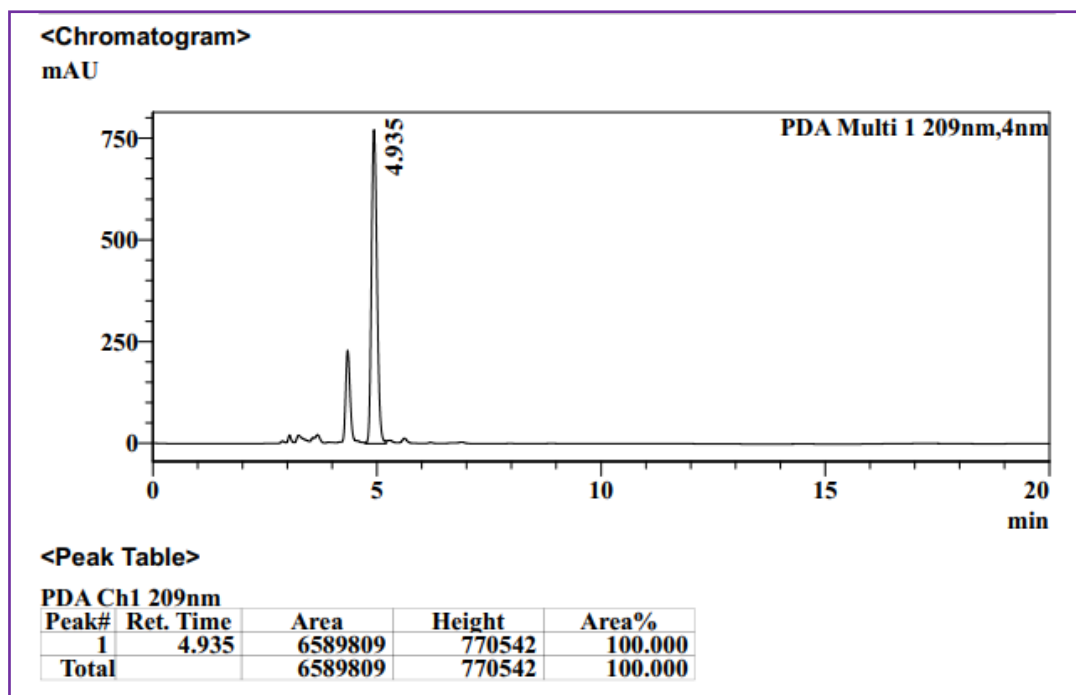


Figure 5.24: HPLC chromatogram of (α , 1*R*)-**10**

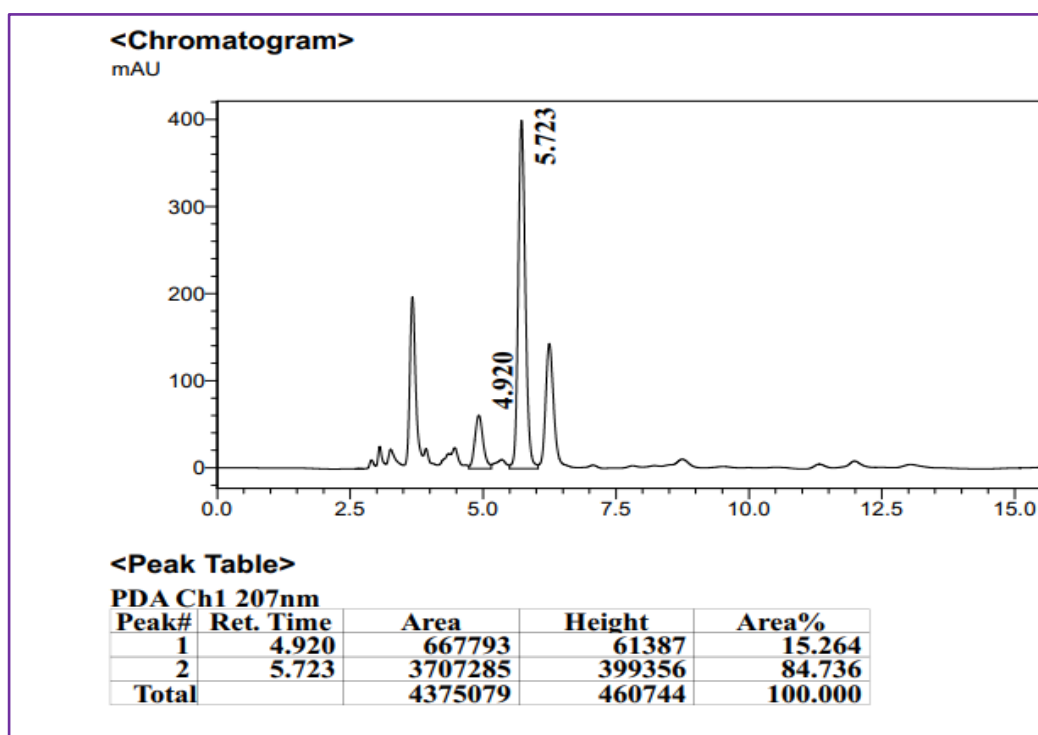


Figure 5.25: HPLC chromatograms of diastereomeric mixture of (α , 1*S*)-**10** and (α , 1*R*)-**10**

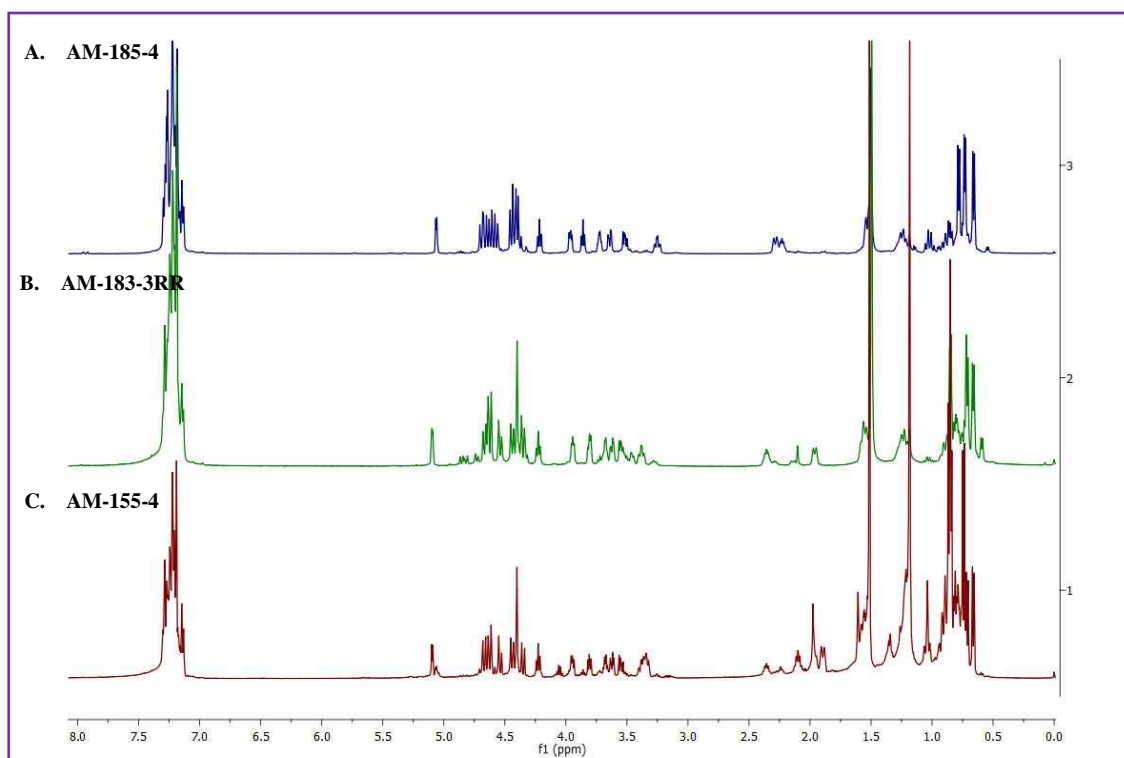


Figure 5.26: ^1H NMR of glycosides (A) (α , 1*R*)-**11** (B) (α , 1*S*)-**11** (C) mixture of (α , 1*S*)-**11** and (α , 1*R*)-**11** catalysed by CBA **1**

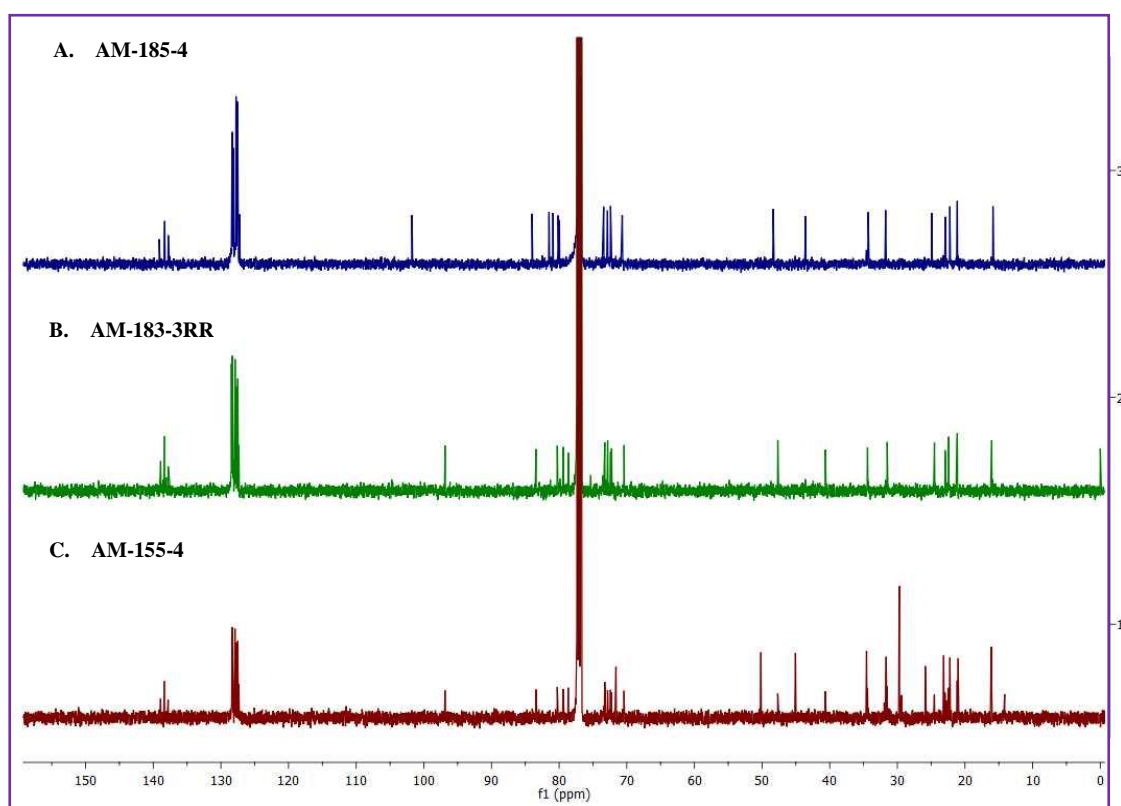


Figure 5.27: ^{13}C NMR of glycosides (A) (α , 1*R*)-**11** (B) (α , 1*S*)-**11** (C) mixture of (α , 1*S*)-**11** and (α , 1*R*)-**11** catalysed by CBA **1**

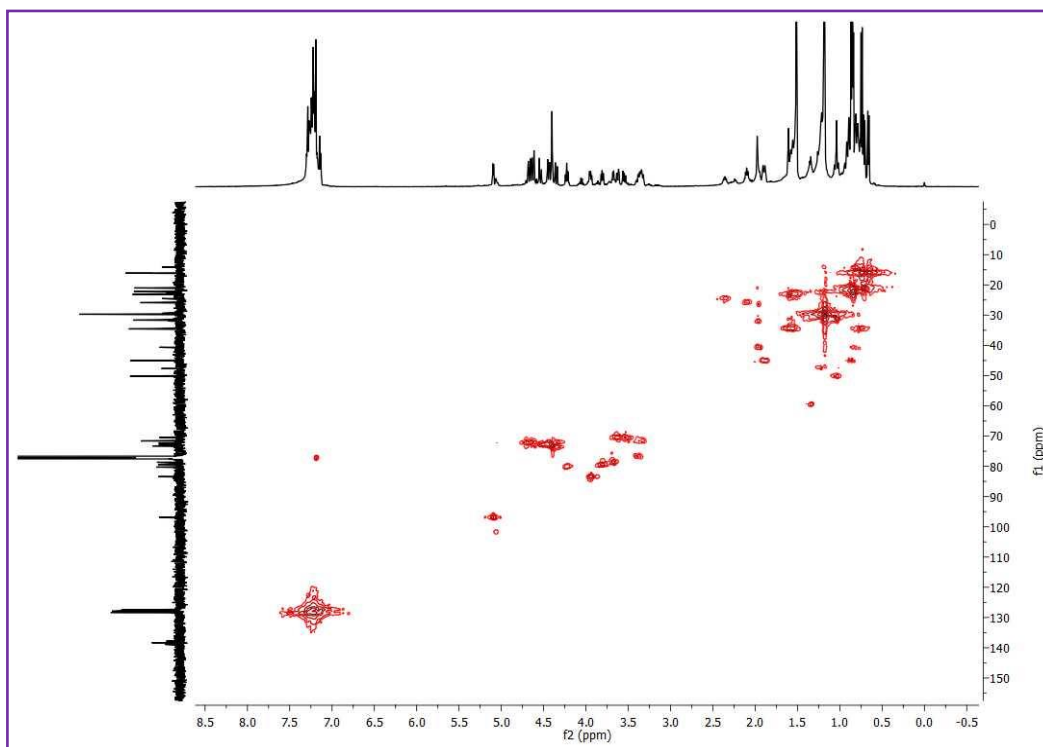


Figure 5.28: HMQC of diastereomeric mixture of (α , 1*S*)-**11** and (α , 1*R*)-**11** catalysed by CBA **1**

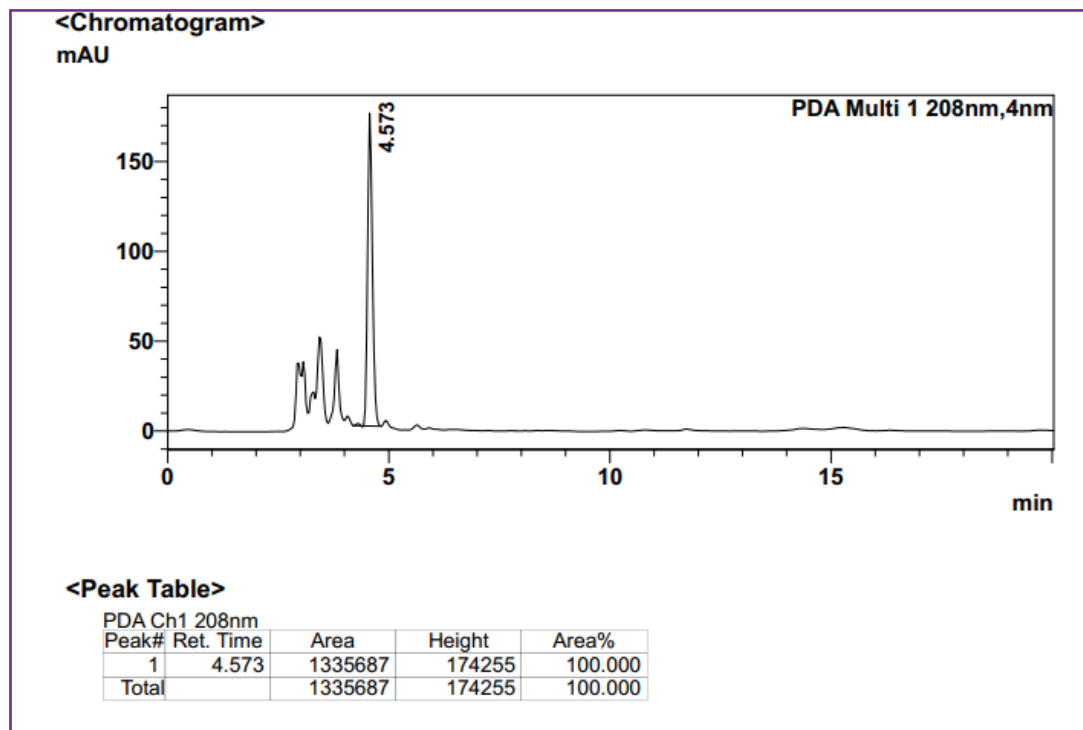


Figure 5.29: HPLC chromatograms of (α , 1*S*)-**11**

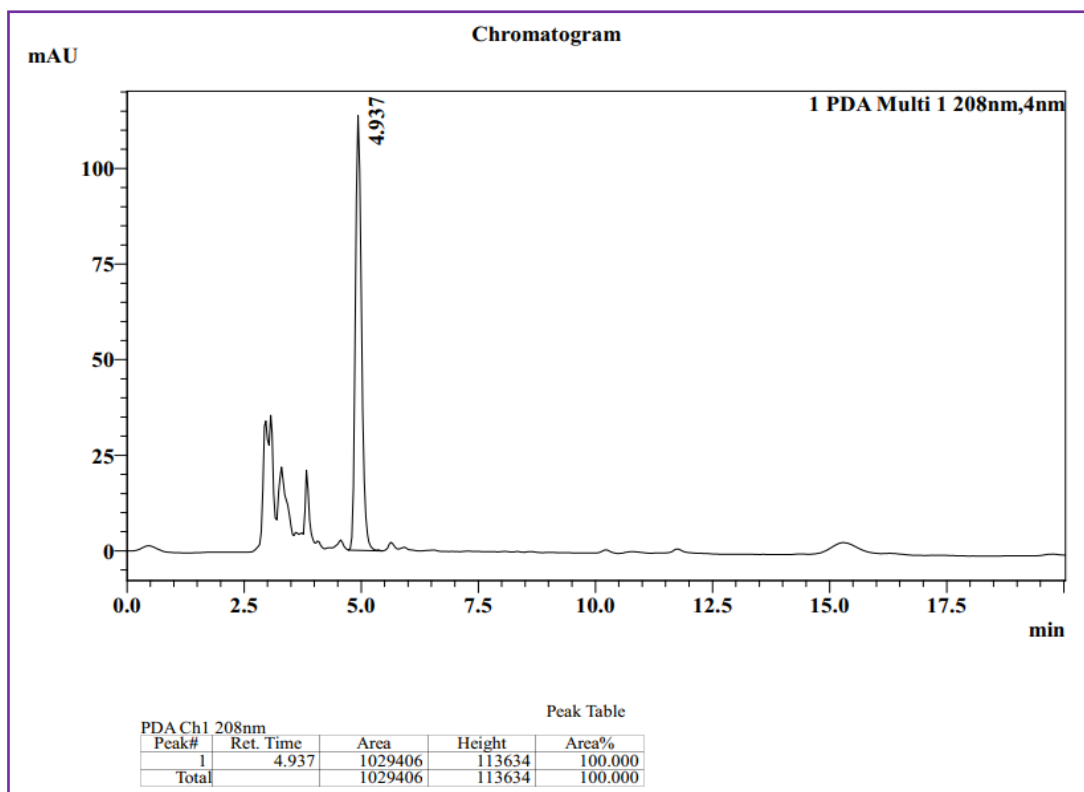


Figure 5.30: HPLC chromatograms of (α , 1*R*)-**11**

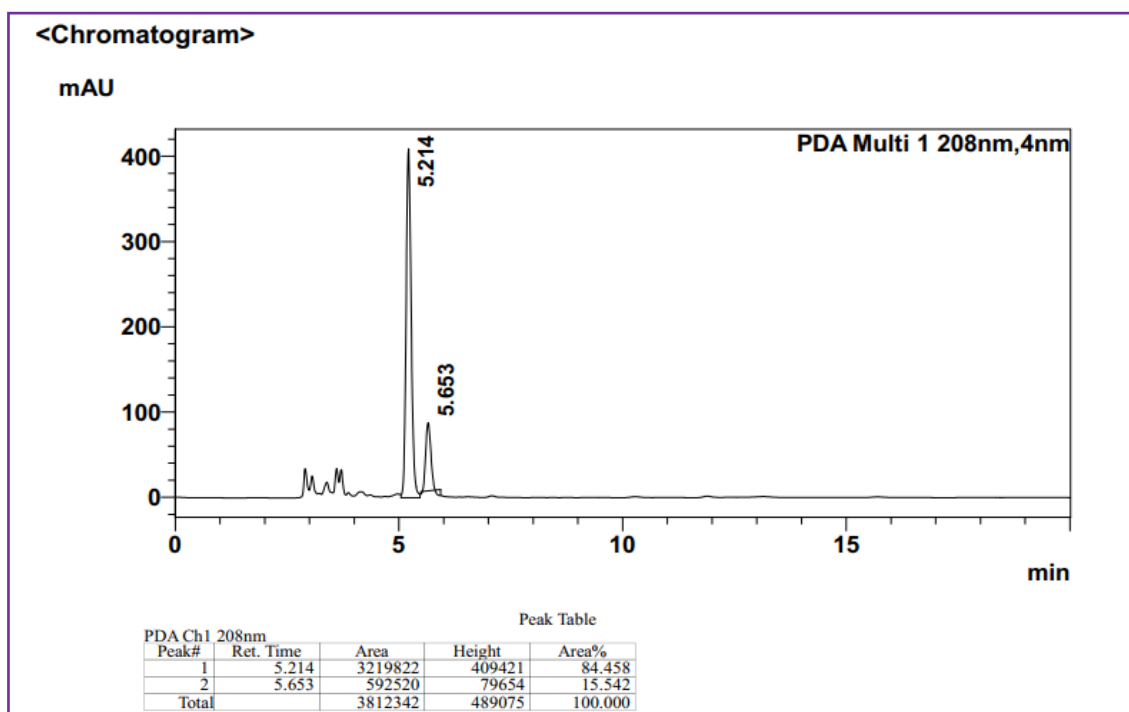


Figure 5.31: HPLC chromatogram of diastereomeric mixture of (α , 1*S*)-**11** and (α , 1*R*)-**11**

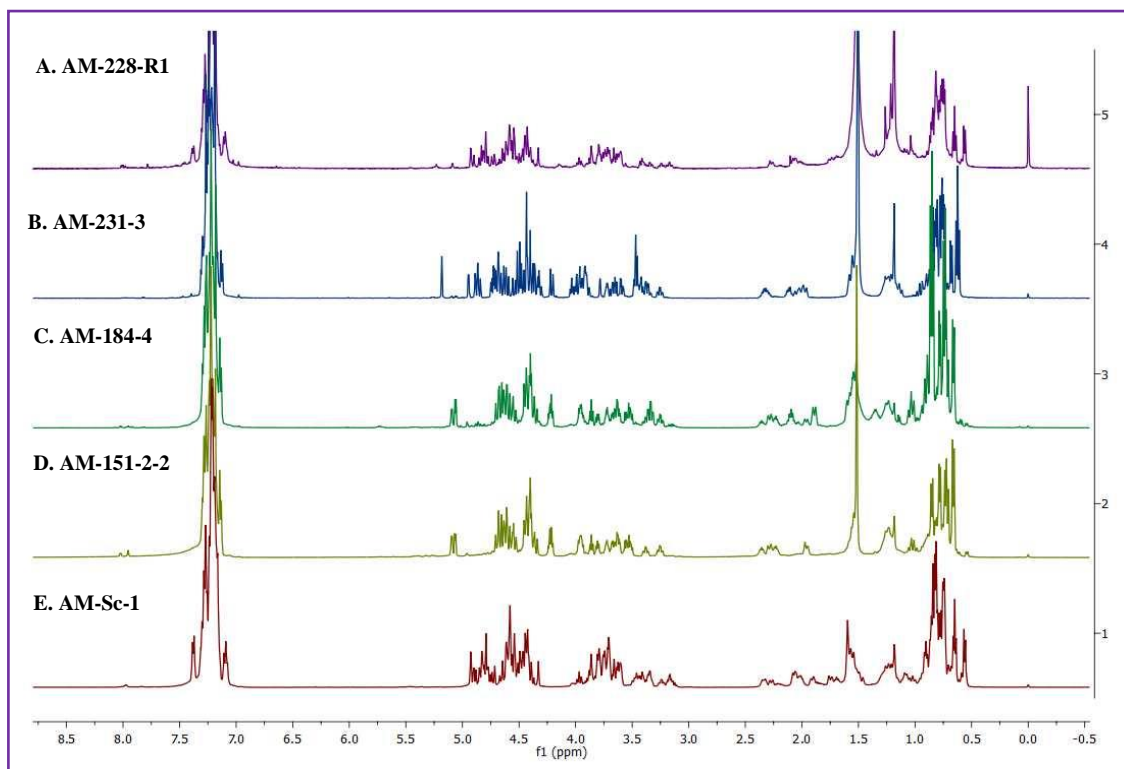


Figure 5.32: ^1H NMR of glycosides catalysed by (A) PCCP (B) $\text{CF}_3\text{SO}_3\text{H}$ (C) (*R*)-2 (D) (*S*)-2 (E) $\text{Sc}(\text{OTf})_3$ (entries 4-8, Table 1)

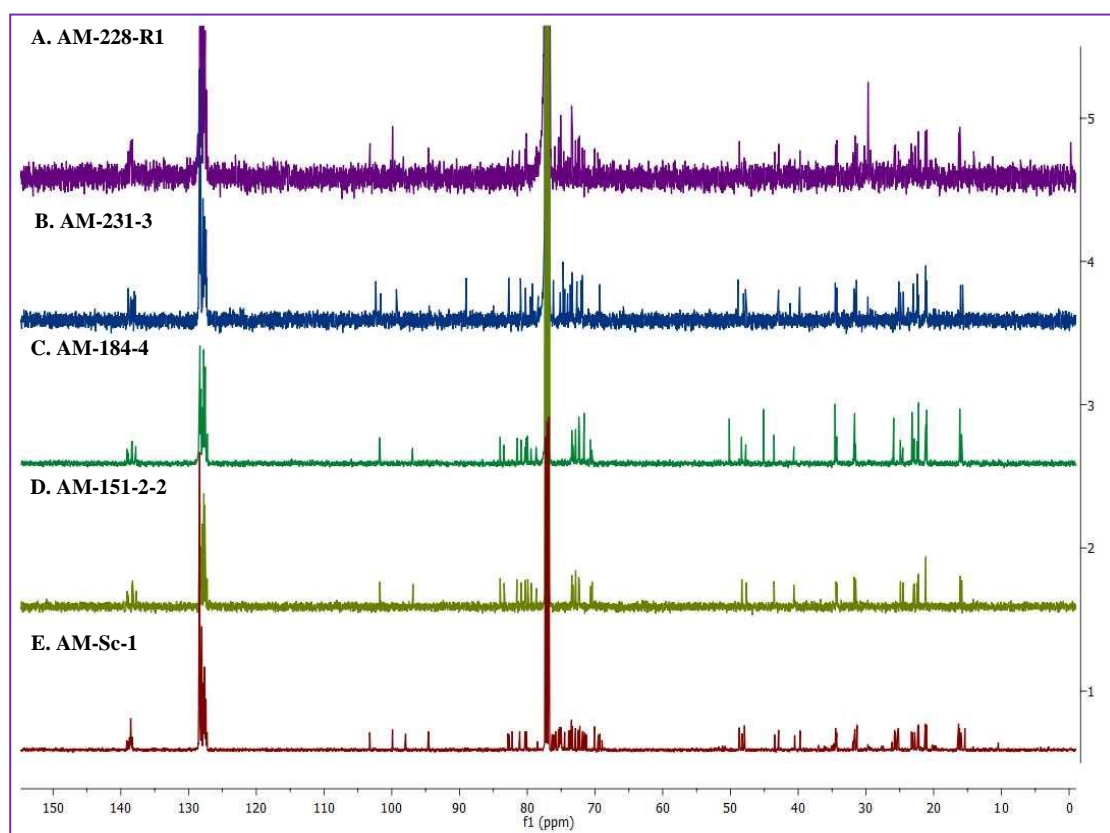


Figure 5.33: ^{13}C NMR of glycosides catalysed by (A) PCCP (B) $\text{CF}_3\text{SO}_3\text{H}$ (C) (*R*)-2 (D) (*S*)-2 (E) $\text{Sc}(\text{OTf})_3$ (entries 4-8, Table 1)

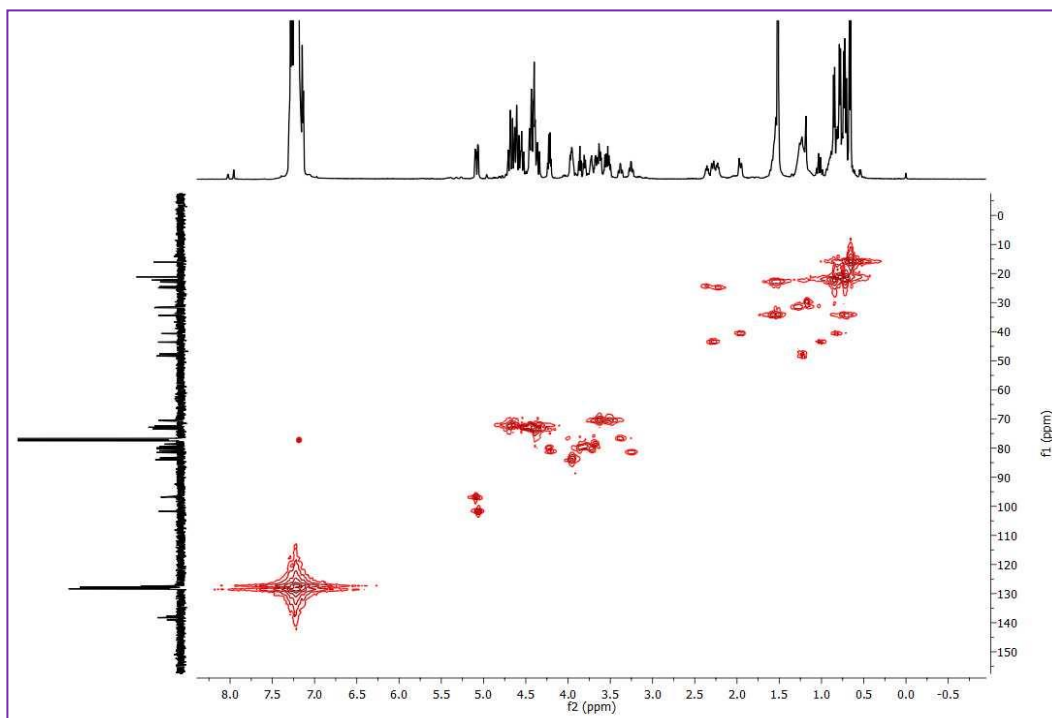


Figure 5.34: HMQC of diastereomeric mixture of (α , 1*S*)-**11** and (α , 1*R*)-**11** catalysed by (*S*)-**2**

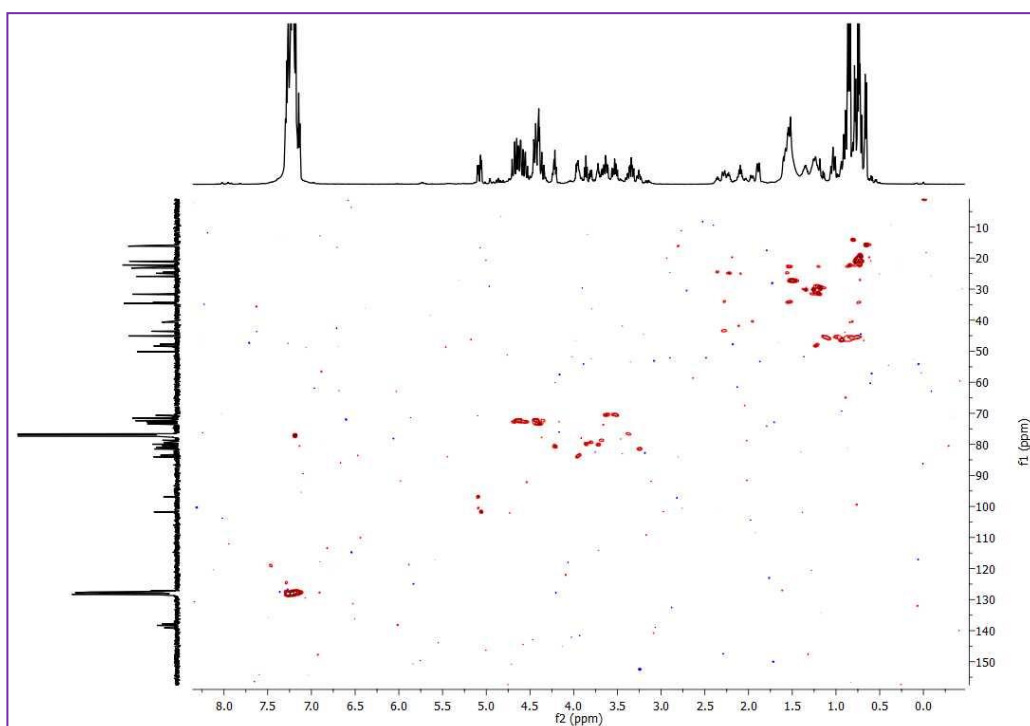


Figure 5.35: HSQC of diastereomeric mixture of (α , 1*S*)-**11** and (α , 1*R*)-**11** catalysed by (*R*)-**2**

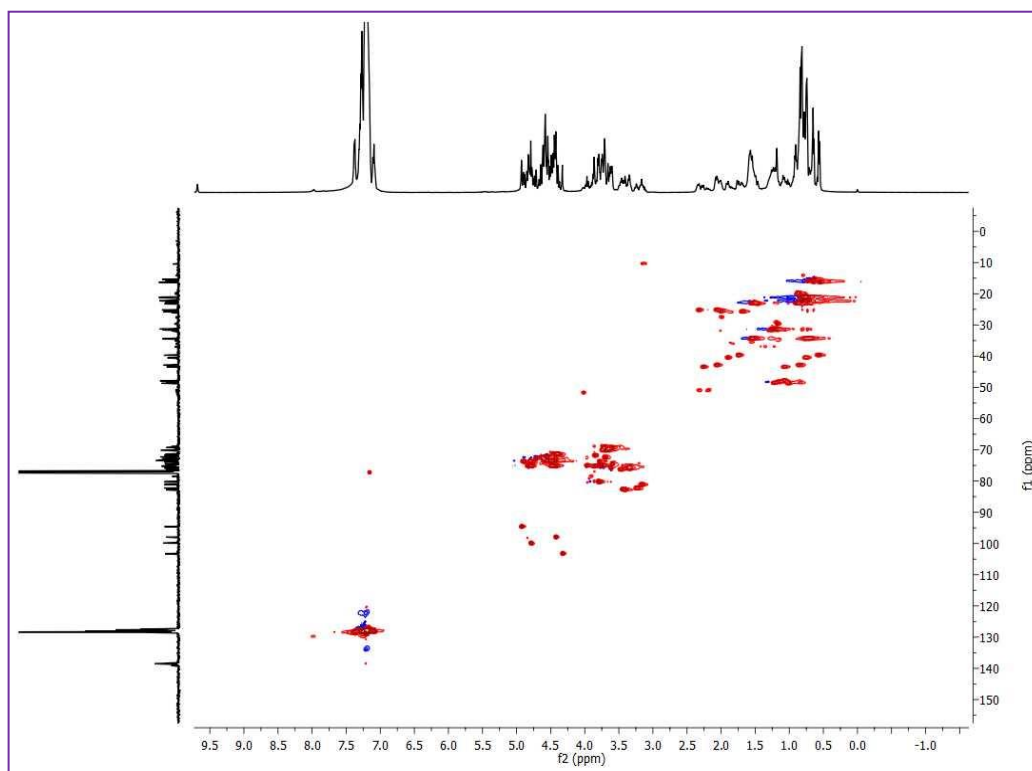


Figure 5.36: HSQC of stereoisomeric mixture of **11** catalysed by Sc(OTf)₃

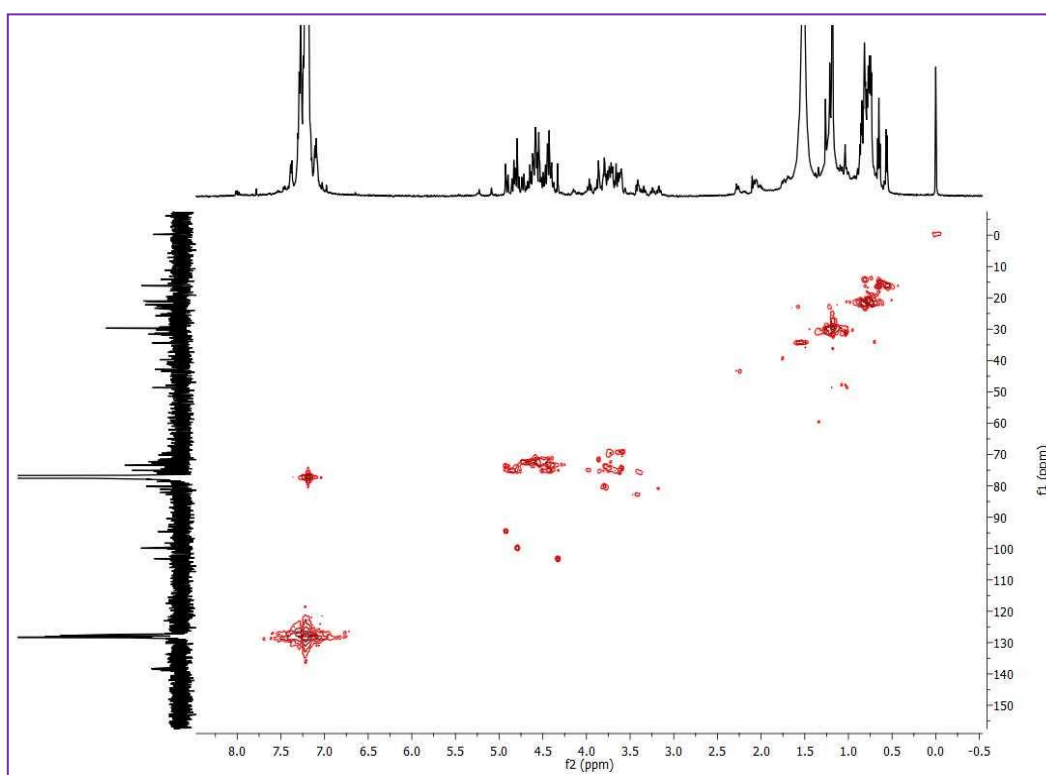


Figure 5.37: HSQC of stereoisomeric mixture of **11** catalysed by PCCP

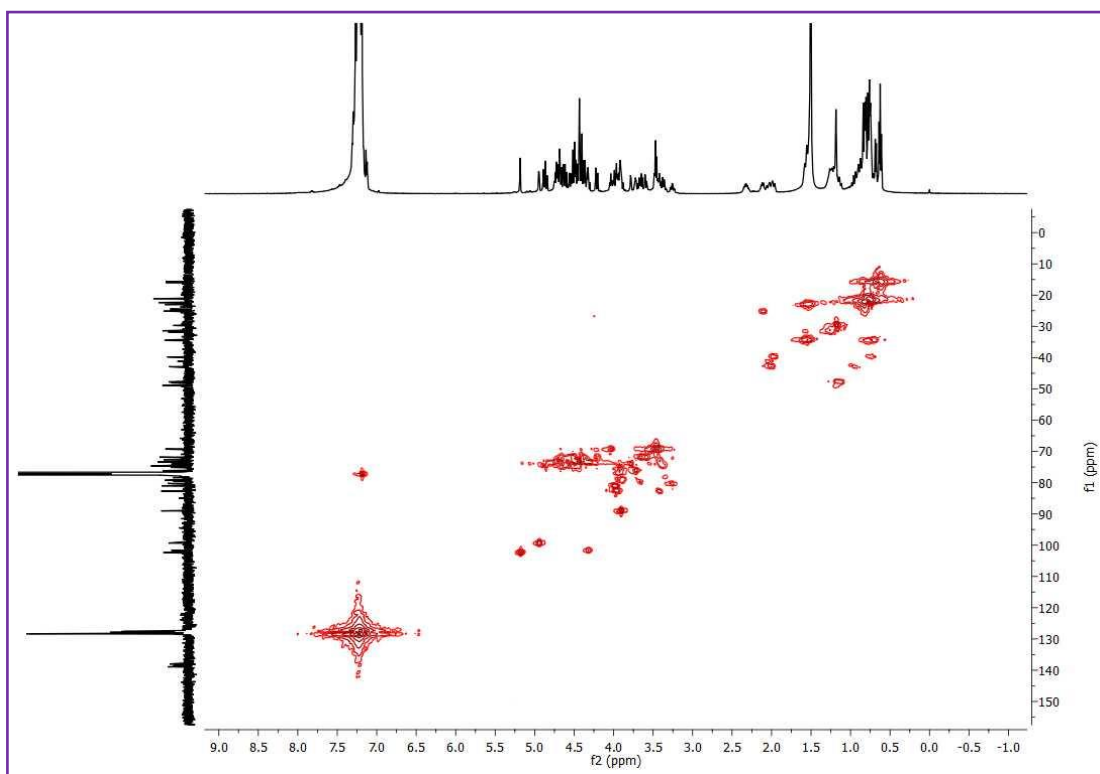


Figure 5.38: HSQC of stereoisomeric mixture of **11** catalysed by CF₃SO₃H

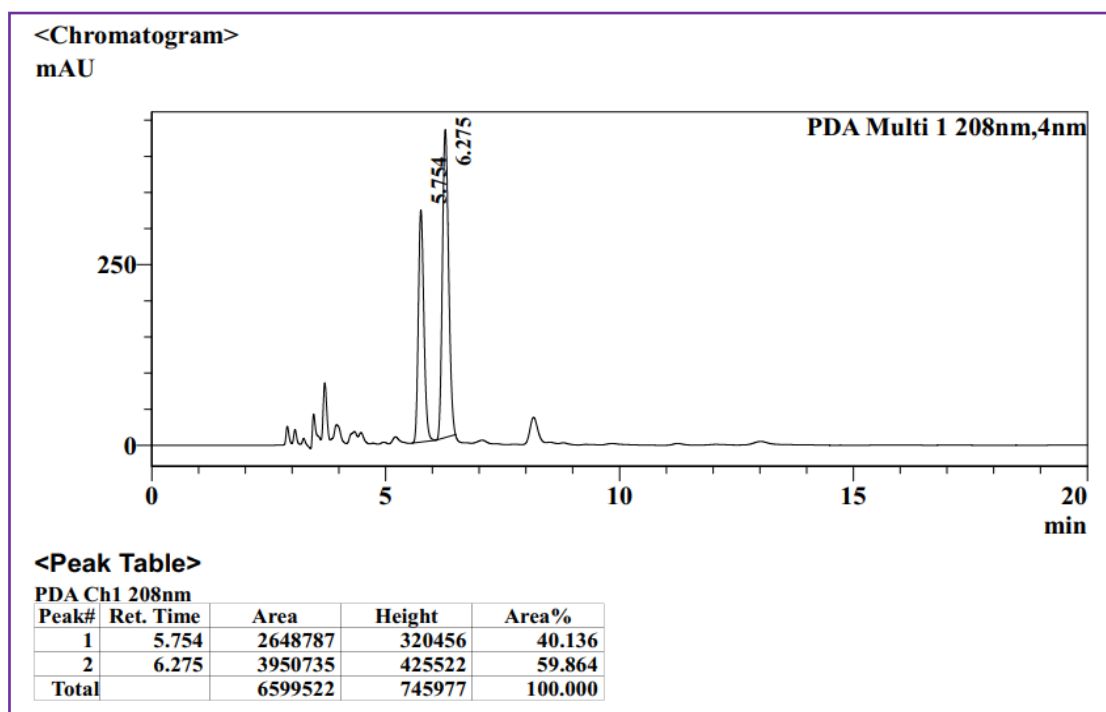


Figure 5.39: HPLC chromatogram of diastereomeric mixture of (α , 1*S*)-**11** and (α , 1*R*)-**11** catalysed by (*R*)-**2**

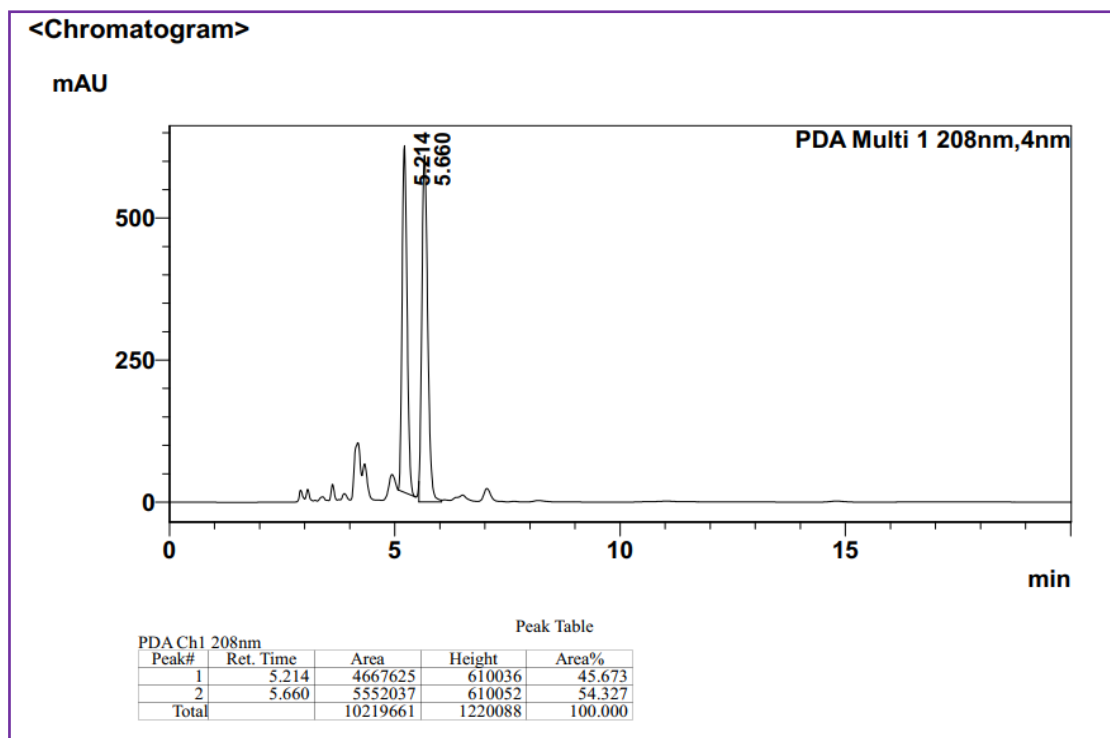


Figure 5.40: HPLC chromatogram of diastereomeric mixture of (α , 1*S*)-**11** and (α , 1*R*)-**11** catalysed by (*S*)-**2**

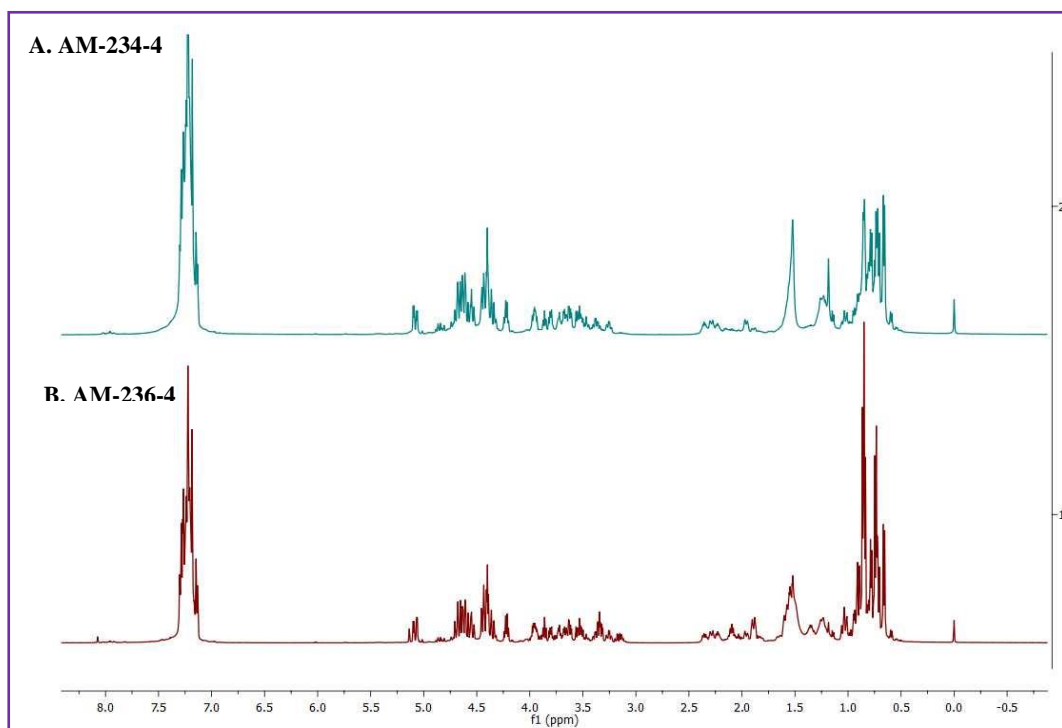


Figure 5.41: ^1H NMR of diastereomeric mixture of (α , 1*S*)-**10** and (α , 1*R*)-**10** catalysed by (A) CBA **3** (B) CBA **4**

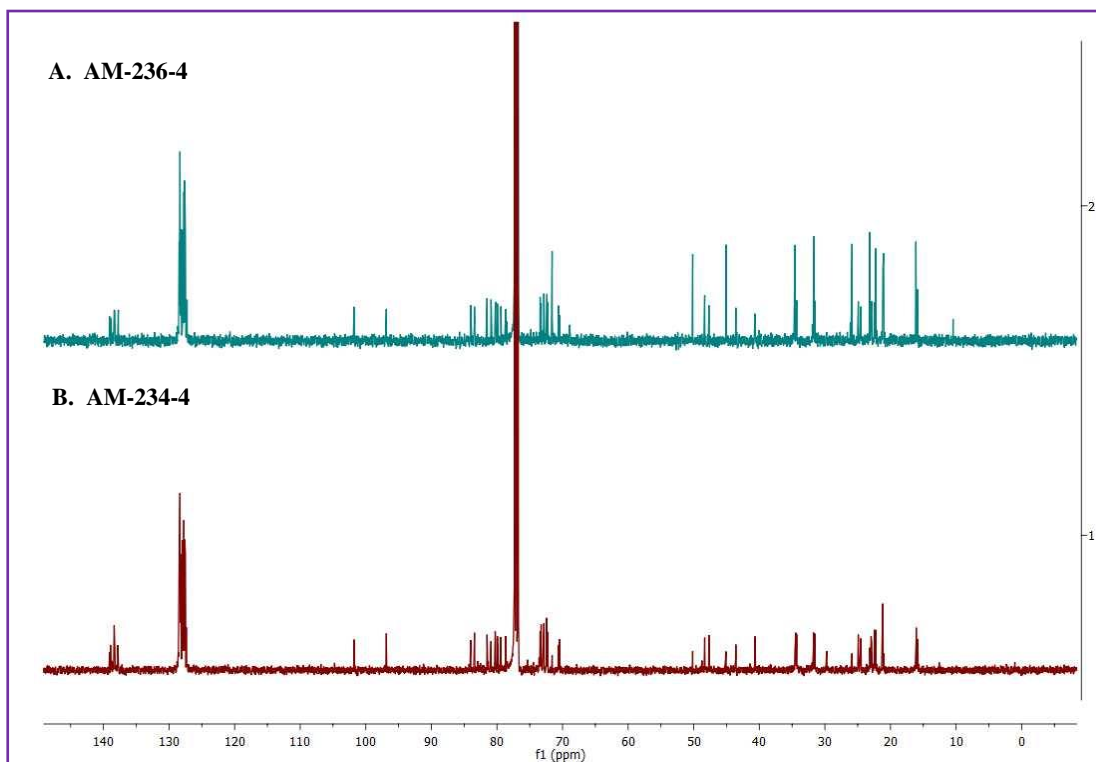


Figure 5.42: ^{13}C NMR of diastereomeric mixture of (α , 1*S*)-**10** and (α , 1*R*)-**10** catalysed by
(A) CBA 4 (B) CBA 3

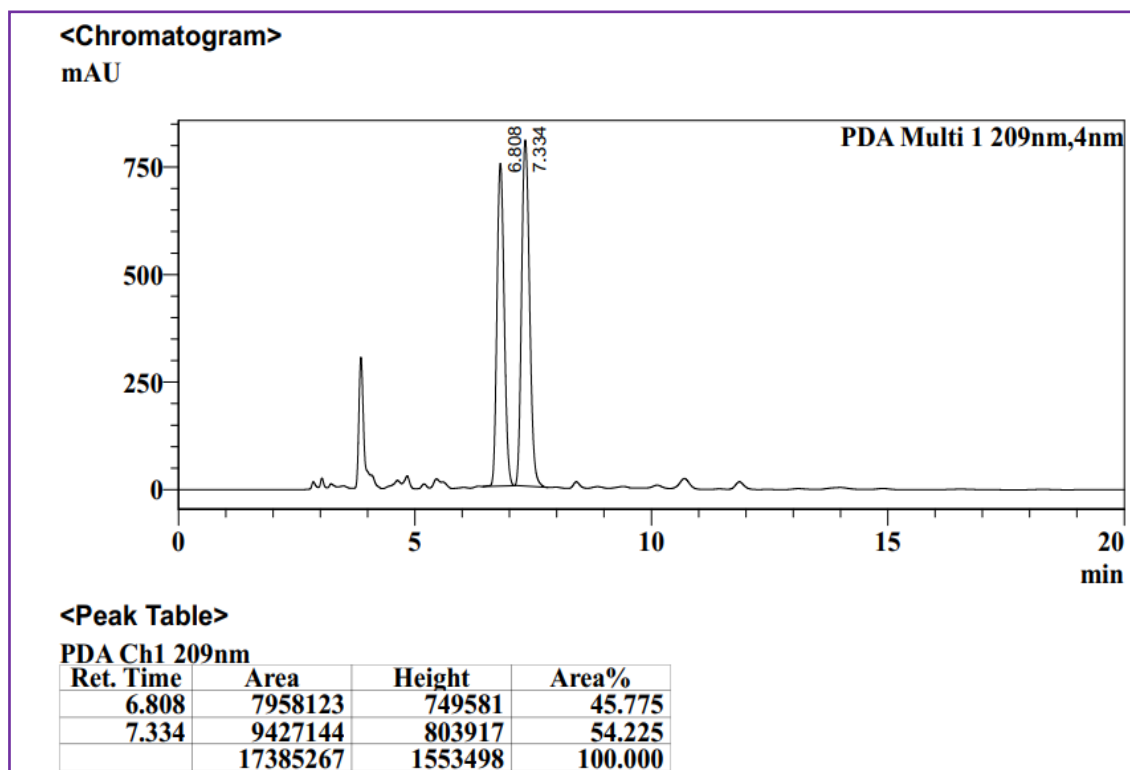


Figure 5.42: HPLC chromatogram of diastereomeric mixture of (α , 1*S*)-**10** and (α , 1*R*)-**10**
catalysed by CBA 3

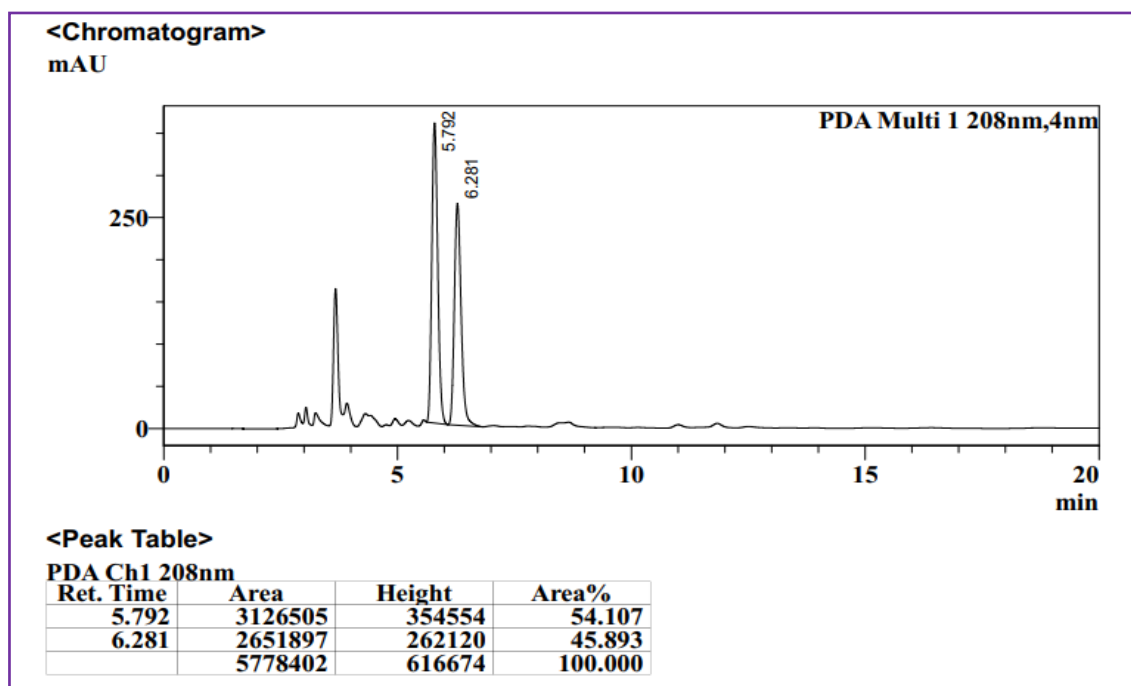
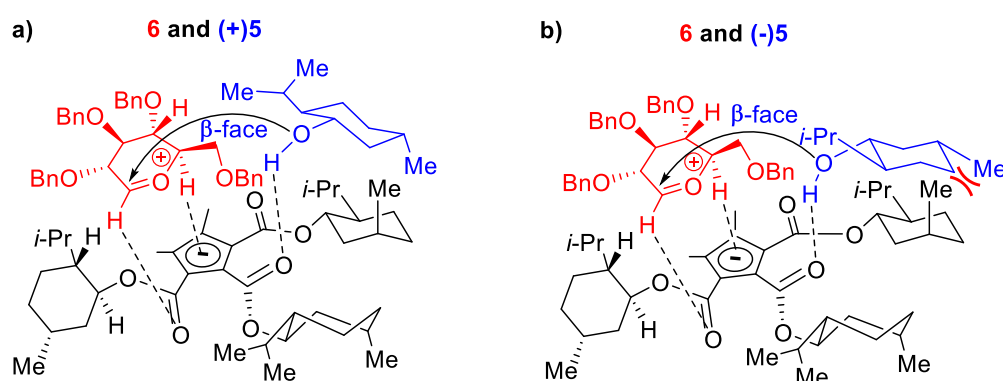


Figure 5.43: HPLC chromatogram of diastereomeric mixture of (α , 1*S*)-**10** and (α , 1*R*)-**10** catalysed by CBA **4**

5.2.4. Mechanistic rationale behind the stereoselectivity of glycosylation

The benzyl protection of NPGs **6-8** was intended to avoid any participation effect during glycosylation, similar to the approach by Toshima et al.¹⁴ Glycosylation, either in the absence of CBA or NIS, did not occur, suggesting the role of CBA catalyst in the activation of NIS. Next, we treated one of the obtained products (β ,1*S*)-**9** with CBA-**1** and NIS under the optimized glycosylation condition without the acceptor \pm **5**. The product (β ,1*S*)-**9** was quantitatively recovered without any isomerization even after 24 h of reaction, which indicates the stereo and diastereoselectivities of the reaction was driven by kinetic control. The mechanistic rationale behind the stereoselectivity is shown in scheme 1 from the positioning of the oxocarbenium ion, generated from NPG activation,²² and menthol on chiral cyclopentadienyl anion platform, in line with the model proposed by Lambert et al. for enantioselective addition on oxocarbenium with the necessary organizational element of H-bonding.²⁰ We surmise the H-bonding interactions of C-H bonds of C1, and C5 carbons adjacent to the oxygen of the oxocarbenium ion and the cyclopentadienyl anion are the conventional and CH/ π H bonding interactions (Scheme 1a). During glycosylation, perhaps, the menthol is positioned in the hydrophobic pocket formed by the (+)-isomenthyl groups and

held by H-bonding with the carbonyl of the catalyst. The organization of the donor and acceptor on the cyclopentadienyl ring, prior to glycosylation, is the key for observed stereo- and diastereoselectivity. As shown in the model, the α/β -stereoselectivity of glycosylation may be governed by the steric hindrance by C2-OBn and C4-OBn groups for the incoming nucleophilic attack on oxocarbenium ion. Accordingly, in the case of glucosyl-NPG **6**, the less hindered β -face is preferred for nucleophilic attack of the menthol oxygen atom, while the mannosyl-NPG **7** and galactosyl-NPG **8** prefer α -face. The β -selectivity with NPG **6** and α -selectivity with NPG **7** and **8** reinforces the proposed model in scheme 1 as a highly conserved catalytic platform with organizational elements to promote stereoselectivity. The rationale for diastereoselectivity is governed by the steric interaction of the all-equatorial conformation of the menthol with the axial-methyl group of (+)-isomenthyl of the catalyst. (-)-Menthol **5** exhibits van der Waals repulsion in the proposed model (Scheme 1b), favouring (+)-menthol **5** in glycosylation (Scheme 1a). Thus, based on the proposed model (Scheme 1), α/β -stereo- and diastereoselectivity with NPGs **6-8** and chiral recognition of racemic menthol **5** (entries 1-3, Table 1) can be rationalized. The choice of ester in the catalyst is essential, which was demonstrated with menthyl esters of CBA **3** and **4** that possess all three groups in the equatorial position of their most stable conformation, causing a lack of diastereoselectivity (entries 9-10, Table 1). By the same token, the PCCP CBA catalyst with (-)-isomenthyl group can offer the opposite chiral recognition; however, due to the lack of commercial availability of (-)-isomenthol, we could not pursue synthesis of the catalyst. The importance of CBA **1** catalysis was obvious in glycosylation; as attempts with chiral phosphoric acid catalysts (*R*)-**2** and (*S*)-**2**, though offered stereoselectivity, there was no appreciable chiral recognition of racemic menthol (entries 4-5, Table 1).



Scheme 3: Rationale for stereo- and diastereocontrol in glycosylation with CBA **1**.

We utilized density functional theory (DFT) calculations to establish a correlation between the suggested mechanism responsible for the oxocarbenium intermediate-assisted transition state, the presence of hydrogen bonding interactions among the three systems, and the electron transitions from the acceptor to the oxocarbenium intermediate. Here we adopt the Gauss View 5.0 [5] program package to establish the atomistic model for the catalyst (CBA-1), oxocarbenium intermediate and the acceptor systems (± 5). A model containing cyclopentadienyl ring as the core for the catalyst, and an oxocarbenium based core for the intermediate were constructed. Based on the above approximation we have developed a model system having 215 atoms and 726 electrons, which is further used for the interaction studies. The developed model was optimized via Density functional theory (DFT) calculation,^{1,2} which was carried out using Gaussian-09 software by minimizing the total energy without symmetry constrain. The electronic structure and bonding interaction existed in the proposed transition state were studied by using Becke three-parameter Lee–Yang–Parr hybrid functional (B3LYP) method. Calculations were performed for the optimized structures of CBA-1, oxocarbenium ion, and menthol using 6-31G* basis set and B3LYP/6-31g (d,p) level of theory. Our experimental analysis aligned seamlessly with DFT assessments, confirming the existence of three significant hydrogen bonding interactions within the optimized geometries. The visual depiction of DFT analysis, as illustrated in Figure 5.44, unveiled precise interactions: A hydrogen bond forms between the hydrogen atom (H39) in the acceptor moiety's hydroxyl group and the catalyst's carbonyl oxygen (O11) at an approximate length of 1.44 Å. Another discernible hydrogen bond interaction exists between the catalyst's carbonyl oxygen (O3) and the hydrogen atom (H54) of the oxocarbenium intermediate, measuring approximately 1.47 Å. Furthermore, a π -hydrogen bond is observed between the catalyst and the oxocarbenium ion (H67) by positioning a dummy atom (O84) at the cyclopentadienyl system's center, with an approximate bond length of 1.96 Å. The consistency of these parameters with findings from prior literature further substantiates the proposed mechanism. Moreover, the electron transition between the oxocarbenium intermediate and the acceptor groups were illustrated by calculating the highest occupied molecular orbitals (HOMO) and the lowest unoccupied molecular orbitals (LUMO) for the optimized geometry. The optimized structure of the materials was visualized using Gauss view version 5.0. HOMO and LUMO energy levels were also evaluated. As given in Table 2, the HOMO energy level (6.40 eV) is concentrated over the acceptor moiety, whereas the LUMO energy level (3.04 eV) is concentrated over the oxocarbenium intermediate.

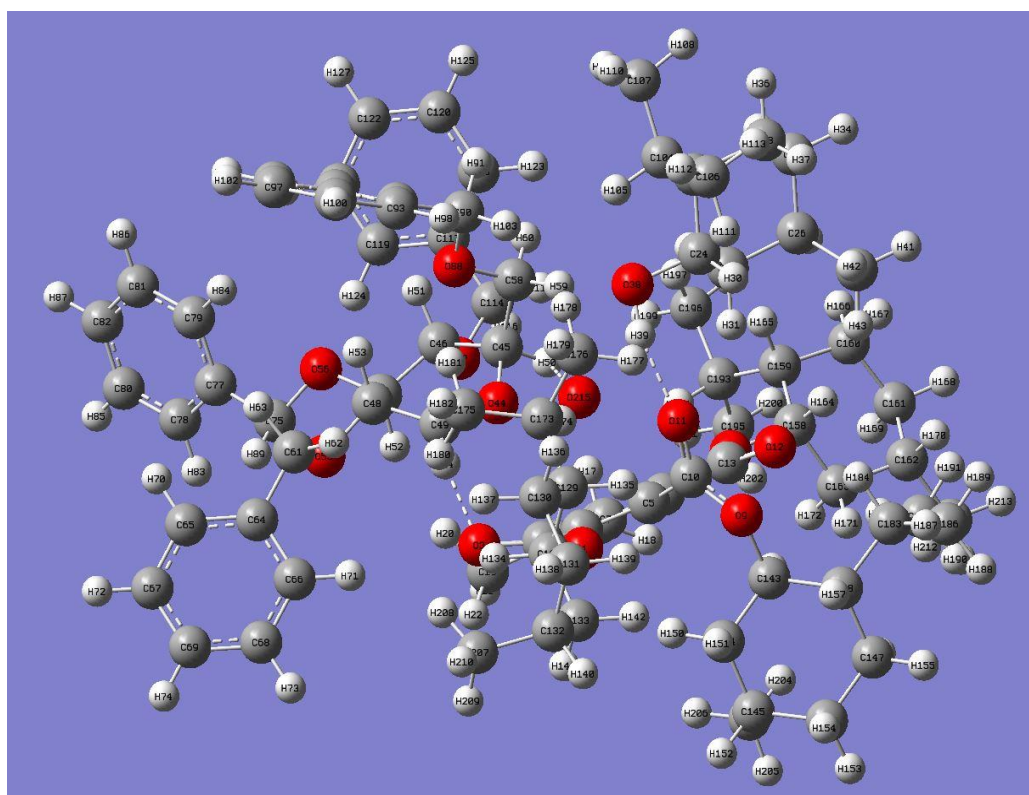
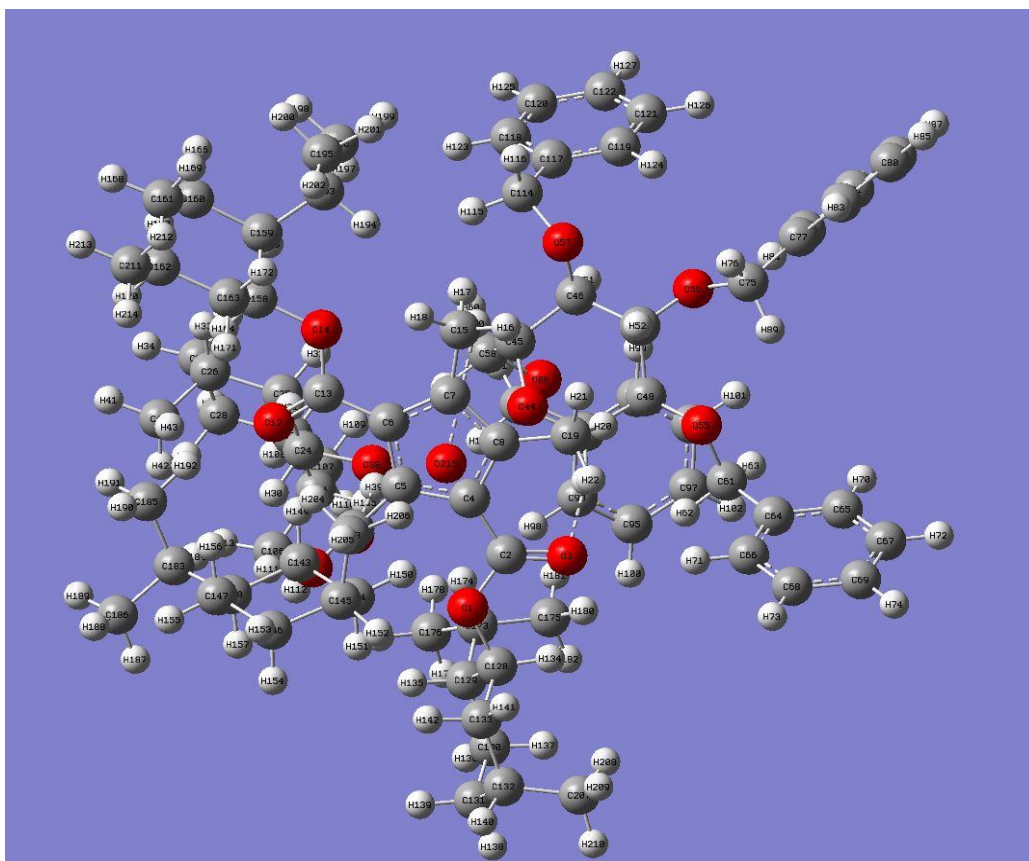


Figure 5.44: B3LYP/6-31 g(d,p) optimised model for the transition state in two different orientations.

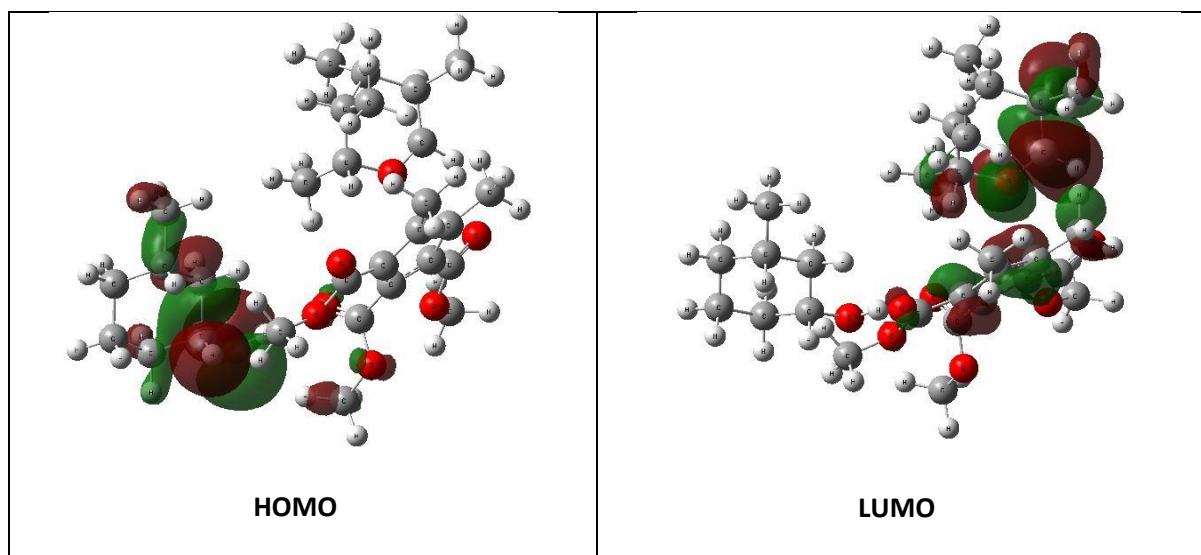
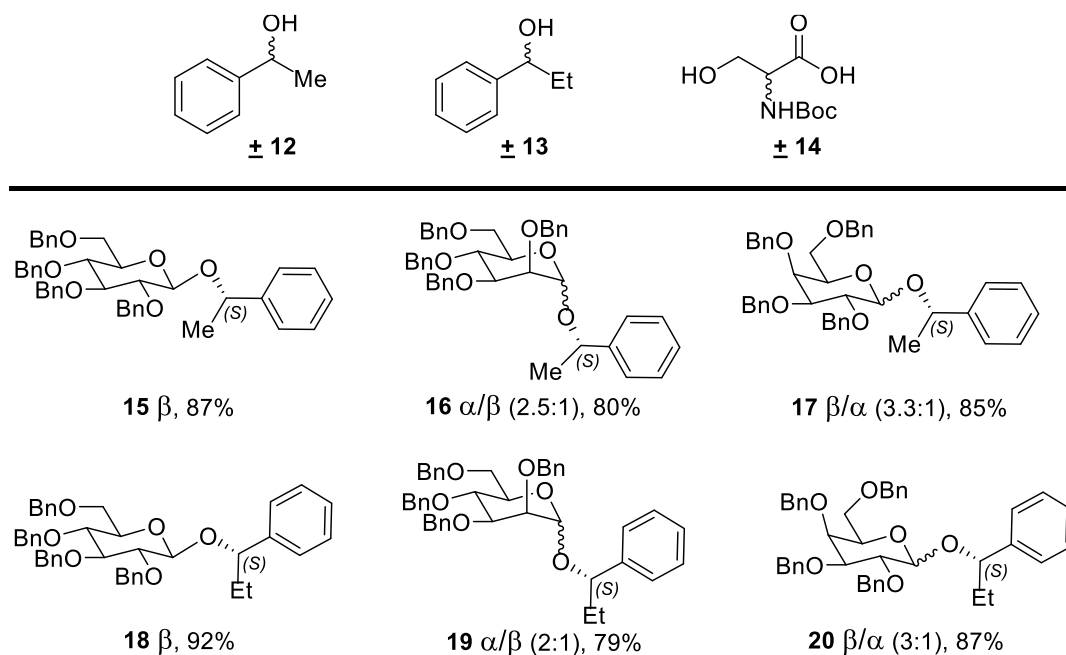


Table 2: HOMO, LUMO energy levels for the transition state

To assess the generality, we explored the chiral recognition with racemic substrates **12**, **13**, and **14** for CBA 1-catalyzed glycosylation reaction with NPGs **6-8** (Scheme 2). Exclusive diastereocontrol in chiral recognition of the S-enantiomers of benzylic alcohols **12** and **13** in the glycosylation reaction afforded **15-20** in excellent yields. Glucosyl-NPG **6** afforded β -anomers **15** and **18** selectively, however, mannosyl-NPG **7** afforded anomeric mixtures **16**, **19**, dominating in α -anomer, and galactosyl-NPG **8** produced anomeric mixtures **17**, **20**, dominating in β -anomer.



^aReaction conditions: To the mixture of 6/7/8 (1.0 equiv.), \pm 12/ \pm 13/ \pm 14 (2.0 equiv.) in CH_2Cl_2 at 0 °C, under 4 Å MS, NIS (2.5 equiv.), CBA 1 (10 mol%) was added and slowly warmed to

room temperature. The reported yields are isolated yields by column chromatography. The ratios were determined from integration of the anomeric protons in ^1H NMR spectra, identified by their respective chemical shifts of the glycosides with pure enantiomers and HMQC spectra, dr is the diastereomeric ratio.

Scheme 4. Diastereocontrol in glycosylation of racemic acceptors **12**, **13** and **14** with CBA **1**

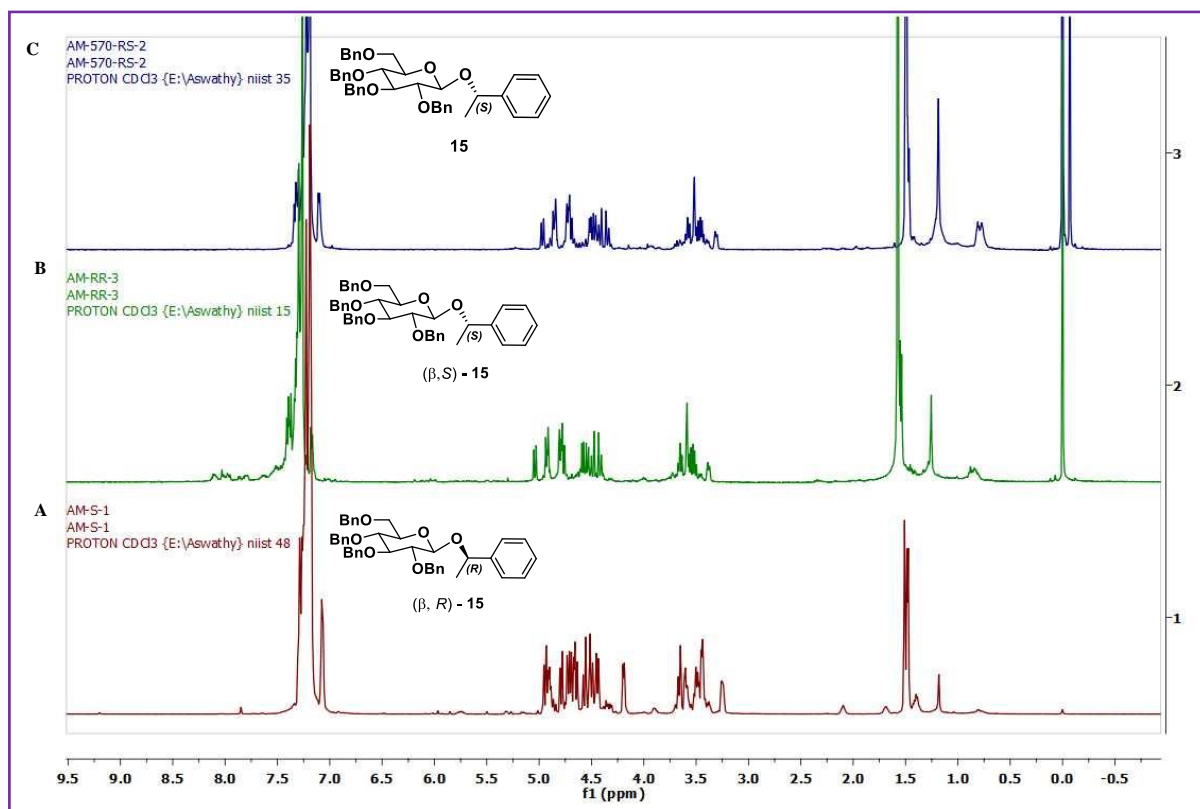


Figure 5.44: ^1H NMR spectra of glycosides of (A) (β , *R*)-**15** (B) (β , *S*)-**15** (C) Compound **15**

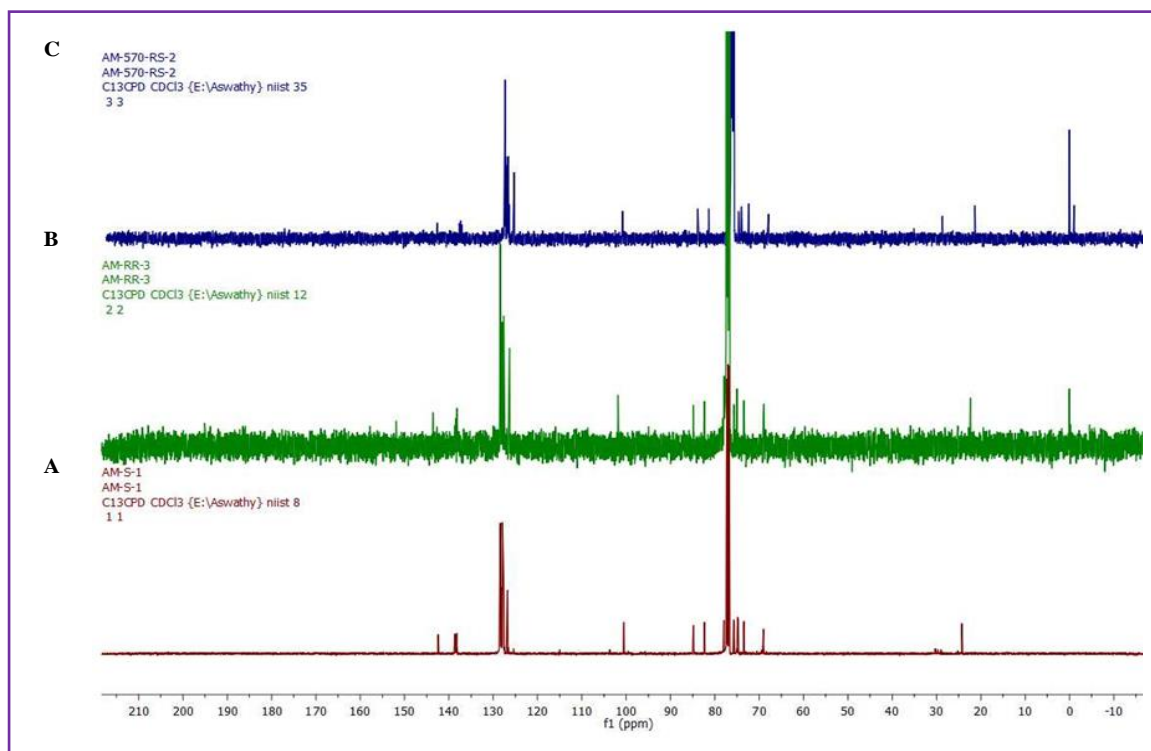


Figure 5.45: ^{13}C NMR of glycosides of (A) (β , *R*)-**15** (B) (β , *S*)-**15** (C) Compound **15**

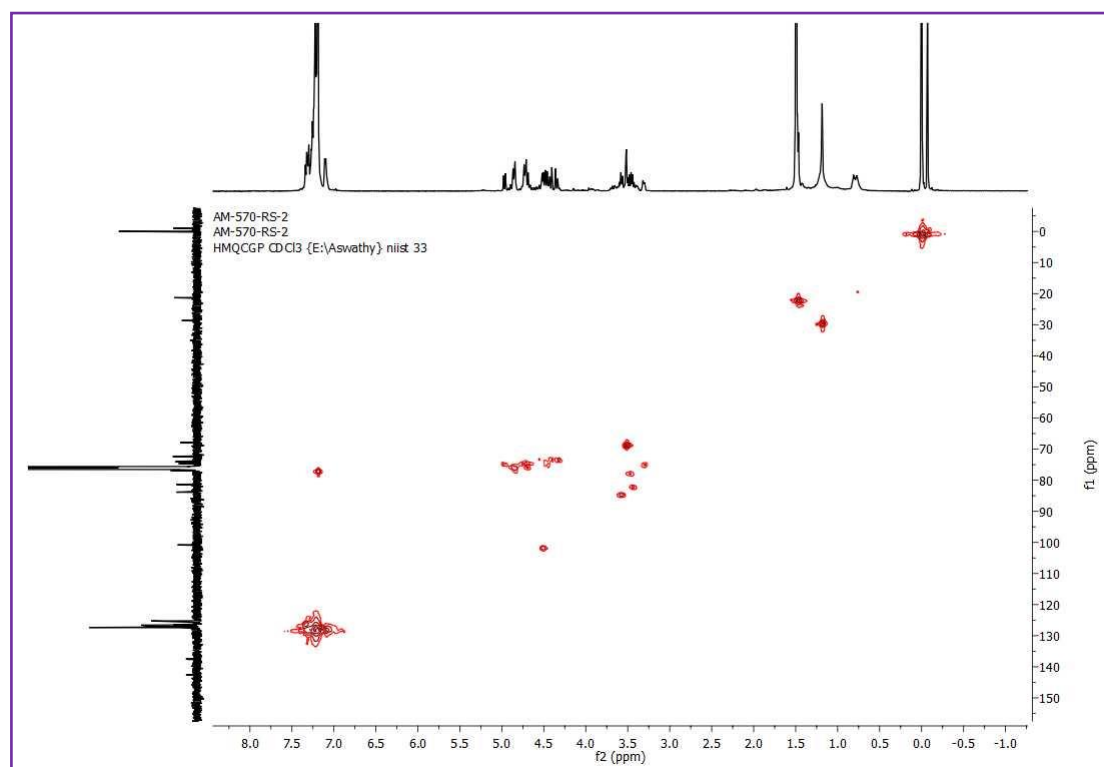


Figure 5.46: HMQC Spectra of compound **15**

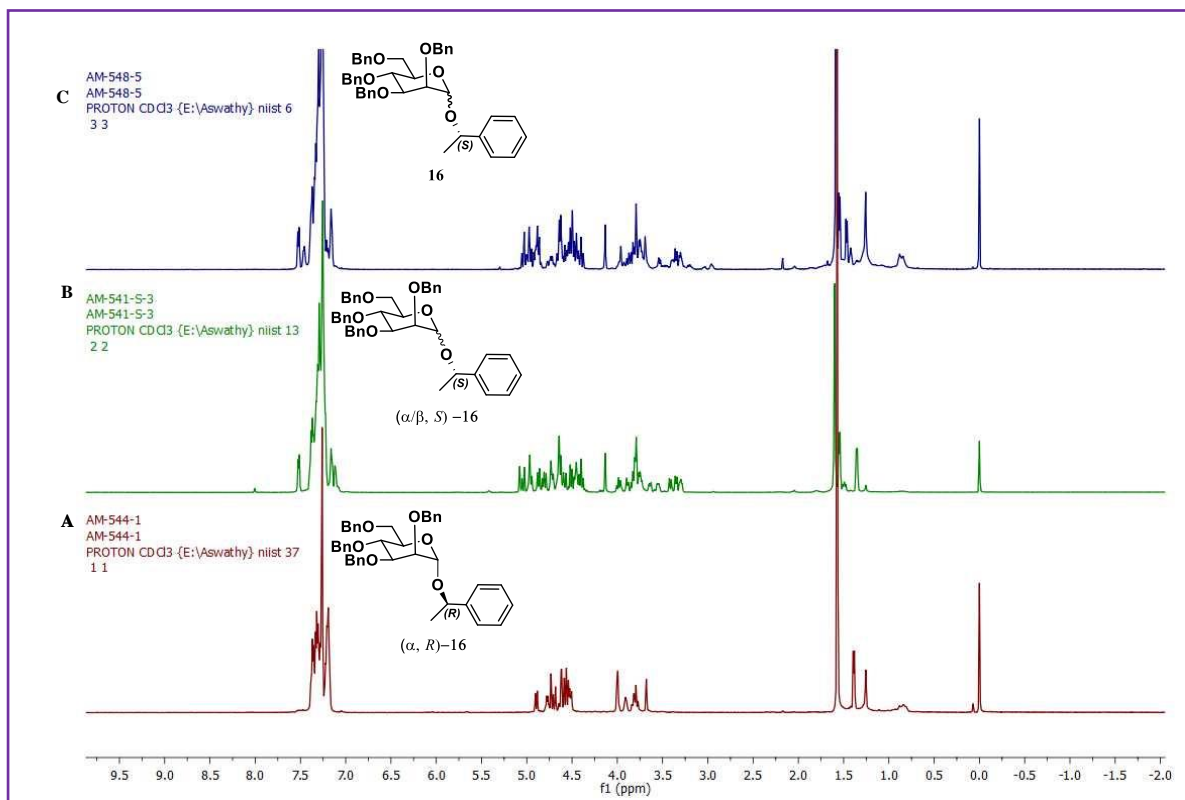


Figure 5.47: ¹H NMR of glycosides of (A) (α, R)-16 (B) (α/β, S)-16 (C) Compound 16

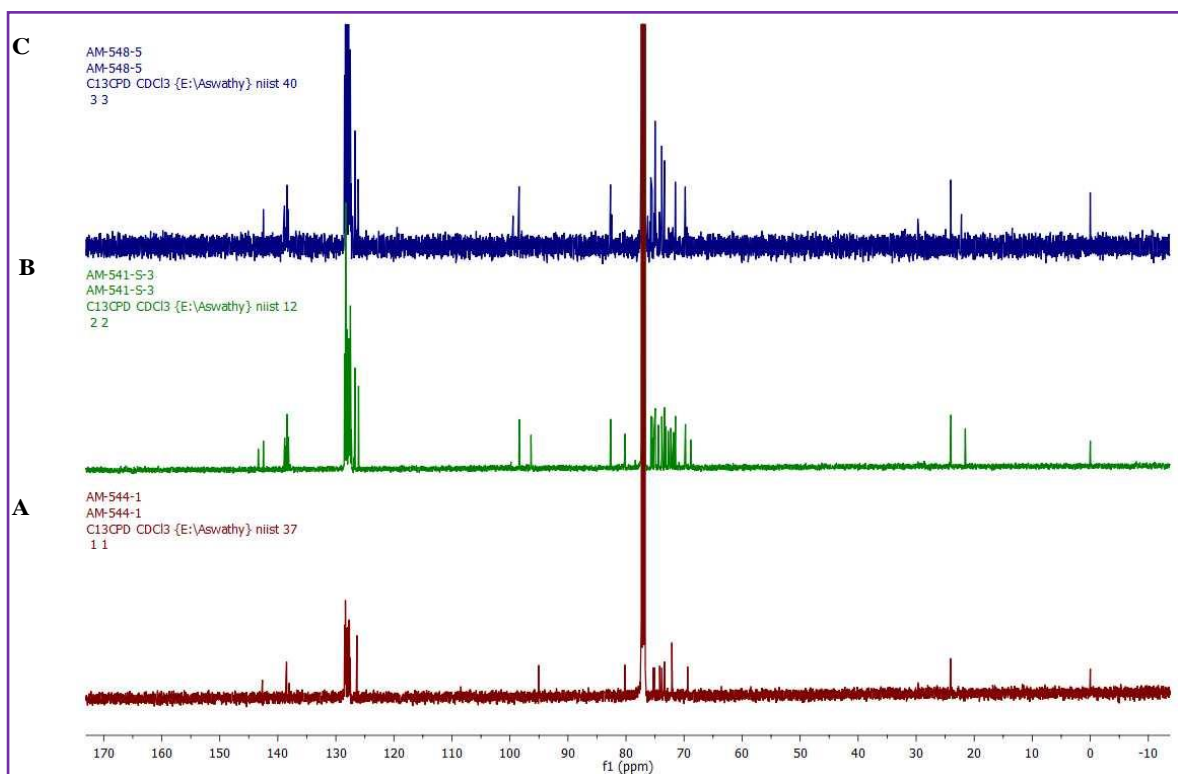


Figure 5.48: ¹³C NMR of glycosides of (A) (α, R)-16 (B) (α/β, S)-16 (C) Compound 16

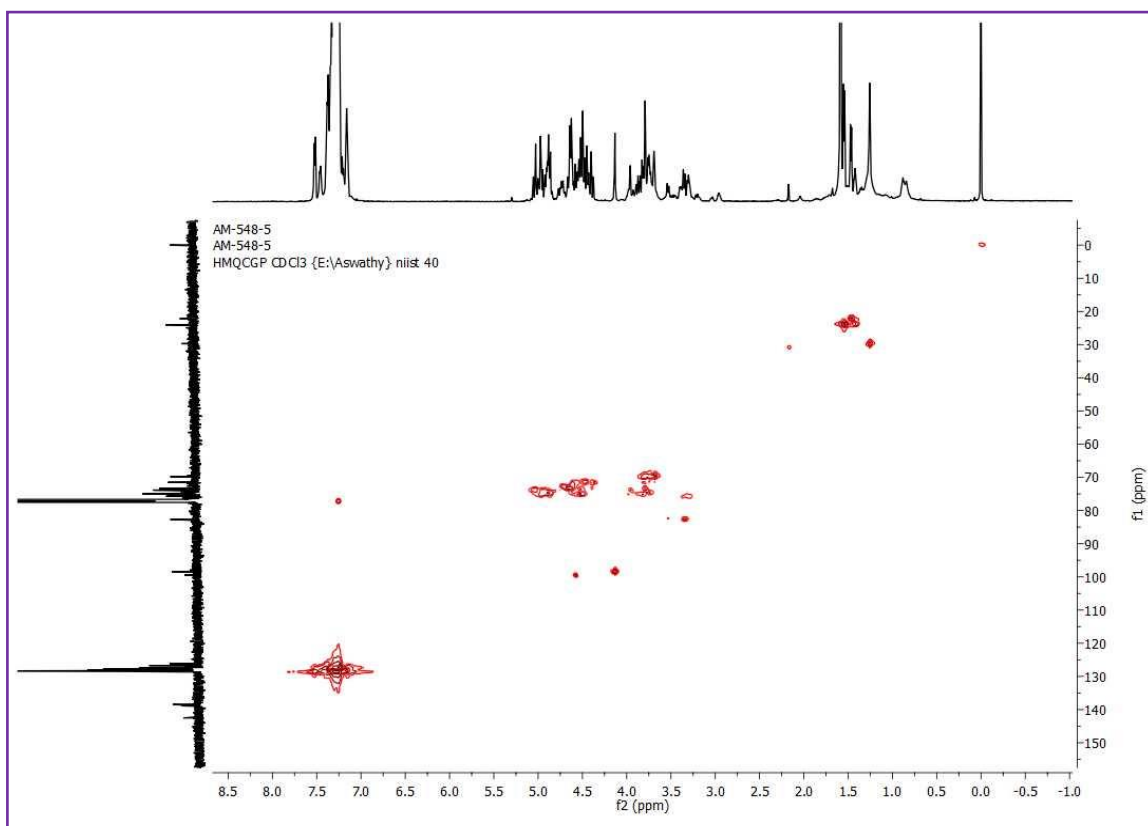


Figure 5.49: HMQC spectra of compound 16

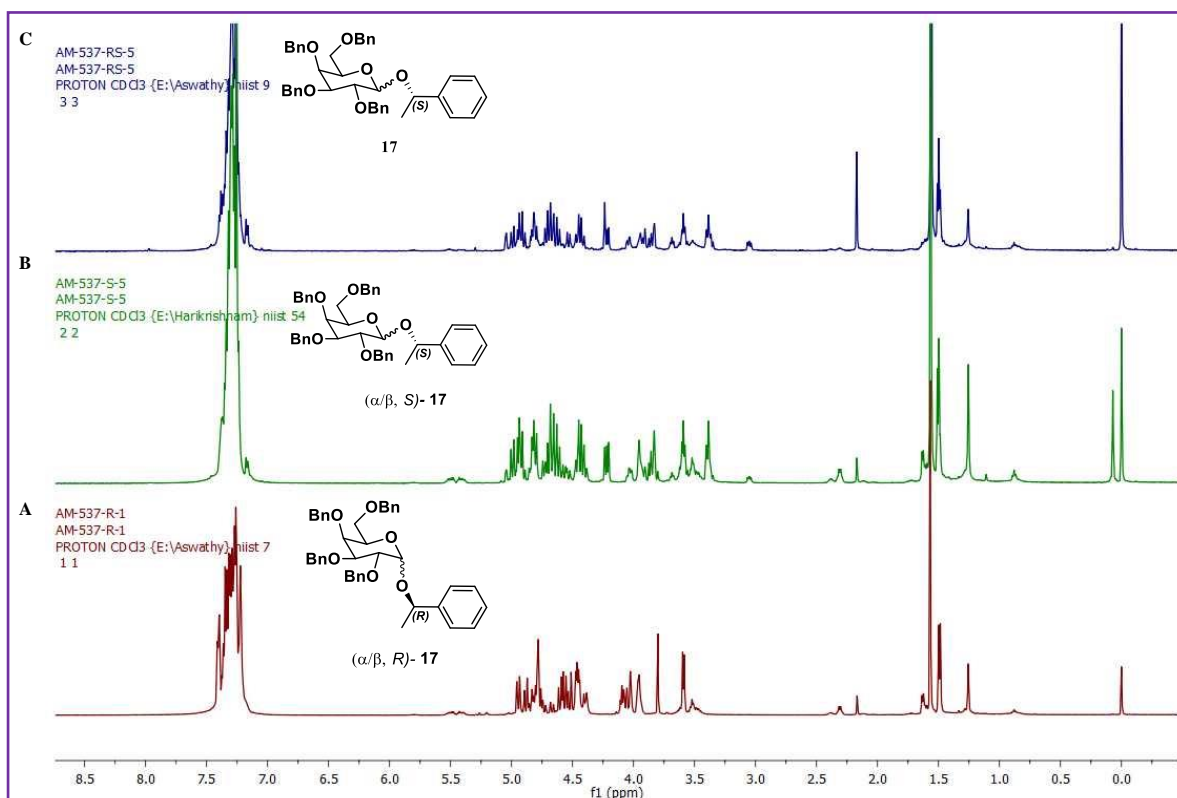


Figure 5.50: ¹H NMR of glycosides of (A) (α/β , R)-17 (B) (α/β , S)-17 (C) Compound 17

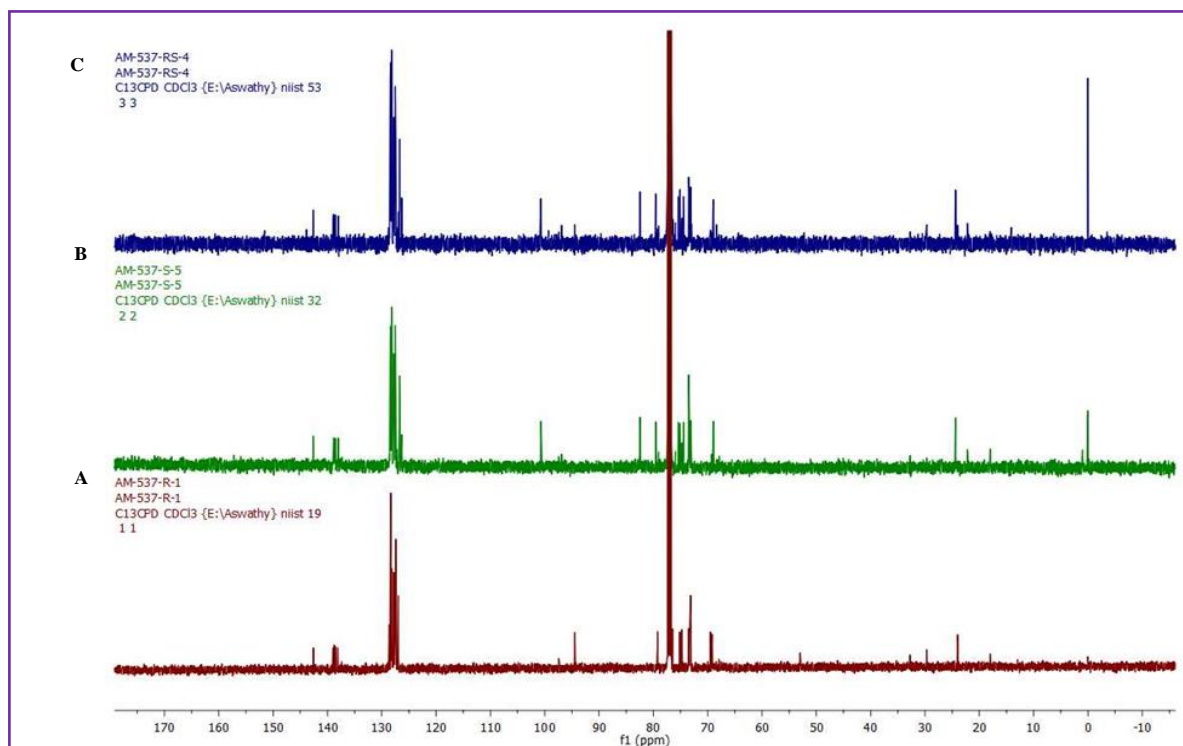


Figure 5.51: ^{13}C NMR of glycosides of (A) (α/β , *R*)-**17** (B) (α/β , *S*)-**17** (C) Compound **17**

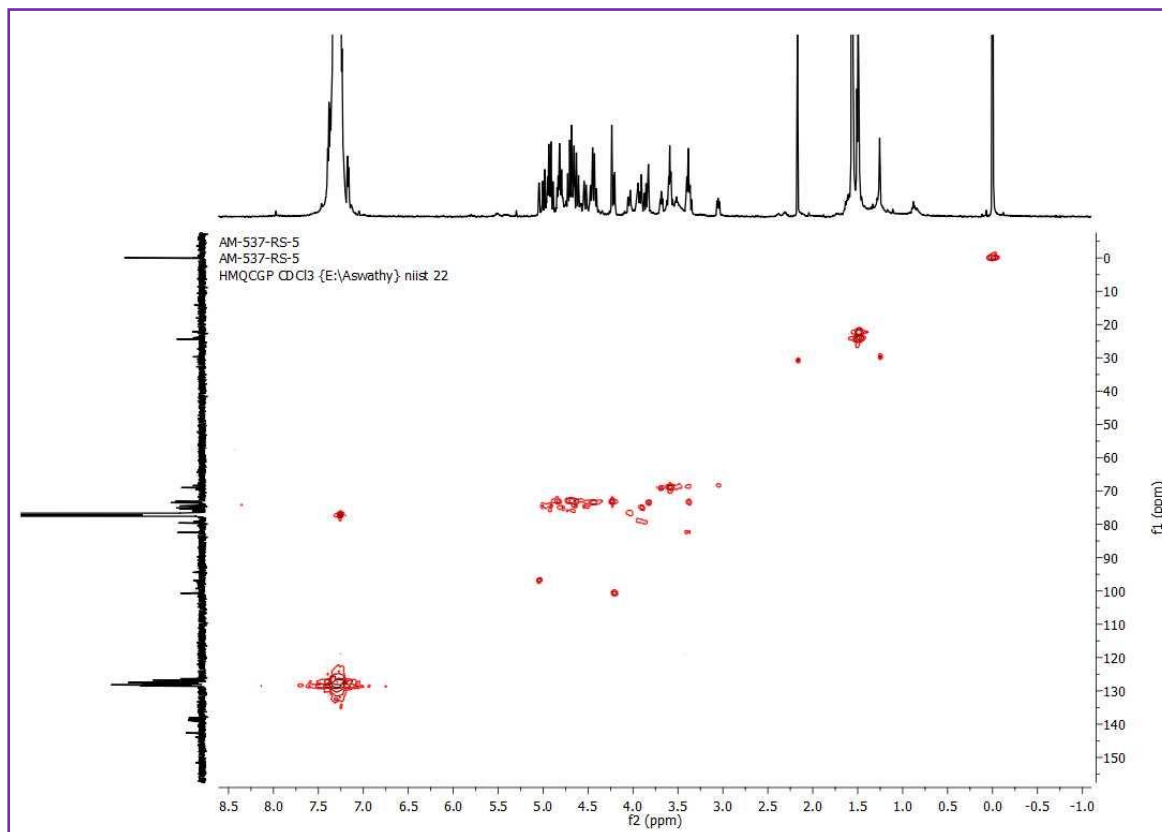


Figure 5.52: HMQC spectra of Compound **17**

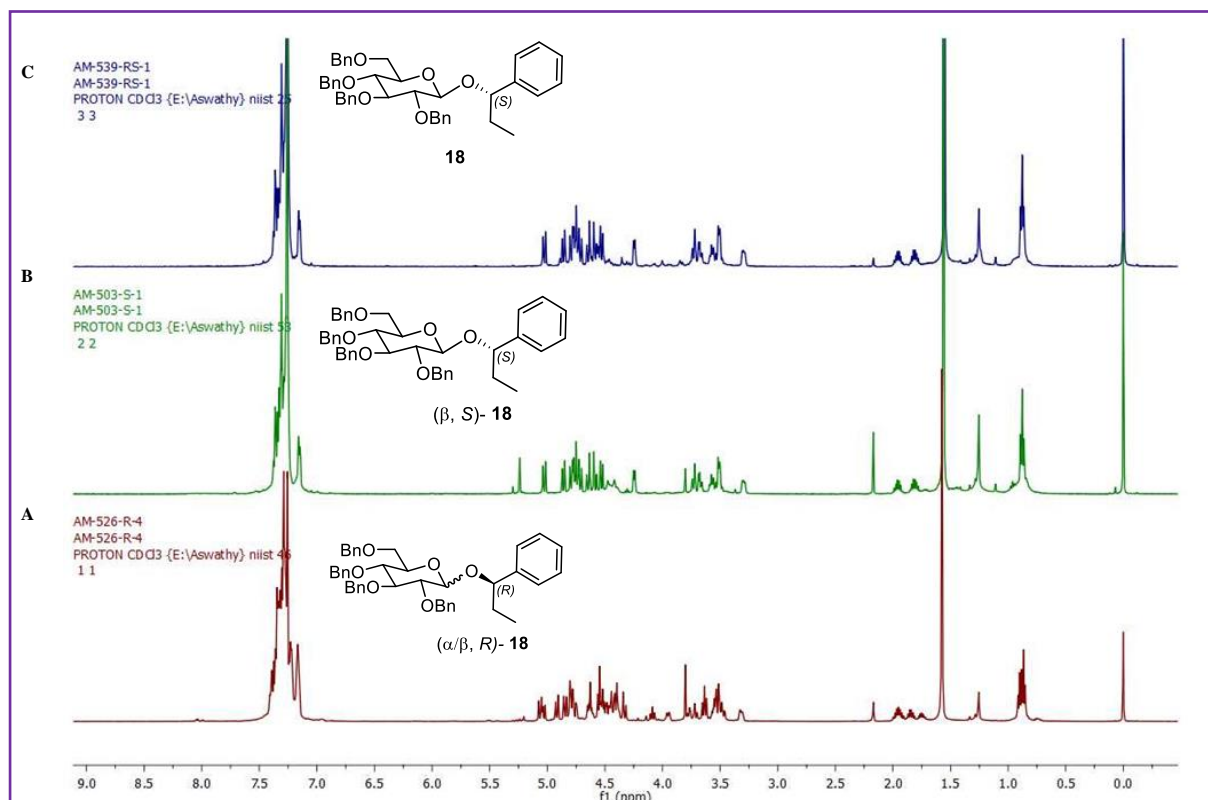


Figure 5.53: ^1H NMR of glycosides of (A) $(\alpha/\beta, R)$ -**18** (B) (β, S) -**18** (C) Compound **18**

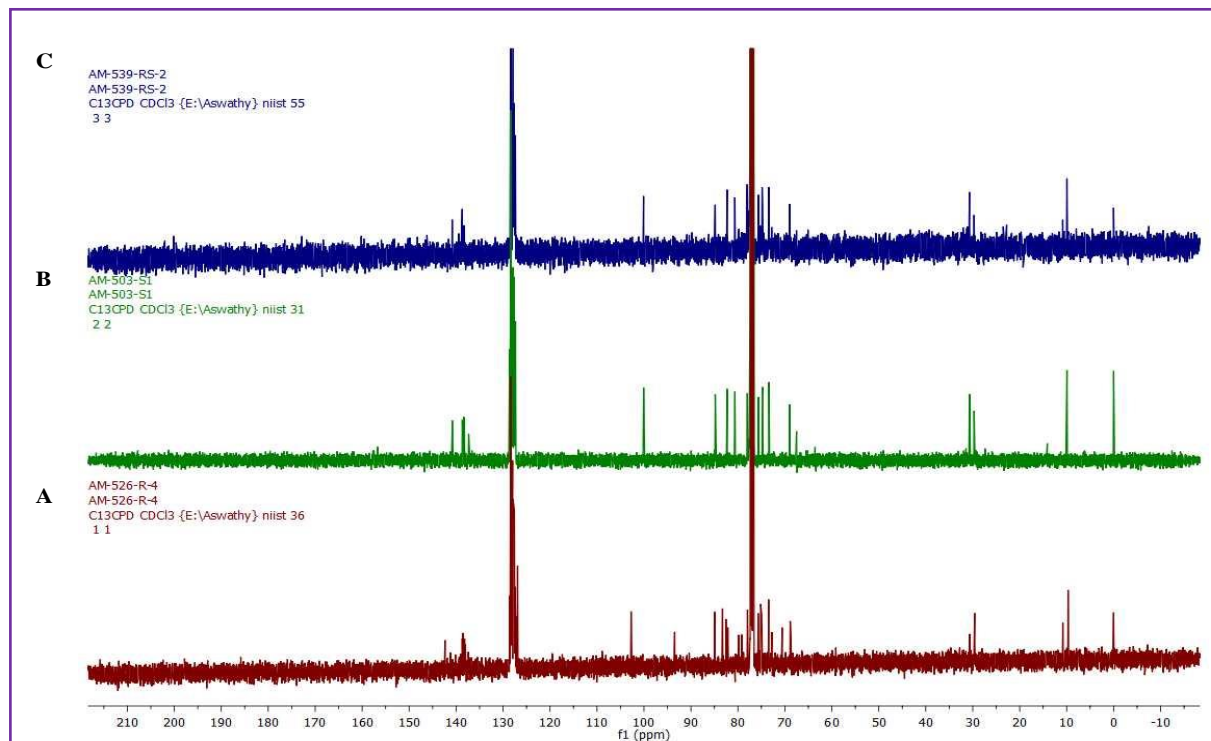


Figure 5.54: ^{13}C NMR of glycosides of (A) $(\alpha/\beta, R)$ -**18** (B) (β, S) -**18** (C) Compound **18**

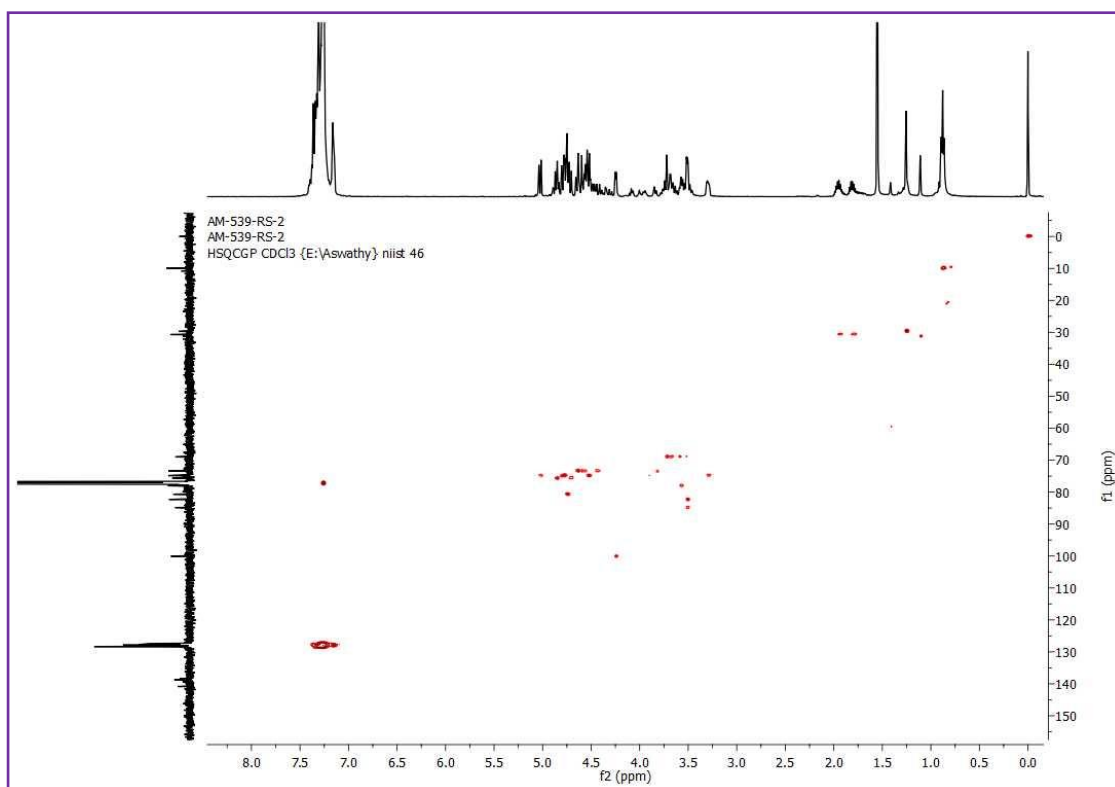


Figure 5.54: HSQC spectra of compound **18**

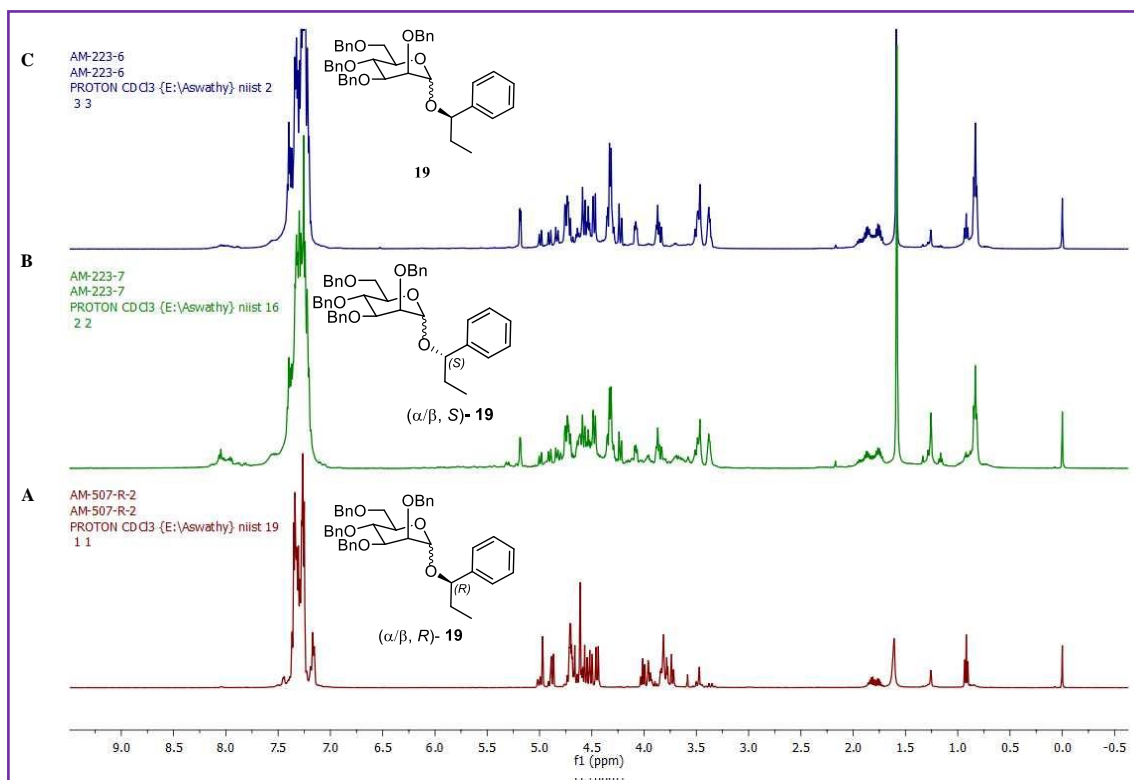


Figure 5.55: ¹H NMR of glycosides of (A) (α/β, *R*)-**19** (B) (α/β, *S*)-**19** (C) Compound **19**

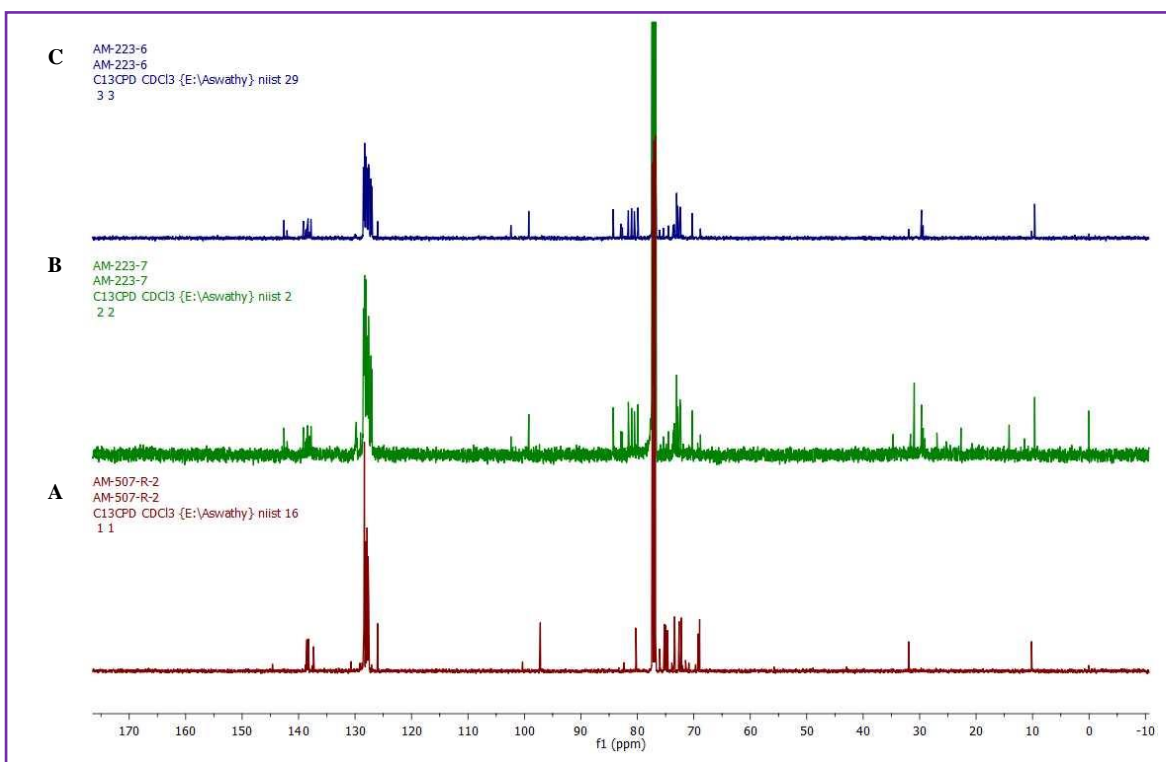


Figure 5.56: ^{13}C NMR of glycosides of (A) (α/β , *R*)-**19** (B) (α/β , *S*)-**19** (C) Compound **19**

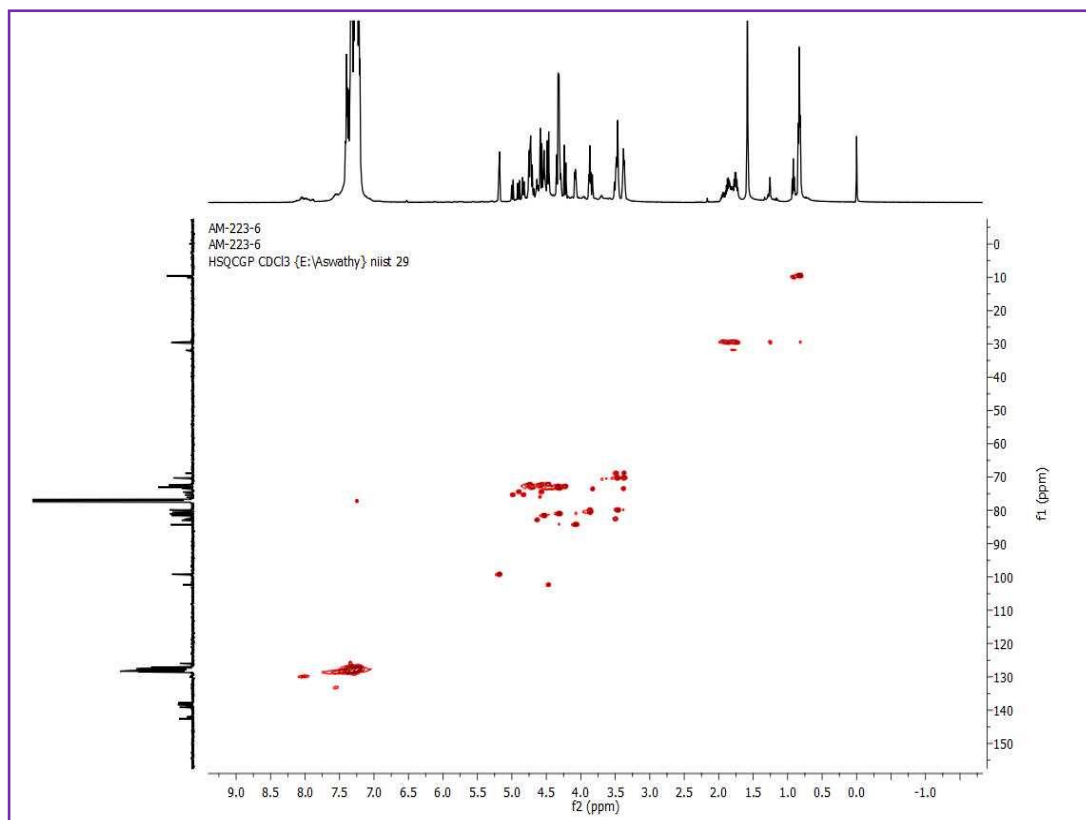


Figure 5.57: HMQC spectra compound **19**

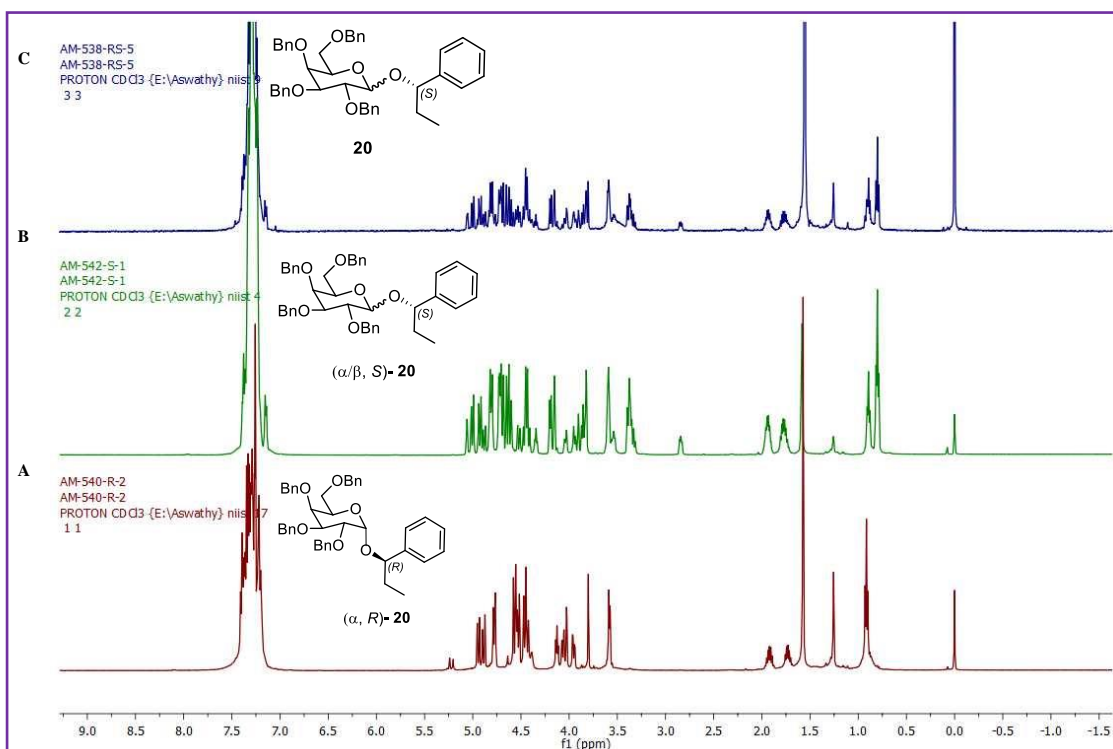


Figure 5.58: ¹H NMR of glycosides of (A) (α, R) -**20** (B) $(\alpha/\beta, S)$ -**20** (C) Compound **20**

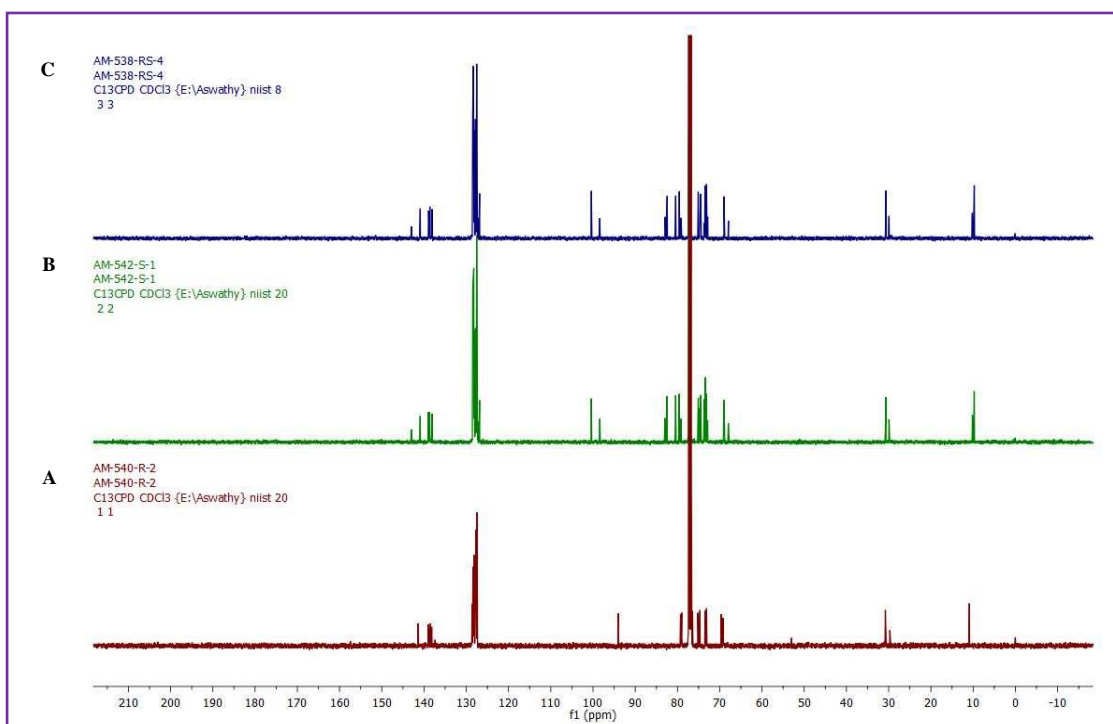


Figure 5.59: ¹³C NMR of glycosides of (A) (α, R) -**20** (B) $(\alpha/\beta, S)$ -**20** (C) Compound **20**

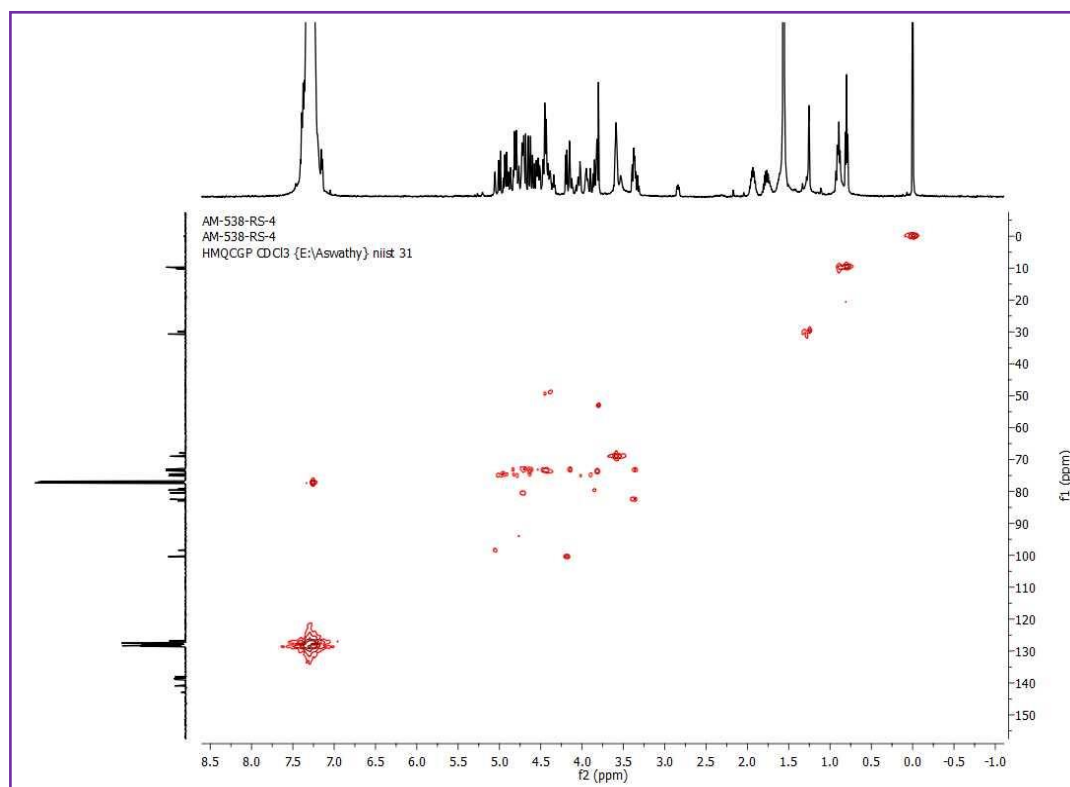
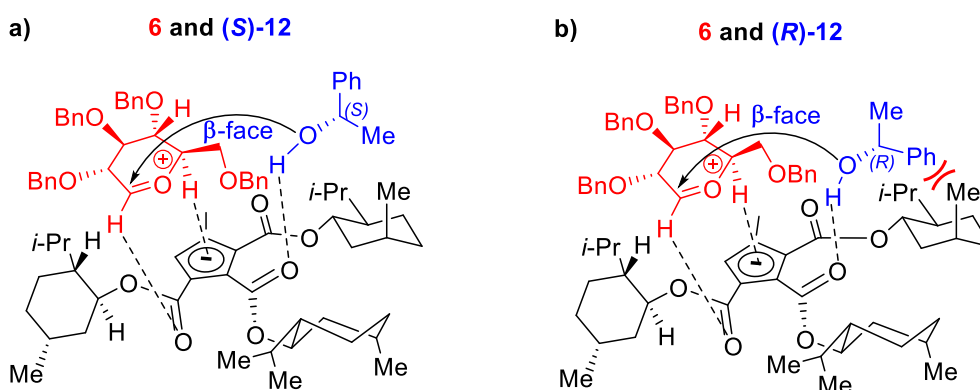


Figure 5.60: HMQC spectra of Compound **20**

Mechanistic rationale for the stereo and diastereocontrol in glycosylation of **12** with CBA **1**



Scheme 5: Rationale for the stereo and diastereocontrol in glycosylation of **12** with CBA **1**.

Interestingly, glycosylation attempts with racemic Boc-protected serine **14**, with free carboxylic acid, also afforded chiral recognition with S-enantiomer in good yields, wherein, glucosyl-NPG **6** afforded α -anomer **21** selectively, and mannosyl-NPG **7** afforded anomeric mixture of **22**, dominating in β -anomer. However, galactosyl-NPG **8** produced α -anomer **23**

selectively, and did not afford chiral recognition unlike its congeners. In line with the mechanistic rationale outlined in scheme 3, the preference for the *S*-enantiomers of benzylic alcohols **12** and **13** in the glycosylation reaction is shown in scheme 5. However, in the case of racemic **14**, intricate secondary interactions arising from the Boc and COOH groups in the transition state for glycosylation reaction dictate the stereo- and diastereoselectivity, which is difficult to comprehend.

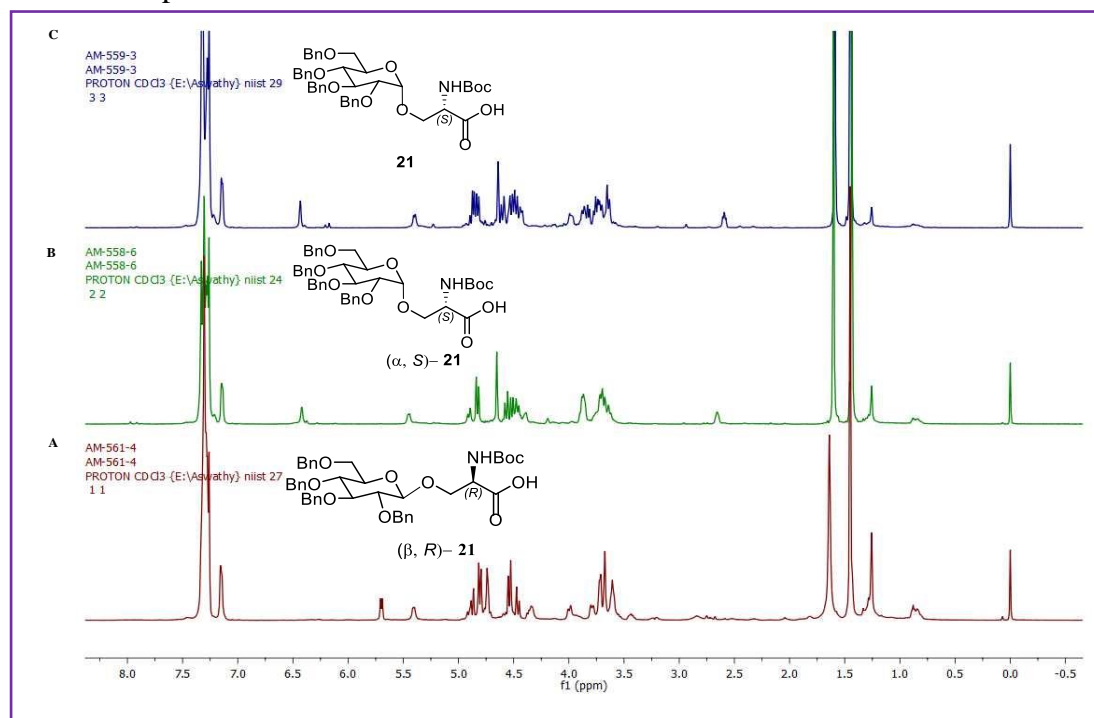


Figure 5.61: ^1H NMR of glycosides of (A) (β , *R*)-**21** (B) (α , *S*)-**21** (C) Compound **21**

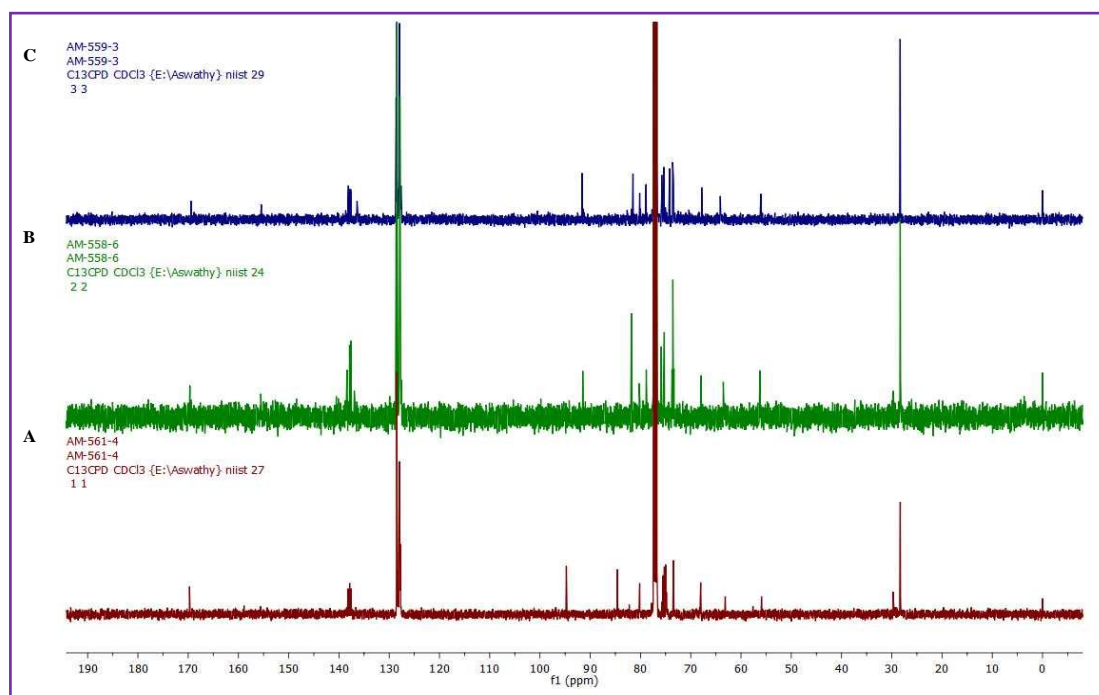


Figure 5.62: ^{13}C NMR of glycosides of (A) (α , *R*)-**21** (B) (α , *S*)-**21** (C) Compound **21**

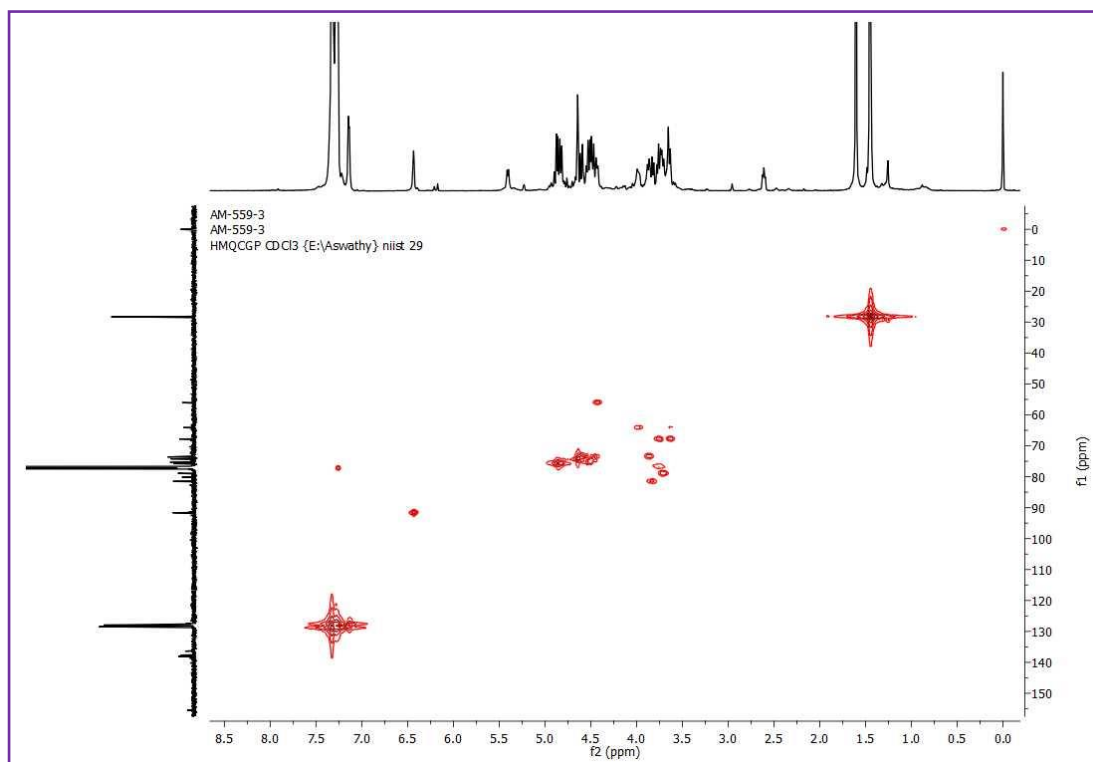


Figure 5.63: HMQC spectra of Compound **21**

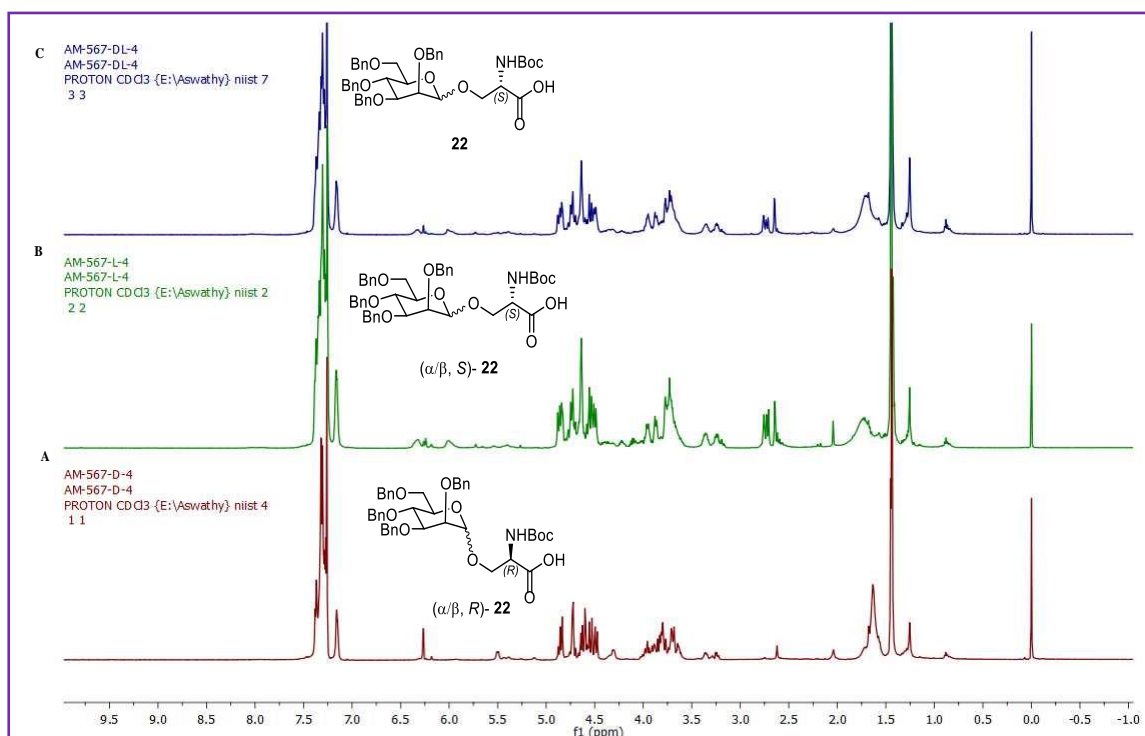


Figure 5.63: ¹H NMR of glycosides of (A) (α/β, *R*)-**22** (B) (α/β, *S*)-**22** (C) Compound **22**

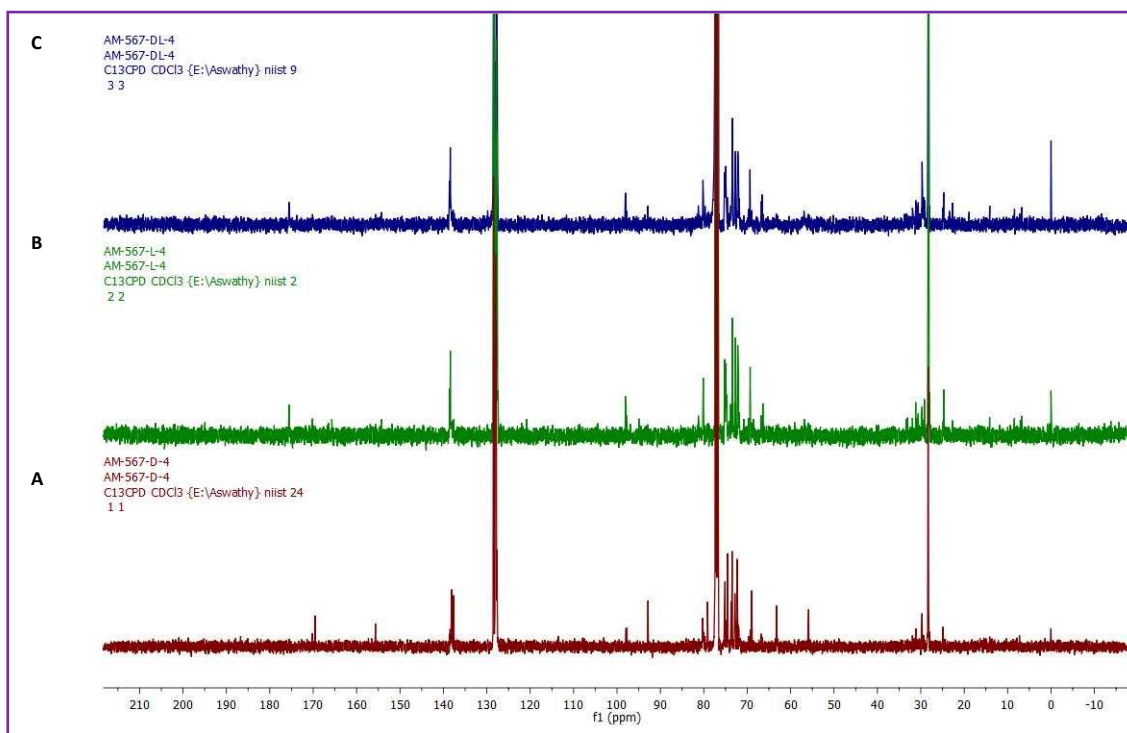


Figure 5.64: ^{13}C NMR of glycosides of (A) (α/β , *R*)-**22** (B) (α/β , *S*)-**22** (C) Compound **22**

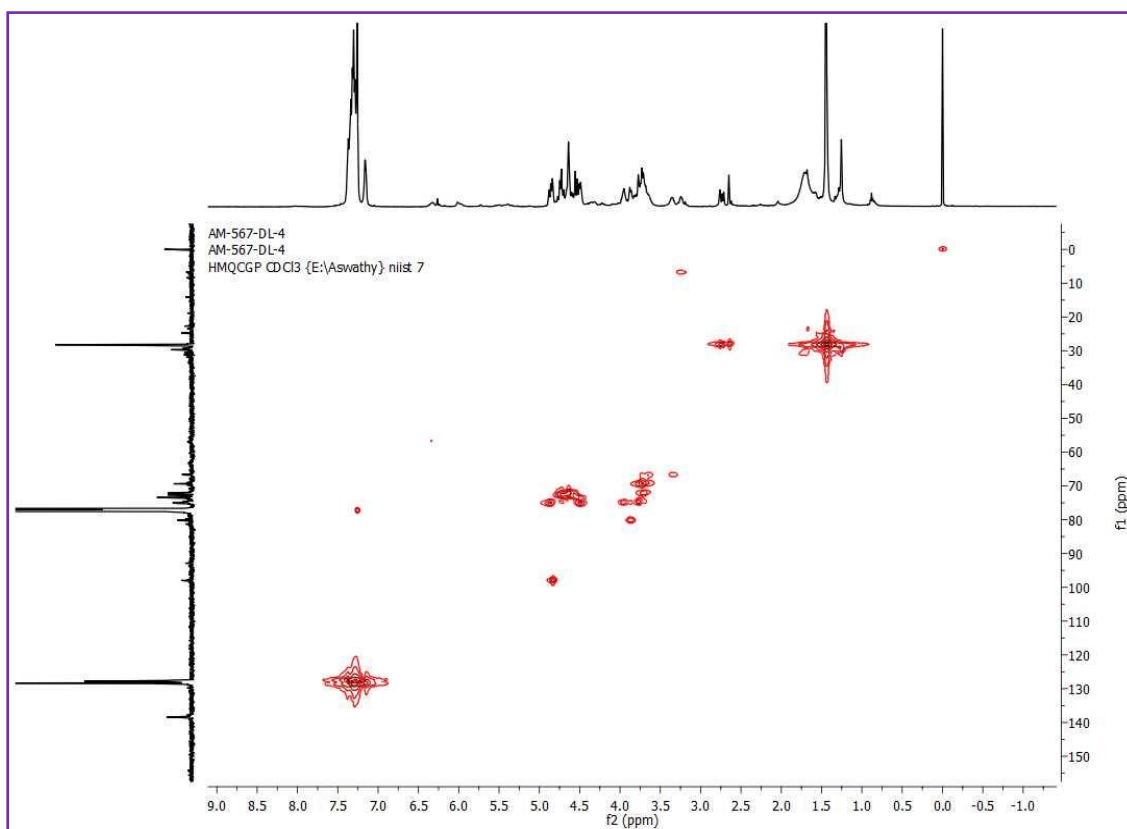


Figure 5.65: HMQC spectra of Compound **22**

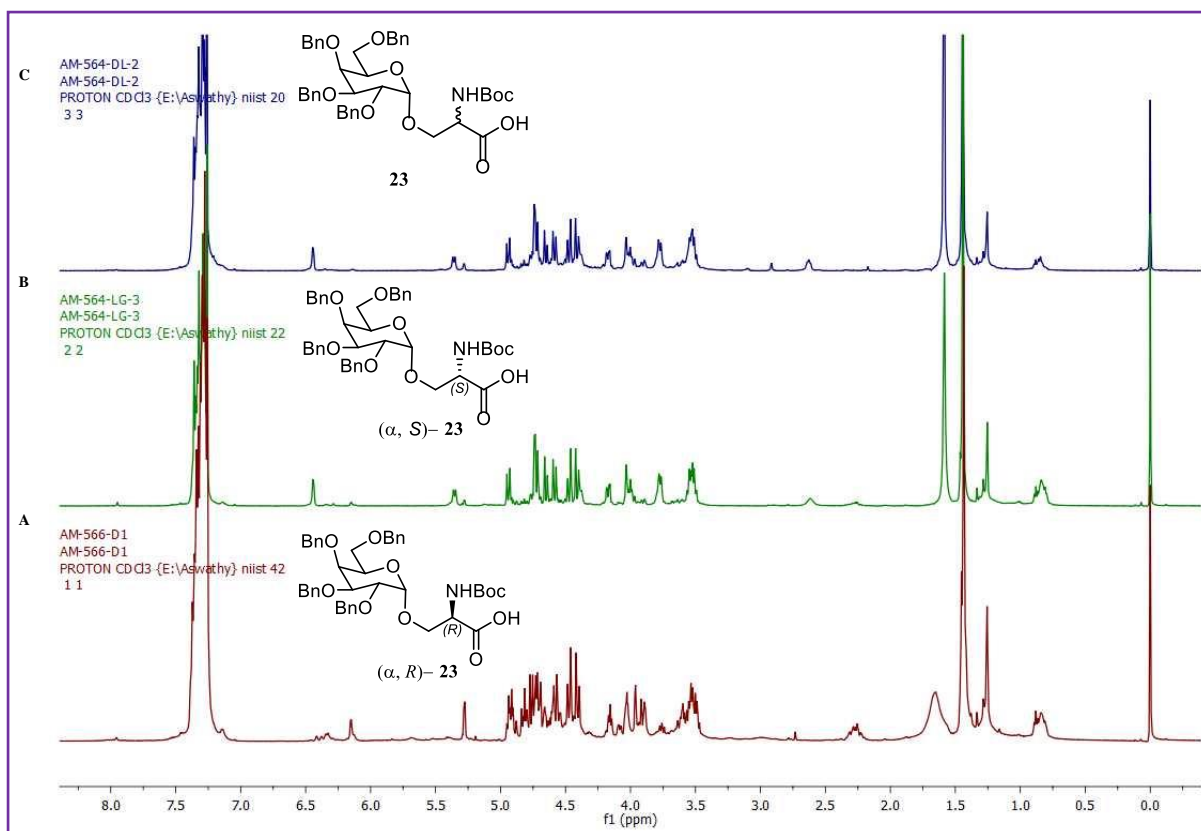


Figure 5.66: ^1H NMR of glycosides of (A) (α, R) -23 (B) (α, S) -23 (C) Compound 23

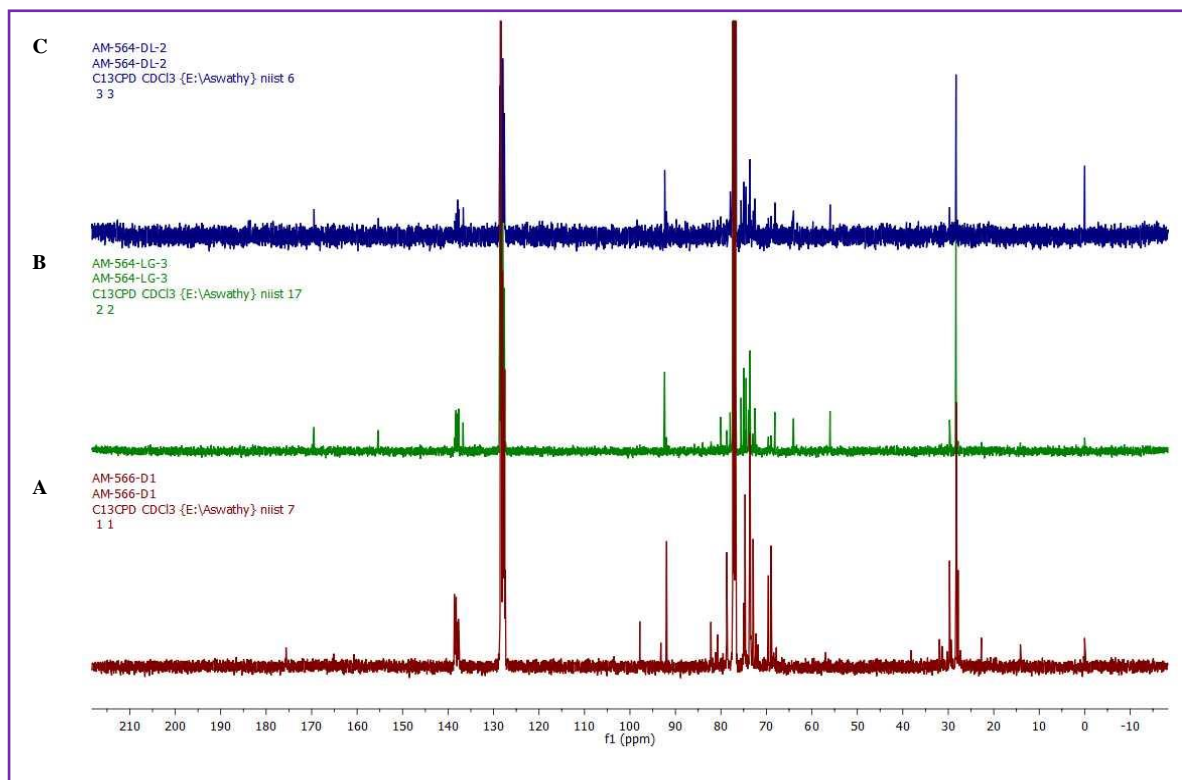
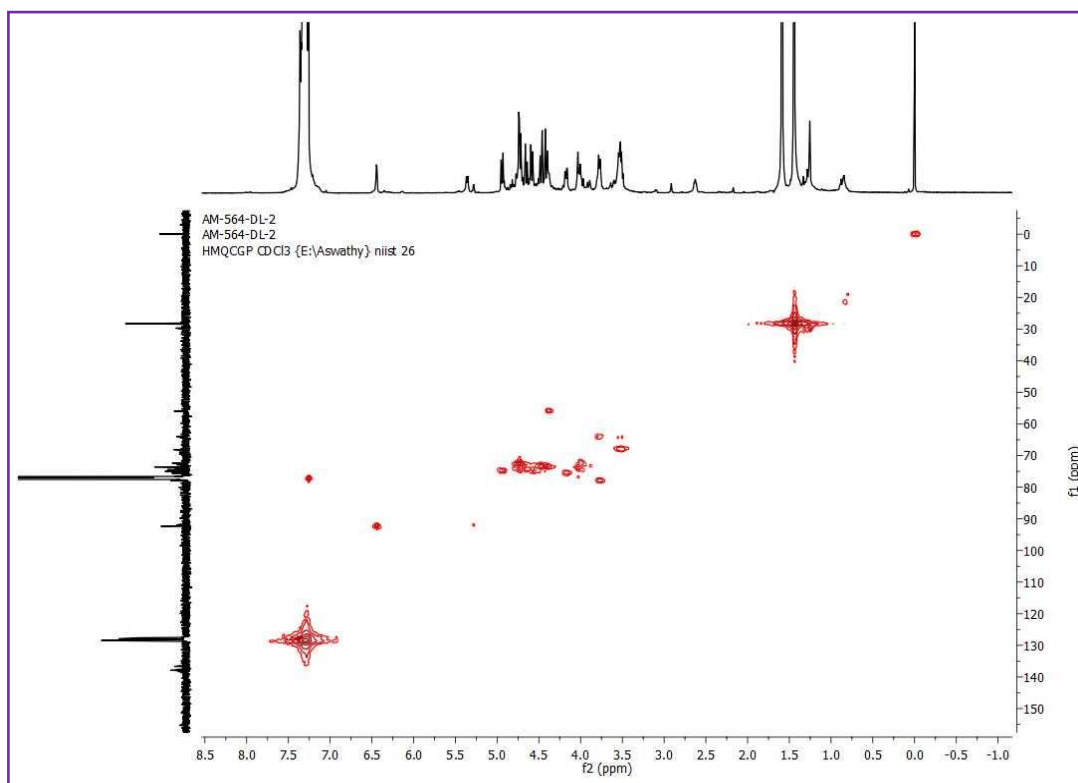


Figure 5.67: ^{13}C NMR of glycosides of (A) (α, R) -23 (B) (α, S) -23 (C) Compound 23



5.4. Conclusions

As noted in the pioneering contribution by Lambert, chiral PCCP BA catalysis can be made more efficient by optimization of the catalyst structure; herein, we modified their original CBA **4** with (-)-menthol to CBA **1** with (+)-isomenthol and evaluated its catalytic role in stereoselective glycosylation with NPG donors in the presence of NIS as the promoter. Apart from α/β -stereoselectivity with NPGs, glycosylation reaction in the presence of CBA **1** was efficient in chiral recognition of the racemic menthol, favouring (+)-menthol, with excellent diastereoselectivity. The stereo- and diastereocontrol observed here with CBA **1** and NPGs is superior to chiral BINOL phosphoric acid-catalyzed glycosylation with trichloroacetimidate donors.¹⁴ The mechanistic model behind CBA **1** catalysis by H-bonding organization of the oxocarbenium ion, generated from NPG activation and menthol with the chiral cyclopentadienyl anion platform, assisted in providing a rationalistic explanation behind the lack of diastereocontrol with other chiral, BINOL-derived and menthyl CBA esters, and non-chiral BAs. This preliminary investigation with CBA **1** catalyst motivated us to explore its utility with other racemic aglycons and the resulting stereo- and diastereocontrol observed in

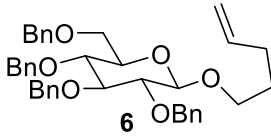
glycosylation with NPGs suggest the potent benefits of CBA in myriad BA-catalyzed synthetic organic transformations.

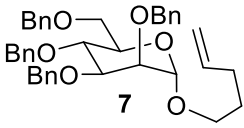
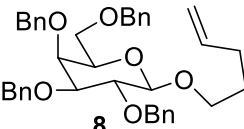
5.5. Experimental Section

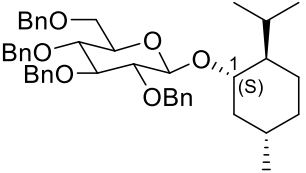
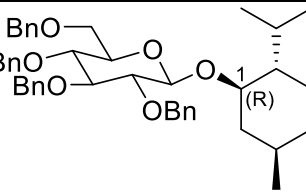
All chemicals were commercially available of the best grade and are used without further purification. Freshly distilled dichloromethane (DCM) over calcium hydride was used for the glycosylation reactions. Thin layer chromatography (TLC) was performed on TLC silica gel 60 F₂₅₄ aluminium sheets purchased from Merck Pvt. Ltd. Silica gel column chromatography (CC) of 100-200 mesh was performed using and mixtures of hexane - ethyl acetate (EtOAc), methanol (MeOH) - DCM were used for elution. Reactions were monitored by TLC and compounds were visualized by a short wavelength UV lamp and by charring the TLC plate after spraying with 15% sulphuric acid in methanol. NMR spectra were recorded with Bruker Ascend™ spectrometer (500 MHz for ¹H NMR, 125 MHz for ¹³C{¹H} NMR) instruments. The chemical shifts δ are given in ppm and referenced to the internal standard TMS. ¹H NMR coupling constants (*J*) are reported in hertz (Hz) and multiplicities are indicated as follows s (singlet), d (doublet), t (triplet), m (multiplet), dd (doublet of doublets), etc. Mass spectra were recorded on ESI-HRMS from Thermo Scientific Exactive mass spectrometer equipped with orbitrap analyzer. Diastereomeric ratios were examined with analytical High-Performance Liquid Chromatography (HPLC) consisting of a Shimadzu LC-20AD system controller, CHIRALPAK AD-H (PartNo.19325, Particle size 5 μ M) (4.6mm ϕ x 250 mmL) column, column oven (CTO-20A), an auto sampler injector (SIL-20AC HT), and a diode array detector (SPD-M20A). The isocratic mobile phase was a mixture of *n*-hexane and 2-propanol (97:3) with a run time of 20 min, flow rate of 0.5 mL/min and monitored by UV (200-400 nm). The solution of glycosides (1 mg/mL) in hexane:2-propanol (9:1) was filtered through a 0.22 μ M PTFE filter; and injected into the HPLC system with a volume of 10 μ L. The column was maintained at a temperature of 25 °C and LC Lab solutions software was used for data acquisition and analysis.

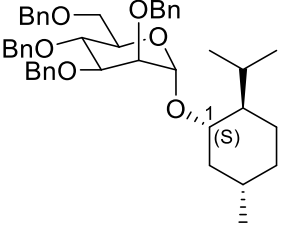
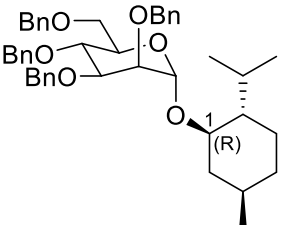
5.6. Spectral data

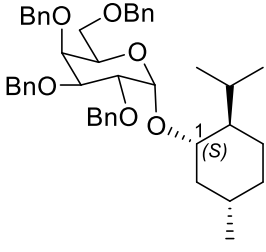
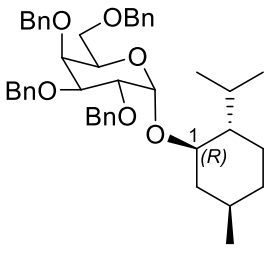
CBA 1	¹ H NMR (CDCl ₃): δ 20.29 (s, 1H), 5.19 (m, 1H), 1.85 – 1.26 (m, 48H), 0.95 (m 48H). ¹³ C{ ¹ H} NMR (CDCl ₃): δ 171.9, 166.5, 162.8, 134.0, 118.7, 106.6, 78.6, 73.4, 72.5, 46.2, 45.6, 43.1, 36.2, 34.3,
-------	---

	30.1, 29.7, 29.1, 27.7, 26.8, 26.2, 25.9, 22.6, 22.4, 21.2, 21.1, 20.9, 20.0, 19.4, 18.2, 17.6 ppm. ESI-HRMS calculated for C ₆₀ H ₉₅ O ₁₀ [M-H] ⁻ : 975.6925; found m/z 975.6929
CBA 3	¹H NMR (CDCl ₃): δ 20.16 (s, 1H), 4.97 (m, 4H), 3.65 – 3.37 (m, 1H), 1.97 – 1.60 (m, 18H), 1.49 – 1.84 (m, 22H), 0.75 – 0.60 (m, 50H). ¹³C{¹H} NMR (CDCl ₃): δ 171.6, 167.7, 163.3, 133.0, 125.0, 107.0, 78.7, 69.6, 53.8, 52.3, 51.7, 45.9, 35.8, 31.9, 31.7, 30.9, 29.7, 29.3, 27.4, 26.0, 22.7, 20.9, 20.0, 18.3, 14.1. ESI-HRMS: calculated for C ₆₀ H ₉₅ O ₁₀ [M-H] ⁻ : 975.6925, found m/z 975.6940.
CBA 4	¹H NMR (CDCl ₃): ¹ H NMR (CDCl ₃): δ 4.77 (s, 5H), 2.21 (m, 3H), 2.03 (m, 5H), 1.65 (d, <i>J</i> = 11.0 Hz, 9H), 1.56 – 1.38 (m, 7H), 1.32 (m, 7H), 1.13 – 0.90 (m, 25H), 0.83 (d, <i>J</i> = 6.1 Hz, 17H), 0.79 (d, <i>J</i> = 5.6 Hz, 17H). ¹³C{¹H} NMR (CDCl ₃): δ 168.00, 116.99, 77.28, 77.03, 76.77, 74.35, 46.36, 38.83, 34.28, 31.70, 25.33, 23.18, 22.66, 21.13, 16.71. ESI-HRMS calculated for C ₆₀ H ₉₅ O ₁₀ [M-H] ⁻ : 975.6925, found m/z 975.6939.
 <p style="text-align: center;">6</p>	¹H NMR (CDCl ₃): δ 7.30 (m, 18H), 7.16 (m, 2H), 5.88 – 5.74 (m, 1H), 5.05 – 4.90 (m, 4H), 4.80 (dd, <i>J</i> ₁ = 14.7 Hz, <i>J</i> ₂ = 11.0 Hz, 2H), 4.72 (d, <i>J</i> = 11.0 Hz, 1H), 4.57 (m, 3H), 4.38 (d, <i>J</i> = 7.8 Hz, 1H), 4.01 – 3.92 (m, 1H), 3.74 (d, <i>J</i> = 10.6 Hz, 1H), 3.69 – 3.61 (m, 2H), 3.56 (m, 2H), 3.45 (t, <i>J</i> = 8.4 Hz, 2H), 2.22 – 2.12 (m, 2H), 1.76 (m, 2H). ¹³C{¹H} NMR (CDCl ₃): δ 138.7, 138.5, 138.3, 138.2, 138.1, 128.4, 128.4, 128.1, 128.0, 127.9, 127.8, 127.7, 127.6, 127.6, 127.6, 114.9, 103.7, 84.8, 82.3, 78.0, 75.7, 75.0, 74.9, 74.8, 73.5, 69.4, 69.1, 30.3, 29.0.

 <p style="text-align: center;">7</p>	<p>¹H NMR (CDCl₃): δ 7.44 – 7.28 (m, 20H), 5.91 – 5.77 (m, 1H), 5.09 – 4.96 (m, 3H), 4.91 (t, <i>J</i> = 4.3 Hz, 1H), 4.79 (m, 2H), 4.67 (m, 2H), 4.64 – 4.58 (m, 1H), 4.58 – 4.47 (m, 3H), 4.42 – 4.32 (m, 1H), 4.10 (m, 1H), 4.05 – 3.99 (m, 1H), 3.94 (s, 1H), 3.89 – 3.84 (m, 1H), 3.75 (m, 1H), 3.70 (m, 1H), 3.64 (m, 1H), 3.60 – 3.55 (m, 1H), 3.41 – 3.32 (m, 1H), 2.16 (m, 2H), 1.72 (m, 2H).</p> <p>¹³C{¹H} NMR (CDCl₃): δ 138.9, 138.7, 138.6, 138.3, 138.2, 138.0, 137.7, 128.5, 128.4, 128.3, 128.2, 128.2, 128.0, 127.9, 127.9, 127.8, 127.7, 127.6, 127.6, 127.4, 114.8, 114.8, 104.0, 100.0, 84.2, 82.3, 81.1, 80.4, 79.7, 79.6, 75.3, 74.5, 73.6, 73.5, 73.4, 73.4, 73.1, 72.4, 72.3, 70.4, 69.4, 68.9, 67.3, 30.4, 30.3, 29.0, 28.7.</p>
 <p style="text-align: center;">8</p>	<p>¹H NMR (CDCl₃): δ 7.27 (m, 20H), 5.80 (dd, <i>J</i>₁ = 16.5 Hz, <i>J</i>₂ = 7.6 Hz, 1H), 5.03 (s, 1H), 5.00 – 4.93 (m, 1H), 4.72 (d, <i>J</i> = 11.7 Hz, 1H), 4.58 – 4.44 (m, 6H), 4.30 (d, <i>J</i> = 11.7 Hz, 1H), 4.12 (d, <i>J</i> = 6.9 Hz, 1H), 4.03 – 3.97 (m, 2H), 3.78 (s, 1H), 3.70 (m, 3H), 3.44 – 3.35 (m, 1H), 2.10 (d, <i>J</i> = 6.8 Hz, 2H), 1.65 (m, 2H) ppm.</p> <p>¹³C{¹H} NMR (CDCl₃): δ 138.5, 138.3, 138.2, 137.9, 137.7, 128.4, 128.4, 128.3, 128.3, 128.3, 128.0, 127.9, 127.8, 127.7, 127.6, 127.6, 114.8, 106.0, 88.6, 82.7, 80.7, 76.3, 73.4, 73.3, 72.0, 71.9, 71.0, 66.9, 30.3, 28.8 ppm.</p> <p>δ 7.20 – 7.09 (m, 19H), 7.00 (m, 2H), 5.67 (m, 1H), 4.90 – 4.74 (m, 4H), 4.61 (m, 4H), 4.51 – 4.28 (m, 4H), 4.23 (d, <i>J</i> = 7.7 Hz, 1H), 3.82 (m, 1H), 3.57 (t, <i>J</i> = 9.9 Hz, 1H), 3.49 (m, 3H), 3.41 (m, 2H), 3.29 (t, <i>J</i> = 8.3 Hz, 2H), 1.98 (m, 2H), 1.60 (m, 2H).</p> <p>¹³C{¹H} NMR (CDCl₃): δ 138.6, 138.5, 138.2, 138.1, 128.4, 128.2, 128.0, 128.0, 127.9, 127.8, 127.7, 127.6, 114.9, 103.7, 84.7, 82.3, 75.7, 75.0, 74.9, 73.5, 69.4, 69.0, 30.3, 29.0.</p>

 <p>(β, 1<i>S</i>)-9</p>	<p>¹H NMR (CDCl₃): δ 7.34 - 7.27 (m, 20H), 4.91 (m, 2H), 4.80 (d, <i>J</i> = 10.7 Hz, 1H), 4.71 (s, 2H), 4.60 (d, <i>J</i> = 11.7 Hz, 1H), 4.46 (m, 2H), 4.41 - 4.34 (m, 2H), 4.32 (d, <i>J</i> = 7.5 Hz, 1H), 4.09 (d, <i>J</i> = 6.7 Hz, 1H), 3.87 (s, 1H), 3.82 - 3.76 (m, 1H), 3.58 (m, 2H), 3.55 - 3.50 (m, 2H), 3.35 (td, <i>J</i>₁ = 10.5 Hz, <i>J</i>₂ = 4.4 Hz, 1H), 2.41 - 2.32 (m, 1H), 2.21 (d, <i>J</i> = 12.4 Hz, 1H), 1.76 - 1.69 (m, 1H), 1.44 (m, 1H), 1.10 (m, 2H), 0.99 (d, <i>J</i> = 6.7 Hz, 2H), 0.98 - 0.92 (m, 3H), 0.87 (d, <i>J</i> = 6.5 Hz, 3H), 0.80 (d, <i>J</i> = 6.9 Hz, 3H), 0.66 (d, <i>J</i> = 6.9 Hz, 3H).</p> <p>¹³C{¹H} NMR (CDCl₃): δ 138.9, 138.7, 138.5, 138.1, 128.4, 128.4, 128.2, 128.1, 127.9, 127.8, 127.6, 104.8, 82.9, 81.3, 79.8, 75.3, 74.4, 73.6, 73.4, 73.0, 69.4, 48.7, 43.6, 34.3, 31.8, 29.7, 24.6, 22.8, 22.3, 21.3, 15.9.</p> <p>ESI-HRMS calculated for C₄₄H₅₄NaO₆ [M+Na]⁺: 701.3818; observed: 701.3836</p>
 <p>(β, 1<i>R</i>)-9</p>	<p>¹H NMR (CDCl₃): δ 7.38 - 7.26 (m, 20H), 4.93 (t, <i>J</i> = 10.7 Hz, 2H), 4.73 (m, 3H), 4.61 (d, <i>J</i> = 11.8 Hz, 1H), 4.44 (d, <i>J</i> = 11.6 Hz, 1H), 4.39 (m, 2H), 3.85 (d, <i>J</i> = 2.5 Hz, 1H), 3.78 - 3.72 (m, 1H), 3.55 (m, 2H), 3.53 - 3.47 (m, 2H), 3.43 (td, <i>J</i>₁ = 10.5 Hz, <i>J</i>₂ = 4.1 Hz, 1H), 2.35 (m, 1H), 2.12 (d, <i>J</i> = 11.7 Hz, 1H), 2.04 (s, 2H), 1.70 - 1.62 (m, 3H), 0.96 (m, 2H), 0.88 (d, <i>J</i> = 5.8 Hz, 6H), 0.75 (d, <i>J</i> = 6.8 Hz, 3H).</p> <p>¹³C{¹H} NMR (CDCl₃): δ 138.9, 138.8, 138.7, 138.0, 128.4, 128.3, 128.3, 128.3, 128.2, 127.9, 127.7, 127.6, 127.5, 127.5, 101.6, 82.7, 79.5, 78.4, 75.2, 74.5, 74.0, 73.6, 73.2, 69.3, 48.1, 41.2, 34.5, 31.5, 29.7, 24.9, 23.1, 22.2, 21.2, 15.7.</p> <p>ESI-HRMS calculated for C₄₄H₅₄NaO₆ [M+Na]⁺: 701.3818; observed: 701.3839</p>

 <p style="text-align: center;">(α, 1S)-10</p>	<p>¹H NMR (CDCl₃): δ 7.25 (m, 18H), 7.14 (m, 2H), 5.10 (d, <i>J</i> = 4.5 Hz, 1H), 4.69 – 4.60 (m, 4H), 4.55 (t, <i>J</i> = 8.1 Hz, 1H), 4.44 (d, <i>J</i> = 11.7 Hz, 1H), 4.40 (s, 2H), 4.35 (d, <i>J</i> = 11.5 Hz, 1H), 4.23 (t, <i>J</i> = 7.7 Hz, 1H), 3.94 (dd, <i>J</i>₁ = 7.5 Hz, <i>J</i>₂ = 4.7 Hz, 1H), 3.81 (dd, <i>J</i>₁ = 7.7 Hz, <i>J</i>₂ = 5.4 Hz, 1H), 3.68 (dd, <i>J</i>₁ = 10.8 Hz, <i>J</i>₂ = 5.3 Hz, 2H), 3.62 (dd, <i>J</i>₁ = 10.2, <i>J</i>₂ = 4.4 Hz, 1H), 3.55 (m, 1H), 3.38 (td, <i>J</i>₁ = 10.6 Hz, <i>J</i>₂ = 4.2 Hz, 1H), 2.36 (m, 1H), 1.96 (d, <i>J</i> = 8.9 Hz, 1H), 1.63 – 1.56 (m, 2H), 1.27 – 1.21 (m, 3H), 0.94 – 0.88 (m, 1H), 0.85 (d, <i>J</i> = 6.5 Hz, 3H), 0.83 – 0.74 (m, 4H), 0.71 (d, <i>J</i> = 7.1 Hz, 3H), 0.66 (d, <i>J</i> = 6.8 Hz, 3H).</p> <p>¹³C{¹H} NMR (CDCl₃): δ 138.9, 138.4, 138.4, 137.8, 128.5, 128.5, 128.3, 128.3, 128.3, 128.3, 128.2, 128.2, 127.9, 127.9, 127.7, 127.7, 127.6, 127.5, 127.5, 127.4, 127.4, 96.9, 83.4, 80.3, 79.4, 78.7, 73.3, 72.8, 72.4, 72.3, 70.4, 47.7, 40.6, 34.4, 31.5, 31.0, 29.7, 24.5, 23.0, 22.4, 21.2, 16.1.</p> <p>ESI-HRMS calculated for C₄₄H₅₄NaO₆ [M+Na]⁺: 701.3818; observed: 701.3823</p>
 <p style="text-align: center;">(α, 1R)-10</p>	<p>¹H NMR (CDCl₃): δ 7.27 (m, 18H), 7.09 (m, 2H), 4.92 (app s, 1H), 4.78 (d, <i>J</i> = 10.5 Hz, 1H), 4.73 (d, <i>J</i> = 12.5 Hz, 1H), 4.60 (d, <i>J</i> = 13.5 Hz, 4H), 4.44 (d, <i>J</i> = 11.4 Hz, 2H), 3.97 (t, <i>J</i> = 9.4 Hz, 1H), 3.79 (dd, <i>J</i>₁ = 9.5 Hz, <i>J</i>₂ = 2.9 Hz, 1H), 3.73 (dd, <i>J</i>₁ = 17.4 Hz, <i>J</i>₂ = 7.0 Hz, 2H), 3.64 – 3.58 (m, 2H), 3.34 (td, <i>J</i>₁ = 10.6 Hz, <i>J</i>₂ = 4.1 Hz, 1H), 2.07 (dd, <i>J</i>₁ = 16.6 Hz, <i>J</i>₂ = 9.3 Hz, 1H), 1.75 (d, <i>J</i> = 12.0 Hz, 1H), 1.21 (s, 2H), 1.07 (dd, <i>J</i>₁ = 22.7 Hz, <i>J</i>₂ = 11.7 Hz, 1H), 0.85 (t, <i>J</i> = 9.2 Hz, 2H), 0.82 (s, 2H), 0.78 (d, <i>J</i> = 7.0 Hz, 3H), 0.72 (m, 2H), 0.64 (d, <i>J</i> = 6.9 Hz, 3H).</p> <p>¹³C{¹H} NMR (CDCl₃): δ 138.7, 138.5, 138.5, 138.4, 128.4, 128.3, 128.3, 128.2, 128.1, 127.8, 127.7, 127.6, 127.6, 127.5, 127.4, 94.6, 80.3, 75.8, 75.4, 75.2, 75.0, 73.5,</p>

	<p>72.9, 72.4, 72.2, 69.2, 47.9, 39.7, 34.5, 31.3, 25.2, 22.8, 22.3, 21.2, 15.4.</p> <p>ESI-HRMS calculated for C₄₄H₅₄NaO₆ [M+Na]⁺: 701.3818; observed: 701.3833</p>
 <p>(α, 1<i>S</i>)-11</p>	<p>¹H NMR (CDCl₃): δ 7.31 – 7.20 (m, 18H), 7.14 (m, 2H), 5.09 (d, J = 3.4 Hz, 1H), 4.65 (m, 3H), 4.54 (d, J = 11.9 Hz, 1H), 4.45 – 4.41 (m, 1H), 4.40 (s, 2H), 4.35 (d, J = 12.0 Hz, 1H), 4.23 (t, J = 7.5 Hz, 1H), 3.97 – 3.92 (m, 1H), 3.83 – 3.78 (m, 1H), 3.68 (d, J = 4.6 Hz, 1H), 3.63 (d, J = 10.8 Hz, 1H), 3.54 (m, 2H), 3.46 (d, J = 11.0 Hz, 1H), 3.38 (t, J = 8.9 Hz, 1H), 2.39 – 2.33 (m, 1H), 2.14 (d, J = 12.8 Hz, 1H), 1.96 (d, J = 11.9 Hz, 1H), 1.55 (m, 2H), 1.22 (m, 3H), 0.85 (d, J = 6.0 Hz, 3H), 0.80 (m, 3H), 0.71 (d, J = 7.1 Hz, 3H), 0.66 (d, J = 6.6 Hz, 3H).</p> <p>¹³C{¹H} NMR (CDCl₃): δ 138.9, 138.3, 137.8, 128.4, 128.3, 128.3, 128.3, 128.2, 127.9, 127.7, 127.6, 127.5, 127.3, 96.9, 83.4, 80.3, 79.4, 78.7, 73.3, 72.8, 72.4, 72.2, 70.4, 47.7, 40.6, 34.4, 31.5, 24.5, 22.9, 22.4, 21.1, 16.1.</p> <p>ESI-HRMS calculated for C₄₄H₅₄NaO₆ [M+Na]⁺: 701.3818; observed: 701.3834</p>
 <p>(α, 1<i>R</i>)-11</p>	<p>¹H NMR (CDCl₃): δ 7.25 (m, 17H), 7.14 (m, 3H), 5.06 (d, J = 4.0 Hz, 1H), 4.64 (m, 5H), 4.46 – 4.36 (m, 5H), 4.22 (t, J = 7.2 Hz, 1H), 3.96 (m, 1H), 3.86 (t, J = 6.7 Hz, 1H), 3.75 – 3.70 (m, 1H), 3.64 (dd, J_1 = 10.4 Hz, J_2 = 3.2 Hz, 1H), 3.52 (dd, J_1 = 10.2 Hz, J_2 = 6.4 Hz, 1H), 3.25 (td, J_1 = 10.5 Hz, J_2 = 4.1 Hz, 1H), 2.31 – 2.21 (m, 2H), 1.53 (d, J = 12.0 Hz, 2H), 1.22 (m, 3H), 1.02 (m, 1H), 0.95 – 0.88 (m, 1H), 0.88 – 0.83 (m, 2H), 0.78 (d, J = 6.9 Hz, 3H), 0.73 (s, 3H), 0.66 (d, J = 6.9 Hz, 3H).</p> <p>¹³C{¹H} NMR (125 MHz, CDCl₃): δ 139.1, 138.3, 137.8, 128.4, 128.3, 128.3, 128.1, 127.8, 127.7, 127.6, 127.5, 127.2, 101.8, 84.0, 81.5, 80.9, 80.1, 80.0, 73.4, 72.9, 72.4,</p>

	72.3, 70.7, 48.4, 43.6, 34.3, 31.7, 24.9, 22.9, 22.3, 21.1, 15.9. ESI-HRMS calculated for C ₄₄ H ₅₄ NaO ₆ [M+Na] ⁺ : 701.3818; observed: 701.3833
--	--

References

- (1) Viladot, J. L.; De Ramon, E.; Durany, O.; Planas, A. Probing the Mechanism of Bacillus 1,3-1,4-β-D-Glucan 4- Glucanohydrolases by Chemical Rescue of Inactive Mutants at Catalytically Essential Residues. *Biochemistry* **1998**, *37* (32), 11332–11342. <https://doi.org/10.1021/bi980586q>.
- (2) Lairson, L. L.; Henrissat, B.; Davies, G. J.; Withers, S. G. Glycosyltransferases: Structures, Functions, and Mechanisms. *Annu. Rev. Biochem.* **2008**, *77* (1), 521–555. <https://doi.org/10.1146/annurev.biochem.76.061005.092322>.
- (3) Kumar, A.; Kumar, V.; Dere, R. T.; Schmidt, R. R. Glycoside Bond Formation via Acid-Base Catalysis. *Org. Lett.* **2011**, *13* (14), 3612–3615. <https://doi.org/10.1021/ol201231v>.
- (4) Chaugule, A. A.; Jadhav, A. R.; Kim, H. RSC Advances Polyvinyl Trisulfonate Ethylamine Based Solid Acid Catalyst for the Efficient Glycosylation of Sugars under Solvent Free Conditions †. *RSC Adv.* **2015**, *5*, 104715–104724. <https://doi.org/10.1039/C5RA20300G>.
- (5) Kobayashi, Y.; Nakatsuji, Y.; Li, S.; Tsuzuki, S.; Takemoto, Y. Direct N-Glycofunctionalization of Amides with Glycosyl Trichloroacetimidate by Thiourea/Halogen Bond Donor Co-Catalysis. *Angew. Chemie - Int. Ed.* **2018**, *57* (14), 3646–3650. <https://doi.org/10.1002/anie.201712726>.
- (6) Yamanoi, T.; Oda, Y.; Matsuda, S.; Yamazaki, I.; Matsumura, K.; Katsuraya, K.; Watanabe, M.; Inazu, T. Synthesis of 1-C-Alkyl-α-d-Glucopyranosides by Lewis Acid- or Brønsted Acid-Catalyzed O-Glycosidation. *Tetrahedron* **2006**, *62* (44), 10383–10392. <https://doi.org/10.1016/j.tet.2006.08.059>.
- (7) Benito-Alifonso, D.; Galan, M. C. Bronsted-and Lewis-Acid-Catalyzed Glycosylation. In *Selective Glycosylation: Synthetic Methods and Catalysts*; Wiley-VCH Verlag GmbH & Co. KGaA: Weinheim, Germany, 2017; pp 155–172.

<https://doi.org/10.1002/9783527696239.ch8>.

- (8) Shirakawa, S.; Kobayashi, S. Surfactant-Type Brønsted Acid Catalyzed Dehydrative Nucleophilic Substitutions of Alcohols in Water. *Org. Lett.* **2007**, *9* (2), 311–314. <https://doi.org/10.1021/ol062813j>.
- (9) Dasgupta, S.; Mukhopadhyay, B. Synthesis of Oligosaccharides Related to a Biodynamic Saponin from *Calamus insignis* as Their Propargyl Glycosides. *European J. Org. Chem.* **2008**, No. 34, 5770–5777. <https://doi.org/10.1002/ejoc.200800834>.
- (10) Karki, G.; Mandal, P. K. Facile Synthesis of Tetrasaccharide Fragments of Bioactive Asterosaponins Novaeguinosides I and II from Starfish *Culcita novaeguineae*. *Arkivoc* **2019**, *2019* (5), 196–210. <https://doi.org/10.24820/ark.5550190.p010.842>.
- (11) Kimura, T.; Sekine, M.; Takahashi, D.; Toshima, K. Chiral Brønsted Acid Mediated Glycosylation with Recognition of Alcohol Chirality. *Angew. Chemie - Int. Ed.* **2013**, *52* (46), 12131–12134. <https://doi.org/10.1002/anie.201304830>.
- (12) Mensah, E.; Camasso, N.; Kaplan, W.; Nagorny, P. Chiral Phosphoric Acid Directed Regioselective Acetalization of Carbohydrate-Derived 1,2-Diols. *Angew. Chemie - Int. Ed.* **2013**, *52* (49), 12932–12936. <https://doi.org/10.1002/anie.201304298>.
- (13) Cox, D. J.; Smith, M. D.; Fairbanks, A. J. Glycosylation Catalyzed by a Chiral Brønsted Acid. *Org. Lett.* **2010**, *12* (7), 1452–1455. <https://doi.org/10.1021/ol1001895>.
- (14) Gould, N. D.; Liana Allen, C.; Nam, B. C.; Schepartz, A.; Miller, S. J. Combined Lewis Acid and Brønsted Acid-Mediated Reactivity of Glycosyl Trichloroacetimidate Donors. *Carbohydr. Res.* **2013**, *382*, 36–42. <https://doi.org/10.1016/j.carres.2013.09.011>.
- (15) Aswathy, M.; Abhijith, B.; Lankalapalli, R. S.; Radhakrishnan, K. V. A Pentacarbomethoxycyclopentadiene (PCCP) Organic Brønsted Acid Catalyzed Stereoselective Glycosidation of N-Pentenyl Orthoesters (NPOE) of D-Glucose and D-Galactose, in Conjunction with N-Iodosuccinimide. *Carbohydr. Res.* **2022**, *522* (September), 108684. <https://doi.org/10.1016/j.carres.2022.108684>.
- (16) Bert Fraser-Reid and J. Cristóbal Lo´pez. Armed–Disarmed Effects in Carbohydrate Chemistry: History, Synthetic and Mechanistic Studies. *Top Curr Chem* **2011**, *310* (June

2011), 1–29. <https://doi.org/10.1007/128>.

- (17) Chirag D. Gheewala, Bridget E. Collins, T. H. L. An Aromatic Ion Platform for Enantioselective Brønsted Acid Catalysis. *Science (80-.)*. **2016**, *351* (6276), 961–965. https://doi.org/10.1142/9781783268993_0002.

ABSTRACT

Name of the student: **Ms. Aswathy M.**

Registration No.: **10CC18A39010**

Faculty of Study: **Chemical Sciences**

Year of Submission: **2023**

AcSIR academic centre/CSIR Lab: **CSIR- National Institute for Interdisciplinary Science and Technology (CSIR-NIIST), TVM, Kerala**

Name of Supervisors: **Dr. K. V. Radhakrishnan & Dr. Ravi Shankar L.**

Title of the thesis: **Exploring the anti-cancer potential of phytochemicals against oral squamous cell carcinoma and developing their glycosylation strategies with organic Brønsted acid**

Natural products can be viewed as a promising tool for the discovery of scaffolds with high structural diversity and various bioactivities that can be directly developed or used as starting points for optimization into novel drugs. Among them, the anti-cancer potential of these ubiquitous moieties were extensively documented and a developing area of research nowadays. In this scenario, our efforts are directed towards the identification of phytochemicals with promising anti-cancer potential from readily available, traditionally highlighted floras.

Chapter 1 deals with an overview of the challenges and opportunities of secondary metabolites in drug discovery process. In addition, this chapter also highlighted the importance of catalytic glycosylation in natural product chemistry. **In chapter 2**, we have explored the anti-cancer potential of a medicinal plant *Dillenia indica* and its active triterpenoids for the inhibition and prevention of oral cancer. We have also elucidated the anti-cancer mechanism of both candidates by various apoptotic and metastatic assays. In chapter **3**, part A deals with the phytochemical profiling *Artocarpus altilis* and second part with anti-cancer mechanism of the bioactives against SAS oral squamous cell carcinoma. Chapter **4** and chapter **5** discussed the glycosylation strategies of the phytochemicals. In chapter **4**, we have utilised a unique organic Bronsted acid, PCCP for the stereo, and regioselective glycosidation of natural products. Chapter **5** describes a stereoselective glycosylation method catalysed by (+)-isomenthol ester of pentacarbomethoxycyclopentadiene (PCCP) as chiral Brønsted acid with *n*-pentenyl glycosides (NPGs) in the presence of *N*-iodosuccinimide as the promoter that offered a chiral recognition of the racemic substrates.

Details of the Publications Emanating from the Thesis Work

Published

1. Exploring the Cytotoxic Effects of the Extracts and Bioactive Triterpenoids from *Dillenia indica* against Oral Squamous Cell Carcinoma: A Scientific Interpretation and Validation of Indigenous Knowledge. **Maniyamma Aswathy**, Kishore Banik, Dey Parama, Parameswaran Sasikumar, Choudhary Harsha, Anuja Gracy Joseph, Daisy R. Sherin, Manojkumar K. Thanathu, Ajaikumar B. Kunnumakkara, and Kokkuvayil Vasu Radhakrishnan. *ACS Pharmacol. Transl. Sci.* 2021, 4 (2), 834–847. DOI: 10.1021/acsptsci.1c0001.
2. Betulinic acid: A natural promising anticancer drug, current situation, and future perspectives. **Maniyamma Aswathy**, Ajesh Vijayan, Uzini D. Daimary, Sosmitha Girisa, Kokkuvayil V. Radhakrishnan, Ajaikumar B. Kunnumakkara. *J. Biochem. Mol. Toxicol.* 2022; e23206. DOI:10.1002/jbt.23206.
3. A pentacarbomethoxycyclopentadiene (PCCP) organic Brønsted acid catalysed stereoselective glycosidation of N-pentenyl orthoesters (NPOE) of D-glucose and D-galactose, in conjunction with N-iodosuccinimide. **Maniyamma Aswathy**, Balan Abhijith, Ravi S. Lankalapalli, Kokkuvayil V. Radhakrishnan. *Carbohydr. Res.*, 2022, 522 (80):108684. DOI: 10.1016/j.carres.2022.108684.
4. α/β -Stereo- and Diastereoselective Glycosylation with n-Pentenyl Glycoside Donors, promoted by N-Iodosuccinimide and Catalyzed by Chiral Brønsted Acid. **Maniyamma Aswathy**, Purushothaman C. Harikrishnan, Sasikumar Parameswaran, Kokkuvayil V. Radhakrishnan, Ravi S. Lankalapalli. *Org. Biomol. Chem.*, 2023, 1-5, DOI: 10.1039/D3OB01633A.
5. Natural prenylflavones from the stem bark of *Artocarpus altilis*: promising anti-cancer agents for oral squamous cell carcinoma targeting AKT/mTOR/STAT3 signaling pathway. **Maniyamma Aswathy**, Dey Parama, Mangala Hegde, Ravi S. Lankalapalli, Ajaikumar B. Kunnumakkara, Kokkuvayil Vasu Radhakrishnan (Communicated).

6. Papers Published from Other Related Works

1. Plant derived bioactive compounds and their potential to enhance adult neurogenesis. Krishnapriya, Parameswaran Sasikumar, **M. Aswathy**, Tripathi Prem Prakash,

- Kokkuvayil Vasu Radhakrishnan, Pulikkaparambil Sasidharan Baby Chakrapani, *Phytomedicine Plus*, 2022, 2 (1),100191. DOI: 10.1016/j.phyplu.2021.100191.
- Lewis acid promoted Regioselective Double Hydro(hetero)arylation of 6,6'-dialkyl Substituted Pentafulvene: A Facile Approach to Bisindole Derivatives, Parameswaran Sasikumar, Bernad Prabha, Sarngadharan Sarath Chand, **Maniyamma Aswathy**, Murali Madhukrishnan, Preethalayam Preethanuj, Eringathodi Suresh, Florian Jaroschik, Kokkuvayil Vasu Radhakrishnan, *Eur. J. Org. Chem*, 2017, 2017, 4469–4474. DOI: 10.1002/ejoc.201700742.
 - Chemoprofiling of *Artocarpus camansi* Blanco. and *Artocarpus lakoocha* Wall. ex. Roxb. and its antidiabetic potential for modulation of digestive enzymes, protein glycation and glucose uptake in L6 myotubes. Sasikumar P, **Aswathy M**, Lekshmi K, Reshmitha T R, Sharathna P, Sanjay S Varma, Meenu M T, Sivan V V, Nisha P, Jayamurthy, Radhakrishnan K V. *J. Med. and Aromatic Plant Sci.*, 2020, 42(3-4), 1-29.

List of Conference Presentations

- Exploration of New Anti-Cancer Leads from *Dillenia indica* against Oral Squamous Cell Carcinoma; A New Insight into Rational Explication of Traditional Wisdom. **Aswathy M**, Ajaikumar B. Kunnumakkara and Radhakrishnan K V. 5th International Conference on Nutraceuticals and Chronic Diseases on Pharmaceuticals and Nutraceuticals for Cancer and Other Chronic Diseases (INCD-2022), University of Delhi, Delhi on October 7-9. **(Best Poster Award)**
- Isolation and characterization of bioactives from *Dillenia indica*". **M. Aswathy**, P. Sasikumar, Diya Anil, Ajaikumar B. Kunnumakkara, K.V. Radhakrishnan. ISP-2019, an International seminar on Phytochemistry organized by college of Pharmaceutical Sciences, Govt.Medical college, Thiruvananthapuram on 29th & 30th March 2019. **(Best Paper Award)**.
- Organic Brønsted acid catalysed stereo and regioselective glycosylation of secondary metabolites" **M. Aswathy**, and K. V. Radhakrishnan. South Zone Students' Research Convention - Anveshan 2020. Bharathidasan University, Tiruchirappalli-620024, Tamil Nadu. Oral presentation

Exploring the Cytotoxic Effects of the Extracts and Bioactive Triterpenoids from *Dillenia indica* against Oral Squamous Cell Carcinoma: A Scientific Interpretation and Validation of Indigenous Knowledge

Maniyamma Aswathy,[#] Kishore Banik,[#] Dey Parama,[#] Parameswaran Sasikumar, Choudhary Harsha, Anuja Gracy Joseph, Daisy R. Sherin, Manojkumar K. Thanathu, Ajaikumar B. Kunnumakkara,* and Radhakrishnan Kokkuvayil Vasu*



Cite This: *ACS Pharmacol. Transl. Sci.* 2021, 4, 834–847



Read Online

ACCESS |



Metrics & More



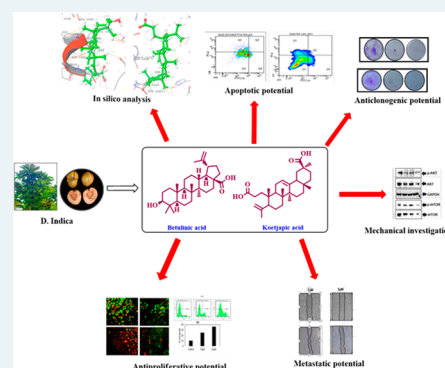
Article Recommendations



Supporting Information

ABSTRACT: Triterpenoids are ubiquitously distributed secondary metabolites, primarily scrutinized as a source of medication and preventive measures for various chronic diseases. The ease of isolation and excellent pharmacological properties of triterpenoids are notable reasons behind the exponential rise of extensive research on the bioactive triterpenoids over the past few decades. Herein, we attempted to explore the anticancer potential of the fruit extract of the ethnomedicinal plant *Dillenia indica* against oral squamous cell carcinoma (OSCC) and have exclusively attributed the efficacy of the extracts to the presence of two triterpenoids, namely, betulinic acid (BA) and koetjapic acid (KA). Preliminary *in vitro* screening of both BA and KA unveiled that the entities could impart cytotoxicity and induce apoptosis in OSCC cell lines, which were further well-supported by virtual screening based on ligand binding affinity and molecular dynamic simulations. Additionally, the aforementioned metabolites could significantly modulate the critical players such as Akt/mTOR, NF- κ B, and JAK/STAT3 signaling pathways involved in the regulation of important hallmarks of cancer like cell survival, proliferation, invasion, angiogenesis, and metastasis. The present findings provide insight and immense scientific support and integrity to a piece of indigenous knowledge. However, *in vivo* validation is a requisite for moving to clinical trials and developing it as a commercial drug.

KEYWORDS: *Dillenia indica*, triterpenoids, OSCC, cytotoxicity



Cancer is one of the leading causes of death worldwide, and according to GLOBOCAN 2018, it accounted for approximately 18.1 million new cases and around 9.6 million deaths globally in the year 2018. Oral cancer, or its predominant form, oral squamous cell carcinoma (OSCC), is a major cause of morbidity and mortality in India. It is one of the most aggressive malignancies occurring globally, affecting approximately 354 864 people every year and causing 177384 deaths per year.^{1–12} Due to its extremely high recurrence rate, the survival rate percentage of oral cancer patients is one of the lowest among all cancer types. Lifestyle factors like chewing tobacco, areca nut, consumption of alcohol, smoking, high intake of red meat, and fermented food are major risk factors of oral cancer and are the prime reason for its high prevalence.^{2,13–16} Despite the significant advancement in the diagnosis and treatment of disease, the incidence of oral cancer is rising quickly due to the lack of sensitive diagnostic methods and effective drugs. The conventional treatment modalities of oral cancer, i.e., surgery, radiation therapy (external beam radiotherapy and/or brachytherapy), and chemotherapy, face

numerous limitations such as adverse side effects, high treatment cost, toxicity to healthy cells, chemoresistance, radio resistance, recurrence of the tumor, and so on.^{2,3,9,12,17} Thus, there has been a growing interest in developing nontoxic and cost-effective treatments for oral cancer, which comprise complementary and alternative therapies. Exploring natural products and their active components, which exhibit significant chemopreventive and chemotherapeutic potential, has been an area of great attraction for researchers all over the world for the last few decades.^{18–25}

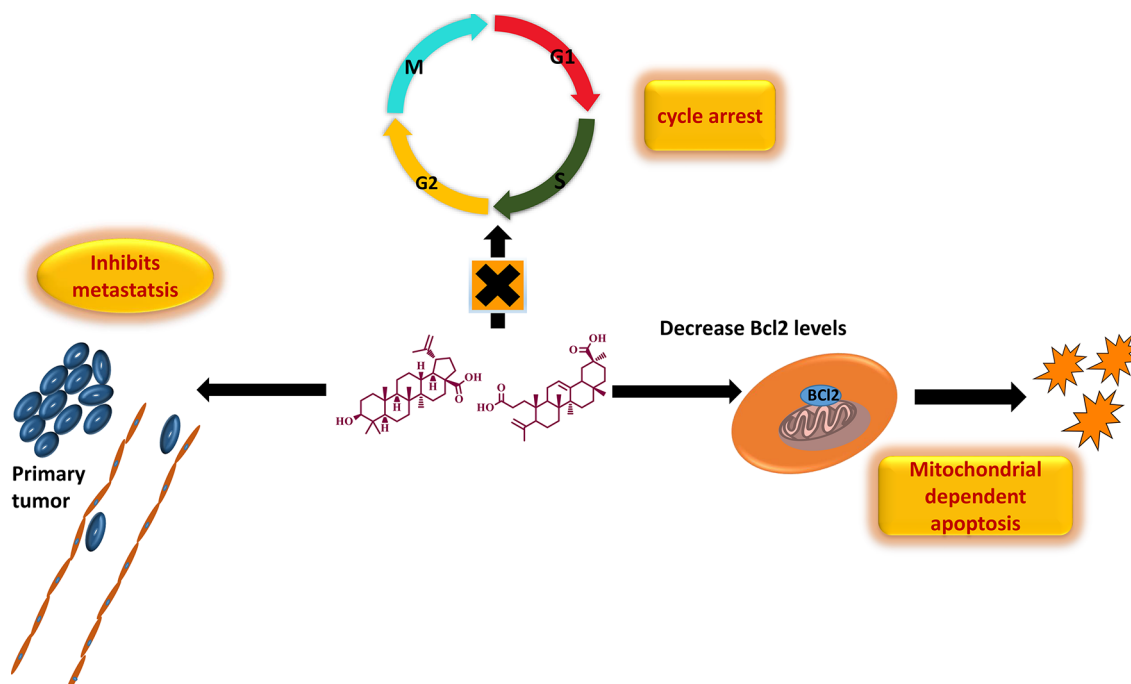
Dillenia indica (DI), commonly known as elephant apple, belonging to the family Dilleneaceae, is typically found in the

Received: January 7, 2021

Published: March 9, 2021



Scheme 1. Triterpenoids from DI Promotes Apoptosis and Inhibits Metastasis



moist forests of the sub-Himalayan region in northeastern India.²⁶ Fruits of the plant are widely used as a traditional medicine among the tribal population of Mizoram for the treatment of mouth ulcer, diarrhea, and jaundice.^{26,27} In addition to this, it is a common culinary ingredient in Assam and is used for preparing jams, pickles, and curries. Besides, the extracts of leaves, fruits, and bark are found to possess medicinal properties and thus are given orally to treat diabetes, cancer, and stomach disorders in the tribal areas of northeastern India.^{28,29} The leaves and bark extracts possess antioxidant potential and are also used as a laxative and an astringent agent.^{30–34} A thorough investigation of the plant chemistry revealed that it was enriched with triterpenoids, especially the pentacyclic triterpenoids belonging to the lupane group.^{35–37} Betulinic acid (BA), a naturally abundant triterpenoid isolated from DI, is reputed as a cytotoxic agent against various malignant tumors.^{38–42} Because of its incredible antitumor potential and nontoxic nature towards normal cells, it was established as an excellent cytotoxic agent in a number of cancer cell lines and entered in preclinical trial 1 phase.

Herein, we documented a scientific validation of indigenous knowledge of DI, and identified novel, safe, cost-effective, and multi-targeted anticancer agents from its fruit extract against OSCC. In addition to this, we also identified the bioactive molecules in the species conferring to the corresponding activity via preliminary cytotoxicity assays and *in silico* screening methods. Two of the identified candidates, viz., BA and KA, belong to the class of pentacyclic triterpenoids (Scheme 1). Even though BA is explored as an anticancer agent against numerous malignant tumors, limited reports are available on its potential against OSCC.^{43,44} To the best of our knowledge, this is the first report on the anticancer potential of KA against OSCC. The anticancer activity of the identified entities was evaluated using various *in vitro* assays such as 3-[4,5-dimethylthiazol-2-yl]-2,5-diphenyltetrazolium (MTT) assay, clonogenic assay, wound healing assay, fluorescent

assisted cell sorting (FACS) analysis, and live and dead assay. Further, Western blot analysis revealed that treatment with DI extracts and compounds significantly modulated multiple signaling pathways such as Akt/mTOR, NF- κ B, and JAK/STAT3, thereby exerting anticancer potential.

RESULT AND DISCUSSION

Extraction Strategy and Isolation Procedure of BA and KA. Initially, the sequential extraction of the fruits of *Dillenia indica* Linn. (900 g) were carried out with methanol (2.5 L) as well as water (500 mL) for 3 days; 45 g of methanol extract (DI-ME Ext) and 11 g of aqueous extract (DI-H₂O Ext) were obtained. As a part of our attempt to validate the integrity of the known medicinal properties popularized among the tribal communities, such as the potential of the fruit of DI to cure mouth ulcers and sores, we first analyzed the antiproliferative potential of the fruit extracts through MTT assay against an oral cancer cell line, SAS. The MTT cell proliferation assay is known to assess the metabolic activity of the cells. The amount of insoluble violet-blue formazan produced via the reduction of MTT tetrazolium salt by mitochondrial dehydrogenases determines the percentage of live cells. In this assay, SAS cells treated with an increasing concentration of DI showed reduced growth and proliferation rates of tumor cells, with IC₅₀ values of 14 and 12 μ g/mL for DI-H₂O Ext and DI-ME Ext respectively (Figure S1).

Because of our keen interest in divulging the phytochemicals in the species which has conferred to the corresponding pharmacological activity, isolation of molecules from DI-ME Ext was performed. For this purpose, DI-ME Ext was preferred over DI-H₂O Ext owing to its lower IC₅₀ value. The isolation procedure involved different chromatographic separation techniques, including thin-layer chromatography (TLC), column chromatography (CC) over silica gel (100–200 and 230–400 mesh), sephadex LH 20, and precipitation methods (Figure S2). Surprisingly, two among the ten isolated molecules showed immense cytotoxicity against SAS cell line

(Figure S3). Both these molecules belong to the category of triterpenoids: BA, [(3 β)-3-hydroxy-lup-20(29)-en-28-oic acid], a pentacyclic triterpenoid is reputed as a cytotoxic agent in various malignant tumor cells and KA is a *seco-A*-ring oleanane group triterpenoid, hitherto uninvestigated from the species, however, reported from the same genus.⁴⁵ Characterization was done with sophisticated NMR techniques (¹H and ¹³C) (Tables S1–S10), and structures of the identified bioactive molecules are represented in Figure 1.

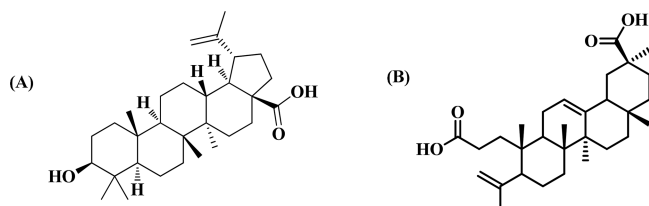


Figure 1. Chemical structures of bioactive molecules (A) BA and (B) KA isolated from DI-ME Ext.

The selection strategy of the entities made by preliminary antiproliferative assay, wherein BA and KA inhibited proliferation at IC₅₀ values of 6 and 20 μ M respectively after 72 h of treatment (Figure S4).

Computational Screening of BA and KA. Next, the screening strategy was further extended to computational simulation tools, where we employed the molecular docking approach to predict the affinity of the previously screened molecules to bind with the selected protein domains involved in regulating the different hallmarks of cancer (Table S11). Moreover, the flexibility and suitability of the molecules inside the binding pocket of the selected receptors were screened by molecular dynamics protocol.

Molecular Docking. BA was docked against the selected proteins: Akt (Protein Data Bank (PDB) ID: 1O6L), p-Akt, mTOR (PDB ID: 4JSP), p-mTOR, MMP-2 (PDB ID: 3AYU), and VEGF-A (PDB ID: 1FLT) (Table S1). It was found that BA showed a better binding affinity with Akt (D/G-score, -7.5 kcal/mol) and mTOR (D/G-score, -8.4 kcal/mol) (Table 1). In the case of 1O6L, the carboxylate group from the ligand forms H-bonds with polar Thr162 (1.8 and 2.1 Å), while with 4JSP, the carboxylate ion forms a salt bridge with positively charged Lys1452. The salt bridge formation is comparatively stronger and in this case, the ligand is deeply buried inside the binding pocket, thus resulting in maximum binding affinity with 4JSP (Figure 2). Subsequently, KA was docked against NF- κ B (1SVC), p-NF- κ B, mTOR (4JSP), p-mTOR, STAT3 (6NJS), p-STAT3, CXCR4 (3ODU), COX-2 (5IKQ), survivin (1E31), MMP-2 (1HOV), and VEGF-A (1FLT) (Table 1). Among these, KA showed a better binding affinity with NF- κ B

(D/G-score, -7.4 kcal/mol), mTOR (D/G-score, -8.1 kcal/mol), and STAT3 (D/G-score, -6.9 kcal/mol) (Table 1). In the binding pocket of 1SVC, one of the carboxylate ions forms H-bonds with positively charged Lys149 (1.9 and 2.2 Å). With 6NJS, one of the carboxylates forms two salt bridges with positively charged Lys573, Lys574, and one H-bond with Lys574 (2.1 Å), and the other carboxylate ion forms H-bond with Asn567 (2.2 Å). Even though two salt bridges are formed with 6NJS, the positioning of the conformer within the binding pocket is not as deep as in the other two cases, which leads to the comparatively lower score with 6NJS. One of the carboxylate ions from KA forms an H-bond with polar Asn1421 (1.8 Å), while the second carboxylate group forms a salt bridge with positively charged Arg2217, eventually contributing to the maximum affinity with 4JSP (Figure 2). The interaction analysis figured out the stability of the ligands inside the binding pocket of the receptor, which is somewhat more in BA as it is well inside the site.

Molecular Dynamics. To visualize the suitability and stability of the ligands inside the binding pocket of the receptor, molecular dynamics simulations were carried out for the complexes 4JSP–BA and 4JSP–KA for 10 000 ps under the OPLS-2005 force field. The RMSD plots (Figure 3) clearly depicts the stability of the complex. Even though the protein shows an initial fluctuation, it is almost stable under 4 Å during the interaction with the BA and KA, whereas the ligands are stabilized inside the protein throughout the trajectory. 4JSP–BA is comparatively more stable with less root-mean-square fluctuations. The P–L histograms (Figure 4) show that the H-bonded interactions are the major force of attraction that holds the ligands inside the protein. The simulation event analysis pointed out the H-bond formation of carboxylate ion of BA with positively charged Lys1452, which lasts for 45% of the simulation time, while that with polar Ser1584 lasts for 49% of the simulation time. However, carboxylate ions of KA form H-bond with positive charged Arg2217 (81 and 96%), hydrophobic Tyr1587 (35%), and polar Ser1584 (52%). Some of the KA residues also form water bridges with both of them. All these factors together subsidize the higher binding affinity of the ligands with mTOR. After evaluating the primary screening based on cancer cell-specific cytotoxicity, followed by molecular docking analysis, the selected candidates were subjected to the next-level studies.

DI Inhibited the Clonogenic Ability of OSCC Cells. We further confirmed the effect of DI on the ability of the individual SAS cells to form colonies by clonogenic assay. Compared with the control, the administration of DI extracts at two different concentrations (10 and 15 μ g/mL) caused a significant reduction in the number of colonies. Besides, the treatment of SAS cells with 10 and 15 μ M concentrations of both BA and KA was able to reduce the number of colonies in

Table 1. D-Score Values and Residues of BA and KA Interacting with Selected Proteins

	Akt (1O6L)		mTOR (4JSP)	
	D-score (kcal/mol)	interacting residues	D-score (kcal/mol)	interacting residues
BA	-7.5	Thr162	-8.4	Lys1452
	NF- κ B (1SVC)		mTOR (4JSP)	
	D-score (kcal/mol)	interacting residues	D-score (kcal/mol)	interacting residues
KA	-7.4	Lys149	-8.1	Arg2217
			Asn1421	Lys573
				Lys574
				Asn567
				STAT3 (6NJS)
	D-score (kcal/mol)	interacting residues	D-score (kcal/mol)	interacting residues
KA	-7.4	Lys149	-8.1	Arg2217
			Asn1421	Lys573
				Lys574
				Asn567

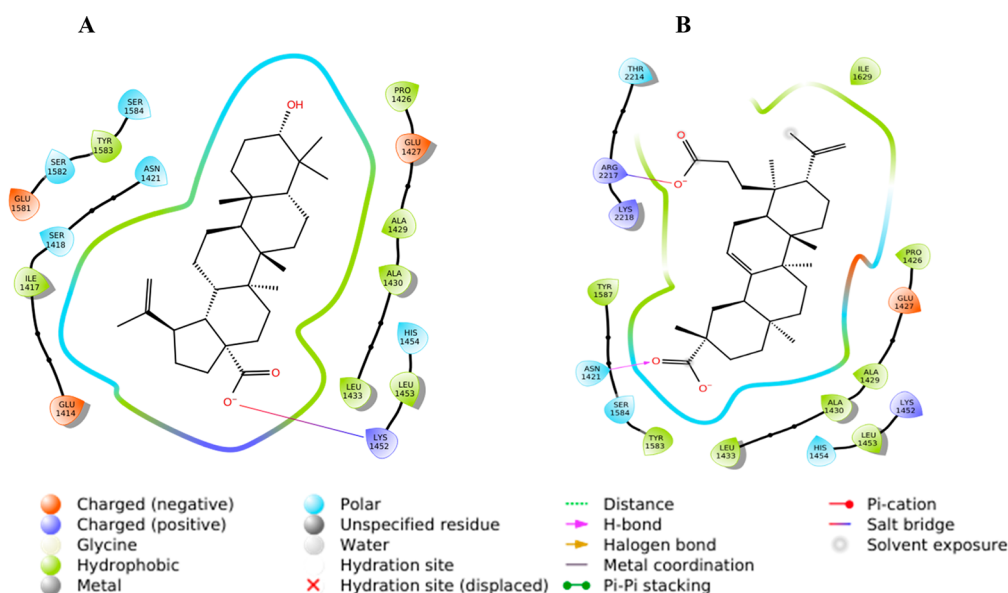


Figure 2. 2D interaction diagrams of (A) BA and (B) KA.

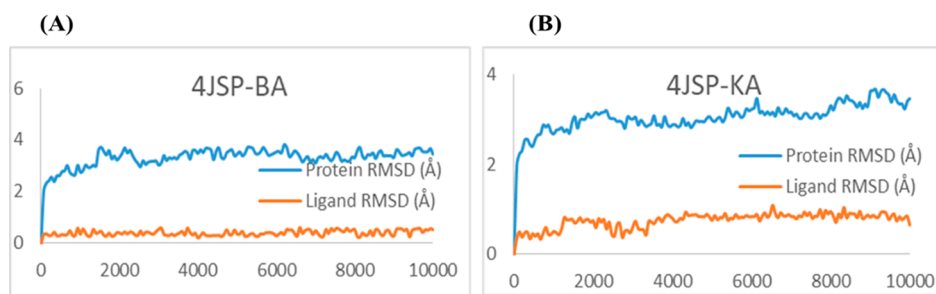


Figure 3. RMSD plots of (A) 4JSP-BA and (B) 4JSP-KA.

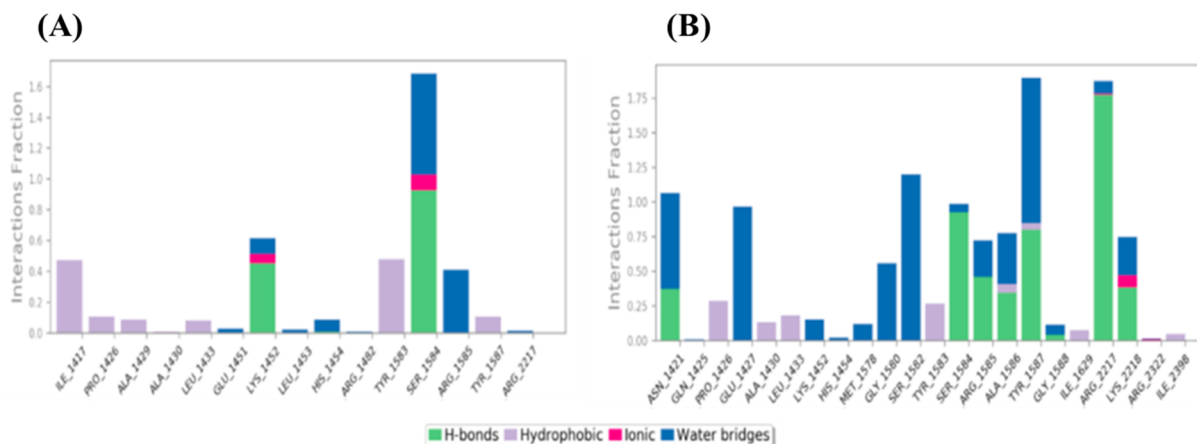


Figure 4. P-L interaction histogram of (A) 4JSP-BA and (B) 4JSP-KA

a dose-dependent manner (Figure 5). In accordance with the clonogenic assay result, it was inferred that KA was superior to BA for inhibiting the colony-forming ability of SAS cells.

DI Induced Cell Death in OSCC Cells. In order to confirm the role of DI in inducing cell death, propidium iodide (PI)-FACS staining was conducted following the treatment of SAS cells with 10 and 20 $\mu\text{g}/\text{mL}$ concentrations of both the extracts. Flow cytometric results revealed that the percentage of cell death increased from 14 to 19% in SAS cells treated with DI-H₂O Ext and from 8 to 10% in SAS cells treated with DI-

ME Ext after 72 h compared with the untreated control. A similar strategy was followed for elucidating the death inducing potential of BA and KA. Our results showed that BA increased the percentage of cell death from 25% at 10 μM to 36% at 25 μM , whereas KA increased the percentage of cell death from 20% at 25 μM to 33% at 50 μM , respectively (Figure 6(1)). Similarly, in the live and dead assay, treatment with DI led to a dose-dependent toxic effect on OSCC cells. Therefore, the results stated that treatment with the extracts, BA and KA resulted in cell death in SAS cells in a dose-dependent manner.

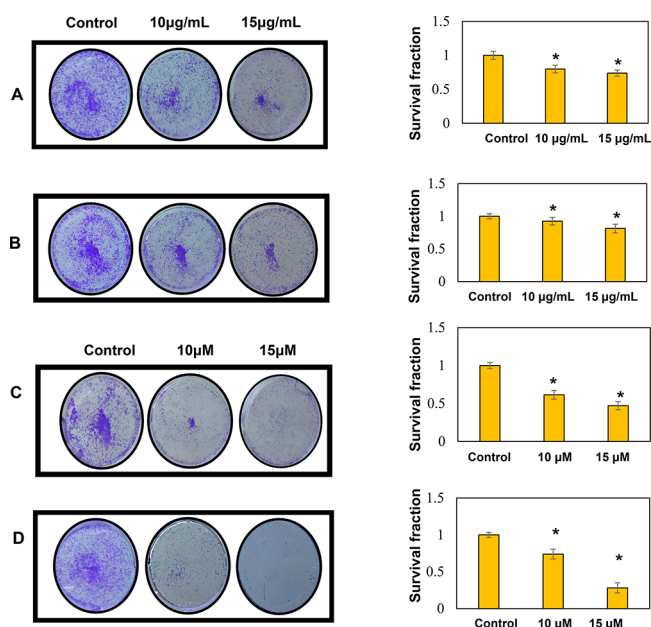


Figure 5. Inhibition of clonogenic potential of SAS cells by (A) DI-H₂O Ext (B) DI-ME Ext (C) BA (D) KA. Untreated cells were kept as the control. Quantification of the number of colonies was done with the help of ImageJ software. Results presented are mean \pm SD of three independent experiments; *, $p < 0.05$ vs control.

Effect of DI in Inducing Apoptosis in SAS Cells. Next, we evaluated the potential of DI in inducing apoptosis in SAS cells using Annexin V assay. SAS cells were treated with 10 and 25 $\mu\text{g}/\text{mL}$ of DI-H₂O Ext and 25 and 50 $\mu\text{g}/\text{mL}$ of DI-ME Ext for 72 h individually. As shown in Figure 7, the percentage of apoptotic cells increased from 1.7% in control to 19.8% under DI-H₂O Ext treatment and from 1% in control to 9% under DI-ME Ext treatment. The percentage of apoptotic cells increased from 3.2% in control to 14.3% in 50 μM BA-treated SAS cells and from 3.2% in control to 12.6% in 50 μM KA-treated SAS cells respectively (Figure 7). These results indicate that BA treatment causes a statistically evident increase in the number of apoptotic cells thus leading to significant growth inhibition in SAS cells.

DI Induced Cell Cycle Arrest in OSCC Cells. To further examine the mechanism of action of DI on SAS cells, the cell cycle distribution was investigated by flow cytometry analysis.

We found that the cells upon treatment with different concentrations of DI-H₂O Ext, DI-ME Ext, BA, and KA showed cell cycle arrest at different phases in comparison to the untreated cells. The SAS cells treated with DI-H₂O Ext and DI-ME Ext exhibited G1 and G2 phase arrest, respectively, while BA and KA treated SAS cells demonstrated S phase arrest. This result indicates that the decrease in cell proliferation and viability of the DI-treated SAS cells may be due to the induction of cell cycle arrest at various phases of the cell cycle (Figure 8).

DI Inhibited the Migration of OSCC Cells. The wound healing analysis of SAS cells showed inhibition in the migration of these cells with an increase in the concentration of DI. The images taken at 12 hr in case of DI-H₂O Ext and DI-ME Ext, or 24 hr in case of BA and KA showed that the wound area was completely healed while the treated cells exhibited changes in cell morphology and a significant reduction in the migration of SAS cells compared to the untreated cells. These results indicate that DI controls the migration of SAS cells (Figure 9).

DI Modulated the Expression of Various Proteins Responsible for Survival, Inflammation, Cell Cycle, Angiogenesis, Migration, and Apoptosis of OSCC Cells and the Involvement of Multiple Signaling Pathways in the Mode of Action. Studies have evidenced that the upregulation of various proteins like MMP-2, COX-2, VEGF, Akt, NF- κ B, CXCR-4, Bcl-2, Survivin, mTOR, and STAT-3 are responsible for enhanced proliferation, survival, angiogenesis, invasion and migration in cancer cells. However, the effect of DI on these gene products in human OSCC cells has not yet been elucidated. COX-2 catalyzes the first step in the synthesis of prostanoids and is often linked with carcinogenesis and inflammatory diseases. It promotes angiogenesis, migration, invasion of tumors, and deregulates apoptosis. As compared to healthy subjects, a significant upsurge in the expression of COX-2 was seen in cancer patients and patients with premalignant lesions.^{45–49} Furthermore, survivin is known to play a critical role in cell survival by regulating cell division and apoptosis. It has been noted that the upregulation of survivin is frequently observed in OSCC samples. This protein is essential for in the development of OSCC and, and it is mostly associated with the more aggressive form.^{50–52} VEGF-A is a 46 kDa heparin-binding homodimeric glycoprotein. It respectively binds to its receptor to promote endothelial cell differentiation and proliferation. Many studies have demonstrated the increase in the expression of VEGFs in different types of

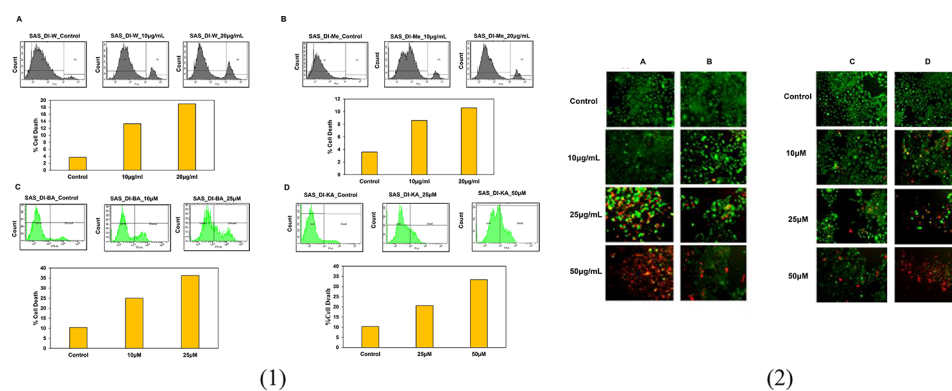


Figure 6. (1) Induction of cell death in SAS cells by (A) DI-H₂O Ext, (B) DI-ME Ext, (C) BA, and (D) KA. Cells were treated with the indicated concentrations for 72 h, followed by PI staining and FACS analysis for the cell death profile. (2) Live and dead assay was performed to evaluate the cytotoxic effect of the indicated concentrations of (A) DI-H₂O Ext, (B) DI-ME Ext, (C) BA, and (D) KA on SAS cells.

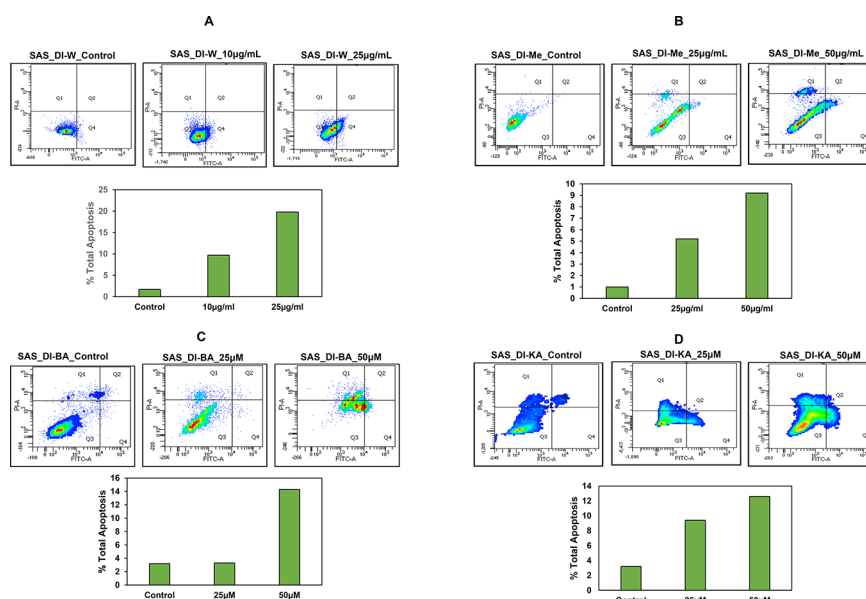


Figure 7. Induction of apoptosis in SAS cells upon treatment with (A) DI-H₂O Ext, (B) DI-ME Ext, (C) BA, and (D) KA. Cells were treated with the indicated concentrations for 72 h, followed by Annexin V staining and FACS analysis.

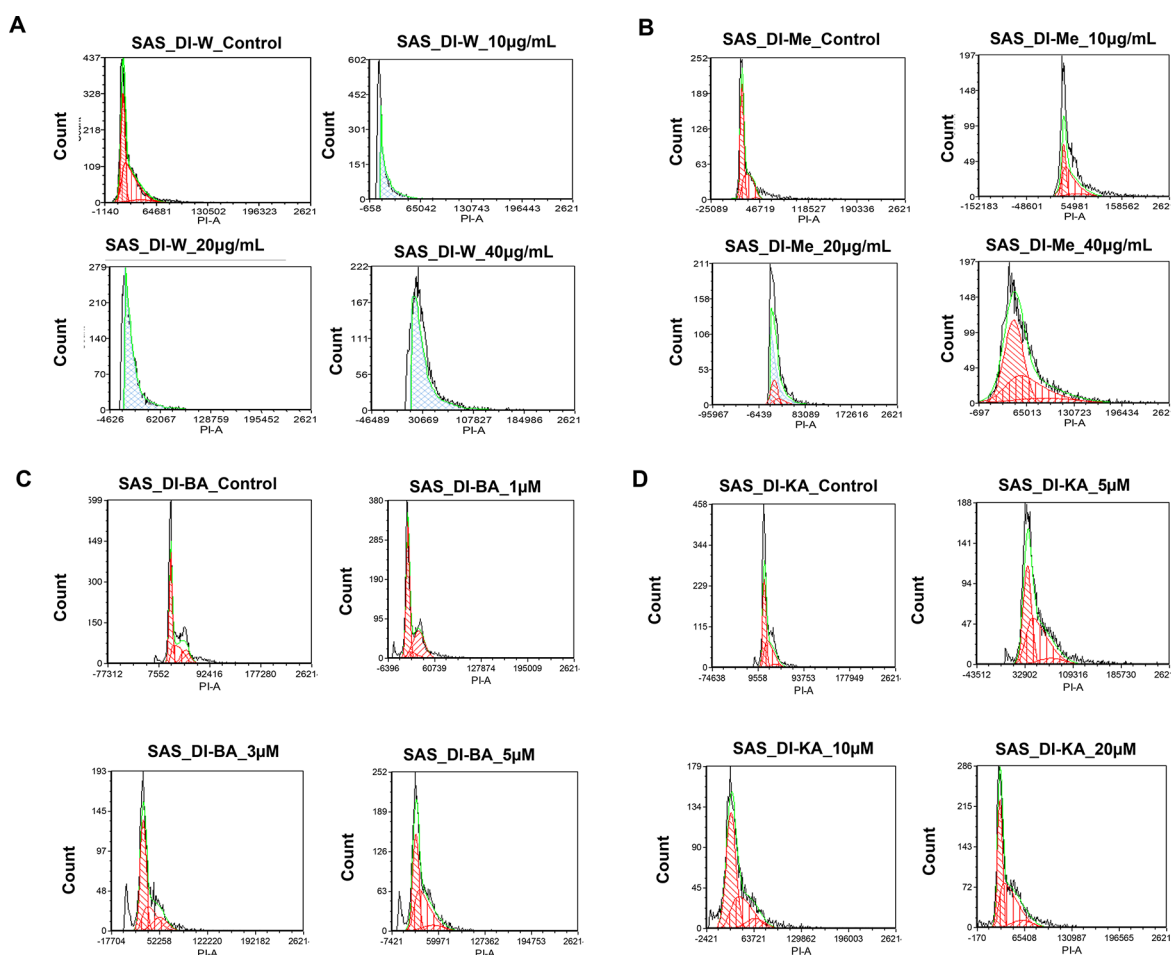


Figure 8. Induction of cell cycle arrest in SAS cells by (A) DI-H₂O Ext, (B) DI-ME Ext, (C) BA, and (D) KA. Percentages of each cell cycle phase were obtained using FCS Express software.

carcinoma. Macrophages, neutrophils, and fibroblasts, upon stimulation by the TGF- β and IL-8, secrete MMPs, and maintain the bioavailability of growth factors, thus promoting

cancer cell proliferation. Furthermore, MMPs cleave the FAS receptors, and modulate the function of natural killer cells and the apoptosis mechanism. They are also known to promote

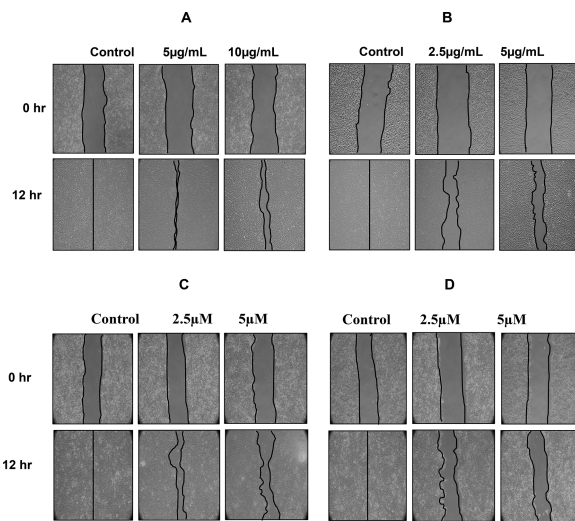


Figure 9. Inhibition of the migration of SAS cells upon treatment with (A) DI-H₂O Ext, (B) DI-ME Ext, (C) BA, and (D) KA. Cells were scratch-wounded and then treated with the indicated concentrations, followed by the recording of wound areas at different timepoints.

angiogenesis and metastasis. Various studies have shown that MMP-2 and MMP-9 are potential diagnostic markers for oral cancer detection.^{53–56} In addition, CXCR4 overexpression in cancer cells contributes to tumor growth, proliferation, invasion, angiogenesis, metastasis, relapse, and chemoresistance. CXCR4 antagonism disrupts tumor-stromal interactions,

reduces tumor growth and metastatic burden, and sensitizes cancer cells to cytotoxic drugs. CXCR4 is the target for not only therapeutic interference but it is also an important candidate for noninvasive checking of disease progression.⁵⁷ Also, Bcl-2 family proteins that regulate the intrinsic mitochondrial apoptosis pathway are activated in response to several stress stimuli, including growth-factor deprivation, cytokine-withdrawal, Ca²⁺-flux, or DNA-damage, caused by UV or gamma-irradiation, but they can also contribute to cell death triggered by members of the tumor necrosis factor family member such as FAS, TNF, or TRAIL. Deregulation of Bcl-2 protein is a frequent feature of human malignant diseases and causal for therapy resistance.^{58,59} NF-κB plays an essential role in inflammatory and immune responses and controls the expression of multiple genes associated with different hallmarks of cancer. The effect of DI on NF-κB as well as the diverse gene products regulated by NF-κB in human OSCC cells has not been elucidated yet. Therefore, in our study, we tried to explicate the effect of DI extracts, BA and KA on the expression of these proteins (Figure 10). Our findings revealed that the SAS cells treated with DI-H₂O Ext exhibited downregulation of VEGF-A, survivin and Bcl-2 via inhibition of the STAT3 pathway. However, similar trend was not observed in case of CXCR4. In addition, SAS cells treated with DI-ME Ext demonstrated downregulation of p-mTOR (S2448), and p-STAT-3 (S727), the crucial constituents of the Akt/mTOR and JAK/STAT signaling cascade. Besides, this extract was also found to inhibit the expression of CXCR4. Further, Western blot analysis showed that the DI constituents,

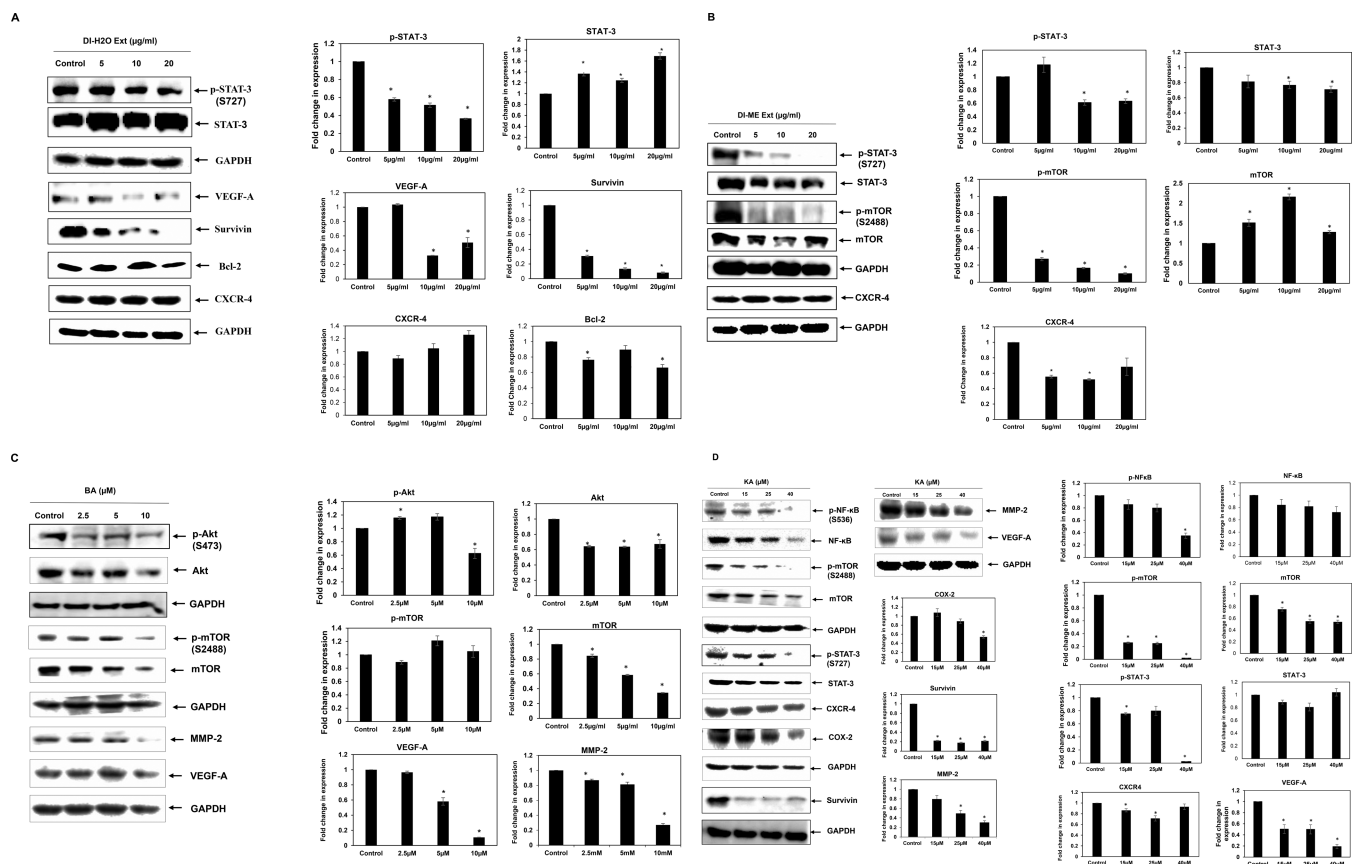


Figure 10. Expression of various proteins in SAS cells upon treatment with (A) DI-H₂O Ext, (B) DI-ME Ext, (C) BA, and (D) KA as examined by Western blot analysis. GAPDH was used as housekeeping control.

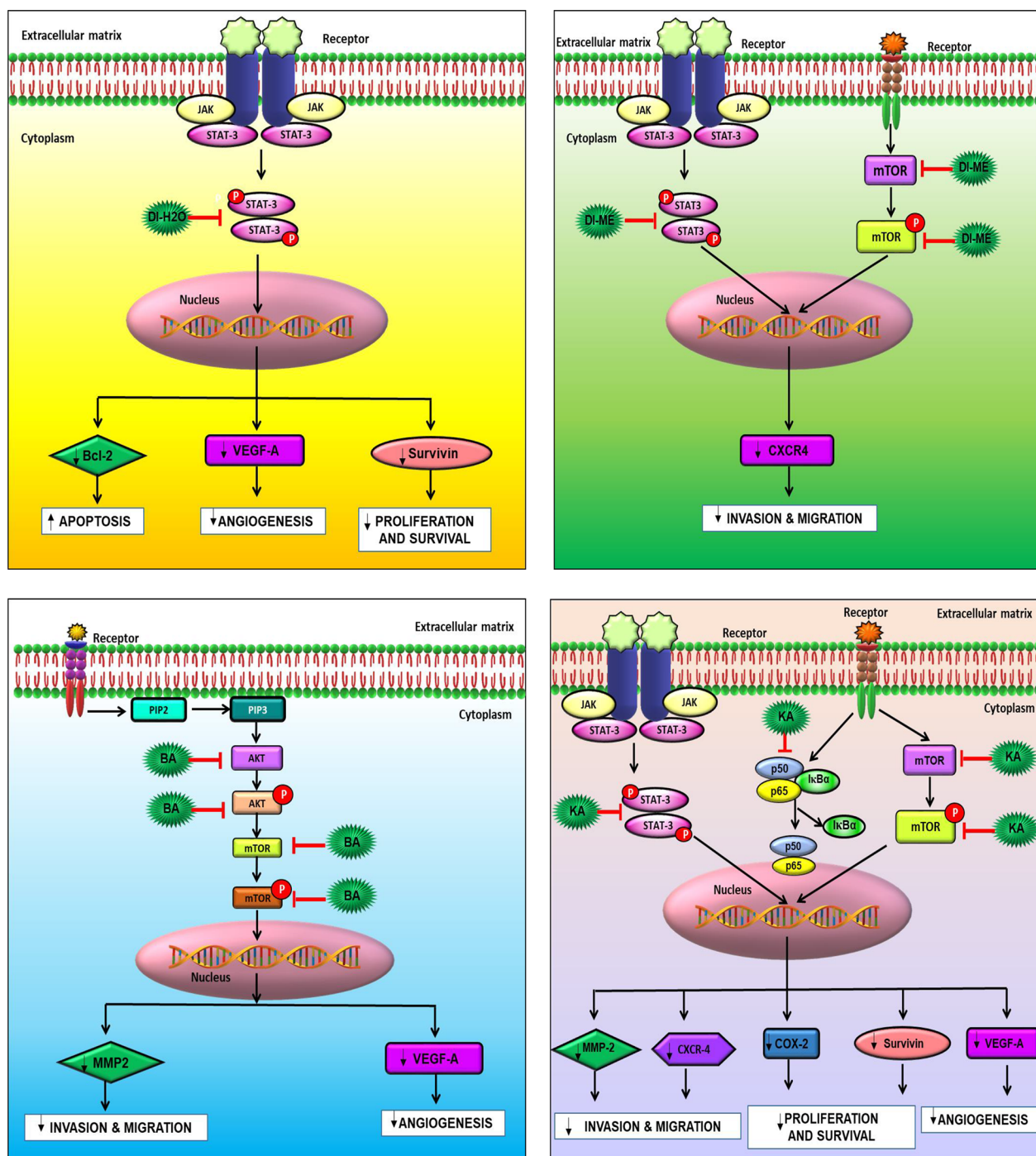


Figure 11. Pathway deciphering the proposed mechanistic mode of action with (A) DI-H₂O Ext, (B) DI-ME Ext, (C) BA, and (D) KA treatment in SAS cells.

BA caused dose-dependent downregulation of the expression of VEGF-A and MMP-2 via inhibition of the Akt/mTOR pathway. Similarly, KA was found to reduce the levels of COX-2, survivin, MMP-2 and VEGF-A through modulation of the NF- κ B, mTOR and STAT3 pathways. A decrease of Bcl-2 expression was observed in DI-H₂O Ext treated SAS cells, indicating that the activation of the mitochondria-dependent apoptotic pathway, at least in part, plays a role in DI-induced apoptosis. Akt1 is a crucial signaling protein involved in cellular survival pathways. It regulates survival by inhibiting apoptosis. The transcription factor NF- κ B is constitutively expressed in head and neck squamous cell carcinoma (HNSCC), and the

persistent expression of this protein is one of the root causes of the cancer cell proliferation, survival, invasion, metastasis, and poor survival of patients. Our results showed that the phosphorylated forms of Akt1 and NF- κ B were significantly downregulated upon treatment with BA and KA respectively. It is possible that both the p-Akt1(S473) and p-NF- κ B (S536) proteins are intracellular targets of DI that mediates its cytotoxic effects on SAS cells. Taken together, our results showed that the DI extracts and their active constituents, BA and KA modulated the expression of several critical proteins involved in the development and progression of OSCC (Figure

11). These results provide an insight into the precise mechanism of action of DI and its constituents (Figure 11).

In summary, we have interpreted indigenous knowledge with scientific criteria and identified new cytotoxic agents against OSCC. The fruit extracts of the ethnomedicinal plant DI might vanquish the adverse side effects of conventional modalities of treatment. In order to recognize the bioactive scaffolds in the plant extract, we performed detailed phytochemical profiling. Ten compounds were isolated and characterized, out of which, five compounds, namely, koetjapic acid, palmarumycin JC1, ferulic acid, 3-oxykojic acid, and 2-(1',2'-dihydroxy)-kojic acid, were reported for the first time from this species. All the isolated molecules were screened through preliminary antiproliferative assay and the leads, BA and KA were identified. They were again subjected to virtual screening based on ligand binding affinity and molecular dynamic simulations for providing theoretical support to the scientific validation. Both of the selected candidates displayed significant anticancer potential *in vitro* by imparting antiproliferative, cytotoxic, anti-clonogenic, anti-metastatic, and apoptotic effects. Our findings were further supported by the reduced expression of various proteins involved in the development and progression of OSCC. However, further *in vivo* studies are required to validate our findings and also elucidate the precise mechanism of action, which may provide a basis for developing chemopreventive and chemotherapeutic strategies for the better management of OSCC.

■ EXPERIMENTAL SECTION

Plant Material. Fruits of DI were collected from Guwahati, Assam, and were identified by the taxonomists of Jawaharlal Nehru Botanical Garden of India, Palode, Thiruvananthapuram, Kerala. A voucher specimen number JNTBGRI 93635 was deposited at the herbarium of JNTBGRI, Kerala.

Cell Line. The OSCC cell line, SAS, was obtained from National Center for Cell Sciences (NCCS, Pune, India). The cells were maintained in DMEM supplemented with 10% heat-inactivated FBS and 1% Penstrep. The cells were grown in an incubator under optimum conditions of 5% CO₂ and temperature at 37 °C.

Reagents. Penstrep, Trypsin EDTA, DMEM medium, and FBS were obtained from Gibco, USA. MTT and PI were obtained from Invitrogen and Sigma-Aldrich respectively, while DMSO used was procured from Merck Life Science Pvt. Ltd. The live and dead assay kit was obtained from Invitrogen, USA. Crystal violet was procured from SRL Pvt. Ltd., India. The Optiblot ECL Detection Kit was procured from Abcam, Cambridge, USA.

Extraction of DI Fruits. Fruits and leaves of DI were collected in March 2018. These were thoroughly cleaned, dried (in an oven maintained at a temperature of 50 °C for 3 days) and powdered. A 1 kg sample of the powdered fruits was extracted with methanol (2.5 L × 48 h) at room temperature thrice and was filtered. The completion of extraction was checked with TLC. The filtrate was concentrated under reduced pressure using a Heidolph rotary evaporator at a temperature of 50 °C yielded 45 g of crude extract. The residue thus obtained was further extracted with water, lyophilized, and yielded 11 g of aqueous extract.

Isolation of Phytochemicals from Methanol Extract. TLC of the methanol extract in various combinations of *n*-hexane–ethyl acetate was studied. The residue was subjected to silica gel (100–200 mesh, Merck) column chromatography

(CC) at different compositions of hexane, ethyl acetate, and methanol to afford 50 fractions (fractions 1–50). Each of these pooled fractions was concentrated by removing the solvent under reduced pressure using a Heidolph rotary evaporator.

Compound 1 (β -sitosterol, 10 mg) was obtained from fractions 1–3 via CC using 5% ethyl acetate–hexane, which recrystallized as white needle-shaped crystals with the same polarity.

Compound 2 (*n*-hentriacontanol, 7 mg) showed an intense spot in a cerium sulfate/phosphoric acid charring solution and was obtained as a white solid in 10% ethyl acetate–hexane.

Compound 3 (lupeol, 20 mg) was isolated from fraction 9 in 20% ethyl acetate–hexane and was further subjected to crystallization.

Compound 4 (betulinic acid, 4g) was obtained from 30% ethyl acetate in hexane as white solid, which was identified as the marker compound of the species.

Compound 5 (koetjapic acid, 17 mg) was isolated from a pool of fractions 30–34 by Sephadex LH 20 column with methanol as the eluent.

TLC of fractions 35–38 eluted from the column in 50–60% ethyl acetate in hexane showed an intense UV active spot, which was further purified by repeated CC by using sephadex LH 20 in methanol, yielding compound 6 (ferulic acid, 15 mg).

Compound 7 (palmarumycins JC1, 40 mg) eluted in 70% ethyl acetate in hexane, which was further purified by using sephadex LH 20 and recrystallized in methanol.

Compound 8 (3-oxykojic acid, 45 mg) and compound 9 ((2-(1',2'-dihydroxy)-kojic acid, 30 mg) were obtained as a mixture of both from fractions 42–44, which were further purified by using Sephadex LH 20.

Compound 10 (β -sitosterol- β -D-glucopyranoside, 30 mg) was obtained from fractions 45–50 as an amorphous solid and was further purified by precipitation using acetone. All molecules were identified by ¹H and ¹³C NMR spectra and HR-ESIMS (Tables S1–S10).

Characterization of Phytochemicals. NMR spectra were recorded on Bruker Avance AMX 500 MHz NMR spectrometer. Chemical shift was reported in parts per million using TMS as an internal standard with solvent residual peaks (CDCl₃: δ_{H} –7.26 ppm, δ_{C} –77.3 ppm), (DMSO-*d*₆: δ_{H} –2.50 ppm, δ_{C} –39.5 ppm), and (acetone-*d*₆: δ_{H} –2.05 ppm, δ_{C} –29.8 ppm). Multiplicities were given as s (singlet); d (doublet); t (triplet); q (quartet); dd (double doublet); and m (multiplet). Coupling constant, *J*, was expressed in Hz. Optical rotation was recorded on Jasco P-1020 polarimeter, and absorbance was recorded on a UV 1800 Shimadzu UV Spectrophotometer. Mass spectra were recorded under ESI-HRMS at 60 000 resolution on a Thermo Scientific Exactive Column, and IR spectra were recorded on Bruker Alpha FT-IR spectrometer. All solvents used for UV, IR, MS, and chromatography were purchased from Sigma-Aldrich and Merck (HPLC-grade). For CC, silica gel with different mesh sizes (100–200 and 230–400) and Sephadex-LH 20 were used.

Computational Screening and Molecular Dynamics Simulation. The optimization and minimization of the proteins, binding site analysis, receptor grid generation, ligand conformation generation, ADME/T screening, molecular docking, and dynamics were done with Schrödinger suite 2020–1.⁶⁰ For this, protein preparation wizard, Sitemap, LigPrep, QikProp, Glide XP docking, and Desmond tools were used in Maestro 11.2 interface in OPLS-2005 force field.⁶¹ The

crystal structures of the proteins were retrieved from the RCSB Protein Data Bank: protein kinase B, Akt (PDB ID: 1O6L); mammalian target of rapamycin, mTOR (PDB ID: 4JSP); matrix metalloproteinase-2, MMP-2 (PDB ID: 3AYU); vascular endothelial growth factor-A, VEGF-A (PDB ID: 1FLT); nuclear factor kappa-light-chain-enhancer of activated B cells, NF- κ B (PDB ID: 1SVC); signal transducer and activator of transcription 3, STAT-3 (PDB ID: 6NJS); C-X-C chemokine receptor type 4, CXCR-4 (PDB ID: 3ODU), cyclooxygenase-2, COX-2 (PDB ID: 5IKQ); and survivin (PDB ID: 1E31).⁶² All these proteins were refined by adding hydrogens/missing side chains, optimized, and minimized. The phosphorylated forms of the Akt, mTOR, NF- κ B, and STAT-3 were generated successively by adding a phosphate group to the corresponding serine residues using build structure protocol. Site map analysis was carried out to identify the suitable binding pockets in the case of these receptors, and the grids were generated around site 1 which were used for further docking. The different conformers of the BA and KA were generated using LigPrep module and screened their ADME/T (Absorption, Distribution, Metabolism, and Excretion/Toxicity) properties by QikProp analysis. The docking simulations were done by Glide docking, and the binding affinities were ranked using docking score (D-score) and glide score (G-score). Molecular dynamics simulations further analyzed the best ones for 10 000 ps using the Desmond module of Schrödinger suite under OPLS-2005 force field.

Cell Proliferation Assay. A total of 2×10^3 SAS cells per 100 μ L media were seeded into each well of two 96-well plates and incubated for 24 h. The cells were then treated with different concentrations of the DI-H₂O Ext, DI-ME Ext, BA, and KA individually, and the MTT assay was performed at 0 and 72 h. A 10 μ L aliquot of MTT at a concentration of 5 mg/mL in PBS was added to each well and incubated for 2 h. Next, the cell culture medium was discarded, and 100 μ L of DMSO was added to each well and incubated for 1 h in the dark. Color conversion of the MTT reaction was measured with a microplate reader at a wavelength of 570 nm. Control cells were defined as 100% proliferation, and the percentage proliferation was calculated to the following formula: (Absorption of treated cells \times 100)/(Absorption of control cells (untreated)).

Colony-Forming Assay. A total of 1×10^3 cells per 2 mL were seeded in a 6-well plate and incubated for 24 h. The cells were then treated with DI-H₂O Ext, DI-ME Ext, BA, and KA separately and incubated for another 24 h. The next day, the media of the wells were replaced with fresh media, and the cells were allowed to form colonies for 9 days. On 9th day, colonies were fixed with ethanol, stained with 0.3% crystal violet (SRL Pvt. Ltd., India) solution for 20 min and washed. Images were captured for each well and the number of colonies was quantified using ImageJ software.

Cell Death Analysis. A total of 2×10^4 SAS cells per 2 mL of media were seeded in a 6-well plate and incubated for 24 h, followed by treatment with different concentrations of DI-H₂O Ext, DI-ME Ext, BA, and KA individually. After 72 h of drug treatment, the media from the wells were collected in labeled 5 \times 77 mm² polystyrene test tubes. Adhered cells were washed with PBS, trypsinized, and collected in their respective tubes. The cell suspension was then centrifuged at 4000 rpm for 10 min at 4 $^{\circ}$ C. After centrifugation, the supernatant was discarded, and the pellet was washed with 1 mL of PBS and centrifuged at 4000 rpm for 10 min, and the step was repeated

twice. Finally, the pellet was suspended in 495 μ L of PBS, and 5 μ L of PI (Sigma-Aldrich) dye was added. The cells were then analyzed in BD FACS Diva software. PI dye is impermeable to the live cells as they have an intact cell membrane and thus emit less fluorescence; however, PI can easily penetrate the dead cells because of the damaged plasma membrane, thereby emitting a high red fluorescence.

Live and Dead Assay. DI-mediated cell death in SAS cells was studied using the Live–Dead assay kit (Invitrogen, USA). The kit contains two fluorescent dyes, calcein-AM and PI. In principle, calcein-AM can enter any cells but labels only live cells. It is converted by cellular cytoplasmic esterases to a highly green-fluorescent calcein. PI is excluded by live cells with an intact membrane but enters dead cells with a broken membrane to stain their nuclei red. Therefore, live cells fluoresce green, whereas dead cells fluoresce red. SAS cells were seeded at 2000 cells per 100 μ L of media in 96-well tissue culture plates. After 24 h, the cells were treated with DI-H₂O Ext, DI-ME Ext, BA, and KA individually. Cells were then stained with the live/dead reagent and incubated at 37 $^{\circ}$ C in the dark for 20 min. Cells were then analyzed under an inverted fluorescence microscope (Olympus, Japan).

Apoptosis Assay. Apoptosis is marked by the translocation and accumulation of the membrane phospholipid phosphatidylserine from the cytoplasmic edge of the membrane to the extracellular surface. The membrane perturbation can be detected by using Annexin V which binds to the phosphatidylserine of the apoptotic cells. A total of 5×10^4 SAS cells per 2 mL of media were seeded in a 6-well plate and incubated for 24 h, followed by treatment with different concentrations of DI-H₂O Ext, DI-ME Ext, BA, and KA individually. After 72 h of drug treatment, the media from the wells were collected in labeled 5 \times 77 mm² polystyrene test tubes. Adhered cells were washed with PBS, trypsinized, and collected in their respective tubes. The cell suspension was then centrifuged at 4000 rpm for 10 min at 4 $^{\circ}$ C. After centrifugation, the supernatant was discarded, and the pellet was washed with 1 mL of PBS and centrifuged at 4000 rpm for 10 min. The PBS was discarded, and 20 μ L of binding buffer was added to the tubes and the tubes were centrifuged again. Then the untreated control was divided into unstained (does not contain either PI or Annexin V) and double-stained (contain both the dyes) tubes, and the positive control was divided into PI-positive and Annexin V-positive tubes. A 2.5 μ L aliquot of Annexin V added to all the tubes except the unstained and PI-positive ones and incubated in the dark for 20 min containing different concentrations of DI. The tubes were incubated in dark for 20 min. Centrifugation was done again, and the supernatant is discarded. A 20 μ L aliquot of binding buffer is added, and 2.5 μ L of PI (Sigma-Aldrich) dye was added. The cells were then analyzed in BD FACS Cell Quest software.

Cell Cycle Analysis. A total of 2×10^5 SAS cells per 2 mL of media were seeded in a 6-well plate and incubated overnight for cell adhesion. The cells were then treated with different concentrations of DI, and the untreated sample was used as a control. Following 24 h of individual treatment of DI-H₂O Ext, DI-ME Ext, BA, and KA, the media was collected in polystyrene tubes, and the adhered cells were washed with PBS twice. Then, 300 μ L of trypsin was added to detach the cells. The detached cells were harvested in their respective tubes and centrifuged at 4000 rpm for 10 min at 4 $^{\circ}$ C. The supernatant was discarded, and the pellet was washed with 1 mL of PBS

and centrifuged at 4000 rpm for 10 min at 4 °C. Then the supernatant was discarded, and 5 mL of 70% ethanol was dropwise added to the pellet under constant vortexing and kept for overnight incubation at 4 °C for fixation. The next day, the suspension was centrifuged at 4000 rpm for 10 min at 4 °C, and the supernatant was discarded. Following the removal of ethanol by centrifugation, the cells were washed twice with PBS and stained with PI/RNase solution for 30 min in the dark. Cell cycle distribution was detected using FACS Celesta (Becton-Dickinson, Franklin Lakes, NJ), and the data were analyzed using FCS Express (BD Biosciences). The fluorescence intensity of the stained cells correlates with the amount of DNA they contain.

Cell Migration Assay. A total of 5×10^5 SAS cells per 2 mL of media were seeded in a 6-well plate and incubated for 12 h to form the monolayer. After the monolayer was formed, the media was replaced with serum-free media and incubated for 8 h. Thereafter, the media was removed, and a vertical scratch or wound was made with the help of a 200 μ L tip at the center of the well. The wells were then washed with PBS twice to remove the debris. Cells were then treated with different concentrations of DI-H₂O Ext, DI-ME Ext, BA, and KA individually. The untreated cells were used as control. The directional migration of SAS cells was observed under an inverted microscope (Nikon T1-SM, Tokyo, Japan), and images were taken at 0 and 12 or 24 h depending upon the healing timepoint of the wound. Images were compared to quantify the migration of SAS cells after treatment.

Western Blot Analysis. A total of 6×10^5 cells per 3 mL of media were seeded in 60 mm culture plates and were allowed to grow for 24 h. The cells were then treated with different concentrations of DI-H₂O Ext, DI-ME Ext, BA, and KA individually and incubated for the next 24 h. Protein was isolated from respective treatment plates using lysis buffer (20 mM HEPES, 2 mM EDTA, 250 mM NaCl, and 0.1% NP40) in the presence of protease inhibitors (2 μ g/mL leupeptin hemisulfate, 2 μ g/mL aprotinin, 1 mM PMSF, and 1 mM DTT) and quantified using Bradford's reagent. Equal amount of protein (30 μ g) was mixed with 5X Laemmli Buffer (250 mM Tris-HCl, 10% SDS, 30% glycerol, 5% β -mercaptoethanol, and 0.02% bromophenol blue) and separated by 12% SDS-PAGE and transferred to nitrocellulose membrane (Biorad) by using a Trans-blot Turbo (Biorad), the membrane was blocked with 5% nonfat skim milk in tris-buffered saline containing 1% tween 20 (TBST). For the phospho-antibodies, the membranes were treated with 5% BSA in tris-buffered saline containing 1% tween 20 to block the nonspecific binding sites. The membranes were then incubated with primary antibodies for MMP-2, COX-2, VEGF-A, Akt1, p-Akt, NF- κ B, p-NF- κ B, CXCR-4, cyclin D1, Bcl-2, survivin, mTOR, p-mTOR, STAT-3, p-STAT-3, and GAPDH overnight at 4 °C. Afterwards, the blots were washed with 1X TBST buffer and then incubated with horseradish peroxidase conjugated secondary antibody for 2 h at room temperature. The bands representing different proteins were visualized with the help of Clarity Western ECL Substrate (Biorad) in a ChemiDoc XRS System (Biorad). GAPDH was used as the housekeeping control.

Statistical Analysis. Statistical analysis was performed using Student's *t* test. All the data are represented as mean \pm standard error (SE). *p* < 0.05 was defined as statistically significant.

■ ASSOCIATED CONTENT

■ Supporting Information

The Supporting Information is available free of charge at <https://pubs.acs.org/doi/10.1021/acspsci.1c00011>.

Isolation procedure, characterization techniques, preliminary MTT screening of both extracts and isolated compounds, computational screening of compounds discussed (PDF)

■ AUTHOR INFORMATION

Corresponding Authors

Ajaikumar B. Kunnumakkara – Cancer Biology Laboratory and DBT-AIST International Center for Translational & Environmental Research (DAICENTER), Department of Biosciences and Bioengineering, Indian Institute of Technology, Guwahati 781 039, Assam, India; orcid.org/0000-0001-9121-6816; Email: kunnumakkara@iitg.ac.in

Radhakrishnan Kokkuvayil Vasu – Chemical Sciences and Technology Division, CSIR-National Institute for Interdisciplinary Science and Technology (CSIR-NIIST), Thiruvananthapuram 695019, India; Academy of Scientific and Innovative Research (AcSIR), Ghaziabad 201002, India; orcid.org/0000-0001-8909-3175; Email: radhu@niist.res.in

Authors

Maniyamma Aswathy – Chemical Sciences and Technology Division, CSIR-National Institute for Interdisciplinary Science and Technology (CSIR-NIIST), Thiruvananthapuram 695019, India; Academy of Scientific and Innovative Research (AcSIR), Ghaziabad 201002, India

Kishore Banik – Cancer Biology Laboratory and DBT-AIST International Center for Translational & Environmental Research (DAICENTER), Department of Biosciences and Bioengineering, Indian Institute of Technology, Guwahati 781 039, Assam, India; orcid.org/0000-0003-2497-8313

Dey Parama – Cancer Biology Laboratory and DBT-AIST International Center for Translational & Environmental Research (DAICENTER), Department of Biosciences and Bioengineering, Indian Institute of Technology, Guwahati 781 039, Assam, India

Parameswaran Sasikumar – Chemical Sciences and Technology Division, CSIR-National Institute for Interdisciplinary Science and Technology (CSIR-NIIST), Thiruvananthapuram 695019, India

Choudhary Harsha – Cancer Biology Laboratory and DBT-AIST International Center for Translational & Environmental Research (DAICENTER), Department of Biosciences and Bioengineering, Indian Institute of Technology, Guwahati 781 039, Assam, India

Anuja Gracy Joseph – Chemical Sciences and Technology Division, CSIR-National Institute for Interdisciplinary Science and Technology (CSIR-NIIST), Thiruvananthapuram 695019, India; Academy of Scientific and Innovative Research (AcSIR), Ghaziabad 201002, India

Daisy R. Sherin – Centre for Computational Modeling and Data Engineering, Indian Institute of Information Technology and Management-Kerala (IIITM-K), Thiruvananthapuram 695581, India

Manojkumar K. Thanathu – Centre for Computational Modeling and Data Engineering, Indian Institute of

Information Technology and Management-Kerala (IIITM-K), Thiruvananthapuram 695581, India

Complete contact information is available at:
<https://pubs.acs.org/10.1021/acspsci.1c00011>

Author Contributions

#A.M., K.B., and D.P. contributed equally to this work.

Notes

The authors declare no competing financial interest.

ACKNOWLEDGMENTS

CSIR Ph.D. student M.A. thanks CSIR for research fellowship. K.B. acknowledges UGC for providing fellowship. M.A. thanks Mathew Dan, Senior Scientist, Plant Genetics Resources Division, JNTBGRI, for providing plant material. A.B.K. acknowledges BT/556/NE/U-Excel/2016 project awarded by Department of Biotechnology, Govt. of India.

ABBREVIATIONS

Bcl-2, B-cell lymphoma 2; BSA, Bovine serum albumin; Ca⁺⁺, Calcium ion; CC, Column chromatography; COX-2, cyclooxygenase 2; CXCR4, C-X-C chemokine receptor type 4; DI, *Dillenia indica*; DMEM, Dulbecco's modified eagle's medium; DMSO, Dimethyl sulfoxide; DTT, Dithiothreitol; EDTA, Ethylenediaminetetraacetic acid; EGFR, Epidermal growth factor receptor; ESI, Electrospray ionization; FACS, Fluorescence-activated cell sorting; FBS, Fetal bovine serum; Fr., Fraction; GAPDH, Glyceraldehyde 3-phosphate dehydrogenase; HEPES, 4-(2-hydroxyethyl)-1-piperazineethanesulfonic acid; HPLC, High-performance liquid chromatography; HRMS, High-resolution electrospray ionization mass spectrometry; IL-8, Interleukin-8; IR, Infrared; JAK2, Janus kinase 2; MMPs, Matrix metalloproteinases; MS, Mass spectrometry; mTOR, Mammalian target of rapamycin; MTT, 3-(4,5-dimethylthiazol-2-yl)-2,5-diphenyltetrazolium bromide; NF- κ B, Nuclear factor kappa B; NMR, Nuclear magnetic resonance; OSCC, Oral squamous cell carcinoma; p38 MAPK, p38 mitogen-activated protein kinase; PBS, Phosphate-buffered saline; PI, Propidium iodide; PMSF, Phenylmethylsulfonyl fluoride; SDS-PAGE, Sodium dodecyl sulfate polyacrylamide gel electrophoresis; STAT, Signal transducer and activator of transcription; TBST, Tris-buffered saline (TBS) and Polysorbate 20 (Tween 20); TLC, Thin-layer chromatography; TNF, Tumor necrosis factor; TRAIL, TNF-related apoptosis-inducing ligand; UV, Ultraviolet; VEGF, Vascular endothelial growth factor

REFERENCES

- (1) Bray, F., Ferlay, J., Soerjomataram, I., Siegel, R. L., Torre, L. A., and Jemal, A. (2018) Global Cancer Statistics 2018: GLOBOCAN Estimates of Incidence and Mortality Worldwide for 36 Cancers in 185 Countries. *Ca-Cancer J. Clin.* 68 (6), 394–424.
- (2) Harsha, C., Banik, K., Ang, H. L., Girisa, S., Vikkurthi, R., Parama, D., Rana, V., Shabnam, B., Khatoon, E., Kumar, A. P., and Kunnumakkara, A. B. (2020) Targeting AKT/mTOR in Oral Cancer: Mechanisms and Advances in Clinical Trials. *Int. J. Mol. Sci.* 21 (9), 3285.
- (3) Singh, A. K., Roy, N. K., Bordoloi, D., Padmavathi, G., Banik, K., Khwairakpam, A. D., Kunnumakkara, A. B., and Sukumar, P. (2020) Orai-1 and Orai-2 regulate oral cancer cell migration and colonisation by suppressing Akt/mTOR/NF- κ B signalling. *Life Sci.* 261, 118372.
- (4) Kunnumakkara, A. B., Thakur, K. K., Rana, V., Bora, B., Banik, K., Khatoon, E., Sailo, B. L., Shabnam, B., Girisa, S., Gupta, S. C., and

Aggarwal, B. B. (2019) Upside and Downside of Tumor Necrosis Factor Blockers for Treatment of Immune/Inflammatory Diseases. *Crit. Rev. Immunol.* 39 (6), 439–479.

(5) Kunnumakkara, A. B., Harsha, C., Banik, K., Vikkurthi, R., Sailo, B. L., Bordoloi, D., Gupta, S. C., and Aggarwal, B. B. (2019) Is curcumin bioavailability a problem in humans: lessons from clinical trials. *Expert Opin. Drug Metab. Toxicol.* 15 (9), 705–733.

(6) Bordoloi, D., Monisha, J., Roy, N. K., Padmavathi, G., Banik, K., Harsha, C., Wang, H., Kumar, A. P., Arfuso, F., and Kunnumakkara, A. B. (2019) An Investigation on the Therapeutic Potential of Butein, A Tetrahydrochalcone Against Human Oral Squamous Cell Carcinoma. *Asian Pac. J. Cancer Prev.* 20 (11), 3437–3446.

(7) Devi Khwairakpam, A., Monisha, J., Roy, N. K., Bordoloi, D., Padmavathi, G., Banik, K., Khatoon, E., and Kunnumakkara, A. B. (2019) Vietnamese coriander inhibits cell proliferation, survival and migration via suppression of Akt/mTOR pathway in oral squamous cell carcinoma. *J. Basic Clin. Physiol. Pharmacol.* 31 (3), 20190162.

(8) Roy, N. K., Parama, D., Banik, K., Bordoloi, D., Devi, A. K., Thakur, K. K., Padmavathi, G., Shakibaei, M., Fan, L., Sethi, G., and Kunnumakkara, A. B. (2019) An Update on Pharmacological Potential of Boswellic Acids against Chronic Diseases. *Int. J. Mol. Sci.* 20 (17), 4101.

(9) Roy, N. K., Monisha, J., Padmavathi, G., Lalhruiatluanga, H., Kumar, N. S., Singh, A. K., Bordoloi, D., Baruah, M. N., Ahmed, G. N., Longkumar, I., Arfuso, F., Kumar, A. P., and Kunnumakkara, A. B. (2019) Isoform-Specific Role of Akt in Oral Squamous Cell Carcinoma. *Biomolecules* 9 (7), 253.

(10) Kunnumakkara, A. B., Bordoloi, D., Sailo, B. L., Roy, N. K., Thakur, K. K., Banik, K., Shakibaei, M., Gupta, S. C., and Aggarwal, B. B. (2019) Cancer drug development: The missing links. *Exp. Biol. Med.* 244 (8), 663–689.

(11) Shabnam, B., Padmavathi, G., Banik, K., Girisa, S., Monisha, J., Sethi, G., Fan, L., Wang, L., Mao, X., and Kunnumakkara, A. B. (2018) Sorcin a Potential Molecular Target for Cancer Therapy. *Transl. Oncol.* 11 (6), 1379–1389.

(12) Monisha, J., Roy, N. K., Padmavathi, G., Banik, K., Bordoloi, D., Khwairakpam, A. D., Arfuso, F., Chinnathambi, A., Alahmadi, T. A., Alharbi, S. A., Sethi, G., Kumar, A. P., and Kunnumakkara, A. B. (2018) NGAL is Downregulated in Oral Squamous Cell Carcinoma and Leads to Increased Survival, Proliferation, Migration and Chemoresistance. *Cancers* 10 (7), 228.

(13) Hanahan, D., and Weinberg, R. A. (2011) Hallmarks of cancer: the next generation. *Cell* 144, 646–674.

(14) Anand, P., Sundaram, C., Jhurani, S., Kunnumakkara, A. B., and Aggarwal, B. B. (2008) Curcumin and cancer: an “old-age” disease with an “age-old” solution. *Cancer Lett.* 267, 133–164.

(15) Dissanayaka, W. L., Pitiyage, G., Kumarasiri, P. V., Liyanage, R. L., Dias, K. D., and Tilakaratne, W. M. (2012) Clinical and histopathologic parameters in survival of oral squamous cell carcinoma. *Oral Surg. Oral Med. Oral Pathol. Oral Radiol.* 113 (4), 518–525.

(16) Lee, J., Taneja, V., and Vassallo, R. (2012) Cigarette smoking and inflammation: cellular and molecular mechanisms. *J. Dent. Res.* 91 (2), 142–149.

(17) Huang, M., Lu, J. J., Huang, M. Q., Bao, J. L., Chen, X. P., and Wang, Y. T. (2012) Terpenoids: natural products for cancer therapy. *Expert Opin. Invest. Drugs* 21 (12), 1801–1818.

(18) Henamayee, S., Banik, K., Sailo, B. L., Shabnam, B., Harsha, C., Srilakshmi, S., Vgm, N., Baek, S. H., Ahn, K. S., and Kunnumakkara, A. B. (2020) Therapeutic Emergence of Rhein as a Potential Anticancer Drug: A Review of Its Molecular Targets and Anticancer Properties. *Molecules* 25 (10), 2278.

(19) Parama, D., Boruah, M., Yachna, K., Rana, V., Banik, K., Harsha, C., Thakur, K. K., Dutta, U., Arya, A., Mao, X., Ahn, K. S., and Kunnumakkara, A. B. (2020) Diosgenin, a steroidal saponin, and its analogs: Effective therapies against different chronic diseases. *Life Sci.* 260, 118182.

(20) Khatoon, E., Banik, K., Harsha, C., Sailo, B. L., Thakur, K. K., Khwairakpam, A. D., Vikkurthi, R., Devi, T. B., Gupta, S. C., and

- Kunnumakkara, A. B. (2020) Phytochemicals in cancer cell chemosensitization: Current knowledge and future perspectives. *Semin. Cancer Biol.* DOI: 10.1016/j.semcancer.2020.06.014.
- (21) Banik, K., Ranaware, A. M., Harsha, C., Nitesh, T., Girisa, S., Deshpande, V., Fan, L., Nalawade, S. P., Sethi, G., and Kunnumakkara, A. B. (2020) Piceatannol: A natural stilbene for the prevention and treatment of cancer. *Pharmacol. Res.* 153, 104635.
- (22) Kunnumakkara, A. B., Banik, K., Bordoloi, D., Harsha, C., Sailo, B. L., Padmavathi, G., Roy, N. K., Gupta, S. C., and Aggarwal, B. B. (2018) Googling the Guggul (Commiphora and Boswellia) for Prevention of Chronic Diseases. *Front. Pharmacol.* 9, 686.
- (23) Ranaware, A. M., Banik, K., Deshpande, V., Padmavathi, G., Roy, N. K., Sethi, G., Fan, L., Kumar, A. P., and Kunnumakkara, A. B. (2018) Magnolol: A Neolignan from the Magnolia Family for the Prevention and Treatment of Cancer. *Int. J. Mol. Sci.* 19 (8), 2362.
- (24) Banik, K., Harsha, C., Bordoloi, D., Laldusaki Sailo, B., Sethi, G., Leong, H. C., Arfuso, F., Mishra, S., Wang, L., Kumar, A. P., and Kunnumakkara, A. B. (2018) Therapeutic potential of gambogic acid, a caged xanthone, to target cancer. *Cancer Lett.* 416, 75–86.
- (25) Banik, K., Ranaware, A. M., Deshpande, V., Nalawade, S. P., Padmavathi, G., Bordoloi, D., Sailo, B. L., Shanmugam, M. K., Fan, L., Arfuso, F., Sethi, G., and Kunnumakkara, A. B. (2019) Honokiol for cancer therapeutics: A traditional medicine that can modulate multiple oncogenic targets. *Pharmacol. Res.* 144, 192–209.
- (26) Sharma, H. K., Chhangte, L., and Dolui, A. K. (2001) Traditional medicinal plants in Mizoram, India. *Fitoterapia* 72 (2), 146–161.
- (27) Rai, P. K., and Lalramnghinglova, H. (2010) Lesser known ethnobotanical plants of Mizoram, North East India: an Indo-Burma hotspot region. *J. Med. Plants Res.* 4 (13), 1301–1307.
- (28) Foo, J. B., Saiful Yazan, L., Tor, Y. S., Wibowo, A., Ismail, N., Armania, N., Cheah, Y. K., and Abdullah, R. (2016) Dillenia suffruticosa dichloromethane root extract induced apoptosis towards MDA-MB-231 triple-negative breast cancer cells. *J. Ethnopharmacol.* 187, 195–204.
- (29) Foo, J. B., Saiful Yazan, L., Tor, Y. S., Wibowo, A., Ismail, N., How, C. W., Armania, N., Loh, S. P., Ismail, I. S., Cheah, Y. K., and Abdullah, R. (2015) Induction of cell cycle arrest and apoptosis by betulinic acid-rich fraction from Dillenia suffruticosa root in MCF-7 cells involved p53/p21 and mitochondrial signalling pathway. *J. Ethnopharmacol.* 166, 270–8.
- (30) Tarak, D., Namsa, N. D., Tangiang, S., Arya, S. C., Rajbonshi, B., Samal, P. K., and Mandal, M. (2011) An inventory of the ethnobotanicals used as anti-diabetic by a rural community of Dhemaji district of Assam, Northeast India. *J. Ethnopharmacol.* 138 (2), 345–350.
- (31) Kritikar, K. R., and Basu, B. D. (2010) *Indian Medicinal Plants, Vol. II*, International Book Distributors, India.
- (32) Abdille, M. H., Singh, R. P., Jayaprakasha, G. K., and Jena, B. S. (2005) Antioxidant activity of the extracts from Dillenia indica fruits. *Food Chem.* 90 (4), 891–896.
- (33) Prasad, P. R. C., Reddy, C. S., Raza, S. H., and Dutt, C. B. S. (2008) Folklore medicinal plants of north Andaman Islands, India. *Fitoterapia* 79 (6), 458–464.
- (34) Das, M., Sarma, B. P., Ahmed, G., Nirmala, C. B., and Choudhury, M. K. (2012) In vitro anti oxidant activity total phenolic content of Dillenia indica Garcinia penducalata, commonly used fruits in Assamese cuisine. *Free Radicals Antioxid.* 2 (2), 30–36.
- (35) Pavanasivam, G., and Sultanbawa, M. U. S. (1975) Flavonoids of some Dilleniaceae species. *Phytochemistry* 14, 1127–1128.
- (36) Banerji, N., Mjumder, P., and Dutta, N. I. (1975) A new pentacyclic triterpene lactone from Dillenia indica. *Phytochemistry* 14, 1447–1448.
- (37) Suokas, E., Hase, T., Liaaen-Jensen, S.ø., Matsutaka, H., and Matsuno, T. (1978) Dry Ozonation of 3beta,28-Diacetoxylupane. A Comment on the Structure of a Pentacyclic Triterpenoid Lactone from Dillenia indica (Linn.). *Acta Chem. Scand.* 32b, 623–624.
- (38) Fulda, S., Jeremias, I., Steiner, H. H., Pietsch, T., and Debatin, K.-M. (1999) Betulinic acid: A new cytotoxic agent against malignant brain-tumor cells. *Int. J. Cancer* 82, 435–441.
- (39) Kumar, P., Bhadauria, A. S., Singh, A. K., and Saha, S. (2018) Betulinic acid as apoptosis activator: Molecular mechanisms, mathematical modeling and chemical modifications. *Life Sci.* 209, 24–33.
- (40) Cai, Y., Zheng, Y., Gu, J., Wang, S., Wang, N., Yang, B., Zhang, F., Wang, D., Fu, W., and Wang, Z. (2018) Betulinic acid chemosensitizes breast cancer by triggering ER stress-mediated apoptosis by directly targeting GRP78. *Cell Death Dis.* 9, 636.
- (41) Mertens-Talcott, S. U., Noratto, G. D., Li, X., Angel-Morales, G., Bertoldi, M. C., and Safe, S. (2013) Betulinic Acid Decreases ER-Negative Breast Cancer Cell Growth In Vitro and In Vivo: Role of Sp Transcription Factors and MicroRNA-27a:ZBTB10. *Mol. Carcinog.* 52, 591.
- (42) Yang, C., Li, Y., Fu, L., Jiang, T., and Meng, F. (2018) Betulinic acid induces apoptosis and inhibits metastasis of human renal carcinoma cells in vitro and in vivo. *J. Cell. Biochem.* 119, 8611.
- (43) Shen, H., Liu, L., Yang, Y., Xun, W., Wei, K., and Zeng, G. (2017) Betulinic Acid Inhibits Cell Proliferation in Human Oral Squamous Cell Carcinoma via Modulating ROS-Regulated p53 Signaling. *Oncol. Res.* 25 (7), 1141–1152.
- (44) Abubakar, S., Khor, B.-K., Khaw, K.-Y., Murugaiyah, V., and Chan, K.-L. (2021) Cholinesterase inhibitory potential of Dillenia suffruticosa chemical constituents and protective effect against Aβ-induced toxicity in transgenic Caenorhabditis elegans model. *Phytomedicine Plus.* 1 (1), 100022.
- (45) Zeng, A., Hua, H., Liu, L., and Zhao, J. (2019) Betulinic acid induces apoptosis and inhibits metastasis of human colorectal cancer cells in vitro and in vivo. *Bioorg. Med. Chem.* 27, 2546–2552.
- (46) Ferrandez, A., Prescott, S., and Burt, R. (2003) COX-2 and colorectal cancer. *Curr. Pharm. Des.* 9 (27), 2229–2251.
- (47) Liu, B., Qu, L., and Yan, S. (2015) Cyclooxygenase-2 promotes tumor growth and suppresses tumor immunity. *Cancer Cell Int.* 15, 106.
- (48) Xiong, B., Sun, T.-J., Yuan, H.-Y., Hu, M. B., Hu, W. D., and Cheng, F. L. (2003) Cyclooxygenase-2 expression and angiogenesis in colorectal cancer. *World J. Gastroenterol.* 9, 1237–1240.
- (49) Elzagheid, A., Emaetig, F., Alkikhia, L., Buhmeida, A., Syrjänen, K., El-Faitori, O., Latto, M., Collan, M., and Pyyhonen, S. (2013) High cyclooxygenase-2 expression is associated with advanced stages in colorectal cancer. *Anticancer Res.* 33, 3137–3143.
- (50) Jaiswal, P. K., Goel, A., and Mittal, R. D. (2015) Survivin: A molecular biomarker in cancer. *Indian J. Med. Res.* 141 (4), 389–397.
- (51) Groner, B., and Weiss, A. (2014) Targeting survivin in cancer: novel drug development approaches. *BioDrugs* 28 (1), 27–39.
- (52) Soleimanpour, E., and Babaei, E. (2015) Survivin as a Potential Target for Cancer Therapy. *Asian Pac. J. Cancer Prev.* 16 (15), 6187–6191.
- (53) Venugopal, A., and Uma Maheswari, T. (2016) Expression of matrix metalloproteinase-9 in oral potentially malignant disorders: A systematic review. *J. Oral Maxillofac. Pathol.* 20 (3), 474–479.
- (54) Patel, B. P., Shah, S. V., Shukla, S. N., Shah, P. M., and Patel, P. S. (2007) Clinical significance of MMP-2 and MMP-9 in patients with oral cancer. *Head Neck.* 29 (6), 564–572.
- (55) Lotfi, A., Mohammadi, G., Tavassoli, A., Mousaviagdas, M., Chavoshi, H., and Saniee, L. (2015) Serum levels of MMP9 and MMP2 in patients with oral squamous cell carcinoma. *Asian Pac. J. Cancer Prev.* 16 (4), 1327–1330.
- (56) Shpitzer, T., Hamzany, Y., Bahar, G., Feinmesser, R., Savulescu, D., Borovoi, I., Gavish, M., and Nagler, R. M. (2009) Salivary analysis of oral cancer biomarkers. *Br. J. Cancer* 101 (7), 1194–1198.
- (57) Chatterjee, S., Behnam Azad, B., and Nimmagadda, S. (2014) The intricate role of CXCR4 in Cancer. *Adv. Cancer Res.* 124, 31–82.
- (58) Youle, R. J., and Strasser, A. (2008) The BCL-2 protein family: opposing activities that mediate cell death. *Nat. Rev. Mol. Cell Biol.* 9, 47–59.

(59) Frenzel, A., Grespi, F., Chmielewski, W., and Villunger, A. (2009) Bcl2 family proteins in carcinogenesis and the treatment of cancer. *Apoptosis: an. Apoptosis* 14 (4), 584–596.

(60) Sherin, D.R., Geethu, C.K., Prabhakaran, J., Mann, J. J., Dileep Kumar, J.S., and Manojkumar, T.K. (2019) Molecular docking, dynamics simulations and 3D-QSAR modeling of arylpiperazine derivatives of 3,5-dioxo-(2H,4H)-1,2,4-triazine as 5-HT1AR agonists. *Comput. Biol. Chem.* 78, 108–115.

(61) Schrödinger, LLC. (2020) *Schrödinger*, release 2020–1, Schrödinger, LLC, New York.

(62) RCSB Protein Data Bank. www.rcsb.org.

Betulinic acid: A natural promising anticancer drug, current situation, and future perspectives

Maniyamma Aswathy^{1,2} | Ajesh Vijayan³ | Uzini D. Daimary⁴ | Sosmitha Girisa⁴ | Kokkuvayil V. Radhakrishnan¹ | Ajaikumar B. Kunnumakkara⁴ 

¹Chemical Sciences and Technology Division, CSIR-National Institute for Interdisciplinary Science and Technology (CSIR-NIIST), Thiruvananthapuram, India

²Academy of Scientific and Innovative Research (AcSIR), Ghaziabad, India

³Department of Chemistry, CHRIST (Deemed to be University), Bangalore, India

⁴Cancer Biology Laboratory, Department of Biosciences and Bioengineering, Indian Institute of Technology, Guwahati, Assam, India

Correspondence

Ajaikumar B. Kunnumakkara, Cancer Biology Laboratory, Department of Biosciences and Bioengineering, Indian Institute of Technology Guwahati, Room # 005, O-Block, Guwahati, Assam 781039, India.
Email: kunnumakkara@iitg.ac.in and ajai78@gmail.com

Kokkuvayil V. Radhakrishnan, Chemical Sciences and Technology Division, CSIR-National Institute for Interdisciplinary Science and Technology (CSIR-NIIST), Thiruvananthapuram 695019, India.
Email: radhu@niist.res.in and radhu2005@gmail.com

Abstract

Natural products serve as the single most productive source for the discovery of drugs and pharmaceutical leads. Among the various chemicals derived from microbes, plants, and animals, phytochemicals have emerged as potential candidates for the development of anticancer drugs due to their structural diversities, complexities, and pleiotropic effects. Herein, we discuss betulinic acid (BA), a ubiquitously distributed lupane structured pentacyclic triterpenoid, scrutinized as a promising natural agent for the prevention, suppression, and management of various human malignancies. Ease of availability, common occurrences, cell-specific cytotoxicity, and astonishing selectivity are the important factors that contribute to the development of BA as an anticancer agent. The current review delineates the mechanistic framework of BA-mediated cancer suppression through the modulation of multiple signaling pathways and also summarizes the key outcomes of BA in preclinical investigations.

KEYWORDS

anticancer, apoptosis, betulin, betulinic acid, cytotoxicity, hydrosolubility, pharmacokinetics

1 | INTRODUCTION

Cancer is a multifactorial malaise that arises due to the dysregulation of multiple signaling pathways and their regulated molecules in the body.^[1-3] The conventional treatment modalities for this disease include surgery, radiation, chemo, immuno, and hormone therapies which are associated with numerous side effects and adverse limitations.^[4-10] The standard anticancer drugs currently available

in the market are nonspecific, cytotoxic, expensive, and inadequate which necessitates the requirement of alternative drugs that are safe, cost-effective, and efficacious.^[11-20] Hence, the development of alternative approaches for the prevention and treatment of cancer becomes imperative.

Since the dawn of current pharmacopeia, natural products have served as a prolific source of potential drug candidates.^[13,16,21-29] The chemicals derived from microbes, plants, and even animals have

Abbreviations: AIF, apoptosis-inducing factor; AKT, protein kinase B; Bax, Bcl-2-associated X protein; CDK, cyclin-dependent Kinases; CHOP, C/EBP homologous protein; ER, estrogen receptor; HIF-1 α , hypoxia-inducible factor-1 α ; MMP, matrix metalloproteinase; $\Delta\Psi_m$, mitochondrial membrane potential; mTOR, mammalian target of rapamycin; MVD, microvessel density; NF- κ B, nuclear factor- κ B; NLRC4, NLR family CARD domain-containing protein 4; PARP, poly (ADP-ribose) polymerase; PI3K, phosphatidylinositol 3-kinase; ROS, reactive oxygen species; Smac, second mitochondria-derived activator of caspases; STAT-3, signal transducer and activator of transcription-3; TIMP-2, tissue inhibitor of metalloproteinases-2; VEGF, vascular endothelial growth factor.

been an invaluable source of therapeutic agents, and the structurally diverse phytochemicals with potent biological activities were the most significant among them, which have been extensively documented.^[17,19,25,30-44] Polyphenolic compounds, including alkaloids and flavonoids, are some of the pleiotropic phytoconstituents that exhibit promising antitumor activities in a plethora of cellular and animal models.^[1,16,24-26,42] In addition, a wide range of polyphenolic secondary metabolites has successively completed different phases of preclinical/clinical trials.^[45-49] For instance, a bioactive ingredient of turmeric, curcumin, is reputed as an excellent therapeutic agent and is presently under human clinical trials for various chronic diseases such as Alzheimer's disease, cancers of the colon, pancreas, and blood cells, myelodysplastic syndromes, and psoriasis.^[16,43,44,50-54] Furthermore, resveratrol, a major phytochemical isolated from grapes and red wine species, has drawn the worldwide attention of many research groups and confronted a huge number of key outcomes of preclinical as well as clinical trials.^[45,55,56] One of the past studies by Newman and Cragg^[56] reported that approximately 60% of the current anticancer drugs were isolated either from natural products or their structural analogs. In addition, various research groups have explored the anticancer properties of the synthetic modifications of isolated natural products for the development of potential drug candidates.^[57] Our research group was intrigued by the tremendous biological potential hidden in these ubiquitous functional moieties, and we commenced our expedition to the fascinating world of natural products by the isolation and screening of phytochemicals from *Zingiber zerumbet* against the α -glucosidase enzyme, aldose reductase enzyme, and their antiglycation properties.^[58] Later, our group also unraveled the isolation of (+) and (-)-hopeaphenol from *Ampelocissus indica* (L.) and *Vateria indica* Linn, isolation of resveratrol oligomers from *Hopea ponga* (Dennst.) Mabb., and so on.^[59] Recently, we reported the isolation of bioactive triterpenoids from the fruit extract of the ethnomedicinal plant *Dillenia indica* which showed cytotoxic effects against oral cancer due to the presence of two triterpenoids, namely, betulinic acid (BA) and koetjapic acid.^[60] Triterpenoids are the oligomers of

isopentenyl pyrophosphate cyclized from squalene, representing one of the largest plant metabolites with various subgroups such as ursane, oleanane, lupane, dammarane, and euphane. In addition, multiple shreds of evidence have reported the promising anticancer properties of biologically potent phytochemicals such as lupeol, taraxasterol, α -amirin, β -amirin, and BA.^[61,62]

BA/ 3β -hydroxy-lup-20(29)-en-28-oic acid (BA), one of the bioactive compounds reported from the family Betulaceae, belongs to the category of triterpenoid with lupane core (Figure 1). The tremendous anticancer potential of this unique phytochemical was disclosed by Pisha et al., in 1995, and thereafter BA has entered as a promising candidate under different phases of preclinical trials as an excellent chemotherapeutic agent.^[63] Moreover, accumulating evidence has also reported the chemosensitizing potential of BA in preclinical settings.^[64] Because of our keen interest in exploring bioactive leads/agents from traditionally highlighted flora, we have emphasized the anticancer properties of BA against oral cancer.^[60] The immense biological potential of the natural products as a selective and excellent therapeutic agent in various cancers has played a pivotal role in its development from a phytoconstituent to a potential anticancer agent.^[65,66] However, lack of aqueous solubility, poor bioavailability, less intestinal permeability, and rapid elimination after oral administration are some of the significant challenges associated with the application of BA as a therapeutic agent.^[67] Nevertheless, various approaches, including structural modifications, combinatorial treatments with other drugs, and various formulations, may be employed to improve the stability and effective transport of this bioactive molecule.

Thus, this review aims to depict the contemporary landscape of BA, within the last few decades, and the molecular mechanism of its chemopreventive and chemotherapeutic potential against various cancers. Particular emphasis has been given to the efficacy of BA in modulating various signaling pathways and its associated oncogenic proteins, which are highly involved in tumorigenesis. In addition, this review also summarizes the anticancer potential of BA in different preclinical studies.

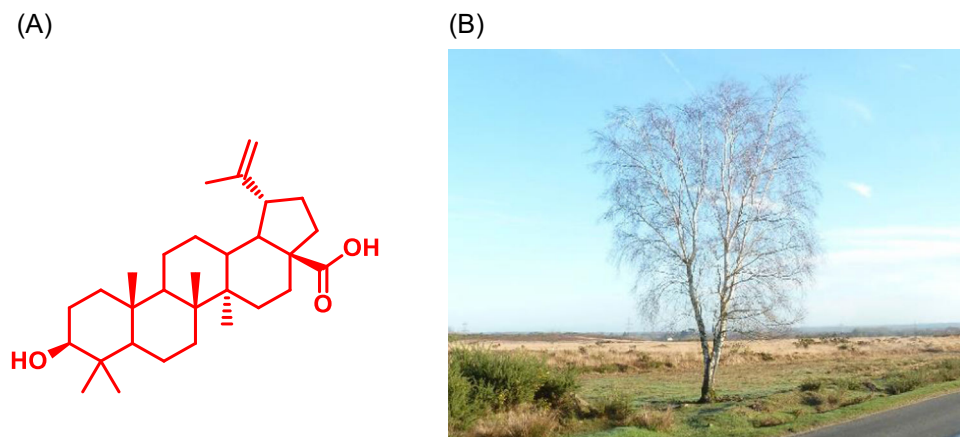


FIGURE 1 (A) Chemical structure of β -betulinic acid (3β -hydroxy-lup-20(29)-en-28-oic acid). (B) Source of betulinic acid, that is, *Betula pendula* (source: discoverlife.org).

2 | BOTANICAL SOURCES OF BA

BA is majorly isolated from the birch tree (*Betula* spp.), through the conventional processes of extraction, isolation, separation, and purification; and via semisynthesis from betulin. The birch tree (*Betula* spp.) from the Betulaceae family is a widely reported source for the isolation of BA. Other sources reported in the literature were from various species including *Alphitonia excelsa* (Rhamnaceae), *Artocarpus integrifolia* (Moraceae), *Dillenia indica* (Dilleniaceae), and *Zizyphus jujube* (Rhamnaceae).^[68,69]

3 | BIOLOGICAL ACTIVITIES OF BA

BA is one of the renowned plant triterpenoids which is shown to possess promising biological activities against various human diseases. It exhibits enormous pharmacological activities against cancer, diabetes, parasitic infections, viruses such as human immunodeficiency virus, and sepsis. BA also acts as an immunomodulatory and antinociceptive agent.^[70–75] Among these, the anticancer activity of BA is the most promising area of research due to its immense potential as a cytotoxic agent and its ease of availability, better selectivity, and low cost of production. The antitumor potential of BA was first disclosed by Pisha et al.,^[63] one of the researchers of the Illinois University of Chicago, in melanoma cancer via induction of apoptosis. Later, Fulda et al.^[76] introduced BA as a novel cytotoxic entity against malignant brain tumors. Numerous studies have also explored the anticancer potential of BA in various breast cancer cell lines through the modulation of multiple signaling pathways. Among them, the anticancer property of BA against MDA-MB231 and MCF-7 breast cancer cell lines was observed to be highly efficacious.^[64,77–85] BA also inhibited pulmonary metastases of breast cancer cells in 4T1 xenograft by inhibiting matrix metalloproteinases (MMPs).^[81] In addition, lactoferrin-attached BA nanoparticles were promptly delivered to triple-negative breast cancer and laryngeal cancer cell lines and inhibited cell growth and induced considerable cell death in MDA-MB-231 and HEP-2 cell lines.^[82] Moreover, BA induced anticancer activity against cervical cancer and rhabdomyosarcoma via induction of apoptosis and inhibition of cell proliferation.^[86,87] In vivo studies also showed that BA suppressed tumor growth in various animal models.^[86,88] In 2021, Wang et al.^[89] reported that BA induced apoptosis in gallbladder cancer cells by repressing stearoyl-CoA desaturase-1 enzyme. In addition, various studies have demonstrated the anticancer potential of BA in several cancer cell lines by inhibiting their proliferation and inducing apoptosis via the activation of caspases.^[66,87,89–103] BA also substantially decreased the viability and migratory potential of pancreatic ductal adenocarcinoma cell lines (Mia PaCa-2, SUI-2, and hTERT-HPNE) without impacting normal pancreatic cells.^[104] Additionally, Soica et al.^[99] reported the anticancer activity of BA complexed with gamma-cyclodextrin in the B164A5 murine melanoma cell line and was found to induce G0/G1 phase cell cycle arrest and suppress cell proliferation. Furthermore, Wang et al.^[100] reported that the efficacy of nanohybrid suspension

of BA in combination with paclitaxel in MCF-7 breast cancer cell line is through the induction of G0/G1 phase cell cycle arrest and inhibition of mitochondrial membrane potential ($\Delta\Psi_m$) and cell migration. Moreover, administration of BA encapsulated liposomes in SW480 colon cancer xenograft suppressed tumor growth and improved the survival outcome. The BA liposomal composition was also found to be bioavailable in this model.^[105] Various in vitro and in vivo studies of BA against various carcinomas are discussed in Table 1 and Table 2, respectively.

4 | MOLECULAR TARGETS OF BA

BA exhibits its anticancer potential by modulating multiple signaling pathways and its downstream targets associated with the different hallmarks of cancer (Figure 2). The most prominent and effectively characterized mechanism is the induction of apoptosis via the mitochondrial-dependent pathway.^[95,106] BA treatment was found to disrupt $\Delta\Psi_m$ and decrease B-cell lymphoma-2 (Bcl-2) and caused the release of cytochrome c (cyt c), the second mitochondrial activator of caspase (Smac), and apoptosis-inducing factor (AIF) into the cytoplasm. BA treatment also leads to the induction of caspases.^[92,114,135,138] Additionally, it was shown to induce apoptosis through suppression of nuclear factor- κ B (NF- κ B) and Janus kinase (JAK)/signal transducer and activator of transcription factor-3 (STAT-3) signaling.^[109] BA was also reported to enhance chemosensitization via glucose-regulated protein 78 mediated pathway.^[64] It suppressed transforming growth factor- β -induced cell growth and proliferation in the Mv1Lu mink lung cancer cell line by upregulating the nuclear translocation of p-Smad2.^[120] In addition to targeting the aforementioned proteins, BA also inhibited some specific targets like estrogen receptors and multidrug resistance proteins in breast cancer.^[142] Furthermore, BA also manifested several mechanistic trajectories including inhibition of vascular endothelial growth factor (VEGF), and STAT-3/hypoxia-inducible factor-1 (HIF-1)/VEGF signaling in hypoxic prostate cancer models^[137] (Figures 2 and 3).

4.1 | Inhibition of topoisomerases

Topoisomerases/DNA topoisomerases are the isomerase enzymes, which play a pivotal role in the topology of DNA during its replication, transcription, recombination, and chromosomal segregation during mitosis.^[143] On the basis of structure and mechanism of action, topoisomerases are broadly classified into two types, topoisomerase I and topoisomerase II. Topoisomerase I cleave only one strand of DNA via the breakage of the opposite strand, while topoisomerase II cleaves both the strands of DNA and is involved in regulating cell growth, proliferation, and apoptosis.^[144] Studies have shown the catalytic inhibition of both topoisomerases I and II by BA.^[145,146] This compound achieved the catalytic inhibition of topoisomerases I via blocking its interaction with oxidatively damaged DNA thereby promoting DNA fragmentation in prostate cancer.^[147] Furthermore,

TABLE 1 In vitro studies of BA against various cancers

Cancer type	Cell line (s)	Active concentrations	Mechanism of action	References				
Bladder cancer	T-24, UMUC-3, 5637	IC ₅₀ = 33.2 µg/ml (UMUC-3)	↑Apoptosis, ↑necrosis, ↓cyclin B1, ↓cyclin A, ↓Cdk2, ↓Cdc2, ↓Cdc25c, ↓MOMP, ↑cleaved PARP, ↑Bax, ↓migration, ↓invasion, ↓slug and snail (T24 and 5637), ↓MMP-9	[90]				
		IC ₅₀ = 28.5 µg/ml (5637)						
Brain tumor	Daoy, D283 Med, D341 Med, MHH1, MHH3, MHH4, MEB1, A172, U118MG, U138MG, U251MG, U343, U373, SK14, SK17, SK19, SK22, SK37, SK49, SK51, SK55, SK60	ED50 = 3 µg/ml (Daoy & D283), 7.5 µg/ml (D341), 9 µg/ml (MHH1), 10 µg/ml (MHH3), 4 µg/ml (MHH4), 15 µg/ml (MEB1), 8 µg/ml (A172), 5 µg/ml (U118), 9.5 µg/ml (U138), 5 µg/ml (U251), 5 µg/ml [343], 6 µg/ml (U373), 12 µg/ml (SK14), 11 µg/ml (SK17), 16 µg/ml (SK19), 8 µg/ml (SK22), 12 µg/ml (SK37), 9 µg/ml (SK49), 7 µg/ml (SK51), 6 µg/ml (SK55), 10 µg/ml (SK60) after 72 h	↑Apoptosis, ↑DNA fragmentation, ↑cyt c release, ↑caspases-3, -8, ↑PARP	[76]				
		U87MG, A172, P3, P5			↓Cell proliferation, ↑DNA damage, ↓Sp1, ↑PERK/CHOP signaling	[98]		
		Breast cancer			MDA-MB-231, MCF-7	IC ₅₀ ≤ 10 µM (24 h)	↓Cell proliferation, ↓migration ↓Cell proliferation, ↑apoptosis, ↓Sp1, ↓Sp3, ↓Sp4, ↑ZBTB10, ↓mRNA-27a, ↑G2/M phase arrest ↓Proliferation, ↑apoptosis ↓Proliferation, ↑apoptosis, ↓Bcl-2, ↓Sp1 ↑GRP78-mediated ER stress, ↑p-PERK, p, ↑CHOP, ↓Proliferation, ↑cytotoxicity ↑GRP78, ↓β-catenin, ↓c-Myc, ↓aerobic glycolysis ↑G0/G1 phase arrest, ↓migration, ↓ΔΨm ↑Apoptosis, ↓proliferation	[78]
						IC ₅₀ = 13.5 µg/ml (48 h)		[79]
						IC ₅₀ = 18.411 µM (MCF-7)		[77]
						IC ₅₀ = 20.465 µM (MDA-MB-231)		[84]
						IC ₅₀ = 2 µg/ml (MDA-MB-231)		[64]
						IC ₅₀ < 20 µM (MDA-MB-231)		[82]
						IC ₅₀ = 19.06 µM (MCF-7), IC ₅₀ = 48.55 µM (MDA-MB-231)		[85]
						IC ₅₀ = 66.75 ± 1.73 µM (24 h) IC ₅₀ = 39.75 ± 2.16 µM (36 h) IC ₅₀ = 30.42 ± 2.39 µM (48 h) IC ₅₀ = 39.83 µg/ml (24 h)		[100]
Cervical cancer	HeLa	IC ₅₀ = 66.75 ± 1.73 µM (24 h)	↑Apoptosis, ↑nuclear condensation, and fragmentation, ↑G0/G1 phase arrest, ↑caspase-3, ↑cleaved PARP, ↓MOMP, ↑ROS generation	[83]				
		IC ₅₀ = 39.75 ± 2.16 µM (36 h)		[87]				
Cervical cancer	SiHa (HPV16)	IC ₅₀ = 30.42 ± 2.39 µM (48 h)	↑Apoptosis, ↑nuclear condensation, and fragmentation, ↑G0/G1 phase arrest, ↑caspase-3, ↑cleaved PARP, ↓MOMP, ↑ROS generation	[92]				
		IC ₅₀ = 39.83 µg/ml (24 h)		[93]				
Cervical cancer	HeLa	IC ₅₀ = 30.42 ± 2.39 µM (48 h)	↓HIF-1α, ↓HIF target genes, ↓VEGF, ↓GLUT1, ↓PDK1, ↑β1, β2, and β5 activities of the proteasome	[93]				
		IC ₅₀ = 39.83 µg/ml (24 h)		[93]				

TABLE 1 (Continued)

Cancer type	Cell line (s)	Active concentrations	Mechanism of action	References
Colorectal cancer	SNU-C5/5FU-R (5-fluorouracil resistant), SNU-C5/IRT-R (irinotecan resistant), SNU-C5/OXT-R (oxaliplatin resistant)	IC ₃₀ = 6 µg/ml (FU) IC ₃₀ = 18 µg/ml (IRT) IC ₃₀ = 100 µg/ml (OXT)	↑Apoptosis, ↑caspase3 ↓Bcl-2	[106]
	RKO, SW480	≥5 µM (48 and 96h)	↓Cell growth, ↓Sp1, ↓Sp3, ↓Sp4, ↓survivin, ↓VEGF, ↓p65, ↓EGFR, ↓cyclin D1, ↑ROS generation, ↓mRNA-27a, ↓ZBTB10	[107]
	HCT116, SW480, HT-29	IC ₅₀ = 178 µM (HCT116, 48 h) IC ₅₀ = 58 µM (SW480, 48 h) IC ₅₀ = 125 µM (HT29, 48 h)	↑Apoptosis, ↑cleaved PARP, ↑p53, ↑AVOs, ↑LC-1 to LC-II, ↑LAMP, ↑autophagy, ↓p-AKT (S473), ↓mTOR (S2448), ↑p53	[108]
	HCT116, SW480, DLD-1	IC ₅₀ = 10 µg/ml (HCT116, 48 h) IC ₅₀ = 50 µg/ml (SW480, 48 h) IC ₅₀ = 40 µg/ml (DLD-1, 48 h)	↑Apoptosis, ↑Bax, ↑cleaved caspase-3, ↓Bcl-2, ↓ΔΨ _m , ↑ROS generation, ↓migration, ↓invasion, ↓MMP-2, ↓MMP-9, ↑TIMP-2	[95]
HT-29	IC ₅₀ = 10 µM (48 h)	↑Apoptosis, ↓p-JAK2, ↓p-STAT-3, ↓p-IKkα/β, ↓p-NF-κB p65, ↓p-IkBα, ↓c-Myc, ↓cyclin D1, ↓Bcl-xL, ↓NF-κB, ↓STAT-3	[109]	
Endometrial Adenocarcinoma	Ishikawa	5 and 10 µg/ml (24 h)	↓Collagen biosynthesis, ↓proliferase activity, ↓integrin-α ₁ and α ₂ , ↓HIF-1α, ↓VEGF	[110]
Gallbladder cancer	NOZ, OCUG, SGC-996, EHGB-1, GBC-5D	IC ₅₀ = 30 µM (72 h, NOZ)	↓Proliferation, ↑apoptosis, ↓SCD 1, ↓Cyt c, ↑cleaved caspases-3, -9, ↑cleaved PARP, ↑Bax, ↓Bcl-2	[89]
Gastric cancer	AGS	IC ₅₀ = 18.25 µg/ml (24 h) 15.86 µg/ml (36 h) 12.99 µg/ml (48 h)	↑Cell proliferation, ↓S phase population, ↑apoptosis, ↓Hiwi, ↓cyclin B1	[111]
	SNU-16, NCI-N87	-	↓Migration, ↓invasion, ↑apoptosis, ↓N-cadherin, ↑E-cadherin	[112]
Hepatocellular carcinoma	BGC-823, MINK45	IC ₅₀ < 30 µM (BGC-823, 48 h) IC ₅₀ < 25 µM (MINK45-7721, 48 h)	↓Migration, ↓cell proliferation, ↓invasion, ↓VASP, ↓NF-κB	[113]
	HepG2, LM3, MHCC97H	2.5–40 µM	↑Apoptosis, ↑nuclear fragmentation, ↓ΔΨ _m , ↓Bcl-2, ↑Bax, ↑cleaved caspase-3, ↑ROS generation, ↓MMP-2, ↓MMP-9, ↑TIMP2	[114]
HepG2, SMIMC-7721	HepG2, SMIMC-7721	IC ₅₀ = 24.8 µM (HepG2, 48 h) IC ₅₀ = 28.9 µM (SMIMC-7721, 48 h)	↑Bax, ↑cleaved caspase-3, ↓Bcl-2, ↑autophagy, ↑LC3B-II, ↑beclin-1, ↓p62, ↓PI3K/AKT/mTOR	[115]
	HUH7, PLC/PRF/5	BA (10 mM) and APO2 (30 ng/ml)	↑Apoptosis, ↑caspases-3, -8, -9, ↑cleaved caspase-3, ↑PARP cleavage, ↓Bcl-2, ↓Mcl-1, ↑p53	[116]
Kaposi's sarcoma	KS	IC ₅₀ = 8.4 µM	↑Cell death, ↓VEGF, ↑apoptosis	[117]

(Continues)

TABLE 1 (Continued)

Cancer type	Cell line (s)	Active concentrations	Mechanism of action	References
Laryngeal carcinoma	HEp-2	IC ₅₀ = 4 µg/ml	↓Cell-proliferation, ↑cytotoxicity, ↑sub-G1 phase arrest, ↑apoptosis	[82]
Leukemia	KG-1A, K562	IC ₅₀ = 10.16 µg/ml (KG-1A) IC ₅₀ = 13.93 µg/ml (K562)	↓ΔΨ _m , ↓caspases-3, -8, ↑ROS/TNF-α pathway	[118]
Lung cancer	A549, H1299	30 µM (36 h)	↓Sp1, ↓cyclin A2, ↑G2/M phase arrest	[119]
	Mv1Lu (Mink animal)	0.6-5 µg/ml	↑p-Smad2/3, ↑PAI-1, ↓TGF-β1-induced cell growth	[120]
	A549, H358, A427	1.3 µg/ml sorafenib and 3 µg/ml BA (Synergism)	↑Apoptosis, ↑CHOP, ↑Bax, ↓Bcl-2, ↓Bcl-xL, ↑caspases-8, -9	[121]
	H460	IC ₅₀ = 50 µM (48 h)	↑Apoptosis, ↓clonogenicity, ↑Bax, ↓Bcl-2, ↑Bax/Bcl-2 ratio, ↑G2/M phase arrest	[122]
	HCC827 and H1975	20 µM BA and 10 µM EGFR TKI	↑Apoptosis, ↑Bax, ↓Bcl-2, ↓survivin, ↑Bax/Bcl-2 ratio	[123]
	HKULC2, H1299, H23	1 µM (91%, 89%, and 86%, respectively, 72 h)	↑G1 phase arrest, ↓cell proliferation, ↓migration, ↑p21, ↑p53, ↓CD133, ↓ALDH, ↓Bcl-2, ↓Mcl-1, ↓c-Myc, ↓ABCG1	[124]
	A549, H358, NCI-H1703	10 µM	↑G1 phase arrest, ↓p21, ↓cyclin D1, ↓cyclin B1, ↓Bcl-2, ↑Bax, ↑Bad, ↑PARP, ↓clonogenicity, ↓p-GSK3β, ↓Wnt/β-catenin pathway, ↓HIF-1α, ↓p53	[125]
Lymphoma	CL-1, CLBL-1 (Canine cell lines)	IC ₅₀ = 23.50 µM (CL-1, 24 h) IC ₅₀ = 18.2 µM (CLBL-1, 24 h) IC ₅₀ = 18.59 µM (D-17)	↓Cell proliferation, ↑S phase arrest, ↑G0/G1 phase arrest	[91]
Melanoma	MEL-1, MEL-2, MEL-3, MEL-4	ED ₅₀ = 1.1 µg/ml (MEL-1) ED ₅₀ = 2.0 µg/ml (MEL-2) ED ₅₀ = 3.3 µg/ml (MEL-3) ED ₅₀ = 4.8 µg/ml (MEL-4)	↓Cell proliferation, ↑apoptosis	[63]
	MelDuWi, MelJless (equine melanoma cell lines), A375	IC ₅₀ = 33.1 µM (MelDuWi, 96 h) IC ₅₀ = 33.4 µM (MelJless, 96 h)	↑Sub-G1-phase arrest, ↑DNA-fragmentation, ↑apoptosis	[66]
	SK-MEL2	IC ₅₀ = 5 to 10 µM (SK-MEL2, 6 days)	↓Sp1, ↓Sp3, ↓Sp4	[126]
	NHEM-neo	IC ₅₀ = 4.6 µM (24 h)	↑Caspase-3, ↑cell death	[96]
	B164A5 (Murine cell line)	-	↓Cell proliferation, ↑G0/G1 phase arrest	[99]
	MelDuWi, eRGO1	IC ₅₀ = 23.6 µM (96 h, MelDuWi) IC ₅₀ = 12.7 µM (96 h, eRGO1)	↓Cell proliferation, ↑apoptosis	[102]

TABLE 1 (Continued)

Cancer type	Cell line (s)	Active concentrations	Mechanism of action	References
Multiple myeloma	KM3 cells	IC ₅₀ = 22.29 µg/ml (12 h) IC ₅₀ = 17.36 µg/ml (24 h) IC ₅₀ = 13.06 µg/ml (36 h)	↑Apoptosis, ↑caspase-3, ↑LC3-II, ↑P62, ↓beclin-1	[103]
	U266, RPMI 8226	IC ₅₀ ~30 µM (U266, 12 h) IC ₅₀ ~40 µM (RPMI 8226, 12 h)	↑Apoptosis, ↑Bax, ↑ cleaved caspases-3, -8, -9, ↑cleaved PARP, ↑cyt c, ↓Bcl-2, ↑ROS generation, ↓NF-κB, ↓p-NF-κB p65, ↓p-IKK/β, ↓p-IkBα, ↑S phase arrest, ↓cyclin A2, ↓Cdk2, ↑p21 ^{waf1/Cip1} , ↑p27 ^{Kip}	[127]
Nasopharyngeal carcinoma	CNE2	-	↑Apoptosis, ↑caspases, ↓Bcl-2, ↓Bcl-xL, ↑cyt c release	[97]
Oral cancer	KB	100 µM	↓Cell proliferation, ↑apoptosis, ↑Bax, ↓Bcl-2, ↑G0/G1 phase arrest, ↓cyclin D1, ↑ROS generation, ↑p53, ↑p-STAT-3	[128]
	CAL-27, Tca-83	IC ₅₀ = 10 µM (24 h)	↓Sp1, ↑PTEN, ↑radiosensitization	[129]
	SAS	IC ₅₀ = 4 µM (72 h)	↓Cell proliferation, ↓clonogenic potential, ↑apoptosis, ↓AKT, ↓p-AKT, ↓mTOR, ↓p-mTOR, ↓MMP-2	[60]
	SCC9, SCC25	8 µg/ml (72 h)	↑Apoptosis, ↑caspases, ↓Bax	[130]
Osteosarcoma	D-17 (canine cell lines)	IC ₅₀ = 18.59 µM	↓Cell proliferation, ↑S phase arrest	[91]
Ovarian cancer	A2780	IC ₅₀ = 44.47 µM (24 h)	↑Nuclear condensation, ↑apoptosis, ↑cleaved caspases-3, -8, -9, ↑Bax, ↓Bcl-2	[131]
Pancreatic cancer	AsPC-1, BxPC-3, capan-1	6 µM (59.8 ± 3.7% [AsPC-1], 24 h 42.2 ± 10.1% [BxPC-3], 24 h 59.7 ± 5.7% [Capan-1], 24 h)	↓Cell viability, ↓cell proliferation, ↑G2 phase arrest, ↑p21, ↓c-Myc, ↓cyclin D1, ↓P13K/AKT, ↓MAPK, ↓clonogenic activity	[132]
	Mia PaCa-2, SUIT-2, hTERT-HPNE	IC ₅₀ = 1.783 µM (Mia PaCa-2, 24 h) IC ₅₀ = 0.505 µM (SUIT-2, 24 h) IC ₅₀ = 5.689 µM (hTERT-HPNE, 24 h)	↓Cell viability, ↓migration, ↓NLR4, ↑APOA1, ↓POLRMT, ↓TACO1	[104]
	BxPC-3, PANC-1, FG	5-20 µM IC	↓Cell proliferation, ↓Sp1, ↓VEGF	[133]
	Mia PaCa-2, PANC-1	IC ₅₀ ~50 µM	↓Cell proliferation, ↓EMT, ↓ invasion, ↓migration, ↓Sox2, ↓Oct4, ↓Nanog, ↑AMPK	[134]
	PANC-1, SW1990	IC ₅₀ = 47 µM (PANC-1, 24 h) IC ₅₀ = 38 µM (SW1990, 24 h)	↓Cell proliferation, ↓invasion, ↓migration, ↑apoptosis, ↑cleaved caspases-3, -8, ↑Bax, ↓Bcl-2, ↓p-mTOR, ↑p-AMPK, ↑autophagy	[135]

(Continues)

TABLE 1 (Continued)

Cancer type	Cell line (s)	Active concentrations	Mechanism of action	References
Prostate cancer	LNCaP	IC ₅₀ = 1–5 μM (LNCaP, 6 days)	↓Sp1, ↓Sp3, ↓Sp4, ↓VEGF, ↓survivin, ↑PARP cleavage, ↑DNA laddering, ↓AR, ↓cyclin D1	[126]
	PC-3	–	↑Apoptosis, ↓NF-κB, ↓p-IκBα, ↓IKKα, ↑PARP cleavage	[136]
	PC-3	25 μM (60%)	↓HIF-1α, ↓p-STAT-3, ↓STAT-3, ↓VEGF	[137]
	LNCaP, DU145, PC3	10 μM (72 h)	↑Apoptosis, ↑cyt c, ↑Smac, ↑AIF, ↑G1/S phase arrest, ↓cyclin A, ↓cyclin B1, ↓cyclin D1, ↓Cdk1, ↓Cdk2, ↓Cdk4, ↓E2F1, ↓Rb, ↑cleaved PARP, ↓AKT, ↓Mcl-1, ↓multiple DUBs, ↓survivin, ↑p27	[138]
	LNCaP, DU145	IC ₅₀ = 38 μM (24 h) IC ₅₀ = 15 μM (48 h)	↑G0/G1 phase arrest, ↑p21/Waf1, ↑Bax, ↓Bcl-2, ↑cyt c release, ↑cleaved caspases-3, -9, ↑cleaved PARP, ↓p-IKKα, ↓IκBα, ↓NF-κB	[139]
Renal cancer	786-O, ACHN	–	↑Apoptosis, ↑Bax, ↓Bcl-2, ↓ΔΨ _m , ↑ROS, ↑MMP-2, ↑MMP-9, ↑Vimentin, ↓TIMP-2, ↑E-cadherin	[88]
Rhabdomyosarcoma	RH-30, RMS-13, RD	IC ₅₀ = 5 μg/ml (RH-30, 72 h) IC ₅₀ = 3.9 μg/ml (RMS-13, 72 h) IC ₅₀ = 9.5 μg/ml (RD, 72 h)	↑Apoptosis, ↓GLI1, ↓GLI2, ↓PTCH1, ↓IGF2	[86]

Abbreviations: AKT, protein kinase B; ALDH, aldehyde dehydrogenases; AMPK, AMP-activated protein kinase; BA, betulinic acid; Bax, Bcl-2-associated X protein; Bcl-xL, B-cell lymphoma-extra large; Cdc 2, cell division cycle 2; Cdk2, cyclin-dependent kinase 2; CHOP, C/EBP homologous protein; cyt c, cytochrome c; EGFR, estimated glomerular filtration rate; EMT, epithelial-to-mesenchymal transition; ER, estrogen receptor; GLUT1, glucose transporter 1; GRP78, glucose-regulated protein 78; HIF-1α, hypoxia-inducible factor-1α; IC₅₀, half-maximal inhibitory concentration; IKKα, IκB kinase α; LAMP, loop-mediated isothermal amplification; MAPK, mitogen-activated protein kinase; MMP, matrix metalloproteinase; ΔΨ_m, mitochondrial membrane potential; mRNA, messenger RNA; mTOR, mammalian target of rapamycin; NF-κB, nuclear factor-κB; NLRP4, NLR family CARD domain-containing protein 4; PARP, poly-ADP-ribose polymerase; PERK, protein kinase R (PKR)-like endoplasmic reticulum kinase; PI3K, phosphatidylinositol 3-kinase; p-AKT, phospho-AKT; p-IKKα/β, phospho-IKKα/β; p-JAK2, phospho-Janus kinase 2; p-mTOR, phosphorylated-mTOR; p-STAT-3, phosphorylated-STAT-3; ROS, reactive oxygen species; SCD-1, stearyl-CoA desaturase 1; Smac, second mitochondria-derived activator of caspases; STAT-3, signal transducer and activator of transcription 3; TIMP-2, tissue inhibitor of metalloproteinases-2; TNF-α, tumor necrosis factor-α; VASP, vasodilator-stimulated phosphoprotein; VEGF, vascular endothelial growth factor; ZBTB-10, zinc finger and BTB domain containing 10.

TABLE 2 In vivo treatments of BA against various cancers

Cancer type	Animal model	Dose/administration	Key outcomes	Refs.
Breast cancer	MDA-MB-231 induced xenograft	Daily intraperitoneal administration of 20 mg/kg/day for 21 days	↓Tumor size, ↓tumor weight, ↑ZBTB10, ↓Sp1, ↓Sp3, ↓Sp4, ↓VEGF, ↓survivin, ↓β2-microglobulin	[79]
	MCF-7 induced xenograft	Daily intraperitoneal administration of 50 and 100 mg/kg (six doses given at 3–4 days intervals)	↓Tumor formation, ↓tumor size, ↓angiogenesis, ↓proliferation, ↓invasion	[77]
	MDA-MB-231 induced xenograft	Daily intraperitoneal administration of 250 mg/kg BA	↑Apoptosis, ↓Ki-67, ↑GRP78, ↑CHOP	[64]
	4T1 induced xenograft	Daily intraperitoneal administration of 10 mg/kg for 21 days	↓Tumor growth, ↓Tumor weight, ↓Ki-67, ↓MMP-2, ↓MMP-9, ↓p-STAT 3, ↓metastasis, ↓MDSCs	[81]
	MDA-MB-231 induced xenograft	Intraperitoneal administration of 250 mg/kg	↓Colony formation, ↓MMP-2, ↓MMP-9, ↓EMT, ↑GRP78, ↓metastasis	[85]
Colorectal cancer	MMTV-PyVT ± mice, MCF-7-Dll xenograft	Intraperitoneal administration of BA 250 mg/kg, q2d	↓Tumor growth, ↓glycolytic activity, ↓cell proliferation, ↑apoptosis, ↑Cav-1	[83]
	SW480 induced xenograft	Intravenous administration of 200 μl of 5 mg/ml BA liposomes three times per week for 3 months	↓Tumor volume, ↑mice survival	[105]
	RKO induced xenograft	Intraperitoneal administration of 25 mg/kg/day every second day for 22 days	↓Tumor volume, ↓tumor growth, ↓tumor weight, ↓Sp1, ↓Sp3, ↓Sp4	[107]
	HCT116 induced xenograft	Daily intraperitoneal administration of 10 and 20 mg/kg for 21 days	↓Tumor growth, ↓MMP-2, ↓Ki-67+, ↑cleaved caspase-3	[95]
	NOZ-induced xenograft	Intraperitoneal administration of 10 and 30 mg/kg/day for 28 days	↓Tumor size, ↓SCD1, ↓PCNA	[89]
Gastric cancer	SNU-16 induced xenograft	Daily intraperitoneal administration of 40 mg/kg for 21 days	↓Metastasis, ↓Ki-67, ↓MMP-2	[112]
	TMZ-resistant U87MG cells induced xenograft	Intraperitoneal administration of 25 mg/kg three times a week for 1 month	↓Tumor growth, ↑survival, ↓Sp1, ↑PERK/CHOP signaling pathway	[98]
Hepatocellular carcinoma	HepG2 induced xenograft	Daily intraperitoneal administration of 5 and 10 mg/kg for 18 days	↓Tumor growth, ↓Ki-67, ↓MMP-2	[114]
	HUH7 induced xenograft	Intraperitoneal administration of the combined dose of 20 mg/kg BA with 100 μg APO2 every 2 days for 21 days	↓Tumor growth, ↑p53	[116]
Lung cancer	A549 induced xenograft	Intravenous administration of 200 μl of 5 mg/ml BA liposomes three times per week for 3 months	↓Tumor growth, ↑survival	[105]
	H1299 induced xenograft	Intraperitoneal administration of 10 mg/kg once every 3 days for 4 weeks	↓Tumor growth	[119]
Melanoma	MEL-2 induced xenograft	Intraperitoneal administration of 50, 250, and 500 mg/kg, every fourth day for 41 days	↓Tumor growth	[63]
	B16F10 induced xenograft	Daily intraperitoneal administration of the combined dose of 10 mg/kg/day BA	↓Lung metastasis	[140]

(Continues)

TABLE 2 (Continued)

Cancer type	Animal model	Dose/administration	Key outcomes	Refs.
Multiple Myeloma	U266 induced xenograft	Intraperitoneal administration of 20 mg/kg at 3-days intervals	↓Tumor volume, ↓tumor growth, ↓NF-κB p65	[127]
Oral cancer	KB induced xenograft	Intraperitoneal administration of 50–150 mg/kg for 3 weeks	↓Tumor volume, ↑p53, ↓p-STAT-3	[128]
Ovarian cancer	SKOV3 induced xenograft	Daily intraperitoneal administration of 40 mg/kg once in a day for 20 days	↓Tumor size, ↓tumor growth, ↓Ki-67, ↓MMP-2, ↓migration	[141]
Pancreatic cancer	FG and PANC-1 induced xenograft	Intraperitoneal administration of 10 mg/kg of BA along with 0.05 mg/kg three times a week	↓Sp1, ↓tumor MVDs, ↓angiogenesis, ↓VEGF, ↓tumor growth	[133]
	PANC-1 induced xenograft	Intragastric administration of 40 mg/kg/d for 30 days	↓Tumor volume, ↓tumor weight, ↓tumor growth	[135]
Prostate cancer	LNCaP induced xenograft	Intragastric administration of 10 and 20 mg/kg/d	↓Tumor growth, ↓tumor weight, ↓mitotic activity, ↓epithelial atypia, ↑necrosis, ↓Sp, ↓VEGF	[126]
	TRAMP transgenic mice	Intragastric administration of 5 and 10 mg/kg 11 times for 14 days	↓Primary tumors, ↑apoptosis, ↓angiogenesis, ↓proliferation, ↓androgen receptor, ↓cyclin D1	[138]
Renal cancer	786-O induced xenograft	Intragastric administration of 5 and 10 mg/kg once daily for 15 days	↓Tumor growth, ↓Ki-67, ↓MMP-9	[88]
Rhabdomyosarcoma	RMS-13 induced xenograft	Intraperitoneal administration of 40 mg/kg every second day for 16 days	↓Tumor volume, ↓tumor growth, ↓apoptosis, ↓hedgehog signaling	[86]

Abbreviations: AKT, protein kinase B; BA, betulinic acid; CHOP, C/EBP homologous protein; Dil, 1,1'-dioctadecyl-3,3,3',3'-tetramethylindocarbocyanine perchlorate; EMT, epithelial-to-mesenchymal transition; GRP78, glucose-regulated protein 78; MDSCs, myeloid-derived suppressor cells; MMP, matrix metalloproteinase; MVD, microvessel density; NF-κB, nuclear factor-κB; PCNA, proliferating cell nuclear antigen; PERK, protein kinase R (PKR)-like endoplasmic reticulum kinase; p-STAT-3, phosphorylated-signal transducer and activator of transcription 3; q2d, every 2 days; SCD-1, stearoyl-CoA desaturase 1; TGF-β1, transforming growth factor-β1; TMZ, temozolomide; VEGF, vascular endothelial growth factor; ZBTB-10, zinc finger and BTB domain containing 10.

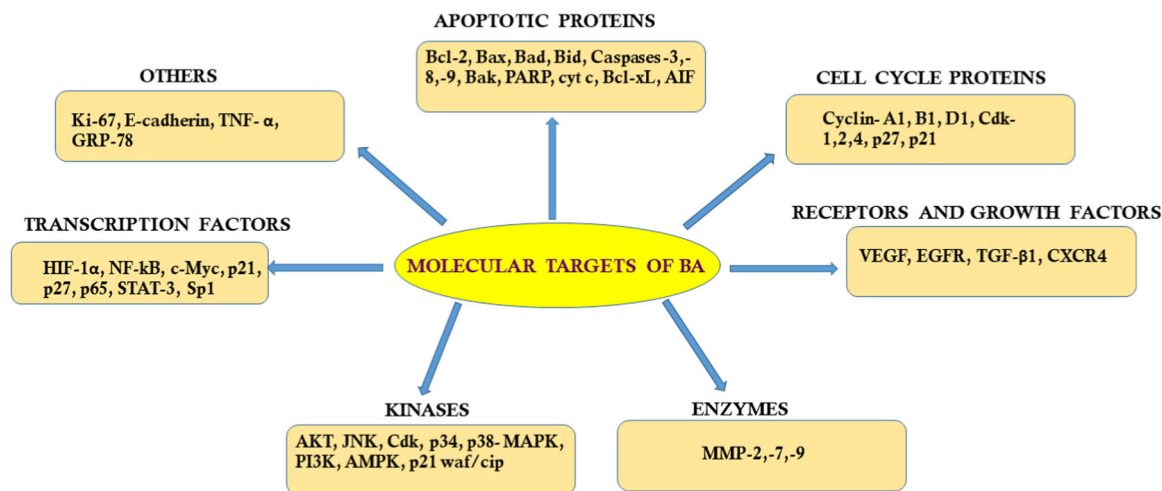


FIGURE 2 Molecular targets of BA. AKT, protein kinase B; AMPK, AMP-activated protein kinase; BA, betulinic acid; Cdk, cyclin-dependent kinase; EGFR, estimated glomerular filtration rate; HIF-1 α , hypoxia-inducible factor-1 α ; JAK, Janus kinase; MAPK, mitogen-activated protein kinases; MMP, matrix metalloproteinase; mTOR, mammalian target of rapamycin; NF- κ B, nuclear factor- κ B; PARP, poly-ADP-ribose polymerase; PI3K, phosphatidylinositol 3-kinase; STAT-3, signal transducer and activator of transcription 3; TGF- β 1, transforming growth factor- β 1; TNF- α , tumor necrosis factor- α ; VEGF, vascular endothelial growth factor.

a halo derivative of BA, 2 α -bromo-dihydrobetulonic acid, acts as a reversible catalytic inhibitor of topoisomerase II α by inhibiting its DNA binding activity in cervical cancer.^[148] BA was also shown to induce cell cycle arrest and apoptosis in MDA-MB-231 breast cancer cells by suppressing topoisomerase I and II.^[149] In addition, BA suppressed aphidicolin induced DNA breakage within RET oncogene, an event of carcinogenic rearrangements found in thyroid cancer, in HTori thyroid epithelial cells.^[150]

4.2 | Mitochondria-mediated apoptosis induction

Apoptosis, also known as programmed cell death, is a genetically regulated process that plays a prominent role in embryonic development and maintenance of tissue homeostasis in multicellular organisms.^[151,152] It removes abnormal, mutated, and damaged cells from the body, and maintains a balance between the death and survival of tissues and cells.^[151,153] The cancer cells have the potential to suppress the apoptotic pathways, thereby increasing their survival, proliferation, migration, and invasion, and finally leading to carcinogenesis. Multiple lines of evidence have shown the efficacy of BA in inducing apoptotic cell death in many cancers.^[87,92,111,114,131,141,154] For example, BA-induced apoptosis in breast, colon, lung, pancreatic, and prostate cancers through the modulation of various proteins such as Bcl-2-associated X protein (Bax), Bcl-2, B-cell lymphoma-extra large (Bcl-xL), poly-ADP-ribose polymerase (PARP), and caspases.^[105,119,133–140] Further, Damle and his group demonstrated the treatment of MCF-7 xenograft mice with BA-induced apoptosis and decreased tumor growth.^[77] Moreover, BA was shown to induce apoptosis in liver cancer, gastric cancer, Kaposi's sarcoma (KS), and leukemia via regulation of $\Delta\Psi_m$ and various molecules such as Bcl-2, Bax, Mcl-1, caspases, reactive

oxygen species (ROS), MMPs, tissue inhibitors of metalloproteinases (TIMP), and p53.^[112–118] Similarly, a study in 2002 by Thurnher et al.^[130] reported that BA-induced apoptosis in head and neck cancer cell lines (SCC9 and SCC25) by elevating the caspases and decreasing Bax expression. Studies have shown that BA could pass through the mitochondrial membrane due to its extreme solubility in lipids and act directly on this organelle.^[85,108] It could decrease $\Delta\Psi_m$, consequently increasing the outer membrane permeability, ROS generation, and downregulation of Bcl-2 family proteins in different cancer cell lines.^[90,92,95,100,114,118] In addition, BA-induced cell cycle arrest and caspase-mediated cell death in T-24, UMUC-3, and 5637 human bladder cell lines via $\Delta\Psi_m$ loss and activation of intrinsic mitochondrial pathway.^[90] This compound also caused caspase-independent apoptosis and cell death in SiHa cervical cell line through nuclear condensation and fragmentation, ROS generation, and mitochondrial membrane disruption.^[92] Moreover, Zeng et al.^[95] reported that BA-induced apoptosis in HCT116, SW480, and DLD-1 human colorectal cancer cell lines through the upregulation of Bax and caspase-3 and repression of Bcl-2, $\Delta\Psi_m$, and ROS generation. BA also induced the expression of proapoptotic proteins like caspases, and Bax, thereby successively killing CNE2 NPC cells.^[97] Furthermore, BA was found to induce apoptosis via the Bcl-2/Bax signaling pathway in lung cancer.^[122,124,125] Moreover, the combined treatment of BA with sorafenib induced cell death in A549, H358, and A427 NSCLC cell lines through the upregulation of C/EBP homologous protein (CHOP), Bax, and caspases and suppression of Bcl-2 and Bcl-xL.^[121] Besides, combination therapy of BA and betulin demonstrated proapoptotic activity against canine T-cell/B-cell lymphomas and canine osteosarcoma.^[91] BA also induced the release of Cyt c, AIF, and Smac from mitochondria to the cytosol which further leads to the activation of caspase-9, caspase-3, and PARP resulting in apoptosis.^[127,138]

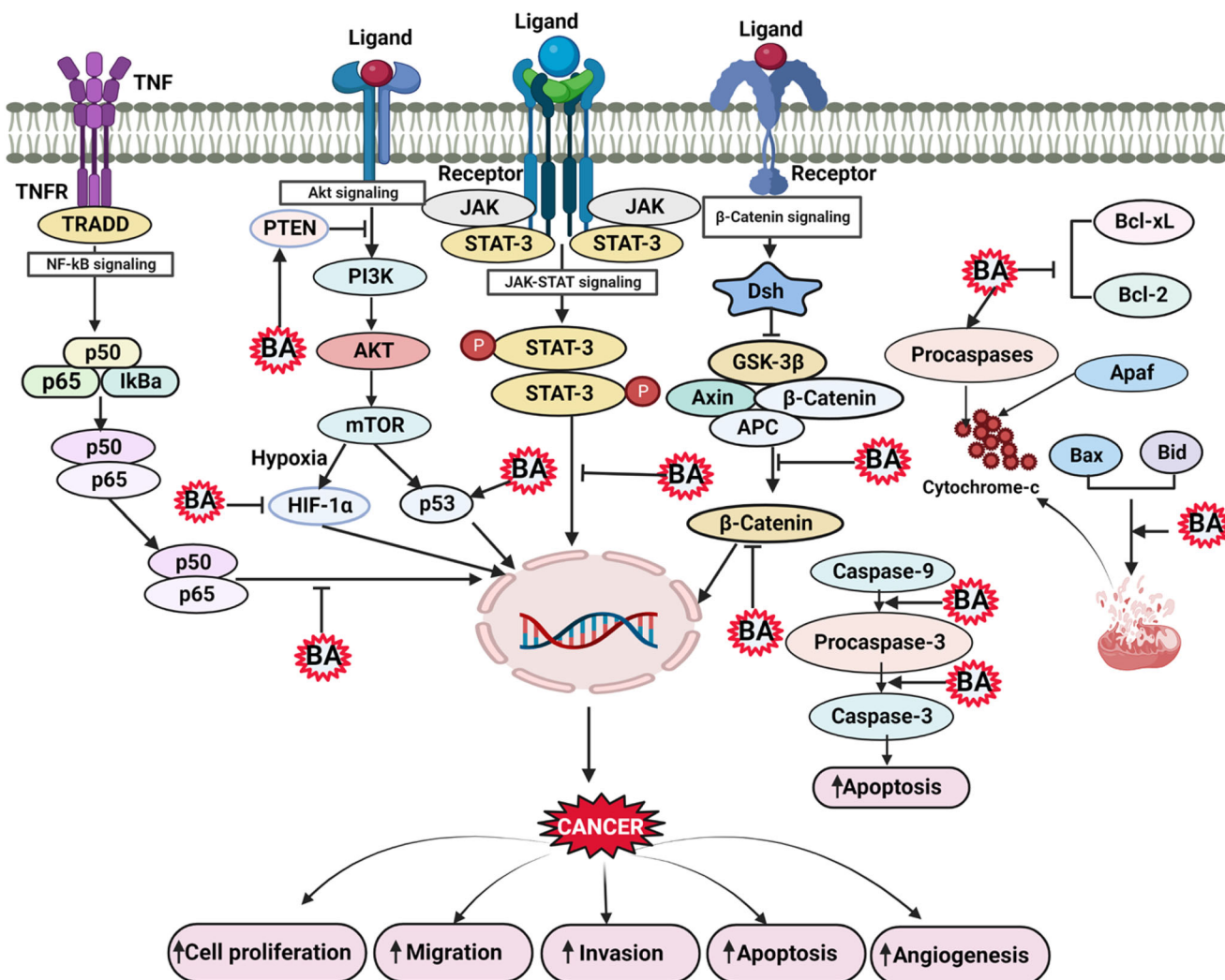


FIGURE 3 Role of BA in multiple signaling pathways involved in the regulation of cancer. AKT, protein kinase B; BA, betulinic acid; HIF-1 α , hypoxia-inducible factor-1 α ; JAK, Janus kinase; mTOR, mammalian target of rapamycin; NF- κ B, nuclear factor- κ B; PI3K, phosphatidylinositol 3-kinase; PTEN, phosphatase and tensin homolog; STAT-3, signal transducer and activator of transcription 3; TNF, tumor necrosis factor; TNFR, tumor necrosis factor receptor.

In addition, BA induced G2/M phase cell cycle arrest and apoptosis in gastric adenocarcinoma cells via the suppression of Hiwi and cyclin B1.^[111] Further, a study by Kim et al.,^[90] showed that BA induced apoptosis in T-24, UMC-3, and 5637 human bladder cancer cell lines by causing cell cycle arrest and cell death via the caspase-dependent mitochondrial apoptotic pathway. Additionally, BA treatment was also shown to activate caspases in brain tumor cell lines by regulating the mitochondrial-dependent apoptotic pathway.^[76] It has also been reported that BA induced apoptosis and inhibited cell viability and proliferation in HepG2, LM3, and MHCC97H HCC cell lines via upregulation of Bax and caspases, and downregulation of Bcl-2 family proteins.^[114] Furthermore, BA induced caspase-dependent apoptosis in ovarian cancer through the activation of caspases-3, -8, and -9, thereby suggesting the involvement of both mitochondria-mediated intrinsic and extrinsic apoptotic pathways.^[131,141] The putative role of BA in inducing apoptosis

was also explored in the KB oral squamous cell carcinoma (OSCC) cell line.^[128] For instance, it was shown that BA induced cell cycle arrest and mitochondrial apoptosis by enhancing the expression of caspases-3, -9, p53, and Bax, and by decreasing the expression of Bcl-2 in this cell line. The same study also reported high ROS generation with BA treatment in these cells.^[128] Thus, BA possesses high potential in inducing apoptosis in various cancer cell lines through the modulation of various molecules associated with the intrinsic and extrinsic apoptotic pathways.

4.3 | Inhibition of VEGF receptor

VEGF is identified as an angiogenesis factor that is specific to the receptors (VEGFR) on the vascular endothelial cells.^[155,156] It is a cascade process that deals with the uncontrolled proliferation of

blood vessels from a pre-existing endothelium and act as a crucial marker in various human disorders, predominantly cancer.^[157,158] Previous studies have reported that VEGF is highly expressed in various malignancies and is known to induce cell proliferation, angiogenesis, migration, and invasion.^[93,133,159] Interestingly, in a recent study, Kim et al.^[93] reported the downregulation of hypoxia-induced HIF-1 α and its targeted genes such as VEGF, glucose transporter 1, and protein 3-phosphoinositide-dependent protein kinase-1 in the HeLa cervical cancer cell line treated with BA. In addition, BA was shown to induce antiangiogenic effect by suppressing VEGF and HIF-1 α in human Ishikawa endometrial adenocarcinoma cells.^[110] Further, in breast cancer, BA inhibited the expression of Sp-regulated VEGF and its receptor, VEGFR, and Sp proteins thereby suppressing cell proliferation and tumor growth in *in vitro* and *in vivo* models, respectively.^[79] In addition, BA was shown to decrease the expression of VEGF, survivin, and Sp regulated genes such as Sp1 transcription factors (Sp1, Sp3 and Sp4), in RKO and SW480 colon cancer cell lines which leads to repression of cell proliferation. *In vivo* study also showed a reduction of tumor growth in SW480 xenograft mice which improved their survival.^[107] Further, a study by Martucciello et al.^[117] demonstrated that BA suppressed cell proliferation in KS cells via VEGF regulation. BA was also shown to induce antiangiogenic responses in prostate cancer, by decreasing the levels of Sp-regulated VEGF and survivin.^[126] Furthermore, a combination of BA and mithramycin A was shown to downregulate the expression of VEGF and Sp1 proteins in pancreatic cancer which resulted in suppression of cell proliferation, angiogenesis, and invasion of pancreatic cancer cells.^[133]

4.4 | Inhibition of STAT-3 activation cascade

STAT-3 is a member of the family of STAT proteins which are activated by cytokines, growth factors, and other polypeptidic ligands. They act as transcriptional activators and modulate the action of major downstream proteins in the cell nuclei after phosphorylation.^[109,160] One of the studies has shown that BA could downregulate the activation of STAT-3 and suppress STAT-3 regulated gene products such as Bcl-xL, Bcl-2, cyclin D1 and survivin, leading to cell death in multiple myeloma.^[160] Further, treatment of BA increased the expression of phosphorylated-STAT-3 (p-STAT-3) via the ROS/p53 signaling pathway in KB OSCC cell lines.^[128] Furthermore, Shin et al.^[137] demonstrated that BA inhibited hypoxia-mediated p-STAT-3 in androgen-independent PC-3 prostate cancer cell line. BA could also induce apoptosis in colorectal cancer via the inhibition of proliferation in HT-29 cells by suppressing the STAT-3 signaling pathway.^[109]

4.5 | Inhibition of NF- κ B signaling

NF- κ B is a transcription factor responsible for modulating a wide range of molecular and cellular processes such as cell survival,

DNA transcription, and cytokine production. It is normally located in the cytosol as a complex with the inhibitory protein I κ B α in an inactive state.^[7,139] Most cancers are associated with the over-expression of NF- κ B. Studies have shown that BA targets different signaling pathways including NF- κ B in colorectal cancer, gastric cancer, and multiple myeloma.^[113,127] It also exhibited substantial dose-dependent cytotoxicity in cancer cells by inhibiting proliferation and causing apoptosis via suppressing the NF- κ B and hedgehog signaling.^[86,113,127] Another study by Gupta et al.^[136] demonstrated that the treatment of human prostate cancer cell line, PC-3, with BA effectively inhibited phosphorylated-NF- κ B. Additionally, BA was shown to induce apoptosis and inhibit cell proliferation and migration of SNU-16 and NCI-N87 gastric cancer cell lines by targeting the NF- κ B signaling pathway.^[112] Besides, BA induced apoptosis and suppressed proliferation in colorectal cancer via inhibition of the NF- κ B signaling pathway.^[109]

4.6 | Induction of autophagy

Autophagy is a natural process of removing unnecessary or dysfunctional components of the cells for maintaining degradation and recycling of cellular components.^[108] Accumulating studies have shown the ability of BA in regulating autophagy and its associated proteins. In line with this, BA was found to induce autophagy in colorectal cancer via inhibition of the protein kinase B/mammalian target of rapamycin (AKT/mTOR) signaling pathway.^[108] In addition, BA inhibited hepatocellular carcinoma and pancreatic cancer by targeting autophagy and apoptotic processes through suppression of the phosphatidylinositol 3-kinase (PI3K)/AKT/mTOR signaling pathway.^[115,135]

4.7 | Effect of BA on Sp transcription factors

Sp1 is the first transcription factor that functions as a transcriptional activator of various genes, including housekeeping genes, cell cycle regulators, and tissue-restricted genes.^[107,161] Sp1 constitutively regulates the expressions of the multiple genes both in normal and tumor cells. It is mostly overexpressed in many types of cancer and is linked to poor prognosis.^[161] Therefore, the suppression of these transcription factors has high potential in the management of cancer. In accordance with this, several studies have reported that BA inhibited the expressions of Sp transcription factors in different cancers.^[98,107,129] BA treatment was shown to induce antitumor activity against the H1299 lung cancer cell line and xenograft by causing degradation of the Sp1 transcription factor.^[119] In addition, this compound suppressed the proliferation of MCF-7, and MDA-MB-231 breast cancer cell lines by modulating Sp1.^[84] Further, a study have also shown that BA-induced chemosensitization in glioblastoma cells via repression of Sp1 and activation of protein kinase R (PKR)-like endoplasmic reticulum kinase/CHOP mechanism.^[98] Furthermore, BA enhanced radiosensitization

in OSCC cells by inducing phosphatase and tensin homolog and Sp1 SUMOylation.^[129] Thus, all the abovementioned findings reveal the prominent role of BA in modulating Sp transcription factors which might be a promising strategy in the management of cancer.

4.8 | Effect of BA on cell cycle proteins

The cell cycle or cell-division cycle is a series of processes that includes DNA replication, partitioning of cytoplasm, and cell division to generate two new daughter cells. Cyclins and cyclin-dependent kinases (Cdks) are the groups of proteins that regulate cell cycle progression through their association in different phases of the cycle.^[162,163] These proteins are highly deregulated in different cancers, therefore the agents targeting these proteins have high potential in the treatment of these diseases.^[163] In line with this, studies have shown the potential of BA in modulating the cell cycle proteins. For instance, BA was shown to downregulate cyclin D1 and induce G2 phase cell cycle arrest in pancreatic ductal adenocarcinoma.^[132] Recently, Yung et al. reported the potential of BA in inhibiting bladder cancer via cell cycle arrest, necrosis, and apoptosis.^[90] BA also substantially decreased the expressions of cell cycle proteins such as cyclin B1, cyclin A, Cdk 2, cell division cycle (Cdc)2, and Cdc25c in bladder cancer.^[90]

5 | PHARMACOKINETICS AND BIOAVAILABILITY OF BA

Pharmacokinetics is essential to understand the movement and distribution of a drug in the body. It helps in determining the absorption and bioavailability of a drug in the biological system.^[164] Previous studies have reported the pharmacokinetics of BA in different experimental settings. For example, Udeani et al.^[165] reported the pharmacokinetics and tissue distribution of BA in CD-1 mice using a two-compartment, first-order pharmacokinetics modeling, in which they identified the peak serum concentration of BA after intraperitoneal administration of 250 or 500 mg/kg doses at 0.146 and 0.228 h, respectively. These administered doses (250 or 500 mg/kg) of BA exhibited distribution volumes of 106 and 108 L/kg with half-lives of 11.5 and 11.8 h, respectively. Intraperitoneal administration of 500 mg/kg BA showed the highest distribution in the fat tissues with 2260 µg/g while the least distributed concentrations were observed in the liver (223.9 µg/g) and kidney (95.8 µg/g) after 24 h.^[165] Another study by Shin et al.^[166] reported that the intraperitoneal administration of a 500 mg/kg dose of BA analysed through liquid chromatography-electrospray ionization mass spectrometry in the melanoma model had the highest concentration at the tumor site (452.2 ± 261.2 µg/g) followed by liver (223.9 ± 80.3 µg/g). Lack of aqueous solubility is one of the major challenges associated with BA, which provides golden opportunities for investigating various formulation techniques to improve its

bioavailability. In this regard, polyvinyl pyrrolidone-BA complex, spray-dried mucoadhesive microparticles, phospholipids nanosome formats, and synthetic modifications are some of the relevant preparation techniques used to overcome the aforementioned drawbacks.^[167-169] Further, liposomes, transdermal applications, nanoemulsions, and slow-release materials are some of the emerging carriers to improve the selectivity, activity, and pharmacokinetics properties of BA without altering its anticancer potential.

6 | CONCLUSION AND FUTURE PERSPECTIVES

Despite the significant advancement in the field of diagnosis and treatment modalities for cancer, it is one of the life-threatening diseases with a significant rate of morbidity and mortality around the globe. High expense, nontargeted action, toxicity to normal cells, and inefficacy still troubles the potency of the currently existing drugs. Extensive research is being carried out globally to develop nature-based therapeutic drugs that are safe, cost-effective, and nontoxic for the treatment of cancer. The phytomolecule BA is one such potential candidate, established as an efficacious chemopreventive and chemotherapeutic agent against various human cancers. The present review summarizes the botanical sources and putative mechanisms of action of BA against various cancers such as the modulation of multiple signaling pathways such as PI3K/AKT/mTOR, NF-κB, JAK/STAT, HIF-1, and hedgehog. BA also modulated the expression of many proteins such as p53, cyclins, Cdks, VEGF, Bcl-2, Bcl-xL, Bax, Bid, MMPs, TIMPs, and Sp. It was also shown to inhibit oxidative stress in different cancers through the modulation of ROS generation. Pharmacokinetics studies have suggested that BA is highly distributed in the fat tissues and the intraperitoneal administration of BA at a dose of 500 mg/kg BA was shown to have a half-life of 11.8 h. However, limited aqueous solubility and poor bioavailability are the major limitations associated with this drug. Nonetheless, these limitations could be managed by structural modifications, combination treatments with other drugs, and different formulations, and complexes. Thus, improving the potency, selectivity, as well as pharmacokinetics properties of BA would help us to develop a potential drug for the prevention and treatment of cancer.

ACKNOWLEDGMENTS

Academy of Scientific and Innovative Research PhD student Maniyamma Aswathy would like to thank CSIR for the research fellowship. The author Uzini D. Daimary would like to thank the Prime Minister's Research Fellowship program, Ministry of Education, Government, of India for providing her with the fellowship.

DATA AVAILABILITY STATEMENT

Data sharing is not applicable to this article as no new data were generated, and the article describes entirely theoretical research.

ORCID

Ajaikumar B. Kunnumakkara  <https://orcid.org/0000-0001-9121-6816>

REFERENCES

- [1] B. Shabnam, G. Padmavathi, K. Banik, S. Girisa, J. Monisha, G. Sethi, L. Fan, L. Wang, X. Mao, A. B. Kunnumakkara, *Transl. Oncol.* **2018**, *11*(6), 1379. <https://doi.org/10.1016/j.tranon.2018.08.015>
- [2] D. Hanahan, R. A. Weinberg, *Cell* **2011**, *144*(5), 646.
- [3] A. B. Kunnumakkara, D. Bordoloi, B. L. Sailo, N. K. Roy, K. K. Thakur, K. Banik, M. Shakibaei, S. C. Gupta, B. B. Aggarwal, *Exp. Biol. Med.* **2019**, *244*(8), 663. <https://doi.org/10.1177/1535370219839163>
- [4] M. Huang, J.-J. Lu, M.-Q. Huang, J.-L. Bao, X.-P. Chen, Y.-T. Wang, *Expert Opin. Investig. Drugs* **2012**, *21*(12), 1801.
- [5] C. Rivera, *J. Oral Res.* **2015**, *4*(1), 8.
- [6] B. Goyal, S. R. M. Yadav, N. Awasthee, S. Gupta, A. B. Kunnumakkara, S. C. Gupta, *Biochim. Biophys. Acta Rev. Cancer* **2021**, *1875*(2), 188502.
- [7] C. Buhrmann, B. Popper, A. B. Kunnumakkara, B. B. Aggarwal, M. Shakibaei, *Nutrients* **2019**, *11*(12), 2904.
- [8] A. B. Kunnumakkara, K. Banik, D. Bordoloi, C. Harsha, B. L. Sailo, G. Padmavathi, N. K. Roy, S. C. Gupta, B. B. Aggarwal, *Front. Pharmacol.* **2018**, *9*, 686. <https://doi.org/10.3389/fphar.2018.00686>
- [9] S. A. Ahmed, D. Parama, E. Daimari, S. Girisa, K. Banik, C. Harsha, U. Dutta, A. B. Kunnumakkara, *Life Sci.* **2021**, *267*, 118814. <https://doi.org/10.1016/j.lfs.2020.118814>
- [10] S. Girisa, B. Shabnam, J. Monisha, L. Fan, C. Halim, F. Arfuso, K. Ahn, G. Sethi, A. B. Kunnumakkara, *Molecules* **2019**, *24*(4), 734. <https://doi.org/10.3390/molecules24040734>
- [11] M. K. Pandey, B. Sung, A. B. Kunnumakkara, G. Sethi, M. M. Chaturvedi, B. B. Aggarwal, *Cancer Res.* **2008**, *68*(13), 5370. <https://doi.org/10.1158/0008-5472.CAN-08-0511>
- [12] A. D. Khwairakpam, Y. D. Damayenti, A. Deka, J. Monisha, N. K. Roy, G. Padmavathi, A. B. Kunnumakkara, *J. Basic Clin. Physiol. Pharmacol.* **2018**, *29*(2), 107. <https://doi.org/10.1515/jbcpp-2016-0132>
- [13] B. H. Babu, H. N. Jayram, M. G. Nair, K. B. Ajaikumar, J. Padikkala, *J. Exp. Clin. Cancer Res.* **2003**, *22*(4), 581.
- [14] B. B. Aggarwal, H. Ichikawa, P. Garodia, P. Weerasinghe, G. Sethi, I. D. Bhatt, M. K. Pandey, S. Shishodia, M. G. Nair, *Expert Opin. Ther. Targets* **2006**, *10*(1), 87. <https://doi.org/10.1517/14728222.10.1.87>
- [15] K. Banik, C. Harsha, D. Bordoloi, B. Laldusaki Sailo, G. Sethi, H. C. Leong, F. Arfuso, S. Mishra, L. Wang, A. P. Kumar, A. B. Kunnumakkara, *Cancer Lett.* **2018**, *416*, 75. <https://doi.org/10.1016/j.canlet.2017.12.014>
- [16] A. Nair, A. Amalraj, J. Jacob, A. B. Kunnumakkara, S. Gopi, *Biomolecules* **2019**, *9*(1), 13. <https://doi.org/10.3390/biom9010013>
- [17] S. Henamayee, K. Banik, B. L. Sailo, B. Shabnam, C. Harsha, S. Srilakshmi, N. Vgm, S. H. Baek, K. S. Ahn, A. B. Kunnumakkara, *Molecules* **2020**, *25*(10), 2278. <https://doi.org/10.3390/molecules25102278>
- [18] E. Khatoon, K. Banik, C. Harsha, B. L. Sailo, K. K. Thakur, A. D. Khwairakpam, R. Vikkurthi, T. B. Devi, S. C. Gupta, A. B. Kunnumakkara, *Semin. Cancer Biol.* **2020**, *80*, 306.
- [19] A. B. Kunnumakkara, A. S. Nair, K. S. Ahn, M. K. Pandey, Z. Yi, M. Liu, B. B. Aggarwal, *Blood* **2007**, *109*(12), 5112. <https://doi.org/10.1182/blood-2007-01-067256>
- [20] D. Bordoloi, N. K. Roy, J. Monisha, G. Padmavathi, B. Kunnumakkara, *Recent Pat. Anticancer Drug Discov.* **2016**, *11*(1), 67.
- [21] D. A. Dias, S. Urban, U. Roessner, *Metabolites* **2012**, *2*(2), 303.
- [22] S. M. Patel, K. C. Nagulapalli Venkata, P. Bhattacharyya, G. Sethi, A. Bishayee, *Semin. Cancer Biol.* **2016**, *40*, 100. <https://doi.org/10.1016/j.semcancer.2016.03.002>
- [23] C. Guruvayoorappan, K. M. Sakthivel, G. Padmavathi, V. Bakliwal, J. Monisha, A. B. Kunnumakkara, *Anticancer Properties of Fruits and Vegetables*, World Scientific Publishing Co., Singapore **2013**, pp. 1–52. https://doi.org/10.1142/9789814508896_0001
- [24] D. Thomas, S. Govindhan, E. C. Baiju, G. Padmavathi, A. B. Kunnumakkara, J. Padikkala, *J. Basic Clin. Physiol. Pharmacol.* **2015**, *26*(5), 485. <https://doi.org/10.1515/jbcpp-2014-0093>
- [25] A. B. Kunnumakkara, C. Koca, S. Dey, P. Gehlot, S. Yodkeeree, D. Danda, B. Sung, B. B. Aggarwal, *Traditional Uses of Spices: An Overview*, World Scientific Publishing Co., Singapore **2009**, pp. 1–24. https://doi.org/10.1142/9789812837912_0001
- [26] C. Harsha, K. Banik, D. Bordoloi, A. B. Kunnumakkara, *Food Chem. Toxicol.* **2017**, *108*(Pt A), 104. <https://doi.org/10.1016/j.fct.2017.07.023>
- [27] B. Choudhury, R. Kandimalla, R. Bharali, J. Monisha, A. B. Kunnumakkara, K. Kalita, J. Kotoky, *Front. Pharmacol.* **2016**, *7*, 3. <https://doi.org/10.3389/fphar.2016.00003>
- [28] D. Parama, M. Boruah, K. Yachna, V. Rana, K. Banik, C. Harsha, K. K. Thakur, U. Dutta, A. Arya, X. Mao, K. S. Ahn, A. B. Kunnumakkara, *Life Sci.* **2020**, *260*, 118182. <https://doi.org/10.1016/j.lfs.2020.118182>
- [29] J. Monisha, G. Padmavathi, N. Kishor Roy, A. Deka, D. Bordoloi, A. Anip, A. B. Kunnumakkara, *Curr. Pharm. Des.* **2016**, *22*(27), 4173. <https://doi.org/10.2174/1381612822666160609110231>
- [30] S. Shah, N. Akhter, B. Auckloo, I. Khan, Y. Lu, K. Wang, B. Wu, Y. W. Guo, *Mar. Drugs* **2017**, *15*(11), 354. <https://doi.org/10.3390/md15110354>
- [31] A. G. Atanasov, S. B. Zotchev, V. M. Dirsch, T. International Natural Product Sciences, C. T. Supuran, *Nat. Rev. Drug Discov.* **2021**, *20*(3), 200. <https://doi.org/10.1038/s41573-020-00114-z>
- [32] D. Kashyap, H. S. Tuli, M. B. Yerer, A. Sharma, K. Sak, S. Srivastava, A. Pandey, V. K. Garg, G. Sethi, A. Bishayee, *Semin. Cancer Biol.* **2021**, *69*, 5.
- [33] E. Lautié, O. Russo, P. Ducrot, J. A. Boutin, *Front. Pharmacol.* **2020**, *11*, 397. <https://doi.org/10.3389/fphar.2020.00397>
- [34] S. Mishra, S. S. Verma, V. Rai, N. Awasthee, S. Chava, K. M. Hui, A. P. Kumar, K. B. Challagundla, G. Sethi, S. C. Gupta, *Cell Mol. Life Sci.* **2019**, *76*(10), 1947. <https://doi.org/10.1007/s00018-019-03053-0>
- [35] D. J. Newman, G. M. Cragg, *J. Nat. Prod.* **2020**, *83*(3), 770. <https://doi.org/10.1021/acs.jnatprod.9b01285>
- [36] V. C. Tripathi, S. Satish, S. Horam, S. Raj, J. Arockiaraj, M. Pasupuleti, D. K. Dikshit, *Semin. Cancer Biol.* **2018**, *18*, 147–166.
- [37] K. Banik, A. M. Ranaware, C. Harsha, T. Nitesh, S. Girisa, V. Deshpande, L. Fan, S. P. Nalawade, G. Sethi, A. B. Kunnumakkara, *Pharmacol. Res.* **2020**, *153*, 104635. <https://doi.org/10.1016/j.phrs.2020.104635>
- [38] D. Bordoloi, J. Monisha, N. K. Roy, G. Padmavathi, K. Banik, C. Harsha, H. Wang, A. P. Kumar, F. Arfuso, A. B. Kunnumakkara, *Asian Pac. J. Cancer Prev.* **2019**, *20*(11), 3437. <https://doi.org/10.31557/APJCP.2019.20.11.3437>
- [39] Y. P. Singh, S. Girisa, K. Banik, S. Ghosh, P. Swathi, M. Deka, G. Padmavathi, J. Kotoky, G. Sethi, L. Fan, X. Mao, C. E. Halim, F. Arfuso, A. B. Kunnumakkara, *J. Funct. Foods* **2019**, *53*, 248. <https://doi.org/10.1016/j.jff.2018.12.020>
- [40] S. B. Muralimanoharan, A. B. Kunnumakkara, B. Shylesh, K. H. Kulkarni, X. Haiyan, H. Ming, B. B. Aggarwal, G. Rita, A. P. Kumar, *Prostate* **2009**, *69*(5), 494. <https://doi.org/10.1002/pros.20899>

- [41] G. Padmavathi, N. K. Roy, D. Bordoloi, F. Arfuso, S. Mishra, G. Sethi, A. Bishayee, A. B. Kunnumakkara, *Phytomedicine* **2017**, *25*, 118. <https://doi.org/10.1016/j.phymed.2016.12.002>
- [42] A. B. Kunnumakkara, B. Sung, J. Ravindran, P. Diagaradjane, A. Deorukhkar, S. Dey, C. Koca, Z. Tong, J. G. Gelovani, S. Guha, S. Krishnan, B. B. Aggarwal, *Int. J. Cancer* **2012**, *131*(3), E292. <https://doi.org/10.1002/ijc.26442>
- [43] S. Gopi, J. Jacob, K. Varma, S. Jude, A. Amalraj, C. A. Arundhathy, R. George, T. R. Sreeraj, C. Divya, A. B. Kunnumakkara, S. J. Stohs, *Phytother. Res.* **2017**, *31*(12), 1883. <https://doi.org/10.1002/ptr.5931>
- [44] A. Amalraj, K. Varma, J. Jacob, C. Divya, A. B. Kunnumakkara, S. J. Stohs, S. Gopi, *J. Med. Food* **2017**, *20*(10), 1022. <https://doi.org/10.1089/jmf.2017.3930>
- [45] J. Tomé-Carneiro, M. Larrosa, A. González-Sarriás, F. A. Tomás-Barberán, M. T. García-Conesa, J. C. Espín, *Curr. Pharm. Des.* **2013**, *19*(34), 6064. <https://doi.org/10.2174/13816128113199990407>
- [46] R. K. Lall, D. N. Syed, V. M. Adhami, M. I. Khan, H. Mukhtar, *Int. J. Mol. Sci.* **2015**, *16*(2), 3350. <https://doi.org/10.3390/ijms16023350>
- [47] J. H. Lee, S. Y. Chiang, D. Nam, W.-S. Chung, J. Lee, Y.-S. Na, G. Sethi, K. S. Ahn, *Cancer Lett.* **2014**, *345*(1), 140. <https://doi.org/10.1016/j.canlet.2013.12.008>
- [48] K. A. Manu, M. K. Shanmugam, L. Ramachandran, F. Li, K. S. Siveen, A. Chinnathambi, M. E. Zayed, S. A. Alharbi, F. Arfuso, A. P. Kumar, K. S. Ahn, G. Sethi, *Cancer Lett.* **2015**, *363*(1), 28. <https://doi.org/10.1016/j.canlet.2015.03.033>
- [49] B. Salehi, Z. Stojanović-Radić, J. Matejić, M. Sharifi-Rad, N. V. Anil Kumar, N. Martins, J. Sharifi-Rad, *Eur. J. Med. Chem.* **2019**, *163*, 527. <https://doi.org/10.1016/j.ejmech.2018.12.016>
- [50] H. Hatcher, R. Planalp, J. Cho, F. M. Torti, S. V. Torti, *Cell Mol. Life Sci.* **2008**, *65*(11), 1631. <https://doi.org/10.1007/s00018-008-7452-4>
- [51] M. Shakibaei, A. Mobasheri, C. Lueders, F. Busch, P. Shayan, A. Goel, *PLoS One* **2013**, *8*(2), 57218. <https://doi.org/10.1371/journal.pone.0057218>
- [52] M. Shakibaei, P. Kraehe, B. Popper, P. Shayan, A. Goel, C. Buhrmann, *BMC Cancer* **2015**, *15*(1), 250. <https://doi.org/10.1186/s12885-015-1291-0>
- [53] S. Girisa, A. Kumar, V. Rana, D. Parama, U. D. Daimary, S. Warnakulasuriya, A. P. Kumar, A. B. Kunnumakkara, *ACS Pharmacol. Transl. Sci.* **2021**, *4*, 647. <https://doi.org/10.1021/acspsci.1c00017>
- [54] A. B. Kunnumakkara, D. Bordoloi, C. Harsha, K. Banik, S. C. Gupta, B. B. Aggarwal, *Clin. Sci.* **2017**, *131*(15), 1781. <https://doi.org/10.1042/CS20160935>
- [55] C. Buhrmann, P. Shayan, A. Brockmueller, M. Shakibaei, *Molecules* **2020**, *25*(18), 4292. <https://doi.org/10.3390/molecules25184292>
- [56] D. J. Newman, G. M. Cragg, *J. Nat. Prod.* **2016**, *79*(3), 629. <https://doi.org/10.1021/acs.jnatprod.5b01055>
- [57] Z. Guo, *Acta Pharm. Sin. B* **2017**, *7*(2), 119.
- [58] K. Ajish, K. Antu, M. Riya, M. Preetharani, K. Raghu, B. Dhanya, K. V. Radhakrishnan, *Nat. Prod. Res.* **2015**, *29*(10), 947.
- [59] P. Sasikumar, K. Lekshmy, S. Sini, B. Prabha, N. A. Kumar, V. V. Sivan, M. M. Jithin, P. Jayamurthy, I. G. Shibi, K. V. Radhakrishnan, *J. Ethnopharmacol.* **2019**, *236*, 196. <https://doi.org/10.1016/j.jep.2019.01.046>
- [60] M. Aswathy, K. Banik, D. Parama, P. Sasikumar, C. Harsha, A. G. Joseph, D. R. Sherin, M. K. Thanathu, A. B. Kunnumakkara, R. K. Vasu, *ACS Pharmacol. Transl. Sci.* **2021**, *4*, 834. <https://doi.org/10.1021/acspsci.1c00011>
- [61] M. H. Ghante, P. G. Jamkhande, *J. Pharmacopuncture* **2019**, *22*(2), 55. <https://doi.org/10.3831/KPI.201.22.007>
- [62] M. Saleem, *Cancer Lett.* **2009**, *285*(2), 109. <https://doi.org/10.1016/j.canlet.2009.04.033>
- [63] E. Pisha, H. Chai, I.-S. Lee, T. E. Chagwedera, N. R. Farnsworth, G. A. Cordell, C. W. Beecher, H. H. Fong, A. D. Kinghorn, D. M. Brown, *Nat. Med.* **1995**, *1*(10), 1046. <https://doi.org/10.1038/nm1095-1046>
- [64] Y. Cai, Y. Zheng, J. Gu, S. Wang, N. Wang, B. Yang, F. Zhang, D. Wang, W. Fu, Z. Wang, *Cell Death Dis.* **2018**, *9*(6), 636. <https://doi.org/10.1038/s41419-018-0669-8>
- [65] R. Prasannan, K. A. Kalesh, M. K. Shanmugam, A. Nachiyappan, L. Ramachandran, A. H. Nguyen, A. P. Kumar, M. Lakshmanan, K. S. Ahn, G. Sethi, *Biochem. Pharmacol.* **2012**, *84*(10), 1268. <https://doi.org/10.1016/j.bcp.2012.07.015>
- [66] G. Liebscher, K. Vanchangiri, T. Mueller, K. Feige, J.-M. Cavalleri, R. Paschke, *Chem.-Biol. Interact.* **2016**, *246*, 20. <https://doi.org/10.1016/j.cbi.2016.01.002>
- [67] P. Rajendran, M. Jaggi, M. K. Singh, R. Mukherjee, A. C. Burman, *Invest. New Drugs* **2008**, *26*(1), 25. <https://doi.org/10.1007/s10637-007-9081-4>
- [68] M. G. Moghaddam, F. B. H. Ahmad, *Asian J. Chem.* **2012**, *24*(11), 4843.
- [69] S. C. Sati, N. Sati, O. P. Sati, *Pharmacogn. Rev.* **2011**, *5*(10), 174. <https://doi.org/10.4103/0973-7847.91115>
- [70] G. A. Birgani, A. Ahangarpour, L. Khorsandi, H. F. Moghaddam, *Braz. J. Pharm. Sci.* **2018**, *54*, e17171.
- [71] S. Fulda, G. Kroemer, *Drug Discov. Today* **2009**, *14*(17), 885.
- [72] Y. Kashiwada, H.-K. Wang, T. Nagao, S. Kitanaka, I. Yasuda, T. Fujioka, T. Yamagishi, L. M. Cosentino, M. Kozuka, H. Okabe, Y. Ikeshiro, C. Q. Hu, E. Yeh, K. H. Lee, *J. Nat. Prod.* **1998**, *61*(9), 1090. <https://doi.org/10.1021/np9800710>
- [73] K. Kinoshita, M. Akiba, M. Saitoh, Y. Ye, K. Koyama, K. Takahashi, N. Kondo, H. Yuasa, *Pharm. Biol.* **1998**, *36*(1), 50.
- [74] T.-J. Song, C.-H. Park, K.-R. In, J.-B. Kim, J. H. Kim, M. Kim, H. J. Chang, *PLoS One* **2021**, *16*(4), 0249109. <https://doi.org/10.1371/journal.pone.0249109>
- [75] M. C. Lingaraju, N. N. Pathak, J. Begum, V. Balaganur, R. A. Bhat, H. D. Ramachandra, A. Ayanur, M. Ram, V. Singh, D. Kumar, D. Kumar, S. K. Tandan, *Cytokine* **2015**, *71*(1), 101. <https://doi.org/10.1016/j.cyto.2014.09.004>
- [76] S. Fulda, I. Jeremias, H. H. Steiner, T. Pietsch, K. M. Debatin, *Int. J. Cancer* **1999**, *82*(3), 435. [https://doi.org/10.1002/\(sici\)1097-0215\(19990730\)82:33.0.co;2-1](https://doi.org/10.1002/(sici)1097-0215(19990730)82:33.0.co;2-1)
- [77] A. A. Damle, Y. P. Pawar, A. A. Narkar, *Indian J. Exp. Biol.* **2013**, *51*, 485.
- [78] C. G. Farcas, C. Dehelean, I. A. Pinzaru, M. Mioc, V. Socoliuc, E.-A. Moaca, S. Avram, R. Ghiulai, D. Coricovac, I. Pavel, P. K. Alla, O. M. Cretu, C. Soica, F. Loghin, *Int. J. Nanomed.* **2020**, *15*, 8175.
- [79] S. U. Mertens-Talcott, G. D. Noratto, X. Li, G. Angel-Morales, M. C. Bertoldi, S. Safe, *Mol. Carcinog.* **2013**, *52*(8), 591. <https://doi.org/10.1002/mc.21893>
- [80] C. Wang, S. Kar, X. Lai, W. Cai, F. Arfuso, G. Sethi, P. E. Lobie, B. C. Goh, L. H. K. Lim, M. Hartman, C. W. Chan, S. C. Lee, S. H. Tan, A. P. Kumar, *Cancer Treat. Rev.* **2018**, *62*, 29. <https://doi.org/10.1016/j.ctrv.2017.10.014>
- [81] A.-Q. Zeng, Y. Yu, Y.-Q. Yao, F.-F. Yang, M. Liao, L.-J. Song, Y.-L. Li, Y. Yu, Y.-J. Li, Y. L. Deng, S. P. Yang, C. J. Zeng, P. Liu, Y. M. Xie, J. L. Yang, Y. W. Zhang, T. H. Ye, Y. Q. Wei, *Oncotarget* **2018**, *9*(3), 3794. <https://doi.org/10.18632/oncotarget.23376>
- [82] A. Halder, M. Jethwa, P. Mukherjee, S. Ghosh, S. Das, A. Helal Uddin, A. Mukherjee, U. Chatterji, P. Roy, *Artif. Cells, Nanomed., Biotechnol.* **2020**, *48*(1), 1362. <https://doi.org/10.1080/21691401.2020.1850465>
- [83] L. Jiao, S. Wang, Y. Zheng, N. Wang, B. Yang, D. Wang, D. Yang, W. Mei, Z. Zhao, Z. Wang, *Biochem. Pharmacol.* **2019**, *161*, 149. <https://doi.org/10.1016/j.bcp.2019.01.016>

- [84] Y. R. Tzenov, P. Andrews, K. Voisey, L. Gai, B. Carter, K. Whelan, C. Popadiuk, K. R. Kao, *J. Clin. Pathol.* **2016**, *69*(6), 518. <https://doi.org/10.1136/jclinpath-2015-203395>
- [85] Y. Zheng, P. Liu, N. Wang, S. Wang, B. Yang, M. Li, J. Chen, H. Situ, M. Xie, Y. Lin, Z. Wang, *Oxid. Med. Cell Longev.* **2019**, *2019*, 8781690. <https://doi.org/10.1155/2019/8781690>
- [86] M. Eichenmüller, B. Hemmerlein, D. Von Schweinitz, R. Kappler, *Br. J. Cancer* **2010**, *103*(1), 43. <https://doi.org/10.1038/sj.bjc.6605715>
- [87] T. Xu, Q. Pang, Y. Wang, X. Yan, *Int. J. Mol. Med.* **2017**, *40*(6), 1669–1678.
- [88] C. Yang, Y. Li, L. Fu, T. Jiang, F. Meng, *J. Cell Biochem.* **2018**, *119*(10), 8611. <https://doi.org/10.1002/jcb.27116>
- [89] H. Wang, F. Dong, Y. Wang, X. Wang, D. Hong, Y. Liu, J. Zhou, *Acta Biochim. Biophys. Sin.* **2020**, *52*(2), 200. <https://doi.org/10.1093/abbs/gmz148>
- [90] S. Y. Kim, H. Hwangbo, M. Y. Kim, S. Y. Ji, D. H. Kim, H. Lee, G.-Y. Kim, S.-K. Moon, S.-H. Leem, S. J. Yun, W. J. Kim, J. Cheong, C. Park, Y. H. Choi, *Molecules* **2021**, *26*(5), 1381. <https://doi.org/10.3390/molecules26051381>
- [91] J. Zhao, R. Li, A. Pawlak, M. Henkowska, A. Sysak, L. Wen, J.-E. Yi, B. Obmińska-Mrukowicz, *In Vivo* **2018**, *32*(5), 1081. <https://doi.org/10.21873/invivo.11349>
- [92] P. Goswami, S. Paul, R. Banerjee, R. Kundu, A. Mukherjee, *Mutat. Res. Genet. Toxicol. Environ. Mutagen.* **2018**, *828*, 1. <https://doi.org/10.1016/j.mrgentox.2018.02.003>
- [93] H.-J. Kim, H.-S. Cho, H. S. Ban, H. Nakamura, *Biochem. Biophys. Res. Commun.* **2020**, *523*(3), 726. <https://doi.org/10.1016/j.bbrc.2020.01.031>
- [94] X. Wang, X. Lu, R. Zhu, K. Zhang, S. Li, Z. Chen, L. Li, *Neurochem. Res.* **2017**, *42*(4), 1130. <https://doi.org/10.1007/s11064-016-2147-y>
- [95] A. Zeng, H. Hua, L. Liu, J. Zhao, *Bioorg. Med. Chem.* **2019**, *27*(12), 2546. <https://doi.org/10.1016/j.bmc.2019.03.033>
- [96] P. Surowiak, M. Drag, V. Materna, M. Dietel, H. Lage, *Mol. Med. Rep.* **2009**, *2*(4), 543. https://doi.org/10.3892/mmr_00000134
- [97] Y. Liu, W. Luo, *Mol. Cells* **2012**, *33*(5), 517. <https://doi.org/10.1007/s10059-012-0022-5>
- [98] W.-L. Lo, T.-I. Hsu, W.-B. Yang, T.-J. Kao, M.-H. Wu, Y.-N. Huang, S.-H. Yeh, J. Y. Chuang, *Cancers* **2020**, *12*(4), 981. <https://doi.org/10.3390/cancers12040981>
- [99] C. Soica, C. Danciu, G. Savoiu-Balint, F. Borcan, R. Ambrus, I. Zupko, F. Bojin, D. Coricovac, S. Ciurlea, S. Avram, C. A. Dehelean, T. Olariu, P. Matusz, *Int. J. Mol. Sci.* **2014**, *15*(5), 8235.
- [100] R. Wang, M. Yang, G. Li, X. Wang, Z. Zhang, H. Qiao, J. Chen, Z. Chen, X. Cui, J. Li, *Colloids Surf., B: Biointerfaces* **2019**, *174*, 270. <https://doi.org/10.1016/j.colsurfb.2018.11.029>
- [101] F. Simone, K.-M. Debatin, *Neoplasia* **2005**, *7*(2), 162. <https://doi.org/10.1593/neo.04442>
- [102] L. A. Weber, J. Meißner, J. Delarocque, J. Kalbitz, K. Feige, M. Kietzmann, A. Michaelis, R. Paschke, J. Michael, B. Pratscher, J.-M. V. Cavalleri, *BMC Vet. Res.* **2020**, *16*(1), 44.
- [103] L.-J. Yang, Y. Chen, J. He, S. Yi, L. Wen, J. Zhao, B.-p. Zhang, G. H. Cui, *Acta Pharmacol. Sin.* **2012**, *33*(12), 1542. <https://doi.org/10.1038/aps.2012.102>
- [104] C.-F. Chiu, H.-Y. Chang, C.-Y. Huang, C.-Z. Mau, T.-T. Kuo, H.-C. Lee, S. Y. Huang, *Molecules* **2021**, *26*(9), 2482. <https://doi.org/10.3390/molecules26092482>
- [105] F. B. Mullauer, L. van Bloois, J. B. Daalhuisen, M. S. Ten Brink, G. Storm, J. P. Medema, R. M. Schiffelers, J. H. Kessler, *Anti-Cancer Drugs* **2011**, *22*(3), 223. <https://doi.org/10.1097/CAD.0b013e3283421035>
- [106] G. R. Jung, K. J. Kim, C. H. Choi, T. B. Lee, S. I. Han, H. K. Han, S. C. Lim, *Basic Clin. Pharmacol. Toxicol.* **2007**, *101*(4), 277. <https://doi.org/10.1111/j.1742-7843.2007.00115.x>
- [107] S. Chintharlapalli, S. Papineni, P. Lei, S. Pathi, S. Safe, *BMC Cancer* **2011**, *11*, 371.
- [108] S. Wang, K. Wang, C. Zhang, W. Zhang, Q. Xu, Y. Wang, Y. Zhang, Y. Li, Y. Zhang, H. Zhu, F. Song, Y. Lei, Y. Bu, *Cell Death Dis.* **2017**, *8*(10), 3087. <https://doi.org/10.1038/cddis.2017.485>
- [109] D. Su, Y.-Q. Gao, W.-B. Dai, Y. Hu, Y.-F. Wu, Q. X. Mei, *Evid. Based Complementary Alternat. Med.* **2017**, *2017*, 5180707. <https://doi.org/10.1155/2017/5180707>
- [110] E. Karna, L. Szoka, J. A. Palka, *Mol. Cell Biochem.* **2010**, *340*(1), 15. <https://doi.org/10.1007/s11010-010-0395-8>
- [111] L.-J. Yang, Y. Chen, Q. Ma, J. Fang, J. He, Y.-Q. Cheng, Q. L. Wu, *Acta Pharmacol. Sin.* **2010**, *31*(1), 66. <https://doi.org/10.1038/aps.2009.177>
- [112] Y. Chen, X. Wu, C. Liu, Y. Zhou, *Cell Biochem. Funct.* **2020**, *38*(6), 702. <https://doi.org/10.1002/cbf.3537>
- [113] X. Chen, X.-n. Yuan, Z. Zhang, P.-j. Gong, W.-n. Yin, Q. Jiang, J. Xu, X. L. Xu, Y. Gao, W. L. Chen, F. F. Chen, Y. H. Tian, L. Wei, J. W. Zhang, *Eur. J. Pharmacol.* **2020**, *889*, 173493. <https://doi.org/10.1016/j.ejphar.2020.173493>
- [114] W. Wang, Y. Wang, M. Liu, Y. Zhang, T. Yang, D. Li, Y. Huang, Q. Li, G. Bai, L. Shi, *J. Cell Mol. Med.* **2019**, *23*(1), 586. <https://doi.org/10.1111/jcmm.13964>
- [115] W. Liu, S. Li, Z. Qu, Y. Luo, R. Chen, S. Wei, X. Yang, Q. Wang, *Am. J. Transl. Res.* **2019**, *11*(11), 6952.
- [116] Y. Xu, J. Li, Q.-J. Li, Y.-L. Feng, F. Pan, *Biomed. Pharmacother.* **2017**, *88*, 349. <https://doi.org/10.1016/j.biopha.2017.01.034>
- [117] S. Martucciello, M. L. Balestrieri, F. Felice, S. Estevam Cdos, A. E. Sant'ana, C. Pizza, S. Piacente, *Chem.-Biol. Interact.* **2010**, *183*(3), 450. <https://doi.org/10.1016/j.cbi.2009.12.012>
- [118] S. K. Dash, S. Chattopadhyay, S. S. Dash, S. Tripathy, B. Das, S. K. Mahapatra, B. G. Bag, P. Karmakar, S. Roy, *Bioorg. Chem.* **2015**, *63*, 85. <https://doi.org/10.1016/j.bioorg.2015.09.006>
- [119] T.-I. Hsu, M.-C. Wang, S.-Y. Chen, S.-T. Huang, Y.-M. Yeh, W.-C. Su, W.-C. Chang, J. J. Hung, *Mol. Pharmacol.* **2012**, *82*(6), 1115. <https://doi.org/10.1124/mol.112.078485>
- [120] C. L. Chen, C. Y. Chen, Y. P. Chen, Y. B. Huang, M. W. Lin, D. C. Wu, H. T. Huang, M. Y. Liu, H. W. Chang, Y. C. Kao, P. H. Yang, *J. Biomed. Sci.* **2016**, *23*(1), 30. <https://doi.org/10.1186/s12929-016-0229-4>
- [121] J. Kutkowska, L. Strzadala, A. Rapak, *Cancer Sci.* **2017**, *108*(11), 2265. <https://doi.org/10.1111/cas.13386>
- [122] X. K. Zhan, J. L. Li, S. Zhang, P. Y. Xing, M. F. Xia, *Oncol. Lett.* **2018**, *16*(3), 3628. <https://doi.org/10.3892/ol.2018.9097>
- [123] J. L. Ko, C. H. Lin, H. C. Chen, W. H. Hung, P. J. Chien, H. Y. Chang, B. Y. Wang, *Environ. Toxicol.* **2018**, *33*(11), 1153–1159.
- [124] H. Zhao, X. Mu, X. Zhang, Q. You, *Med. Sci. Monit.* **2020**, *26*, 922092. <https://doi.org/10.12659/MSM.922092>
- [125] J. Kutkowska, L. Strzadala, A. Rapak, *Chem.-Biol. Interact.* **2021**, *333*, 109320. <https://doi.org/10.1016/j.cbi.2020.109320>
- [126] S. Chintharlapalli, S. Papineni, S. K. Ramaiah, S. Safe, *Cancer Res.* **2007**, *67*(6), 2816. <https://doi.org/10.1158/0008-5472.CAN-06-3735>
- [127] M. Shen, Y. Hu, Y. Yang, L. Wang, X. Yang, B. Wang, M. Huang, *Oxid. Med. Cell Longev.* **2019**, *2019*, 5083158. <https://doi.org/10.1155/2019/5083158>
- [128] H. Shen, L. Liu, Y. Yang, W. Xun, K. Wei, G. Zeng, *Oncol. Res.* **2017**, *25*(7), 1141. <https://doi.org/10.3727/096504017X14841698396784>
- [129] D.-Y. Yuan, Z. Meng, K. Xu, Q.-F. Li, C. Chen, K.-Y. Li, B. Zhang, *Oncol. Rep.* **2017**, *38*(4), 2360.
- [130] D. Thurnher, D. Turhani, M. Pelzmann, B. Wannemacher, B. Knerer, M. Formanek, V. Wacheck, E. Selzer, *Head Neck* **2003**, *25*(9), 732. <https://doi.org/10.1002/hed.10231>
- [131] D. Lee, S. R. Lee, K. S. Kang, Y. Ko, C. Pang, N. Yamabe, K. H. Kim, *Biomolecules* **2019**, *9*(7), 257. <https://doi.org/10.3390/biom9070257>

- [132] J. Kutkowska, L. Strzadala, A. Rapak, *Int. J. Mol. Sci.* **2018**, 19(10), 3234.
- [133] Y. Gao, Z. Jia, X. Kong, Q. Li, D. Z. Chang, D. Wei, X. Le, H. Suyun, S. Huang, L. Wang, K. Xie, *Cancer Res.* **2011**, 71(15), 5182. <https://doi.org/10.1158/0008-5472.CAN-10-2016>
- [134] L. Sun, J. Cao, K. Chen, L. Cheng, C. Zhou, B. Yan, W. Qian, J. Li, W. Duan, J. Ma, D. Qi, E. Wu, Z. Wang, Q. Liu, Q. Ma, Q. Xu, *Int. J. Oncol.* **2019**, 54(1), 98. <https://doi.org/10.3892/ijo.2018.4604>
- [135] Y. Guo, H. Zhu, M. Weng, C. Wang, L. Sun, *BMC Complementary Med. Ther.* **2020**, 20(1), 178. <https://doi.org/10.1186/s12906-020-02976-7>
- [136] T. Rabi, S. Shukla, S. Gupta, *Mol. Carcinog.* **2008**, 47(12), 964. <https://doi.org/10.1002/mc.20447>
- [137] J. Shin, H.-J. Lee, D.-B. Jung, J. H. Jung, H.-J. Lee, E.-O. Lee, S. G. Lee, B. S. Shim, S. H. Choi, S. G. Ko, K. S. Ahn, S. J. Jeong, S. H. Kim, *PLoS One* **2011**, 6(6), 21492. <https://doi.org/10.1371/journal.pone.0021492>
- [138] T. Reiner, R. Parrondo, A. de Las Pozas, D. Palenzuela, C. Perez-Stable, *PLoS One* **2013**, 8(2), 56234. <https://doi.org/10.1371/journal.pone.0056234>
- [139] E. Shankar, A. Zhang, D. Franco, S. Gupta, *Molecules* **2017**, 22(2), 264. <https://doi.org/10.3390/molecules22020264>
- [140] N. Sawada, K. Kataoka, K. Kondo, H. Arimochi, H. Fujino, Y. Takahashi, T. Miyoshi, T. Kuwahara, Y. Monden, Y. Ohnishi, *Br. J. Cancer* **2004**, 90(8), 1672. <https://doi.org/10.1038/sj.bjc.6601746>
- [141] L. Liao, C. Liu, X. Xie, J. Zhou, *J. Food Biochem.* **2020**, 44(7), 13278. <https://doi.org/10.1111/jfbc.13278>
- [142] R. Luo, D. Fang, P. Chu, H. Wu, Z. Zhang, Z. Tang, *Biomed. Pharmacother.* **2016**, 84, 1321. <https://doi.org/10.1016/j.biopha.2016.10.018>
- [143] J. J. Champoux, *Annu. Rev. Biochem.* **2001**, 70(1), 369. <https://doi.org/10.1146/annurev.biochem.70.1.369>
- [144] J. L. Delgado, C.-M. Hsieh, N.-L. Chan, H. Hiasa, *Biochem. J.* **2018**, 475(2), 373. <https://doi.org/10.1042/BCJ20160583>
- [145] A. R. Chowdhury, S. Mandal, B. Mitra, S. Sharma, S. Mukhopadhyay, H. K. Majumder, *Med. Sci. Monit.* **2002**, 8(7), 254.
- [146] T. Syrovets, B. Büchele, E. Gedig, J. R. Slupsky, T. Simmet, *Mol. Pharmacol.* **2000**, 58(1), 71. <https://doi.org/10.1124/mol.58.1.71>
- [147] A. Ganguly, B. Das, A. Roy, N. Sen, S. B. Dasgupta, S. Mukhopadhyay, H. K. Majumder, *Cancer Res.* **2007**, 67(24), 11848. <https://doi.org/10.1158/0008-5472.CAN-07-1615>
- [148] S. Ghosh, S. Mukhopadhyay, M. Sarkar, A. Mandal, V. Das, A. Kumar, B. Giri, *Chem.-Biol. Interact.* **2017**, 268, 68. <https://doi.org/10.1016/j.cbi.2017.02.015>
- [149] F. M. Bar, M. A. Khanfar, A. Y. Elnagar, H. Liu, A. M. Zaghoul, F. A. Badria, P. W. Sylvester, K. F. Ahmad, K. P. Raisch, K. A. El Sayed, *J. Nat. Prod.* **2009**, 72(9), 1643. <https://doi.org/10.1021/np900312u>
- [150] L. W. Dillon, L. C. Pierce, C. E. Lehman, Y. E. Nikiforov, Y. H. Wang, *PLoS One* **2013**, 8(9), 75741. <https://doi.org/10.1371/journal.pone.0075741>
- [151] D. A. Nedopekina, R. R. Gubaidullin, V. N. Odnokov, P. V. Maximchik, B. Zhivotovsky, Y. P. Bel'skii, V. A. Khazanov, A. V. Manuylova, V. Gogvadze, A. Y. Spivak, *MedChemComm* **2017**, 8(10), 1934. <https://doi.org/10.1039/c7md00248c>
- [152] S. Girisa, S. Henamayee, D. Parama, V. Rana, U. Dutta, A. B. Kunnumakkara, *Mol. Biomed.* **2021**, 2(1), 21. <https://doi.org/10.1186/s43556-021-00035-2>
- [153] S. Fulda, K. M. Debatin, *Curr. Opin. Pharmacol.* **2004**, 4(4), 327. <https://doi.org/10.1016/j.coph.2004.02.005>
- [154] F. B. Mullauer, J. H. Kessler, J. P. Medema, *Apoptosis.* **2009**, 14(2), 191. <https://doi.org/10.1007/s10495-008-0290-x>
- [155] D. W. Leung, G. Cachianes, W.-J. Kuang, D. V. Goeddel, N. Ferrara, *Science* **1989**, 246(4935), 1306. <https://doi.org/10.1126/science.2479986>
- [156] N. Ferrara, W. J. Henzel, *Biochem. Biophys. Res. Commun.* **1989**, 161(2), 851. [https://doi.org/10.1016/0006-291x\(89\)92678-8](https://doi.org/10.1016/0006-291x(89)92678-8)
- [157] T. Matsumoto, S. Bohman, J. Dixelius, T. Berge, A. Dimberg, P. Magnusson, L. Wang, C. Wikner, J. H. Qi, C. Wernstedt, J. Wu, S. Bruheim, H. Mugishima, D. Mukhopadhyay, A. Spurrkand, L. Claesson-Welsh, *EMBO J.* **2005**, 24(13), 2342. <https://doi.org/10.1038/sj.emboj.7600709>
- [158] Q. Y. Zhang, S. Y. Tao, C. Lu, J. J. Li, X. M. Li, J. Yao, Q. Jiang, B. Yan, *Mol. Med. Rep.* **2020**, 21(6), 2571. <https://doi.org/10.3892/mmr.2020.11056>
- [159] C. D. Mohan, H. Bharathkumar, K. C. Bulusu, V. Pandey, S. Rangappa, J. E. Fuchs, M. K. Shanmugam, X. Dai, F. Li, A. Deivasigamani, K. M. Hui, A. P. Kumar, P. E. Lobie, A. Bender, S. Basappa, G. Sethi, K. S. Rangappa, *J. Biol. Chem.* **2014**, 289(49), 34296. <https://doi.org/10.1074/jbc.M114.601104>
- [160] M. K. Pandey, B. Sung, B. B. Aggarwal, *Int. J. Cancer* **2010**, 127(2), 282. <https://doi.org/10.1002/ijc.25059>
- [161] K. Beishline, J. Azizkhan-Clifford, *FEBS. J.* **2015**, 282(2), 224. <https://doi.org/10.1111/febs.13148>
- [162] M. Malumbres, M. Barbacid, *Nat. Rev. Cancer* **2009**, 9(3), 153. <https://doi.org/10.1038/nrc2602>
- [163] E. Verma, A. Kumar, U. D. Daimary, D. Parama, S. Girisa, G. Sethi, A. B. Kunnumakkara, *J. Funct. Foods* **2021**, 86, 104660.
- [164] L. Z. Benet, G. Levy, B. L. Ferraiolo, *Pharmacokinetics: A Modern View*, Springer Science & Business Media, New York **2012**. <https://doi.org/10.1007/978-1-4613-2799-8>
- [165] G. O. Udeani, G. M. Zhao, Y. Geun Shin, B. P. Cooke, J. Graham, C. W. Beecher, A. D. Kinghorn, J. M. Pezzuto, *Biopharm. Drug Dispos.* **1999**, 20(8), 379. [https://doi.org/10.1002/1099-081x\(199911\)20:8<30.0.co;2-c](https://doi.org/10.1002/1099-081x(199911)20:8<30.0.co;2-c)
- [166] Y. G. Shin, K. H. Cho, S. M. Chung, J. Graham, T. K. Das Gupta, J. M. Pezzuto, *J. Chromatogr. B: Biomed. Sci. Appl.* **1999**, 732(2), 331. [https://doi.org/10.1016/s0378-4347\(99\)00291-1](https://doi.org/10.1016/s0378-4347(99)00291-1)
- [167] C. Godugu, A. R. Patel, R. Doddapaneni, J. Somagoni, M. Singh, *PLoS One* **2014**, 9(3), 89919. <https://doi.org/10.1371/journal.pone.0089919>
- [168] T. P. Castor, *Curr. Drug Delivery* **2005**, 2(4), 329. <https://doi.org/10.2174/156720105774370195>
- [169] R. Mukherjee, V. Kumar, S. K. Srivastava, S. K. Agarwal, A. C. Burman, *Anti-Cancer Agents Med. Chem.* **2006**, 6(3), 271. <https://doi.org/10.2174/187152006776930846>

How to cite this article: M. Aswathy, A. Vijayan, U. D. Daimary, S. Girisa, K. V. Radhakrishnan, A. B. Kunnumakkara, *J Biochem. Mol. Toxicol.* **2022**, e23206. <https://doi.org/10.1002/jbt.23206>



A pentacarbomethoxycyclopentadiene (PCCP) organic Brønsted acid catalyzed stereoselective glycosidation of *N*-pentenyl orthoesters (NPOE) of *D*-glucose and *D*-galactose, in conjunction with *N*-iodosuccinimide

Maniyamma Aswathy^{a,b}, Balan Abhijith^a, Ravi S. Lankalapalli^{a,b,*},
Kokkuvayil V. Radhakrishnan^{a,b,*}

^a Chemical Sciences and Technology Division, CSIR-National Institute for Interdisciplinary Science and Technology (CSIR-NIIST), Thiruvananthapuram, 695019, India

^b Academy of Scientific and Innovative Research (AcSIR), Ghaziabad, 201002, India

ARTICLE INFO

Dedicated with respect to Dr. Bert Fraser-Reid for his pioneering contributions and comradeship

Keywords:

Glycosidation
Organic Brønsted acid
PCCP
N-Pentenyl orthoesters
Stereoselectivity

ABSTRACT

Herein, we report our preliminary results in utilizing the organic Brønsted acid, pentacarbomethoxycyclopentadiene (PCCP), for catalysing the glycosidation with *n*-pentenyl orthoesters (NPOE) of *D*-glucose and *D*-galactose in the presence of *N*-iodosuccinimide (NIS). Benzoyl and benzyl protection in *D*-glucosyl NPOEs led to 1,2-*trans* glycosides, while acetyl protection in NPOE led to a mixture of 1,2-*cis* and *trans* glycosides with >75% *cis* selectivity, and *D*-galactosyl NPOEs led to 1,2-orthoesters. Substrate scope was demonstrated with acceptors of natural product relevance. This article highlights the prospect of utilizing the organic Brønsted acid, PCCP, for stereoselective glycosidation.

1. Introduction

The success and efficiency of glycosidation reactions depends on several factors, starting from protecting groups to match-mismatch between glycosyl donors and acceptors [1,2]. Though there are number of methods available for glycosidation, based on different types of donors, there exists the need to have a robust method for stereoselective and regioselective glycosidation [3]. Pioneering studies from a number of laboratories suggests that O-2 protecting group has a profound influence on the control and extent of stereoselective glycosidation [3–5]. Reports also points to the fact that the results of glycosidation reactions cannot be predicted based on reactivity of donors and acceptors alone [6].

As part of our ongoing interest in natural products of phyto-origin, attaching the saccharide appendages to the aglycones with complete regio- and stereoselectivity is a formidable challenge and requires more focused investigation. Fraser-Reid et al. have utilized the nuanced activation of donors and donor-acceptor matching to simplify the oligosaccharide assembly utilizing *n*-pentenyl glycosyl donors (NPGs)

and *n*-pentenyl orthoesters (NPOEs) [7–9]. The versatile use of NPG and NPOE by utilizing Lewis acids such as ytterbium and scandium triflates are also reported by Fraser-Reid et al. [10–12]. In this context, we were impressed by the pioneering report by Lambert et al. on synthesis of an organic Brønsted acid, pentacarbomethoxycyclopentadiene (PCCP, Fig. 1), which is efficiently utilized for catalysing various organic reactions [13]. They have also shown that the pKa of PCCP can be manipulated by changing the five ester groups leading to chiral and achiral PCCP derivatives [14]. There is only sporadic information available on utilizing organic Brønsted acid for saccharide coupling [15–19]. We have initiated our studies on utilizing PCCP (A/B, Fig. 1), the unique organic Brønsted acid for glycosidation reaction using NPOEs, the preliminary results of our investigations are discussed in this article.

2. Results and discussion

Our initial experiment involved glycosidation using benzoyl (Bz)

Abbreviations: PCCP, pentacarbomethoxycyclopentadiene.

* Corresponding authors. Chemical Sciences and Technology Division, CSIR-National Institute for Interdisciplinary Science and Technology (CSIR-NIIST), Thiruvananthapuram, 695019, India.

E-mail addresses: lavishankar@niist.res.in (R.S. Lankalapalli), radhu2005@gmail.com (K.V. Radhakrishnan).

<https://doi.org/10.1016/j.carres.2022.108684>

Received 15 March 2022; Received in revised form 16 September 2022; Accepted 22 September 2022

Available online 27 September 2022

0008-6215/© 2022 Elsevier Ltd. All rights reserved.

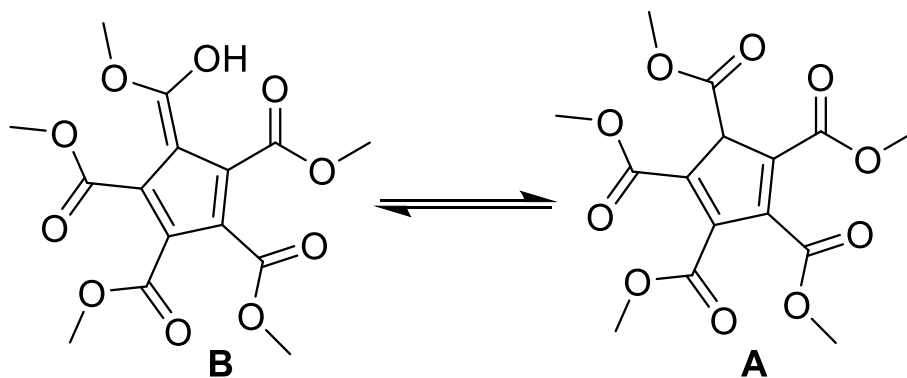


Fig. 1. Structure of organic Brønsted acid pentacarbomethoxycyclopentadiene (PCCP).

protected NPOE of *D*-glucose (**1a**, Fig. 2) with a naturally occurring secondary alcohol (+)-isomenthol (**2a**, Fig. 2), a major component of the wild mint *Mentha arvensis*, a species of flowering plant in the mint family Lamiaceae. Reaction of **1a** and **2a** in the presence of a catalytic amount of PCCP (0.01 mol%) and NIS (3.5 equiv.) in dichloromethane at 0 °C to room temperature afforded the glycoside **3aa** (Scheme 1) in moderate yield, even after stirring the reaction mixture for 24 h. Hence, we optimized the reaction conditions by varying the time, temperature, and solvents (see, Supporting Information, Table S1). The optimized reaction condition for glycosidation of **2a** (1 equiv.) with **1a** (1.5 equiv.) in the presence of PCCP (0.01 mol%), NIS (3.5 equiv.) in dichloromethane (9 mL) and 4 Å molecular sieves (powdered), under inert atmosphere, from 0 °C to room temperature for a duration of 48 h afforded 1,2-trans glycoside **3aa** in 93% yield (Scheme 1).

The first successful glycosidation reaction with catalytic PCCP and NIS prompted for investigation of substrate scope of the reaction with *D*-glucose NPOEs bearing benzyl, benzoyl, and acetyl protection, and various aglycones comprising natural products cholesterol **2b**, betulinic acid **2c**, methyl cholate **2e**, deoxymethyl cholate **2f**, and methylglycoside acceptors **2d**, **2g-h** (Fig. 2), which afforded 1,2-trans glycosides **3** in good to excellent yields (entry 1–5, Table 1). The effect of protecting groups on the stereochemical outcome of glycosidation was apparent. Benzoyl (**1a**) and benzyl (**1b**) protected NPOEs selectively afforded 1,2-trans glycosides **3**, whereas, acetyl protected NPOE **1c** led to 1,2-cis and trans glycoside mixture of **4ce:3ce** (1:0.3) and **4cf:3cf** (1:0.33) (entry 6–7, Table 1). However, NPOEs bearing benzoyl, benzyl protection on *D*-galactose (**1d** and **1e**) with the aforementioned aglycones, invariably, led to formation of 1,2-orthoester adducts (entry 8–13, Table 1). The glycosylated products/1,2-orthoesters were identified from the coupling constants of the anomeric protons in the ¹H NMR spectra. Anomeric protons of the 1,2-orthoester products exhibit a coupling constant of 5–5.5 Hz, compared to 1,2-trans and 1,2-cis glycosides that exhibit 7–9 and 1–4 Hz, respectively.

The reactivity order of the three OH groups in cholic acid was investigated by various research groups [20,21]. In the present study, a regioselective glycosidation of **2e** with **1a** at C3 position was the only product observed in 96% yield. Compound **3ae** was confirmed by comparison with respective chemical shifts in ¹³C NMR spectra of hydroxy bearing carbons of **2e**, which are 71.9, 68.4, and 73.0 ppm for C3, C7, and C12, respectively. The chemical shifts of C3, C7, and C12 of **3ae**

are 80.7, 68.0, and 72.8 ppm, respectively, which confirms the C3 regioselectivity of the glycosidation. A similar ¹³C NMR chemical shift analysis was carried out to confirm the C3 regioselectivity of the products **3ac**, **3be**, **3ce**, **4ce**, **3cf**, **4cf**, **5df**, **5ec**, and **5ef**. Additionally, experiments were conducted with common Lewis acids (10 mol%) in conventional glycosidation of **2a** with **1a** to ascertain the efficiency of PCCP catalyst. Reactions catalyzed by Sc(OTf)₃ and Yb(OTf)₃ afforded 1, 2-orthoester adduct **5aa** in 90 and 93% yields, respectively, similar to a report by Fraser-Reid et al. [6], interestingly, Zn(OTf)₂ afforded the 1, 2-trans glycoside **3aa** in 85% yield.

Control experiments were conducted to decipher the role of PCCP in conjunction with NIS in the glycosidation reaction, where attempts with either PCCP (0.01 mol%) or NIS (3.5 equiv.) resulted in no reaction, which shows that activation of NIS by PCCP as the driving force behind generation of iodonium ion. Interestingly, repetition of the optimized reaction condition by replacing PCCP with other Brønsted acids viz. BINAP or triflic acid at 10 mol% did not yield the glycosidated product. Fraser-Reid et al. described that the activation of NPOE results in the initial formation of oxocarbenium (I) and dioxolenium (III) cations, which are interchanged via trioxolenium (II) ion (Scheme 2) [22]. The second role of PCCP, perhaps, is to enhance the nucleophilicity of the acceptor by hydrogen bonding similar to chiral phosphoric acids [23], resulting in 1,2-trans glycoside bond formation with I or II or III to afford **3** by S_N2 attack, the steric difference in C2 benzoyl ester versus acetyl ester can be the reason behind 1,2-cis selectivity with **1c** donor for the formation of **4**. The rationale behind formation of 1,2-orthoester **5** from **1d/1e** could be owing to an intramolecular stabilization of oxocarbenium ion (I) from C4 ether or ester, which ensure nucleophilic addition by acceptor alcohol on disarmed C2 ester IV. As reported by Fraser-Reid et al. on reactivity of NPOEs in the presence of Lewis acids [6], Sc(OTf)₃ and Yb(OTf)₃ afforded 1,2-orthoester adduct **5aa**. However, the rationale behind the formation of 1,2-trans glycoside **3aa** in the presence of Zn(OTf)₂ can be attributed to the spontaneous release of triflate, due to sheer size of zinc compared to the other two metals, followed by formation of a glycosyl triflate intermediate [24] from oxocarbenium ion I and subsequent nucleophilic S_N2 attack by the alcohol acceptor.

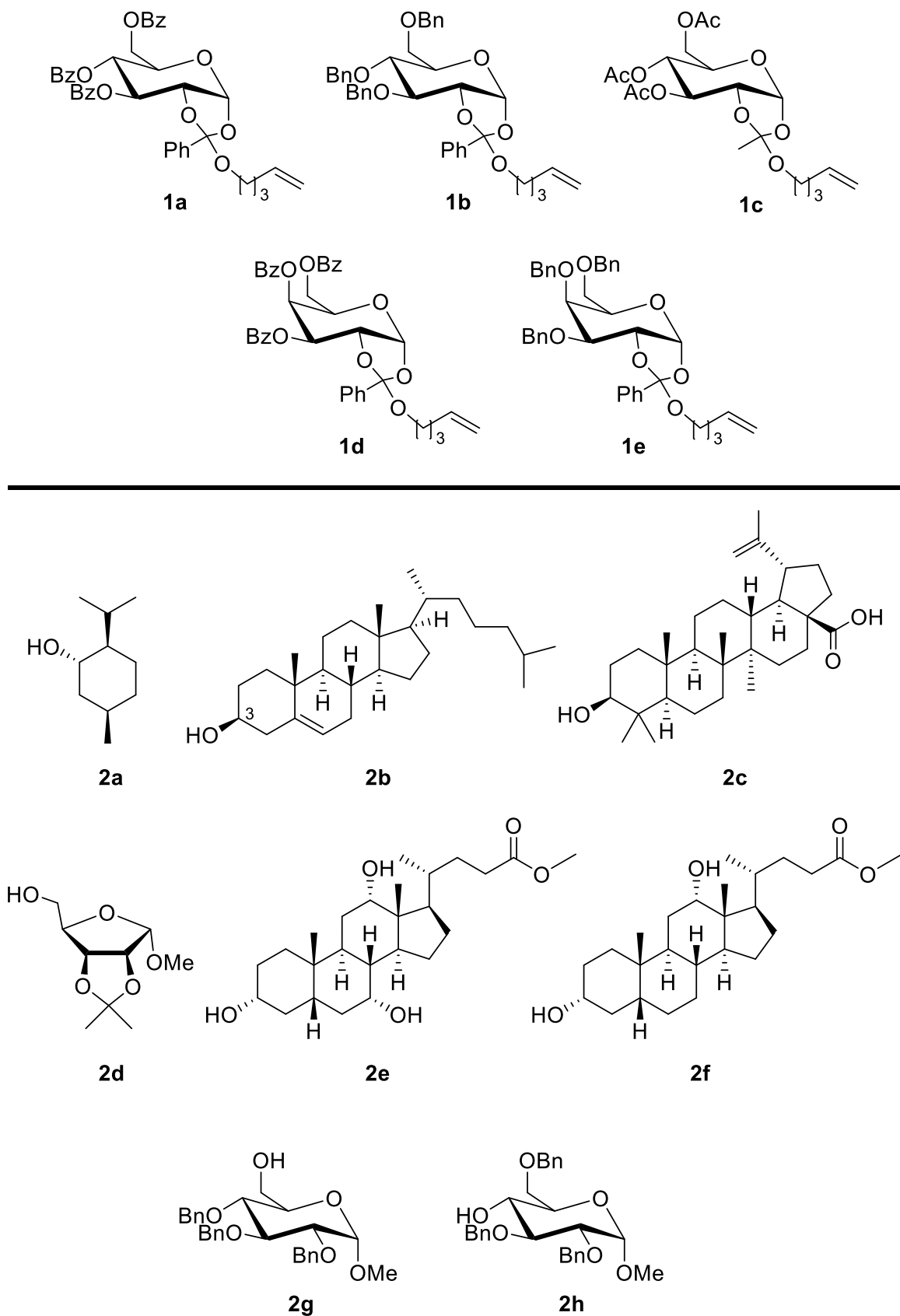
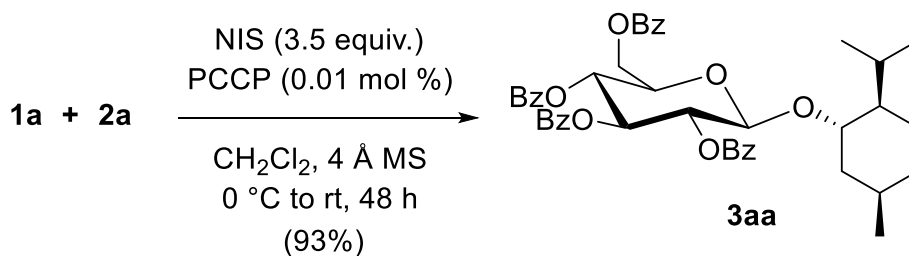


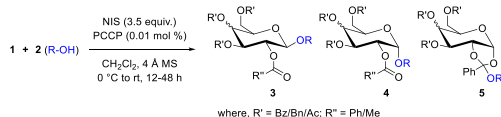
Fig. 2. Structures of NPOE donors and acceptors.



Scheme 1. PCCP catalyzed glycosidation of 2a with NPOE 1a.

Table 1

Substrate scope of glycosidation reactions catalyzed by PCCP using NPOE donors.^a



Entry	Glycosyl Donor	Glycosyl acceptor	Product(s)	Yield ^b (%)
1	1a	2b	3ab	76 (94)
2	1a	2c	3ac ^c	71 (89)
3	1a	2e	3ae ^c	96
4	1b	2a	3ba	79 (90)
5	1b	2e	3be ^c	91 (93)
6	1c	2e	3ce:4ce ^c (0.3:1)	92
7	1c	2f	3cf:4cf ^c (0.33:1)	92
8	1d	2f	5df ^c	68 (85)
9	1d	2h	5dh	93
10	1e	2c	5ec ^c	63 (91)
11	1e	2d	5ed	67 (86)
12	1e	2f	5ef ^c	61 (76)
13	1e	2g	5eg	92

^a Reaction conditions: To the mixture of 1 (1.5 equiv.), 2 (1 equiv.) in CH₂Cl₂ at 0 °C, under 4 Å MS, PCCP (0.01 mol%), NIS (3.5 equiv.) were added, and slowly warmed to room temperature.

^b Isolated yields by column chromatography (yields in parenthesis represent values based on recovered 2).

^c C3 position glycosidated.

3. Conclusions

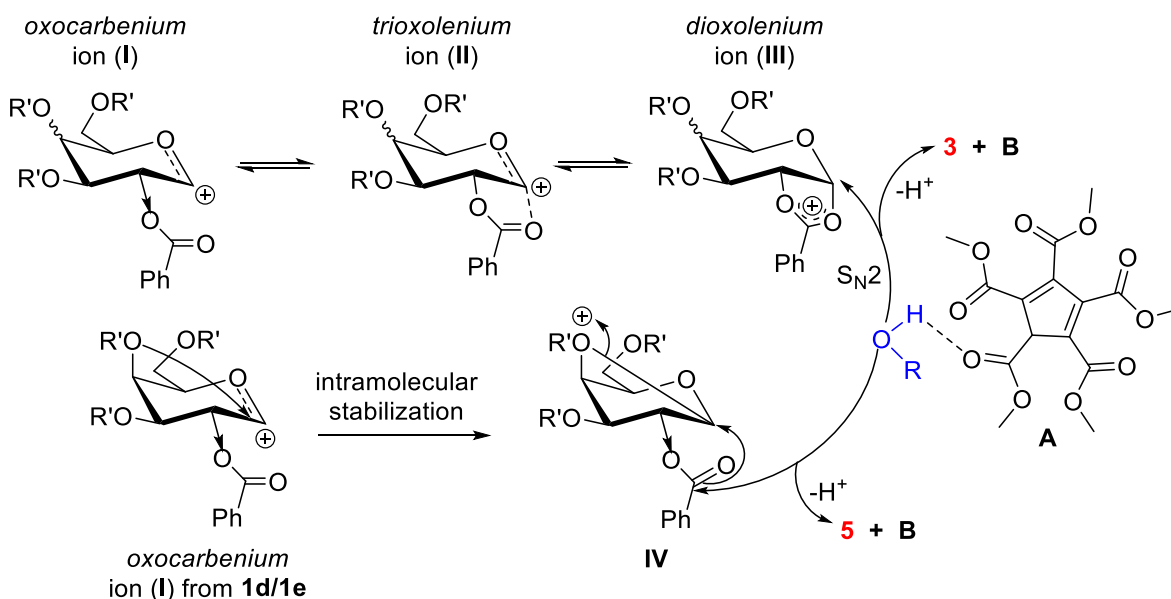
In conclusion, our preliminary investigation in utilizing the organic Brønsted acid PCCP for catalysing the glycosidation with NPOEs in conjunction with NIS led to the formation of 1,2-trans glycosides with D-glucose, and variation of C2 position with acetyl group led to cis-selectivity. However, the D-galactose based-NPOEs, afforded 1,2-orthoester products, and a reasonable mechanism behind the reactivity difference with donors is provided. Lewis acids such as Sc(OTf)₃ and Yb(OTf)₃ afforded 1,2-orthoester product in contrary to reaction with PCCP catalyst and D-glucosyl NPOEs 1a/1b/1c. To maintain the utility of the method towards glycosidation of natural products, attempts with cholic acid derivatives afforded a C3 regioselectivity and 1,2-trans stereoselectivity in excellent yields. Though the glycosidation with D-galactosyl donors led to 1,2-orthoesters, our preliminary studies showed the utility of PCCP in glycosidation with D-glucosyl NPOEs. Based on the results of this study, an expansion of the method with chiral Brønsted acids for stereoselectivity, diastereoselectivity with racemic alcohol acceptors for resolution is currently under progress, which will be communicated shortly.

Declaration of competing interest

The authors declare that they have no known competing financial interests or personal relationships that could have appeared to influence the work reported in this paper.

Data availability

Data will be made available on request.



Scheme 2. Plausible mechanism.

Acknowledgements

ACSIR research student M. A. thanks CSIR for research fellowship. Thanks are due to Ms. Viji S., Ms. Saumini Mathew for ESI-HRMS and NMR analysis.

Appendix A. Supplementary data

Supplementary data to this article can be found online at <https://doi.org/10.1016/j.carres.2022.108684>.

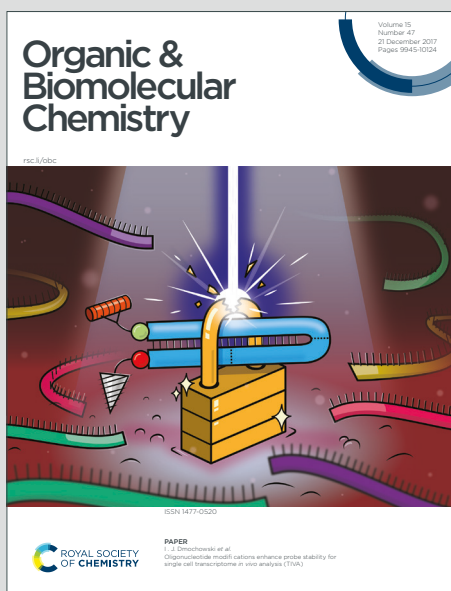
References

- [1] S. Manabe, Y. Ito, Optimizing glycosylation reaction selectivities by protecting group manipulation, *Curr. Bioact. Compd.* 4 (2008) 258–281, <https://doi.org/10.2174/157340708786847861>.
- [2] B. Fraser-Reid, J.C. Lopez, K.V. Radhakrishnan, M. Mach, U. Schlueter, A. Gomez, C. Uriel, Reciprocal donor acceptor selectivity (RDAS): a new concept for “matching” donors with acceptors, *Can. J. Chem.* 80 (2002) 1075–1087, <https://doi.org/10.1139/v02-137>.
- [3] M.M. Nielsen, C.M. Pedersen, Catalytic glycosylations in oligosaccharide synthesis, *Chem. Rev.* 118 (2018) 8285–8358, <https://doi.org/10.1021/acs.chemrev.8b00144>.
- [4] G. Sureshkumar, S. Hotha, Propargyl 1,2-orthoesters as glycosyl donors: stereoselective synthesis of Propargyl 1,2-orthoesters as glycosyl donors: stereoselective synthesis of 1,2-trans glycosides and disaccharides, *Tetrahedron Lett.* 48 (2007) 6564–6568, <https://doi.org/10.1016/j.tetlet.2007.07.015>.
- [5] B. Fraser-Reid, J.C. Lopez, K.V. Radhakrishnan, M. Mach, U. Schlueter, A. M. Gomez, C. Uriel, Unexpected role of O-2 “protecting” groups of glycosyl donors in mediating regioselective glycosidation, *J. Am. Chem. Soc.* 124 (2002) 3198–3199, <https://doi.org/10.1021/ja012383m>.
- [6] K.N. Jayaprakash, S.R. Chaudhuri, C.V.S.R. Murty, B. Fraser-Reid, Regioselective strategies mediated by lanthanide triflates for efficient assembly of oligomannans, *J. Org. Chem.* 72 (2007) 5534–5545, <https://doi.org/10.1021/jo070018t>.
- [7] M. Mach, U. Schlueter, F. Mathew, B. Fraser-Reid, K.C. Hazen, Comparing n-pentenyl orthoesters and n-pentenyl glycosides as alternative glycosyl donors, *Tetrahedron* 58 (2002) 7345–7354, [https://doi.org/10.1016/S0040-4020\(02\)00671-3](https://doi.org/10.1016/S0040-4020(02)00671-3).
- [8] Z. Yang, W. Lin, B. Yu, Rearrangement of sugar 1,2-orthoesters to glycosidic products: a mechanistic implication, *Carbohydr. Res.* 329 (2000) 879–884, [https://doi.org/10.1016/S0008-6215\(00\)00242-1](https://doi.org/10.1016/S0008-6215(00)00242-1).
- [9] J.G. Allen, B. Fraser-Reid, n-Pentenyl glycosyl orthoesters as versatile intermediates in oligosaccharide synthesis. The proteoglycan linkage region, *J. Am. Chem. Soc.* 121 (1999) 468–469, <https://doi.org/10.1021/ja9832358>.
- [10] T. Buskas, E. Söderberg, P. Konradsson, B. Fraser-Reid, Use of n-pentenyl glycosides as precursors to various spacer functionalities, *J. Org. Chem.* 65 (2000) 958–963, <https://doi.org/10.1021/jo9909554>.
- [11] B. Fraser-Reid, P. Konradsson, D.R. Mootoo, U. Udodong, Direct elaboration of pent-4-enyl glycosides into disaccharides, *J. Chem. Soc. Chem. Commun.* (1988) 823–825, <https://doi.org/10.1039/c39880000823>.
- [12] A. Arasappan, B. Fraser-Reid, n-pentenyl glycoside methodology in the stereoselective construction of the tetrasaccharyl cap portion of leishmania lipophosphoglycan, *J. Org. Chem.* 61 (1996) 2401–2406, <https://doi.org/10.1021/jo9520102>.
- [13] T.H.L. Chirag D. Gheewala, Bridget E. Collins, An aromatic ion platform for enantioselective Brønsted acid catalysis, *Science* 351 (80) (2016) 961–965, https://doi.org/10.1142/9781783268993_0002.
- [14] C.D. Gheewala, M.A. Radtke, J. Hui, A.B. Hon, T.H. Lambert, Methods for the synthesis of functionalized pentacarboxycyclopentadienes, *Org. Lett.* 19 (2017) 4227–4230, <https://doi.org/10.1021/acs.orglett.7b01867>.
- [15] D. Benito-Alifonso, M.C. Galan, Brønsted- and lewis-acid-catalyzed glycosylation, in: *Sel. Glycosylations Synth. Methods Catal.*, Wiley-VCH Verlag GmbH & Co. KGaA, Weinheim, Germany, 2017, pp. 155–172, <https://doi.org/10.1002/9783527696239.ch8>.
- [16] D.J. Cox, M.D. Smith, A.J. Fairbanks, Glycosylation catalyzed by a chiral Brønsted acid, *Org. Lett.* 12 (2010) 1452–1455, <https://doi.org/10.1021/ol1001895>.
- [17] L. Meng, P. Wu, J. Fang, Y. Xiao, X. Xiao, G. Tu, X. Ma, S. Teng, J. Zeng, Q. Wan, Glycosylation enabled by successive rhodium(II) and Brønsted acid catalysis, *J. Am. Chem. Soc.* 141 (2019) 1–6, <https://doi.org/10.1021/jacs.9b04619>.
- [18] D. Liu, S. Sarrafpour, W. Guo, B. Goulart, C.S. Bennett, Matched/Mismatched interactions in chiral Brønsted acid-catalyzed glycosylation reactions with 2-deoxy-sugar trichloroacetimidate donors, *J. Carbohydr. Chem.* 33 (2014) 423–434, <https://doi.org/10.1080/07328303.2014.927882>.
- [19] S. Traboni, E. Bedini, A. Silipo, G. Vessella, A. Iadonisi, Solvent-free glycosylation from per-O-acylated donors catalyzed by methanesulfonic acid, *Eur. J. Org. Chem.* 2021 (2021) 5669–5676, <https://doi.org/10.1002/ejoc.202101121>.
- [20] X. Hu, Z. Zhang, X. Zhang, Z. Li, X. Zhu, Selective acylation of cholic acid derivatives with multiple methacrylate groups, *Steroids* 70 (2005) 531–537, <https://doi.org/10.1016/j.steroids.2004.11.015>.
- [21] P.S. Dangate, C.L. Salunke, K.G. Akamanchi, Regioselective oxidation of cholic acid and its 7 β epimer by using o-iodoxybenzoic acid, *Steroids* 76 (2011) 1397–1399, <https://doi.org/10.1016/j.steroids.2011.07.009>.
- [22] B. Fraser-Reid, S. Grimme, M. Piacenza, M. Mach, U. Schlueter, Orthoesters versus 2-O-acyl glycosides as glycosyl donors: theoretical and experimental studies, *Chem. Eur. J.* 9 (2003) 4687–4692, <https://doi.org/10.1002/chem.200304856>.
- [23] T. Kimura, M. Sekine, D. Takahashi, K. Toshima, Chiral Brønsted acid mediated glycosylation with recognition of alcohol chirality, *Angew. Chem., Int. Ed.* 52 (2013) 12131–12134, <https://doi.org/10.1002/anie.201304830>.
- [24] E.T. Sletten, Y.J. Tu, H.B. Schlegel, H.M. Nguyen, Are Brønsted acids the true promoter of metal-triflate-catalyzed glycosylations? A mechanistic probe into 1,2-cis-aminoglycoside formation by nickel triflate, *ACS Catal.* 9 (2019) 1–30, <https://doi.org/10.1021/acscatal.8b04444>.

Organic & Biomolecular Chemistry

Accepted Manuscript

This article can be cited before page numbers have been issued, to do this please use: M. Aswathy, N. K. Mohammad Sadiq, P. C. Harikrishnan, S. Parameswaran, K. V. Radhakrishnan and R. S. Lankalapalli, *Org. Biomol. Chem.*, 2023, DOI: 10.1039/D3OB01633A.



This is an Accepted Manuscript, which has been through the Royal Society of Chemistry peer review process and has been accepted for publication.

Accepted Manuscripts are published online shortly after acceptance, before technical editing, formatting and proof reading. Using this free service, authors can make their results available to the community, in citable form, before we publish the edited article. We will replace this Accepted Manuscript with the edited and formatted Advance Article as soon as it is available.

You can find more information about Accepted Manuscripts in the [Information for Authors](#).

Please note that technical editing may introduce minor changes to the text and/or graphics, which may alter content. The journal's standard [Terms & Conditions](#) and the [Ethical guidelines](#) still apply. In no event shall the Royal Society of Chemistry be held responsible for any errors or omissions in this Accepted Manuscript or any consequences arising from the use of any information it contains.

α/β -Stereo- and Diastereoselective Glycosylation with *n*-Pentenyl Glycoside Donors, Promoted by *N*-Iodosuccinimide and Catalyzed by Chiral Brønsted Acid

Received 00th January 20xx,
Accepted 00th January 20xx

DOI: 10.1039/x0xx00000x

Maniyamma Aswathy,^{a,b} Mohammed Sadik N. K.,^c Purushothaman C. Harikrishnan,^a Sasikumar Parameswaran,^a Kokkuvayil Vasu Radhakrishnan,^{a,b,*} and Ravi S. Lankalapalli^{a,b,*}

A stereoselective glycosylation method catalyzed by (+)-isomenthol ester of pentacarbomethoxycyclopentadiene as chiral Brønsted acid with *n*-pentenylglycosides (NPGs) in the presence of *N*-iodosuccinimide as the promoter is described that offered a chiral recognition of the racemic substrates.

Hydrolysis of the glycosidic bond by glycosidases or glycosylation by glycosyltransferases is governed by acid-base catalysis by amino acids Asp, Glu, and Tyr as the catalytic residues in the active site.^{1,2} Intuitively, Brønsted acids (BAs) can act as enzymes when used with appropriate glycosyl donors for synthetic glycosylation. Activation of glycosyl donors by Lewis acids is dominant in glycosylation compared to BA-based promoters that were employed, in general, for 1-hydroxy and trichloroacetimidate glycosyl donors.^{3–10} Sulfuric acid immobilized on silica as BA in combination with *N*-iodosuccinimide (NIS) was utilized to activate a thioglycoside for the synthesis of tetrasaccharide fragments.^{11–13} Further, glycosylation attempts were made with chiral BA (CBA) activation to achieve α/β -stereoselectivity, which includes a tetrazole-amino acid ionic liquid,⁹ chiral binaphthol (BINOL) phosphoric acids,^{14–16} and peptide bearing carboxylic acid groups in combination with MgBr₂ Lewis acid.¹⁷

Recently, we reported the catalytic utility of the BA-PCCP (pentacarbomethoxycyclopentadiene) for stereoselective glycosylation with *n*-pentenyl orthoesters (NPOE) of β -glucose and β -galactose in the presence of NIS.¹⁸ Oxidative hydrolysis of *n*-pentenyl glucoside (NPG) with *N*-bromosuccinimide to a hemiacetal is an outcome of a serendipitous observation by Fraser-Reid,¹⁹ which led to the inception of NPG and NPOE glycosyl donors. BA-PCCP catalysis was a pioneering contribution by Lambert et al., who prepared the chiral version of this BA by appending naturally occurring (-)-menthol as an

ester and showed its utility in Mukaiyama-Mannich and oxocarbenium aldol reactions in an enantioselective manner.²⁰ Toshima et al. utilized chiral BINOL phosphoric acid as BA, resulting in an enantioselective catalysis for glycosylation with trichloroacetimidate donors and racemic acceptors, affording excellent α/β -stereo- and diastereoselectivity.¹⁴ Inspired by these two reports, we present our findings on stereoselective glycosylation with NPG donor in the presence of NIS, by efficient chiral catalyst from (+)-isomenthol ester of PCCP, which offered chiral recognition of racemic aglycones viz. menthol, benzylic alcohols, and Boc-protected serine.

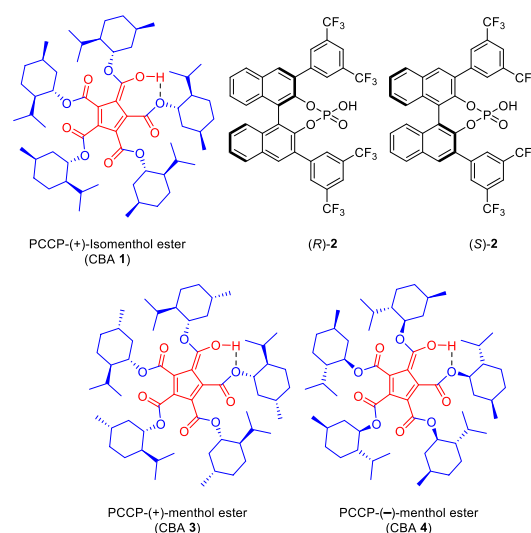


Figure 1. Chiral Brønsted Acids (CBAs).

CBA **1** (Figure 1) was synthesized from PCCP and (+)-isomenthol as per the reported procedure.²⁰ Racemic menthol **5** was chosen as the acceptor for exploring the chiral recognition in glycosylation reaction catalyzed by CBA **1**. The initial glycosylation attempt was performed with benzyl-protected glucosyl-NPG **6** and **5** in the presence of NIS

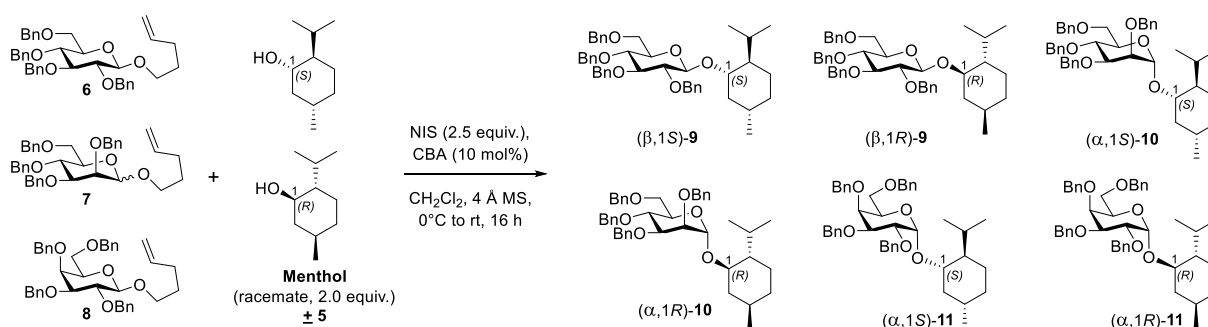
^a Chemical Sciences and Technology Division, CSIR-National Institute for Interdisciplinary Science and Technology (CSIR-NIIST), Thiruvananthapuram-695019, India

^b Academy of Scientific and Innovative Research (AcSIR) Ghaziabad-201002, India.

^c Department of Applied Chemistry, CUSAT, Kochi-22.

E-mail: radhu2005@gmail.com, ravishankar@niist.res.in Electronic Supplementary Information (ESI) available: ¹H, ¹³C and 2D NMR, experimental procedures, Computational studies, NMR spectral data, HPLC chromatograms. See DOI: 10.1039/x0xx00000x

COMMUNICATION

Table 1. Glycosylation reaction of benzyl protected NPGs **6/7/8** and racemic menthol **5**.^a

Entry	Donor	Activator	Yield (%) ^b	Ratio of diastereomeric glycosides (%) ^c					
				(β,1S)-9	(β,1R)-9	(α,1S)-10	(α,1R)-10	(α,1S)-11	(α,1R)-11
1	6	1	92	86.8%	13.2%	-	-	-	-
2	7	1	85	-	-	84.7%	15.3%	-	-
3	8	1	94	-	-	-	-	84.5%	15.5%
4	8	(<i>R</i>)- 2	90	-	-	-	-	40.1%	59.9%
5	8	(<i>S</i>)- 2	83	-	-	-	-	45.7%	54.3%
6	8	Sc(OTf) ₃	86	Neither stereoselective nor diastereoselective					
7	8	PCCP	73	Neither stereoselective nor diastereoselective					
8	8	CF ₃ SO ₃ H	35	Neither stereoselective nor diastereoselective					
9	7	3	90	-	-	54.2%	45.8%	-	-
10	7	4	85	-	-	45.9%	54.1%	-	-

^aReaction conditions: To the mixture of **6/7/8** (1.0 equiv.), **5** (2.0 equiv.) in CH₂Cl₂ at 0 °C, under 4 Å MS, NIS (2.5 equiv.), CBAs (10 mol%) activators other than CBA (15 mol%) were added and slowly warmed to room temperature. ^bIsolated yields by column chromatography. ^cRatio of diastereomeric glycosides obtained from the area% of HPLC chromatogram.

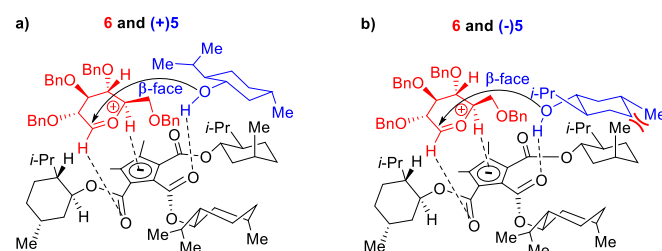
and CBA **1** (10 mol%), under the optimized reaction conditions of our previous report with BA-PCCP,¹⁸ which afforded β-glycoside **9** in 92% yield (entry 1, Table 1). The diastereomeric ratio of (β, 1*S*)-**9** and (β, 1*R*)-**9**, determined by computing the area percentage of both the peaks in the HPLC chromatogram and by comparison with the retention times of respective glycosides of each enantiomer of menthol (see the Supporting Information), were found to be 86.83% and 13.17%, respectively (entry 1, Table 1). Thus, apart from β-selectivity with CBA **1**, chiral recognition of the racemic menthol favouring glycosylation of (+)-menthol afforded (β,1*S*)-**9** with a diastereomeric excess of 74%. Glycosylation with mannosyl-NPG **7** (α, β mixture) in the presence of CBA **1** afforded glycoside **10** with the expected α-stereoselectivity

(entry 2, Table 1). It is interesting to note that glycosylation with the less studied galactosyl-NPG **8** produced glycoside **11** with α-stereoselectivity (entry 3, Table 1). Once again, chiral recognition favoured glycosylation of (+)-menthol to afford diastereoselective products (α,1*S*)-**10** and (α,1*S*)-**11**, with both showing a diastereomeric excess of 69% (entry 2 & 3, Table 1). The results of glycosylation with CBA **1** motivated us to compare its role in α/β-stereo- and diastereoselectivity with other chiral and non-chiral BAs under the optimized glycosylation conditions.¹⁸ Galactosyl-NPG **8** is rarely explored for glycosylation reactions compared to NPGs **6** & **7**. Hence, glycosylation with NPG **8** and BINOL-derived chiral phosphoric acid catalysts (*R*)-**2** and (*S*)-**2** (Figure 1) were attempted, which

also afforded α -glycoside **11** like CBA **1**; however, the diastereoselectivity was poor and slightly favoured glycosylation of (-)-menthol (entry 4 & 5, Table 1). Glycosylation attempt with NPG **8** in the presence of Lewis acid activator $\text{Sc}(\text{OTf})_3$, a conventional activator for NPG donors,²¹ and BAs such as achiral PCCP and triflic acid afforded neither stereoselectivity nor diastereoselectivity (entry 6-8, Table 1). In all three attempts, we observed the formation of the *R/S* mixture of both α and β glycosides of corresponding NPGs. To assess the importance of the selection of (+)-isomenthol in CBA synthesis, CBA **3** and CBA **4** (Figure 1) were synthesized from (+)-menthol and (-)-menthol, respectively. NPG **7** was chosen to study the effect of steric hindrance of the β -face of oxocarbenium ion on glycosylation in the presence of both CBA **3** and CBA **4** catalysts, α -glycosides **10** were produced as an outcome with no diastereoselectivity.

The benzyl protection of NPGs **6-8** was intended to avoid any participation effect during glycosylation, similar to the approach by Toshima et al.¹⁴ Glycosylation, either in the absence of CBA or NIS, did not occur, suggesting the role of CBA catalyst in the activation of NIS. Next, we treated one of the obtained products (β ,1S)-**9** with CBA-**1** and NIS under the optimized glycosylation condition without the acceptor \pm **5**. The product (β ,1S)-**9** was quantitatively recovered without any isomerization even after 24 h of reaction, which indicates the stereo and diastereoselectivities of the reaction was driven by kinetic control. The mechanistic rationale behind the stereoselectivity is shown in Scheme 1 from the positioning of the oxocarbenium ion, generated from NPG activation,²² and menthol on chiral cyclopentadienyl anion platform, in line with the model proposed by Lambert et al. for enantioselective addition on oxocarbenium with the necessary organizational element of H-bonding.²⁰ We surmise the H-bonding interactions of C-H bonds of C1, and C5 carbons adjacent to the oxygen of the oxocarbenium ion and the cyclopentadienyl anion are the conventional and CH/ π H bonding interactions (Scheme 1a).²³ During glycosylation, the menthol is positioned in the hydrophobic pocket formed by the (+)-isomenthyl groups and held by H-bonding with the carbonyl of the catalyst. The organization of the donor and acceptor on the cyclopentadienyl ring, prior to glycosylation, is the key to the observed stereo- and diastereoselectivity. As shown in the model, the α/β -stereoselectivity of glycosylation is governed by the steric hindrance by C2-OBn and C4-OBn groups for the incoming nucleophilic attack on oxocarbenium ion. Accordingly, in the case of glucosyl-NPG **6**, the less hindered β -face is preferred for nucleophilic attack of the menthol oxygen atom, and galactosyl-NPG **8** preferred the α -face. While the mannosyl-NPG **7** exhibited the conventional α -selectivity. The β -selectivity with NPG **6** and α -selectivity with NPG **7** and **8** reinforces the proposed model in Scheme 1 as a highly conserved catalytic platform with organizational elements to promote stereoselectivity. The rationale for diastereoselectivity is governed by the steric interaction of the all-equatorial conformation of the menthol with the axial-methyl group of (+)-isomenthyl of the catalyst. (-)-Menthol **5** exhibits van der Waals repulsion in the proposed model (Scheme 1b), favoring (+)-menthol **5** in glycosylation

(Scheme 1a). Thus, based on the proposed model (Scheme 1), α/β -stereo- and diastereoselectivity with NPGs **6-8** and chiral recognition of racemic menthol **5** (entries 1-3, Table 1) can be rationalized. The choice of ester in the catalyst is essential, which was demonstrated with menthyl esters of CBA **3** and **4** that possess all three groups in the equatorial position of their most stable conformation, causing a lack of diastereoselectivity (entries 9-10, Table 1). By the same token, the PCCP CBA catalyst with (-)-isomenthyl group can offer the opposite chiral recognition; however, due to the lack of commercial availability of (-)-isomenthol, we could not pursue synthesis of the catalyst. The importance of CBA **1** catalysis was obvious in glycosylation; as attempts with chiral phosphoric acid catalysts (*R*)-**2** and (*S*)-**2**, though offered stereoselectivity, there was no appreciable chiral recognition of racemic menthol (entries 4-5, Table 1).

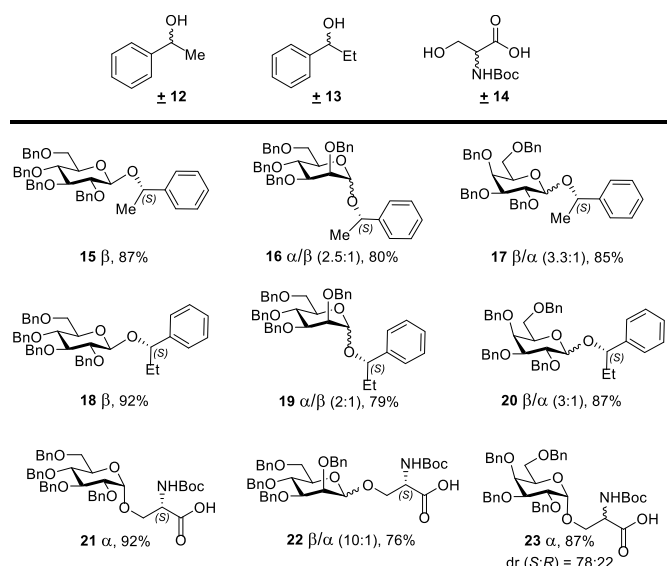


Scheme 1. Rationale for stereo- and diastereocontrol in glycosylation with CBA **1**.

We utilized density functional theory (DFT) calculations to establish a correlation between the suggested mechanism responsible for the oxocarbenium intermediate-assisted transition state, the presence of hydrogen bonding interactions among the three systems, and the electron transitions from the acceptor to the oxocarbenium intermediate. Our experimental analysis aligned seamlessly with DFT assessments, confirming the existence of three significant hydrogen bonding interactions within the optimized geometries. The visual depiction of DFT analysis, as illustrated in Figure (S1) (see supporting information), unveiled precise interactions: A hydrogen bond forms between the hydrogen atom (H39) in the acceptor moiety's hydroxyl group and the catalyst's carbonyl oxygen (O11) at an approximate length of 1.44 Å. Another discernible hydrogen bond interaction exists between the catalyst's carbonyl oxygen (O3) and the hydrogen atom (H54) of the oxocarbenium intermediate, measuring approximately 1.47 Å. Furthermore, a π -hydrogen bond is observed between the catalyst and the oxocarbenium ion (H67) by positioning a dummy atom (O84) at the cyclopentadienyl system's center, with an approximate bond length of 1.96 Å. The consistency of these parameters with findings from prior literature further substantiates the proposed mechanism.²³ Moreover, the electron transition between the oxocarbenium intermediate and the acceptor groups were illustrated by calculating the highest occupied molecular orbitals (HOMO) and the lowest unoccupied molecular orbitals (LUMO) for the optimized geometry. As given in Table S1 (See supporting information), the HOMO energy level (6.40 eV) is concentrated over the acceptor moiety, whereas the LUMO energy level (3.04 eV) is concentrated over the oxocarbenium intermediate.

Which confirms the nucleophilic as well as electrophilic nature of the acceptor and intermediate system respectively.

To assess the generality, we explored the chiral recognition with racemic substrates **12**, **13**, and **14** for CBA **1**-catalyzed glycosylation reaction with NPGs **6-8** (Scheme 2). Exclusive diastereocontrol in chiral recognition of the S-enantiomers of benzylic alcohols **12** and **13** in the glycosylation reaction afforded **15-20** in excellent yields. Glucosyl-NPG **6** afforded β -anomers **15** and **18** selectively, however, mannosyl-NPG **7** afforded anomeric mixtures **16**, **19**, dominating in α -anomer, and galactosyl-NPG **8** produced anomeric mixtures **17**, **20**, dominating in β -anomer. Interestingly, glycosylation attempts with racemic Boc-protected serine **14**, with free carboxylic acid, also afforded chiral recognition with S-enantiomer in good yields, wherein, glucosyl-NPG **6** afforded α -anomer **21** selectively, and mannosyl-NPG **7** afforded an anomeric mixture of **22**, dominating in β -anomer. However, galactosyl-NPG **8** produced α -anomer **23** selectively and did not afford chiral recognition, unlike its congeners. In line with the mechanistic rationale outlined in Scheme 1, the preference for the S-enantiomers of benzylic alcohols **12** and **13** in the glycosylation reaction is shown in Scheme S3 (Supporting Information). However, in the case of racemic **14**, intricate secondary interactions arising from the Boc and COOH groups in the transition state for glycosylation reaction dictate the stereo- and diastereoselectivity, which is difficult to comprehend.



^aReaction conditions: To the mixture of **6/7/8** (1.0 equiv.), \pm **12/13/14** (2.0 equiv.) in CH_2Cl_2 at 0 °C, under 4 Å MS, NIS (2.5 equiv.), CBA **1** (10 mol%) was added and slowly warmed to room temperature. The reported yields are isolated yields by column chromatography. The ratios were determined from integration of the anomeric protons in ^1H NMR spectra, identified by their respective chemical shifts of the glycosides with pure enantiomers and HMQC spectra (see the Supporting Information), dr is the diastereomeric ratio.

Scheme 2. Diastereocontrol in glycosylation of racemic acceptors **12**, **13** and **14** with CBA **1**. View Article Online
DOI: 10.1039/D3OB01633A

In conclusion, as noted in the pioneering contribution by Lambert, chiral PCCP BA catalysis can be made more efficient by optimization of the catalyst structure; herein, we modified their original CBA **4** with (-)-menthol to CBA **1** with (+)-isomenthol and evaluated its catalytic role in stereoselective glycosylation with NPG donors in the presence of NIS as the promoter. Apart from α/β -stereoselectivity with NPGs, glycosylation reaction in the presence of CBA **1** was efficient in chiral recognition of the racemic menthol, favouring (+)-menthol, with excellent diastereoselectivity. The stereo- and diastereocontrol observed here with CBA **1** and NPGs are superior to chiral BINOL phosphoric acid-catalyzed glycosylation with trichloroacetimidate donors.¹⁴ The mechanistic model behind CBA **1** catalysis by H-bonding organization of the oxocarbenium ion, generated from NPG activation and menthol with the chiral cyclopentadienyl anion platform, assisted in providing a rationalistic explanation behind the lack of diastereocontrol with other chiral, BINOL-derived and menthyl CBA esters, and non-chiral BAs. The present investigation with CBA **1** catalyst motivated us to explore its utility with other racemic aglycons and the resulting stereo- and diastereocontrol observed in glycosylation with NPGs suggest the potent benefits of CBA in myriad BA-catalyzed synthetic organic transformations.

Author contributions

K. V. R. conceived and supervised this project. M. A. performed a major portion of the synthesis. M.S. performed theoretical calculations. P. C. H. and S. P. performed a minor portion of the synthesis. R. S. L. supervised this project and wrote the original draft of the manuscript which was edited by all the authors.

Acknowledgement

AcSIR student M. A. thanks CSIR for the fellowship and Mr. Billu Abraham and Ms. C.P. Devika for help with HPLC and Deepa Sebastian for the help in interpreting theoretical calculations. Financial support from DST, Science, and Engineering Research Board, India (Grant number: CRG/2020/004993) is gratefully acknowledged.

Conflicts of interest

The authors declare that they have no conflict of interest.

Notes and references

- J.-L. Viladot, E. de Ramon, O. Durany and A. Planas, *Biochemistry*, 1998, **37**, 11332–11342.
- L. L. Lairson, B. Henrissat, G. J. Davies and S. G. Withers, *Annu Rev Biochem*, 2008, **77**, 521–555.
- A. Kumar, V. Kumar, R. T. Dere and R. R. Schmidt, *Org Lett*, 2011, **13**, 3612–3615.
- H. Hinou, N. Saito, T. Maeda, M. Matsuda, Y. Kamiya and S.-I. Nishimura, *J Carbohydr Chem*, 2011, **30**, 575–586.
- A. A. Chaugule, A. R. Jadhav and H. Kim, *RSC Adv*, 2015, **5**, 104715–104724.

- 6 Y. Kobayashi, Y. Nakatsuji, S. Li, S. Tsuzuki and Y. Takemoto, *Angew. Chem. Int. Ed.*, 2018, **57**, 3646–3650.
- 7 T. Yamanoi, Y. Oda, S. Matsuda, I. Yamazaki, K. Matsumura, K. Katsuraya, M. Watanabe and T. Inazu, *Tetrahedron*, 2006, **62**, 10383–10392.
- 8 T. Yamanoi, S. Matsuda, I. Yamazaki, R. Inoue, K. Hamasaki and M. Watanabe, *Heterocycles*, 2006, **68**, 673–677.
- 9 S. Delacroix, J.-P. Bonnet, M. Courty, D. Postel and A. N. van Nhien, *Carbohydr Res*, 2013, **381**, 12–18.
- 10 S. Shirakawa and S. Kobayashi, *Org Lett*, 2007, **9**, 311–314.
- 11 S. Dasgupta and B. Mukhopadhyay, *European J Org Chem*, 2008, **2008**, 5770–5777.
- 12 G. Karki and P. K. Mandal, *Arkivoc*, 2019, **2019**, 196–210.
- 13 G. Karki, H. Kumar, R. Rajan and P. K. Mandal, *Synlett*, 2016, **27**, 2581–2586.
- 14 T. Kimura, M. Sekine, D. Takahashi and K. Toshima, *Angew. Chem. Int. Ed.*, 2013, **52**, 12131–12134.
- 15 D. Liu, S. Sarrafpour, W. Guo, B. Goulart and C. S. Bennett, *J Carbohydr Chem*, 2014, **33**, 423–434.
- 16 D. J. Cox, M. D. Smith and A. J. Fairbanks, *Org Lett*, 2010, **12**, 1452–1455. VIEW ARTICLE ONLINE
DOI: 10.1039/D3OB01633A
- 17 N. D. Gould, C. Liana Allen, B. C. Nam, A. Schepartz and S. J. Miller, *Carbohydr Res*, 2013, **382**, 36–42.
- 18 M. Aswathy, B. Abhijith, R. S. Lankalapalli and K. V. Radhakrishnan, *Carbohydr Res*, 2022, **522**, 108684.
- 19 B. Fraser-Reid and J. C. López, in *Top Curr Chem*, 2011, vol. 301, pp. 1–29.
- 20 C. D. Gheewala, B. E. Collins and T. H. Lambert, *Science (1979)*, 2016, **351**, 961–965.
- 21 K. N. Jayaprakash and B. Fraser-Reid, *Synlett*, 2004, 301–305.
- 22 B. Fraser-Reid, G. Anilkumar, M. R. Gilbert, S. Joshi and R. Kraehmer, in *Carbohydrates in Chemistry and Biology*, Wiley-VCH Verlag GmbH, Weinheim, Germany, 2000, pp. 135–154.
- 23 M. Nishio, *Phys. Chem. Chem. Phys.*, 2011, **13**, 13873–13900.